SEVENTH EUROPEAN CONFERENCE ON CONTROLLED FUSION AND PLASMA PHYSICS

Volume I

Lausanne, 1-5 September 1975
Centre de Recherches en Physique des Plasmas (CRPP)
Ecole Polytechnique Fédérale de Lausanne, Switzerland

SEVENTH EUROPEAN CONFERENCE ON CONTROLLED FUSION AND PLASMA PHYSICS

VOLUME I

CONTRIBUTED PAPERS

Lausanne, 1-5 September 1975

Centre de Recherches en Physique des Plasmas (CRPP)

Ecole Polytechnique Fédérale de Lausanne, Switzerland

These Proceedings (Vol. 1: Contributed Papers, Vol. 2: Invited and Supplementary Papers) will be distributed free of charge to all registered participants. They will also be sold at the price of 40 Swiss Francs after the Conference. Orders should be placed with the Conference Secretariat, during the meeting, or sent to the Centre de Recherches en Physique des Plasmas, Ecole Polytechnique Fédérale de Lausanne, Avenue des Bains 21, CH-1007 Lausanne, Switzerland, after the meeting.

21986

C O N T E N T S

P R E F A C E

This volume contains the Contributed Papers of the Seventh European Conference on Controlled Fusion and Plasma Physics, to be held in Lausanne, Switzerland, 1-5 September, 1975. Previous conferences in this series were held in Munich (1965), Stockholm (1967), Utrecht (1969), Rome (1970), Grenoble (1972) and Moscow (1973).

The Conference is organized by the "Centre de Recherches en Physique des Plasmas", Ecole Polytechnique Fédérale de Lausanne, under the auspices of the Plasma Physics Division of the European Physical Society (EPS).

The papers contained in this book have been selected for presentation by the Paper Selection and Programme Committee. The responsibility for the contents of the contributions is exclusively that of the authors.

Invited and Supplementary Papers will be published after the Conference, in Vol. II of the Proceedings.

The Organizing Committee

COMMITTEES AND SUPPORTING ORGANIZATIONS

ORGANIZING COMMITTEE

E.S. Weibel, Chairman

K. Appert, Finances

A. Heym, Communication

F. Hofmann, Conference Secretary

F. Troyon, Scientific Secretary

PAPER SELECTION AND PROGRAMME COMMITTEE

H.A.B. Bodin, Culham, U.K.

B. Lehnert, Stockholm, Sweden

C. Mercier, Fontenay-aux-Roses, France

G. Wolf, Jülich, Federal Republic of Germany

FINANCIAL SUPPORT

The organizations listed below have contributed financially to the Conference. Their support is gratefully acknowledged:

Département Fédéral de l'Intérieur, Berne

Ecole Polytechnique Fédérale de Lausanne

Etat de Vaud

Ville de Lausanne

MEASUREMENT OF THE ENERGY CONFINEMENT TIME IN TFR
FOR VARIOUS VALUES OF THE SAFETY FACTOR

by the TFR Group
(presented by P. PLATZ)
ASSOCIATION EURATOM-CEA SUR LA FUSION
Département de Physique du Plasma et de la Fusion Contrôlée
Centre d'Etudes Nucléaires
Boîte Postale n° 6. 92260 FONTENAY-AUX-ROSES (FRANCE)

Abstract. The energy confinement time τ_E has been studied as function of the toroidal magnetic field (25; 33; 40; 50 kG) or safety factor (3.6; 4.8; 6.0; 7.0) at constant plasma current (140 kA). τ_E starts at 15 ms and saturates at 20 ms.

The following analysis concerns several days of experimental work spread over six weeks. The value q(a) of the safety factor at the limiter radius a (= 20 cm) has been varied by changing the toroidal magnetic field, B, and keeping the plasma current, I , approximately constant. We have also tried to have the $N_e l$ product (HCN laser interferometer) nearly the same for all types of the discharge ; this was done by injecting a neutral gas pulse during the current rise. Table I summarizes the characteristics of the discharge in the stationary state (t = 150 ms).

B (kG)	25	33	40	50
I (kA)	140	141	134	145
q (a)	3.6	4.8	6.0	7.0
V (volts)	2.7	2.08	1.85	1.85
$N_e l$ (10^{15} cm^{-2})	1.53	1.4	1.35	1.25

TABLE I

Radial profiles of the electron temperature, T_e, have been measured at least up to r = 12 cm by Thomson scattering. As the toroidal magnetic field (and the safety factor) increases, the T_e profiles become more and more peaked as shown in Fig. 1. As 90 % of the total thermal electron energy is contained in the r$\leq$12 cm region, T_e profiles have been measured for r> 12 cm only for two values of B (25 and 40 kG) rather than systematically. Fig. 2 contains data obtained at 40 kG with various gratings in the spectrum analyzer (lower half-space only).

Measurements of the ion temperature via charge exchange neutrals (up to 13 cm on both sides of the equatorial plane) have shown an increase in core values and profile-narrowing for increasing values of B. Finally, spectroscopic measurements (systematically on O VI, Fe XV, N V, C III ; occasionally on Mo XIII and XIV) have not shown a clear-cut dependence of the impurity situation on B. Fig. 3 summarizes the $T_{e,i}$ measurements. The core electron temperature is a linear function of B while the mean electron and core ion temperatures show a distinctly weaker dependence (probably $B^{1/3}$).

In Table II the thermal energy content per cm discharge length of electrons (W_e) and ions (W_i) is given (N_e=N_i), together with the poloidal beta, the effective charge of the plasma ions (from the resistivity anomaly) and the energy confinement time, $\tau_E = (W_e + W_i)\, 2\pi R\, I^{-1}\, V^{-1}$. Note that τ_E increases with B (due to a decrease of V·I rather than an increase of $(W_e + W_i)$ but seems to saturate. This situation is further analyzed in Fig.4, where

B (kG)	25	33	40	50
W_e (J/cm)	5.2	5.1	5.3	5.4
W_i (")	3.6	3.2	3.0	3.1
$W_e + W_i$	8.8	8.3	8.3	8.5
β	0.6	0.57	0.61	0.54
Z_{eff}	5.4	4.4	4.6	4.2
τ_E (ms)	14,5	17,5	20,5	19,5

TABLE II

experimental τ_E(●) is compared to values calculated for anomalous electron heat losses. At present it is not clear if the discharge is best described by a 10 fold enhanced pseudoclassical diffusion loss (X) (the apparent B-dependence is due to the varying $N_e l$ product) or a dissipative trapped electron instability (o)[1]. However, at higher values of the plasma current, the latter seems to dominate, especially in the 400 kA/60 kG discharge. Finally we note that we have also observed temperature relaxations inside the q = 1 region (both from X ray signals, A(t), and from Thomson scattering). The sawtooth-like behaviour of the normalized fluctuations $\frac{\Delta A}{A}$ and $\frac{\Delta T_e}{T_e}$ diminishes with increasing B($\frac{\Delta A}{A} \approx B^{-1.6}$) or decreasing radius of the q = 1 surface (Fig. 1). In the 25 kG runs where $\Delta T_e/T_e$ is greatest (0.2) about 20 % of the total ohmic power is evacuated in this way.

Although this loss mechanism is not the most important one, it cannot be excluded that the relaxation controls in a sensitive way the energy content, i.e. the energy confinement time.

References

1. B.B. Kadomtsev, O.P. Pogutse ; in Review of Plasma Physics, Vol.5 .

See also TFR papers at this Conference, presented by M. Chatelier, C. De Michelis, and D. Launois.

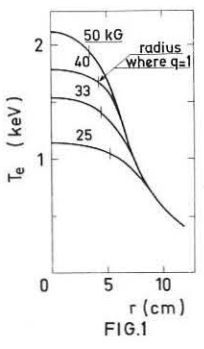

FIG.1

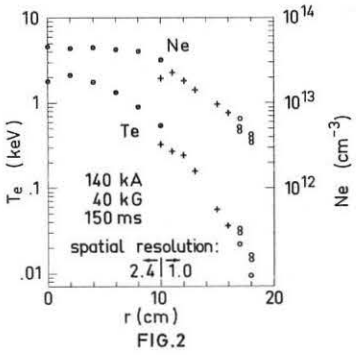

FIG.2

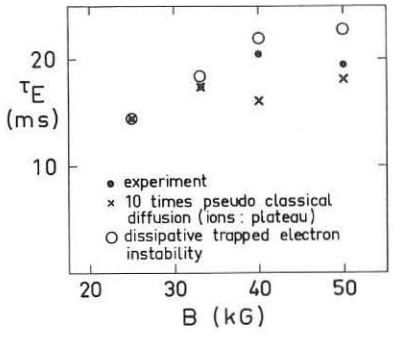

FIG.4

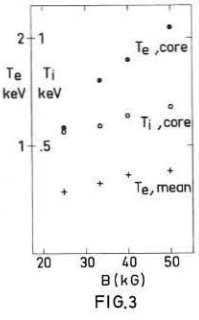

FIG.3

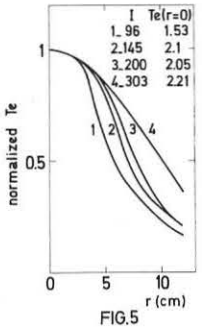

FIG.5

Very recently we have done experiments at constant B (50 kG) and varying I as summarized by Table III.

TABLE III

I (kA)	96	145	200	303
V (volts)	1.85	1.85	1.75	1.88
q (a)	10	7	4.8	3.3
$N_e l$ (10^{15}cm^{-2})	1.07	1.25	1.88	2.51
W_e (J/cm)	2.7	5.4	8.1	13
W_i (J/cm)	1.6	3.1	4.5	8
β	0.62	0.54	0.42	0.3
Z_{eff}	3.6	4.2	2.7	3.55
τ_E (ms)	15	19.5	22	22.7

from Tables I + II

The normalized T_e profiles are given in Fig.5. Combined with Fig.1 it is deduced that the width (FWHM) of the T_e profiles increases linearly with $[q(a)]^{-1}$.

THE IONS IN T.F.R. THROUGH ANALYSIS OF FAST NEUTRALS AND NEUTRON EMISSION.

T.F.R. Group presented by M. Chatelier
ASSOCIATION EURATOM-CEA SUR LA FUSION
Département de Physique du Plasma et de la Fusion Contrôlée
Centre d'Etudes Nucléaires
Boîte Postale n° 6. 92260 FONTENAY-AUX-ROSES (FRANCE)

a) Neutral and neutron measurements of the ion temperature.

The ion temperature has been measured by energy analysis of fast neutrals escaping from the plasma (H_o, D_o) and by neutron flux measurements (D_o). For fast neutrals analysis a one-channel electrostatic analyser provides 8 successive ion temperature measurements during one discharge. The neutron flux is measured with $B.F._3$ detectors and silver activation counters which can both be moved around the torus in order to measure the toroidal distribution of the neutron emission. Indeed a large non-uniform neutron flux (10^{10}n per pulse) is usually detected whose maximum is located near the molybdenum diaphragm. This flux is strongly correlated with the existence of runaway electrons in the plasma. This non-thermonuclear flux may be explained [1] by supposing that energetic runaway electrons (E = 10 MeV) create bremstrahlung γ photons in the molybdenum which in turn produce photo dissociation of its nucleus with neutron emission : $\gamma + {}_z M_o^A \rightarrow n + {}_z M_o^{A-1}$. A runaway current of less than 1 kA due to 10 MeV electrons is required to explain the observed flux. In some discharges hard X rays are not observed and the neutron flux (10^7 - 10^8 n per pulse) seems close to a true thermonuclear flux. In that case we have compared the two measurements of the ion temperature. As seen in the T.4 Tokomak [2] the neutron flux is less than required to explain the ion temperature deduced from neutral flux analysis. One can understand this fact supposing that the deuteron density is less than the electron density which is the only one measured. With a plasma current of 140 kA (minor radius a = 17 cm) the ion temperatures are similar (Fig. 1) if we introduce a $Z_{eff} = 3 - 4$ due to fully ionized oxygen. With a plasma current of 300 kA (a = 20 cm) Z_{eff} has to be increased up to 6. These results are consistent with other Z_{eff} determinations. In order to do more correct correlations between the two measurements the ion temperature profile has to be known and this has been done by tilting the analyser which can look at the plasma from -16 cm to + 16 cm in a plane perpendicular to the magnetic axis (looking angle 30 - 40').

b) Ion temperature radial profile.

As already observed by Petrov [3] on T.3 measurements of the ion radial temperature profile by fast neutrals analysis taking the slower slope of neutral distribution function, without an Abel inversion (which is justified by numerical simulation [5]) also give in T.F.R. a non-symmetric profile (Fig. 2). In one direction the ion temperature always decreases with radius whereas in the other direction we observe a greater number of energetic neutrals (2 keV < E) than in a Maxwellian distribution. When the main toroidal magnetic field is reversed the radial profile is also reversed which shows that influence of fast neutrals reflected on the vacuum chamber cannot easily explain the results.

b.1) Decreasing temperature part of the profile.

This part has a profile very different from the electron temperature profile and looks more like the density profile (Fig.3). At the center $T_e(o) / T_i(o)$ is always of order of 2 - 3 but when the radius increases the two profiles merge at a radius larger than 12 cm.

For 140 kA when the main toroidal field was increased [4] the profile shrank but the temperature did not change very much at radius larger than 10 cm.

For 50 kG when the plasma current had been changed from 100 kA up to 300 kA we observed a general increase of the ion temperature (Fig. 4) as well as the electron temperature.

When we have measured the profile for two limiter radius (17 cm and 20 cm) for the same plasma current (140 kA) the width at half maximum was equal for equal safety factor at the limiter radius.

In absence of other ion temperature measurements, these profiles have been compared with simulation calculations made by Mercier and Soubbaramayer [5]. Agreement is good only in the case when the numerical density profile is similar to the density profile measured by Thomson scattering, results being very sensitive to the recycling coefficient.

b.2) Increasing "temperature" part of the profile.

The analyser receives neutrals which are emitted from the plasma with $V_\perp \gg V_{//}$, that is, sees particles which follow "banana" trajectories or are localized in the local mirror of the configuration ($\delta B/B = 6\ \%$ at the plasma boundary). The observed asymmetry is in the ion magnetic drift direction. "Banana" particles cannot give real asymmetry because of the low neutral density measured in T.F.R. ($n_{H_o} < 10^8$ up to 12 - 13 cm), so the charge exchange lifetime is much larger than the banana drift time.

The asymmetry is only observed for particles whose energy is larger than 2 keV having low collision frequency with other ions. Nevertheless , taking into account Z_{eff} value which is larger than one, the displacement along a localized trajectory is short (few cm), collisions fastly detrapping the particles. It is possible that the electric field present in the plasma (the plasma is negatively charged) helps to maintain the particles in the localized space, the electric drift bringing particles in increasing $\delta B/B$ space. Measurements of ion temperature profile have to be done with the analyser not placed in the median plane between two main toroidal coils in order to decrease the contribution of localized particles in the observed signal.

References.

[1] Barber et al .. Physical Review 116, (1959), 1551.
[2] E.P. Gorbunov et al. 6th European Conference on Controlled Fusion and Plasma Physics, (1973) Paper 1.11
[3] Petrov. Soviet Physics Technical Physics 13, (1968), 708
[4] T.F.R. Group presented by P. Platz. This Conference.
[5] C. Mercier et Soubbaramayer. This Conference.

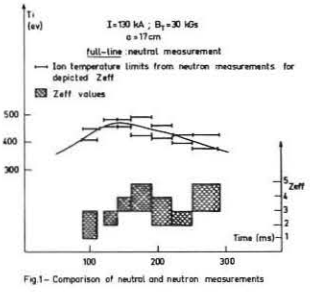

Fig.1 - Comparison of neutral and neutron measurements

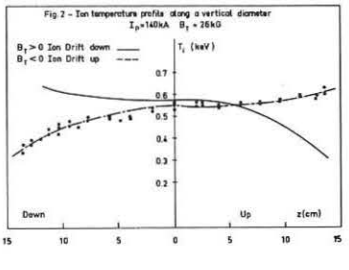

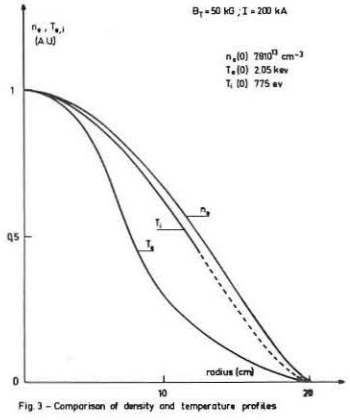

Fig. 3 - Comparison of density and temperature profiles

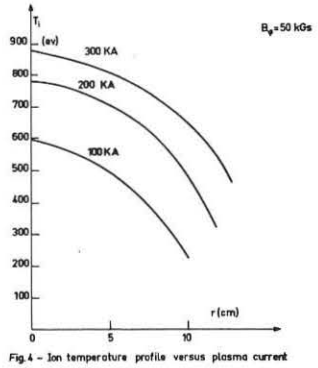

Fig. 4 - Ion temperature profile versus plasma current

DYNAMICS OF HIGH ENERGY RUNAWAY ELECTRONS IN ORMAK*

H. Knoepfel†, D. A. Spong‡, and S. J. Zweben§
Oak Ridge National Laboratory, Oak Ridge, Tennessee, U.S.A.

Abstract: Hard x-rays at the 10-MeV level produced by high energy runaways in ORMAK can be understood by an examination of the single-particle confinement properties of this species. The results of numerical orbit calculations and of hard x-ray measurements from ORMAK discharges are presented and discussed.

Introduction

Recent experimental results[1] have shown that in ORMAK a group of runaway electrons exists in normal, moderately low-density discharges that is characterized by: very high final energies (in the 10-MeV range); being generated at early times (0.5-10 ms) and preferentially on the outer magnetic surfaces (10-20 cm); and being stably contained during most of the discharge (up to 80 ms). This class of high energy runaway electrons complements and extends previous information on runaways in toroidal discharges[2] and could have some distinct consequences on the operation of future tokamak devices. In this paper we analyze the dynamics of the high energy runaways and present related experimental results.

Theoretical Model

The orbit of a high energy electron consists of a fast gyration about field lines at the relativistic electron gyrofrequency superimposed on a slower drift motion and movement along field lines. The combination of the motion along field lines and the guiding center drift then results in orbits whose projection on a minor cross section is depicted in Fig. 1, where the various shifts and radii are also defined. The vertical drift is caused predominately by the curvature in the toroidal field (since runaways have $v_{\parallel} \gg v_{\perp}$) and leads to an outward displacement of the orbits away from flux surfaces. This shift is approximately given by $d_\gamma \simeq r_c \rho_{LP}/R$, where R is the major radius and ρ_{LP} is the poloidal Larmor radius. For example, for a flat current density discharge, $j_o = I/\pi r_L^2$, we obtain $d_\gamma \simeq r_L^2 I_A/2RI$, where $I_A = 17\sqrt{\gamma^2 - 1}$ [kA] is the Alfvén current and γ the relativistic energy parameter. The orbits with radii r_{ci} that just intersect the outer limiter are defined by $r_{ci} + d_\gamma + d_p = r_L$, from which we obtain

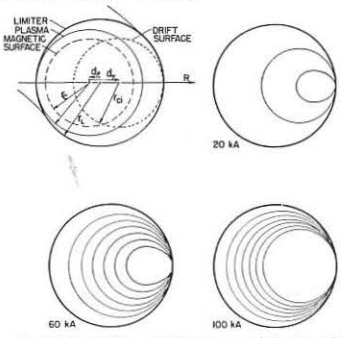

Fig. 1. Drift Orbits of Electrons with Kinetic Energies of 2 (Outermost Orbits), 4, 6,...MeV.

$$\frac{I_A}{I} \simeq \frac{2R}{r_L}\left[1 - \frac{r_{ci}}{r_L} - \frac{d_p}{r_L}\right] \qquad (1)$$

This equation provides the relation between the (unknown) radius r_{ci} of the runaway electron lost at the limiter and its (measurable) kinetic energy $W_k = 0.51(\gamma - 1)$ [MeV] (see Fig. 2, where $d_p = 0$, $r_L = 23$ cm).

In Fig. 1 we show some of the numerically calculated drift orbits for an ORMAK type B current profile $[j(r) = j_o[1 - (r/r_L)^3]]$, which are just intersecting the limiter. The intersection curve, deduced from the numerically calculated shifts, is plotted in Fig. 2. The question arises, whether the mean radius r_{ci} of the orbit when intersecting the limiter has exactly the same value as its radius r_c before acceleration. An examination of the time evolution of runaway electron drift orbits based on the constants of motion in an applied electric field shows that as the particles gain energy and displace outward their minor radius also increases. This effect has been taken into account in the broken curve in Fig. 2. The number of runaways ΔS_R driven into the limiter per unit time as a consequence of the orbit shift is given by

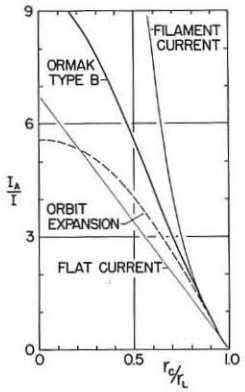

Fig. 2. Intersection Condition.

$$\frac{\Delta S_R}{\Delta t} = 4\pi^2 R r_c n_r \frac{\Delta r_c}{\Delta t}, \qquad (2)$$

where $r_c(t)$ can now be expressed through the curves in Fig. 2 as a function of measurable quantities $[\gamma(t), I(t)]$, and $n_r(r_c)$ is the runaway density.

Experimental Results

Measurement of bremsstrahlung spectra produced by the high energy runaway electrons hitting the target were made with two scintillation detector systems and the results compared with the data from other ORMAK[3] diagnostics. The bremsstrahlung produced by high energy runaways can be basically understood in terms of the (outward) shift of their orbits by $d_p + d_\gamma$, where d_p is the (measurable) shift of the whole plasma column.

In Fig. 3 the maximum runaway energy (deduced from the bremsstrahlung measurement) is shown to increase during the steady part of the discharge, and only slightly less than the free fall curve. This shows that runaways at the MeV-level move around the discharge practically as free electrons. From the broken curve in Fig. 2 we deduce the correlation between energy (γ), time and radius r_c (plotted on the bottom abscissa); from the measured number of runaways hitting the target (S_R) we find, through Eq. (2), the runaway density as a function of radius (Fig. 3).

To have information on the energy and intensity of the runaways dumped towards the end of the discharge (after the voltage pulse ends) we analyze in Fig. 4 the scintillation spectrum obtained from normal ORMAK discharges with three curves constructed from experimental data for monoenergetic electrons of 10 MeV (curve a), 10 and 5 Mev (b), 10 and 8 MeV (c). We conclude that towards the end, the discharge contains within the radius of $r_c \leq 16$ cm a group of about 10^{13} runaway electrons with energies around 10 MeV. In addition, there are less intense energy components in the 4 to 9 MeV range, with a total number of runaways of about the same order (10^{13}). These high energy runaway intensities (determined to within a factor of 3) are typical for discharges with line averaged plasma densities of $\bar{n}_e = 1.5\ 10^{13}$ cm^{-3}. About ten times larger intensities are obtained at $\bar{n}_e = 1\ 10^{13}$ cm^{-3}.

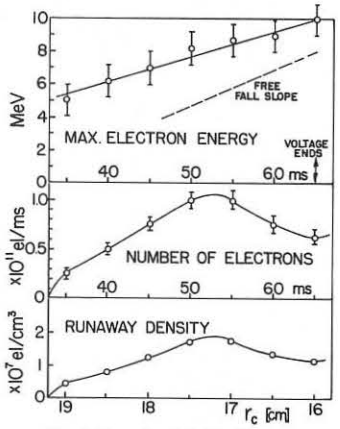

Fig. 3. Experimental Results.

In conclusion we can say that the measurement of hard x-rays provides a powerful and direct method to detect the high energy runaways produced in tokamak discharges. In conjunction with theoretical models on the generation and acceleration of runaways, this method may also provide a sensitive diagnostic probe of the electric field, temperature, and density within the plasma.

Acknowledgment

It is a pleasure to acknowledge the many direct and indirect contributions to this work by all the members of the ORMAK group.

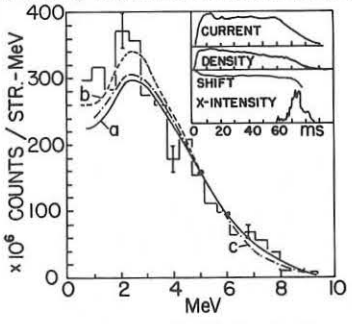

Fig. 4. Analysis of Scintillation Spectrum. Typical values of plasma current, density, and shift at 30 ms are: 100 kA, 1.5 10^{13} cm^{-3} - 2.0 cm.

References

*Research sponsored by the Energy Research and Development Administration under contract with the Union Carbide Corporation.

†On leave from Laboratorio Gas Ionizzati (Euratom-CNEN), Frascati, Italy.

‡ORAU Participant from the University of Michigan, Ann Arbor, Michigan.

§ORAU Participant from Cornell University, Ithaca, New York.

[1] H. Knoepfel and S. J. Zweben, submitted for publication (1975).

[2] D. A. Spong, J. F. Clarke, J. A. Rome, and T. Kammash, *Nucl. Fusion* 14, 397 (1974).

[3] L. A. Berry et al., *Fifth IAEA Conf. on Plasma Physics and Controlled Nuclear Fusion Research* (Tokyo, 1974), IAEA-CN-33/ A 5-1.

EXPERIMENTS ON PLASMA COMPRESSION IN THE TUMAN-2 DEVICE

V.K.Gusev, V.A.Ipatov, M.G.Kagansky, S.G.Kalmykov,
G.T.Razdobarin, K.G.Shakhovetz, I.D.Shpritz

A.F.Ioffe Physico-Technical Institute, Leningrad, USSR

Abstract. Experiments on compression of the tokamak plasma by fast increasing toroidal magnetic field are described. The plasma is shown to be "frozen" in the magnetic field for a time of order $\sim 100\,\mu$s or more. The compressed column is maintained during ~ 2 ms. Oscillations in compressed plasma are strongly reduced.

In the first experiments /1,2/ it has been shown that the effective compression of a plasma column can be carried out by a fast increasing toroidal magnetic field. However the plasma parameters typical for the stable tokamak regime of operation have not been achieved because of poor vacuum. Improved vacuum conditions have made it possible to obtain the substantially higher plasma parameters in the present experiments.

Ohmic heating in a quasi-stationary magnetic field precedes compression. The filling pressure is about 10^{-4} Torr in hydrogen. The current pulse time is 5 ms. An MHD-stable discharge with a loop voltage $U_p = (3\div4)$ V typical for tokamaks turns out to be achieved only when the safety factor at the limiter is $q_l \geq 5$. Under the usual conditions the plasma current I_p is 5 kA for toroidal field strength $H_\theta = 4$ kG. During 2 ms after the breakdown, the plasma parameters vary substantially remaining thereafter approximately constant. During this period an average electron density is $\bar{n} = (5\div7) \times 10^{12}$ cm^{-3}, and the electron temperature at the centre of the plasma, $T_0 = (100\div150)$eV. Spectral and Thomson scattering data show the temperature profile to be narrower than the limiter (the limiter diameter is 16 cm) (Fig.1). It can be approximated by a parabola $T(r) = T_0\left[1-\left(\frac{r}{a}\right)^2\right]$ where a = 5 cm. Assuming the conductivity $\sigma(r) = 1.1 \times 10^{13}\, T^{3/2}(r)$ we find the calculated resistivity of the plasma column to be $(0.4\div0.6)\ m\Omega$, while the experiment yields $(0.6\div0.8)\ m\Omega$ and $Z_{eff} = 1.5\div2.0$. The safety factor at the boundary $q_a = 2.5$ and $q = 1$ at the centre in agreement with /3/, the value of β_I being 0.6. The energy life time τ_E is about $(150\div200)\,\mu$s in rough agreement with $\tau_E = 3.6 \times 10^{-8}\, a^2\, H_\varphi$ /4/. Thus the plasma parameters obtained are typical for a tokamak plasma.

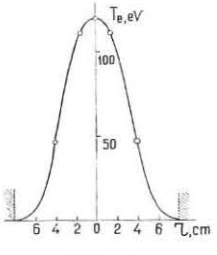

Fig. 1.

The compression is switched on at 2.5 ms after the beginning of ohmic heating. The toroidal field increases up to a maximum during $125\,\mu$s. The maximum magnitude of field exeeds that during the ohmic heating by a factor of 2÷5. The time behaviour of the toroidal field in a typical discharge is shown in Fig.2. A crow-bar of the toroidal field winding is produced to obtain a compressed plasma column for ~ 2 ms. The plasma current is maintained constant.

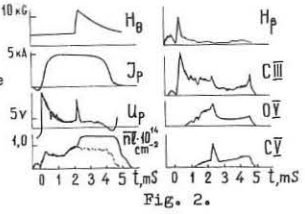

Fig. 2.

The rise of the column inductance and β_I due to compression should cause an outward shift of the plasma. This phenomenon has been observed experimentally and to remove it, the transverse field is increased from 15 G up to 30 G in compression. Besides, a shift of the plasma column from the equatorial plane has been observed. This shift (typically ~ 2 cm) is likely to be caused by stray magnetic field H_R.

Basing on microwave measurements (Fig.2) the plasma can be considered to be "frozen" in the magnetic field during compression. In Fig.2 a damping of oscillations in the plasma and prolonged confinement of a high density plasma is shown.

The appearance of spikes due to compression is characteristic of OV and CV spectral line oscillograms (Fig. 2). It can be seen from the measurements of intensity along various chords that spectral lines of OV and CV "burn out" in the central region of the compressed plasma column. It is worth mentioning that in another discharge regime with a lower current ($I_p = 2.5$ kA, $\bar{n} = 1.5 \times 10^{12}$ cm^{-3}, $T_0 \simeq (40\div50)$ eV) the "burn out" of the OV line is absent during the compression, change in OV line radial profile describing mainly the compression of matter. The results of such experiments are presented in Fig.3. Here curve 1 is the profile of the OV line before compression, 2, 3, 4 - 130, 300, 600 μs after the beginning of compression, respectively. It is clear that in compression the OV line is radiated only from a narrow region near the axis.

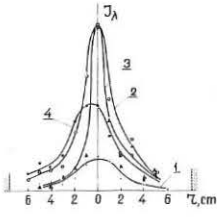

Fig. 3.

During the compression, the current radius a decreases while the loop voltage increases. This can be easily seen in Fig.2 and, in more detail, in Fig.4. The compression rate has been shown experimentally to be close to that of a "frozen-in" plasma throughout the time of compression. This result is valid over a wide range of field rise rates. Current diffusion is likely to be negligible. Consequently, the safety factor at the column boundary should be constant. However a strong damping of plasma oscillation amplitude is observed experimentally. It can be seen in the U_p and OV traces (Fig.1) and, in particular, in the trace of the time derivative of the poloidal magnetic field $\dot{H}_\varphi$ (Fig.4).

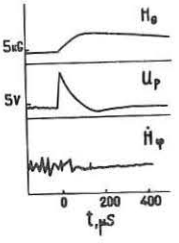

Fig. 4.

Thus, stable confinement of compressed plasma in a tokamak-type trap has been shown in the present experiments. During the compression, the amplitude of the plasma oscillations is strongly reduced. Experiments on heating and thermoinsulation of the plasma will be described in the next report.

/1/ E.L.Berezovsky et al., Proc. III Int. Symp. Toroidal Plasma Confinement, Garching, 1973, B 19.

/2/ Berezovsky E.L. et al., Zh.Tech.Fis. 45, 543 (1975).

/3/ D.L.Dimock et al., Nucl. Fusion 13, 271 (1973).

/4/ Gorbunov E.P. et al., Nucl. Fusion 10, 43 (1970).

HEATING AND THERMOINSULATION OF THE PLASMA COLUMN IN ADIABATIC COMPRESSION IN THE TUMAN-2 DEVICE

E.L.Berezovsky, V.K.Gusev, V.A.Ipatov, M.G.Kagansky, S.G.Kalmykov, A.I.Kislyakov, G.T.Razdobarin, K.G.Shakhovetz, I.D.Shpritz

A.F.Ioffe Physico-Technical Institute, Leningrad, USSR

Abstract. Data on plasma heating during a fast increase of the toroidal magnetic field are discussed. An essential improvement of energy confinement in plasma compression is found. The ion component heating follows an adiabatic law. The electron heating is more intensive.

The description of the experiment is given in /I/. The electron temperature is determined from plasma conductivity measurements, spectroscopic measurements and Thomson scattering of ruby laser light. The ion temperature is obtained from an energy analysis of charge exchange atoms. The plasma density is determined by microwave (λ = 4 mm) interferometer measurements.

Most of the data are obtained in a typical regime, plasma current I_p = 5 kA, toroidal magnetic field during ohmic heating H_o = 4 kG and increasing up to H_c = I2 kG in I25 μs at compression. Before compression, the mean density is $\bar{n}_e$ = = (5÷7) x 10^{12} cm^{-3}, the electron temperature on the column axis is T_e = (I00÷I50) eV and ion temperature - T_i = 30 eV. The energy confinement time is equal to τ_E = (I50÷200) μs.

During compression, plasma conductivity increases. Measurements are made at the maximum of the compression field when the inductive voltage may be neglected. The current radius is taken as $r_c = r_o\sqrt{H_o/H_c}$ according to /I/. The results of conductivity measurements for compressed column are shown in Fig. I. Here σ_c is the conductivity for compressed plasma and σ_o, before compression. The data are given for different compression coefficients $\alpha = H_c/H_o$ and for different plasma currents. The experimental results are shown by curve 2, curve I giving the conductivity change for the pure adiabatic compression $\sigma_c/\sigma_o = \alpha$. One can see the heating to be more intensive. The initial plasma conductivity is σ_o = (2÷6) x 10^{15} CGSE. In the typical regime α = 3 the conductivity temperature increases from 50 up to I50 eV (assuming Z_{eff} = const).

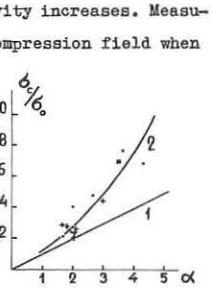

Fig. I.

Measurements of the electron temperature by Thomson scattering are made at the centre of the discharge chamber. Typically, T_e is (II0± 20) eV in ohmic heating, (I90± 30) eV at the maximum of compression and (280± 40) eV - 320 μs later, in the crow-bar period. A displacement of the plasma column from the equatorial plane is observed /I/ during compression. Therefore T_e measured at the centre of the chamber at maximum compression corresponds to the temperature at the column periphery. We suppose the temperature on the plasma axis to be close to that measured in crow-bar period. It is in agreement with the data obtained by other methods.

The CV (λ = 227I Å) line intensity measurements are made in a cross-section of the plasma column. The CV line oscillograms are shown in Fig.2 for central chord (I) and for chords at 2 cm (2) and 4 cm (3) from it outward. If the decrease of the CV line intensity during compression is connected with ionisation the electron temperature may be determined from the ionisation time $\tau = \frac{1}{n_e \langle \sigma_i v_e \rangle}$.

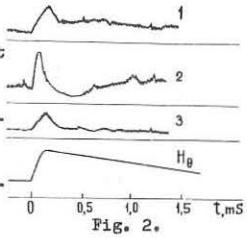

Fig. 2.

Taking the ionisation rate coefficients from /2/ a value $T_e \geq$ 300 eV can be obtained for the hottest column region.

Thus a 3-fold temperature rise is obtained in the typical regime (α = 3). The increase of the temperature is $\frac{T_c}{T_o} = \alpha^{\frac{2}{3}} \simeq$ ≃ 2 for pure adiabatic process. The additional electron heating is caused by an improvement of energy confinement. The ion temperature increases at compression from 30 up to 55 eV in agreement with the expected value. The classical electron-ion energy - transfer time is ≃ 5 ms and the fast electron heating cannot affect the ion heating.

The fact that the plasma column heated by magnetic compression does not cool during ≃ 0.5 ms in crow-bar period is of great interest. It means there is an essential increase of the energy confinement time. A calculation gives the value τ_E = (600÷800) μs, i.e. 4÷5 times longer than in the ohmic heating period. For comparison, in the TM-3 whose geometrical dimensions are close to those of Tuman-2 τ_E = 600 μs is obtained at a plasma current I_p = 30 kA /3/.

There are two ways of explaining this result. An improvement of thermal insulation may be caused by removal of the plasma column from the limiter. Calculations shows /4/ that in such case a rise of energy confinement and the heating above adiabatic level may occur at plasma compression. Another possibility is connected with a decrease of transport coefficients. It may be connected with damping of plasma oscillations at compression /I/. The neoclassical theory gives for our case $\tau_E \simeq$ 2 ms. The difference from experimental value τ_E = (0.6÷0.8) ms may be due to radiative losses in the compressed column.

The experimental data obtained in the typical regime are summarized in Fig. 3. Thus experiments show that at a fast rise of the toroidal magnetic field from 4 kG up to I2 kG the electron temperature increases from I00 eV up to 300 eV, and the ion temperature from 30 eV up to 55 eV. The ion heating is in a good agreement with the expected adiabatic compression law, the electron heating being more intensive. An essential improvement of the plasma thermoinsulation is found in comparison with the usual tokamak for wich the formula $\tau_E = 3.6 \times 10^{-8}\, a^2\, B_\varphi$ /5/ is characteristic.

	OHMIC HEATING	Compression
H_φ, kG	4	12
J_p, kA	5	5
U_p, v	4	3
$\bar{T}_e$, eV	50	150
T_e, eV	110	300
T_i, eV	30	55
$\bar{n}_e$, 10^{13} cm^{-3}	0,5	~1,5
β_J	0,6	1,6
τ_E, mS	150	600
τ-$d H_\varphi$, mS	180	100

Fig. 3.

References.

/I/. V.K.Gusev et al., Proc. of present conf.
/2/. Y.J.Galushkin et. al., Proc. 4 Int.Conf. on Plasma Phys. and Contr.Nucl.Fus.Res., Madison, I97I, F-6.
/3/. Strelkov W.S., Proc. 5 Europ.Conf.Fus. and Plasma Phys., Grenoble, I972, v.II.
/4/. Y.N.Dnestrovskii et al., Pis. v Zh.Eksp. i Teor.Fiz., I3, 697 (I97I).
/5/. Gorbunov E.P. et al., Nucl.Fus., I0, 43 (I970).

TOKAMAKS

SHAPING AND COMPRESSION EXPERIMENTS IN A SMALL, MULTIPOLE TOKAMAK

G. Cima+, C.W. Gowers++, G.E.S. Harding, R.E. King, H. Krause+++, D.C. Robinson, P.A. Wolfe++, A.J. Wootton.
+ Institute of Physics, Milan Italy; ++ AWRE Aldermaston, U.K.;
+++ IPP Garching, W. Germany
Euratom-UKAEA Association for Fusion Research, Culham Laboratory, Abingdon, Oxon. U.K.

ɔstract First results from TOSCA (R = 30, a = 10cm) with $B_\phi \simeq 7.5$ kG, $\simeq 20$ kA, and $\bar{n}_e$ between 0.6 and 5×10^{13} cm^{-3} are presented. Equilibria ıve been established using either an externally imposed vertical field or / connecting the windings to simulate a conducting shell. Minor radius com- :ession and shaped cross section experiments are described.

evice and Diagnostics TOSCA has been built to investigate fast B_ϕ compres- ional heating and shaping using multipole windings without a conventional ıell in the pursuit of higher β in a Tokamak. Fig.1 illustrates the wind- ıgs and indicates the diagnostics used[1].

quilibrium Discharge initiation by a filament required an average vertical ield (B_v) inside the vacuum vessel $\lesssim$ 10 G. Equilibria have been established or 1 msec, both with and without a limiter, by connecting the 16 E windings a a 4:1 series parallel arrangement to simulate a shell. The impedance of he windings causes a current redistribution which produces a B_v; better ontrol of the plasma position is achieved by energising the B_v windings o oppose this field. Fig.2 shows results from such a discharge. The easured displacement results from an outward motion due to: (1) the hoop orce; (2) the externally applied B_v and (3) the leakage of plasma flux hrough the resistive shell ($\tau \simeq 2$ ms), and an inward motion due to the edistribution of the E-winding current. The latter motion eventually ecomes so large that the discharge is terminated, as in Fig.2. Operation t 8:1 series - parallel and 16:1 (all in series) with B_v equilibrium ontrol has been obtained.

Better displacement control has been obtained by connecting E-windings to 14 in 4:1 series - parallel, and energising windings 1 and 16 to pro- ide the correct vertical field; the results are shown in Fig.3. In this ase $B_v \propto I_p$ and the displacement is small. The discharge is terminated y a slow decay of plasma current after the available volt seconds are onsumed. Compared with the discharge of Fig.2 the fluctuations of the oloidal and radial field are reduced substantially to $\Delta B/B \lesssim 2\%$ indicating

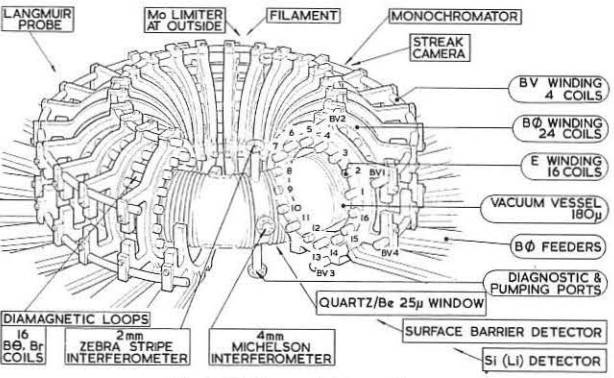

Fig.1 Windings and diagnostics

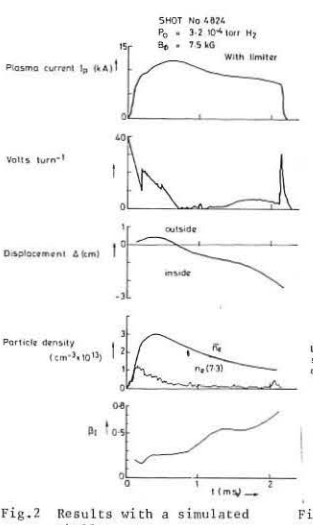

Fig.2 Results with a simulated shell

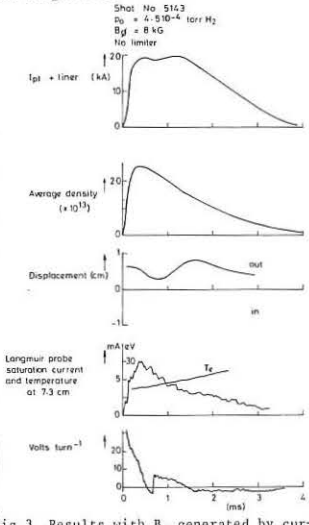

Fig.3 Results with B_v generated by currents in the two outer E windings

improved stability in spite of a larger plasma current.

Plasma Parameters The peak value of the average electron density, measured with the two interferometers, was approximately proportional to the filling pressure, and always decayed. Langmuir probe measurements showed a similar time dependence of the electron density at 7.3 cm radius, with electron temperatures of 20 eV. Diamagnetic loop measurements showed that β_I varied between 0.3 and 0.5 ± 0.05, depending on the initial conditions, and rose to $\lesssim$ 1.0 towards the end of the discharge. With a 20 kA plasma current the diamagnetic temperature at peak current varied between 60 and 300 eV, depending on the density ($\bar{n}_e \simeq 1$ to 5×10^{13}cm^{-3}), and the conductivity temperature was $\lesssim$ 60 eV. For $q(a) \lesssim 3.5$ a disruptive instability terminated the discharge. About 20 μsec before the start of the negative going voltage spike x-ray emission was detected. Magnetic field and density perturbations at the plasma edge were only observed after the start of the spike, indicating an internal origin for the phenomena.

Operating regimes similar to those in T6[2] have been obtained, in which positive voltage spikes occur. Spikes with risetimes of 2 to 10 μsec were measured, accompanied by hard x-ray emission. Perturbations in the poloidal field only at the bottom of the torus were observed; the density and diamagnetic measurements showed that there was no additional heating.

Compression B_ϕ has been increased by up to a factor 2 (eg 6 to 12 kG) in 150 μsec for a variety of initial conditions and the different equilibria. No density increases or outward displacements were found for plasma currents < 10 kA. Above this value the estimated energy confinement time was $\simeq$ the compression time and current decreases of up to 15% were recorded. Fig.4 shows the measured increase in the displacement (outward) associated with compression as a function of the compression ratio $C_r = B_\phi^f / B_\phi^i$ for two equilibria. Also shown, as solid lines are the theoretical displacements expected for an

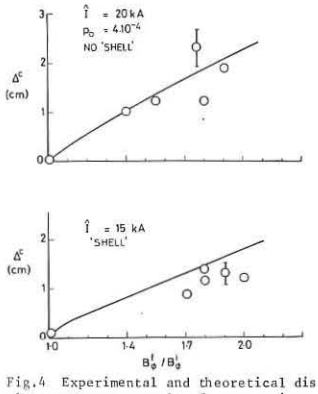

Fig.4 Experimental and theoretical displacements as a result of compression: upper with applied B_v; lower with simulated shell

adiabatic compression assuming $\beta_I^i = 0.5$ and a parabolic current density distribution in the plasma. For β_I constant the theoretical displacements would be reduced by a factor $\simeq 2$. Preliminary results from the Langmuir probe indicated a marked reduction of electron density near the wall. The 4 mm interferometer showed a 25-30% increase (ie a change of 3¼ to 4 fringes) of the initial phase shift ($\bar{n}_e = 2.3 \times 10^{13}$ cm^{-3}) for C = 1.7. This is consistent with an adiabatic compression; similar results were obtained on TM1[3] and TUMAN-2[4]. In all cases compression did not affect the gross stability as indicated by field and density fluctuations. The rms voltage fluctuations were reduced, although sometimes a small negative voltage spike ($\sim$ 1 V) occurred, indicating a plasma current redistribution.

Shaping Windings 1 and 16 were energised with current parallel to the plasma current to generate a separatrix. The short lived plasma produced oscillated in major radius. Equilibrium calculations show that the plasma was probably n = 0, m = 1 unstable.

Conclusions Equilibria have been obtained using either an externally imposed vertical field or by connecting the windings to simulate a conducting shell. Compression experiments indicate a reduction of electron density near the wall with an increase in microwave phase shift and an outward displacement corresponding approximately to those calculated assuming an adiabatic compression. Shaping experiments with a separatrix on the outside of the toroidal column lead to unstable motion.

Acknowledgement Technical assistance by J. Fessey and R. Peacock is gratefully acknowledged.

References

(1) R E King et al. 8th SOFT Conference p.57, 1974.
(2) V S Vlasenkov et al. Nucl. Fusion 13, p.509, 1973.
(3) D P Ivanov, D S Parfenov, Proc. Conf. on Plasma Phys. and Controlled Nuclear Fusion Research, Culham, vol.2, 595, Vienna 1966.
(4) E L Beresovsky et al. 3rd International Symposium on Toroidal Confinement, Garching, 1973, paper B-19.

EMPIRICAL TOKAMAK SCALING

J. Hugill
Culham Laboratory, Abingdon, Oxon, OX14 3DB, UK
(Euratom/UKAEA Fusion Association)

Abstract Data from various experiments are fitted to three types of empirical scaling laws, for which τ_E varies as a^2, a or a^0. The results are used to predict the performance of future large tokamaks.

Symbols R = major radius (m), a = limiter radius (m), I = plasma current (A), q_a,q_o = safety factors at limiter and magnetic axis, n_e,n_i = mean electron and ion densities (m^{-3}), T_e,T_i = mean electron and ion temperatures (eV), V_R = resistive loop voltage (V), β_θ = poloidal beta, τ_E = plasma energy/input power (s), B_φ = toroidal field (T), Z_{eff} = effective ion charge.

Introduction This paper attempts to predict the performance of future large tokamaks by using empirical expressions derived from the data of present experiments (Table I). Attention is restricted to hydrogen discharges, for which there was no large anomalous resistance due to turbulence. The implicit assumption is that the physics of the discharge will be unchanged in larger devices; a big assumption. However, no specific physical models are assumed, a priori.

The two basic parameters of interest are the plasma pressure which can be sustained by ohmic heating alone, and τ_E. The latter allows an estimate of the additional heating required to reach a specified condition.

TABLE I

Experiment	Main parameters R(m)	a(m)	I(kA)	$n_e(10^{19}m^{-3})$	Symbol on Graphs	References
T3 and T3a	1.0	0.1-0.17	36-90	0.9-2.7	Δ	1,2
T4	1.0	0.17	110-180	1.0-3.0	o	3,4
ST	1.09	0.06-0.14	10-100	0.8-3.3	□	5,6,7,8,9
ATC (uncomp[d])	0.88	0.17	60-80	0.6-2.1	•	10,11
ORMAK	0.8	0.23	95-160	1.2-2.0	*	12,13
CLEO-Tokamak	0.9	0.12-0.18	34-72	1.0-2.4	x	14
TFR	0.98	0.17-0.2	103-300	1.6-3.5	⊗	15,16
PULSATOR	0.7	0.12	44	1.1	⊙	17
ALCATOR	0.54	0.10	190	1.5	▽	18

Effect of Varying q_a q_a is an independent variable, but q_o tends to be near unity. The ratio determines the basic geometry of the discharge. It has been found on T3 and T4(1), and, more recently on TFR(16), that τ_E increases as q_a increases up to ~ 6, then remains constant. Conversely, when $q_a \leq 2$, τ_E decreases sharply and large disruptive instabilities are seen. For 90% of the data analysed here $3 < q_a < 5.5$, as shown in Fig. 1, a value which gives optimum plasma parameters for a given B_φ. In this sense, q_a is not a proper independent parameter.

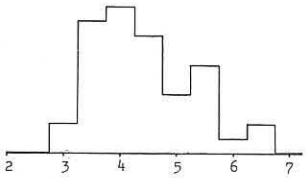

Fig. 1. Histogram of q_a.

Effect of Varying n Many experiments of moderate size now show that τ_E, β_θ vary as n_e^α, where $\alpha \sim 0.4$ in the early Russian experiments (1), to ~ 0.8 in ST (5), and 1.0 in Ormak (12) and Alcator (18). This implies the amount of plasma in the discharge does not have a big effect on the energy loss rate, or on T_e. It confirms the idea that particle balance and energy balance are controlled by nearly independent processes. In some experiments (14,16) n_e increases linearly with I, possibly due to plasma-wall interaction.

Scaling with I and a It is difficult to disentangle the effects of increasing I and a independently, since larger experiments tend to run higher current discharges. In any case, the range of a is limited to a factor ~ 3. Therefore, three possible types of scaling are tested, for which τ_E varies approximately as a^2(A), a(B) or a^0(C). We always have $\tau_E = 3\mu_o IR\beta_\theta/8V_R$, so a knowledge of V_R, or the plasma conductivity, is sufficient to relate τ_E and β_θ. It is remarkable that 95% of the data points considered have $2 < V_R < 4$, but it is not possible to distinguish the constancy of V_R from that of V_R/R,

Type A was first suggested by workers on TM3 and T3 in the form

$$\tau_E \sim a^2 n_e^{0.3} B_\theta \sim a\, n_e^{0.3} I$$

A test of this scaling is shown in Fig. 2. It does not look very convincing, and the corresponding scaling for $\beta_\theta \sim n_e^{0.4} I^{-0.3}$ predicts a plasma resistivity lower than classical for large devices. The mean value of τ_E/aI is $\sim 5 \times 10^{-7}$ ($sm^{-1}A^{-1}$).

Type B is illustrated in Fig. 3. 85% of the data is within a factor of 2 of the expression $\tau_E = 8 \times 10^{-26} n_e I^{\frac{1}{2}}$; though a higher exponent for I, up to about 1, would fit the data equally well.

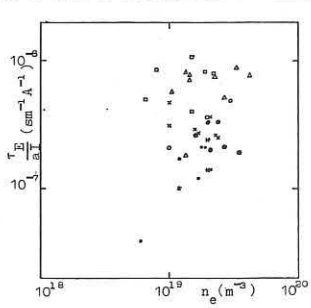

Fig. 2. Type A scaling.

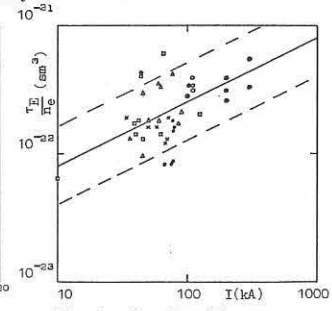

Fig. 3. Type B scaling

Type C is illustrated in Fig. 4. The data fits the expression

$T = T_e + (n_i/n_e)\, T_i = 1700$ [mean ohmic power density (MW/m^{-3})]^2

which leads to

$\tau_E = 10^{-23} n_e T^{\frac{1}{2}}$.

This expression is similar to that suggested by recent results in Alcator (18), and also agrees with the scaling found on ATC (11), in the form $\beta_\theta/n_e Z_{eff}^{\frac{1}{2}} = 5.8 \times 10^{-16}/I$, if $Z_{eff} = (T/T_o)^{3/2}$.

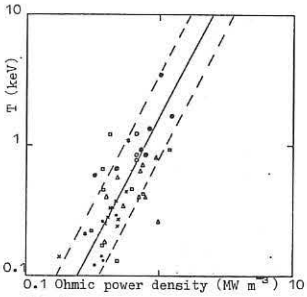

Fig. 4. Type C scaling

Table II shows the results of applying the three types of scaling to PLT (Princeton large torus) and JET (Joint European torus), assuming $Z_{eff} = 4$.

Conclusions There is presently insufficient data to choose between scalings of type B or C, but type A looks improbable. Type C scaling favours the high field, high current density type of experiment.

TABLE II

Experiment	Scaling	τ_E(s)	T(eV)	β_θ	V_R(v)
PLT	A	0.23	1400	0.28	0.75
R = 1.3 m, a = 0.45 m	B	0.08	920	0.19	1.43
I = 1 MA, $n_e = 10^{20}$ m^{-3}	C	0.024	570	0.12	3.0
JET	A	1.63	1300	0.30	0.59
R = 2.96 m, a = 1.25 m	B	0.13	470	0.11	3.0
I = 2.6 MA, $n_e = 10^{20}$ m^{-3}	C	0.014	190	0.04	12

References

1. E.P. Gorbunov et al, Nuclear Fusion 10 (1970) 43.
2. A.M. Anashin et al, JETP 33 (1971) 1127/Zh ETF 60 (1971) 2092.
3. L.A. Artsimovich et al, Nuclear Fusion Special Supplement (1972) 41.
4. V.V. Afrosimov et al, JETP Letts 18 (1973) 300/Zh ETF Pis. Red. 18 (1973) 510.
5. Princeton Plasma Physics Laboratory Report MATT Q29 (1972) 14-19.
6. D.L. Dimock et al, Princeton PPL Report MATT-906 (1972).
7. W. Stodiek 5th Conf on Controlled Fusion and Plasma Physics, Grenoble, Vol II (1972) 1.
8. E. Hinnov et al, 3rd Int Symp on Toroidal Plasma Confinement, Garching Paper B13 (1973).
9. D.D. Dimock et al, Plasma Phys and Controlled Nuclear Fusion Research I (1971) 451.
10. Princeton Plasma Physics Laboratory Report MATT Q30 (1973) 21.
11. P.E. Stott et al, submitted to Nuclear Fusion (1975).
12. L.A. Berry et al, Proceedings of the Toyko Conference IAEA-CN-33/A5-1 (1974).
13. G.G. Kelley et al, 3rd Int Symp on Toroidal Confinement, Garching Paper B3-I (1973).
14. J.G. Cordey et al, Culham Laboratory Preprint CLM-P 407 (1974).
15. T.F.R. Group, 6th Conf on Controlled Fusion and Plasma Physics, Moscow, Vol II (1973) 20.
16. P. Lecoustey, J.P. Girard, Private communications (1974, 1975).
17. O. Klüber, Private communication (1974).
18. B. Montgomery, B. Coppi, Private communications (1974, 1975).

DEVELOPMENT AND APPLICATIONS OF THE FONTENAY TRANSPORT CODE.

C. Mercier, Soubbaramayer
ASSOCIATION EURATOM-CEA SUR LA FUSION
Département de Physique du Plasma et de la Fusion Contrôlée
Centre d'Etudes Nucléaires
Boîte Postale n° 6. 92260 FONTENAY-AUX-ROSES (FRANCE)

Abstract. The use of the Tokomak plasma transport code to simulate existing experiments suggests empirical scaling laws for the transport coefficients. The condition on the local safety factor $q < 1$ plays an important role. Numerical investigations show that this condition may be avoided by a suitable additional heating.

1. Introduction .

A one-dimensional transport code is in use at Fontenay since many years [1] and two new features have been recently added to the model : heating by high energy neutral beam and diffusion of heavy impurities. The neutral injection is adapted to cylindrical symmetry taking into account the two inclination angles of the beam with the cross section plane and the meridian plane. The impurity diffusion approach combines heavy atom diffusion equation with coronal model and includes four types of impurities (oxygen, carbon, iron and molybdenum). We present here three applications of the model.

2. Simulation of existing experiments.

The main discharges on existing Tokomaks have been simulated with our code and have shown that the electrons are experiencing two types of turbulence increasing the transport coefficients : one in the current rise phase (skin relaxation if the skin exists) and the second in the quasi stationary state due to $q < 1$ in the near axis region of the plasma. These turbulent effects are superposed on a transport coefficient which is already anomalous. This is summarized by the empirical formula for the particle diffusion D and the electron thermal conductivity K_e

$$(1) \quad K_e = D = a\, \nu_{ee}\, r_{re}^2 \,(1+q^2)\,\lambda(\rho)$$

$a \simeq 400$, ν_{ee} electron collision frequency, r_{re} electron Larmor radius relative to the toroidal magnetic field, $\lambda(\rho)$ enhancement factor :

$$(2) \quad \begin{cases} \lambda(\rho) \simeq 3 \text{ to } 5 \text{ for } \rho \gtrsim \rho_c \;\; \dfrac{dJ}{d\rho}(\rho=\rho_c) = 0 \;\; \text{(Skin relaxation)} \\ \lambda(\rho) \simeq 5 \text{ to } 10 \text{ for } q(\rho) \lesssim 1 \;\; \text{(Internal disruption)} \end{cases}$$

(J is the current density). Due to this enhancement one obtains a stationary state.

The ions have a neoclassical three regimes behaviour

(3) K_i = Neoclassical.

but it should be emphasized that up to now Tokomak experiments are in plateau regime.

3. Investigation of the internal disruption.

The computations with the formula (1) show that the electron temperature and the current density peak more and more towards the axis and the value $q = 1$ is always reached on the axis. As illustration, one can prove analytically, with a simplified stationary equation, that this happens essentially when the Ohmic heating is the only source balancing the thermal loss given by formula (1).

When $q_{axis} < 1$, the observations on TFR [2] are perfectly simulated by increasing periodically K_e by a factor 10 during a short pulse. The formula (1) with the enhancement of internal disruption appears as an average of a periodic process. We have found empirically on TFR experiments that in the case of internal disruption, a better representation of this average is the following formula :

$$(4) \quad K_e = D \sim Z_{eff}\,(n_e A_i q)^{-\frac{1}{2}}\, T_e^{-\frac{3}{4}}$$

The dependency of K_e upon the atomic mass A_i suggests that the internal disruption is MHD nature.

4. Effect of an additional heating.

The peaking of the temperature may be attenuated by creating an additional heat source at the edge region of the plasma. This may be practically achieved, for instance by energetic neutral beam heating. We have investigated the effect of this additional heating on the q profile according to the angle of injection. It is obvious that the peaking is not much altered when the beam is directed towards the axis. But if the beam is inclined by a non zero angle α on the meridian plane, heat is deposited preferentially at the edge region of the plasma and the temperature profile is flattening.

This results are illustrated in the Fig. 1 where we have plotted q_{axis} versus beam inclination angle α . The example considered is a case of TFR with 140 kamps, 40 kG ($q_{edge} \simeq 6$). The three curves correspond to three values of the beam intensity (10 amps, 20 amps, 30 amps), the energy of the beam being 30 keV. Numbers in brackets designate the corresponding average ionic temperature. One can notice that it is easy to obtain $q_{axis} > 1$ with a relatively small inclination α of the beam. But for α exceeding some limit $\alpha_{critical}$ ($\alpha_{critical}$ depends upon the intensity), the profile is again very peaked. In the neighbourhood of $\alpha_{critical}$ both the two states may be reached depending upon the past evolution of the discharge.

Let us point out that it is not always favourable for the plasma performance to avoid $q_{axis} < 1$ by inclining the neutral beam. There is a balance between the decreasing of the heat deposit due to $\alpha \neq 0$ and the increasing of transport coefficient due to $\alpha = 0$, $q_{axis} < 1$. In the example considered, with $\alpha = 0$, a turbulence, relatively small, increases the value of q_{axis} up to 1 and the average ionic temperature is the highest in spite of an internal disruption still present.

References.

[1] C. Mercier, Soubbaramayer, Fifth Conference on Controlled Fusion and Plasma Physics, Grenoble 1972. The computations are carried out with the collaboration of J.P. Boujot and J.P. Morera (CISI, France).

[2] TFR Group See this Conference.

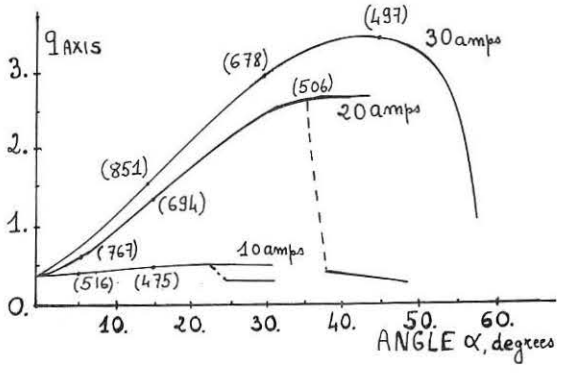

Fig. 1 - q_{axis} vs beam inclination angle .

NUMERICAL COMPUTATION OF TOROIDAL EQUILIBRIA WITH ANISOTROPIC PRESSURE

A. Taroni, Centro di Calcolo CNEN, Bologna

A. Sestero, Associazione Euratom-CNEN, Frascati (Roma)

Abstract: A numerical iteration scheme is presented for the calculation of toroidal plasma equilibria with anisotropic pressure. An application is made to the TEE experiment in Juelich.

The scalar pressure equilibrium theory may not be adequate for the description of experimental situations in which the temperature is sufficiently high to prevent the complete isotropization of the plasma pressure, or in which a certain degree of anisotropy is maintained by the particular plasma heating method that is employed. The equilibrium theory of such anisotropic plasmas has been investigated in the framework of a lowest-order guiding center model (see, e.g., Ref.1). In the toroidal axisymmetric case one has to solve the following equation [1] for the stream function ψ of the poloidal magnetic field, generally with ψ given at the plasma boundary,

$$\frac{\partial^2\psi}{\partial r^2} + \frac{\partial^2\psi}{\partial z^2} - \frac{1}{r}\frac{\partial\psi}{\partial r} = -\frac{r^2}{\sigma}\frac{\partial p_{//}}{\partial\psi} - \frac{L}{\sigma^2}\frac{dL}{d\psi} - \frac{1}{\sigma}\nabla\sigma\cdot\nabla\psi \qquad (1)$$

Cylindrical co-ordinates r,φ,z have been used and

$$\sigma = \frac{1}{\mu_0} + \frac{p_\perp - p_{//}}{B^2}\,, \quad \frac{\partial p_{//}}{\partial B} + \frac{p_\perp - p_{//}}{B} = 0\,, \quad L = \mu_0\sigma I \qquad (2)$$

Here μ_0 is the vacuum magnetic permeability, B is the modulus of the magnetic field, I is the stream function of the poloidal current, $p_{//}$ and $p_\perp$ are the "parallel" and "perpendicular" pressure, respectively, one of which can be specified arbitrarily as a function of ψ and B, while the other one must be derived from it by means of the second of eqs. (2). We recall that in terms of the above quantities the magnetic field $\underline{B}$ and the current density $\underline{J}$ have the following expressions:

$$\underline{B}_T = \mu_0\frac{I}{r}\underline{e}_\varphi\,, \quad \underline{B}_p = \frac{1}{r}\nabla\psi\times\underline{e}_\varphi$$
$$\underline{J}_T = \left(\frac{r}{\mu_0\sigma}\frac{\partial p_{//}}{\partial\psi} + \frac{L}{\mu_0\sigma^2 r}\frac{dL}{d\psi} + \frac{1}{\mu_0\sigma r}\nabla\sigma\cdot\nabla\psi\right)\underline{e}_\varphi\,, \quad \underline{J}_p = \frac{1}{r}\nabla I\times\underline{e}_\varphi \qquad (3)$$

with the subscripts T and p referring as usual to the "toroidal" and "poloidal" part, respectively. Notice that second derivatives of the unknown ψ enter in the last term of eq. (1) through the factor $\nabla\sigma$; for a discussion of this circumstance in relation to the permanence of the elliptic character of the equation, see Ref.2.

The choice of the arbitrary functions $p_{//}(\psi,B)$ and $L(\psi)$ specifies a plasma model. For convenience, we shall factorize a costant number α out of $p_{//}$ and L^2:

$$p_{//} = \alpha\,\hat{p}_{//}\,, \quad L^2 = \alpha\,\hat{L}^2 \qquad (4)$$

so that eq. (1) becomes:

$$\frac{\partial^2\psi}{\partial r^2} + \frac{\partial^2\psi}{\partial z^2} - \frac{1}{r}\frac{\partial\psi}{\partial r} = -\alpha\left(\frac{r^2}{\sigma}\frac{\partial\hat{p}_{//}}{\partial\psi} + \frac{\hat{L}}{\sigma^2}\frac{d\hat{L}}{d\psi}\right) - \frac{1}{\sigma}\nabla\sigma\cdot\nabla\psi \qquad (5)$$

While $\hat{p}_{//}(\psi,B)$ and $\hat{L}(\psi)$ are chosen arbitrarily, the factor α is determined together with the solution ψ by prescribing the value of the total toroidal current, $\int_S J_\varphi\,dS$, where S is the (meridian) cross section of the plasma. The numerical solution of this problem is obtained by an iteration technique analogous to that described in Ref.3 for the scalar pressure case. A simplified version of the method, valid only in the low-β limit, has been considered elsewhere [4].

As an application, we shall present some results obtained with the following choice of $\hat{p}_{//}$ and $\hat{L}$:

$$\hat{p}_{//}(\psi,B) = \frac{1}{2\mu_0}\left(1 + bB\psi\right)\psi^2\,, \quad \hat{L}^2(\psi) = \frac{1}{\mu_0^2}\,c\,\psi^2 + L_c^2\,, \qquad (6)$$

where b, c and L_c are constants. Within this model one easily derives

$$p_\perp = \frac{\alpha}{2\mu_0}\psi^2\,, \quad \frac{p_\perp}{p_{//}} = \frac{1}{1+bB\psi} \qquad (7)$$

We impose $\psi = 0$ on the plasma boundary; it easily follows that also $p_{//}$, $p_\perp$ and J_φ are zero at the plasma boundary. As for the meaning of the constants L_c and c, one can see that they are related to the value of the vacuum toroidal field and to the poloidal β, as in the isotropic pressure case. The constant b is related to the degree of anisotropy $p_\perp/p_{//}$, as it appears from the second of relations (7). If desired the number b can also be changed (as done with α) at each iteration so as to keep constant, e.g., the degree of anisotropy at the magnetic axis.

The choice (6) was made with the purpose of approaching the experimental situation of the TEE machine of Juelich Laboratory where a maximum degree of anisotropy $\frac{p_\perp}{p_{//}}$ has been observed near the magnetic axis, while $p_\perp \approx p_{//}$ at the plasma boundary. The results presented here were obtained by using input data for the numerical computation based on the physical parameters of TEE, in particular:

$\beta_p = 3$, $\frac{p_\perp}{p_{//}} = 2$ at the magnetic axis, major radius R=25 cm., plasma radius a = 7 cm, vacuum toroidal field at the center $B_{oT} = 4.5$ kG, total toroidal current $I_\varphi = 25$ kA. It was found, as it appears from figs.1 and 2, a shift between the current axis and the magnetic axis that can, at least partially, explain the experimental findings on TEE [5]. In the figures solid lines represent level lines for $p_{//}$ (fig.1) and for I (fig.2) whereas dotted lines are level lines for ψ.

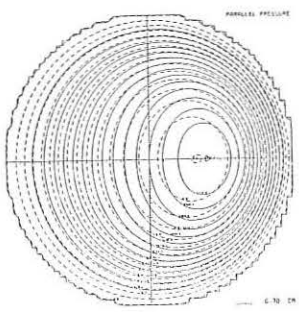

Fig. 1

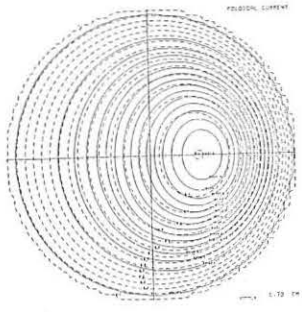

Fig. 2

REFERENCES

[1] H. Grad, Phys. Fluids, 10, 137 (1967)

[2] H. Grad, New York University Report, NYO 1480/50 (MF-48), 1966

[3] G. Cenacchi, A. Taroni, A. Sestero, Nuovo Cimento, 25 B, 279 (1975)

[4] A. Sestero, A. Taroni, to be published

[5] P.G. Carolan, M. Korten, F. Sand, G. Waidmann, submitted to XII Int. Conf. on Phenom. in Ionized Gases, Eindhoven, 1975.

PARTICLE TRANSPORT DUE TO POLARIZATION OF TRAPPED PARTICLES BY INDUCTION ELECTRIC FIELD IN A TOKAMAK

R.K. Varma
Physical Research Laboratory, Ahmedabad 380 009, India

Abstract: The induction electric field in a tokamak leads to a polarization of the trapped particles. The particle transport due to this polarization electric field is calculated and is found to be radially inwards. This helps to explain some of the experimental observations.

It is now well known[1] that trapped particles in a tokamak suffer a radially inward drift of magnitude cE_φ / B_θ, where E_φ is the toroidal electric field and B_θ is the azimuthal field. This drift can be easily reduced by applying the conseration of canonical angular momentum to trapped particles.

It has been stated[1] that as the trapped particles move radially inward they would leave the passing particles where they are. However, experimental results on the tokamak[2] seem to indicate an inward motion of more or less plasma as a whole, whereas the trapped particles constitute only a fraction $\sqrt{r/R_0}$ of the total number of particles.

We propose here a mechanism whereby plasma as a whole moves radially inwards, but perhaps with a speed smaller than cE_φ / B_θ. The physical mechanism is that the trapped particles in a tokamak get polarized under the influence of the induction toroidal electric field E_φ. The polarization field in (γ, θ) plane, turns out to be in such a direction that the γ-component of the resulting E X B drift is radially inwards. Since it obviously depends on the number of trapped particles and, for a given E_φ field, on the magnitude of the maximum of the mirror field, the effect will be more important for tokamaks with smaller aspect ratio R/r, and therefore for those of the reactor type.

Trapped Particle Density Distribution in the (γ, θ) plane

Because of the axisymmetry of the tokamak geometry, the trapped particle distribution will obviously be φ-independent. In the presence of the toroidal electric field (also axisymmetric) the effective trapping potential is modified. For the trapped particles, the toroidal electric field can be taken to be derivable from a potential which is given by

$$\bar{\Phi} = -\int d\ell\, E_{\parallel} = -\int d\theta\, r B_\varphi E_\varphi / B_\theta$$
$$= -\left(r B_0 E_0 / B_\theta\right)\left(\theta + 2\epsilon \sin\theta\right) \qquad (1)$$

where ℓ represents the coordinate along the field line and in the usual notation $B_\varphi = B_0\left(1+\epsilon\cos\theta\right)^{-1}$, $E_\varphi = E_0\left(1+\epsilon\cos\theta\right)^{-1}$ and $R = R_0\left(1+\epsilon\cos\theta\right)$, $\epsilon = r/R_0$. The above expression for $\bar{\Phi}$ stands conveniently normalized to $\bar{\Phi} = 0$, for $\theta = 0$.

The energy of a trapped particle is now given in the usual notation by $\mathcal{E} = \frac{1}{2} m v_{\parallel}^2 + \mu B + q\bar{\Phi}$ so that the effective trapping potential is $\mu B + q\bar{\Phi}$. A particle is trapped if $\mathcal{E} < \left(\mu B + q\bar{\Phi}\right)_{max}$ where $\left(\mu B + q\bar{\Phi}\right)_{max}$ is the lower maximum of the potential with respect to θ. For a given μ, the maximum and the minimum of the potential are easily found to be given by

$$\theta_{min} = \sin^{-1}\left(q E_0 R_0 / \mu B_\theta\right)$$
$$\theta_{max} = \pi - \sin^{-1}\left(q E_0 R_0 / \mu B_\theta\right) \qquad (2)$$

For a certain $\mu = \mu_{min} = q R_0 E_0 / B_\theta$, $\theta_{max} = \theta_{min}$ the potential well degenerates into a point of inflexion, and no trapping occurs for $\mu < \mu_{min}$. For a given value $\mu > \mu_{min}$, the energy for the trapped particles will lie in the range $\mathcal{E}(min) < \mathcal{E} < \mathcal{E}(max)$, where $\mathcal{E}(min)$ is the value of the energy of a particle at the bottom of the well, $\theta = \theta_{min}$ with $v_{\parallel} = 0$, and $\mathcal{E}(max)$ similarly is the value at the maximum

Because of the inward Ware drift, the spatial density distribution of trapped particles in the presence of the induction electric field E is non-stationary. In what follow, we calculate the polarization electrostatic field due to an "instantaneous" distribution of trapped particles in the (γ, θ) plane.

If we assume a Maxwellian distribution in the energy and for simplicity, a δ-function distribution, $\delta\left(\mu - \mu_0\right)$, we obtain the spatial distribution in (γ, θ) plane

$$n_T^j = n_0 \left\{ \exp\left[-\left(\mu_0 B/T + q\bar{\Phi}/T\right)\right]_{\theta=\theta_{max}} \operatorname{erf}\left[\frac{1}{T}\left\{\mu_0\left(B(\theta_{max}) - B\right) + q\left(\bar{\Phi}(\theta_{max}) - \bar{\Phi}\right)\right\}\right]^{1/2} - \exp\left[-\left(\mu_0 B + q\bar{\Phi}\right)/T\right] \cdot \operatorname{erf}\left[\frac{1}{T}\left\{\mu_0\left(B(\theta_{min}) - B\right) + q\left(\bar{\Phi}(\theta_{max}) - \bar{\Phi}\right)\right\}\right]^{1/2} \right\} \qquad (3)$$

where $\operatorname{erf} x = 2/\sqrt{\pi}\int_0^x dy\, e^{-y^2}$ is the error function. The electrostatic potential ϕ_T due to the trapped particles is given by

$$\nabla^2\left(\epsilon\phi_T\right) = -4\pi e\left(n_T^i - n_T^e\right) \qquad (4)$$

$\epsilon = 1 + 4\pi n_0 M c^2 / B^2$ is the dielectric constant. Eqn. (4) can be solved for the potential ϕ_T and the electrostatic field and the EXB drift obtained. Since n_T^i of Eqn. (3) is the expression for $\delta\left(\mu - \mu_0\right)$ the solution ϕ_T of Eqn. (4) can be considered as a Green's function for any arbitrary distribution in μ.

Numerical solutions of the deifts are obtained for some distributions in μ. It is easily to see geometrically that the drift is radially inward.

References

1. A.A. Ware, Phys. Rev. Lett. 25, 15, (1970)

2. E.P. Gorbunov, in Proceedings of Conference on Plasma Physics and Controlled Nuclear Fusion Research Novosibirsk U.S.S.R. 1968 (International Atomic Energy Agency, Vienna, Austria, 1969), Vol. II, 629, (1969).

DETERMINATION OF CONDUCTIVITY AND Z_{eff} PROFILES IN THE T.F.R. DEVICE

T.F.R. GROUP PRESENTED

by P.PLINATE

ASSOCIATION EURATOM-CEA SUR LA FUSION
Département de Physique du Plasma et de la Fusion Contrôlée
Centre d'Etudes Nucléaires
Boite Postale n° 6 . 92260 FONTENAY-AUX-ROSES (FRANCE)

The radial conductivity profile is determined by inducing, along the plasma, a weak oscillating electric field $E_\sim = U_\sim/2\pi R$ so as to create a skin effect in the plasma.[1] The $\sigma_{//}(r)$ profile is deduced from the measurement of the plasma inductance $L_\sim = \frac{U_\sim}{dI_\sim/dt}$ for several frequencies.[2,3,4]

The model used for the interpretation of the experimental results implies :

- a radial conductivity profile of the form : $\sigma_{//}(r) = \sigma_o\, e^{-(r/r_o)^n}$
  r_o characteristic length of the plasma.
- a stationary plasma.
- an axisymetric plasma centered on the torus axis.

If $E_\sim(r,t)$ is given by : $\frac{1}{r}\frac{\partial}{\partial r}\left[r \frac{\partial E_\sim}{\partial r} \right] = i\omega\mu\sigma(r)\, E_\sim$ (1)

then

$$L_\sim = \mu R \,\mathrm{Log}\frac{b}{a_o} + \frac{\mu R}{a_o}\frac{E_\sim(a_o,t)}{\left[\frac{\partial E_\sim(r,t)}{\partial r}\right]_{r=a_o}} \qquad (2)$$

For the steady state of the plasma, $L_\sim$ depends only on the frequency $f = \omega/2\pi$ and the parameters σ_o, n and r_o characterizing the conductivity profile.

Measurements of $L_\sim$ have been mainly performed together with the T_e and n_e profiles[5] during the current plateau of a 140 KA - 25 KG discharge.

Figure 1 shows the experimental $L_\sim$ values plotted against the parameter $u = \mathrm{Log}(\bar\sigma f a_o^2)$; $\bar\sigma = \frac{I}{U}\cdot\frac{2R}{a_o^2}$ (3) is the average conductivity, I being the main current in the plasma induced by the electric field $E_o = U/2R$ measured along the copper shell.

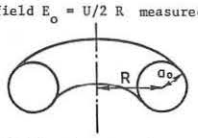

The inductance $L_\sim$ decreases as the frequency increases, showing that a skin effect has indeed been imposed on the current profile.

For the explored frequency range of 30 Hz to 6 000 Hz, the a.c. plasma impedance is primarily inductive. The amplitude of the modulation $I_\sim$ is very small compared with the main current I, i.e. 2% at 40 Hz ; and even at these low frequencies, no measurable macroscopic modification of the plasma can be observed.

The comparison between the experimental values $L_\sim(u)$ and the curves computed from the above defined model gives a range of the values σ_o , r_o and n determining the possible conductivity profiles.

σ_o is given by : $$\sigma_o = \frac{a_o^2\,\bar\sigma}{2\int_o^a e^{-(r/r_o)^n} r\,dr} \qquad (4)$$

For $r \gtrsim 7$ cm , all these profiles are close to one another ; but, near the axis, an indetermination exists which is removed in the following way : we assume that the electric field inducing the main current in the discharge is radially constant and equal to E_o ; so

$$J(r) = E_o\,\sigma(r) = J_o\, e^{-(r/r_o)^n} .$$

The J_o value equal to $E_o\sigma_o$ is determined by the condition $q(o)\simeq 1$ deduced from the internal disruprions study.[6] Thus

$$J_o = \frac{B_T}{R}\,\frac{2}{\mu_o}\,\frac{1}{q(o)}$$

On the other hand, the condition :

$$I = \int_o^{a_o} 2\pi J_o\, e^{-(r/r_n)^n} r\,dr \qquad (5)$$

has to be met.

So, the $\sigma(r)$ and $J(r)$ profiles are unambiguously determined (Fig.2) by $n = 2.7$, $r_o = 11.1$ cm and $\sigma_o = 9\ 10^6$ mho-m or $J_o = 4\ 10^6$ A/m^2 .

Figure 3 shows the variation of q(r) defined by :

$$q(r) = \frac{B_T}{R}\,\frac{1}{\mu_o}\,\frac{r^2}{\int_o^r J(r)\, r\,dr} \qquad (6)$$

Then, if we assume that $\sigma(r)$ is given by the Spitzer's classical formula :

$$\sigma(r) = 10^9\,\frac{Y_E(Z_{eff})}{Z_{eff}(r)}\,\frac{T_e(r)^{3/2}}{\mathrm{Log}\,\Lambda}\ \left|\begin{matrix}\mathrm{KeV}\\ \mathrm{ohm}\\ \mathrm{m}\end{matrix}\right. \qquad (7)$$

the Z_{eff} profile is defined using the T_e and n_e profiles and the above experimental determination (r) as described in figure 4. Z_{eff} appears as nearly constant equal to 7.5 for $r \lesssim 10$ cm (with an uncertainty of the order of the deviation of q(o) from unity) and then decreases.

References

1 - D.P. IVANOV and S.S. KRACILNIKOV, Plasma diagnostics, Moscow 1963.

2 - D.P. IVANOV, A.E. LENEVA and D.S. PARFENOV, On the measurement of conductivity radial distribution of a plasma ring I.A.E. 2077 Moscow 1971.

3 - A.N. DELLIS and J.C. HOSEA, Radial profile of plasma resistivity determined from a.c. impedance measurements in the S.T. Tokomak, Dec. 1973 Matt. 969.

4 - P. PLINATE and M. RIGOULAY, Mesure de la distribution radiale de conductivité dans T.F.R. Rapport EUR.CEA n°771 (to be published).

5 - T.F.R. Group, Measurement of energy confinement time in T.F.R. for various values of the safety factor ; paper presented by P. PLATZ at this conference.

6 - T.F.R. Group, Experimental studies and numerical simulation of the evolution of a discharge in T.F.R. phenomena of internal disruptions ; paper presented by D. LAUNOIS at this conference.

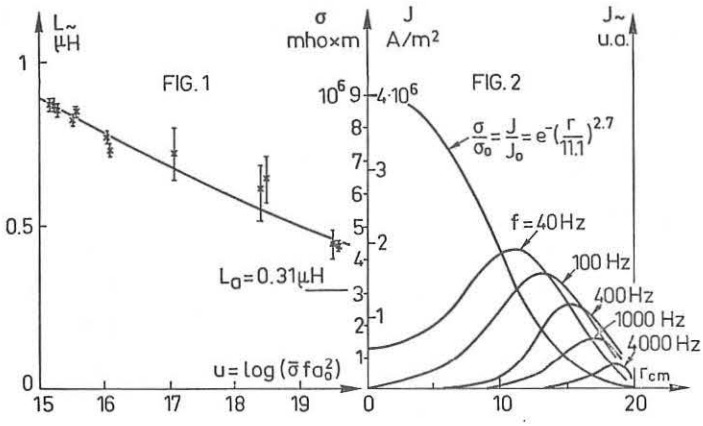

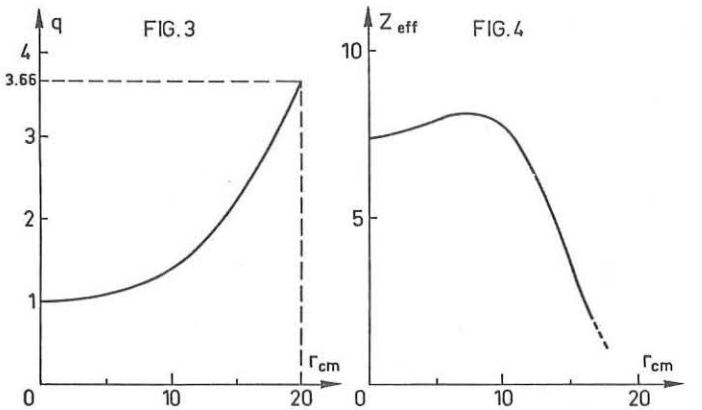

FIRST RESULTS ON PETULA TOKAMAK

PETULA GROUP*

ASSOCIATION EURATOM-CEA
Département de Physique du Plasma et de la Fusion Contrôlée
Service IGn - Centre d'Etudes Nucléaires
B.P.85 - Centre de Tri - 38041
GRENOBLE CEDEX (France)

ABSTRACT : Tokamak discharges of 40 to 65 kA have been achieved in the PETULA installation using a metallic liner. Measurements of $T_e(r,t)$, $n_e(r,t)$.. at 50 kA and 16 KGauss are reported.

INTRODUCTION. PETULA is a moderate size Tokamak designed for R.F. heating, especially T.T.M.P. heating. In order to get the penetration of the high frequency electromagnetic field inside the plasma, the vacuum vessel will be made of six identical alumina sectors, each of 30° arc length, connected to six observation and pumping ports by stainless steel bellows. Six coils located between the copper shell and the alumina sectors will produce a 3% modulation of the toroïdal magnetic field. During the construction phase we decided to use the anticipated interval between the completion of the toroïdal field system and the alumina vacuum vessel to carry out some experiments with the usual metallic liner. Apart from the obvious aim of testing PETULA and its diagnostics these experiments allow us a reference for direct comparison with the existing Tokamak discharges and that which we will have with the alumina liner.

APPARATUS. Main dimensions of the torus are : Large radius 72 cm, maximum limiter radius 15 cm. Toroïdal magnetic field is produced by means of 24 bitter coils : its maximum value with existing rectifier is 16 KGauss which will be increased to 25 KGauss next year for the second phase of the experiment. Current is induced by discharging a capacitor bank into different sets of coils which are coupled to the plasma through a 0,5 Wb central transformer core with six return limbs. Coil configuration can be changed in order to vary vertical field. A 2 cm thick copper shell with about 50ms e-folding time is used to stabilize the plasma discharge. Its 23 cm radius was a compromise between desirable stabilizing effect and dissipation produced by the R.F. coils to be located inside. The whole machine is divided into six identical parts. Each part has a large horizontal port (15 x 45 cm^2) for diagnostics and pumping as well as smaller vertical ones, adjacent to a 0.5 mm thick stainless steel bellows.

EXPERIMENTAL RESULTS. As a standard Tokamak, PETULA has been in operation since February. After a few weeks it was found that the maximum current in stable regime was 65 kA, with a density of 3 $10^{13} cm^{-3}$ and 580 eV electron temperature. However most results were obtained at 50 kA with B_ϕ = 16 KGauss. Typical results are presented in Fig. 1 as a function of time. Radial profiles of n_e and T_e along a vertical line are given in fig. 2. Base pressure is in the range 1-5 10^{-8}Torr and hydrogen filling pressure is 8 10^{-4}Torr. Measurements of electron temperature, T_e, by Thomson scattering show that it increases to a maximum of 410 eV pretty well following the evolution of discharge current which reaches its peak of 50 kA at 30 msec whereas the density, n_e, peaks at 4.2 $10^{13} cm^{-3}$ at 40 msec. The radial profile for t > 10 msec shows neither skin effect nor pronounced peaking since at r = 12 cm, T_e > 100eV. Magnetic probes and radial profiles measurements show a downward displacement due to toroïdal field errors which has now been corrected by a steady state radial field. Average density obtained by scattering is in good agreement with interferometric results at 2 mm. T_i by line broadening measurements of O_{VII} 1638 Å, N_V 1238.8 and C_{IV} 1548, show maxima of 180, 100 and 50 eV respectively. Radial profiles which will be so obtained are to be compared to T_i measured by charge exchange. Calculations based upon our measurements at maximum current show that $\bar{Z}_{eff}$ lies between 3.8 and 4.8 for arc voltages between 4 and 5 volts, β poloïdal is 0.4, and the energy confinement time is 1.6 msec.

NUMERICAL SIMULATION. Using the numerical code developped at Fontenay-aux-Roses by Mercier, Soubbarameyer and Boujot, a first attempt has given a correct simulation of the time evolution of the mean electron density and T_e, T_i on the axis (fig. 1). The energy confinement time is then about 1 ms and β poloïdal between 0.25 and 0.30. These results have been obtained assuming ions in the plateau regime and setting the electron thermal conductivity in the Pfirsch-Schlüter one but increased by a factor 2000. This factor was moreover enhanced in the central part of the plasma to take into account induced turbulence when q is less than unity.
This work will be completed in order to get a better simulation of the T_e radial profile which is presently more peaked than the experimental one thus explaining the low computed value of β poloïdal.

* - R. BARDET - M. BERNARD - G. BRIFFOD - M. CLEMENT - R. FRANK - A. GAUTHIER - M. GREGOIRE - P. GRELOT - M. HESSE - F. PARLANGE - D. PINET - E. PORROT - G. REY - J. WEISSE.

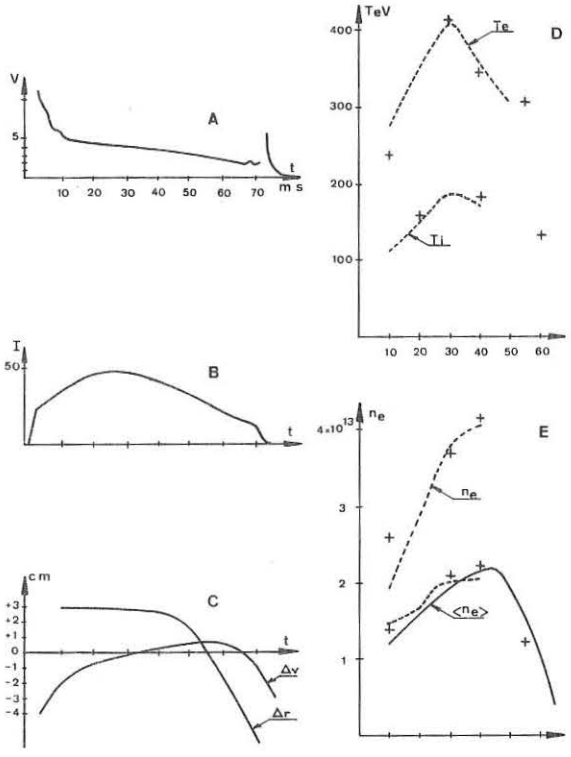

Fig. 1 - A typical 50 kA discharge ; A) loop voltage, B) plasma current, C) radial and vertical displacement, D) electron and ion temperature : + experimental results (Thomson scattering and Doppler broadening of O_{VII} line), E) peak and average electron densities + Thomson scattering results ; solid line : 2 mm interferometry.
On d and e, dashed line are discharge simulation results.

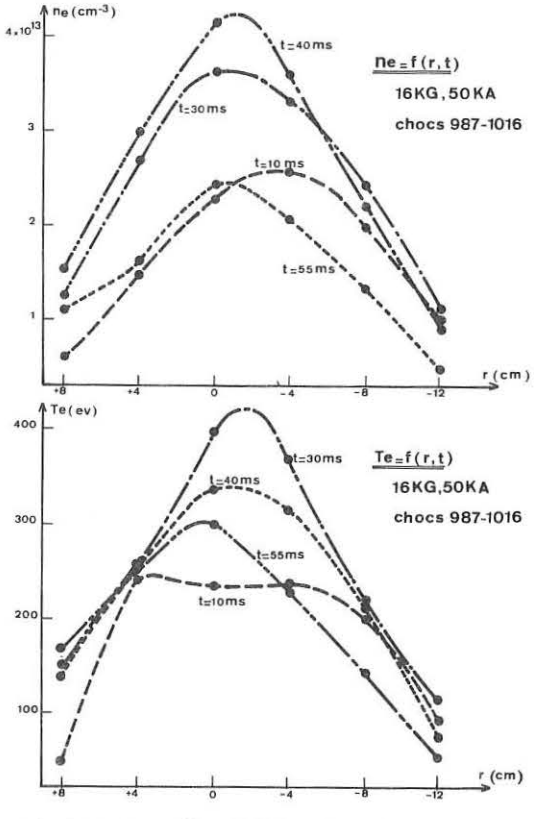

Fig. 2 - Radial profiles of electron temperature and density along a vertical chord at R = 72 cm.

CORRELATION EFFECTS IN CYCLOTRON RADIATION FROM PLASMAS.

K. Audenaerde and F. Engelmann

Lab. Gas Ionizzati (Euratom-CNEN), C.P.65, Frascati, Italy.

Abstract : The dispersion and correlation effects on the optical constants for cyclotron radiation are evaluated for equilibrium plasmas ($T_e \lesssim 10$ keV) for arbitrary densities. It is shown that in cases of practical interest dispersion dominates and attenuates the emissivity. The results are consistent with Kirchhoff's law.

Cyclotron radiation is an important energy loss mechanism of a magnetically confined high temperature plasma.[1-5] So far detailed studies have been devoted essentially to the regime where the plasma density is low enough that correlations between electrons do not influence the emission. In such a situation the optical constants of the plasma are proportional to the plasma density.

In this paper we study cyclotron emission for the case of arbitrary density. The plasma is assumed to be homogeneous and stationary, the ions forming an immobile background. The typical electron velocities v are taken small compared to the light speed c so that all results can be taken in lowest significant order in $(v/c)^2$. Having in mind applications to laboratory plasmas with temperatures below 10 keV, the final formulae are written in a form, where the contributions of different harmonics are separated.

The quantity of interest is the spectral emissivity $\eta_\omega^{(i)}(\hat{\underline{S}})$, in the polarization modes i=1,2 , of light of frequency ω ,defined in an elementary cone $d\Omega_S$ about the Poynting vector $\underline{S}$. As this is difficult to calculate in a direct way, we computed a quantity $\eta_\omega^{(i)}(\hat{\underline{k}})$, closely related to the spectral emissivity, but defined with respect to an elementary cone $d\Omega_k$ about the wave vector $\underline{k}$. Both quantities are linked by

$$\eta_\omega^{(i)}(\hat{\underline{S}})\, d\Omega_S = \eta_\omega^{(i)}(\hat{\underline{k}})\, d\Omega_k \qquad (1)$$

It may be shown that

$$\frac{d\Omega_k}{d\Omega_S} = \frac{n_r^2}{n^2}\,.\,\cos\beta \qquad (2)$$

where n is the refractive index, n_r the ray refractive index, the angle included between the wave and Poynting vectors and the sign ^ denotes unit vectors. The quantity $\eta_\omega^{(i)}(\hat{\underline{k}})$ can be calculated from

$$\eta_\omega^{(i)}(\hat{\underline{k}}) = \frac{\rho^2}{\delta V'}\left\langle \underline{S}^{(i)}(\omega,\underline{r})\right\rangle .\hat{\underline{k}} \qquad (3)$$

where

$$\left\langle \underline{S}^{(i)}(\omega,\underline{r})\right\rangle = \frac{2\pi}{T}\frac{e^2}{16\pi^3\omega}\left\langle \underline{k}^{(i)}\underline{E}^{(i)*}(\omega,\underline{r}).\underline{E}^{(i)}(\omega,\underline{r}) - \underline{k}^{(i)}.\underline{E}^{(i)}(\omega,\underline{r})\underline{E}^{(i)*}(\omega,\underline{r})\right\rangle + \text{complex conjugate} \qquad (4)$$

is the average spectral energy flux density at a point $\underline{r}$, created by the sources in a volume $\delta V'$ around the position $\underline{r}'$ and $\underline{\rho} = \underline{r}-\underline{r}'$, the $k^{(i)}$'s are solutions of the dispersion relation, $\underline{E}^{(i)}(\omega,\underline{r})$ being the Fourier component of the corresponding electric field amplitude of the mode i, T the observation time and e the elementary charge.

For linearly stable plasmas, the amplitude $\underline{E}^{(i)}(\omega,\underline{r})$ can be expressed in terms of the "free current sources" $\underline{J}^L$ by using the Klimontovich approach[6] and following a method due to Baldwin et al.[7]. Neglecting ternary correlations between electrons, one may start with the linearized Klimontovich equation

$$\left(\frac{\partial}{\partial t} + \underline{v}.\frac{\partial}{\partial \underline{r}} - \frac{e}{M_e}\frac{\underline{v}\times\underline{B}_0}{c}.\frac{\partial}{\partial \underline{v}}\right)\delta\nu - \frac{en_e}{M_e}\left(\underline{E}_1 + \frac{\underline{v}\times\underline{B}_1}{c}\right).\frac{\partial f}{\partial \underline{v}} = 0 \qquad (5)$$

where $\delta\nu = \nu - n_e f$ is the difference between the fine-grained density ν and its statistical average $\langle\nu\rangle = n_e f$, f being the distribution function of the electron velocities $\underline{v}$, normalized accorfing to $\int d^3v\, f = 1$ and independent of position $\underline{r}$ and time t, $\underline{B}_0$ is the (constant) external magnetic field, $\underline{E}_1$ and $\underline{B}_1$ the self-consistent electromagnetic fields, and n_e and M_e, respectively, the electron density and mass. The solution of this equation has the structure

$$\delta\nu = \delta\nu^L + \delta\nu^E \qquad (6)$$

where $\delta\nu^L$ is the solution of the homogeneous part of eq.(5) satisfying the initial conditions adopted and, hence, contains the electron dynamics disregarding their interaction forces, whereas $\delta\nu^E$ describes the effects of the self-consistent fields. In particular, the dynamics is to be considered for asymptotically large times. Decomposing the current density in an analogous way, and using Maxwell's equations to eliminate electric and magnetic field quantities, one finds eventually for the spectral emissivity :

$$\eta_\omega^{(i)}(\hat{\underline{k}}) = \frac{c^2k^{(i)3}\omega}{4\pi^2}A_{mn}\left[\frac{T^A_{pm}T^{A*}_{nq}}{\frac{\partial\Delta}{\partial k}}\right]_{\underline{k}=\underline{k}^{(i)}}\frac{\left\langle J_p^L(\omega,\underline{k}^{(i)})J_q^{L*}(\omega,\underline{k}^{(i)})\right\rangle}{T\,\delta V'} \qquad (7)$$

where $A_{mn} = \delta_{mn} - \hat{k}_m\hat{k}_n$, $\underline{\underline{T}}$ is the dispersion tensor, Δ its determinant and the superscript A denotes the matrix of complements. The correlation function of the free current density can be calculated from its definition, yielding

$$\frac{\left\langle \underline{J}^L(\omega,\underline{k})\underline{J}^L(\omega,\underline{k})\right\rangle}{T\,\delta V'} = 2\pi n_e e^2\int d^3v\, f(v_\perp,v_\parallel)\,\delta(\omega-kv_\parallel-n\omega_c)\,J_n^2\left(\frac{kv_\perp}{\omega_c}\right)\underline{v}^{(n)}\underline{v}^{(n)*} \qquad (8)$$

with

$$\underline{v}^{(n)} = \left(\frac{n\omega_c}{k_\perp}\,,\,-i\frac{J_n'}{J_n}v_\perp\,,\,v_\parallel\right) \qquad (9)$$

For special cases a complete analytic treatment is possible : for low density plasmas, i.e. in the limit where $\alpha^2 \equiv \frac{\omega_p^2}{\omega^2} \ll 1$, the known results are confirmed. For propagation perpendicular to the static magnetic field, it results for the extra-ordinary mode (i=1, say) and for the m^{th} harmonic :

$$\eta_{\omega,m}^{(1)}(\hat{\underline{k}}) = \frac{\omega^2\Theta}{8\pi^3c^2}\frac{\pi}{2^m}\frac{\omega_p^2}{c}\frac{m^{2m-1}}{(m-1)!}\left(\frac{\Theta}{M_ec^2}\right)^{m-1}\varphi_m^{(X)}(\omega)\left[\frac{(1-\alpha^2)^2m^2-1}{(1-\alpha^2)m^2-1}\right]^{m-1/2}\left(1+\frac{\alpha^2m}{(1-\alpha^2)m^2-1}\right)^2 \qquad (10)$$

while the ordinary mode is about a factor $.1(v_{th}^2/c^2)$ weaker. In the latter equation, $\varphi_m^{(X)}(\omega)$ represents the line profile of the extra-ordinary mode, in which the relativistic effect prevails. The correction factor between square brackets describes dispersion effects, while the one between parentheses accounts for correlation effects. In the lower left area of the CMA-diagram (8) (i.e. for not too high plasma densities), the dispersion reduces the emissivity by a factor like 2 (2nd harmonic at half the cut-off density, i.e. at $\alpha^2=.25$) or 12.6 (5th harmonic at $\alpha^2=.4$). On the contrary, the correlation amplifies the emissivity by a factor 1.5 resp. 1.33 at the same parameter values. Thus the overall effect is a rather strong attenuation.

For arbitrary directions of propagation the effect has been studied numerically and shows the same tendencies.

The relative absorptivity α_ω has been calculated independently from the dispersion relation by means of the definition

$$\alpha_\omega = 2\,\mathrm{Im}\,k\,.\,\cos\beta \qquad (11)$$

Both analytical (for low density or propagation at $\vartheta=90^o$) and numerical (for arbitrary densities and directions) results are in agreement with Kirchhoff's law

$$\eta_\omega(\hat{\underline{S}}) = I_{bb}\,n_r^2\,.\,\alpha_\omega \qquad (12)$$

where I_{bb} represents vacuum black body intensity. It is noteworthy that from eqs.(2-11-12) a Kirchhoff-like relation

$$\eta_\omega(\hat{\underline{k}}) = I_{bb}\,.\,2\,\mathrm{Im}\,k \qquad (13)$$

follows for the quantity $\eta_\omega(\hat{\underline{k}})$.

Acknowledgment : One of the authors (K.A.) did benefit from a Euratom scholarship.

References :

(1) Trubnikov, B.A., Plasma Physics and the Problem of Controlled Thermonuclear Reactions, 3,122(1959).
(2) Drummond, W.E., Rosenbluth, M.N., Phys. Fluids, 6,276(1963).
(3) Rosenbluth, M.N., Nuclear Fusion, 10,340(1970).
(4) Pakhomov, V.I.,Aleksin, V.F.,Stepanov, K.N., Sov.Physics-Techn.Physics, 6,856(1962).
(5) Engelmann, F.,Curatolo, M., Nuclear Fusion 13,497(1973).
(6) Klimontovich, IU.L., J.Exptl.Theoret.Phys.(USSR),33,982(1957)
(7) Baldwin, D.E.,Bernstein, I.B., Weenink, M.P.H., Advances in Plasma Physics, 3,1(1969).
(8) Allis, W.P.,Buchsbaum, S.J., Bers, A., Waves in anisotropic Plasmas, M.I.T.Press, Cambridge 1963.

MEASUREMENTS OF THE ELECTRON CYCLOTRON EMISSION FROM THE TFR TOKAMAK PLASMA AND COMPARISON WITH THEORY

TFR Group* and NPL Submillimetre Wave Group**
(presented by A.E. Costley**)

*ASSOCIATION EURATOM-CEA SUR LA FUSION
Département de Physique du Plasma et de la Fusion Contrôlée
Centre d'Etudes Nucléaires
Boite Postale n° 6. 92260 FONTENAY-AUX-ROSES (FRANCE)

**DIVISION OF ELECTRICAL SCIENCE
National Physical Laboratory
TEDDINGTON, Middlesex (ENGLAND)

Abstract. We present measurements of the electron cyclotron emission from the TFR tokamak plasma. The emission is, as predicted [1], self-absorbed but contrary to recent predictions [2, 3] has the same frequency spectrum both along and at right angles to a major radius and peaks at a frequency $\sim \omega_{pe}$ in addition to $n\omega_{ce}$. We suggest possible causes for the discrepancies.

Measurements of the electron cyclotron emission from the CLEO tokamak plasma have shown that the emission in not as expected [4]. In particular, the radiation crossing the plasma/vacuum boundary is not polarized probably because of reflections of the radiation within the torus, and can be an order of magnitude above the predicted power level probably because of the presence of suprathermal electrons. In this paper we present measurements of the emission in the frequency range $0.5\omega_{ce} < \omega < 4\omega_{ce}$ from the TFR plasma. (See [5] for measurements of the emission and $\omega \sim 2\omega_{ce}$ at high resolution). The new measurements, while confirming the theoretical prediction of significant self-absorption of the radiation [1], show some further discrepancies between experiment and expectation.

Two discharge conditions are investigated : (A) toroidal flux density $B_\phi \sim 2.6$ T, central electron density $n_{eo} \sim 5 \times 10^{19}$ m^{-3}, central electron temperature $T_{eo} \sim 1.1$ keV, major radius $R_o = 0.98$ m, minor radius $a_o = 0.20$ m and duration $\tau \sim 350$ ms ; (B) $B_\phi \sim 3.9$ T, $n_{eo} \sim 5 \times 10^{19}$ m^{-3}, $T_{eo} \sim 1.9$ keV, $R_o = 0.98$ m, $a_o = 0.20$ m, and $\tau \sim 350$ ms. In both conditions the runaway level and degree of plasma/wall interaction are low.

The measurements are made by observing the plasma both along (direction (1)) and at right angles (direction (2)) to a major radius (Fig.1). Radiation from the plasma is directed with overmoded light-pipes (diameter $\sim 10\ \lambda_{MAX}$) into two-beam polarization type interferometers. The path-differences within the interferometers are scanned rapidly (usually in 10 ms) and the resulting interference patterns are detected with Putley indium antimonide detectors. Subsequent Fourier transformation of the interference patterns and calibration of the apparatus yield the emission spectra ($I(\omega)$).

The emission spectra observed along a major radius under discharge conditions (A) and (B) are shown in Figs 2 and 3 respectively. As expected emission peaks occur at harmonics of the electron cyclotron frequency (ω_{ce}) for the magnetic field B_o at the centre of the plasma. Since for condition (A) $I(\omega_{ce}) < I(2\omega_{ce})$ and for (B) $I(\omega_{ce}) < I(2\omega_{ce}) < I(3\omega_{ce})$, significant self-absorption of the radiation occurs.

In addition, an emission peak occurs at $\omega \sim \omega_{pe}$ under condition (B), where ω_{pe} is the plasma frequency corresponding to n_{eo}. Spectra obtained at later times in the discharge duration show that the amplitude of this peak decays with a time constant ~ 100 ms.

The emission spectra observed simultaneously in two directions of observation under condition (A) are shown in Fig. 4. The spectra have been normalized at $\omega = 2\omega_{ce}$. Nearly identical spectra are also observed under condition (B).

The predictions of the theory of tokamak cyclotron emission [2,3] for the emission along a major radius are shown in Figs. 1 and 2 for comparison with experiment . (Again the spectra have been normalized at $\omega = 2\omega_{ce}$). In the associated computations the measured values of B_ϕ, n_{eo}, and T_{eo}, with assumed parabolic profiles for the latter two, are used, and the effect of wall reflections whicn maintain the angle between the radiation vector and the magnetic field are included. In addition, the presence of ports is taken into account by reducing the conductivity value for the reflectivity of the wall material by an appropriate factor f = surface area of ports/surface area of torus, polarization scrambling is included by introducing a transfer fraction p between the two possible polarizations at each reflection, and reflection of the extraordinary mode fundamental in the upper hybrid region is included by reducing the calculated value with polarization scrambling by a factor ~ 2 (see [4] for details).

The theory predicts that the emission line at $2\omega_{ce}$ should be optically thick under both discharge conditions and so $I(2\omega_{ce})$ should be equal to twice the single mode black-body level (I_{BB}) for the measured T_{eo} (twice, because of polarization scrambling). Preliminary estimates based on a microwave calibration of the complete system used to detecte the emission in direction (1) (i.e. interferometer, detector, light-pipe and coupling to torus), give the level of the emission at this frequency to be within an order of magnitude of 2 I_{BB} in both cases.

The agreement between experiment and prediction is evidently good for the relative heights of the harmonics and suggests that a measurement of the frequency spectrum of the emission would be a useful diagnostic for $T_{eo}(t)$ under low runaway conditions [6]. However, three substantial discrepancies exists : (i) the apparent isotropy of the emission, (ii) the peak in the emission at $\omega \sim \omega_{pe}$, and (iii) the relatively narrow experimental line widths particularly for the non optically thick (n = 3) lines [7]. Reflections of the radiation within the torus which change the angle between the radiation vector and the magnetic field may be the cause for (i) and (iii), while the occurrence of a collective phenomenon may be the source for (ii).

We wish to thank the Culham Laboratory, UKAEA, for supporting the major part of this work.

[1] B.A. Trubnikov and V.S. Kudryavtsev, proc. 2nd UN Conf. Peaceful Uses of Atomic Energy (Geneva) 31, 93 (1958).
[2] M.N. Rosenbluth, Nucl. Fusion 10, 340 (1970).
[3] F. Engelmann and M. Curatolo, Nucl. Fusion 13, 497 (1973).
[4] A.E. Costley, R.J. Hastie, J.W.M. Paul, and J. Chamberlain, Phys. Rev. Letts. 33, 13, 758-761 (1974).
[5] TFR Group, Paper presented by R. Cano at this Conference.
[6] Note that the agreement is good even for the fundamental where one of the basic assumptions of the theory (ω_{pe}^2 c/ ω^2 V_{th} << 1) is violated.
[7] Note that because of the finite resolution (R) of the Fourier spectrometer the real line widths must be less than those shown in the figures.

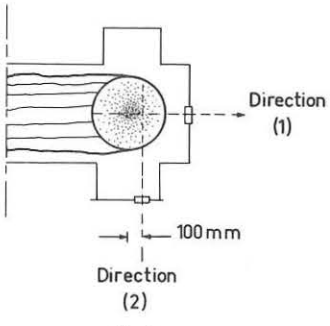

Fig 1

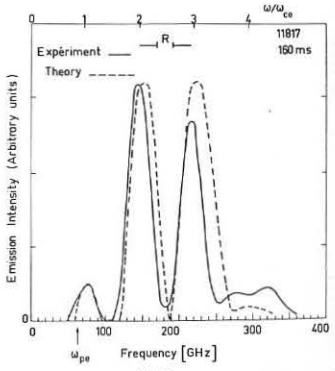

Fig 2

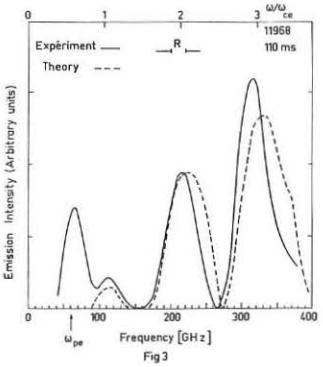

Fig 3

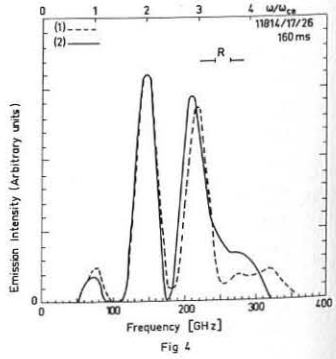

Fig 4

ELECTRON TEMPERATURE RADIAL PROFILE DEDUCED FROM CYCLOTRON EMISSION IN TFR.

TFR Group presented by R. Cano.
ASSOCIATION EURATOM-CEA SUR LA FUSION
Département de Physique du Plasma et de la Fusion Contrôlée
Centre d'Etudes Nucléaires
Boite Postale n° 6. 92260 FONTENAY-AUX-ROSES (FRANCE)

Abstract. Measurements of the radial profile of the electron cyclotron radiation at the second harmonic in the TFR device are reported. Comparison of these measurements with the theory for a weakly inhomogeneous hot plasma gives the electron temperature profile. The resulting temperature profiles and their time evolution are compared with those obtained from Thomson scattering measurements.

Electron cyclotron radiation measurements at the second or higher harmonics have been proposed as a means of evaluating the electron temperature and its time evolution [1]. Previously, the validity of the conventional hot plasma theory for the propagation and absorption of an electromagnetic wave at the second harmonic of the electron cyclotron frequency in a homogeneous magnetic field has been verified in the C Stellarator [2]. Measurements of the cyclotron emission have been reported in CLEO [3] and TFR [4]. In a toroidal device, taking advantage of the radial inhomogeneity of the magnetic field, a simple spectral analysis of the emitted radiation is required to obtain a local measurement of the electron temperature.

In this paper we report measurements of the radial profile of the second harmonic electron cyclotron radiation carried out in the TFR device. The experimental arrangement is illustrated in fig. 1. The emitted radiation in the extraordinary polarization is measured perpendicularly to the magnetic field in the direction of the large radius R. The horn is connected to a superetherodyne receiver through a 4 m length 3 cm rectangular oversized waveguide. Two local oscillators have been used covering the band from 120 to 160 GHz. After mixing, the signal goes through a pass band video amplifier (F_o = 375 ± 125 MHz) followed by a diode rectifier and an audio amplifier (dc to 30 kHz frequency band). For a given value of the toroidal magnetic field we select at each shot the frequency of the local oscillator F_o and we measure the emission in the band $F_o \pm \Delta F$ (ΔF = 125 MHz). Supposing that the strong interaction between the plasma and radiation of frequency F_o is localized in the region where $F_o = 2 F_c(r)$ (where F_c is the electron cyclotron frequency) we obtain the radial profile of the emission shown in fig. 2.

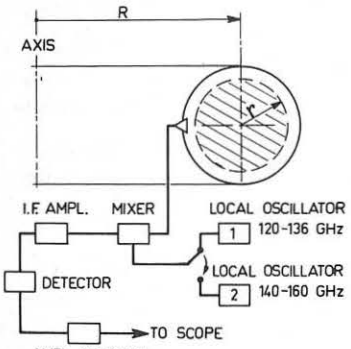

Figure 1.
Experimental Scheme.

The specific intensity for the extraordinary polarization at the second harmonic is given by :

$$I = \frac{\omega_c^2 k T_e}{8\pi^3 c^2} \left| 1 - e^{-\tau(r)} \right|$$

where [2]

$$\tau(r) = 4\pi^2 \left(\frac{6 - \gamma}{6 - 2\gamma} \right)^2 \gamma \frac{k T_e(r)}{2 mc^2} \frac{R(r)}{\lambda} \quad , \quad \omega_o = 2\pi F_o$$

$$\gamma(r) = \frac{\omega_p^2(r)}{\omega_c^2(r)} \quad , \quad \lambda = \frac{c}{F_o}$$

For the experimental conditions of fig. 2 at r = 0 using the density given by the microwave interferometer $n_e = 6 \times 10^{13} cm^{-3}$, the temperature given by Thomson scattering T_e = 1,25 keV we obtain $\tau(0) = 35$. Therefore the condition of an optically thick layer ($\tau > 1$) is satisfied over the majority of the plasma cross section. ($r \lesssim 15cm$).

Under the conditions of antenna-plasma matching the power measured by the receiver is $P(\omega) = k T_e(r) \frac{\Delta\omega}{2\pi}$ where $\Delta\omega/2\pi$ is the band of the video amplifier. Calling L the distance from the surface of blackbody to the antenna, A the linear dimension of the antenna aperture and D the transverse dimension of the blackbody the conditions of matching given by $A^2/4\lambda < L < AD/2\lambda$ are satisfied in the region of the measured emission profile.

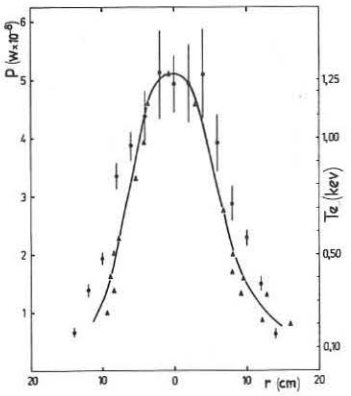

Figure 2
Power radiated at 2nd harmonic vs.radius (▲) and electron temperature by Thomson scattering (ϕ)
I = 140 kA, B_T = 26 kG, t = 150 ms.

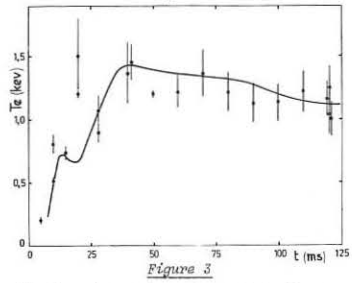

Figure 3
Electron temperature at r = 0 vs.time measured by cyclotron emission (curve) and by Thomson scattering (points) for the conditions of fig. 2. The emission is normalized to Thomson scattering at t = 120 ms.

Taking into account the sensitivity of the receiver (2×10^6 m V/m W) and the losses of the transmission line we found at r = 0 P = 0.5×10^{-7} watt and T_e = 1.4 ± 0.3 keV in good agreement with 1.25 ± 0.2 keV given by Thomson scattering measurements.

In fig. 2 the temperature profile obtained by cyclotron emission is compared to the Thomson scattering profile. The emission profile has been measured in the equatorial plane whereas the Thomson scattering is in the vertical plane 2 cm outside the geometrical axis. A somewhat narrower profile is obtained by the emission measurements.

In fig. 3 we show the time evolution of the cyclotron emission at r = 0 measured during one shot compared with the value of T_e given by Thomson scattering (one shot is needed for each Thomson scattering point). The condition of black body emission is fulfilled approximatly 10 ms after the beginning of the discharge. The dispersion of the Thomson scattering points during the first 25 ms can be attributed to the narrower temperature profile normally observed at the beginning of the discharge and to the displacement of this profile early in time.

Emission more than two orders of magnitude larger than the previous measurements has been observed for particular discharge conditions. X-rays measurements suggest that the discharge is then dominated by runaway electrons thus the measurement of the spectrum in this case could yield information about the suprathermal electron population.

In conclusion, for low runaway working conditions of the TFR, the radial profile and the time evolution of the second harmonic cyclotron radiation seems in good agreement with the hot plasma theory of radiation in thermodynamic equilibrium. The local electron temperature is then readily obtained by the emission measurements.

References :

[1] F. Engelmann, M. Curatolo, Nuclear Fusion 13 497 (1973).
[2] E.B. Meservey, S.P. Schlesinger, Phys. of Fluids 8 , 500 (1965).
[3] A.E. Costley, R.J. Hastie, J.W.M. Paul, J. Chamberlain, Phys. Rev. Letters 33, 758 (1974).
[4] TFR Group, Paper IAEA CN 33/A6 - 2, 5th Conf. on Plasma Physics and Controlled Nuclear Fusion Research, Tokyo (1974).

ELECTRON TEMPERATURE RADIAL PROFILE DEDUCED FROM CYCLOTRON EMISSION IN TFR.

TFR Group presented by R. Cano.
ASSOCIATION EURATOM-CEA SUR LA FUSION
Département de Physique du Plasma et de la Fusion Contrôlée
Centre d'Etudes Nucléaires
Boîte Postale n° 6. 92260 FONTENAY-AUX-ROSES (FRANCE)

Abstract. Measurements of the radial profile of the electron cyclotron radiation at the second harmonic in the TFR device are reported. Comparison of these measurements with the theory for a weakly inhomogeneous hot plasma gives the electron temperature profile. The resulting temperature profiles and their time evolution are compared with those obtained from Thomson scattering measurements.

Electron cyclotron radiation measurements at the second or higher harmonics have been proposed as a means of evaluating the electron temperature and its time evolution [1]. Previously, the validity of the conventional hot plasma theory for the propagation and absorption of an electromagnetic wave at the second harmonic of the electron cyclotron frequency in a homogeneous magnetic field has been verified in the C Stellarator [2]. Measurements of the cyclotron emission have been reported in CLEO [3] and TFR [4]. In a toroidal device, taking advantage of the radial inhomogeneity of the magnetic field, a simple spectral analysis of the emitted radiation is required to obtain a local measurement of the electron temperature.

In this paper we report measurements of the radial profile of the second harmonic electron cyclotron radiation carried out in the TFR device. The experimental arrangement is illustrated in fig. 1. The emitted radiation in the extraordinary polarization is measured perpendicularly to the magnetic field in the direction of the large radius R. The horn is connected to a superetherodyne receiver through a 4 m length 3 cm rectangular oversized waveguide. Two local oscillators have been used covering the band from 120 to 160 GHz. After mixing, the signal goes through a pass band video amplifier (F_0 = 375 ± 125 MHz) followed by a diode rectifier and an audio amplifier (dc to 30 kHz frequency band). For a given value of the toroidal magnetic field we select at each shot the frequency of the local oscillator F_0 and we measure the emission in the band $F_0 \pm \Delta F$ (ΔF = 125 MHz). Supposing that the strong interaction between the plasma and radiation of frequency F_0 is localized in the region where $F_0 = 2 F_c(r)$ (where F_c is the electron cyclotron frequency) we obtain the radial profile of the emission shown in fig. 2.

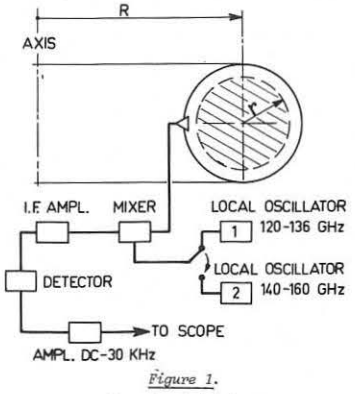

Figure 1.
Experimental Scheme.

The specific intensity for the extraordinary polarization at the second harmonic is given by :

$$I = \frac{\omega_0^2 k T_e}{8\pi^3 c^2} \left| 1 - e^{-\tau(r)} \right|$$

where [2]

$$\tau(r) = 4\pi^2 \left(\frac{6-\gamma}{6-2\gamma}\right)^2 \gamma \frac{k T_e(r)}{2 mc^2} \frac{R(r)}{\lambda} \quad , \quad \omega_0 = 2\pi F_0$$

$$\gamma(r) = \frac{\omega_p^2(r)}{\omega_c^2(r)} \quad , \quad \lambda = \frac{c}{F_0}$$

For the experimental conditions of fig. 2 at r = 0 using the density given by the microwave interferometer $n_e = 6 \times 10^{13} cm^{-3}$, the temperature given by Thomson scattering T_e = 1,25 keV we obtain $\tau(0) \simeq 35$. Therefore the condition of an optically thick layer ($\tau > 1$) is satisfied over the majority of the plasma cross section. ($r \lesssim 15$cm).

Under the conditions of antenna-plasma matching the power measured by the receiver is $P(\omega) = k T_e(r) \frac{\Delta\omega}{2\pi}$ where $\Delta\omega/2\pi$ is the band of the video amplifier. Calling L the distance from the surface of blackbody to the antenna, A the linear dimension of the antenna aperture and D the transverse dimension of the blackbody the conditions of matching given by $A^2/4\lambda < L < AD/2\lambda$ are satisfied in the region of the measured emission profile.

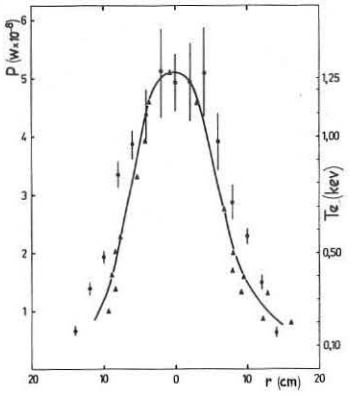

Figure 2
Power radiated at 2nd harmonic vs.radius (▲) and electron temperature by Thomson scattering (ϕ)
I = 140 kA, B_T = 26 kG, t = 150 ms.

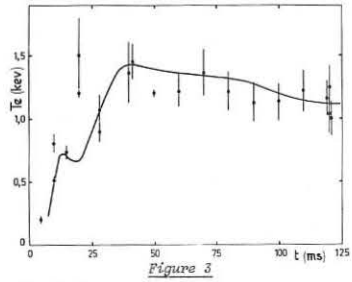

Figure 3
Electron temperature at r = 0 vs.time measured by cyclotron emission (curve) and by Thomson scattering (points) for the conditions of fig. 2. The emission is normalized to Thomson scattering at t = 120 ms.

Taking into account the sensitivity of the receiver (2×10^6m V/m W) and the losses of the transmission line we found at r = 0 P = 0.5×10^{-7}watt and T_e = 1.4 ± 0.3 keV in good agreement with 1,25 ± 0.2 keV given by Thomson scattering measurements.

In fig. 2 the temperature profile obtained by cyclotron emission is compared to the Thomson scattering profile. The emission profile has been measured in the equatorial plane whereas the Thomson scattering is in the vertical plane 2 cm outside the geometrical axis. A somewhat narrower profile is obtained by the emission measurements.

In fig. 3 we show the time evolution of the cyclotron emission at r = 0 measured during one shot compared with the value of T_e given by Thomson scattering (one shot is needed for each Thomson scattering point). The condition of black body emission is fulfilled approximatly 10 ms after the beginning of the discharge. The dispersion of the Thomson scattering points during the first 25 ms can be attributed to the narrower temperature profile normally observed at the beginning of the discharge and to the displacement of this profile early in time.

Emission more than two orders of magnitude larger than the previous measurements has been observed for particular discharge conditions. X-rays measurements suggest that the discharge is then dominated by runaway electrons thus the measurement of the spectrum in this case could yield information about the suprathermal electron population.

In conclusion, for low runaway working conditions of the TFR, the radial profile and the time evolution of the second harmonic cyclotron radiation seems in good agreement with the hot plasma theory of radiation in thermodynamic equilibrium. The local electron temperature is then readily obtained by the emission measurements.

References :

[1] F. Engelmann, M. Curatolo, Nuclear Fusion 13 497 (1973).
[2] E.B. Meservey, S.P. Schlesinger, Phys. of Fluids 8 , 500 (1965).
[3] A.E. Costley, R.J. Hastie, J.W.M. Paul, J. Chamberlain, Phys. Rev. Letters 33, 758 (1974).
[4] TFR Group, Paper IAEA CN 33/A6 - 2, 5th Conf. on Plasma Physics and Controlled Nuclear Fusion Research, Tokyo (1974).

DYNAMIC STABILIZATION OF A DISRUPTIVE INSTABILITY IN TOKAMAKS

R.A.Demirkhanov, A.G.Kirov, V.P.Sidorov, A.I.Astapenko, E.M.Lomakin, N.I.Malykh

Institute of Physics and Technology, Sukhumi, U S S R

ABSTRACT: The paper present the results of experimental studies on suppressing the disruptive instability by means of stabilization in a tokamak using a longitudinal alternative current. Stabilization is realized at $\tilde{J}_p/\bar{J}_p \leq 0{,}2$. The experimental results are analyzed on the basis of a theory of combined stabilization.

As it is well-known, the disruptive instability occuring in tokamaks is an obstacl to lowering the safety factor below: $q \simeq 2{,}5$. The investigations of this instability in "T-6" /1/ indicate that a helical MHD-instability is a cause of its occurence. These instabilities can be suppressed by the dynamic stabilization using h.f. fields and feedbacks. The paper /2/ presented the preliminary results on stabilization of helical instabilitis in tokamak "RT-4" by h.f. fields. The present paper gives more detailed results on dynamic stabilization studies of the tokamak discharge disruptive instability by a h.f. current at higher freguencies and wider range of plasma parameter variations. A possible mechanism of the effect observed is discussed.

The experimental machine 'RT-4" is a tokamak in which a longitudinal h.f. current can be excited in addition to the discharge quasistationary current. There is no liner in the machine, and the casing serves as a vacuum chamber and a primary winding of an air-transformer which excites both quasistationary and h.f. currents in the plasma.

In a circuit exciting h.f. currents, the casing forms a part of inductance of the oscillating contour fed by the self-oscillator. The power dissipated in the oscillating contour is ~4 Mwatt.

The machine magor radius R = 20cm, the minor one a_p =4 cm, $b_{cas.}$= 4,5 cm.

The experiments have been carried out in the following range of variation parameters plasma:

B_z = 8÷20 KG; $\bar{J}_p$ = 6÷25 ka; $\tilde{J}_{pstabil.}$= 0÷5 ka; q=8÷2

$n_e = 3.10^{13}$÷10^{14} cm^{-3}; j_{max}= 600 a/cm^2, $\omega = 5.10^5$ sec^{-1}

Conclusions on the discharge stability have been drawn on the basis of loop voltage, plasma current and plasma volume X-radiation analysis. Density measurements have been carried out using a laser three-mirror interferometer at the wave λ = 337 μm which allowed us to measure the concen trations from 3.10^{12} to 10^{16} cm^{-3}.

In Fig. IA typical traces of a "purely" tokamak discharge are shown at $q_{min} \simeq 2$ and $\bar{J}_{p_{max}}$= 20 ka. The current front shows the steps corresponding to the instantaneous q-values, and the loop voltage indicates the oscillations developing at the moment of the current pass the step. The plasma volume X-radiation analysis shows that the common monotonous-rising signal has the oscillations correlated with loop-voltage and current oscillations. On developing these oscillations the plasma density slightly rises. When the current grows further the loop-voltage and X-ray signal oscillations begin to damp and the discharge becomes more quiescent; afterwards the loop voltage decreases a little and undergoes a sharp spike. Simultaneously, we observe X-radiation blow-out, a small "peak" of the plasma current and density growth, i.e., a whole set of phenomena characteristic of the disruptive instability.

When generating an additional h.f. current of a certain value in the plasma, the diagnostic signal oscillations disappear and the disruptive instability does not develope.

Fig. I B shows such traces of the discharge stabilized by h.f. currents. Fig. I C shows an envelope of the stabilizing h.f. current.

Stabilization is of threshold type and is realized in a whole range of q=2÷8 at $\tilde{J}_p/\bar{J}_p \leq 0{,}2$. When $\tilde{J}_p/\bar{J}_p \ll 0{,}2$ the oscillations slightly change their amplitudes but when approaching the threshold value, considerable spikes in the loop voltage disappear and there remain only small ones and completely disappear at $\tilde{J}_p/\bar{J}_p \leq 0{,}2$.

In a poorly set regimes when the chamber walls release a considerable flux of impurities and a neutral gas, the stabilization condition gets worse and $\tilde{J}_p/\bar{J}_p \simeq 0{,}25$.

In stabilized regimes, we observe plasma conductivity growing I.5 times at $Te_6 \simeq 80$ ev and $n_e \simeq 6$÷8.10^{13}cm^{-3}.

The experimental dependences obtained show that the value which is necessary to stabilize the field disruptive instability:

1. slightly depends on the plasma density n_e,
2. grows together with the plasma current $\bar{J}p$,
3. decreases on increasing the quasistationary field B_z.

Fig. 2 shows the experimental points reflecting the dependence of the value $h_{crit} = \tilde{B}_\varphi/\bar{B}_\varphi$ which is necessary to realize the stability at the given q. It is evident that h_{crit} slightly depends upon q. The comparison of the dependence of h_{crit} with the theory of a "purely" dynamic stabilization /3/ (Curve I in Fig.2) shows some divergence in the region of small q.

We suppose that the observed effect of the disruptive instability suppression can be treated in terms of the theory of combined stabilization of plasma MHD-instabilities using h.f. fields and feedbacks. As a matter of fact, on imposing a h.f. field on the plasma column, plasma shows perturbations containing spatial and temporal harmonics. The automatic control system receives and amplifies each harmonic separately. A well-conducting copper casing in "RT-4" probably acts as an automatic control system with each harmonic amplification factor being equal to I. The h.f. field amplitude necessary for the MHD mode stabilization m, as it follows from the theory considering the case in "RT-4", is given by the expression:

$$h^2_{crit} = \frac{\tilde{B}^2_\varphi}{B^2_\varphi} = \frac{\{1-(a/b)^{2|m|}\}^2}{|m|\{|m|-1+(|m|+1)(a/b)^{2|m|}\}} \qquad (I)$$

In order to make direct comparison with the experimental values of h_{crit}, it is necessary to know $h_{crit}(q)$. It follows from the theory that the range of instable

$$m - \frac{1-(a/b)^{2|m|}}{2} + \Delta(\hat{h}^2) > nq > m - \frac{1-(a/b)^{2|m|}}{2} - \Delta(\hat{h}^2)$$

with $\Delta(\hat{h}^2) \to 0$ at $\hat{h}^2 \to \hat{h}^2_{crit}$. Thus, at $\hat{h}^2 = \hat{h}^2_{crit}$ the equality m = nq is fulfilled within the accuracy not less than IO %. Thus, expression (I) gives the dependence of $\hat{h}^2_{crit}(nq)$. Experimental and theoretical dependences of $h_{crit}(nq)$ at n = I are given in Fig.2; it shows that the theory and experiment coincidence is rather good.

We express our acknowledgements to V.B.Myburov for help in developing and setting the h.f. system and to I.S.Fursa for continuous help in operation.

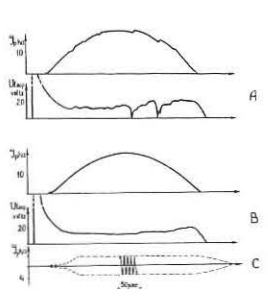

Fig.I

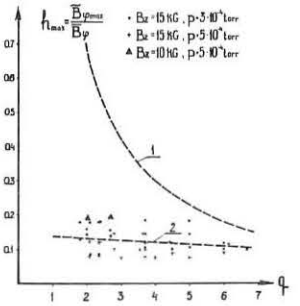

Fig.2

REFERENCES:

I. V.S.Vlasenkov et al., YI European Conf. on Contr. Fusion and Plasma Physics, 1973, vol I, p.55.

2. R.A.Demirkhanov et al., YI European Conf. on Contr. Fusion and Plasma Physics, 1973, vol I, p. 171.

3. V.P.Sidorov, T.R.Soldatenkov, Dokl. Acad. Nauk. USSR, 215, p. 321, 1974.

INSTABILITY HEATING IN THE LT-3 TOKAMAK

M. G. Bell, I. H. Hutchinson and J. D. Strachan

The Australian National University, Canberra, A. C. T., Australia.

Abstract: In the Canberra tokamak, appreciable ion heating has been observed at the disruptive instability. Experiments on LT-3 have been aimed at evaluating the potential for using such heating to bring a reactor plasma to ignition.

Ion Heating: In the small tokamak, LT-3 (major radius R = .4 m, aperture radius a = 0.085 m, toroidal magnetic field $B_\phi \leq 1$T, gas currents $I_\phi \leq$ 25 kA, $T_e \sim T_i \sim 50$ eV, and $n_e \sim 3 \times 10^{13}$ cm^{-3}) the ion temperature can be deduced from measurements of the thermal Doppler broadening of impurity lines. The results from OV2781 Å broadening during an unstable discharge indicate a rapid rise in the ion temperature at the disruptive instability which then decays over a period of 150μs (fig. 1). The heating is observed to increase both with the plasma current and the toroidal magnetic field.

The poloidal beta, $\beta_I = 8\pi^2 a^2 \overline{n(T_e + T_i)} / \mu_o I_\phi^2$, has been observed to change only marginally at the disruptive instability under most conditions and may be a decrease or an increase of up to 30% depending on I_ϕ and B_ϕ. Observations of the emission from the successive ionization stages of oxygen (OI to OVI) indicate that the electron temperature falls at the disruptive instability by a factor of 2 or 3.

The Heating Mechanism: The disruptive instability is known to follow a shrinking of the plasma current profile. In about 10μs, the plasma expands to fill the torus and the current profile flattens. We believe that the ions are heated by current driven turbulence created by the high toroidal electric field, E_ϕ, induced by the expansion. This field is seen as the negative spike in the loop voltage.

Although the total plasma current remains constant, the redistribution of the current is associated with a reduction in the stored magnetic energy by $\left[2W_p \ln(r_1/a)/\beta_I\right]$ where W_p is the initial plasma kinetic energy and r_1 is the initial plasma radius. Up to 20% of this change in magnetic energy finds its way into the ions.

One possible energy transfer mechanism is by ion cyclotron drift waves. Magnetic probes at the plasma edge have picked up oscillations at the ion cyclotron frequency during the negative voltage spikes (fig. 2). Work on the Princeton Q-machine[1] at lower electric fields indicates that this form of turbulence could account for the magnitude of the observed temperature rise in LT-3.

Reactor Implications: The mean kinetic energy in a tokamak plasma is $\overline{n(T_e + T_i)} = \frac{1}{2\mu_o} \frac{\beta_I}{q^2(a)} \left(\frac{a}{R}\right)^2 B_\phi^2$ where q(a) is the aperture safety factor. Ignition requires the achievement of a high value of n and T_i; the quantities β_I and q(a) are limited by the fundamental plasma behaviour while (a/R) and B_ϕ are limited by technology. To achieve ignition within these constraints, it is desirable to increase T_i/T_e. The ion heating and electron cooling associated with the disruptive instability does, in fact, increase this ratio. By ohmically heating a reactor to its limiting value and then inducing a single disruptive instability it might be possible to achieve ignition.

The distribution of the turbulent heating through the plasma depends on the induced electric field, whose profile is more favourable than that for an externally applied electric field. We expect that E_ϕ will be sufficient to excite ion cyclotron drift waves close to the minor axis.

The injection of impurities may be the major impediment to this reactor concept since the disruptive instability can cause the plasma to interact with the walls. The influx of impurities at the disruption has been difficult to assess on LT-3 but our impurities enter primarily early in the discharge when the current profile is hollow and also during the "oscillatory phase" which follows the disruption. It should be noted that the disruption may have the favourable effect of redistributing the impurities evenly through the torus and thus remove any impurity concentration from the torus centre[2].

Following each disruptive instability is an oscillatory phase which lasts for 200μs during which the ion temperature decays. The rate of temperature decay is reduced by increasing the toroidal magnetic field. The minimum decay rate is consistent with the electron-ion equilibration time which is also about the energy confinement time for an LT-3 size device.

We have been able to truncate this oscillatory phase (fig. 3) by reducing the current slightly so that the q(a) rises above 4 and the plasma re-enters the stable regime. Unfortunately for this marginally unstable regime in LT-3 the toroidal current is so low that appreciable ion heating has not been observed.

The authors would like to thank Professor B. S. Liley whose ideas motivated this study.

References:

(1) M. Yamada et al., Phys. Rev. Lett. 34, 650 (1975).

(2) B. B. Kadomtsev, Sixth European Conf. on Contr. Fusion and Plasma Phys. (Moscow) Vol II, pg 1 (1973).

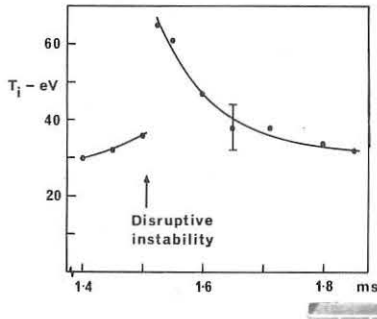

Figure 1a). OV ion temperature in unstable discharge (current = 15 kA, magnetic field = .9T).

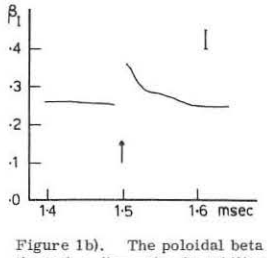

Figure 1b). The poloidal beta through a disruptive instability.

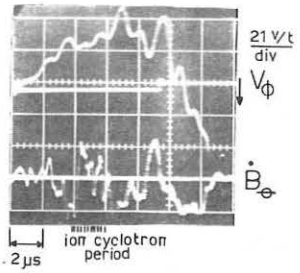

Figure 2. Plasma oscillations during the negative voltage spike.

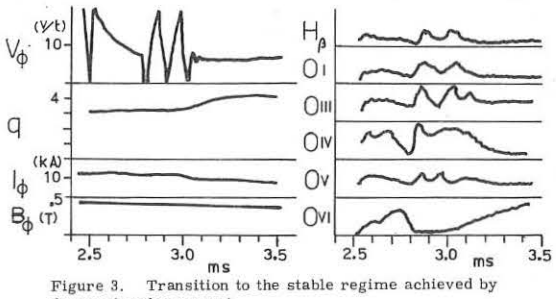

Figure 3. Transition to the stable regime achieved by decreasing the current.

INJECTION OF A HIGH INTENSITY REB INTO A TOKAMAK

M. Masuzaki, A. Mohri, T. Tsuzuki, A. Nishizawa and K. Ikuta
Institute of Plasma Physics, Nagoya University
Nagoya, Japan

Abstract: A high intensity relativistic electron beam(REB) was successfully injected into a tokamak plasma. The behaviour of the plasma-beam system depended upon the relative directions of the toroidal magnetic field, the Ohmic-current and the beam current. Energy density of up to 6.4×10^{15} eV/cm^3 was transferred to the plasma, which corresponds to the efficiency of about 5 %. A global motion of the plasma-beam system was observed.

Introduction: Recent successes of the injection of high intensity REB's into toroidal fields[1,2,3] have made it possible to investigate experimentally whether REB's can be injected and trapped into toroidal plasmas such as tokamak plasmas without serious disturbances and whether they can heat plasmas effectively as in the case of linear plasmas[4]. In this paper, some preliminary results of our experiment concerning these problems are reported.

Experimental details: Fig.1 shows a schematic drawing of the experimental setup which mainly consists of a tokamak SPAC-II[5] and a REB source Phoebus-I[6]. The characteristics of SPAC-II are: the major radius 28 cm; the inner radius of a liner, made of stainless-steel bellows of 0.3 mm thick, 6.7 cm; the inner radius of a limiter 5.5 cm; and the inner radius of aluminum shell of 1.5 cm thick 8 cm. The typical parameters in this experiment were: the peak of the toroidal magnetic field B_t 10 KG; the vertical magnetic field B_v several tens of gauss; the peak of the Ohmic-current I_p around 10 KA; the averaged electron density, measured by a HCN laser interferometer[7], $1 \sim 3 \times 10^{13}$ cm^{-3}; and the electron conduction temperature, assuming $Z_{eff}=2$, around 60 eV; the filling pressure of deuterium gas being several times 10^{-4} torr.

Fig.1

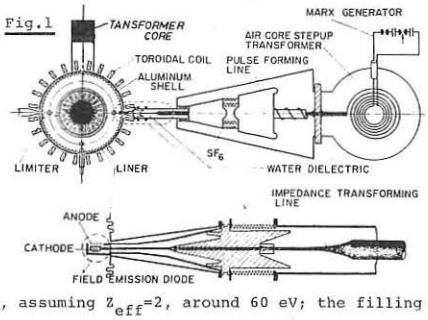

A diode was located near the limiter on the meridian plane as shown in Fig.1, the head of its housing protruding 1 cm into the torus from the limiter. The diode consists of a carbon cathode, the dimensions of the emitting surface being 1.8 cm × 1.5 cm, and a grid anode; it ejects electrons parallel to the toroidal magnetic field. The diode voltage, the diode current and the FWHM of the pulse were typically 500 KV, 13 KA and 40nsec, respectively. The diode characteristics were the same with and without the plasma. The beam was injected, in most of the experiment, at the quiescent stage of the tokamak plasma. During the experiment, all four combinations of the directions B_t and I_p, the direction of the beam current I_b being fixed, were tried with almost the same plasma parameters.

Results: The magnetic measurements by fast magnetic probes placed just inside the liner showed that the behaviour of the plasma after the beam injection depended strongly upon the directions of B_t and I_p. For example, the variation of the toroidal field between the plasma and the liner ΔB_{te}, which showed the diamagnetic behaviour of the plasma-beam system under the assumption that the toroidal magnetic flux was conserved inside the liner during the characteristic time of the behaviour of the plasma-beam system, had the following inclination: $\Delta B_{te}(\downarrow\uparrow\downarrow) > \Delta B_{te}(\uparrow\downarrow\downarrow) \gtrsim \Delta B_{te}(\downarrow\downarrow\downarrow) > \Delta B_{te}(\uparrow\uparrow\downarrow)$, where the first, the second and the third arrows in the bracket means the directions of B_t, I_p and I_b, respectively. Fig.2 shows a typical signal for the case $(\downarrow\uparrow\downarrow)$, the peak value being 6.4×10^{15} eV/cm^3 with the efficiency of about 5 %.

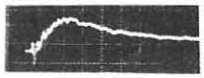

Fig. 2

VER:3.2x10^{15}eV·cm^{-3}/D.
HOR:200nsec/D.

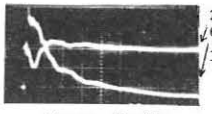

Upper: Upside
Lower: Downside

Fig. 3 $\downarrow I_p \uparrow I_b$

The variation of the poloidal field ΔB_p depended more complicatedly upon the field configuration. However, it was evident that part of B_p was due to the motion of the plasma-beam system. For example, Fig.3, which shows typical signals of the probes placed at the upside and the downside of the plasma for the case of $(\downarrow\uparrow\downarrow)$, exhibits that in this case there was an upwards motion. The direction of the motion was reversed with a reversal of B_t. This fact suggests that there was an excess of negative charges in the major-axis-side of the plasma and the electric potential surfaces did not coincided with the magnetic surfaces. The observed hard X-rays from a tungsten-wire target of 1 mm dia., inserted horizontally into the plasma. showed that the energetic electrons had the inclination to concentrate in the major-axis-side of the plasma column.

Conclusive Remarks: The experimental results mentioned above show the successful trapping of the injected REB into the plasma. An another evidence of this is that the rather long duration of emissions of hard X-rays from the limiter and the liner as shown in Fig. 4. The poloidal displacement between I_b and the return current due to plasma resistivity may be responsible for the trapping[8].

500nsec/D.
Fig. 4

References:

[1] A. Mohri, M. Masuzaki, T. Tsuzuki and K. Ikuta, Phys. Rev. Letter 34, 574(1975).

[2] J. Benford, B. Ecker and V. Bailey, Phys. Rev. Lett. 33, 574(1974).

[3] P. Gilad, B. R. Kusse and T. R. Lockner, Phys. Rev. Lett. 33, 1275(1974).

[4] For example, C. Ekdahl, M. Greenspan, R. E. Kribel, J. Sethian and C. Wharton, Phys. Rev. Lett. 33, 346(1974)

[5] Y. Hamada and A. Mohri, Jpn. J. Appl. Phys. 13, 1624(1974).

[6] A. Mohri. K. Ikuta, M. Masuzaki, T. Tsuzuki, S. Fujiwaka, K. Ukegawa and T. Kato, Institute report IPPJ-T-23(1975).

[7] A. Nishizawa, M. Masuzaki, A. Mohri and J. Fujita, to be published.

[8] R. N. Sudan, Report of Laboratory of Plasma Physics, Ithaca LPS-135(1973).

The Divertor Experiment on the Heliotron-D Device

K. Uo, O. Motojima, A. Iiyoshi and S. Morimoto
Plasma Physics Laboratory, Faculty of Engineering
Kyoto University, Gokasho, Uji, Japan

Abstract: The Heliotron-D device has an intrinsic magnetic limiter and a built-in divertor because of the characteristics of the magnetic field configuration of the helical heliotron. We report the computer calculation of the separatrix region and the experimental results which confirm these characteristics.

The Heliotron-D device has an intrinsic magnetic limiter and a built-in divertor because of the characteristics of the magnetic field configuration of the helical heliotron. Therefore, it has a great advantage to overcome the problems of the protection of the first wall and the impurity concentration.[1][2] The first kind magnetic surface of the heliotron is eliptic and it has two ridges of the separatrix at the farthest place from the helical conductor. Its rotational transform and shear are large and these contribute greatly to the stable confinement of the plasma.[3][4][5] Using the magnetic lines of force in the separatrix region, it is possible to set a divertor. The configuration of the separatrix region of the Heliotron-D for $\alpha^* = B_{to}/B_{h\nu 0} = 0$ is shown in Fig.1, S, where B_{to} and $B_{h\nu 0}$ are the magnetic flux densities of the toroidal field and the toroidal component of the helical field respectively. The finite width of the separatrix region is attributed to the toroidal effect. To extract the incoming impurity atoms, the divertor layer of the heliotron is thick enough to ionize them within the layer. Where we use the term divertor layer as a layer of the plasma stream which escapes from the scrape-off layer along the magnetic lines of force in the separatrix region and the scrape-off layer is a part of the separatrix region just outside the confining region. The plasma diffuses during the excursion along magnetic lines of force. Therefore, the width of the divertor layer is wider than the width of the separatrix region. However, since the length of the magnetic lines of force in the separatrix region connecting the scrape-off layer with the opposite side of the helical conductor is shorter than the toroidal radius, the increment of the width of the divertor layer due to the diffusion is rather small in the heliotron. The width along the long axis of the magnetic surface and the width along the short axis are about 4cm and 1cm respectively. The magnetic lines of force in the separatrix region fill the region S in a very complicated way.[4][8] If we scale up the dimensions of the device up to the future reactor design, the width of the separatrix region will be more than 10cm.[6] This value is wide enough to ionize the incoming neutral atoms and this means that the heliotron type divertor achieves a high divertor efficiency. The width of the separatrix region can be varied if we change the aspect ratio and the pitch number of the helical conductor.

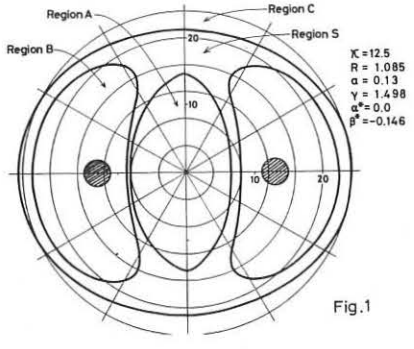

Fig.1

The measurement by the double probe shows that there is a side density peak at the location of the separatrix region away from the confining region. This side peak corresponds to the divertor layer. Shapes of the side peaks are shown in Fig.2 for the several magnetic flux densities. Abscissa X is the distance from the magnetic axis. The width of the side peak is almost independent of the plasma density. The shape does not change greatly and this fact means that in our experimental conditions $T_e \sim 30eV$, $I_{oh} \sim 5kA$, $N_e \sim 1 \times 10^{13} cm^{-3}$, the width of the divertor layer is determined mainly by the width of the separatrix region itself and it does not depend on the plasma diffusion during the excursion along the magnetic lines of force in the separatrix region. This result gives a great advantage to construct a divertor. Fig.3 shows the dependence of the ratio of the density of the side peak, n_s, to that of the main plasma, n_o, on the magnetic flux density. The ratio decreases as the magnetic flux density increases. In the case of our experiment, the increase of the magnetic flux density gives rise to the increase of the plasma density.

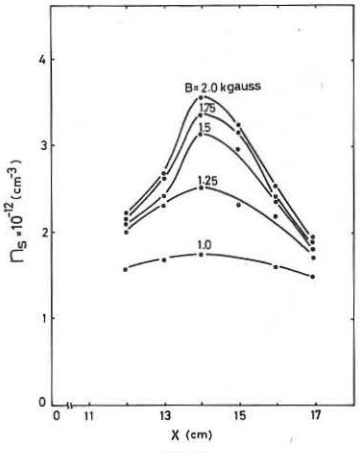

Fig.2

Since the increase of the density of the side peak is smaller than that of the confining region, the above result is attributed mostly to the improvement of the plasma confinement. All these experimental results approve the presence of the divertor layer of the Heliotron-D device.[7]

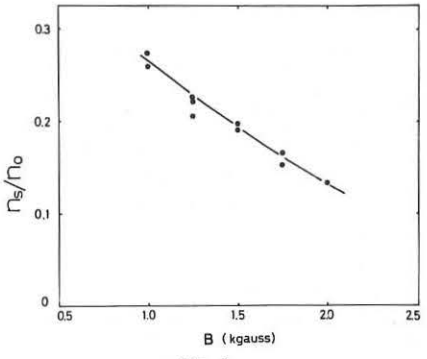

Fig.3

Reference

(1) V. A. Vershkov and S. V. Mirnov, Report IAE-2298 Kurchatov Institute of Atomic Energy, Moscow, 1973

(2) S. Von Goeler, W. Stodiek, H. Fishman, S. Grebenshchikov and E. Hinnov, MATT-1081, January 1975

(3) K. Uo, Nucl. Fusion, 13 (1973) 661

(4) K. Uo, J. Plasma Physics, 13 (1971) 243

(5) K. Uo, S. Morimoto, S. Konoshima, M. Koyama and A. Iiyoshi, Phys. Rev. Lett., 31 (1973) 986

(6) A. Iiyoshi and K. Uo, 5-th Int. Conf. on Plasma Physics and Controlled Nuclear Fusion Research Tokyo, Paper IAEA-CN-33/G4 (1974)

(7) O. Motojima, A. Iiyoshi and K. Uo, To be published.

(8) C. Gourdon, et al, Nucl. Fusion, 11 (1971) 161

A Concept for a Moving Magnetic Limiter

K.v. Hagenow, K. Lackner

Max-Planck-Institut für Plasmaphysik, 8046 Garching bei München,

Federal Republic of Germany

Abstract: To suppress the skin effect during the current-rise phase in a large tokamak, one would like to enforce proportionality between the cross-sectional area of the discharge and the plasma current. In the case of a divertor tokamak this would imply a proper variation of the postion of the separatrix, acting as a moving magnetic limiter. For a tokamak with localized divertor fields, which decay rapidly towards the plasma center - like in the ASDEX and PDX experiments - this perfect magnetic limiter behaviour cannot be achieved over a large range of currents without changing the position of the plasma center.

The following arguments are illustrated at hand of a configuration similar to ASDEX in the approximate position of the divertor coil triplet. (Fig. 1a) The detailed arrangement of divertor coils as well as the ratio of divertor currents to nominal plasma current have however be changed to produce a stagnation point sufficiently far away from these coils to allow approximately 3 m of space for blanket and shielding if the small and large plasma radius were to be scaled to typical fusion reactor dimensions of 6 and 17 m, respectively. It was the purpose of the study of this configuration to decide whether essential points of the ASDEX concept - like localized divertor fields, self-similar plasma shapes for different plasma currents in spite of time-independent operation of the multipole coil currents, and nearly circular flux surfaces in the plasma interior - can be maintained in such an extrapolation.

In the corresponding vacuum field configuration the magnitude of B rises rapidly - in fact exponentially - in the direction towards the divertor.As a result of this, changes in the plasma currents around their nominal value result in only small motion of the stagnation point. The cross-sectional area therefore initially changes much too slowly and much too fast at later stages to correspond to a perfect limiter behaviour. An also quantitatively very similar result holds for the PDX configuration. Eliminating from the presented design the so-called multipole compensation coils - which compensate the field of the divertor coils over the inner region of the plasma column - would result in some improvement in this respect, but at the cost of drastic changes in the plasma shape and the displacement-stability behaviour for different plasma currents.

The above results refer to the technically desireable case of constant currents in the divertor coils. The separatrix could be forced farther inward during the lower plasma current phase by increasing these divertor currents. Computing the factor by which these currents would have to be increased to enforce perfect magnetic limiter behaviour as a function of plasma currents show that this option is inconvenient and expensive even if used only during the last half of the current rise, and impossible to use over a larger range of plasma currents. In order to enforce perfect limiter behaviour over a factor of 5 in plasma currents one would need in the present design initially divertor currents 5 times as large as for the final plasma currents.

An effective and cheap way to vary the plasma cross-section in a programmed way consists in shifting the plasma column by proper magnetic fields into the vicinity of one of the divertor coils. For the present configuration - like for ASDEX - this suggests a shift of the plasma column in vertical direction. Figures 1a-d show a corresponding set of equilibrium configurations computed by the code described in [1] for plasma currents of 1/8, 1/4, 1/2 and full nominal value, where the displacement of the plasma column has been chosen properly in each case so as to make the cross-sectional area proportional to the plasma currents.

A simple model for the scaling of the radial fields required for the proper shift of the plasma column shows that their value never exceeds more than a few percent of the vertical B-field required to balance the hoop-force at full plasma current. Of course this mode of operation cannot be simply extrapolated to arbitrarily small plasma currents without additional investigations, as for small plasma currents the increasing vicinity of the divertor coils together with the decrease in the vertical field required for balancing the hoop force will make the multipole fields increasingly dominant over the whole plasma cross-section, possibly violating at some point the condition for displacement stability.
All equilibria shown in Fig.1 were found to be stable against rigid vertical displacement [2]. As no code is presently available for testing numerically computed configurations against generalized displacements, equilibrium calculations were carried out for neighbouring, displaced equilibria. These calculations, which do not take into account the stabilizing influence of poloidal and toroidal flux conservation indicate that the equilibria 1 c and 1 d might be unstable.

If these results were to be confirmed by a more consistent analysis, and if no feedback system were to be employed, a mode of operation would be appropriate in which the discharge is formed at the mid-plane and is left to grow till the discharge area corresponds to 1/2 the final plasma cross-section. For the present configuration this would happen at about 18% of the nominal plasma current. During the rise of I_p from 18% to 50% of its nominal value the plasma column is shifted vertically in such a manner that the cross-sectional area remains constant. During the last phase of the current rise between 50 and 100% the plasma column is shifted back to the center maintaining propotionality between plasma current and cross-sectional area.

[1] K.v. Hagenow, K. Lackner, Computation of Axisymmetric MHD Equilibria, 7th Conference on Numerical Simulation of Plasmas

[2] K. Lackner, A.B. Macmahon, Nucl. Fusion 14 (1974) 575

"This work was performed under the terms of the agreement on association between the Max-Planck-Institut für Plasmaphysik and EURATOM".

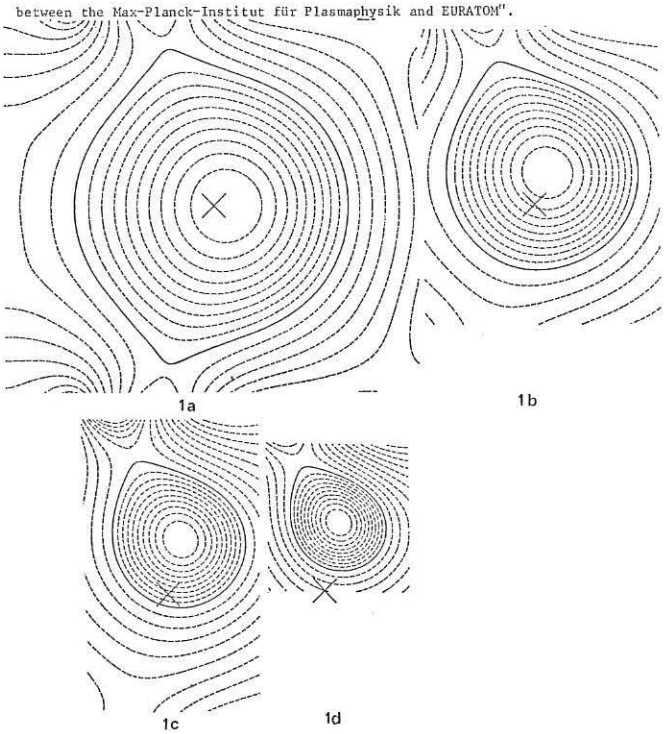

1a 1b 1c 1d

A MAGNETOHYDRODYNAMIC THEORY OF DIVERTORS*

A. H. Boozer

Princeton University, Plasma Physics Laboratory
Princeton, N.J. 08540 USA

Abstract: A two-fluid MHD divertor model is studied with zero ion temperature. The electrons are shown to leave the divertor much closer to the main plasma body than the ions. The divertor width is found comparable to the ion gyroradius calculated with the electron temperature.

The importance of divertors for controlling impurities has been recognized since stellarator experiments in the 1950's. However, divertor theory has remained remarkably primitive and been based on the theory of planar discharges.

A planar discharge is a one-dimensional system with the electrons held at a constant temperature, T_e. Plasma is created from a background neutral gas and flows to neutralizing walls, which are two parallel infinite planes. An electrostatic sheath forms at the walls to equalize the ion and electron currents. With the usual assumption of zero temperature ions, there are two primary results. The ions enter the sheath at a velocity $C_s = (T_e/m_+)^{1/2}$ with m_+ the mass associated with a positive charge. The jump in electrostatic potential $\Delta\phi$ across the sheath is approximately $3.5\ T_e/e$.

These two basic planar discharge results were assumed to apply to divertors. However, FM-1 experiments at Princeton have given potential jumps between a divertor plasma and its neutralizer which vary from less than $5\ T_e/e$ near the main plasma body to greater than $20\ T_e/e$ on the outer edges of the divertor [1].

The electron-ion current ratio to the neutralizing walls is exponentially dependent on the potential jump. Consequently these experiments are in sharp disagreement with the traditional divertor assumption that the ratio is unity on each field line. The experimental plasma flow velocity to the neutralizing walls, $\sim C_s/3$, is, however, in approximate agreement with the theory.

Plasma discharge theory does not apply to a divertor because a divertor is intrinsically two dimensional. Plasma diffuses from the main plasma body onto open magnetic field lines and then flows along the field lines to netralizing walls. In the Figure the simplest two-dimensional divertor-like system is illustrated. We have studied this system under the assumption of zero ion temperature with two fluid MHD equations. The electron mean free path λ_e is assumed to satisfy $(m_+/m_e)^{1/2} \gg L/\lambda_e \gg 1$. The major results are:

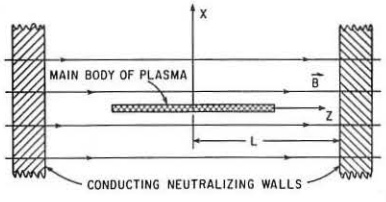

Figure. The Divertor Model. The main body of the plasma is surrounded by a uniform z directed magnetic field. The main plasma is assumed to be of infinitesimal extent in the x direction, but of a size comparable to L in the z direction. All quantities are independent of y.

(1) The electric field E_x is of constant magnitude for scales less than $\rho_+(T_e)$, the ion gyroradius calculated with the electron temperature. This implies $e\Delta\phi/T_e$ is not constant.

(2) The electrons flow to the walls in a region of approximate width $\rho_e L/\lambda_e$, ρ_e being the electron gyroradius. The flow is near the main plasma body.

(3) The ions flow to the walls in a region of approximate width $\rho_+(T_e)$. This is also the divertor width. It is substantially wider than the usual estimate $(D_\perp L/C_s)^{1/2}$ which classically gives $(\rho_+\rho_e L/\lambda_e)^{1/2}$.

(4) The ion flow velocity into the electrostatic sheath is C_s.

(5) The pressure on a field line is lower by $1/\sqrt{2}$ at the electrostatic sheath than at the center of the divertor $(z=0)$.

Even though the electron and ion currents to the walls are concentrated in different regions of the divertor, the integrated flux is the same for the two species. Quasi-neutrality is assumed to hold throughout the divertor except in the Debye length scale electrostatic sheath near the neutralizing walls. The electrons in the outer parts of the divertor form a stagnant fluid confined by large potentials compared to the electron temperature

The two fluid MHD analysis with zero ion temperature required the solution of five coupled, nonlinear, vector equations — two kinetic equations, two continuity equations, and one energy equation. The reason the one-dimensional theory fails can, however, be easily seen. The $\hat{y}$ component of the kinetic equation formed by summing the equations for the two species is $m_+ n \vec{v}\cdot\vec{\nabla} v_y + j_x B/c = 0$ while $v_y = -cE_x/B$. If δ is the divertor width, the fall in electron temperature across the divertor means $e|E_x| \approx T_e/\delta$ for equal electron and ion currents on each field line. Using $\vec{v}\cdot\vec{\nabla} \approx C_s/L$, we find $|j_x| \approx enC_s(\delta/L)(\rho_+/\delta)^2$. The ion continuity equation implies $v_x \approx C_s\delta/L$, so the current across the divertor reaches env_x for $\delta \approx \rho_+(T_e)$. This means the electrons are not moving across the divertor for $\delta \lesssim \rho_+(T_e)$. Since divertors are generally assumed to have dimensions comparable to ρ_+, one-dimensional theory cannot apply.

* Work supported by United States Energy Research and Development Administration Contract E(11-1)3073.

[1] Princeton University Plasma Physics Laboratory 1973 Annual Report MATT-Q-31, p. 10.

NEUTRAL INJECTION IN TOKAMAKS*

John Sheffield

EURATOM-UKAEA, Culham Laboratory, Abingdon, Oxon, England.

Abstract: The requirements of adequate beam penetration and equilibrium limitations to the total contained pressure are combined in determining for a Tokamak, (a) the maximum neutral power that may be injected, (b) the maximum beam fusion power that may be generated.

Constraints on neutral injection. It is generally agreed that the injected power should not be deposited near the plasma edge because this will lead to high conduction losses and increased wall bombardment. With the criterion that the radial power deposition should be a good match to the ohmic power profile it is found that we should operate with injection energies for which there are less than two mean free paths for trapping ($F_1 \leq 2$) up to the plasma centre. This estimate is supported by preliminary investigations with transport codes. At high energies $\varepsilon_o >> 10$ keV the cross sections for ionisation and charge exchange are approximately proportional to Z_{eff};[1][2] but the detailed variation with impurity content for all energies is not yet established. For injection of hydrogen, with the ionisation rate taken as proportional to Z_{eff}.

$$F_1 \simeq \frac{0.17\, na}{\sin\theta}\left(Z_{eff} - 1 + \frac{107A_b}{\varepsilon_o}\right) \quad 20 \leq \frac{\varepsilon_o}{A_b} \leq 100 \text{ keV} \tag{1}$$

this is a modification of a formula given by Sweetman[3]

If in addition the charge exchange rate is proportional to Z_{eff}

$$F_1 \simeq \frac{18na}{\sin\theta}\,\frac{Z_{eff}\,A_b}{\varepsilon_o}\,, \quad 20 \leq \frac{\varepsilon_o}{A_b} \leq 200 \text{ keV} \tag{2}$$

this is calculated in a cylindrical approximation, $\theta = 90^o$ is perpendicular injection, and $\sin\theta = \left(\frac{a}{4R}\right)^{\frac{1}{2}}$ represents injection tangential to the axis.

The ratio of fast ion energy density to plasma energy density is

$$\Gamma = \frac{P_{in}\, t_s}{0.19\, nTa^2R} \tag{3}$$

where the time for fast ions to slow down to thermal energies is

$$t_s = \frac{4.4 \times 10^{-2} A_b\, T^{\frac{3}{2}} \ell n}{n\, Z_b^2}\left(1 + \left(\frac{\varepsilon_o A_i}{15A_b T}\right)^{\frac{3}{2}}\right) \tag{4}$$

In the steady state where the plasma is supported by injection

$$\Gamma \simeq \frac{t_s}{2\tau_E} \tag{5}$$

In general no instability problems are expected[4] for approx.

$$\Gamma \leq 1 \text{ and } V_b < V_{Alfven}$$

The beam adds to the plasma pressure and we can expect similar limitations to apply to the total pressure as apply to β_p

$$\beta_p(1+\Gamma) \leq \begin{cases} 1, \\ \text{or } \sqrt{\frac{R}{a}} \quad \text{(ref (5))} \quad \beta_p = \frac{0.2\, a^2 nT}{I^2} \\ \text{or } \frac{R}{a} \qquad (6) \end{cases} \tag{6}$$

Maximum injected power The power to support the plasma at a given (n) and T is

$$P = \frac{0.096\, a^2\, RnT}{\tau_E} \tag{7}$$

We combine (7) with (4), (5) and (6) to obtain

$$P_m \simeq \frac{1.1 \times 10^2\, RI^4\, \beta_p^2\, Z_b^2\, \Gamma}{a^2 A_b\, \Gamma^{\frac{3}{2}}\, \ell n\left\{1 + \left(\frac{\varepsilon_o A_i}{15A_b T}\right)^{\frac{3}{2}}\right\}^{\frac{2}{3}}} \tag{8}$$

For a given (T) and (ε_o) and with $\beta_p(1+\Gamma)$ fixed this has a weak maximum at $\Gamma = 1$.

We arrange (8) using the penetration constraint (1) and

$$\frac{P_m}{R\Gamma} \simeq \frac{1.5 \times 10^2 (F_1 \sin\theta)^2 Z_b^2}{A_b T^{\frac{1}{2}} \ell n\left(1 + \left(\frac{\varepsilon_o A_i}{15A_b T}\right)^{\frac{3}{2}}\right)^{\frac{2}{3}}\left(Z_{eff} - 1 + \frac{107A_b}{\varepsilon_o}\right)^2} \tag{9}$$

This is plotted below for the example of a 200 keV deuterium beam and a tritium plasma. To a good approximation P_m is independent of (T) and (ε_o) and for D→T (40→200 keV)

$$P_m \simeq \frac{16\,(F_1 \sin\theta)^2\, R\Gamma}{Z_{eff}^2} \tag{10}$$

and for H → H (20 → 100 keV) we may inject about 4 x more power The impurity effects occur because for a given injection energy we must reduce (n) when (Z_{eff}) is increased, to ensure good beam penetration, and at the lower density we must then reduce the injected power if we are operating at the maximum allowed value of Γ.

Maximum beam-fusion power Computations of Q, the ratio of fusion power generated to injected beam power[7], show that peak Q, which for D → T occurs at $\varepsilon_o \sim 150$ keV, is $Q \simeq 0.23\,T$, so that

$$P_f \simeq \frac{3.7(F_1 \sin\theta)^2\, R\,\Gamma\, T}{Z_{eff}^2} \tag{11}$$

Symbols

n ($\times 10^{13}$ cm^{-3}), mean density; $T_e = T_i = T$ (keV), temperature; R,a (m), major and minor plasma radii; I (MA), plasma current; τ_E (s), energy confinement time; ε_o (keV), injection energy; A_b, Z_b, atomic number and charge of beam ion, A_i, Z_i, atomic number and charge of plasma ion; P (MW), power; P_m (MW), maximum injected power; P_f (MW), maximum beam fusion power; θ, mean injection angle, F_1, number of trapping lengths to plasma centre

References:

(1) E. McDaniel (1964) Collision Phenomena in Ionised Gases, p.328. John Wiley Inc., New York.

(2) H. Schiff (1954). Can. J. Phys. 32. 6. (P. Moriette (1974), 7th Jugoslav Conference on the Physics of Ionised Gases. p.43).

(3) D. R. Sweetman (1972) Nuclear Fusion 13, 157.

(4) H. L. Berk et al, (1974) IAEA Conference Tokyo, Japan. IAEA-CN-33/G2-3.

(5) A. A. Galeev, R. Z. Sagdeev, (1971). Soviet Physics - JETP Letters 13, 113.

(6) V. D. Shafranov (1966) Reviews of Plasma Physics (2) p.103.

(7) J. G. Cordey, W. Core, J. Sheffield (1975). Submitted to Nuclear Fusion.

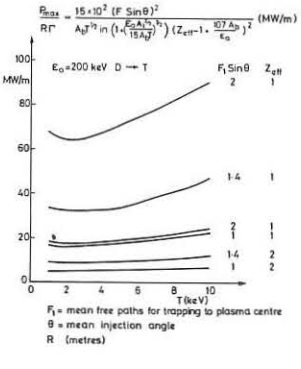

ENERGY MULTIPLICATION AND TRANSPORT IN A TWO-COMPONENT TORUS *

J. Killeen, K. D. Marx, A. A. Mirin, M.E. Rensink

Lawrence Livermore Laboratory, Livermore, California, U.S.A.

Abstract: A study of plasma behavior in the two-component torus has been made using a variety of theoretical and computational models. We study the effects of energy clamping, fast compression, impurities and radial transport on the slowing down and energy multiplication of the injected beam.

The basic physics of a two-component torus (TCT) reactor has been given by Dawson, et.al.[1] Refinements and variations on this concept have been described by Furth and Jassby.[2] In this paper we present some results on energy multiplication and transport in a TCT.

A two-dimensional multi-species Fokker-Planck code has been used to calculate the time-dependent velocity-space distribution functions for all plasma components. The kinetic equation, which we solve numerically, is of the form

$$\frac{\partial f_a}{\partial t} + \frac{\dot{R}}{R}\left[-(1 - \frac{1}{2}\sin^2\theta)\ v\frac{\partial f_a}{\partial v} + \frac{1}{2}\sin\theta\cos\theta\frac{\partial f_a}{\partial \theta}\right] = \left(\frac{\partial f_a}{\partial t}\right)_c + S_a + L_a \qquad (1)$$

where (v,θ) are spherical coordinates in velocity space. The $\dot{R}/R$ term is due to major radius compression; $\left(\frac{\partial f_a}{\partial t}\right)_c$ is the non-linear Fokker-Planck collision term

$$\frac{1}{\Gamma_a}\left(\frac{\partial f_a}{\partial t}\right)_c = -\frac{\partial}{\partial v_i}\left(f_a\frac{\partial h_a}{\partial v_i}\right) + \frac{1}{2}\frac{\partial^2}{\partial v_i \partial v_j}\left(f_a\frac{\partial^2 g_a}{\partial v_i \partial v_j}\right), \qquad (2)$$

where the Rosenbluth potentials are given by

$$g_a = \sum_b \left(\frac{Z_b}{Z_a}\right)^2 \ln\Lambda_{ab}\int f_b(\underline{v}')\,|\underline{v} - \underline{v}'|\,d\underline{v}', \qquad (3)$$

$$h_a = \sum_b \frac{m_a + m_b}{m_b}\left(\frac{Z_b}{Z_a}\right)^2 \ln\Lambda_{ab}\int f_b(\underline{v}')\,|\underline{v} - \underline{v}'|^{-1}\,d\underline{v}', \qquad (4)$$

The source term S_a is used to represent the injection of collimated mono-energetic deuteron beams into the tritium plasma, and the loss terms L_a represent the effects of finite particle and energy confinement times,

$$L_a = -\frac{f_a}{\tau_p} + \frac{1}{v^2}\frac{\partial}{\partial v}\left[\left(\frac{1}{\tau_{E_a}} - \frac{1}{\tau_p}\right)\frac{v^3 f_a}{2}\right]. \qquad (5)$$

For pulsed systems the "breakeven" experiment is defined to occur during the interval when the bulk plasma energy losses are compensated by energy input from the deuteron beam. The energy multiplication factor Q_b is then just the ratio of the fusion energy produced (17.6 MeV per reaction) and the initial energy in the deuterons. A relatively simple scenario for TCT operation is shown schematically in Figure 1. A slow adiabatic compression follows the beam injection pulse in order to "clamp" the deuteron energy at the optimum value for fusion reactions, as shown in Figure 2. For a tritium plasma with initial density $n = 2.5 \times 10^{13}$ and temperature $T = 4$ keV and energy confinement time $\tau_E = 200$ msec we find an energy multiplication factor $Q_b = 0.86$. Breakeven ($Q_b \geq 1$) can be achieved by minor changes in the plasma parameters. For a simple scenario, with no compression, the effects of alpha-particle heating and impurities (carbon and oxygen) are given in Table I. Energy multiplication has also been studied for other possible TCT scenarios including energy clamping, the use of both heating and fusion beams, and fast compression and de-compression cycles in various combinations, as well as steady-state TCT operation.

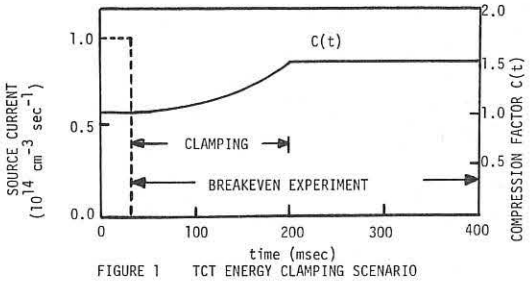

FIGURE 1 TCT ENERGY CLAMPING SCENARIO

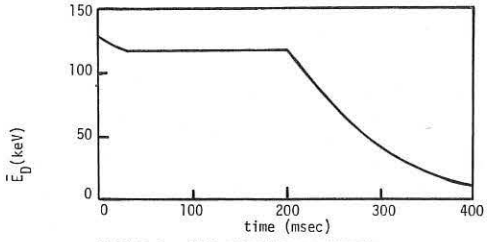

FIGURE 2 MEAN ENERGY PER DEUTERON

TABLE I

Effect of Impurities and Alphas on Q:

$E_D = 200$ keV , $T_e = T_i = 6.7$ keV , $n_e\tau_E = 2 \times 10^{13}$ cm^{-3}sec

PLASMA SPECIES	Z_{eff}	Q
e-D-T	1.0	1.08
e-D-T-α	1.0	1.09
e-D-T-α-C	2.0	0.92
e-D-T-α-C-O	2.7	0.84

A radial transport code[3] has been coupled to a new Fokker-Planck code with spatial dependence so as to yield information on the energetics of a TCT as a function of both space and time. Fokker-Planck equations describe the energetic deuterium beam component as well as α-particles at each flux surface while a fluid transport model describes the bulk plasma. The deposition of a tangentially injected deuterium beam is computed self-consistently with the bulk plasma profile and appropriate source terms are introduced into the deuterium Fokker-Planck equation. Energy transfer to the Maxwellian bulk plasma is based on the detailed form of the deuteron distribution function at each point in space and time.

REFERENCES:

1. Dawson, J. M., Furth, H. P., and Tenney, F. H., Phys. Rev. Lett. 26 (1971) 1156.

2. Furth, H. P., and Jassby, D. L., Phys. Rev. Lett. 32 (1974) 1176.

3. Keeping, P. M., Grimm, R. C., and Killeen, J., Proc. 5th European Conf. on Controlled Fusion and Plasma Physics, CEA Grenoble (1972).

* This work was performed under the auspices of the Energy Research & Development Administration

ENERGY BALANCE STABILITY OF A THERMONUCLEAR PLASMA

Ya.I.Kolesnichenko, S.N.Reznik, V.A.Yavorsky
Institute for Nuclear Research,
Academy of Sciences of the Ukrainian SSR, Kiev, USSR

Abstract: The stability of steady-state development of a thermonuclear reaction in an inhomogeneous plasma is investigated. The treatment is made assuming the plasma energy lifetime τ_E to be short compared with the charged-particle confinement time τ_n.

The condition of steady-state development of the self-sustaining thermonuclear reaction is essentially dependent on the fact whether the energy release from the reaction at any point in the plasma exceeds the energy losses due to radiation or there is a region where the reverse situation takes place. In other words the form of the function

$$G(T) = Q_{fus} - Q_{rad} \qquad (1)$$

is essential, where $Q_{fus} = \mathcal{E}_\alpha \frac{n_i^2}{4} \langle \sigma v \rangle$, $\mathcal{E}_\alpha$ = 3.5 Mev (for D-T reaction); Q_{rad} is the plasma energy losses due to bremsstrahlung per unit time and unit volume; n_i is the ion density; T is the plasma temperature.

If $G(T) > 0$ in the whole range of the plasma the steady-state thermonuclear combustion is possible at any small transverse plasma dimension a. However, there may exist the upper limit for a /1,2/. Then if a exceeds some value a_{max} the thermal equilibrium of plasma and its environment cannot be realized (see Fig.1 where dependence of T_m on a following from the stationary energy balance equation is given under the condition $G(T) > 0$; T_m and T_s are the plasma temperatures at the central region and at the boundary, respectively). At $a > a_{max}$ the self-acceleration of the thermonuclear reaction will take place. This process in its initial stage is similar to heat explosion /3,4/.

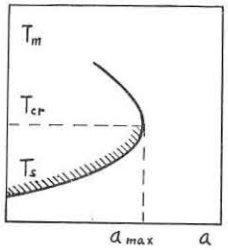

Fig.1

The characteristic dependence of T_m on a when $G(T) < 0$ at the peripheral plasma region as represented in Fig.2 /2/. In this case the steady-state developmnet of the thermonuclear reaction is realizable if $a > a_{min}$. At $a < a_{min}$ the cooling of plasma and extinguishing of the thermonuclear reaction occur.

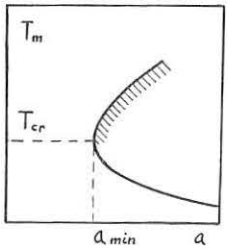

Fig.2

Apparently, the fulfilment of the mentioned restrictions for the transverse plasma dimension may be insufficient to steady-state development of the thermonuclear reaction. It is necessary that the equilibrium state be stable. If the equilibrium state is unstable then depending on the kind of the fluctuations of the plasma parameters ether the falling of the plasma temperature or the rising of it will take place; other effects are possible as well.

The stability of thermonuclear combustion was studied in /5-9/. In /5,6/ the plasma was assumed to be spatially homogeneous; in /7,8/ the problem was considered with account for the plasma inhomogeneity, however, a special kind of the fluctuations of the plasma parameters was chosen and insufficiently correct method was applied. The general conclusion made in the works /5-8/ is that, if $T_s \ll T_m$, thermonuclear combustion may be stable only at sufficiently high plasma temperature. Mathematically rigorous solution of the problem of the energy balance stability of an inhomogeneous plasma was made in the work /9/. The main results of the work are as follows.

Due to $\tau_E \ll \tau_n$, in studying of the most rapidly developing perturbations it is sufficient to confine oneself to the taking into account of the plasma temperature fluctuations δT. If the thermonuclear reaction is developed in the cylindrical plasma column the arbitrary perturbation may be represented as:

$$\delta T = \sum_{\vec{\sigma}} C_{\vec{\sigma}} R_{\vec{\sigma}}(r)\, e^{-\lambda_\ell t + i k_z z + i m \varphi} \qquad (2)$$

where $\vec{\sigma} = \{i,m,k\}$; $l=1,2,\ldots$; $m=0,\pm1,\ldots$; $R_{\vec{\sigma}}$ are the eigenfunctions of the linearized energy balance equation which satisfy the boundary condition $R_{\vec{\sigma}}\big|_s = 0$; λ_ℓ are the eigenvalues corresponding to $R_{\vec{\sigma}}$; $C_{\vec{\sigma}}$ are arbitrary constants.

The analysis shows that fluctuations with $m=0, k_z = 0$ are the most unstable i.e. the most rapidly growing and existing in the largest temperature range. These fluctuations are growing over the whole temperature region, where $da/dT_m < 0$ and only the perturbations of the form $\delta T = C_{\lambda_1} R_{\lambda_1}$ are excited. The fluctuations $\delta T = \sum_\ell C_{\lambda_\ell} R_{\lambda_\ell}$, $l \neq 1$, are always damped. If $|d\ell n a / d\ell n T_m| \ll 1$ then instability is characterized by the increment

$$\gamma \sim \frac{G(T_m)}{n_m a} \frac{da}{dT_m} \qquad (3)$$

where $n_m = n(r=0)$. For example, if the function $a(T_m)$ has a minimum (Fig.2) then these perturbations will increase at $T_m < T_{cr}$, where T_{cr} is the value of the temperature T_m at which $a(T_m) = a_{min}$. It should be noted that in homogeneous plasma approximation the formula (3) may be obtained with $T = T_m$, but in this approximation the minimum of the function $a(T)$ is lower than T_{cr}. The perturbations with $m \neq 0$ and $k_z \neq 0$ can increase if $da/dT_m < 0$. However they are excited not in the whole range of T_m, where this inequality is satisfied (for instance, at $T_m = T_{cr}$ the perturbations with $m \neq 0$, $k_z \neq 0$ are damped). Thus the thermonuclear combustion is stable if $da/dT_m > 0$ (shaded region in Fig.1,2).

Acknowledgement: The authors wish to express their gratitude to V.D.Shafranov for his useful discussion of the work.

References:

/1/ Kolesnichenko, Ya.I., Atomnaja Energija 31 (1971) 295
/2/ Kolesnichenko, Ya.I., Nuclear Fusion 12 (1972) 419
/3/ Vant Hoff, J.H., "Etudes de dynamique chimique", Amsterdam (1884).
/4/ Frank-Kamenetsky, D.A., Diffusija i teploperedacha v himicheskoi kinetike (Diffusion and heat transfer in chemical kinetics), Moscow (1967)
/5/ Mills, R.G., LA-4250 (1969)
/6/ Ohta, M., Yamato, H., Mori, S., in Plasma Physics and Controlled Nuclear Fusion Research (Proc.Conf.Madison 1971)
/7/ Kolesnichenko, Ya.I., Reznik, S.N., Nuclear Fusion 13 (1973) 167.
/8/ Ohta, M., Yamato, H., Mori, S., Journal of Nucl.Science and Technology, Japan, 10 (1973) 353
/9/ Kolesnichenko, Ya.I., Reznik, S.N., Yavorsky, V.A., Nuclear Fusion, to be published.

DISTRIBUTION OF α-PARTICLES IN LARGE TOKAMAK AND REACTOR PLASMAS

D. Pfirsch, D. Düchs

Max-Planck-Institut für Plasmaphysik, 8046 Garching bei München, Federal Republic of Germany

Abstract: The behavior of fusion-created α-particles is described by a time-dependent, two-dimensional (minor torus radius r , energy E) distribution function F_α (r,E,t) which is obtained by solving a Fokker-Planck type kinetic equation. The background plasma is consistently computed from a Tokamak transport code [2].

This paper extends the work of Ref. [1] in two directions: (1) The treatment of the radial diffusion of α-particles has been refined, and (2) the kinetic equation for F_α is solved simultaneously with a set of transport equations for the background plasma.

1. Radial diffusion of α-particles

In Ref. [1] it was assumed that F_α could be approximated by a sum of Maxwellian distributions. For each one of these, neoclassical (or other) fluxes could then be calculated. It turned out that in some important cases (e.g. relatively rapid changes in the production rate of α's) F_α can only very poorly be described by such a sum . This is especially true at high energies. At low energies, however, where the collisions between α's and background ions (rather than electrons) dominate, a Maxwellian approximation of F_α is very good.

For the time being we thus split F_α into two parts at the energy $\bar{E}$ [3], where the effect of collisions with the ions starts to exceed the electronic influence: $F_\alpha = F^{(1)} + F^{(2)}$

The Maxwellian distribution $F_M^{(1)}$ which is constructed using

(1) $n^{(1)} = \int_0^{\bar{E}} F^{(1)}(E)\, dE$ and $T^{(1)} = \frac{2}{3}\frac{1}{n^{(1)}} \int_0^{\bar{E}} E F^{(1)} dE$,

then serves to calculate neoclassical particle ($n^{(1)} \underline{v}_{nc}^{(1)}$) and heat ($\underline{q}_{nc}^{(1)}$) fluxes.

For energies above $\bar{E}$ two effects seem to operate: friction with the background electrons causes antidiffusion because of shrinking banana orbits, and residual pitch angle scattering leads to a regular diffusion which is reduced, however, by $\frac{R}{r}$ relative to neoclassical diffusion. Even the latter would be small compared with $n^{(1)} \underline{v}_{nc}^{(1)}$ and $\underline{q}_{nc}^{(1)}$ because of the increased "temperature". In view of this situation neglecting the fluxes for $E > \bar{E}$ seems to be a reasonble assumption until an adequate theory has been developed.

Since we do not want to restrict the theory to neoclassical fluxes, the procedure of including the fluxes in the kinetic equation for the α-particles [1] is kept.

However, the weighting with energy E has been changed to a more appropriate form.The kinetic equation now reads:

$$(2)\quad \frac{\partial F_\alpha}{\partial t} + \frac{\partial}{\partial E}(L F_\alpha) - \frac{\partial^2}{\partial E^2}(D F_\alpha) = Q\,\delta(E-E_0) - \operatorname{div}_r\left(\sum_{i=1}^{2} F^{(i)} \underline{v}^{(i)} + \sum_{i=1}^{2} F^{(i)} \underline{q}^{(i)} \frac{2}{3 n^{(i)} T^{(i)2} - 4 S^{(i)}}\left(3T^{(i)} - 2E\right)\right)$$

The quantities $n^{(i)}$, $T^{(i)}$ and $S^{(i)}$ are defined by analogy with Eq. (1) and with

$$(3)\quad S^{(1)} = \int_0^{\bar{E}} E^2 F^{(1)}(E)\, dE .$$

For some estimates we also insert anomalous particle and heat fluxes.

2. Transport model for the background

Equation (2) is solved simultaneously with a set of transport equations for background electrons, hydrogenic ions (and neutrals), as well as impurities. In addition to the terms described in [2], we include energy loss due to cyclotron radiation and enhanced diffusion in regions with safety factor $q < 1$.

The neoclassical confinement time of the α-particles considerably increases in comparison with the model of Ref. [1]. This was to be expected because at the same temperature the α-particles will diffuse neoclassically with the gradient of the hydrogenic ions.

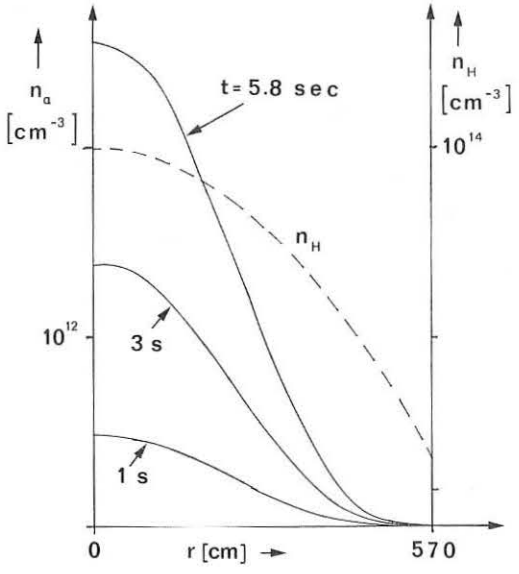

In Fig. 1 density profiles of neoclassically diffusing α-particles are shown for constant (in time) background plasma the parameters of which conform with case IV,(b) in Ref. [1] except for a slightly different n_H-profile. The results might be compared with Fig. 2 of Ref. [1]. Radial diffusion speeds are of the order of 1cm s^{-1}.

[1] D.F. Düchs, D. Pfirsch, in Plasma Physics and Controlled Nuclear Fusion Research (Proc. 5th Int. Conf., Tokyo, Japan, 1974), paper IAEA-CN-33/A17-1.

[2] D.M. Meade, H.P. Furth, P.H. Rutherford, F.G.P. Seidl, and D.F. Düchs, in Plasma Physics and Controlled Nuclear Fusion Research (Proc. 5th Int. Conf., Tokyo, Japan, 1974) paper IAEA-CN-33/A15-4.

[3] A. Nocentini, M. Tessarotto, F. Engelmann, Frascati Report LGI/R/TEO/73.3/E, p.6

"This work was performed under the terms of the agreement on association between the Max-Planck-Institut für Plasmaphysik and EURATOM".

COLLIDING-BEAM TOKAMAK PLASMAS

D. L. Jassby, R. M. Kulsrud, Y. C. Sun

Plasma Physics Laboratory, Princeton University,

Princeton, N. J. 08540, U.S.A.

Abstract. We consider the properties of a tokamak plasma in which all ions are tangentially injected to form two "thermal" velocity distributions, oppositely displaced in velocity along the magnetic axis, so that head-on collisions between ions in opposite distributions are maximized.

Coulomb and nuclear interactions among beam ions are becoming significant in present beam-injection experiments in tokamaks, where n_{beam}/n_e is as large as 0.1. In the case of 15-keV D^o beams injected into a D plasma in the ATC device, by injection both parallel and anti-parallel to the magnetic axis, head-on collisions between oppositely directed beam ions resulted in a doubling of the fusion power output, even for $n_{beam}/n_e \sim 0.01$ [1]. In the following we consider a tokamak plasma where all ions are injected via neutral beams, and those ions which have decelerated by Coulomb drag on the plasma electrons are removed from the plasma in a time that is short compared to their slowing-down time. Then $n_{beam}/n_e \sim 1$. In particular, we consider the case of two oppositely directed distributions of D and T ions, which together with space-charge neutralizing electrons form a colliding-beam tokamak plasma (CBT). A preliminary discussion of this scheme was given in Ref. [2], where it was shown that the absence of substantial cold-ion population results in an increase in fusion gain Q over that of a target-plasma reactor (TCT), while the injection energy can be 3 to 4 times smaller (vis., 50-60 keV), because head-on collisions predominate.

Consider a steady-state tokamak plasma into which energetic neutrals are injected parallel and anti-parallel to the magnetic axis. The neutrals are trapped by charge-exchange with ions travelling in the same direction, by impact ionization on oppositely travelling ions, and by electron ionization. Neutrals generated by successive charge-exchange are trapped up to the third or fourth generation, for realistic geometries (e.g., $n_e a \sim 3 \times 10^{15}$ cm^{-2}, $R/a \geq 4$), so that for injection voltages in the optimal range, 5-10% of the injected energy is eventually lost by charge-exchange.

The energetic ions are assumed to be confined until they decelerate to an energy $2T_e$ by Coulomb drag on the electrons. Ions with energy $W < 2T_e$ are assumed to be lost at a rate τ_E^{-1}, where τ_E is the electron energy confinement time. T_e is maintained entirely by power deposition from the fast ions, so that T_e and n_e are determined by τ_E and the ion source strength S. For $T_e \lesssim 10$ keV, the slowing-down time of the fast ions is several times longer than τ_E. Microinstabilities, such as drift instabilities, preferentially cause diffusion of thermal ions and electrons [3], and would be useful for eliminating cold ions at a rate $\sim \tau_E^{-1}$. By means of a magnetic divertor, the inward flow rate of cold neutrals and ions from the wall can be kept small compared to the large rate of particle injection by the beams.

The ion velocity distribution functions f(v) have been calculated with a multi-species two-dimensional Fokker-Planck code. Fig. 1 shows a polar plot of the steady-state f(v) contours for a CBT plasma operating in DT, in which the injection energies W_o are 60 keV for D and 40 keV for T (relative collision energy = 168 keV). S and $n_e\tau_E$ are of sufficient magnitude that $T_e = 6.0$ keV. Evidently f(v) for each beam resembles a displaced Maxwellian, which results from the strong Coulomb interaction among beam ions. The beam "temperature" is about 14 keV, with $T_\perp$ slightly greater than $T_\parallel$. These relatively broad ion distributions are apparently stable to electrostatic and electromagnetic modes [2].

The fusion power gain Q is calculated by integrating the fusion reactivity over the D and T velocity distributions, and dividing by the injection power. Fig. 2 shows T_e and Q as a function of $n_e\tau_E$; specifying

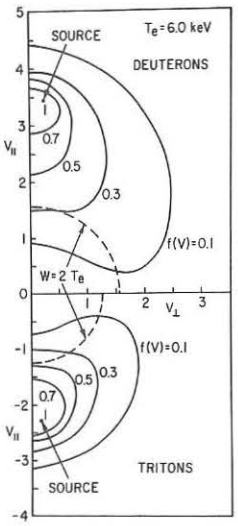

Figure 1

$n_e\tau_E$ and n_e determines both T_e and S. Q = 1 ("break-even") is attained at $n_e\tau_E = 1.6 \times 10^{12}$cm^{-3} and $T_e = 3.4$ keV. For $T_e \geq 4$ keV, Q may be substantially larger than in TCT operation, while the required $n_e\tau_E$ may be substantially less [3]. The required ion confinement time is $\tau_h/\tau_E \simeq (\bar{W}_o - \frac{3}{2}T_e)/1.5\,T_e \gg 1$. This condition on τ_h/τ_E seems compatible with experimental results from beam-injected tokamaks [4].

The principal effect of an impurity population is enhanced pitch-angle scattering, which undermines the advantage of head-on collisions. We find that for $W_o = 60$ keV (both D and T), $T_e = 5.0$ keV, and iron impurity, Q is reduced by 33% and 46% for $Z_{eff} = 2$ and 3, respectively.

Solution of the steady-state momentum balance equations for CBT operation have been carried out for mean particle velocities directed as shown in Fig. 3. The electron drag on the tritons overwhelms the acceleration of the tritons by the electric field, so that continuous injection is required to maintain the triton velocity. If $Z_{eff} = 1$, any imbalance in toroidal ion current is exactly compensated by the shift in the electron velocity distribution required to maintain momentum balance. But if $Z_{eff} > 1$, because of impurities or significant electron trapping, a toroidal current can be maintained even when E = 0.

For the same total pressure in CBT and TCT operation, and for $\bar{\Gamma} \sim 1$ in the TCT [3], it is easy to show that the fusion power density in

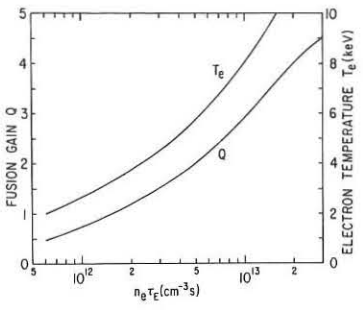

Figure 2

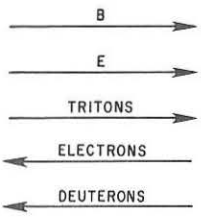

Figure 3

either mode of operation is very similar. However, the maximum size of a CBT reactor would have to be considerably smaller than the maximum possible size of a TCT reactor, because adequate penetration by the lower energy CBT beams demands a smaller plasma radius. It would appear that the lenient requirements on injection voltage and $n_e\tau_E$ for $Q \sim 1$ make the CBT mode of operation particularly appropriate for application in near-term toroidal devices.

This work was supported by U.S.E.R.D.A. Contract E(11-1)-3073.

References

[1] H. P. Eubank, unpublished.

[2] R. M. Kulsrud and D. L. Jassby, PPPL Report MATT-1114 (January 1975).

[3] H. L. Berk, et al., paper G2-3, Fifth Intern. Conf. on Plasma Physics and Controlled Nuclear Fusion Research (IAEA, Tokyo, 1974).

[4] K. Bol, et al., ibid., paper A4-1; L. A. Berry, et al., ibid., A5-2.

THE RADIAL BUILD UP OF PLASMA BY NEUTRAL INJEKTION INTO TOROIDAL CONFIGURATIONS

H.D. Falter, W. Henkes

Institut für Kernverfahrenstechnik, Kernforschungszentrum,
D 75 Karlsruhe, Germany

Abstract: The radial build up of plasmas in toroidal reactor configurations is computed for injected beams of finite diameter. Beams with a homogenous current tend to produce MHD-unstable, "hollow" plasmas, whereas beams with a current density peaked on the beam axis behave similar to pencil beams considered before (1).

In a previous paper (1) we proposed to start a fusion reactor by the build up of a high temperature, high density plasma by injection of neutral particles with an energy of the order of 10 keV, (2). The problem of particle penetration is circumvented by radial build up of the plasma, that is by creating a plasma of high density and small radius near the magnetic axis which in turn grows in radius until the reactor is filled. In this paper we first investigate the influence of a finite beam diameter on plasma build up, in contrast to (1) where we assumed a pencil beam. Then we discuss the influence of charge exchange neglected before.

For computation of build up we restrict ourselves to the case of injection tangential to the magnetic axis (3), called "parallel injection" in (1). All dimensions and assumptions are the same as in (1). We simulate a beam of finite cross section by subdividing the injected current into a number of individual beamlets as shown in Fig.2. Since trapped particles distribute over a magnetic surface it is sufficient to place these beamlets on one side of the magnetic axis. This corresponds roughly to a physical beam of circular cross section with its axis tangent to the magnetic axis. Its diameter is twice the width occupied by the beamlets. To simulate a beam of constant current density the currents of the beamlets are chosen proportional to the beam radius. On the other hand beamlets with equal currents will correspond to a physical beam with the current density peaked on the axis.

In Fig.3 we compare the results for three different beams at the same time after the start of injection. For comparison we also show the result for a single pencil beam, curve d, (case 7 of (1)). Curve a is for a beam with 5 cm radius and constant current density, curve b for the same radius but a peaked beam profile, while curve c is for a beam of 10 cm radius with constant current density. Beam b builds up the density nearly as fast as the pencil beam while beams a and c fall far behind. Both beams with a constant current density profile produce a plasma density distribution with a minimum near the magnetic axis. This kind of distribution is not in stable equilibrium. Figs. 4-5 show the further development in time of the plasma density. With a pencil beam (Fig.3d) we get a plasma radius of 10 cm and a density of $3 \cdot 10^{14}$ cm^{-3} after only 0.04 sec, while with the beam of 10 cm radius (Fig.5) a density of $1.7\ 10^{14}$ cm^{3} ist obtained only after 0.24 sec, and the density distribution at this time looks highly forbidding.

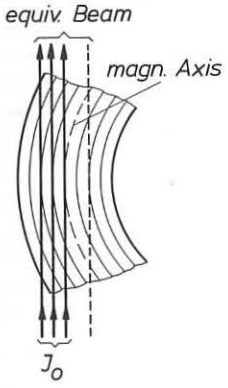

Fig.2: Simulation of a beam of a finite diameter by pencil beams.

Once the plasma density and radius have grown sufficiently large so that the injected beam is completely absorbed we can use the following approximation for the density at the plasma edge:

$$n = (J\, r^{1/2} \cos\alpha / 2\pi^2\, R^{5/2} d\, \sigma_{01})^{1/3} \qquad (1)$$

Here J is the injected current (Atoms/sec), α its angle of incidence on the plasma surface, a the minor, and R the major plasma radius, $D = dn(R/r)^{3/2}$ the Diffusion constant and σ_{01} the cross section for electron loss.

Charge exchange between a high energy atom of the beam and a high energy plasma ion does not contribute to plasma build up but it does contribute to the attenuation of the incident beam. Part of the neutrals produced by charge exchange will leave the plasma before being reionized. This will result in a reduction of the trapped particle current to be used in Equ. (1). The fraction γ of the injected current leaving the plasma at its surface is approximately

$$\gamma \approx (\sigma_{10} + \sigma_{01} - \sqrt{\sigma_{10}\sigma_{01} + \sigma_{01}^2})/(\sigma_{10} + \sigma_{01} + \sqrt{4\,\sigma_{10}\sigma_{01} + \sigma_{01}^2}) \qquad (2)$$

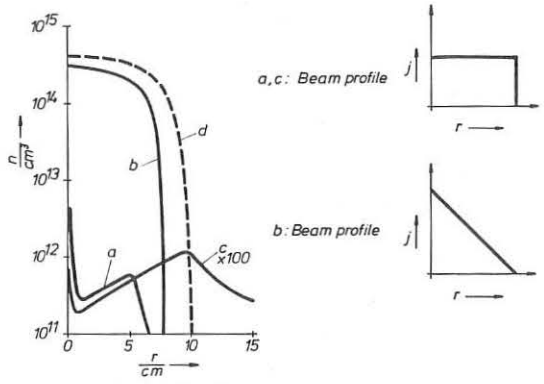

Fig.3: Plasma density distribution after 0.04 sec of injection.
a. Beam with 5 cm radius, constant current density j.
b. Beam with 5 cm radius, current density j peaked on the axis.
c. Beam with 10 cm radius, constant current density j.
d. Pencil beam (case 7 of (1)).

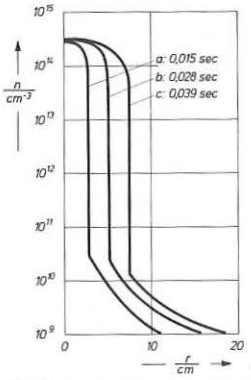

Fig.4: Development of plasma density in time. Beam like in Fig.3b.

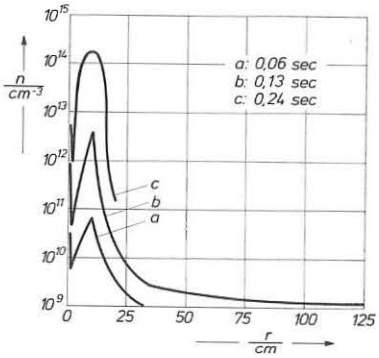

Fig.5: Development of plasma density in time. Beam like in Fig.3c.

Here σ_{10} and σ_{01} are cross sections for electron capture and electron loss respectively. For $\sigma_{10} = 5\sigma_{01}$ we find $\gamma = 0.22$, that is the trapped current is 22% lower than the beam current. The second effect of charge exchange is a reduction in the penetration depth which results in a steeper gradient at the plasma edge and a larger diffusion current toward the outside. Taking into account both effects we find for $\sigma_{10} = 5\sigma_{01}$ a reduction of the plasma density by only 40% compared to the case of $\sigma_{10} = 0$. Since a fraction of the energetic neutrals formed by charge exchange will be in excited states their cross section for reionization will be larger and the influence of charge exchange further reduced.

Conclusion

The concept of radial build up of a plasma in a toroidal fusion reactor does not rely on the existence of pencil beams, but plasmas of high density may be produced by beams of finite radius. By computations we find, though, that during build up the plasma can assume a density distribution with $\frac{dn}{dr} > 0$. The effect is most pronounced for a large beam radius and is enhanced by a large cross section for beam attenuation, as for instance charge exchange. Positive density gradients can be avoided only by injecting beams of small radius and with a high current density on their axis in order to feed enough particles into the region close to the magnetic axis. The method of cluster ion acceleration should be well suited to produce such beams of high current density at moderate energies (ca. 10-20 keV/atom) (4). The effect of charge exchange of beam particles with hot plasma particles is not expected to change the computatational results by more than a factor of 2.

REFERENCES

(1) FALTER, H. HENKES, W., 6th Europ. Conf. on Controlled Fusion and Plasma Phys. (Proc. Conf. Moscow, 1973) 385

(2) Plasma buildup in smaller experimental devices has been discussed by several authors, e.g.
BICKERTON, R.H., DROGMAN, Nucl. Fusion 6 (1966) 287
FUTCH, A.H., DAMM, C.C., Plasma Phys. 9 (1967) 423
FUMELLI, M., GIRARD, J.P., BOURDON, Eur.-Report Eur-CEA-FC-432 (1967)

(3) In the case of a fusion reactor the difference between magnetic and drift axis can be safely ignored.

(4) HENKES, W., Phys. Lett. 12 (1964) 322

A CHRONICLE OF ION-CURRENT INSTABILITIES - OLD & NEW

Ronald W. Landau

Queens College of the City University of New York
Flushing, N.Y. 11367

and

Plasma Physics Laboratory, Princeton University
Princeton. New Jersey 08540

ABSTRACT

When $T_\perp = 0$, counter-streaming ion currents are unstable if the streaming velocity is greater than the ion thermal velocity. For this instability, $\omega_r = 0$ and $\omega_i \approx 16\Omega_+$. Even when streaming ions are only 1% of the stationary ions there is instability, but now $\omega_r \approx (\Omega_+\Omega_-)^{1/2}$ while $\omega_i \approx 4\Omega_+$. In all this $T_{\parallel,+} = T_{\parallel,-}$.

There has been considerable interest recently in using neutral beams to heat plasmas in a new generation of Tokomaks to achieve marginal power production. the neutral beams are very monoenergetic and when converted to ions are also very monoenergetic. the earlier proposals[1,2] envisage injection of low-density ions but more recent[3] suggestions have pointed out that less energetic beams are required if one preferentially removes low-energy ions, so that the 'plasma' consists of two counterstreaming ion beams. Owing to the importance of the above ideas we have looked carefully at the instabilities of counterstreaming ion beams flowing along the magnetic field.

We assume a uniform magnetic field $\vec{B}_o$ along the z direction and of infinite extent in the other two directions, traversed by two counterstreaming ion beams flowing along the magnetic field $\vec{B}_o$. All parallel (along $\vec{B}_o$) temperatures, i.e. of ions and electrons are equal, ($T_{\parallel,+} = T_{\parallel,-}$) and are given by Maxwellian distributions while all perpendicular temperatures are zero ($T_\perp = 0$). Setting $T_\perp = 0$ gives no singularities, simplifies the algebra by eliminating $n \geq 2$ Bessel functions, and gives maximum growth rates since the instabilities considered propagate mainly perpendicular to the magnetic field. We define the wave vector $\vec{k} = k_\perp i + k_\parallel k$ and consider two ion beams of density εn each, with equal and opposite velocities V_+, passing through a stationary ion background of density $(1-2\varepsilon)n$ and electron background of density n. The symmetrical situation insures that there is no zero-order current and hence finite β effects may be treated consistently.

1. All Ions Stream, $T_\perp = 0$. In the first part we assume $\varepsilon = 1/2$, i.e. all the ions counterstream. Using the infinite medium dispersion relation as given e.g. by Landau and Cuperman[4] together with Barberio-Corsetti's[5], computer program for $Z(\zeta)$, we have solved the dispersion relation on the computer. The maximum growth rate for the $\omega_r = 0$ mode is shown by the top two curves in Fig.1. The mass ratio $\mu \equiv m_+/m_- = 1837$ is used and also the definitions

$\tau \equiv T_{\parallel,+}/T_{\parallel,-}$ $\quad \theta \equiv k_\parallel/k_\perp$ $\quad \beta \equiv 4\pi n T_\parallel/B_o^2$

$\omega_p \equiv 4\pi ne^2/m_-$ $\quad \Omega_\pm \equiv |e|B_o/m_\pm c$ $\quad \bar{\omega}_p \equiv \omega_p/\Omega_-$

$1/a_\pm \equiv k_\parallel \tilde{R}_{\parallel,\pm}$ $\quad \tilde{R}_{\parallel,\pm} \equiv \sqrt{2}\,\bar{v}_{\parallel,\pm}/\Omega_\pm$ $\quad \bar{v}_\parallel^2 \equiv T_\parallel/m$

$\phi \equiv \angle\vec{k},\vec{B}_o$ $\quad \tilde{V}_+ \equiv V_+/\sqrt{2}\,\bar{v}_{\parallel,+}$ $\quad z \equiv \omega/\Omega_- \equiv b + i\gamma$

where $\pm V_+$ is the velocity of each stream. Quantities without subscripts refer to electrons. The curve marked 100% gives the $\omega_r = 0$ growth rate, γ_m, maximized as a function of 'a', for $\varepsilon = 1/2$ i.e. 100% ions streaming. The growth rate is a maximum for $\theta \sim 0$ and for $\bar{\omega}_p \gg 1$. The $\bar{\omega}_p$ dependence is shown in Fig.2. (We have not explored the τ dependence.) The ES curve in Fig.1 gives the maximum growth rate obtained when the electrostatic (ES) equation is used, and does not differ much from the $\beta = .1$ growth rate. The maximum wave number occurs for $a \sim \tilde{V}_+ \gg 1$. Since also $z \ll 1$ and $a_+ \ll \tilde{V}_+$, it is possible to use the asymptotic expressions for all the Z functions occuring in the ES equation (p.224 of Stix[6]), to obtain the simple result in the $\theta \sim 0$, $\bar{\omega}_p \gg 1$ limit,

$$(2 + 2\bar{\omega}_p^2) = \sum_{+,-} \omega_{p,+}^2/(\omega \pm k_\parallel V_+)^2 \qquad (1)$$

This ES equation has the form of the two-stream instability and may use Stix[6] p.113 to obtain the maximum growth rate, (since $1/2(2\mu)^{1/2} = .83 \times 10^{-2}$).

$$\gamma \equiv \omega_i/\Omega_- = .83 \times 10^{-2}\,\bar{\omega}_p/(1 + \bar{\omega}_p^2)^{1/2} \qquad (2)$$

which occurs at a wave number $k_\parallel \tilde{R}_\parallel \equiv 1/a = (3/8)^{1/2}\tilde{V}_+ = .612\,\tilde{V}_+$. The locus of wave numbers for maximum growth is shown in Fig.3 by the dashed curve for $\beta = .1$, which is close to the ES value just given. Similarly, the maximum growth rate given by (2) is close to that shown in Fig.1, while the $\bar{\omega}_p$ dependence is also given accurately, as shown by the $\tilde{V}_+ = 10$ and 2.5 curves of Fig.2.

2. Equal Temperatures $T_\perp = T_\parallel$. The solution for the $T_\perp = T_\parallel$ case has been obtained by Weibel[7] and is shown by the 'Weibel' dash in Fig.1. His marginal stability criterion is shown in Fig.3, insert, plotted vs. $1/a_+ = \mu^{1/2}/a$. It is possible to approximately reproduce Weibel's results by setting $\theta \neq 0$ with $1/(\theta a_+)^2 = 4e^{-\lambda}I_1(\lambda) \approx 1$, but then the ES results are obtained only for $\beta \approx 10^{-5}$. For $\beta = .01$ The growth rate is 4 × larger. Since it is not clear that Weibel's results are optimised (he chooses $\lambda = 3$) we can say only that the instability threshold lies in the range $1 < \tilde{V}_+ < 8$.

3. Weak Beam, $T_\perp = 0$. When the percentage of streaming ions is low, $\varepsilon \ll 1$, then keeping lowest order terms in the ES equation gives a cubic. It may, however, be solved approximately and one obtains a maximum growth rate and real part given by

$$\gamma_m = (\sqrt{3}/2^{4/3})W\varepsilon^{1/3}/\mu^{1/2} = 1.6 \times 10^{-2}\varepsilon^{1/3}W, \quad \omega_{r,m}\mu^{1/2}/\Omega_- = (1-\varepsilon^{1/3}/2^{4/3})W$$

with $W \equiv \bar{\omega}_p/(1 + \bar{\omega}_p^2)^{1/2}$ which is quite close to the values given in Fig.1 and 2. Note that the real part is near the LHy frequency.

These two instabilities are in addition to the Drummond-Rosenbluth ion-cyclotron instability.

We are grateful for encouragement from and conversations with Profs. T.H. Stix, P.H. Rutherford, C.S. Liu and H.Berk.

1. J. M. Dawson, H. P. Furth and F. H. Tenney, Phys. Rev. Lett. 26, 1156 (1974)
2. H. P. Furth and D. L. Jassby, Phys. Rev. Lett. 32, 1176 (1974)
3. R. M. Kulsrud and D. L. Jassby, Matt-1114, (1975), Princeton Plasma Lab. Report
4. R. W. Landau and S. Cuperman, J. of Plasma Phys. 6 495 (1971)
5. P. Barberio Corsetti, Matt-773 (1970) Princeton Plasma Lab. Report
6. T. H. Stix "The Theory of Plasma Waves" (McGraw-Hill, N.Y. 1962)
7. E. S. Weibel, Phys. Fluids 13, 3003 (1970)

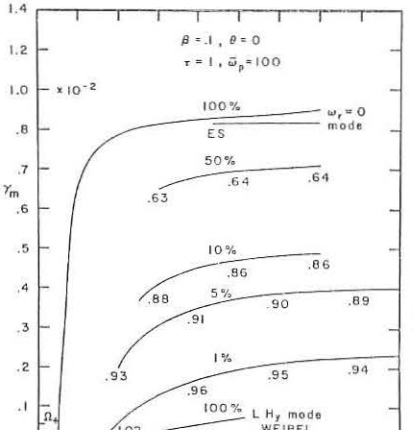

Fig. 1. Maximum growth rates for optimum 'a' and θ. Optimum $\theta \neq 0$ for the LHy mode. The % streaming ions is indicated. ($2\varepsilon \times 100$ = % streaming). The numbers under the curves give ω_r in units of $(\Omega_+\Omega_-)^{1/2}$. The Ω_+ dash indicates $\omega_i = \Omega_+$.

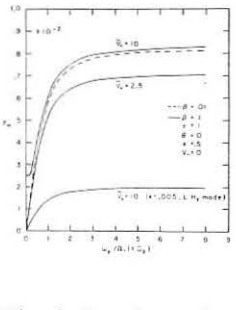

Fig. 2. Dependence of γ_m on $\bar{\omega}_p \equiv \omega_p/\Omega_-$. Note that $\varepsilon = .005 \rightarrow 1\%$ streaming, is valid for the bottom curve only.

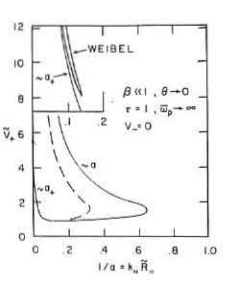

Fig. 3. Marginal stability for the $\omega_r = 0$ mode. The solid curves marked ~a, a_+ are the $\tilde{V}_+ = a$ and $\tilde{V}_+ = a_+$ curves valid for $\tilde{V}_+ > 3$. The insert axis is labelled in units of $1/a_+ = \mu^{1/2} \cdot 1/a$.

FEEDBACK STABILIZATION OF TRAPPED PARTICLE INSTABILITIES

A. K. Sundaram & A. Sen
Physical Research Laboratory
Ahmedabad 380 009
India

Abstract: We study the possible suppression of trapped particle instabilities of the magnetic type by using feedback controlled neutral beam injection. We find that the potentially dangerous dissipative trapped particle modes may be effectively quenched by means of a positive feedback with 90° phase.

Feedback stabilization schemes using electrostatic probes have been widely considered for the suppression of various electrostatic instabilities in a plasma [1]. However the use of material probes limits their applicability to plasmas of moderate density and temperature. The possibility of neutral beam injection to provide feedback controlled volume sources of particle and momentum density was first suggested by Chen and Furth [2] as an alternate method for suppressing low frequency plasma instabilities. In this paper we use their model to study the suppression of some of the harmful instabilities that arise in closed magnetic devices due to the presence of trapped particles [3]. These particles which undergo unfavourable drifts in the curved magnetic fields give rise to growing flute type perturbations very similar to those found in adiabatic traps. In essence, the trapped particles behave like a distinct species in the system attaining their own local equilibrium with a reduced temperature ($\cong \sqrt{\epsilon}\, T_j$ where $\epsilon = r/R$ is the ratio of minor to major radius) while the transiting particles provide a background of high dielectric constant. The basic idea of the feedback stabilization scheme is to sense the growing perturbations of the trapped particles (by an independent system of optical or microwave beams) and then appropriately modulate the intensity of an incident neutral beam. The neutral beam gets ionized by its interaction with the plasma and thus acts as a source for particle and momentum density. We concern ourselves mainly with the effect of "density smoothing" provided by the particle source and ignore the effects of the momentum source. Our present calculations are based on modified fluid equations [3] (which retain most of the essential features of trapped particle instabilities in an approximate sense) and we study the effect of neutral beam injection by including a source term of the form

$$S = -i\omega_f n_1 \qquad (1)$$

n_1 stands for density perturbation and ω_f is in general complex. The magnitude of ω_f gives the gain of the feedback system and the phase is given by $\theta = \arg(iS/n_1)$. Positive(negative) feedback implies negative (positive) ω_f. Our results are summarised below for three principal instabilities.

1. Collisionless trapped particle instability: This is basically the ordinary flute instability, which for trapped particles arises when the magnetic drift has the unfavourable sign ($\omega_* \omega_d < 0$; $\omega_d \cong \frac{cTk}{eBR}$ and ω_* is the diamagnetic drift frequency). For a simple isothermal situation ($T_e = T_i$) we get the following dispersion relation,

$$\omega^2 - \omega\omega_f - \omega_d^2 + \omega_f^2 - \sqrt{\epsilon}\,\omega_*\omega_d = 0 \qquad (2)$$

Stabilization can be achieved by positive feedback applied at 180° phase and with a gain of $\omega_f > \epsilon^{1/4}(\omega_*\omega_d)^{1/2}$

2. Dissipative trapped particle instabilities: Particle collisions can give rise to new trapped particle instabilities which are more dangerous than the collisionless instabilities, as they do not depend on the sign of curvature of the magnetic field. Since in most fusion devices the collision frequencies are comparable to the characteristic frequencies of plasma motion, we next consider the stabilization of two major types of dissipative modes.

(a) Trapped ion instability: It evolves out of the collisionless flute instability and is characterized by $\frac{\nu_i}{\epsilon} < \omega < \frac{\nu_e}{\epsilon}$ with $\frac{\omega}{k_\parallel} < (\epsilon T_i/m_i)^{1/2}$ where ν is the collision frequency. Our dispersion relation is ($\tau = \frac{T_e}{T_i}$),

$$\frac{1+\tau}{\sqrt{\epsilon}} = \frac{(\omega-\omega_f)\tau + \omega_{*e}}{\omega-\omega_f} + \frac{\omega-\omega_f-\omega_{*e}+i\nu_e/\epsilon}{\omega-\omega_f+i\nu_e/\epsilon} \qquad (3)$$

This instability can be suppressed by a positive feedback applied at 90° phase with a gain of $\omega_f > \epsilon^2\,\omega_{*e}^2/\nu_e(1+\tau)^2$

(b) Trapped electron instability: This is very similar to the drift dissipative instability and arises due to the loss of trapped electrons through collisions. For $\sqrt{T_i/m_i} < \frac{\omega}{k_\parallel} < \sqrt{\epsilon T_e/m_e}$ and $\omega_{*e} < \nu_e/\epsilon$ we obtain a simplified dispersion relation

$$\left(\frac{\omega_{*e}}{\omega}-1\right)\left(\frac{i\nu_e}{\epsilon}-\omega_f\right) = \sqrt{\epsilon}\left[\omega_{*e}\left(1-\frac{2\nu_e^2}{\epsilon^2\Omega_e^2}\cdot\frac{1-\frac{3}{2}\eta_e}{}\right) - \frac{i\nu_e}{\epsilon}+\omega_f\right] \qquad (4)$$

where $\eta_e = d\ln T_e/d\ln n_e$, Ω_e is the electron cyclotron frequency. Stability can be attained by positive feedback (90° phase) with a gain of $\omega_f > \omega_{*e}\left[1-\frac{2\nu_e^2}{\epsilon^2\Omega_e^2}\left(1-\frac{3}{2}\eta_e\right)\right]$ or a negative feedback at 180° phase with a gain of $\omega_f > \nu_e/\epsilon$

We note that it is possible to simultaneously suppress both the dissipative modes by means of positive feedback at 90° phase. In an actual situation it is possible to utilize additional parameters such as the momentum source arising from the beam to suppress a larger variety of trapped particle modes simultaneously. Calculations incorporating the momentum source and using the kinetic theory are in progress.

References:

[1] Feedback and Dynamic Control of Plasmas, ed. T. K. Chu and H. W. Hendel, AIP, N. Y. 1970.

[2] F. F. Chen and H. P. Furth, Nuclear Fusion, 9, 364 (1969).

[3] B. B. Kadomtsev and O. P. Pogutse, Nuclear Fusion, 11 67, (1971).

" GRAD B DRIFT INSTABILITY " IN A TOKAMAK

T. Dodo and O. Okada
Central Research Laboratory, Hitachi Ltd., Tokyo 185, Japan
Y. Terashima
Institute of Plasma Physics, Nagoya University, Nagoya 464, Japan

A new type of instability, caused by the charge separation due to the grad B drift in a torus, is analyzed with an electrostatic approximation. This instability will explain the fluctuations of the poloidal mode number m = 4,3,2 on the rational surfaces q = 4,3,2 observed prior to the disruptive instability in tokamaks.

In the experiments[1)2)] in tokamaks, fluctuations with poloidal mode number m = 4,3,2 are observed with corresponding safety factor q = 4,3,2. In low shear stellarators, the particle confinement time is observed to become smaller at the rational surfaces.[3)4)] The analysis in the following is aimed to present an explanation of the mechanism of these fluctuations.

The instability presented in this analysis is driven by the charge separation due to grad $|B|$ drift of ions and electrons in the opposite direction. Fluctuations are amplified in the region with bad magnetic field curvature and are suppressed in the good curvature region. The electron flow along the magnetic field lines acts to neutralize the charge unbalance and stabilizes this instability. As the parallel wave number $k_{//}$ of the fluctuations tends to zero, the parallel phase velocity of the instability exceeds the thermal velocity of electrons, and the electron flow is not enough to neutralize the charge unbalance produced by grad $|B|$ drift. The growth rate of the order ϵ^2 is obtained from the difference of the growth rate in the bad region and the damping rate in the good region, though the parallel wave length is much larger than the connection length qR_0.

The fluid equations of motion and continuity of the ions and electrons are analyzed in the usual toroidal coordinate system. The equilibrium radial distribution of the q-value and the gradient of the density and the electrical potential are assumed to be constant and the eigen value problem in the radial direction (- shear stabilization-) will be treated in a later paper. The standard perturbation calculation for the density and the electrical potential are carried out in which the toroidal effect of the order of ϵ are included. The perturved quantities $(\tilde{n}, \tilde{\phi})$ are expressed as $\exp i(m\theta + n\zeta - \omega t) \cdot \Sigma(\tilde{n}_l, \tilde{\phi}_l) \exp(il\theta)$, where θ is the poloidal direction and ζ the toroidal direction. The amplitude function $\tilde{n}_l \exp(il\theta)$ expresses the poloidal variation of the density fluctuation amplitude.

When $k_{//} \simeq 0$, the dispersion equation is given approximately as,

$$\Omega^2 + \Omega(1-g^2/2)(T_i/T_e) + g^2(1+T_i/T_e)(T_i/T_e)^2/(2b) \simeq 0, \qquad (1)$$

where $\Omega = \omega/\omega_*$, $g = V_{gm}/V_* \simeq \epsilon$, $V_* = \kappa T_e/(eB_0)$, $\kappa = -\nabla n_0/n_0$, $\omega_* = (m/r)V_*$, $V_{gm} = 2T_e/(eB_0R_0)$, $\epsilon = r/R_0$, $b = (m/r)^2(T_i/M\bar{\nu}_i^2)$. The imaginary part in the dispersion equation (1) is omitted because the collision frequencies ν_{ei}, ν_{ii}, ν_{in} are small and the instability at $k_{//} = 0$ is the so-called reactive instability.[7)] The instability occurs when

$$2g^2\{1+(T_i/T_e)\} \simeq \epsilon^2 > b. \qquad (2)$$

For the standard tokamaks, as the parameter b, which expresses finite Larmor radius effect, is usually small (10^{-4} for B_T = 30 kG, T_i = 100eV), the inequality is satisfied.

The parameters of T_e 350eV, T_i 100eV, n_i 10^{13} cm^{-3}, R 1m and r 0(10cm), represent typical tokamak plasma now in operation. The mean free path of electrons is 3×10^3 cm and longer than qR_0, but is still in the plateau regime. In Fig. 1, a growth rate of the order of ω_* is shown at the rational surface $k_{//} = 0$. Experimental observations of fluctuations with m = 4, 3, 2 might be explained with the "grad $|B|$ drift instability" shown in Fig. 1. As ϵ increases, Ω_i increases and the instability tends to be very dangerous. When $k_{//}$ is not small, Ω_i in Fig. 1 is smoothly connceted to the usual resistive drift mode.

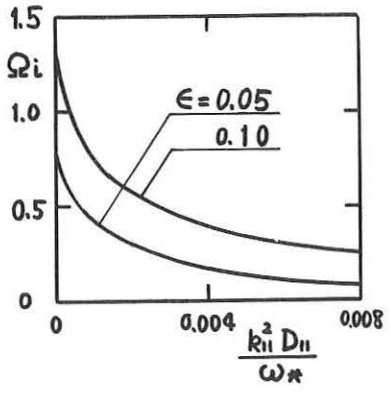

Fig. 1. Growth rate of fluctuations with m = 3 and n = -1. $\frac{k_{//}^2 D_{//}}{\omega_*}$ is the non-dimensional diffusion coefficient along the magnetic field.

In Fig. 2, Ω_r is shown as a function of $k_{//}$ where E/B is a parameter. When E/B increases, Ω_r increases but the functional relation is not linear. When E = 0, Ω_r at $k_{//} = 0$ is in the direction of an ion diamagnetic rotation. The figure shows that the direction of wave propagation is not the direct result of a sign of E_r. The growth rate Ω_i is scarcely affected by E/B.

In Fig. 3, the locus of Ω in the complex plane (Ω_r, Ω_i) is shown for $V_{E/B}$ = 0. Poloidal mode number m is 3 at $k_{//} \simeq 0$, while at large $k_{//}$, the resistive drift with m = 2 is approached and the dominant mode becomes m = 2. The transition takes place on the locus near $q \simeq 3.03$. The poloidal distribution of fluctuation amplitude is symmetric except near the transition. The poloidal symmetry at the rational surface is the remarkable feature of the grad $|B|$ drift instability in comparison with the trapped particle instabilities[5),6)] in which the fluctuation is strongly localized in the region with bad magnetic field curvature.

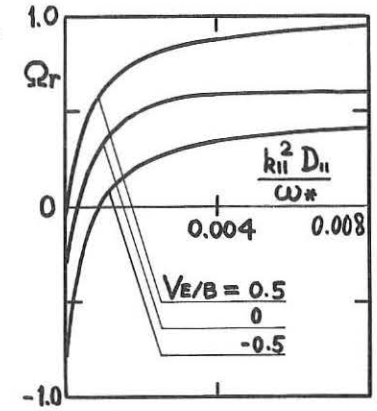

Fig. 2. Frequency of fluctuations with m = 3 and n = -1, ϵ = 0.05. $V_{E/B}$ represents normalized E x B drift velocity.

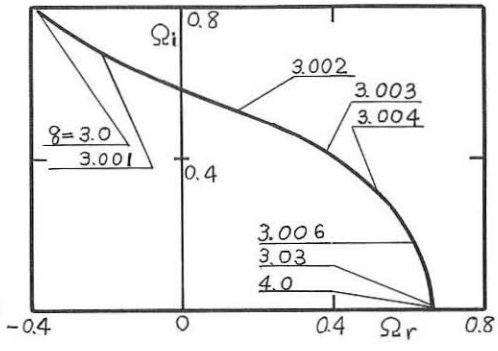

Fig. 3. Root locus of the mode with m = 3 and n = -1 at ϵ = 0.05.

The grad $|B|$ drift instability has been shown in the present analysis to have a large growth rate of the order of ω_* in the plateau regime. The amplitude of the oscillation distributes nearly uniform over the poloidal angle θ, because the electron mean-free-path is much longer than the connection length. The trapped particle instabilities are characterized with the amplitude strongly localized in the bad curvature region. Experimentally observed fluctuations in tokamaks[1),2)] now in operation in the plateau regime, might be explained with the grad $|B|$ drift instability.

On the rational surface where the parallel wave number is zero, the energy of the magnetic field perturbation is also zero, and the effect of the magnetic field perturbation is negligible.

REFERENCES

1) L. A. Artsimovich, Nuclear Fusion 12 (1972) 215
2) J. C. Hosea, et al., IAEA, Madison Vol. 2, 425 (1971)
3) G. Grieger, et al., IAEA, Madison Vol. 3, 37 (1971)
4) K. Miyamoto, et al., IAEA, Tokyo CN-33 B-5-1 (1974)
5) B. B. Kadomtsev and O. P. Pogutse, Sov.Phys. JETP 24 (1967) 1172
6) B. B. Kadomtsev and O. P. Pogutse, Sov.Phys. Doklady 14 (1969) 470
7) A. Hasegawa, Phys. Rev. 169 (1968) 204.

Heating Process in Experiments of Plasma Injection and Adiabatic Compression (PIACE)

S. Gotô, T. Uyama, N. Satomi and H. Itô
Plasma Physics Laboratory, Faculty of Engineering
Osaka University, Suita, Osaka, Japan

Abstract: Heating process of a keV deuterium plasma produced by rapid magnetic compression of colliding plasma streams is experimentally studied. In early stage of ion heating an electrostatic shock with high Mach number is observed. Main heating is dominated by the inward movement of the strong sheet current.

Introduction: Magnetic compression of a plasma produced by an encounter of two plasma streams ejected by plasma guns has been tried in our laboratory [1][2]. In this experiment, both ion and electron temperatures increase rapidly and reach 2∿5 keV within 1 μs inspite of wide variations of intial T_i, T_e and n_e. Final densities are 6×10^{15}∿5×10^{15} ions/cc and any serious mass motion is not observed in implosion phase. Up to the present, our ion heating is found to be divided into two stages in time: first one with a heating rate ∿1 eV/ns and second one with that of 10 eV/ns as shown in fig.1. Although this process has been partly discussed by a theoretical work, more detailed experimental data are presented here especially for early stage of plasma heating which leads to succeeding main heating [2][3].

Experiments: The initial plasma is produced by an encounter of two plasma streams ejected by theta guns of the same performance. The translational energy of each stream along 1 kG guide-field is rapidly converted into the thermal energy and a plasma with $T_i>T_e$ is obtained in the region surrounded by a one-turn coil of 1 m length. By choosing some appropriate time later than gun firing time, a rapidly increasing discharge through the compression coil is started. In this experiment, we selected only one time point 13 μs when T_i of the initial plasma is 100 eV which is the maximum in course of one plasma encounter. T_i and T_e were determined by spectroscopic method and laser scattering. Time and spatially resolved variations of B_z and E_r were measured by specially designed very fine probes. Results obtained by probe measurements are given in fig.2 and fig.3 respectively.

Discussion: Magnetic profiles until 160 ns are that of a so-called laminar shock with a high Mach number(> 3). This is understood by a fact that some plasma flow with a velocity ∿1×10^7cm/s from the surface of the plasma column towards the wall exists at the initial time. The ion temperature at the axis begins to increase after the foot of the shock reaches r=0(t=160ns, T_i∿200eV). The behavior of E_r is explained as follows. Just after B_z penetrates into the plasma, electrons begin to drift towards the axis with a velocity $v_r=(E_\theta/B_z)$ while ions are left or lost at the wall because of their large Larmor radius ρ_i. Then E_r is formed and begins to move by ambipolar effect. During ω_{ci} is small, the ion upstream is strong enough to compensate the loss at the wall. From observation, v_r is nearly constant(1.0∿1.2×10^7cm/s) up to 160ns. Ions penetrating through the shock are accelerated by E_θ near the wall for $2/\omega_{ci}$ and returned into the plasma without touching the wall when $\rho_i<(E_\theta/B_z)(2/\omega_{ci})$. This condition is fully satisfied at $t\gtrsim100$ ns, and heating by reflected ions are expected. At t=160 ns, E_r reaches the boundary of the initial plasma(r∿2 cm) where ρ_i is already small. Then the supply of ions to the shock becomes smaller and E_r is necessarily diminished. Nextly, by strong E_θ at the wall, same kind of process begins once more. In this phase, however, the movement of E_r does not deviate from that of the strong sheet current around the heated plasma column which ceases at the time of the maximum T_i.

It is concluded that our two-stage ion heating corresponds exactly to this temporal behavior of the radial electric field. E_r observed here seems to denote very imcoplete plasma boundary in phase I. However, only excess ions of the line density 10^8∿10^9/cm are necessary to produce it. This number is too small to produce some appreciable density hump in implosion phase(n_0∿10^{14} ions/cc). In phase II, ion heating is still supported by adiabatic compression or Fermi acceleration by the movement of the strong current sheet.

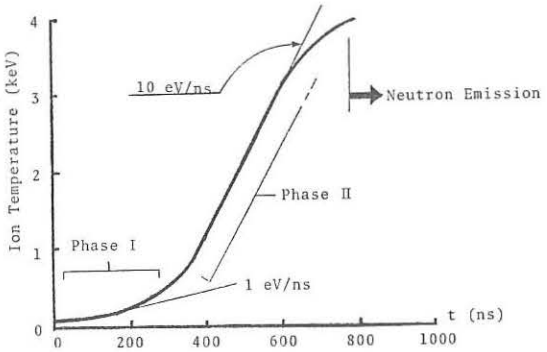

Fig.1. Typical T_i behavior in two-stage ion heating.

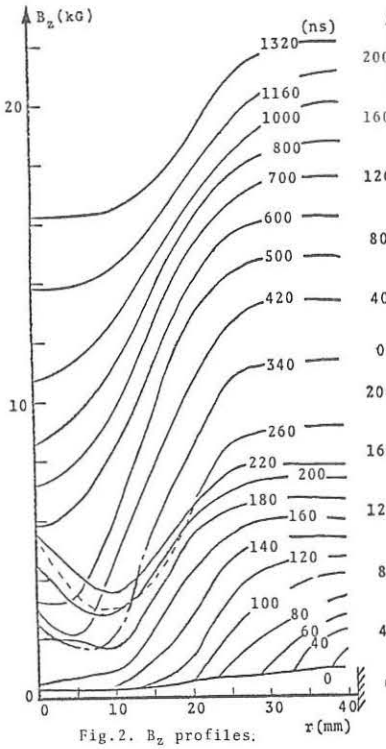

Fig.2. B_z profiles.

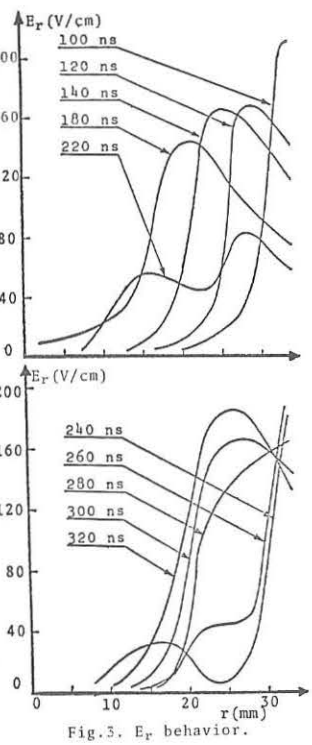

Fig.3. E_r behavior.

References
[1] H. Kishimoto, S. Gotô, H. Itô, Phys. Rev. Lett. 31(1973)1120.
[2] H. Itô, S. Gotô, H. Kishimoto, N. Satomi, M. Ushio, T. Uyama, IAEA-CN-33/E8-5 5th International Conf. on Plasma Physics and Controlled Nuclear Fusion Research(1974).
[3] H. Itô, "KAKUYUGO-KENKYU", Circular in Japanese 32(1974)144.
[4] D. Biskamp, Nuclear Fusion 13(1973)719.

THEORETICAL AND EXPERIMENTAL RESULTS OF HIGH TEMPERATURE PLASMA INVESTIGATIONS IN PULSED ELECTROMAGNETIC TRAPS

Lavrent'ev O.A., Kalmykov A.A., Sidorkin V.A., Azovskii Yu.S., Zaitsev B.V., Ovcharenko L.I., Sappa N.N., Stepanenko I.A., Potapenko V.A., Komarov A.D., Skibenko A.I., Fomin I.P., Pankrat'ev Yu.I., Volovin S.A., Naboka V.A., Nozdrachev M.G., Novikov M.N., Slavnii A.S.

Physical-Technical Institute, Kharkov, U.S.S.R.

1. Introduction

In this paper we consider the accumulation processes and plasma heating in electromagnetic traps [1] with pulsed magnetic fields. Plasma is produced with a generating gas ionization by electrons directly in the trap volume. Ions are accumulated and confined in the potential well of space electron charge whereas electrons are confined by outer electric and magnetic field. The removing velocity of slow electrons from the trap determines the accumulation and plasma heating efficiency. It follows from the fact that injection current and the indtroduced plasma power are confined by the space charge of the electrons already accumulated in the trap. The new electrons of outer injection can be introduced only instead of waste electrons, leaving the trap due to the diffusion across the magnetic field. By increasing the magnetic field the electron diffusion velocity would not be sufficient for reaching the limiting plasma parameters for time period of the magnetic field pulse duration.

To force the accumulation processes and plasma heating it is necessary to apply the methods of enforcing removal of slow electrons from the trap, for example, the excitation of diocatron instability [2] in magnetic gap region.

2. Experimental device and diagnostics

The experiments on high temperature plasma accumulation have been carried out at the devices of two types:Jupiter 1A,Jupiter 1M,BK-4.The design and parameters of the first two devices were reported [3,4]. They have a magnetic configuration of the contrary-engaged solenoids, an annular gap, two axial holes were blocked by electrostatic mirrors,the electron injection was through the axial holes. The latter is a multigap electromagnetic trap. Magnetic configuration is produced by current bars,which are located along a cylinder surface and by two coaxial solenoids on the ends. All magnetic gaps are blocked by electrostatic mirrors.Electron injection is through the radial gaps. Design and parameters of the device are given [5].

Plasma density is measured over the total number of the charged particles in the trap, with 8-mm interferometer, by potassium neutral beam. Plasma temperature is determined from the energetic spectra of charged and neutral particles.The life time is evaluated from the ratio of the total number of electron in the trap to the injection current.Energetical time is determined from the ratio of the total power contents in plasma to the injection power. Plasma boudary and loss localization of charged particles were determined by electrostatic probes.The potential well depth of space electron charge is evaluated by means of corpuscular methods.

3. The principal results

Table I shows the experimental result on plasma accumulation in the electromagnetic traps.

Device	Ju 1A	Ju 1M	BK-4
magnetic field,H, KGS	8	10	3
injection power, E_k,keV	5	7	1
injection current, I,A	0.1	0.1	0.3
plasma volume , V, l	0.3	0.2	1.0
density, n, cm^{-3}	4.10^{12}	5.10^{12}	2.10^{11}
ion temperature, T_i, keV	0.8	1	0.25
life time τ_k , msec	1.0	5	0.05
$\tau_* = (\nu_{ie} + \nu_{in})^{-1}$	1.7	5.3	0.4

Two regimes of accumulation are found, they have different velocities of neutral gas introduction into plasma. In the first regime, Fig.1a, we note a monotonic build-up of density, as a time accumulation function, for the velocity of neutral gas introuction into plasma $7 \cdot 10^{16}$ particles/sec.

During the injection 8.75 msec it is confined with a magnetic field plateau extension, $6 \cdot 10^{14}$ particles are introduced. Average density $2 \cdot 10^{12} cm^{-3}$ consists of 30% critical Brillouin one, $n_{cr} = H^2/4\pi mc^2$. In the second regime, Fig.1b, the velocity is $3.5 \cdot 10^{17}$particles/sec, a monotonic accumulation is disturbed by partial density breakdowns. Development of diocotron instability due to slow electron accumulation in magnetic gap region may be a possible reason of the breakdown, the monotonic accumulation build-up restores. During the injection 3.5 msec 10^{15} particles are introduced into plasma.The main density $4 \cdot 10^{12} cm^{-3}$ consists of 60% critical Brillouin one. It is close to the limit and is defined by a sagging of potential space electron charge in the magnetic gap.A further increase of injection duration leads to the exponential rise of ion current through the annular gap. Measurements of the energetic ion spectra with different devices have confirmed a linear dependence Ti on the electron injection energy with proportionality coefficient close to the theoretical one. The life time was compared with the theoretical estimations [6] taking into account electron diffusion in space coordinates and in the velocity space.

Discrepancy between experimental life time and the theoretical estimations for BK-4 is explained by local electron losses on the ends, we have found them experimentally. Also it have been found the life time increases linearly with the increasing of the distance between the end solenoids.

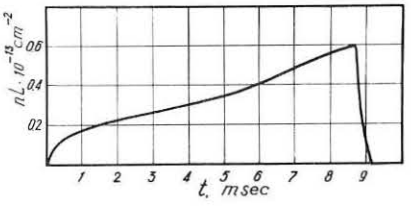

Fig.1a. $p = 2 \cdot 10^{-6}$torr

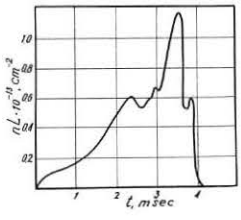

Fig.1b. $p = 10^{-5}$torr, hydrogen

REFERENCES

1. Lavrent'ev O.A. Uk.Ph.J. 8, 1963, 446.
2. Levy R.H., Gallen I.D., Ph.El.8, 1965, 2298.
3. Lavrent'ev O.A. et al. Reports on VI European Conference on Plasma Physics and the Problems of Controlled Thermonuclear Fusion", p.251, 1973.
4. Azovskii Yu.S., et al. "The Electromagnetic Trap "Jupiter IM", "Plasma Physics and Problems of Controlled Thermonuclear Fusion", vol.1 Academy of Sciences of the Ukrainian SSR, Kharkov (1973), 8-9.
5. Lavrent'ev O.A. et al. Ukr.Ph.J. 19, 1974, 1278.
6. Dolan T.Y. Electromagnetic confinement, University, Missouri-Rolla, 1973.

RESULTS FROM THE ELMO BUMPY TORUS* IN A THEORETICAL CONTEXT

C. L. Hedrick, R. A. Dandl, R. A. Dory, H. O. Eason, G. E. Guest, G. R. Haste, H. Ikegami, E. F. Jaeger, N. H. Lazar, D. G. McAlees, D. H. McNeill, D. B. Nelson, L. W. Owen

Oak Ridge National Laboratory, Oak Ridge, Tennessee USA

Abstract: Theoretical and experimental results from the ELMO Bumpy Torus will be discussed with particular emphasis on macroscopic stability and transport.

The ELMO Bumpy Torus (EBT) is a steady state device [1] composed of a linked set of twenty four 2-to-1 mirrors, arranged to form a torus with plasma heated by microwave power. The plasma has two basic components; a mirror confined, high beta, hot electron plasma, forming hollow annuli between each pair of coils; and a moderate temperature toroidal plasma that threads each of the electron annuli. Experiments carried out during the past year have demonstrated the validity of the basic EBT premise: that plasma currents produced by the high-beta hot-electron annuli can provide macroscopically stable plasma confinement by creating average minimum-B. EBT has also exhibited confinement of particles and energy for 10's of milliseconds, high plasma purity, and no perceptible difficulties with field errors or convective cells. This paper summarizes the principal experimental and theoretical features of the EBT research program.

Stability

Three distinct, reproducible modes of operation, the C-, T- and M-Modes are observed at successive lower ambient gas pressure. The C-Mode has a relatively high level of density fluctuations while the T-Mode is quiet. Theory predicts that when the hot electron component beta is in excess of about 15%, the local gradient in magnetic intensity should reverse and satisfy the relevant stability criteria. Experimentally the transition between the C- and T-Modes occurs for beta on the order of 15%.

Ideal MHD and guiding center theory would predict that the macroscopic modes of most importantance are pressure driven ballooning modes. These theories are not applicable to the annuli themselves, since $\omega_d, \omega_* > \Omega_i$. A more correct, but geometrically simplified Vlasov analysis shows that the annuli are stabilized when the poloidal drift frequency of the electrons exceeds the ion cyclotron frequency. If the annuli are considered to be rigid an MHD variational stability analysis of the toroidal core plasma shows that ballooning modes can only occur if the beta of the toroidal core exceeds a critical value comparable to the beta in the annuli. These results confirm that the present values of beta for the toroidal core are not limited by gross stability requirements.

Transport and Heating

In the EBT plasma, electrons are heated by microwave power at frequencies of 18 GHz and 10.6 GHz. The 18 GHz is resonant (electron cyclotron frequency) for constant B surfaces on each side of the mirror midplanes, while the 10.6 GHz source can provide lower off-resonant heating as well as profile heating. Ions are heated by Coulomb collisions with hot electrons. In the T-Mode, typical values of the plasma parameters are n_e(toroidal) $\sim$ 1-5 $\times 10^{12}/cm^3$; T_e(toroidal) $\simeq$ 150 eV; T_i(toroidal) $\simeq$ 75 eV; $\tau > 30$ msec; n_e(annulus) $\cong 2.5 \times 10^{11}/cm^3$; T_e(annulus) $\cong$ 250 keV; $\beta \cong 0.4$.

For a theoretical estimate of operating conditions in the quiet T-Mode, a simple point model has been developed in which radial variations are characterized by typical scale lengths. We assume a neoclassical lifetime for ions as derived by Kovrizhnikh [2] for the bumpy torus. To maintain charge neutrality, the loss rate of electrons must equal that for ions, requiring an ambipolar electric field in the radial direction. If the rate at which electrons transfer energy to ions is that of classical Coulomb collisions, the electron and ion temperatures and particle lifetimes can be calculated as functions of charged particle density.

The results for a density of 2×10^{12} cm^{-3} suggest ion and electron temperatures of 60 and 150 eV and particle lifetimes of about 20 msec. For weak ambipolar electric fields, the calculated particle lifetimes exhibit a strong inverse dependence on ion temperature, characteristic of the collisional regime. Higher electric fields and higher poloidal drift frequencies are required to attain the collisionless regime where confinement time increases with ion temperature.

While this model gives results which are consistent with typical parameters in the T-Mode, more detailed knowledge is needed of electron dynamics, ambipolar fields, diffusion coefficients and microwave power deposition to permit an unambiguous comparison with experiment. To upgrade the theory accordingly, we have devised a strategy based on the following circular relations:

1. Equilibrium magnetic fields depend on the pressure profile.
2. Guiding-center drift orbits depend on the equilibrium magnetic field and ambipolar electric fields.
3. Transport rates, which together with sources and sinks determine the profile, depend on the guiding center drift orbits.

3D equilibrium codes have been developed and are being improved and operated to gain insight into the effect of finite beta on guiding-center drift orbits. The effect of finite-beta and electric fields on guiding-center drifts is significant. To determine the resulting effect on transport phenomena and study the effects of microwave heating, a kinetic model of transport has been formulated using a Fokker-Planck equation to determine the radial dependence of the distribution function and ambipolar electric field. This is being implemented. Ultimately the loop represented by 1), 2) and 3) above will be closed with transport and the pressure profiles then being determined self-consistently.

The fluid-model computer codes developed in support of the tokamak program at Oak Ridge will have relevance to EBT, especially for questions of neutral and impurity effects. The EBT experiments have demonstrated the importance of the reflux of gas from the cavity wall in determining the source of particles required to maintain the plasma. The dominant source of fresh ion-electron pairs is energetic neutral hydrogen, recirculated at the wall. Experiments provide estimates of the principal impurities; these suggest that impurity ions drift to a wall (and are collected there) faster than they can diffuse inward, thus providing the observed high purity of the EBT toroidal plasma.

A central research objective unifies all the experimental and theoretical work on EBT reported here: to gain a working understanding of any mechanisms responsible for the loss of particles and energy from the system. Given the encouraging confirmation of the arguments advanced in proposing the EBT experiment, [3] we contemplate a sequence of devices to confirm the present scaling. The next step calls for a moderate increase in magnetic field to perform scaling experiments using the existing torus. The second step would involve a large increase in the magnetic field and a new torus. These steps require development (already underway) of appropriate high frequency microwave power sources.

References

*Research sponsored by the U. S. Energy Research and Development Administration under contract with Union Carbide Corporation.

[1] R. A. Dandl, et al, "The ELMO Bumpy Torus Program", ORNL-TM-4941 (June 1975) and references cited therein.

[2] L. M. Kovrizhnikh, Sov. Phys. - JETP 29, 475 (1969).

[3] R. A. Dandl, et al, "The ELMO Bumpy Torus Experiment", ORNL-TM-3694 (November 1971).

EXPERIMENT ON THE HF ELIMINATION OF THE CONE LOSSES IN THE MIRROR MACHINE

V.D.Dougar-Jabon, K.S.Golovanivsky, V.I.Karyaka
Plasma Physics Laboratory, Patrice Lumumba University, Moscow W-302, U.S.S.R.

Abstract: A hydrogen plasma was axially injected into the mirror configuration. A standing electromagnetic wave was excited in one of the mirrors. It was shown, that in accordance with the relativistic theory under the fulfilment of the ECR condition and when the gradient of the magnetic field in the resonance zone is sufficiently small, the decreasing of the cone losses by two orders was not accompanied by HF heating of the confined plasma.

Introduction: In the previous publications of our group /I-IV/ it was shown both theoretically and experimentally that the quasiadiabatic reflection of a plasma can be achieved by the mirror magnetic field supplemented by resonant HF field. The aim of the present experiments was to confine the externally injected plasma inside the mirror configuration with one or both mirrors supplemented by HF field under ECR conditions.

Experimental device: The experiments were conducted on a device shown in Fig.1. The distance between the mirrors was 56cm, mirror ratio R=1,5 , B_{max}=1,2KGs. Plasma generated by the coaxial gun during 60 μsec penetrated into the trap through the right mirror. Plasma parameters: hydrogen, bunch length about 800cm, diameter 4cm, density $n_{max}=6.10^{9}cm^{-3}$, parallel energy of ions $W_{i\parallel}$=100eV, electron temperature T_e=15eV, the background pressure 3.10^{-6}torr. The magnetron (P=500W,f=2,375GHz) excited the cylindrical cavities in the mode TE_{111}(E=150V/cm). The ECR condition was fulfilled at the central plane of the cavity. The mean magnetic field gradient in this region was equal to 10Gs/cm. Diagnosis: Langmuir and diamagnetic probes, electrostatic analyser of energy of the ions passing through the left mirror and appliances for HF measurement.

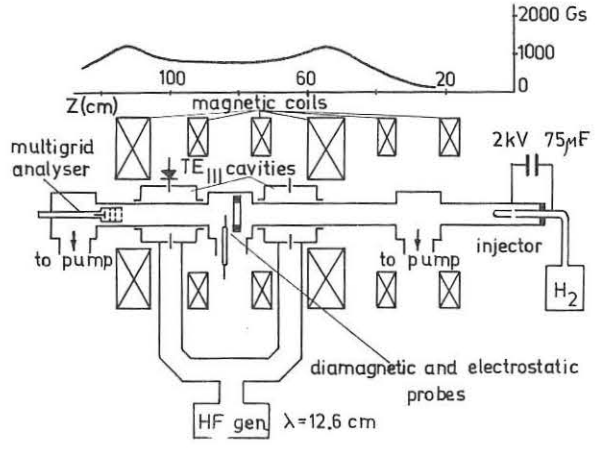

Fig. 1.

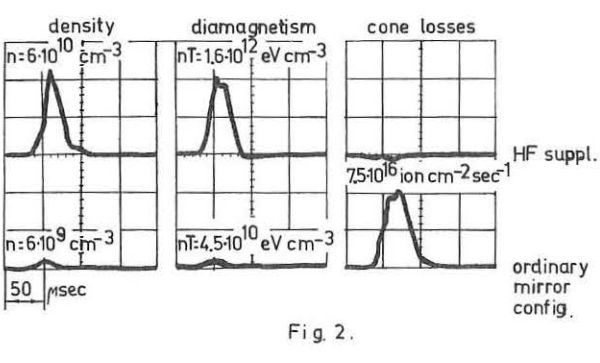

Fig. 2.

Results: In the absence of HF field the injected plasma passed along the axis without being trapped. This is illustrated in the lower traces of the Fig.2 presenting the ionic current registered by the probe in the centre of the machine, diamagnetic probe signal and the ionic flow coming to the analyser. The measured value of the ionic flow through the left mirror $N=7,5.10^{16}cm^{-2}sec^{-1}$ corresponds to the whole flow of the injected plasma, which indicates that all the injected plasma passes through the loss cone of the left mirror. The density and electron temperature probe measurements are in good agreement with the diamagnetic probe data, when the perpendicular inhomogeneity of the plasma is taken into account. When the HF field is created only in the left mirror (the upper traces in the Fig.2) the plasma density in the trap increasing during the whole time of injection reaches the value of $6.10^{10}cm^{-3}$ and decreases later during the characterestic time 25μsec. Simultaneously, nT signal increases to the value $1,6.10^{12}eV/cm^{3}$ and decreases later during the same characterestic time. As it is seen, the ion cone losses through the left mirror disappear practically completely. The widening of the plasma was studied by the simultaneous registration of the signals from two probes situated in the central plane at different distances from the axis. It was established that the confined plasma widened with the velocity 6.10^{6}cm/sec, which corresponds to the coefficient of the perpendicular diffusion $D_{\perp\,exp} = 0,7.10^{5}cm^{2}sec^{-1}$. The Langmuir probe measurements showed that the electron temperature of confined plasma was 17eV which within the limits of the experimental accuracy coincides with the electron temperature of the injected plasma. Comparison of the signals from the electrostatic and diamagnetic probes showed that in the confined plasma the ion temperature reached 38eV (while determining T_i , the mean value of nT measured by the diamagnetic probe was taken to be equal to half of nT in the centre of the plasma).

Discussion: The absence of the electron heating indicates that plasma does not absorb HF energy. The ionic component of the plasma cannot obviously absorb HF energy at the applied frequency. It follows then, that the heating of the ionic component is due to the compression of the long plasma bunch by the inertia forces when the bunch comes to a stop in the trap. From the energy balance it can be easily shown that about 36% of the longitudinal energy of the injected plasma bunch gets transformed into the perpendicular ion energy. As a consequence, the plasma leakage back to the injector should considerably decrease even in the absence of the HF field in the right mirror. We convinced ourselves in this fact by removing the right mirror. We carried out experiments when the HF field was present in the right mirror also. This led to the elimination of the cone losses through this mirror as a result of which the particle's life time in the trap increased by a factor two. In this case the plasma losses were determined by the perpendicular diffusion. The classical diffusion coefficient under the above said experimental conditions was $D_{\perp cl}=10cm^{2}sec^{-1}$which is considerably less than the experimentally obtained value. It follows then, that the diffusion was of non-classical character. An estimation of the Bohm's diffusion coefficient leads to the value $D_{\perp B}=3.10^{5}cm^{2}sec^{-1}$. The comparison of this value and experimental quantity $D_{\perp} = 0,7.10^{5}cm^{2}sec^{-1}$ allows us to conclude that the diffusion of Bohm's type plays an essential role in the perpendicular widening of the confined plasma. One of the basic results of the experiments is that the reflection of the electrons from the mirror with local ECR is quasiadiabatic. This is a consequence of the fulfilment of the condition for relativistic phase autofocusing effect /1/ $\frac{\partial \beta}{\partial z} < \left(\frac{eE}{2m_0cV_{i\parallel}}\right)^{2} B_0 |z-z_0|$.
In the experiments, the l.h.s. of the inequality was less than the r.h.s. by a factor four. In conclusion, we note that in the described experiments the plasma kinetic pressure exceeded the pressure of the HF field by three orders.

References:

I. K.S.Golovanivsky, Physics Letters, 44A, 3, 1973.
II. K.S.Golovanivsky, V.P.Milantiev, Plasma Physics, 16, 549, 1974.
III. K.S.Golovanivsky, L.A.Pokhmelnykh, V Europ. Conf. on Contr. Fusion and Plasma Physics, Grenoble, 1972.
IV. V.D.Dougar-Jabon, K.S.Golovanivsky, L.A.Pokhmelnykh, VI Europ. Conf. on Contr. Fusion and Plasma Physics, Moscow, 1973.

Max-Planck-Institut für Plasmaphysik
8046 Garching bei München

Electrostatic Confinement and Heating of Ions in Magnetic Mirror Field

Y. Nishida and S. Kawamata

Electrical Engineering, Utsunomiya University, Utsunomiya, Japan

K. Ishii

Institute of Plasma Physics, Nagoya University, Nagoya, Japan

Abstract: Electrostatic ion stoppering at the mirror point is achieved accompaning strong ion heating at the same time. When ions are heated, the many plasma satellites around the HeII line are observed, relating to the high frequency modulation of the spectrum.

Collisional losses from the ends of mirror machines place substantial restrictions on the confinement time of a plasma in such a open-end device. Because of these losses, it has been shown that it would be difficult to build a fusion reactor based on a mirror machine.[1] However, in recent years, various proposals have been made to utilize rf or dc electric fields to reflect escaping particles back into the system.[2~5] All of these proposals have difficulties to build the strong electric field in a plasma system. Effective ion heating in a mirror machine in steady state have been reported by using modified Penning type discharges.[6,7] The ion heating would be resulted from the ExB type instabilities or the beam plasma interactions. However, the precise mechanisms are not clarified yet partly because the plasma production and the heating regions are not separated.

In this paper a simple electrostatic ion confinement system in a mirror machine is proposed accompaning strong ion heating at the same time. In Fig.1 the schematic of ion confinement system is shown with diagnostic systems used. Region II is the plasma producing section which is the TPD-I machine in Nagoya University. Region I is the ion heating section where the ions are trapped electrostatically as well as the magnetic mirror field and heated.

The helium plasma produced in II diffuses into the heating section through orifices O_o and O_1, where orifice O_o is floating electrode with a hole of 30 mmϕ. Orifices O_1 and O_2 with a hole of 30 mmϕ can be biased at a desired potential. Orifices O_3 and O_4 with a hole of 20 mmϕ are made from insulator and protect the direct coupling between the plasma source region and the heating. In region I the plasma density n_o with a diameter about 20 mmϕ ranges $10^{11} < n_o < 10^{14}$ cm^{-3} under the neutral pressure of $(0.5\text{-}1.0)\times10^{-3}$ Torr, and ion temperature T_i and electron temperature T_e are about 30 eV and 15~30 eV at the column center, respectively. By changing the discharge current between 10-50 A, we can controle the plasma density.

The profiles of density, potential and T_e are measured by means of Langmuir probes in a rather low density case, while in rather high density the probes are melted and only T_i is measured from the Doppler broadening in HeII (4686 Å) line. The results in both cases can be discussed at the same time, as the abrupt changes between them have not been observed. End loss of ions from the mirror point is measured by probe P_2 which is settled at 3 mm apart from the column center and biased fully negative.

For heating the plasma we apply the strong DC field (V_H) at the electrode H, and V_o at O_1 and O_2, separately. In the case of O_1 and O_2 at floating potential, we can heat the ions selectively as the previous results.[6,7] Typical example is shown in Fig.2. From this results we may say that the threshold voltage for heating exists at around 300 V, and that ions are heated up to about 300 eV which is 10 times the initial value.

End losses from the mirror point are decreased untill about 10~15 % of the initial value as shown in Fig.3, when V_H is applied. In this figure, an ordinate shows the ion saturation current of probe P_2. At some value of V_H, say V_H= 1.3 kV at I_d=10 A, the breakdown occures within the heating region because of the rather high neutral pressure. We may say from these results that the plasmas are confined within the heating section by the positively biased orifices O_1 and O_2, and the heating electrode H.

The floating potential V_f and the density profiles estimated from ion saturation current I_{si} are shown in Fig.4. This result shows that the electric fields exist in the plasma, bringing about the ExB plasma rotation.

Measuring the Doppler broadening of HeII line, we observed the many satellites around HeII line, when ions are heated strongly. Typical example of the spectrum is shown in Fig.5. This phenomena could be related to the high frequency modulation[8,9] of HeII line by the strong instabilities occured in the plasma.

The electrostatic field is built through the electron currents flowing into the electrodes across the magnetic field, when V_H and V_o are applied. The machine is constructed so that the electron currents from the source along the magnetic field lines are suppressed as small as possible. This is essential for heating as well as confining the ions within the heating region.

Particles are adiabatically reflected if

$$v_{//}^2 < 2eV_o/M + v_\perp^2(R-1) \qquad (1)$$

at the mirror point and

$$v_\perp^2 < 2eV_H/M \qquad (2)$$

at the surface of the heating electrode, where $v_{//}$ and $v_\perp$ are the parallel and perpendicular velocities at the center of the machine, V_o and V_H are the potential of the orifices and the heating electrodes, respectively, R is the mirror ratio and M is the ion mass. At the surface of the orifices O_1 and O_2, the conbined condition of Eqs.(1) and (2) are necessary. The physical mechanisms of the ion heating have not been understood, although they are similar to the previous works.[6,7]

References

1 D.V.Sivukin, Plasma Phys. 8, 607 (1966).
2 A.A.Ware and J.E.Faulkner, Nucl. Fusion 9, 353 (1969).
3 C.J.H.Watson andL.G.Kuro-Petravic, Phys. Rev. Lett. 27, 1231 (1968).
4 R.W.Moir, W.I.Barr, and R.F.Post, Phys. Fluids 14, 2531 (1971).
5 B.B.McHarg,Jr and N.E.Oakes, Phys. Fluids 17, 1923 (1974).
6 J.R.Roth, Phys. Fluids 16, 231 (1973).
7 I.Alexeff et al, Phys. Rev. Lett. 25, 848 (1970).
8 M.Baranger and B.Mozer, Phys. Rev. 123, 25 (1961).
9 W.S.Cooper III and R.A.Hess, Phys. Rev. Lett. 25, 433 (1970).

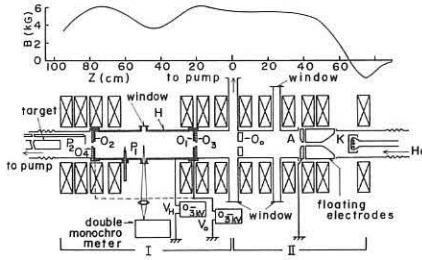

Fig.1. Experimental apparatus.

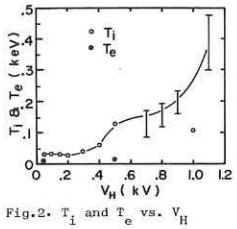

Fig.2. T_i and T_e vs. V_H

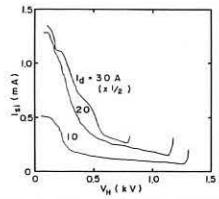

Fig.3. End loss from mirror point measured by probe P_2.

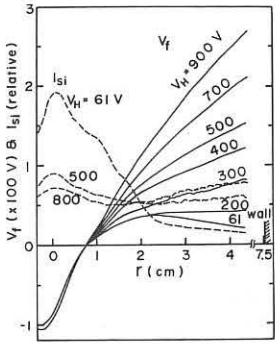

Fig.4. Potential and density profile in a radial direction.

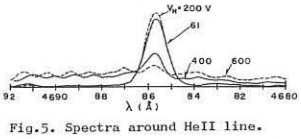

Fig.5. Spectra around HeII line.

NUMERICAL ANALYSIS OF THE PLASMA CONFINEMENT IN THE MIRROR MACHINE WITH LOCAL ECR

V.P.Milantiev, V.A.Tourikov
Patrice Lumumba University, Moscow W302, USSR

Abstract: Numerical solution of the averaged motion equations of ensemble of the charged particles with chaotic initial phases at the beginning of the cavity in the mirror machine with the conditions of local electron cyclotron resonanse (ECR) in one of the mirrors is presented. It is shown that under some values of the parameters reversible reflection of the particles by combined mirror and long enough confinement of the plasma take place.

The motion of electrons in the mirror in the presence of standing HF wave we describe by an averaged relativistic equations [1]-[2]:

$$\frac{dA_1}{d\tau} = g\frac{E(Z)}{\sqrt{\Omega(Z)}}\cos\varphi \qquad \frac{dA_2}{d\tau} = g\frac{E(Z)}{\sqrt{\Omega}}\sin\varphi$$

$$\frac{d\dot{Z}}{d\tau} = -\frac{\alpha}{\gamma}\frac{d\Omega}{dZ}(A_1^2+A_2^2), \quad \frac{d\varphi}{d\tau} = \frac{\Omega_0}{\gamma} - 1, \quad \frac{dZ}{d\tau} = \dot{Z} \qquad (1)$$

Here dimensionless variables are inroduced:

$$(X,Y,Z) = \frac{\omega}{c}(x,y,z), \quad \tau = \omega t, \quad \dot{X} = V_x = \frac{dX}{d\tau} = \frac{v_x}{c}, \ldots$$

$$g = \frac{eE_0}{mc\omega}, \quad \Omega = \frac{eB_0}{mc\omega}, \quad \gamma = \sqrt{1+\Omega(A_1^2+A_2^2)}, \quad \alpha = \frac{m}{M} = 0{,}5449\cdot10^{-3}$$

M is the mass of ion (hydrogen atom), ω is the frequency, E_0 is the amplitude of HF field, given by $E = E_0 E(Z)\cos\tau$.

Stationary magnetic field is given as follows

$$\vec{B} = \{-\frac{X}{2}\frac{dB_0}{dZ}, -\frac{Y}{2}\frac{dB_0}{dZ}, B_0(Z)\}$$

The influence of ions is accounted by the application of the model of "tensorial" mass [3].

The initial conditions for system (1) are:

$$A_1(0) = -\frac{V_{\perp 0}\cos\nu_0}{\sqrt{\Omega(0)}}, \qquad A_2(0) = \frac{V_{\perp 0}\sin\nu_0}{\sqrt{\Omega(0)}}$$

$$\dot{Z}(0) = \sqrt{2\alpha W_z(0)}, \qquad \varphi(0) = 0$$

Here $V_{\perp 0} = \sqrt{V_{x0}^2 + V_{y0}^2}$, $V_{x0} = V_{\perp 0}\cos\nu_0$, $V_{y0} = V_{\perp 0}\sin\nu_0$

$W_z(0)$ is initial (dimensionless) parallel energy.

The system (1) is used for numerical investigation of the motion of the particles.

The profile of stationary magnetic field is choosen as follows:

$$\Omega = \begin{cases} \alpha_1 Z^2 + \beta_1 & \text{if} \quad -\frac{L}{2} \le Z \le 0 \\ \alpha_2 Z^2 + \beta_2 & \text{if} \quad 0 < Z \le Z_{r1} \\ -\lambda(Z-Z_r)^2 + 1 & \text{if} \quad Z_{r1} < Z \le Z_r \\ \lambda(Z-Z_r)^2 + 1 & \text{if} \quad Z_r < Z \le Z_{r2} \\ \alpha_3 Z^2 + \beta_3 & \text{if} \quad Z_{r2} < Z \le \frac{L}{2} \end{cases} \qquad (2)$$

where L is the length (dimensionless) of the trap, Z_r is the point of classical ECR ($\Omega_0 = 1$), Z_{r1}, Z_{r2} are boundary coordinates of the cavity, L_r is the length of the cavity. Coeffitients $\alpha_1, \alpha_2, \alpha_3$ are defined by the continuity conditions on the boundaries of the given domaines and depend on parameters of the trap. Parabolic profile $\Omega(Z)$ is choosen for its simplisity of calculations. Outside the cavity adiabatic motion of the particles takes place. For given $\Omega(Z)$ the quantity $Z(\tau)$ takes the form

$$Z = a\sin(\omega_z\tau + \beta) \qquad (3)$$

where a, β, ω_z are defined by initial conditions and parameters of the trap.

The profile of the magnetic field in the cavity is most optimal with regards to efficiency of the reflection properties of the combined mirror [4].

The amplitude of electric HF field in the cavity is given as follows $E(Z) = \frac{\pi}{L_r}\sin(Z - Z_{r1})$

By help of(1)-3) dynamics of particles ensemble, which start at some initial moment of time in the plane $Z = -\frac{L}{2}$ with different initial parallel energies and an initial zero perpendicular energy was investigated. Uniform distribution of initial parallel energies of the particles was considered. The deflection is about 10 % of the value of the mean energy. In adiabatic region expression (3) was used.

At the beginning of the cavity initial phase ν_0 was given by help of programm generator of random numbers. So the process of phase randomization was modelled. In the result of calculations the dependence on time of the average perpendicular ensemble energy $\overline{W_\perp}$, average parallel energy $\overline{W_z} = \frac{M}{Q}\overline{v_z^2}$ and the particles number N were obtained.

It is stated that with some values of parameters reversible motion of plasma takes place, which is an important factor in the use two-cavities system. In the absence of the energy recuperation, in the process of multiple reflection from the mirrors, permanent escaping of particles from the trap occurs. With values of the parameters closed to the boundary of the region, in which the condition of reversibility of the reflection is fulfilled, long confinement of the particles in the trap takes place. The results of numerical calculations for that case are presented in Fig.1 . Averaged perpendicular and parallel energies of the particles, gained after first reflection from the combined mirror, remain nearly constant after consequitive reflections. Averaged life- time of the particles in the trap is approximately 10^6 periods of HF field.

References

[1]. E.Canobbio, Nuclaer Fusion, 1969, No9, 27.
[2]. V.P.Milantiev, V.A.Tourikov, Book of Abstracts, II Int.Conf. on Plasma Theory, Kiev, 1974.
[3]. R.Bardet, T.Consoli, E.Geller, Nuclear Fusion, 1965, 5, 7.
[4]. K.S.Golovanivsky, Phys.Lett., 1973, A44, No3, 190.

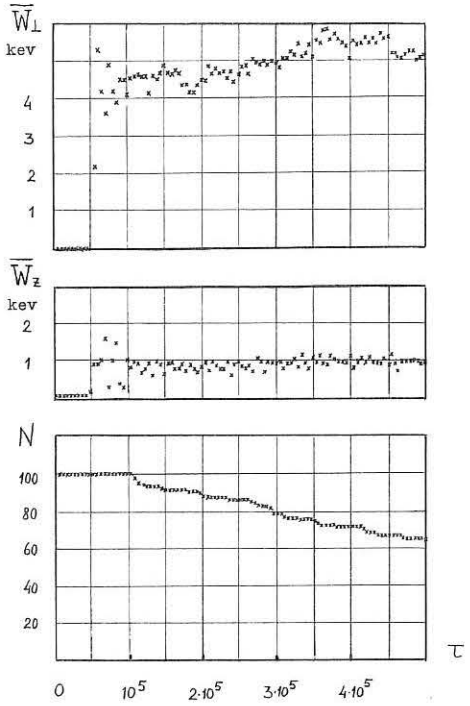

FIG. 1. $g = 10^{-4}$, $\lambda = 0.02$, $R = 2.0$, $R_0 = 1.5$, $\overline{W}_{z0} = 0.1$ kev.

NUMERICAL SIMULATION OF NEUTRAL INJECTION ON A HOT ELECTRON MIRROR TARGET PLASMA

C. GORMEZANO - G. MELIN - F. WERKOFF

ASSOCIATION EURATOM-CEA
Département de Physique du Plasma et de la Fusion Contrôlée
Service IGn - Centre d'Etudes Nucléaires
B.P.85 - Centre de Tri - 38041
GRENOBLE CEDEX (France)

ABSTRACT : In the case of neutral injection on a hot electron target plasma, the use of the existing Fokker-Planck codes is greatly complicated by the fact that the scale of the energies of the confined ions is very large. To avoid this difficulty we use a multi-species model, in which the particle losses are described by a differential system.

1 - INTRODUCTION : It has been pointed out /1/ that a hot electron plasma in a mirror machine could be used as a convenient target plasma to produce a hot ion plasma by fast neutral injection. We present a numerical simulation of neutral injection on a CIRCE-type target plasma. Such a plasma /2/ should be able to achieve the target requirements (sufficiently high density, low gas pressure), assuming it is possible to inject and trap a plasma in the distorted field of a minimum B magnetic configuration by electron heating.

2 - ANALYTICAL MODEL AND HYPOTHESIS. The main problem arises from the transition of this target plasma dominated by hot electrons with a negative potential to a final plasma which is a hot ion plasma with a positive potential. It is possible to use classical Fokker-Planck codes to study the behaviour of the plasma during the neutral injection, but the scale of energies and times for the different species is very large. Cold ions and hot electrons of the target have to balance with cold electrons and hot ions resulting from the neutral injection ; characteristic times lie between a few μs and several ms. So the resolution of FP equations should need prohibitive computation times. To overcome this difficulty we have to find equations which are more readily integrable. By integrating analytically the FP equations /3/ over the velocity space, the coulombian diffusion can be described by two equations for density and energy of each species a

$$\left(\frac{dn_a}{dt}\right)_{coul.} = -n_a \Gamma_a \sum_b n_b K_{ab} \qquad \left(\frac{dn_a \bar{v}_a^2}{dt}\right)_{coul.} = -n_a \Gamma_a \sum_b \left(L_{ab} + M_{ab}\right) \quad (1)$$

with $\Gamma_a = \frac{4\pi e^4}{m_a^2} \mathrm{Log}_e \Lambda$, K_{ab} is the particle diffusion coefficient of species a on species b, L_{ab} and M_{ab} the energy diffusion and equipartition coefficients. Analytical approximations of the distribution functions are written, taking into account the ambipolar potential ϕ. For particles having $q_a \phi > 0$, which are not confined by the potential, we use the Ben Daniel's approximation /4/ with hyperbolic coordinates ($u_a^2 = v_a^2 - \alpha_a^2$, $\xi_a = v_{//}/u_a$, $\alpha_a^2 = \frac{2q_a\phi}{m(R-1)}$ /5/) to yield the distribution functions. For particles having $q_a \phi < 0$, no losses occur if $v_a^2 < 2|q_a\phi|/m_a$ and the distribution function is near the maxwellian /6/, /7/ ; if $v_a^2 >> 2|q_a\phi|/m_a$, the ambipolar potential is neglected. Knowing the distribution functions, the coefficients K, L, M can be calculated from the Rosenbluth potentials /3/ (here we only consider the isotropic part). So we have to solve the differential system (1) for each species instead of the whole system of coupled FP equations. The model keeps only 4 species, using the subscripts hereafter referenced: 1 cold ions and 3 hot electrons from target plasma, 2 hot ions and 4 cold electrons from neutral beam, 0 neutral beam (H^0), n background neutral gas (H^0). The equations for density n and energy E (the subscript s stands for source) are for a hydrogen plasma :

$$\frac{dn_1}{dt} = -n_1\Gamma_1 \sum_{b=1}^{4} n_b K_{1b} - \frac{I_{0\alpha}}{eV} \frac{n_1 \langle \bar{\sigma}_{ex}^{i} v_r \rangle_{10}}{S_{ex} + S_{ion}} + \mathcal{J} - n_1 n_n \langle \bar{\sigma}_{ex}^{A} v_r \rangle_{1n}$$

$$\frac{dn_2}{dt} = -n_2\Gamma_2 \sum_{b=1}^{4} n_b K_{2b} + \frac{I_{0\alpha}}{eV}\left(1 - \frac{n_2 \langle \bar{\sigma}_{ex}^{i} v_r \rangle_{20}}{S_{ex} + S_{ion}}\right) - n_2 n_n \langle \bar{\sigma}_{ex}^{A} v_r \rangle_{2n}$$

$$\frac{dn_3}{dt} = -n_3\Gamma_3 \sum_{b=1}^{4} n_b K_{3b} + \mathcal{J}$$

$$\frac{dn_4}{dt} = -n_4\Gamma_4 \sum_{b=1}^{4} n_b K_{4b} + \frac{I_{0\alpha}}{eV} \frac{S_{ion}}{S_{ex} + S_{ion}}$$

$$\frac{d(n_1E_1)}{dt} = -n_1\Gamma_1 \sum_{b=1}^{4} n_b \left(L_{1b} + M_{1b}\right) - E_1 \frac{I_{0\alpha}}{eV} \frac{n_1 \langle \bar{\sigma}_{ex}^{i} v_r \rangle_{10}}{S_{ex} + S_{ion}} + \mathcal{J} E_{1s} - n_1 E_1 n_n \langle \bar{\sigma}_{ex}^{A} v_r \rangle_{1n}$$

$$\frac{d(n_2E_2)}{dt} = -n_2\Gamma_2 \sum_{b=1}^{4} n_b \left(L_{2b} + M_{2b}\right) + E_{0s} \frac{I_{0\alpha}}{eV} - E_2 \frac{I_{0\alpha}}{eV} \frac{n_2 \langle \bar{\sigma}_{ex}^{i} v_r \rangle_{20}}{S_{ex} + S_{ion}} - n_2 E_2 n_n \langle \bar{\sigma}_{ex}^{A} v_r \rangle_{2n}$$

$$\frac{d(n_3E_3)}{dt} = -n_3\Gamma_3 \sum_{b=1}^{4} n_b \left(L_{3b} + M_{3b}\right) + \mathcal{J} E_{3s}$$

$$\frac{d(n_4E_4)}{dt} = -n_4\Gamma_4 \sum_{b=1}^{4} n_b \left(L_{4b} + M_{4b}\right) + E_{4s} \frac{I_{0\alpha}}{eV} \frac{S_{ion}}{S_{ex} + S_{ion}}$$

J being the particle flux to maintain the target plasma density, V the plasma volume, I_0 the equivalent beam current (H^0), α the beam attenuation factor $\alpha = 1 - \exp\left(-\frac{d}{v_0}(S_{ex} + S_{ion})\right)$, S_{ex}, S_{ion} the absorption coefficients of fast neutrals : $S_{ex} = n_1 \langle \sigma_{ex}^{i} v_r \rangle_{10} + n_2 \langle \sigma_{ex}^{i} v_r \rangle_{20}$

$$S_{ion} = n_1 \langle \sigma_{ion}^{i} v_r \rangle_{10} + n_2 \langle \sigma_{ion}^{i} v_r \rangle_{20} + n_3 \langle \sigma_{ion}^{e} v_r \rangle_{30} + n_4 \langle \sigma_{ion}^{e} v_r \rangle_{40}$$

Simplifying assumptions for ion losses by charge exchange on neutral gas neglecting wall desorption and burn out effect were made since our primary interest is understanding the behaviour of the ambipolar potential. This potential is calculated to ensure the plasma charge neutrality at each step. This step is adjusted in order to reach the required precision in a few iterations and is varied in a range which usually reaches a factor 10^4.

3 - RESULTS. The target parameters are : $n_1 = n_3 = 2.10^{13} cm^{-3}$, $E_3 = 30$ keV, $E_2 = 400$ eV, R = 3, d = 15 cm, V = 5 l. The time duration, t_t, where the target plasma density is maintained constant, can be adjusted. The results are shown in figs. 1 through 4 for a permanent hot neutral injection. To describe the plasma confinement quality, we introduce the parameter S which is the ratio between the calculated term (nτ) and the theoretical one /8/.

4 - CONCLUSION. The accuracy of this method is less than that of a complete FP code. However the calculation shows that it is possible to build up a convenient hot ion plasma by neutral beam injection on a hot electron target plasma. The results show that the hot electron population increases the ambipolar potential ; the target plasma density must not be maintained for a too long time.

REFERENCES. /1/ - R.J. COLCHIN, Nucl. Fusion, 11, 329 (1971).
/2/ - R. BARDET et al., V^th Conf. Pl. Phys., TOKYO (1974).
/3/ - M.N. ROSENBLUTH et al., Phys. Rev., 107, 1 (1957).
/4/ - D.J. BEN DANIEL, W.P. ALLIS, Pl. Phys., 4, 31 (1962).
R.F. POST, M.N. ROSENBLUTH, Phys. Fluids, 9, 730 (1966).
/5/ - F. WERKOFF, EUR-CEA-FC 687, 56 (1973).
/6/ - A.H. FUTCH et al., Pl. Phys., 14, 211 (1972).
/7/ - V.P. PASTUKHOV, Nucl. Fus., 14, 3 (1974).
/8/ - T.K. FOWLER, M. RANKIN, Pl. Phys., 8, 121 (1966).

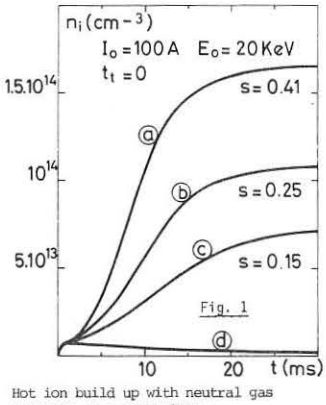

Hot ion build up with neutral gas pressure as a parameter - a : Pn = 0, b : Pn = 3.10^{-8} torr, c : Pn = 5.10^{-8} torr, d : Pn = 10^{-7}torr

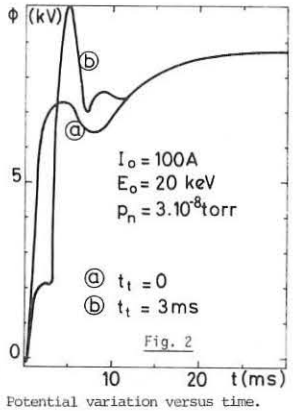

Potential variation versus time.

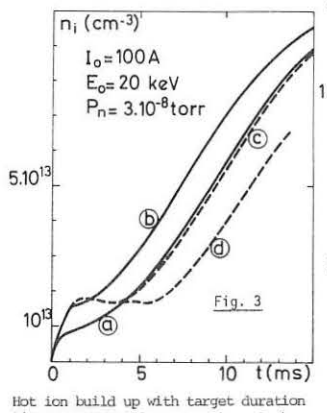

Hot ion build up with target duration time as a parameter - a : t_t = 0, b : t_t = 1ms, c : t_t = 3ms, d : t_t = 5ms.

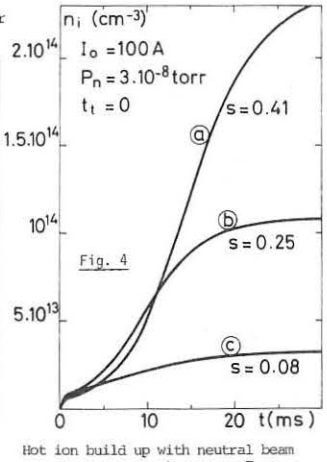

Hot ion build up with neutral beam energy as a parameter - a : E_o = 40keV, b : E_o = 20keV, c : E_o = 10keV

Feedback Stabilization of

Weakly Turbulent Mirror Plasma*

T. Kammash and N. A. Uckan

University of Michigan, Ann Arbor, Mich., U.S.A.

Abstract: A feedback control in which the local potential perturbation is used as a control variable is examined for possible utilization in the stabilization of a weakly turbulent mirror-confined plasma. A set of quasilinear equations with the appropriate feedback is derived and then applied to loss cone mirror instabilities. It is shown that the particle diffusion into the loss cone can be sufficiently fast with modest feedback that the instability could be attenuated before the particles can escape through the mirrors.

The use of feedback stabilization in which the control variable is the potential rather than the density fluctuation has recently been studied within the frame work of linear theory and its effectiveness tested by application of the results to well known mirror instabilities[1]. In this paper we examine the use of this type of feedback in a weakly turbulent (where the energy density in the field fluctuations is much smaller than the mean particle kinetic energy density) plasma by deriving the appropriate quasilinear equations and the corresponding diffusion tensor for an infinite collisionless plasma situated in a constant magnetic field.

The basic equations are the Vlasov-Poisson equations with feedback i.e

$$\frac{\partial f_j}{\partial t} + \underline{v}\cdot\frac{\partial f_j}{\partial \underline{r}} + \frac{q_j}{m_j}\left[\underline{E}(\underline{r},t) + \frac{1}{c}(\underline{v}\times\underline{B})\right]\cdot\frac{\partial f_j}{\partial \underline{v}} = 0 \quad (1)$$

$$\nabla\cdot\underline{E} = 4\pi\sum_j q_j\int f_j\, d^3v \quad (2)$$

where

$$\underline{E}(\underline{r},t) = \underline{E}(\underline{r},t) + \underline{E}_f(\underline{r},t) \quad (3)$$

is the total electric field vector and E_f is the feedback field which can be expressed as

$$\underline{E}_f = \int\int d\underline{r}'\,dt'\, H(\underline{r}-\underline{r}', t-t')\,\underline{E}(\underline{r}',t') \quad (4)$$

with H being the transfer function of the feedback system which we take to be a real function of its arguments. Carrying out the usual Fournier Analysis by first writing

$$f_j(\underline{r},\underline{v},t) = F_{oj}(\underline{v},\chi) + \sum_{\underline{k}} f_{j\underline{k}}(\underline{v},t)\, e^{i\underline{k}\cdot\underline{r}} \quad (5)$$

where $\chi = x + v_y/\Omega$ is included to allow for mild spatial inhomogeneity and assuming that the perturbed electric field can be written as

$$\underline{E}_{\underline{k}}(t) = \underline{E}_{\underline{k}}(0)\exp\int_0^t S_{\underline{k}}(\tau)\,d\tau \quad (6)$$

with

$$S_{\underline{k}}(t) = -i\omega_{\underline{k}}(t) + \gamma_{\underline{k}}(t) \quad (7)$$

we obtain, after neglecting the mode coupling term[2], a dispersion equation in the form

$$\epsilon(\underline{k},S_{\underline{k}}) = \left[1 - \frac{1}{2}\frac{\partial S_{\underline{k}}}{\partial t}\frac{\partial^2}{\partial S_{\underline{k}}^2}\right]\left[\epsilon_{F_o}(\underline{k},S_{\underline{k}}) + \epsilon_{f_o}(\underline{k},S_{\underline{k}})\right] \quad (8)$$

In the above expression the quantities ϵ_{F_o} and ϵ_{f_o} are lengthy, but ϵ reduces to the appropriate form in the absence of feedback. If we now define

$$F_j(\underline{v},t) = F_{oj}(\underline{v},\chi) + f_{jo}(\underline{v},t) \quad (9)$$

and invoke the usual assumptions of quasilinear theory we obtain

$$\frac{\partial F_j}{\partial t} = \left(\frac{\partial}{\partial \underline{v}} + \frac{\hat{\underline{e}}_z}{\Omega_j}\times\frac{\partial}{\partial \underline{r}}\right)\cdot\left[\underline{\underline{D}}_j\cdot\left(\frac{\partial}{\partial \underline{v}} + \frac{\hat{\underline{e}}_z}{\Omega_j}\times\frac{\partial}{\partial \underline{r}}\right)F_j\right] \quad (10)$$

where the diffusion tensor is given by

$$\underline{\underline{D}}_j = \sum_{\underline{k}}\sum_{n=-\infty}^{\infty}\left(\frac{q_j}{m_j}\right)^2\frac{|\mathcal{E}_{\underline{k}}(t)|^2}{k^2}\frac{J_n^2\left(\frac{k_\perp v_\perp}{\Omega_j}\right)}{S_{\underline{k}}(t) + i\underline{k}_z\underline{v}_z + in\Omega_j}\,\underline{\alpha}_{jn,\underline{k}}\,\underline{\alpha}_{jn,\underline{k}} \quad (11)$$

with

$$\underline{\alpha}_{jn,\underline{k}} = \frac{n\Omega_j}{v_\perp}\hat{\underline{e}}_\perp + \underline{k}$$

$$|\mathcal{E}_{\underline{k}}(t)|^2 = |E_{\underline{k}}(t)|^2\left[1 + |H_{\underline{k}}(S_{\underline{k}})|^2 + H_{\underline{k}}H_{-\underline{k}}\right] \quad (12)$$

having taken the applied magnetic field to be along the $\hat{z}$-direction. The standard equation for the wave growth[2] along with eq. (10) constitute the desired quasilinear equations and we readily note that

$$D_j)_{\text{feedback}} > D_j)_{\text{no feedback}}$$

so that the diffusion time in velocity space is shorter with feedback than it is without it.

We apply the above results to the Post - Rosenbluth[3] loss cone instability using the equilibrium ion distribution function suggested by Galeev and Sagdeev[4] and the results reflecting the effect of feedback on the growth rate and the spectral energy density are shown in figures (1) and (2). The extent of feedback stabilization depends on the value of H which for present day amplification systems can be of the order of 100.

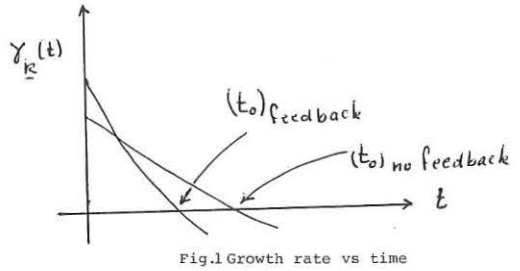

Fig.1 Growth rate vs time

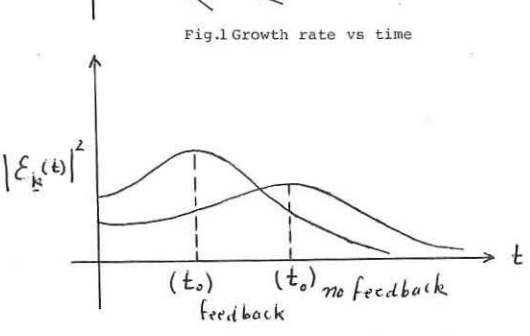

Fig. 2 Wave energy density vs time

*Work supported by U. S. ERDA

1. T. Kammash and N. A. Uckan, Nuclear Fusion (to be published)

2. R. C. Davidson, Methods in Nonlinear Plasma Theory Academic Press, N. Y. 1972, p. 151

3. M. N. Rosenbluth and R. F. Post, Phys. Fluids 8, 547 (1975)

4. R. Z. Sagdeev and A. A. Galeev, Nonlinear Plasma Theory W. A. Benjamin Inc. N. Y. 1969, p. 65

PARAMETERS OF SCREW PINCHES IN SPICA

R.J.J. van Heijningen, C. Bobeldijk, J.A. Hoekzema, P.C.T. van der Laan, D. Oepts, J.W.A. Zwart, W. Kooyman, and D.J. Maris

Association Euratom-FOM, FOM-Instituut voor Plasmafysica Rijnhuizen, Jutphaas, The Netherlands

Abstract: Experimental results of screw-pinch discharges in SPICA[1,2] (aspect ratio R/r = 0.6/0.2) are given. A deuterium plasma column characterized by $T_e = T_i = 50$ eV, $n_e = 7 \times 10^{21}$ m^{-3}, and $\beta = 0.20$, has been confined for about 100 μs. Turbulence and current depletion in the low-density region outside the pinch are discussed.

Since the last publication of SPICA results[3] the experimental program has been concentrated around the control of β in order to improve MHD-stability[4]. A better control of β was made possible by the introduction of a higher bias field strength. At filling pressures of 10 mTorr D_2 the value of β can be varied down to 0.2 without spoiling the shock heating effect of the implosion. At low filling pressures the snow-plough implosion does not develop well, which is probably due to ineffective preionization.

Care has been taken to avoid magnetic field errors due to holes and gaps in the copper shield. Inevitable large holes such as pumping ports (diameter 74 mm) are closed during plasma operation. Especially the local vertical stray fields in the poloidal gap have been successfully minimized. These fields are due to transverse currents in the feed flange which arise if the poloidal distribution of currents differs from the externally applied one. As long as gross stability maintains, these fields can be kept well below 0.01 T, as shown in Fig. 1, where the output of monitor coils in the gap is given. The variation of the signal is mainly due to horizontal movement of the column. These coils are very sensitive to macroscopic instabilities. If no plasma current flows, the local vertical field amounts to 0.04 T. Horizontal stray fields due to up-down asymmetry of the current supply are negligible (less than 0.001 T). It is estimated that the aperture of the current-carrying plasma could be as large as 93% of the bore of the copper shield.

Figure 1 shows a series of data obtained from one shot. The bank voltages are: $V_\theta = 40.7$ kV, $V_z = 26.8$ kV (70% of the maximum energy). The initial pressure is 10 mTorr D_2, the toroidal field B_z is 1.2 T, the bias field 0.127 T. Most data are sampled and stored during the discharge, using fast AD-converters with local memory (2.5 MHz frequency response). Long-term storage and analysis of the data is performed by an optically coupled PDP-15 (32k) computer[5]. Only 40 μs of this discharge is sampled to avoid loss of details during the implosion phase. In shots like this the plasma column maintains much longer (∿ 100 μs), as can be inferred from the density (He-Ne interferometer[6]) and the streak photographs. Although these photographs show irregular flares of light in the outside region, there is little influence on the column density or on the position as measured by the sin-cos coils[7]. The output signals of the sin-cos coils are related to displacements by direct comparison with a streak picture.

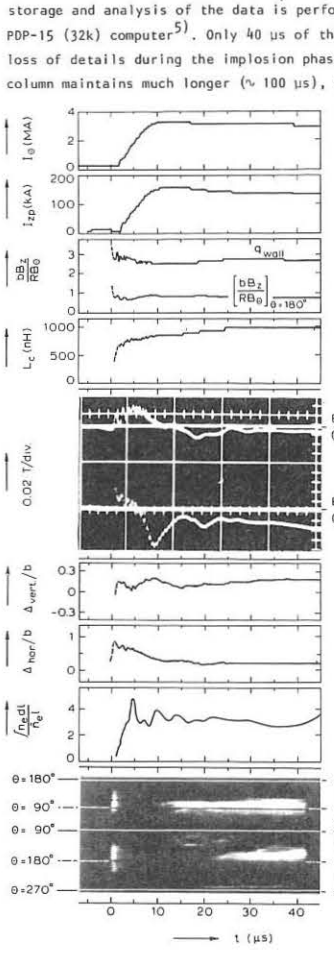

Fig. 1.

Typical set of data from one SPICA screw-pinch discharge in D_2. From top to bottom are displayed with the same sweep speed: main coil current; plasma current; safety factor q and local pitch; internal plasma inductance ($\int V_z dt / I_{zp}$); vertical stray magnetic fields in the poloidal gap of the copper shield; vertical and horizontal displacement of the pinched column; linear compression of the pinch; streak picture of the total visible light emission. The poloidal angle Θ is 0 at the inside of the torus.

Local T_e and n_e have been determined from 90° Thomson scattering[8] at a position slightly off the tube axis (0.04 m), at t = 10 μs. For the discharge shown in Fig. 1 the measured values, $T_e = 50$ eV, $n_e = 7 \times 10^{21}$ m^{-3} (β = 0.20) are roughly peak values of the radial distribution (see Fig. 2). T_e is in agreement with the predictions from simple implosion theory. The density corresponds to a linear compression of 3.3 which agrees well with the line density results. The photomultiplier signals are registered with an 8-channel, charge-sensitive, gated AD-converter. Calibration of the photomultipliers is performed with a tungsten ribbon lamp. The relative sensitivities of the different channels are monitored by means of a pulsed light-emitting diode. Absolute calibration required for density measurements is obtained from Rayleigh scattering by neutral nitrogen at pressures of 5 to 10 Torr.

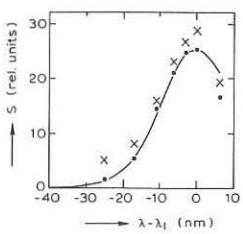

Fig. 2. Thomson-scattering measurement for the discharge of Fig. 1, at t = 10 μs.
+ observed intensities
• corrected for plasma radiation and laser stray light.
The curve represents a Gaussian fit correponding to T_e = 50 eV, $n_e = 7 \times 10^{21}$ m^{-3}.

The value of q at the wall decreases in this particular discharge from 2.8 initially to about 2.2 after a quarter period (10 μs). By proper programming of the predischarge and the main currents $q_{wall}(t)$ can be made approximately constant or increasing. In a well-conducting outside plasma this should lead to a corresponding profile of the pitch as a function of r[9]. For a flat profile the current density is almost homogeneous, which implies a total toroidal inductance of 420 nH in the torus[10]. In practice the measured inductance is in between 500 nH and 900 nH, which indicates a vacuum region outside the constant pitch region with a width up to 0.10 m. The value of q at the plasma boundary is then about 1/2 or 1/3 of q_{wall}, which approaches the Kruskal-Shafranov limit.

The equilibrium position of the plasma is good, in fact even better than expected from calculations to first order in the inverse aspect ratio[11]. This indicates that the force-free currents immediately outside the pinched column develop well[3]. In screw-pinch discharges, in contrast with Θ-pinch and Z-pinch discharges, hard X-rays are produced, presumably due to runaway electrons in the low-density region. These may be expected as soon as the drift velocity of the electrons exceeds the electron thermal velocity ($v_{de} > v_{the}$). For SPICA the maximum current density, for q ≈ 1.4 outside the plasma, is equal to $j = n e v_{de} = 2.8 \times 10^6$ A/m^2. Measurements in earlier screw-pinch experiments[12,13] suggest that during the first few μs the density outside the column may indeed be low enough to invoke the condition $v_{de} > v_{the}$ despite the fact that j has not yet reached its maximum value. The resulting turbulence (accompanied by runaways) could then be responsible for the current depletion, although other mechanisms like current scrape-off during the horizontal motion cannot be excluded. Recent measurements show that better preionization can make the X-ray emission completely disappear.

Acknowledgement: The authors gratefully acknowledge the technical help in the reconstructions, repairs, and measurements by Messrs. P.J. Busch, G. van Dijk, A.C. Griffioen, W.J. Mastop, P.H.M. Smeets, and A.B. Sterk.

This work was performed under the Euratom-FOM association agreement with financial support from ZWO and Euratom.

References

[1] C. Bobeldijk, R.J.J. van Heijningen, P.C.T. van der Laan, Proc. 3rd Int. Symp. on Toroidal Plasma Confinement, Garching (1973) G5.

[2] R.J.J. van Heijningen et al., EUR 5182e, Proc. 8th Symp. on Fusion Technology, Noordwijkerhout (1974) 341.

[3] C. Bobeldijk et al., IAEA Proc. 5th Int. Conf. on Plasma Physics and Controlled Nuclear Fusion Research, Tokyo (1974) E9-1.

[4] R.F. de Vries et al., Proc. 3rd Eur. Conf. on Contr. Fusion and Plasma Physics, Utrecht (1969) 88.

[5] W. Kooyman, EUR 5182e, Proc. 8th Symp. on Fusion Technology, Noordwijkerhout (1974) 477.

[6] F.P. Küpper et al., Rev. Sci. Instr. 44 (1973) 954.

[7] R.J.J. van Heijningen et al., Plasma Physics 14 (1972) 205.

[8] G.D. Khoe et al., Rijnhuizen Report 73-77 (1973).

[9] P.C.T. van der Laan, Proc. 3rd Eur. Conf. on Contr. Fusion and Plasma Physics, Utrecht (1969) 87.

[10] P.C.T. van der Laan et al., IAEA Proc. 4th Int. Conf. on Plasma Phys. and Controlled Nuclear Fusion Research, Madison (1971) 1, 217.

[11] C. Bobeldijk, Plasma Physics 10 (1968) 567.

[12] C. Bobeldijk et al., IAEA Proc. 3rd Int. Conf. on Plasma Physics and Controlled Nuclear Fusion Research, Novosibirsk (1968) 1, 287.

[13] P.C.T. van der Laan, A. Nijsen-Vis, W. Kooyman, Rijnhuizen Report 72-72 (1972).

REVERSED FIELD PINCHES SET UP BY NATURAL AND DRIVEN FIELD REVERSALS

E P Butt, C W Gowers*, A Mohri#, A A Newton, D C Robinson, A J L Verhage, M R C Watts, Li Yin-An□, H A B Bodin

Euratom-UKAEA Association for Fusion Research, Culham Laboratory, Abingdon, Oxon, U.K.
*AWRE Aldermaston #Institute of Plasma Physics Nagoya, Japan □Inst. of Physics, Academy of Sciences of China, Peking, The People's Republic of China.

Abstract Recent experiments on HBTX I are reported. The relaxation towards a lower energy state, which starts with a helical kink, and can lead to the natural generation of reversed field (self reversal) is described; many of the theoretically expected trends have been identified.

Introduction Studies of reversed field pinches on HBTX I and details of the machine have been reviewed[1]. Recently Thomson scattering experiments have been carried out which show that when the filling pressure, p_o, is reduced from 40-13.5 mtorr $T_e \propto p_o^{-1}$, and the line density varies as p_o. Total radiation measurements confirm that radiation is unimportant in most conditions as a source of energy loss in RFP discharges. In the remainder of this paper we describe observations on self reversal in pinches.

Self Reversal Self reversal is explained as a consequence of the natural relaxation of the plasma towards a state of minimum magnetic energy, which, according to Taylor's β=0 model[2], is a Bessel function distribution. The variation of field reversal ratio $F(t)=B_z(\text{wall},t)/B_z(\text{wall}, t=0)$ with $\theta(t)=B_\theta(\text{wall},t)/B_z(t)$ (averaged over plasma) according to the Bessel function model and a high-β variant (HBM[3]) to represent possible high-β behaviour are shown on Fig 1. ("wall" is the inside surface of the quartz torus, dimensions R = 100 cms, a = 6.0 cms). Stable high-β RFP configurations are expected to lie in or near the shaded area. Theory[2] indicates that in the final relaxed state (a) F<0 (ie RFP configuration) when θ>1.2 . (b) There is an upper limit

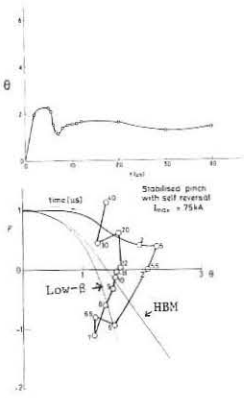

Fig 1 (above) θ vs time and (below) locus of (F,θ) time steps shown in μsec, for stabilised z-pinch at 75 kA.

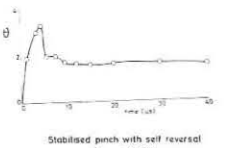

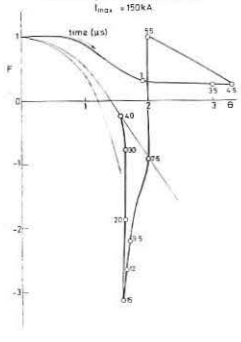

Fig 2 (above) θ vs time and (below) locus of (F,θ), time steps in μsec, for stabilised z-pinch at 150 kA

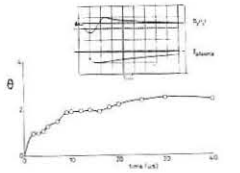

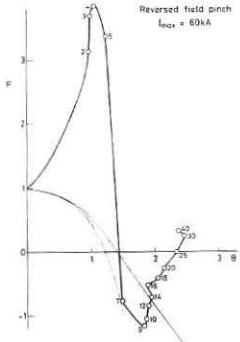

Fig 3 (above) θ vs time showing, inset, waveforms and (below) locus of (F,θ), time steps in μsec, for a driven RFP

of θ = 1.56, and raising the applied volt seconds further drives helical deformations of increasing amplitude but does not change θ (see also Lees and Rusbridge[4] and Kadomtsev[5]). The effect of finite beta is to raise the value of θ at which these transitions occur. The measured value of $\theta(t)$ and the locus (F,θ) are compared with theory in Figs 1-3. Since theory assumes β=0 and a perfect flux conserving shell at the plasma boundary, whereas experimentally $\beta \sim 0.4$ and there is a flux reservoir outside the plasma boundary this comparison is intended to identify qualitative trends.

Fig 1 is for a stabilised z-pinch (SZP) with no applied reversal, in which the current is driven to give an initial value of $\theta_i \sim 2.2$ at 5 μsec and then crowbarred. Fig 2 is for an SZP with $\theta_i \sim 3.5$ at 4.5 μsec in which the driving E_z field is maintained and the I_z current continues to rise for about 15 μsec; Fig 3 is for an RFP with applied reversal programmed so that $\theta_i \sim 1.8$ at 7 μsec. It is found that (1) the locus of (F,θ) tends to move towards the shaded area during the relaxation , independently of the initial values, and then dwells there. This involves a rapid reduction in θ and F; F becomes < 0 when $\theta_i > 2$ (2) θ relaxes to between 1.5 and 2.0 and stays near these values for the remainder of the decay time. (3) very large negative values of F (Fig 2) are associated with strong unstable helical deformations. (4) the fluctuation level was lowest for discharges programmed to lie near the final relaxed state. Plasmas stable throughout the decay have been obtained at 60 kA (Fig 3), compared with 40 kA previously[6], by a new programming sequence in which the applied reversed field was produced on the second half cycle of the fast B_z bank (see inset in Fig 3), leading to better control of the plasma compression at higher currents. The plasma radius is 4.5 cm and that of the metal wall 7.5 cm so no gross m=1 mode is expected and none observed. The decay of the magnetic field configuration appears to be controlled by diffusion. In this case θ increases slowly at later times because B_z decays faster than B_θ. At higher currents such diffusion is usually followed by a secondary relaxation which reduces θ once more[1].

Studies have been made of the relaxation process for $\theta_i \gtrsim 2$ using electrical measurements and calibrated streak photographs. Firstly, an m=1 helical kink grows (Figs 4 and 5) as expected because at $\theta_i \gtrsim 2$ the plasma is

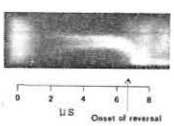

Fig 4 Streak picture of continuum emission from 125 kA self reversed pinch

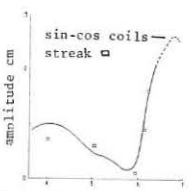

Fig 5 Amplitude of m=1 instability. Stabilised z-pinch.

too compressed for wall stabilisation to be effective. The wavelength and growth rate of this instability agree with numerical predictions using ideal MHD[7]; dissipative MHD gives a similar result for modes with wavelengths >6 cm at these compression ratios: compressed SZP and RFP with $\theta_i > 2$ have very similar properties. Secondly, the kink grows to a large amplitude (radial field component, $B_r \sim$ main field B at r = 2 cm) (Fig 5) and generates flux in the core of the plasma which reduces θ; the total toroidal flux is conserved hence B_z falls in the outer regions. Field reversal can occur at this stage, an effect discussed by Kadomtsev[5].

Finally the helical column breaks up within a microsecond and the current redistributes itself to give a more diffuse RFP plasma, with approximate axisymmetry and no strong helical components ($B_r \lesssim 0.2$-0.3 B). This is to be compared with the axisymmetric relaxed state predicted theoretically[2] when θ<1.56. The optical and electrical data are complex to interpret during and immediately after this process which is not yet well understood, but dissipation is evidently involved. The reversed field once generated usually decays in 30-40 μsec at currents above 100 kA. Sometimes there is evidence of successive decays in field reversal followed by regeneration. Self reversal has only been observed in HBTX I for initial values of $\theta_i > 2$, ie for plasmas which strongly violate kink stability conditions so it is not surprising that the relaxation begins with a large amplitude kink. At $\theta_i \lesssim 2$ weak kink instabilities were observed and the field in the outer region was reduced but not reversed; this is believed to be due to the B_z flux reservoir outside the plasma. It is not possible to say from the present results whether relaxation leading to self reversal can occur without a helical kink instability. In slow experiments such as Zeta[1,3] self reversal leading to axisymmetric RFP states took place both at lower values of θ when no gross kink instability was observed, and at higher values of θ in kink unstable conditions.

Conclusion Experiments on the relaxation leading to self reversal have demonstrated many of the expected trends on HBTX I. Self reversal occurs when the initial value of θ exceeds 2, which corresponds to strongly kink unstable plasmas and the relaxation begins with a helical m=1 instability which grows to large amplitude, followed by a rapid current redistribution towards a diffuse approximately axisymmetric RFP. A limiting value of θ is observed.

References
1) Butt, E.P., Gowers, C.W., Gribble, R.F., Li Yin-An., Newton, A.A., Robinson, D.C., Verhage, A.J.L., 5th IAEA Conf on Plasma Physics and Controlled Nuclear Fusion, Tokyo, 1974, CN-33/E9.2.
2) Taylor, J.B., 5th IAEA Conf on Plasma Physics and Controlled Nuclear Fusion, Tokyo, 1974, CN-33 Post deadline paper
3) To be published
4) Lees, D.J., Rusbridge, M.G., Proc 4th Int Conf on Ionisation Phenomena in Gases, Uppsala, 2 (1959) 954.
5) Kadomtsev, B.B., Proc Conf on Plasma Physics and Controlled Nuclear Fusion Research, Salzburg, 1961, CN-10/227.
6) Robinson, D.C., Crow, J.E., Gowers, C.W., Halsted, G.F., Verhage, A.J.L., Bodin, H.A.B., Proc RPS Conf on Contr Fusion and Plasma Physics, Grenoble 1 (1972) 47.
7) Robinson, D.C., Verhage, A.J.L., 2nd International Congress on Waves and Instabilities on Plasmas, Innsbruck, 1975, Book of Abstracts, P-9.

EXPERIMENTAL STUDIES OF FIELD REVERSAL

A.Buffa, S.Costa, G.F.Nalesso and G.Malesani
Centro di Studio sui Gas Ionizzati
del Consiglio Nazionale delle Ricerche e dell'Università di Padova
(Associazione Euratom-CNR) - Padova (Italy)

Abstract: A number of experiments on toroidal Z pinches, with different values of initial bias field and various degrees of control on the external "flux reservoir" has been performed. In many cases the plasma drives a reversal associated with an instability of the toroidal field near the walls. A first analysis of the collected data is presented.

Introduction: A series of diffused pinches with high values of toroidal current has been produced in the Eta Beta device, operating in Mode II [1], in which the fast θ circuit produce the preionization (in its first quarter of period) as well as the bias field B_{z_o}.

The evolution of the magnetic field profiles (measured by a set of 6 complanar coils) and of the first space harmonica of B_z and B_θ at the vessel's periphery (measured by small coils distributed along a minor circumference of the torus according to the sine-cosine law) have been observed and put in correlation with the variations of the toroidal field outside the plasma ($B_{z_{ext}}$). Experimental evidence of the "self-reversal" of $B_{z_{ext}}$ for a large variety of initial conditions (bias, pressure and compression ratio) has been observed in connection with the growth of an m=1 large amplitude kink instability.

Further experiments and a more detailed analysis of the collected data are in progress.

Experimental Observations: In a first series of experiments (p=40 mtorr H_2) the value of B_{z_o} has been progressively reduced thus increasing the pinch parameter $\Theta_M = (\mu_o \hat{I}_z R_{cb}) / (2 \phi_{z_{tot}})$ measured at peak current, 1.5 μs after the start of I_z (R_{cb} is the equivalent wall radius evaluated at the crow-bar point). The reduction of B_{z_o} gives stabilized Z pinches that show higher and higher compression ratios (see Table I; the figures are averaged over a number of shots). In all cases it has been observed that, after the start of I_z, the average field at the edge of the container $B_{z_{ext}}$, decreases not only during the dynamic phase of the pinch, but also during the following 1 or 2 μs, down to a minimum, $B_{z_{min}}$, that within a given range of parameters is negative (self-reversal).

The reduction of $B_{z_{ext}}$, steady from the beginning, shows sharp variations associated with the appearance of an asymmetry in the pinch and also with the occurrence of interactions with the wall. The $B_{z_{ext}}$ values (even if positive) compared with the total flux, within the crow-bar point of the circuit, $\phi_{z_{tot}}$ (the equivalent area is about twice the area inside the quartz), point out that the flux inside the pinch becomes higher than the value initially present in the tube (see fig. 1): this additional flux seems always larger than allowed by any simple model. The creation of this additional flux may be put in correlation with the instability, which the sine-cosine probes show to appear short time after the I_z maximum (indipendently from the application of the crow-bar to the fast I_z circuit). This instability can be recognized as a fast growing, high amplitude m=1 mode, at least when the compression ratio $Rw/Rp \gtrsim 3$ (Rw=radius of the metall wall), with $KR \simeq 2$, (wave lenght $\simeq 18$ cm.). The starting time of the instability is practically indipendent from the initial bias, while the growth time τ (assumed equal to the time to get the maximum of the coil's signal) seems related to the compression ratio. The minimum observed growth time is $\tau_{min} \simeq 0.4$ μs.

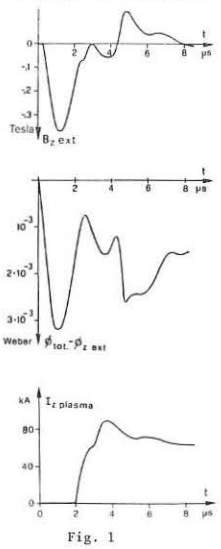

Fig. 1

In our experimental condition, a negative value of $B_{z_{ext}}$ is achieved by self-reversal only with $\Theta \gtrsim 1.6$ (all parameters measured at the flux conserving wall). The RFP-like configuration lasts only for a few microseconds. Two coils, both measuring B_z external, placed in two different positions at 180 degrees along the torus, show a different degree of field reversal: the latter appears as a "local" phenomenon associated with the strong, fast rising instability. This fact is also confirmed by a good correlation between all the signals (streaks, magnetic profiles, $B_{z_{ext}}$ and sine-cosine coils). When the bias field is too low, the reversal is not always clearly observable, which can be explained with a too high compression ratio.

The β_θ of this plasma seems to range from 0.6 to 1, but the error in this measure can be of a factor two. Experiments have been made also at different filling pressures, 20 and 80 mtorr H_2. The main features of the discharge don't vary essentially. It is possible to notice an increasing start time of the instability as well as of the growth time with pressure, the last one more clear at 80 mtorr, probably due to the lower temperature of the obtained plasma.

In an other series of experiments we used a "semi-programming" technique in which the crow-bar of the fast θ circuit was applied after the start of the I_z current, in order to have a larger flux trapped in the plasma (and therefore a small compression ratio) and reduce thereafter $B_{z_{ext}}$ to small (but not of opposed sign) values. The influence of the flux reservoir between the quartz and the flux conserving wall is thus reduced. In these conditions the reversal of $B_{z_{ext}}$ is always obtained. The main differences from the previous experiments is that reversal lasts for longer times (at least 10 μs) following an instability which can't be identified as a pure m=1 mode, and has a smaller amplitude.

In most of the studied cases, the history of the discharge in the Taylor "Z-Θ" plane [2], after an initial driven phase, relaxes towards the region of minimum energy equilibria (evaluated with a simple sharp boundary model, that includes the effect of a finite β_θ [3]. Examples are shown in figs. 2,3,4; here $\Theta = (\mu_o I_z R_{cb})/(2\phi_{z_{tot}})$, and $Z = (B_{z_{ext}} \pi R_{cb}^2)/(\phi_{z_{tot}})$.

Conclusion: Experimental evidence of a tendency of stabilized Z-pinches to relax toward RFP-like configurations following a strong kink instability has been observed. The duration of the self reversal is only few microseconds, while in recent experiments [4] it has been observed for many tens of micro seconds. This can be explained with the short rise time of I_z current in our device which dominated the first phase of the pinch so that the instability and related self reversal start after I_z maximum and can't be sustained be the rise of the current. Due to the large flux reservoir outside the quartz, a high compression ratio is necessary in order to get a large energy available for the reversal. In other situations (reduction of external flux by "semi-programming") a larger self reversal period is observed related to a weaker instability.

We wish to thank prof. G.Rostagni for many usefull discussions.

TABLE I

P (mtorr)	B_{z_o} (kG)	$B_{z_{min}}$ (kG)	$\hat{I}_z$ (kA)	Θ_M	R_w/R_p	Start of instab. (μs)	Growth time (μs)	KR (R=5.7 cm)
20	1.5	-0.35	75	1.3	-	1.0	1.0	1.6
	1.0	-0.7	75	1.5	-	1.5	0.6	2.0
	0.85	-0.7	65	1.6	-	1.5	0.5	2.0
	0.65	-0.9	65	2.4	-	1.2	0.5	1.9
	0.35	-1.0	60	3.3	-	1.0	-	-
40	2.4	0.9	130	1.38	2.0	1.5	1.0	2.5
	1.8	0.2	125	1.5	2.0	1.7	1.5	2.2
	1.0	-0.2	100	1.6	2.7	1.5	0.5	2.0
	0.7	-1.4	90	2.0	2.7	1.5	0.4	2.0
	0.6	-2.0	80	2.5	>3.0	1.5	0.6	-
	0.3	-0.7	80	2.9	>3.0	1.5	0.5	-
80	1.5	-0.01	125	1.7	2.0	-	-	-
	0.9	-0.55	115	3.5	-	2.2	1.0	2.4
	0.4	-1.2	105	3.9	3.0	2.2	1.0	1.8
	0.25	-0.6	95	5.2	>3.5	2.2	1.2	1.8
	0.15	-0.27	90	10.0	>3.5	2.5	1.0	-

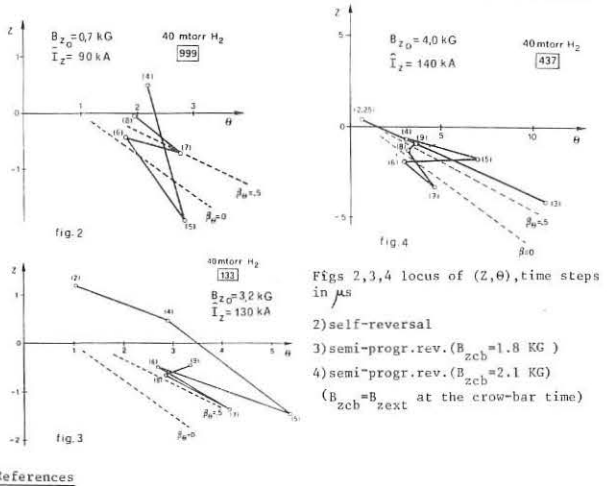

Figs 2,3,4 locus of (Z,Θ), time steps in μs
2) self-reversal
3) semi-progr.rev. (B_{zcb}=1.8 KG)
4) semi-progr.rev. (B_{zcb}=2.1 KG)
($B_{zcb}=B_{zext}$ at the crow-bar time)

References
[1] Buffa,A., et alii - 5th IAEA Conf.-Tokyo 1975; CN-33/E9-3
[2] Taylor,J.B. - 5th IAEA Conf.-Tokyo 1975; post deadline paper
[3] Ortolani,S., Rostagni,G. - UPee Report 75/04 - Padova 1975
[4] Robinson,D.C.,Verhage,A.J.L. - 2nd Congr.Waves Instab. on Plasma-Innsbruck '75

STABILITY AND TEMPERATURE MEASUREMENTS ON ZT-1*

by

D. A. Baker, L. C. Burkhardt, J. N. Di Marco, P. R. Forman, A. Haberstich, R. B. Howell, H. J. Karr, S. Ortolani,** and A. E. Schofield

Los Alamos Scientific Laboratory
of the University of California
Los Alamos, New Mexico U.S.A.

ABSTRACT

Analysis of the magnetic field profiles set up in the ZT-1 pinched plasma, demonstrated that the degradation of the stability of these profiles with time, can be attributed to diffusion. Ion temperature measurements of Doppler broadened He II have determined its scaling over a range of both I_z and $\dot{I}_z$.

We report the behavior of the toroidal z-pinch experiment, ZT-1, operated in the current range 20 to 95 kA with rates of rise between 10^{10} and 2×10^{11} A/s. The experiment was operated with a gas filling of 20% He and 80% D_2 at 40 to 120 mTorr. The He was added to allow ion temperature to be determined from Doppler broadening of He II lines. The formation and time evolution of the reversed field profiles were investigated by varying the rate of change of the reversing field and its timing with respect to the start of the axial current I_z. The rate of reversal of the toroidal magnetic field was controlled by the initial voltage on the reverse field capacitor bank. Magnetic field profiles were obtained from coils inserted into the plasma at 1 cm intervals; five coils measured B_θ and five coils measured B_z.

Flux and Pitch Measurements: For the programming work the $\dot{B}_\theta$(wall) is 3.2×10^5 T/s and the $\dot{B}_z$ varies up to 1.5×10^5 T/s. From magnetic field profiles the motion of flux tubes and the time behavior of the pitch of the magnetic field lines were obtained. It is observed that there is motion of the poloidal and toroidal flux tubes with respect to each other, the poloidal flux penetrating more rapidly. During the interval explored, ~ 1 μs with respect to the onset of I_z, the timing is unimportant. Values of the pitch, $P = rB_z/B_\theta$, greater than ~ 0.03 m are not affected by the rate of reversal of the magnetic field or its timing. The evolution of the small values of pitch, i.e., $P \sim 0.015$ m, is modified by the rate of reversal. During the discharge, the larger values of pitch are seen to disappear on axis, see Fig. 2, an effect that can only result from diffusion of the magnetic field. Under these conditions the pitch profile cannot be programmed into the discharge by a matching of the pitch at the wall to the pinch motion, by assuming that the flux tubes are "frozen" into the plasma.

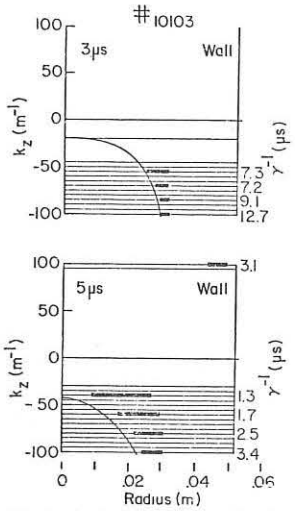

Fig. 1. Stability diagram of a 40 mTorr discharge with low PI and delayed B_z reversal. k_z is the axial wavenumber, and γ^{-1} the growth time of unstable m = 1 modes.

MHD Simulation: The stability diagram shown in Fig. 1 is produced from probe data under the assumptions of cylindrical geometry, ideal incompressible MHD, and equilibrium. Only the fastest growing m = 1 modes are considered. The lines crossing the diagram horizontally are unstable axial wavenumbers k_z. Five of the unstable k_z's are analyzed for normal modes. The width and location of these modes are indicated by heavy horizontal bars and their growth times are shown on the right hand side of the diagram. The remaining curve in the diagram is the locus of $-1/P$.

The results of several such stability analyses indicate fairly good initial MHD stability followed by a gradual deterioration of the stability conditions. This late behavior has been tentatively attributed to diffusion. A one dimensional resistive MHD calculation was performed to simulate the experiment. The magnetic field profiles measures at 3 μs, corresponding to the data of Fig. 1, have been entered as initial conditions, and the code was run for 2 μs discharge time. The initial radial dependence of the ion and electron temperatures was assumed to be parabolic with $T_i = T_e$ = 20 eV on axis, and 10 eV at the wall. The initial density profile followed from pressure balance. The expression for the electrical resistivity tensor was varied until the calculated profiles approximated those measured at 5 μs. The calculated magnetic field profiles were then analyzed for stability. The resulting stability diagram at 5 μs was found to be almost identical to the one obtained experimentally. This shows the slow change in the ideal MHD stability of the pinch can be interpreted on the basis of a diffusion model. The value of the electrical resistivity necessary to duplicate the experiment is essentially classical on axis with a 100-fold exponential increase towards the wall of the discharge tube. There is an enhanced energy loss due to the electron thermal conductivity being linearly related to the electrical resistivity. No other losses were allowed in the calculation. Radial measurements of the electron density and temperature will be needed to identify the nature of the transport coefficients.

A comparison of the measured parallel and perpendicular current densities at the intermediate time of 4 μs shows the parallel current is much larger than the perpendicular current over most of the interior of the discharge. It has been suggested[1] that the lower hybrid drift instability may be responsible for an anomalous resistivity which could cause the observed fast diffusion in ZT-1. This instability is driven by the perpendicular electron drift velocity and can give anomalous resistivity even when $T_i > T_e$.

New experimental conditions have been explored in which higher bias fields are used and both the B_z and B_θ fields rise in approximately 2 μs. Sharper, slower diffusing profiles, having improved stability diagrams for the early times, are observed as compared to previous discharges. These data are being analyzed and results will be presented at the meeting.

Ion Temperature Measurements: Ion temperatures have been determined from the width of the Doppler broadened 468.6 nm line of He II. Comparison of the broadening of the 320.2 nm He II line with that of the 468.6 nm He II line confirms that the broadening of the latter is mainly Doppler broadening.[2] Additional measurements with impurity ions, C, Ne, N, and Ar, indicate the helium and deuterium ion temperatures should be the same.

The deuterium ion temperature was determined as a function of I_z and $\dot{I}_z$ for several values of initial bias field. T_i was observed to decrease with increasing initial bias field, while it increases approximately linearly with both I_z and $\dot{I}_z$. Typically $T_i/\dot{I}_z = 1.7 \times 10^{-10}$ eVs/A. A graph of the temperature dependence upon I_z is shown in Fig. 3. The temperature plotted is that measured after the implosion of the pinch. The ion temperature is then approximately constant or slowly decreasing in time. The line shapes of impurity ions during the formation of the pinch are not Gaussian but rather are double peaks suggestive of directed motion associated with imploding fronts. This velocity compares reasonably well with that obtained from streak photographs.

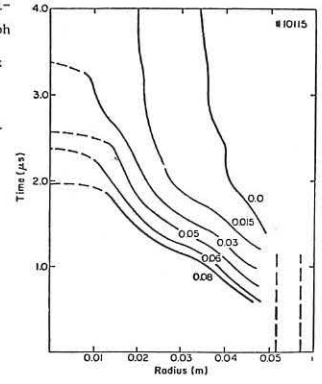

Fig. 2. Radial time dependence of specified values of pitch.

* Work performed under the auspices of the U.S.ERDA.

**On leave of absence from Centro di Studio sui Gas Ionizzati del Consiglio Nazionale delle Ricerche e dell'Universita di Padova (Associazione Euratom-CNR)-Padova (Italy).

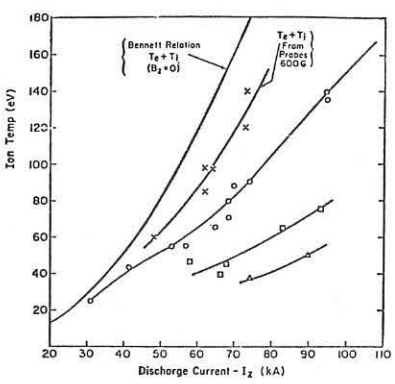

Fig. 3. Ion temperature vs. discharge current for several bias fields. Circles are 0.06 T, squares 0.105 T and triangles 0.15 T.

REFERENCES:

1. N.T. Gladd and R. C. Davidson, "Anomalous Transport Properties Associated with the Lower-Hybrid-Drift Instability," to be published Phys. of Fluids.
2. H. R. Griem and H. J. Kunze, "Stark Broadening of Two Ionized-Helium Lines by Collective Electric Fields in a Laboratory Plasma," Phys. Rev. Lett 23, 1279 (1969).

CONFINEMENT OF HIGH β PLASMA IN TPE-1 (REVERSED FIELD PINCH)

K. Ogawa, T. Shimada, S. Kiyama, Y. Hirano,
Y. Maejima and I. Hirota

Electrotechnical Laboratory, Tanashi, Tokyo, Japan

Abstract: The experimental study of the confinement of the high β toroidal pinch plasma in the reversed field pinch configuration. The experiment is carried out on ETL TPE-1 (R= 40cm, a=5cm, $I_p \sim 100$kA). The main object of this paper is to describe how the RFP configuration is set up by the fast programing of the currents (z and θ).

Introduction: ETL TPE-1 is the experimental apparatus for the confinement of a high β toroidal plasma in an axisymmetric magnetic system. The experimental results of equilibrium and stability in a screw pinch configuration in the range of plasma temperature of over 100eV ~ 30eV were reported at IAEA Tokyo Conference.[1] The short summary of the remarkable results that (1) in the low q value region ($q<1$, high current region), it was not be able to confine the stable equilibrium plasma in the toroidal screw pinch configuration due to the MHD kink instability, (2) in high q value region ($q>1$), the stable plasma in the so-cald high β tokamak configuration was confined in a rather longer period, typically, 40 ~ 50 μsec. However, in this case β value in the confinement phase is only several percent in this rather slender torus. So, the special characteristics of the fast compression obtaining the high temperature, high density and high β plasma in the early dynamic phase was losed in the transient to the confinement phase from the dynamic phase. The energy loss in this process was so large and this loss was inevitable in order to that the plasma establishes itself in the stable configuration, (3) In order to obtain the stable pinch plasma the special concerns in our experiments were paied to the followings; (a) by changing the bias toroidal magnetic field β_p value was controlled for obtaining a adequate toroidal equilibrium, so the plasma did not pinch so strongly and T_e does not rise so big and (b) the radial distributions of q value was controlled by changing the time duration between the starts of z and θ pinches (z procedes), so that the pitch minimum configuration might not appear.

Thus, if we want to obtain a higher β plasma ($\beta \gtrsim 20\%$) in a stable toroidal configurations by the fast pinch, we must have a very fat torus(even so, probablly, $\beta \sim 10\%$), or dynamically controll the plasma in the compression phase so that it may don't lose it's energy, for example, by the application of the pulse vertical magnetic field.

On the other hand, the stable RFP which has been studied by several groups[2),3),4)], is obtained with a high β value,i.e. 0.3 ~ 0.4 and does work with higher plasma current ($q < 1$). This configuration has usually a large bias field and $\beta_p < 1$ because of $|B_z| = |B_\theta|$, so no problem is in obtaining the equilibrium.

Table 1

Electrical Parameters for R.F.P. (R=40cm, r=5cm)

circuits			II	III
θ	$V_{\theta\,max}$	(kV)	40	40
	$\frac{3}{4}$	(μsec)	2.6	3.9
	$I_{\theta\,max}$	(kA)	2.2 (30 u.)	2.0 (40 u.)
	RIPPLE OF CROWBAR	(%)	19.5	8.6
Z	$V_{z\,max}$	(kV)	40	40
	$\frac{3}{4}$	(μsec)	2.8	3.94
	$I_{z\,max}$	(kA)	270 (16 u.)	197 (16 u.)
	RIPPLE OF CROWBAR	(%)	15.5	8.4
Bias	$B_{z\,max}$	(kG)	2.2	4

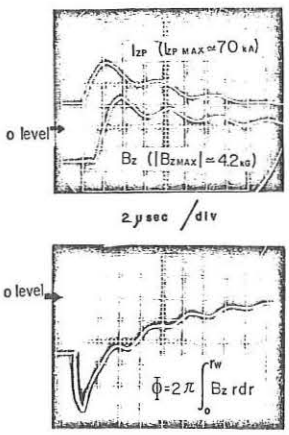

Fig. 1
He, $p_0 = 5.0$ m Torr, B_z bias $= 2.2$ kG

Experiments of RFP: TPE-1 was recently arranged for the RFP experiments from the SP experiments reported before.

Table 1 is the electrical parameters of RFP in TPE-1. So far, the experiments were mostly in the RFP-II parameters shown in Table 1. Helium gas was used for the experiments in the filling pressure of 30 ~ 50mTorr.

The examples of the oscillograms of the plasma current, the magnetic field at wall and the total flux over the cross section are shown in Fig.1.

The RFP configuration in TPE-1 is set up by the fast programming of the coil currents. First of all, the bias B_z field is applied, then the plasma is pre-ionized by the high frequency z and θ discharges. At the appropriate value of bias B_z field, the main z discharge precedes the main θ discharge which reverses B_z field. This time delay ($\tau_{z\text{-}\theta}$) is important to generate a stable configuration. The both currents (z and θ) are crowbared at their maximum where the stable configuration might be generated.

Fig.2 shows the measured time history of the magnetic field configuration.

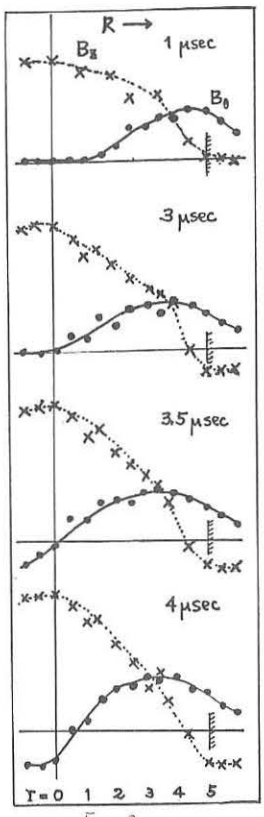

Fig. 2.
He, $p_0 = 5.0$ m Torr, B_z bias $= 2.2$ kG.
$I_{zp\,max} \simeq 70$ kA, $|B_{z\,max}| = 4.2$ kG.

Discussions: The preliminary experiments of RFP in TPE-1 are successfully being done. The RFP configuration set up in TPE-1 is close to the stable one with high β theoretically predicted. In this case, T_i is 20eV at 4μsec ~ 4.5μsec evaluated from the Doppler broadenning of H_e II 4686 Å. T_e rises linearly to 12eV from 2eV(at 1μsec). The time described in this paper is from the start of z discharge. After 5μsec, the magnetic flux (Φ) diffuses rappidly due to the strong instability originated from the ripple of the currents. This is also clearly observed by the streak pictures. The bank is now rearranged for RFP-III shown in Table 1. The ripple will be reduced and the stability will be improved and we hope, we can investigate the transport phenomena of stable RFP.

Fig.3 shows the RFP configuration calculated by the computer simulation of the one dimensional two fluids plasma model with the RFP-III parameters in TPE-1.

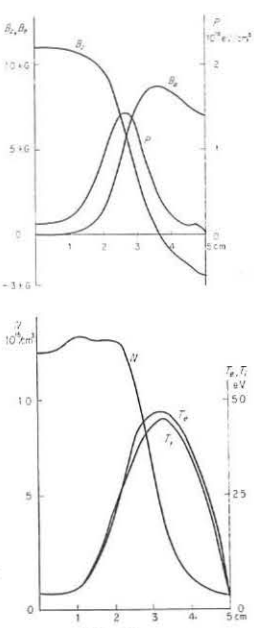

Fig. 3.
D_2 gas, $N_e = 5 \times 10^{15}$/cm.
B_z bias $= 4$ kG, $I_{zp} \simeq 70$ kA (max),
$|B_{z\,max}| \simeq 4$ kG

Acknowledgement: The authors would like to express their thanks to Mr.s S.Takeda and Y.Sato for their helps of engineering problems. They also wish to thank Dr. T.Tamaru for his support.

References:

1) K.Ogawa et al.; 5th IAEA Conference, Tokyo, 11-15 Nov.(1974) CN-33/E9-4.
2) E.P.Butt et al.: ibid. CN-33/E9-2.
3) D.A.Baker et al.; ibid. CN-33/E3.
4) A.Buffa et al.; ibid. CN-33/E9-3.

The Belt Pinch II Experiment with Improved Shock Heating

O. Gruber, R. Wilhelm
Max-Planck-Institut für Plasmaphysik, Garching, Germany, Euratom Association.

Abstract: In the Belt Pinch II experiment plasma stability was obtained in a noncircular-high ß-Tokamak configuration for around 20 MHD growth-times at critical q-values ($q \approx 3$), comparable to those of low β circular Tokamaks. This decisive question is investigated further in the new 160 kV shock-heated version at longer confinement times and higher temperatures.

In the first experimental step of the Belt Pinch II (40 kV shock heating) device the energy confinement time was limited by impurity radiation to $\tau_E \simeq 30$–40 µs. Thus the ohmic heating by poloidal and toroidal plasma currents could sustain the high-ß-phase ($\langle\beta\rangle \gtrsim 50$ %) only for around 50 µs. The strong influence of the mentioned loss mechanism has been demonstrated by an admixture of a fraction of oxygen comparable to the natural oxygen content of the discharge (typically 0,4 % at $\langle n_e\rangle \approx 7.10^{14}$ cm^{-3}). In this case the ß-decay was increased as expected.

A first improvement was obtained using a lower filling pressure (2 mTorr instead of 5 mTorr D_2). At average densities of about $\langle n_e\rangle \approx 3.10^{14}$ cm^{-3} but practically constant impurity level the influence of the radiation was reduced and the ohmic heating becomes more effective. First measurements indicate a slower decay of the plasma diamagnetism at somewhat increased temperatures (40–60 eV). Now a further improvement for the compressional heating is obtained using the fast high voltage system at these low densities.

The technical concept is shown in Fig. 1. At the end of the preionization phase an homogeneous plasma with $\langle n_e\rangle \approx 3$–$6.10^{13}$ cm^{-3} is achieved, which corresponds to an ionization degree of 50 to 60 %. In addition the transmission line is magnetized so that the preionization bank is decoupled from the main bank. Furthermore the transformer core is saturated in such a way that a complete flux reversal by the heating bank is possible. When the main bank and the heating bank are fired the sum of both voltages appears at the coil. The energy content of the heating bank and the iron cross section are chosen so that the first compression and the following ringing is in resonance with the bouncing plasma at a density range of about $\langle n_e\rangle \approx 2.10^{14}$ cm^{-3}. After a final saturation produced by the main bank the heating bank is decoupled from the main circuit. Then the toroidal magnetic field is kept constant by the crowbar system in the main bank (see Fig. 2).

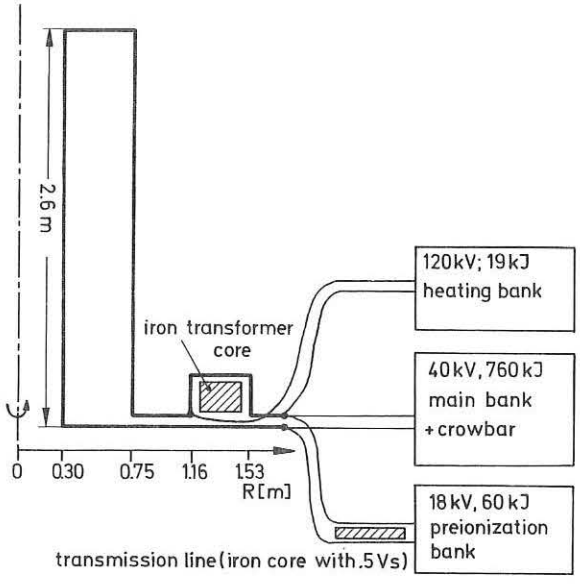

Fig. 1: Electrical Circuits

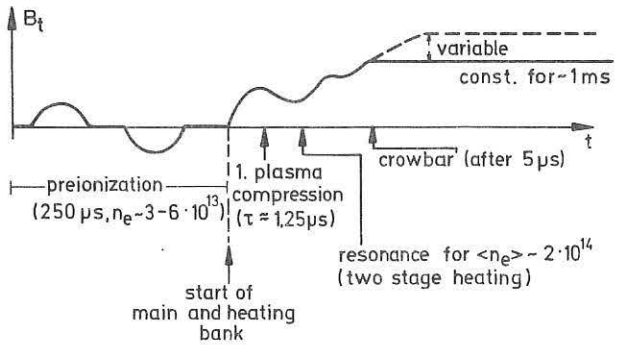

Fig. 2: Toroidal Fields

Using this technique a temperature range above 100 eV (after therma lisation) should be obtainable. Under these conditions the lower ionization stages of the impurities (i.e. oxygen I-VI) are burned out and the radiation losses are reduced by more than an order of magnitude. As a consequence the ohmic heating due to the toroidal and poloidal currents should overcome the radiation losses. Thus the stability behaviour in the Belt Pinch can be investigated during longer confinement times.

Based on an earlier work of Düchs a diffusion code was developed including different energy loss mechanisms/1/ (radiation, effects of neutrals, heat conduction). This code will be used to find in the experiments those plasma parameters which are compatible with an approximately constant temperature during the unavoidable ß-decay at $\beta_{pol} > 1$, and without particle injection. This would open to the Belt Pinch the range of lower β-values ($\beta \simeq 10$–20 %) amd β_{pol} -values lower than the aspect ratio, but higher than 1. The results of these experiments will be reported at the conference.

Reference

/1/ G. Becker, D. Düchs, APS-Conference, Albucherque, Bull. APS, 19, II (1974)

ENERGY AND ß-EVOLUTION DURING THE INITIAL CONFINEMENT PHASE IN THE TEE COMPACT TOROIDAL EXPERIMENT

P.G. Carolan, M. Dembinski[+], M. Korten, F. Sand[x], F. Waelbroeck, G. Waidmann

Institut für Plasmaphysik der Kernforschungsanlage Jülich GmbH
Association EURATOM-KFA

[+] Institute of Fundamental Technological Research/Warshaw

[x] Laboratori Gas Ionizzati, Frascati (Roma)

Abstract

The energy evolution and the behaviour of the plasma parameters ß, $ß_e$, T_i, n_e during the initial confinement phase of the TEE experiment will be described. Several energy loss mechanisms are discussed and their relative importance for the energy decay in the TEE experiment is estimated.

In the TEE compact torus experiment (R = 25 cm, a = 9.5 cm) the behaviour of a high-ß tokamak-like plasma is investigated. The vacuum vessel cross section is circular. Fast magnetic compression generates a plasma with initial ß-values higher than obtained so far in tokamak experiments. The main characteristics of the experiment have been described earlier [1]. For the present set of investigations a toroidal field maximum of B_φ = 4.5 kG is chosen which is reached in 1,8 /us. The fast rising fields limit the effect of an adiabatic compression which would increase the R/a value. Moreover, small positive bias fields ($B_\varphi^o \approx 100$ G) and small filling pressures (1./.2 mTorr) were used to restrict ß to the maximum tolerable value expected from equilibrium theory, $ß \approx \frac{a}{Rq^2}$. The energy and ß-evolution is studied in the quasi-stationary phase after crowbar of the main discharge.

The diagnostics used to study the evolution of plasma parameters and energy losses are magnetic probes inserted into the plasma to measure spatially resolved poloidal and toroidal magnetic fields [2], Doppler-broadening of impurity lines which yield the ion temperature, magnetic coils on the outside of the vacuum vessel which give the position of the toroidal current, a 2-mm microwave interferometer to obtain the spatial resolved electron density, and spectroscopic methods to determine the impurity concentration and the neutral particle density. A laser-light Thomson scattering diagnostic to obtain the electron temperature is in preparation.

The plasma behaviour and the energy evolution in the quasi-stationary phase after crowbar was investigated using ion-temperature measurements and magnetic probe measurements applying tokamak equilibrium theory [2]. At crowbar time, the main plasma parameters can be characterized as follows: R ≈ 27 cm, a ≈ 7 cm, ion temperature T_i = 120./.150 eV, $\bar{n}_e \approx 1.\ 10^{14}\text{cm}^{-3}$, toroidal plasma current I_p = 20./.25 kA, $ß_p \lesssim 3$, q(a) = 2./.3, ß = 3./.10%, plasma energy $\mathcal{E}_p \approx 100$ J, degree of ionisation $\alpha \approx 50\%$. The plasma toroidal current I_p decays in $\tau_I \approx 60$ /us (e-folding time), but the energy of the plasma is lost much faster.

Assuming equilibrium, the energy development can be derived from poloidal field measurements which gives a decay time constant of $\tau_e \approx 10$ /us (Fig. 1). A similar result is obtained for the poloidal $ß_p$ which comes down to 1 in about 10 /us and then remains almost constant, $ß_p \lesssim 1$. The temporal behaviour of the ion temperature shows a similar dependence; T_i is less then 50 eV after 6 to 10 /us (Fig. 2). Measurements of the toroidal ΔB_φ field [3] confirm the fact that the "diamagnetic" energy is lost preferentially, whereas at the field maximum it contains about 50% of the total plasma energy.

Several loss mechanisms are suggested to explain the fast energy decay. Centrifugal momentum to the outside during the implosion phase could be a reason for wall contact in the earlier confinement time which may cause plasma energy losses that could be reduced only if field programming is improved to provide a better control of the plasma position. Moreover, after crowbar, perturbations of the toroidal symmetry have been observed which have approximately the length of the torus and could be interpreted as kink modes which are predicted for a high-ß tokamak for an aspect ratio of A = 4 with a stability margin for the critical ß-value between 3% and 6% [4]. Poloidal field measurements, too, show strong plasma movements in the first 15 /us after crowbar, as can be seen in the plot of lines with equal poloidal flux versus time (Fig. 3).

Radiation losses due to impurity lines were estimated not to contribute dominantly to the energy decay. The most prominent impurity elements were found to be carbon with 0.3% and oxygen with 0.75%. Considering oxygen to be here the most dangerous impurity, radiation losses can be estimated according to [5]. As an upper limit, energy loss of about 0.20 J/ /us could be emitted as line radiation of oxygen ions.

However, energy loss due to charge exchange processes plays a more dominant role. The total neutral particle density was measured by the absolute determination of the D_α-line radiation to be $n_N \approx 2.5.10^{13}\text{cm}^{-3}$ at crowbar time. Then, after a few /us, n_N drops to a nearly constant value of $n_N \approx 1.10^{13}\text{cm}^{-3}$. It may be concluded that plasma-wall-interaction causes a continuous influx of neutral particles which leads to an average charge exchange energy loss of about 10 J/ /us. According to [6] the plasma should be in the diffusive regime with an outer layer of $L_n \approx 4$ cm thickness, and a large plasma volume must be considered to be in wall contact. Strong losses due to neutral particle transport must be expected. This is corroborated by the observed increase of the electron density after crowbar, because for these temperatures the ionization rate is not very much lower than the rate for charge exchange processes.

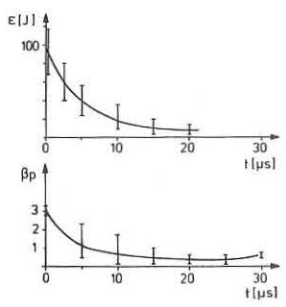

Fig. 1

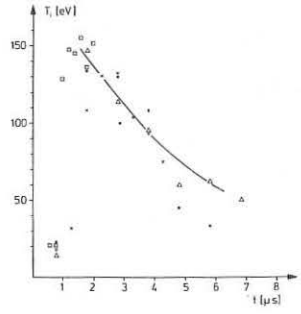

Fig. 2

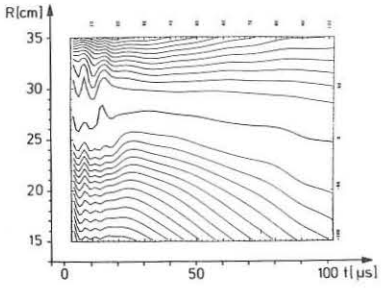

Fig. 3

[1] P. Noll, M. Korten, E. Kugler, F. Sand, F. Waelbroeck, G. Waidmann: Proc. 6th Europ. Conf. Contr. Fusion Plasma Physics, Moscow, 1973

[2] M. Korten, P.G. Carolan, F. Sand, F. Waelbroeck: Report KFA-Juel-1190 (to be published)

[3] P.G. Carolan, M. Korten, F. Sand, G. Waidmann: Submitted to: XIIth Int. Conf. on Phenomena in Ionized Gases, Eindhoven, 1975

[4] J.P. Freidberg, J.P. Goedbloed, W. Grossmann, F.A. Haas: Proc. Vth Conf. Plasma Physics Contr. Nucl. Fusion Res., Tokyo, 1974

[5] W. Engelhardt, G. Bateman: Proc. 5th Europ. Conf. on Contr. Fusion and Plasma Physics, Moscow, 1973

[6] G. Podesta, F. Engelmann: Proc. 3th Int. Symp. Pl. Conf., Garching, 1973

Effects of Pulsed Vertical Field
on the Fast High Beta Tokamak Experiment

K. Hirano, S. Kitagawa, M. Mimura and Y. Kita
Institute of Plasma Physics, Nagoya University
Nagoya, JAPAN

Abstract: The pulsed vertical field, having the same rise time as that of the plasma current, is applied to suppress violent toroidal drift which appears at the beginning of the discharge. It is found that proper value of the vertical field is effective to improve plasma parameters.

The fast axisymmetric toroidal pinch-STP with small aspect ratio is constructed to improve the limit of the density and temperature which is observed in the present tokamak discharges. Various scaling laws for tokamak show that high density is the key point to obtain longer confinement time. Our present purpose is to study the tokamak configuration around the density of $10^{15}/cm^3$. The schematic drawing of our STP system is shown in Fig.1. The major and minor radius of the STP is 25 cm and 10 cm respectively. The coils to excite the pulsed vertical field are fixed inside the copper shell. The maximum vertical field strength is 500 G at the tube axis and its rise time is equal to that of the plasma current. Most of the experiments reported here are carried out under the toroidal field of 8 to 10 kG with the plasma current from 60 to 100 kA. The usual operating D_2 pressure is 10^{-2} torr. A typical example of horizontal streak photographs, showing the effect of pulsed vertical field, are given in Fig.2. It is seen that the pulsed vertical field moves the plasma to the major axis. The instantaneous poloidal field distribution just inside the copper shell is measured by means of eight small pick-up loops. The results are also shown in Fig.2: the correlations between these two measurements are easily seen. In accordance with the streak picture, poloidal field distribution is evidently shifted to inner side of the torus. In case of no vertical field, however, poloidal field distribution suggests that the plasma is rapidly split into two parts and that it perhaps contacts the wall, which is presumable from the strong light emission observed when the deformation reaches its maximum. The surface q value at the instant of the maximum m=2 distortion happened to be 2. Note that such a strong m=2 deformation is not seen when the pulsed vertical field is applied. The magnetic probes inserted into the plasma show diamagnetic effect when the vertical field is applied, while, with no vertical field, probe signals become paramagnetic. The local β value proved to drop very quickly as soon as the strong m=2 distortion appears. The typical β value with the vertical field ranges from 6 to 10 % and no catastrophic decay of β is observed. Since obtaining the above encouraging results, the following several modifications of our STP have been done:

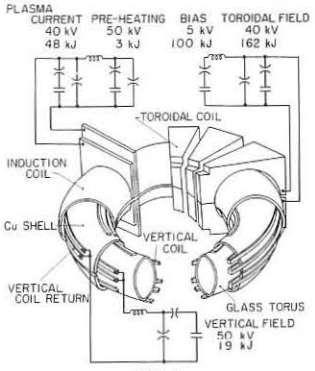

Fig.1
A schematic drawing of the STP apparatus

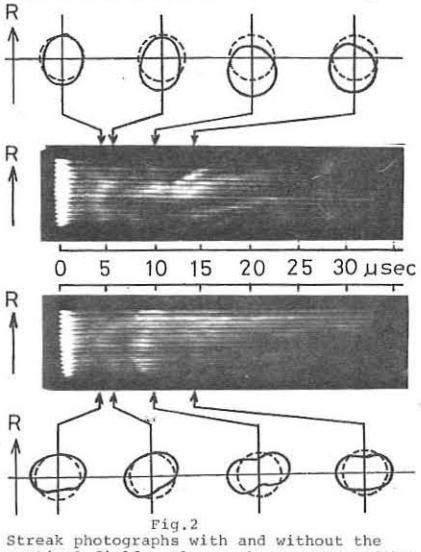

Fig.2
Streak photographs with and without the vertical field. Plasma shapes measured by 8 pick-up loops are also illustrated.

(1) In order to obtain complete ionization, series capacitor for power crowbar is inserted into the pre-heating circuit. Consequently 10 kA pre-heating current, the rise time of which is 3μsec, is sustained for 30μsec without decay.

(2) A series inductance is inserted into the driving circuit of the plasma current so that the decay of the current can be moderated. As can be seen in Fig.3, the decay rate of the plasma current is much decreased.

(3) Freidberg predicted[2] that the shape of the plasma cross-section may change at every different toroidal position. In order to check his prediction small pick-up loops inside the shell is increased from 8 to 60 for the purpose of studying the accurate plasma shapes. A typical streak photograph after this modification is shown in Fig.4. Although the results are preliminary and the parameters are not optimized yet, no sign of violent instability nor toroidal drift is seen on the picture. In accordance with this picture no violent behaviour appears on the trace of the magnetic probe signal inserted into the plasma.

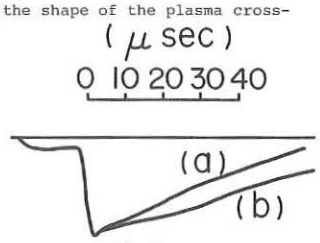

Fig.3
Waveforms of plasma current: (a) without series inductance b) with series inductance.

The authors acknowledge Prof. K. Takayama and Prof. H. Yoshimura for their continuous encouragement.

References

(1) Kei-ichi Hirano et al. Tokyo meeting IAEA-CN-33/E9-5 (1974, Tokyo)

(2) Freidberg, private communication

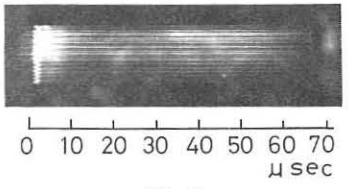

Fig. 4
Streak photograph of the plasma after modification of the apparatus. In this case maximum plasma current and toroidal field is 100 kA and 8 kG, respectively. In order to take the bright photograph 30 % Helium gas is introduced into D_2 gas.

Z-PINCH EXPERIMENTS WITH A NOVEL INDUCTIVE ENERGY STORAGE SYSTEM

I.R. Jones, E.L. Murray, M.G.R. Phillips, P.G. Weber
The Flinders University of South Australia
Bedford Park 5042 South Australia

ABSTRACT: A description is given of the generation of a Z-pinch using a novel circuit which both produces large initial power inputs and inhibits secondary wall breakdown.

INTRODUCTION: The Los Alamos Z-pinch group observed in 1968 (1) that none of the Z-pinch experiments performed to that date had achieved the initial power inputs realised in the larger θ-pinches. A large power input produces a high degree of shock heating and reduces the interval when the plasma loses energy rapidly by bound state transitions. Increasing the initial power input to a Z-pinch by increasing the charging voltage on a conventional capacitor bank is ineffective since a large fraction of the initial voltage remains between the electrodes after the pinched plasma has been formed. This causes a secondary breakdown near the discharge tube wall which screens the central plasma column from the compressing magnetic field (2). The problem becomes more acute the higher the initial bank voltage. The Los Alamos group avoided this problem by using a magnetic energy storage circuit and an exploding foil switch to transfer the current to the discharge tube (3). This paper describes the generation of a Z-pinch using a novel circuit (4) which both produces the desired fast initial current rise and inhibits secondary breakdown. This circuit is much more convenient to use than the Los Alamos circuit. Some preliminary measurements on the properties and stability of the pinched discharge are presented.

APPARATUS: The discharge tube was 10 cm in diameter (i.d.) and had ring electrodes at each end separated by 50 cm. The ring electrodes allowed streak and framing pictures to be taken through end windows. The return current conductor consisted of an aluminium mesh wrapped around the exterior of the discharge vessel. Discharges were made in preionized deuterium at filling pressures, P_F, of 12-35 mTorr, with quasi-steady axial magnetic fields, B_o, of up to 4 KGauss. Fig. 1a shows an idealised form of the circuit used to produce the Z-pinch. L_p is the load inductor (discharge tube plus some transmission cables). The capacitor C_F is chosen to give the desired rise time, $\tau_R = (\pi/2)(L_p C_F)^{\frac{1}{2}}$. The inductor L_S and the capacitor C_S serve for energy storage and are chosen such that $L_S \gg L_p$ and $C_S \gg C_F$. At the beginning of the operating sequence, all switches are open and the capacitors C_S and C_F are charged to the voltages $V_S = +I(L_S/C_S)^{\frac{1}{2}}$ and $V_F = -I(L_p/C_F)^{\frac{1}{2}}$ respectively, where I is the desired current. At the time $t_A = -(\pi/2)(L_S C_S)^{\frac{1}{2}}$ the switch A is closed and at the time $t_C = -(\pi/2)(L_p C_F)^{\frac{1}{2}}$ the switch C is closed. Thus, at t=0, the currents I_S and I_p have reached equal magnitude I, while the voltages on both capacitors are zero. At this time the switch B is closed thus linking the inductors into a loop in which the current I circulates indefinitely while the capacitors remain uncharged (See Fig. 1b). In our present prototype apparatus C_F = 2.06 μF; C_S = 5400 μF; L_p = 391 nH; L_S = 1.84 μH; V_S = 1400 V; and V_F = 20000 V. In practice, stray inductances modify the situation and the actual current pulse through L_p has the form shown in Fig. 1c. The voltage across the discharge tube is also shown in Fig. 1c; note that the voltage gradient does not exceed ± 40 volts/cm after the initial voltage pulse.

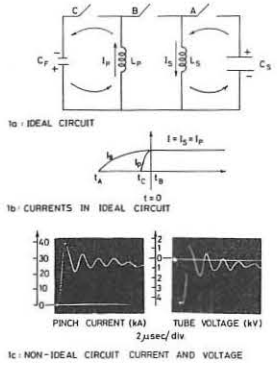

Fig. 1.

MEASUREMENTS: Fig. 2 shows a streak photograph of the Z-pinch and a series of framing pictures, both taken with P_F = 35 mTorr D_2 and B_o = 1.3 KGauss. The photographs have been time-correlated with the current waveform. These pictures show that the plasma pinches to the axis of the discharge tube in about 1 μsec and thereafter remains grossly stable and cylindrical in shape for about 4-5 μsec. The onset of instabilities can then be seen. There is no evidence for secondary wall breakdown. Magnetic field measurements have been made using a probe which slides inside a ceramic tube (2mm o.d.) located across a discharge tube diameter at the mid-plane. Fig. 3 shows the radial field profiles at t = 2 μs in a discharge having P_F = 35 mTorr and B_o = 1.3 KGauss. Note that these profiles were constructed from many experimental shots; the smoothness of the data reflects the reproducibility of the discharges. The j_z radial profile, deduced from the B_θ profile, shows that the total discharge current is nearly uniformly distributed over the cross section of the plasma column at this time. Again, no evidence for secondary breakdown at the discharge tube wall is seen in the magnetic probe data.

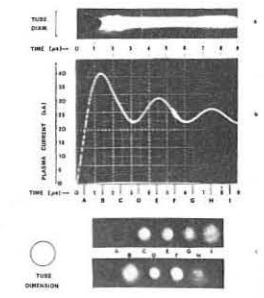

Fig. 2.

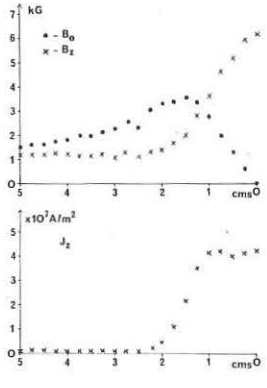

Fig. 3.

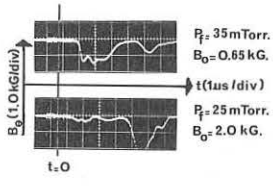

Fig. 4.

that the electron temperature in this discharge is approximately 10 ev. A measure of the gross stability of the discharge was obtained by examining the value of B_θ at r=0. Its value should remain zero until an instability displaces the pinched current channel. Typical measurements are shown in Fig. 4 for two different discharges conditions.

Further measurements will be made on the plasma using Thomson scattering and holographic interferometry. A one-dimensional hydromagnetic code (5) is being used to interpret and predict the plasma characteristics in the stable regime of the pinch.

References:

(1) DiMarco, J.N., Burkhardt, L.C., LASL Rept LA-4075-MS (1968)

(2) Bodin, H.A.B., Newton, A.A., Peacock, N.J., Nuc. Fusion 1, 54 (1960)

(3) DiMarco, J.N., Burkhardt, L.C., J. Appl. Phys. 41, 3894 (1970)

(4) Weibel, E.S., Jones, I.R., Rev. Sci. Instr. 32, 972 (1961)

(5) Hofmann, F., I.A.E.A. Conference, Madison, Vol I, 267 (1971)

FAST THETA-PINCH PLASMA HEATING EXPERIMENTS

A.B.Andrezen, V.A.Burtsev, V.N.Litunovsky, V.G.Smirnov

D.V.Efremov Scientific Research Institute of Electrophysical Apparatus, Leningrad, USSR

Abstract: The main aspects of the experiments described below are the following: shock plasma heating study, diagnostics method development of fast plasma process investigation, as well as the design of the electrotechnical apparatus for creation of high fast-rising magnetic fields.

Initially plasma heating investigation in a Θ-pinch discharge was carried out in a general way with the direct condenser battery power supply of the coil. The main purpose of this investigation is not to obtain high plasma parameters, but to work out the holographic plasma interferometry method in the well-known physical conditions.

The three-turn coil has the inner diameter d=12 cm and the length l=35 cm. In the experiments the condenser battery with the capacity C=8 μF and the voltage of 50 kV have been used. The self period of the discharge loop is T=12μsec. The initial longitudinal magnetic field up to B=3 kgauss can be created. In these investigations the preliminary gas ionization has not been carried out. As is known, in these conditions at the beginning of the first half-wave of the discharge current in the chamber the cylindrical shock wave is generated, providing the cylindrical shock wave is generated, providing the sufficient gas preionization for the effective plasma collapse in the second half-wave of the current [1].

In fact, the measurements, carried out by the magnetic probing, fast photography and the holographic discharge interferometry [2] showed that at the end of the first half-wave of the current the plasma laver is formed, which captures the longitudinal magnetic field. The plasma cylindrical layer pinching continues at the beginning of the second half-wave of the current, but by the inverse sign field, the captured field value at the chamber axis being increased.

When the captured field is fully dissipated, the electron density profile becomes single-hilled, and the pseudopressure is changed into the proper plasma pressure (fig.1). At this moment the plasma temperature estimation on the pressure balance condition gives (Te+Ti)$\lesssim$100 eV.

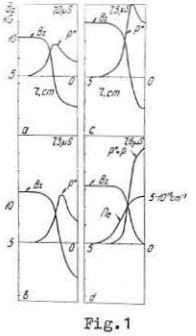

Fig.1

In fig.2 the typical interferogram and the results of itstreatment are given for the time of the captured field disappearance. The figure shows the plasma column decay with protuberance forming.

To increase the effectiveness of the shock plasma heating it is necessary, that increasing time of the piston magnetic field be sufficiently smaller than that of the shock wave path to the chamber axis. At the chamber radiud of some cm the field rising time should be of the order of microsecond fraction. The usual circuits of the direct coil supply from the condenser batteries to carry out the similar experiments are not suitable.

The high voltage artificial lines are used to obtain the fast rising magnetic fields for the effective shock plasma heating in Los Alamos laboratory [3]. In the described experiments the inductive energy storage method with the current switching into the coil by the fast-acting foil breakers [4] is developed.

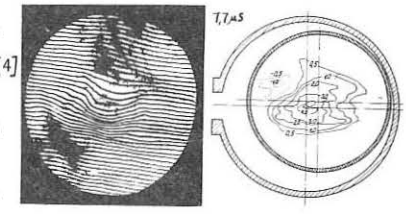

Fig.2

As the experiments carried out earlier showed [5], the fast-acting breakers on the principle of the electrical foil explosion in the arc-damping media allow to create the currents in the inductive loads at the rising time much lower than the quarter-period of the small inductive condenser batteries. To this end a number of experimental investigations have been carried out in order to work out the foil breaker design, to study their operating characteristics and to determine the optimum arc-damping media [6,7].

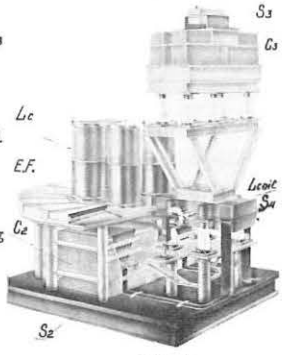

Fig.3

The experimental installation "Utro" has been designed for investigation of the shock plasma heating, that is, the plasma envelope implosion by the high fast rising magnetic field. The equivalent electrical circuit and the layout of the installation are presented in fig.3. The one-turn coil has the inner diameter d=7 cm and the length l=50 cm. It has two longitudinal cuttings, to one of which the "fast" part of the power supply system is connected, consisting of low inductive condenser battery C_1, capacitive inductance L_c and foil breakers E.F. At the latter explosion the current is spread into the coil L_{coil} after the spark gap S_4 triggering.

The initial longitudinal magnetic field B_{zo} is created by the "slow" battery C_2. The discharge current I_2 flows through the foil breakers not yet exploded. To increase the effective capture of the initial field by plasma the longitudinal electrical discharge system with the condenser battery supply C_3 is used.

In fig.4 the oscillograms of the signals, taken at the discharge absence from Rogowski belt, the voltage divider on the foil breakers and the magnetic probe, installed on the chamber axis.

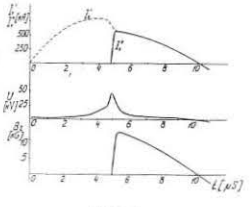

Fig.4

REFERENCE

1.Kolb A.C. At Proc.2-nd U.N.Conf.on Peauful Uses of Atomic Energy, Geneva, 1958.

2.Smirnov V.G.,Smirnov A.G.,Preprint T-0194,NIIEFA,1974.

3.An Engineering Design Study of a Reference Theta-Pinch Reactor (RTPR) Report LA 5336, AWL-8019.

4.Shenk G. 5-th Symposium on Fusion Technology,Oxford,1968.

5.Andresen A.B. et al. Pribori i technika eksperimenta, No.4, 146 (1973).

6.Burtsev V.A.et al.,Preprint T-0224, NIIEFA, 1974.

7.Burtsev V.A.et al., Preprint T-0223,NIIEFA, 1974.

SCYLLAC "DERATED" FEEDBACK SECTOR EXPERIMENTS*

E. L. Cantrell, W. R. Ellis, B. L. Freeman, K. B. Freese, R. F. Gribble, W. D. Gutscher, F. C. Jahoda, K. J. Johnson, R. Kristal, K. J. Kutac, J. R. McConnell, G. Miller, W. E. Quinn, and R. E. Siemon

Los Alamos Scientific Laboratory, University of California
Los Alamos, New Mexico

Abstract: A 120° sector of the Scyllac torus has been "derated" for feedback stabilization experiments to reduce the m = 1 instability growth rates to values which are compatible with the response time of the feedback system. Initial plasma studies are given and compared with the predictions of an MHD model. Plasma stabilization experiments will be reported.

I. INTRODUCTION. Scyllac experiments have been performed in toroidal sectors [1], R = 2.4 and 4.0 m, and in a full torus [2] (R=4.0 m) to study the high-β plasma equilibrium and stability and their scaling. These experiments have demonstrated the existence of the high-beta, ℓ = 1,0 toroidal equilibrium and have shown the following: (1) Theta-pinch plasma heating mechanisms are unaffected by the toroidal curvature and the presence of ℓ=1 and ℓ=0 equilibrium fields during the implosion; (2) The plasma column takes up a helical, bumpy toroidal shape and comes into an equilibrium position as predicted by theory, and remains stably confined for 6 to 10 μs; (3) The period of stable confinement is terminated by an m = 1 unstable motion of the plasma column, whose properties are those of the theoretically predicted m = 1 instability; (4) Measurements of the magnetic field, plasma beta, radius, and relative density profile confirm in detail the theoretical predictions of a high-β toroidal equilibrium and its scaling; (5) Measurements of the toroidal mode structure of the m = 1 instability show the existence of at least five toroidal modes (theory predicts a maximum of six) and confirm the theoretical fall-off of the unstable displacement amplitude past n = 3; (6) No indication of higher order poloidal instability modes than m = 1 has been seen, in agreement with FLR criteria; and (7) The major divergence of the observed plasma behavior from theoretical predictions is the initial period of quiescent equilibrium before m=1 instability onset.

Two methods for stabilizing the m = 1 instability in Scyllac have been proposed: feedback (FB) and wall stabilization. Since in the present Scyllac experiments the ratio a/b of plasma to wall radius is too small (∿ 0.1) for wall stabilization, feedback control has been chosen for plasma stabilization. Computer studies indicate that $\gamma\tau \leq 0.5$ ($\gamma\tau$ is the product of instability growth rate and FB delay-risetime) is required for controlling the instability, while Scyllac, with improved FB modules, has $\gamma\tau \gtrsim 0.8$. In order to reduce γ to a value which is compatible with the FB system ($\gamma\tau \sim 0.4$), the main field has been reduced to ∿ 17 kG and plasma parameters derated accordingly. Initial feedback experiments [2] are being performed in an 8-m sector, following preliminary studies of the derated plasma.

II. EXPERIMENTAL ARRANGEMENT. An "8-m sector" of the Scyllac torus, with a major radius 4.0 m, subtended angle 120°, and coil arc length 8.38 m, has been modified for the initial feedback stabilization experiments. The wavelength (62.8 cm) of the ℓ = 1,0 equilibrium fields has been selected to minimize the growth rate of the m = 1 instability and the required feedback field. The ℓ=1 helical ($B_{\ell=1}/B_o$ = 0.095) and ℓ=0 bumpy ($B_{\ell=0}/B_o$ = 0.147) fields were produced by machining the inner surface of the compression coil to coincide with the desired ℓ=1,0 flux surface. We define a position of maximum field strength as a "land" region ($B=B_0+B_{\ell=0}$ = 19.4 kG) and a position of minimum field strength as a "groove" region ($B=B_o-B_{\ell=0}$ = 14.4 kG). A small reversed bias field (∿ 140 G) has been used in some experiments to improve the plasma profiles for better equilibrium.

III. RESULTS: A. Plasma Parameters. Plasma measurements with B_o ∿ 17 kG give the following parameters: (1) plasma densities of 2 - 4 x 10^{16} cm^{-3} from both side-on holographic and coupled-cavity interferometry; (2) plasma radii of 0.9 - 1.1 cm from luminosity profiles and side-on holographic interferometry; (3) plasma beta at the column center of 0.6 - 0.7 from combined excluded flux and luminosity profiles; (4) plasma electron temperatures of 130 - 150 eV from Thomson scattering ($T_i = T_e$ in the derated collisional plasma); (5) plasma confinement times of 15 - 25 μs; (6) ℓ=0 plasma distortion, δ_o=0.2; (7) ℓ=1 plasma distortion, δ_1= 1.0 - 1.4; and (8) growth rate of m = 1 instability, $\gamma_1 \sim 0.2 - 0.3 \times 10^6$ s^{-1}.

B. Plasma Equilibrium Relations. The approach of the plasma column to MHD equilibrium is shown in Fig. 1. The upper part of the figure shows the time behavior of the average plasma radius, $\langle a\rangle = (\bar{a}_L + \bar{a}_G)/2$, where $\bar{a}_L$ is the plasma radius in a land region averaged over four discharges, and similarly for $\bar{a}_G$ in a groove region. The center part of the figure shows the time variation of the average plasma beta in the center of the column, $\langle\beta\rangle = (\bar{\beta}_L+\bar{\beta}_G)/2$, where $\bar{\beta}_L$ and $\bar{\beta}_G$ refer to averages over four discharges. The solid line shows for comparison the theoretical beta value for toroidal equilibrium derived from sharp-boundary theory with the design values of h, R, $B_{\ell=1}$, and $B_{\ell=0}$, and the experimental curve for $\langle a\rangle$. Agreement is better than 5%.

The lower part of Fig. 1 shows the approach of the plasma column to axial pressure equilibrium (nkT = constant) using experimental curves for $(\bar{B}_L/\bar{B}_G)$ and $(\bar{B}_G/\bar{B}_L)^2$. In pressure equilibrium these curves will coincide. Also shown for comparison is the vacuum design ratio $(B_G/B_L)^2 = (1-B_{\ell=0}/B_o)^2/(1+B_{\ell=0}/B_o)^2 = 0.553$. The equilibration time is lengthened by the presence of the ℓ=0 bumps in the plasma column, and the MHD "sloshing" period is ∿ 5 μs. Error bars in each case refer to standard deviation from the mean because of variations between discharges.

C. Transverse Plasma Motions. The streak photographs of Fig. 2 show the plasma forming a well-defined column and taking up an equilibrium position with initial δ_1 helical oscillations, $\omega_o = kv_A(2-\beta)^{1/2}$, which damp in ∿ 7 μs. The column equilibrium position is helically shifted horizontally outward in land regions, inward in groove regions and vertically halfway between land and groove regions. The helical shift suggested in Fig. 2(L) and 2(G) is exaggerated owing to different plasma motion at these widely separated positions. Plasma confinement is terminated by an outward m=1 motion at ∿ 25 μs. The m=1 growth rate from the streak photographs is ∿0.2-0.3 x 10^6 s^{-1}, in agreement with sharp-boundary theory.

Figure 3 compares the measured land and groove plasma trajectories with the predictions of a sharp-boundary MHD model. The model consists of a set of coupled differential equations for the plasma column displacement ξ and surface distortions δ_o and $\delta_{\pm 1}$ as functions of time, assuming in this case a=1 cm, n=3x10^{16} cm^{-3}, B_o=17 kG, and β=0.77. Damping of the oscillations, which normally is not present in sharp-boundary MHD theory, has been included empirically to agree with experiment. The plasma column is assumed to be cylindrical at t=0, when the $B_{\ell=1}$ and $B_{\ell=0}$ fields are applied instantaneously. At later times, not shown in Fig. 3, the calculated trajectories go to the inner wall exponentially with a growth rate of ∿0.3x10^6 s^{-1}. Two possible explanations of the reversing plasma motion seen in the streaks are (1) several toroidal n-modes (n=kR=2πR/λ) are being excited, which locally carry the plasma first one way and then the other. The calculated motions in Fig. 3 allow only for the longest wavelength (n=0) mode; and (2) the plasma beta decreases at later times due to end effects. The MHD model has also been used to simulate the feedback stabilization and indicates that a helical ℓ=2 feedback field is functionally superior to a bumpy ℓ=0 field due to the formative time of the plasma distortion in the latter case. Feedback stabilization experiments including studies of the effectiveness of ℓ=0 and ℓ=2 feedback fields are being performed.

REFERENCES

[1] W. R. Ellis et al., Nuclear Fusion 14, 841 (1974).

[2] E. L. Cantrell et al., Paper CN-33/E1-2, Fifth IAEA Conf. on Plasma Phys. and Controlled Nuclear Fusion Research, Tokyo, Japan, Nov. 1974.

* Work performed under the auspices of the U.S. Energy Research and Development Administration.

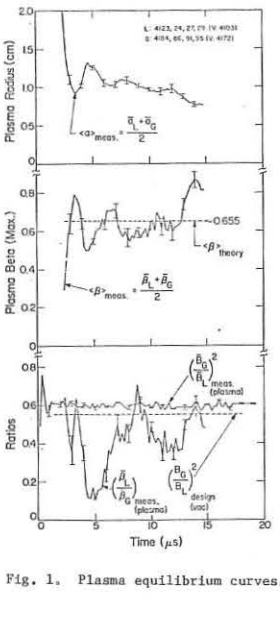

Fig. 1. Plasma equilibrium curves.

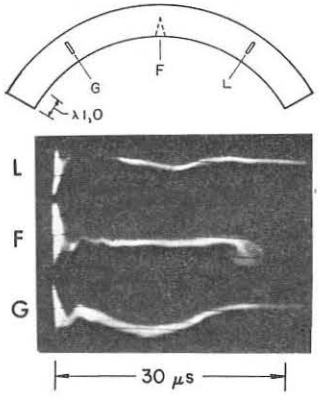

Fig. 2. Simultaneous streak photographs (4603): L-Land, horizontal plane; F-Front, vertical; G-Groove, horizontal.

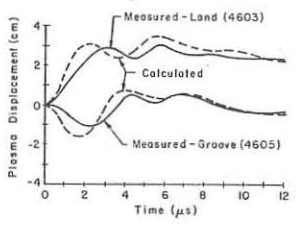

Fig. 3. Measured and computed plasma trajectories (same ℓ=1,0 wavelength).

STAGED THETA PINCH EXPERIMENTS

R. K. Linford, J. N. Downing, R. F. Gribble,
A. R. Jacobson, D. A. Platts, and K. S. Thomas

University of California, Los Alamos Scientific Laboratory
Los Alamos, New Mexico, USA

Abstract: Two concepts are presented for producing theta pinch plasmas with larger ratios of plasma radius to discharge tube radius than are produced in standard theta pinches. The experiments for testing these concepts and preliminary results are described.

Previous theta pinches have performed initial implosion heating of the ions and subsequent adiabatic compression with a single capacitor bank power supply. Projected theta-pinch feasibility experiments and fusion reactors, however, will require separation of the two functions to achieve greater efficiency and to allow for wall stabilization of toroidal theta pinch plasmas.[1] Wall stabilization requires that the ratio of plasma radius to wall radius be larger than in conventional theta pinches. The Staged Theta Pinch program is designed to study the technological and physics problems associated with producing fat plasmas and separating the implosion heating from the adiabatic compression.

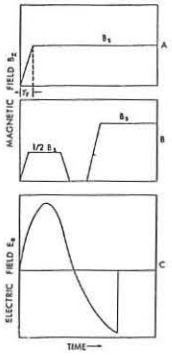

Fig. 1. Driving fields assumed by Freidberg, Morse and Ribe [1] for (a) simple implosion heating, (b) free-expansion heating, and (c) programmed E_θ heating of a theta-pinch plasma.

Several methods of implosion heating have been proposed. Freidberg, Morse and Ribe [1] presented three concepts indicated in Fig. 1 which was taken from their paper.[2] No specific circuits were proposed to produce these waveforms, but the plasma dynamics were analyzed for each case. Since the free expansion case appeared most promising, one of the authors of this paper [3] designed a circuit which simulates the field behavior in Fig. 2b. The resulting circuit, shown in Fig. 2a, is being used in the Staged Theta Pinch (STP) experiment described later in the paper.

Recently, the resonant heating implosion process was proposed by one of the authors [4] which theoretically produces plasma parameters very similar to those resulting from the STP circuit. However, the advantage of resonant heating is the efficiency and simplicity of the circuit shown in Fig. 2b. The circuit is topologically the same as the circuits used in present theta pinches such as Scyllac, but the component sizes are chosen so that the natural resonance of the imploding and expanding plasma can be used as the second "resonant loop" thus necessitating only one properly tuned implosion bank. The crowbarred field decays exponentially on a much longer time scale than the implosion process, which would allow the slowly rising compression field of future experiments to take over.

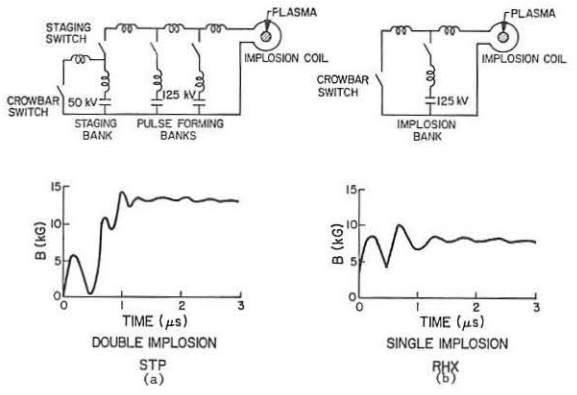

Fig. 2. Circuit diagrams and theoretical magnetic field behavior for (a) the STP experiment and (b) the RHX experiment.

These two implosion heating circuits are being experimentally tested. The principal experiment in the program is the 4.5-m-long linear Staged Theta Pinch (STP). It uses a relatively low energy, high-voltage capacitor bank to produce the theta-pinch plasma. A lower voltage, higher energy capacitor bank is used to contain the plasma and provide a variable amount of adiabatic compression. The experiment will be capable of producing high temperature plasmas with a much larger ratio of plasma radius to discharge tube radius than is possible in conventional theta pinches. Plasma experiments will include a study of the effect of magnetic field amplitude and time history on plasma formation, the properties of the plasma formed, and later, studies of the effect of helical magnetic fields on plasma stability. If the ratio of plasma radius to coil radius can be made large enough, the effect of plasma stabilization by image currents in the coil walls will be observable. The resonant heating concept is being tested on the 0.9 m RHX (Resonant Heating Experiment) which uses components similar to those in the STP experiment.

Preliminary results obtained from the Staged Theta Pinch program are:

1. Plasmas have been successfully imploded using the STP form of the implosion circuit.
2. Holographic interferometric data indicate that the flutes seen during the implosion phase in the Scylla 1B experiment are not present.[5]
3. Theta pinch preionization is used to produce 45% to 80% preionization with only minor radial dependence from 3 mTorr to 11 mTorr. The highest percentage of ionization was observed at the lower pressures.
4. Field gradients similar to Scylla 1B [5] and the STP prototype [6] were observed between the main plasma column and the discharge tube wall.

References

[1] J. P. Freidberg, R. L. Morse, and F. L. Ribe, "Staged Theta Pinches with Implosion Heating," Symp. Tech. of Controlled Thermonuclear Fusion Experiments and Engineering Aspects of Fusion Reactors, Austin, Texas, Nov. 20-22, 1972.

[2] The paper [1] contains an error in the calculation of the relative size of the two pulses of implosion field for the "free-expansion" case, but the numerical factor has been corrected in Fig. 1b.

[3] R. F. Gribble

[4] R. K. Linford

[5] K. F. McKenna, R. Kristal, and K. S. Thomas, Phys. Rev. Letters 32, 409 (1974).

[6] R. F. Gribble, J. E. Hammel, I. Henins, F. C. Jahoda, R. Kristal, R. K. Linford, J. Marshall, K. F. McKenna, A. R. Sherwood, and K. S. Thomas in Plasma Physics and Controlled Nuclear Fusion Research (International Atomic Energy Agency, Vienna, 1975), Paper CN-33/E 8-4.

On the Influence of the Walls in Theta Pinch Experiments with Low Filling Densities.

W. Engelhardt, W. Köppendörfer, M. Münich, J. Sommer

Max-Planck-Institut für Plasmaphysik, Garching, Germany, EURATOM Association.

Abstract: The neutron emission from a theta pinch with series of discharges in hydrogen and deuterium shows a dominant role of the discharge vessel walls at low filling pressure. At 4 mTorr about half of the filling gas enters the vessel directly whereas the other half is exchanged over the walls. The gas absorbed at the walls amounts to 10^{16} cm^{-2}.

1.) Introduction.

Theta pinch discharges were carried through in a 1 m long and 20 cm diameter vessel at 4 mTorr filling pressure. A specially shaped magnetic field pulse allowed to produce plasmas with low compression ratios /1/. The decay and rise of neutron emission in dependence on discharges in deuterium and hydrogen revealed the influence of the quartz vessel walls.

First the experimental procedure of producing the plasma is described. After this, results from neutron measurements are presented. Finally, the observations are interpreted by means of a simple model.

2.) Plasma Preparation.

Two axial discharges with 80 and 120 kV served for breakdown and preheating. For good reproducibility and for facilitating breakdown, the discharge tube was filled up to 10 mTorr filling pressure and the gas then pumped off through a throttle valve with an 1/e pressure decay time of 1.5 seconds. At the moment when 4 mTorr were reached, breakdown, preheating and main discharge were successively triggered. For full ionization, a ringing preheating discharge of 50 kA maximum current was necessary. After 25 microseconds before the electron line density started to fall below the filling density value of 4 mTorr the theta pinch bank was discharged.

3.) Neutron Measurements

Fig. 1 shows the neutrons emitted by the theta pinch plasma as measured by a scintillation counter for a number of successive discharges. In region I, values for discharges in hydrogen which followed a long operating period in deuterium are plotted. Region II gives the rise of neutron emission if deuterium filling is used again after 25 hydrogen fillings. Region III confirms the decay shown by region I.

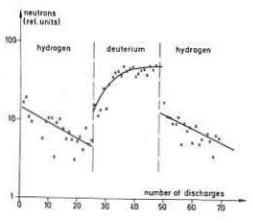

Fig. 1:
Neutron emission of a series of discharges in hydrogen and deuterium

In order not to introduce errors by the filling system, the latter was carefully pumped and flushed whenever the filling gas was changed.

Two features become evident from the data of Fig. 1:

1) The number of neutrons jumps when the filling gas is changed.

2) For a 1/e decay of the neutron emission as shown by region I and III, typically 25 discharges are necessary. A similar number is needed for the rise in region II.

4.) Discussion

The results can be interpreted quantitatively by means of a simple model. It assumes that a fraction α of the filling gas enters the discharge volume directly. The other fraction $1-\alpha$ enters a reservoir. The reservoir gives gas of a certain composition determined by its momentary content to the discharge tube. The reservoir represents the walls. The decay in region I and III can then be described as a function of the discharge number z:

$$N_z = N_{(z=-1)} (1-\alpha)^2 \exp\left\{-(1-\alpha)\frac{n_o}{n_F} R_G \cdot z\right\}$$

$N_{(z=-1)}$ is the number of neutrons emitted by the last preceding deuterium discharges, n_o the filling density and n_F the number of particles absorbed by the quartz walls per cm^{-2}. R_G is the radius of the discharge tube. α is determined by

$$\frac{N_{z=+1}}{N_{z=-1}} = (1-\alpha)^2 .$$

n_F is obtained from the slope of the curves in region I and III.

For the conditions described above, $\alpha = 0.51$ and $n_o = 3 \cdot 10^{16}$ cm^{-2} were obtained. Half of the filling gas is thereafter exchanged through walls which contain a large amount of hydrogen and deuterium absorbed. One cause for the latter may be the breakdown and preheating discharges which cause energetic particles to impinge on the walls.

The model described assumes same ión temperatures for hydrogen and deuterium discharges. It assumes further stationarity, i.e. the amount of gas entering the vessel before the discharge has to leave it again. The first assumption has not been proved. The second is essentially confirmed by pressure measurements. Interesting minor deviations cannot be discussed here.

References:

/1/ W. Braun, et al., Tokyo Conference, IAEA-CN-33/E2 1974

Fast Plasma Compression in Slit Metal Vessels

A. Eberhagen, H. Herold, R. Wilhelm

Max-Planck-Institut für Plasmaphysik, Garching, Germany, EURATOM Association.

Abstract: The applicability of slit metal vessels for fast magnetic plasma compression is experimentally investigated. The scaling law for the limiting E-fields as function of pressure, gap width and material is given and special problems associated with long way arcing at low pressures are discussed.

Fast magnetic plasma compression has commonly been conducted in discharge vessels made of dielectrics such as quartz or ceramics. With increase in size and energy of such experiments, however, severe difficulties are to be expected with such materials, particularly when the plasma parameters approach fusion conditions. Investigations have been taken up, therefore, to establish the limits of the applicability of properly slit metal vessels in fast compression experiments.

The studies were started on a 15 kJoule thetapinch with B_{max} (with crowbar) = 29 kGauss, $(dB/dt)_{max}$ = 26 kGauss/μsec, U_{coil} = 19 kVolt, coil diameter = 10.5 cm, coil length = 20 cm. With this equipment plasma temperatures of 20-50 eV and densities in the 10^{15}-10^{16} cm^{-3} range were produced depending on the deuterium filling pressure p_o = 5-50 mTorr.

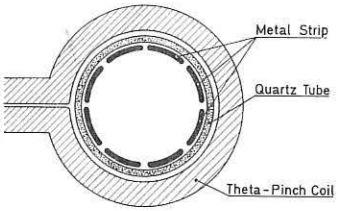

Fig. 1 Schematic of Slit Metal Vessels

The discharge vessel was constructed as follows: Inside a quartz tube, which serves as the vacuum chamber, bare metal strips were fixed to the inner surface. These strips were arranged parallel to the magnetic field. Their number (1-22), thickness (1.5- 5.0 mm) and the gaps between them (s = 1.5 - 8.5 mm) were varied in the course of the experiments.

The operational procedure in the experiments was as follows: The deuterium gas was pre-ionized either by an rf-cable- and a subsequent theta-discharge or, at lower filling pressure, by a z-pinch. Then the main bank was fired. Its charging voltage - and the corresponding voltage difference induced across the strip gaps - was varied from shot to shot to find the limiting voltage at which arcing across the gaps was just avoided. This critical voltage U_c could be identified rather clearly with help of a set of diagnostic methods consisting of side-on and end-on framing and smear pictures, diamagnetic signals from two axial positions, photomultiplier signals from spectral lines characteristic of the strip metal under investigation, etc.. Below the critical figures the fast thetapinch discharges in vessels with properly slit metal walls developed in essentially the same way as in dielectric vessels. Typical values of the induced critical field strength $E_c = U_c/s$ were in the range of 1-10 kV/cm with the metal covering the inner metal surface up to 99 %.

For the experimental conditions mentioned it turned out that all the individual results obtained can be summarized by the simple empirical formula:

$$E_c \times (p_o \cdot s)^{\alpha} = K = \text{const.}$$

This finding is demonstrated by Fig. 2, which, as an example, presents the experimental results (indicated by crosses: +) for slit stainless steel vessels (strip thickness: 3 mm, p_o : 5-50 mTorr). Obviously the exponential α exhibits an additional slight dependency on the filling pressure p_o, increasing with lower filling pressures from $\alpha = 1/2$ at the upper pressure range investigated ($p_o \gtrsim 15$ mTorr). For $p_o \approx 5$-10 mTorr

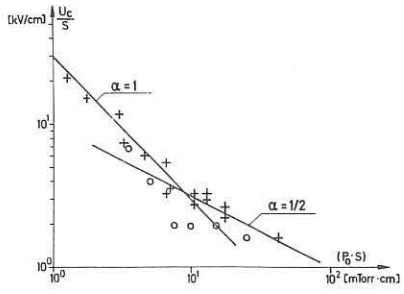

Fig. 2: E_c-$(p_o \cdot s)$ relationship for slit stainless steel vessels

$\alpha = 1$ was established with the consequence that the critical voltage difference U_c became independent of slit width s. The magnitude of the constant K varied with the metal chosen for the strips and the radius of their surface curvature at the gaps, i.e. with the strip thickness. In particular, with slit metal vessels of brass or stainless steel E_c is about 50 % higher than with aluminium.

Insertion of insulators into the gaps had little effect on U_c (glass, ceramics, protolin). Only with some commercial materials (e.g. plexiglass, trovidur) were partially reduced critical figures E_c found, possibly due to the occurrence of sliding sparks. Corresponding results for plexiglass in the gaps are indicated in Fig. 2 by open circles: o .

A compact vessel with slit stainless steel walls (inner diameter: 7.5 cm, two slits with glass as insulators) surrounded by protolin for mechanical rigidity and vacuum tightness was finally constructed with the experience gained. With this prototype the applicability of slit metal vessels in fast thetapinch discharges was demonstrated at $p_o \gtrsim 5$ mTorr according to expectation. A helically slit metal vessel (length: 100 cm, larger inner diameter: 60 cm) was built for the current Garching beltpinch experiments. It is now being prepared for testing.

At filling pressures $p_o \lesssim 5$ mTorr difficulties are envisaged for slit metal vessels in fast compression experiments due to the tendency of the exponent α to increase towards lower filling pressures. At given induced voltage differences arcing is then no longer to be expected on the "short way" across the slit gaps but rather on the "long way" between two more distant points of the inner metal surfaces on both sides of the slits. Due to the potential distribution across each strip, however, the limiting voltage will now depend not only on p_o, but also on the strip width itself, as well as on the vessel radius.

These problems are presently being investigated in the pressure range $1 \lesssim p_o \lesssim 5$ mTorr with an enlarged stainless steel vessel (inner diameter: 40 cm, length: 80 cm) of the type described. First experiments with large strip widths (only two slits) indeed indicate (Fe-lines and end-on framing pictures) that at the very beginning of the fast thetapinch discharge the slit gaps are shortened on the "long way" by relatively broad and diffuse plasma bridges. Shortly thereafter (about 1 μsec), however, these concentrate in the slit region, becoming bright, heavy arcs similar to those observed in the cases of $p_o \gtrsim 5$ mTorr. A report on experiments to overcome these difficulties by varying the strip widths used in the slit metal vessels will be given at the conference.

STABILITY OF THETA-PINCH PLASMA IN MULTIPLE MIRROR FIELD

S.Shiina, T.Itagaki, K.Saito, T.Karakizawa, Y.Osanai,
J.Todoroki, I.Kawakami, H.Yoshimura

Department of Physics and Atomic Energy Research Institute,
College of Science and Engineering, Nihon University, Tokyo, Japan

Abstract: The stability of corrugated theta-pinch plasma in multiple mirror field is studied. It is found from the detailed measurement of plasma parameters and plasma dynamics that the plasma is stable against m=1 flute instability for a longer time than the theoretical growth time, because of some stabilizing effects.

To confine a high-beta plasma a new toroidal magnetic configuration with closed magnetic lines of force has been proposed[1]. The magnetic configuration is constructed by an appropriate superposition of ℓ=0, ℓ=±1, ℓ= ±2, ·····helical magnetic fields. The toroidal equilibrium condition can be achieved, for example, by modifying the toroidal multiple mirror field with a copper shell, which is rolled around the discharge tube and has a longitudinal gap of an angle beyond a critical value. In this case we expect that a copper shell plays a role of enhancing the wall stabilizing effect[2,3], because of lowering the effective ratio of wall to plasma radius. The studies of the stability in a periodic system are useful for investigating the stability in toroidal system, since the two systems have a common feature of altanative stabilizing and destabilizing regions. From this point of view, we have studied the stability of corrugated theta-pinch plasma confined in linear multiple mirror field. We had already reported that the helium plasma was stable against m=1 flute mode during the confinement. In this experiment, the plasma parameters and plasma dynamics are measured for hydrogen plasma, in order to compare with the sharp boundary M.H.D. model for m=1 mode of corrugated theta-pinch plasma[4].

The linear multiple mirror field is produced by forty-two single turn coils, total length and inner diameter of which are 1 m and 13 cm, respectively. The external magnetic field reaches the maximum value of 1.77 T with a rise time of 19 μs, then is crowbarred with decay constant of 140 μs. The period and the mirror ratio of multiple mirror field are 28.8 cm and 1.52, respectively. The filling gas pressure is 30 mTorr H_2, preionized by Z-discharge through 1.6 m between two electrodes. The ratio of plasma pressure to external magnetic pressure, β, is measured by a diamagnetic probe placed on magnetic axis. The electron temperature and density are measured by 90° Thomson scattering of a ruby laser beam. The ion temperature is determened from the measured values of β, T_e and n_e. The corrugation amplitude of plasma is determined from both plasma radii at stabilizing(good) and destabilizing(bad) region, which are taken through side slits by S.T.L. streak camera. Also, the time histories of the intensity of Bremsstrahlung (visible light) from plasma are observed at both regions in order to confirm the macroscopic plasma behavor along magnetic lines of force.

Fig. 1 shows the time histories of β, T_e and T_i at the central part of plasma column(corresponds to bad region), where two species of β values are plotted, one from a diamagnetic probe, the other from laser scatterring by assuming T_i=T_e. The difference between two β values comes from assumption T_i=T_e, so that, T_i is higher by a few times than T_e. The β ratio from a diamagnetic probe has the maximum value of 0.64 at pinch time, then decreases with increasing external magnetic field, while T_i, T_e keep the values nearly constant with time. The produced plasma is stable against m=1 mode during observation(for 50 μs). The higher m modes are weakly unstable so that the plasma is deformed not being in contact with discharge tube wall. The theoretical growth time, which is based on the sharp boundary M.H.D. model for m=1 mode, is expected to be about 3 μs for plasma parameters of T_i=7 ev, β=0.1, δ_*(normalized corrugation amplitude)=0.25, in the absence of wall stabilization effect. The diffuseness of plasma boundary (radial profile) leads to faster growth time. The corrugation amplitude is determined from the maximum and minimum plasma radii taken by the streak photographs, as shown in Fig. 2. The observed plasma stability can not be explained by end effect only [5], because of two reasons that an arrival time of Alfven wave to central region from end region is about 8 μs after pinch time and that the plasma is stable even in the case of removing the end part. Because of interest in stabilizing effect, the plasma dynamics along magnetic lines of force are investigated in both good and bad regions. Fig. 3 shows the time histories of T_e and n_e, and Fig. 4 of Bremsstrahlung intensity(6940 Å) from plasma, in both regions. The temporal behaivors of n_e, and Bremsstrahlung intensity have the same time correlation between both regions. This time correlation means the existence of axial plasma flow that the plasma contracts to bad region after radial contraction, thereafter expands to good region, and then contracts to bad region again. The flow velocity is nearly of 2.4 cm/μs, smaller than the Alfven velocity. The ratio of β value in bad region to that in good region oscillates with time, as shown in Fig. 5. This oscillation indicates that the plasma does not achieve axial pressure equilibrium. Therefore, the observed plasma stability would be, as one possible effect, due to the dynamical axial flow driven by the lack of axial pressure equilibrium.

REFERENCES

[1] T.ITAGAKI, T.KARAKIZAWA, K.SAITO, S.SHIINA, J.TODOROKI, 5th Conf. Plasma Phys. Controlled Nucl. Fusion Research (Tokyo,1974) IAEA-cn-33/E7-3.

[2] J.P.FREIDBERG, B.M.MARDER, H.WEITZNER, Nuclear Fusion 14, 809(1974)

[3] E.FUNFER, M.KAUFMANN, W.LOTZ, J.NEUHAUSER, G.SCHRAMM, U.SEIDEL, Nuclear Fusion 15, 133(1975)

[4] F.A.HAAS, J.A.WESSON, Phys. Fluids 10, 2245(1967)

[5] T.MIYAMOTO, S.HAMADA, H.OHONISHI, J. Phys. Soc. Japan 23, 1131(1969)

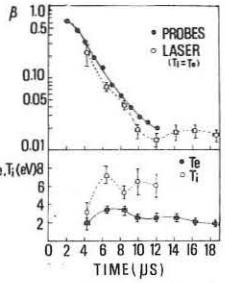

Fig. 1. The time histories of β value, T_e and T_i by diamagnetic probe and Laser scattering at central bad region.

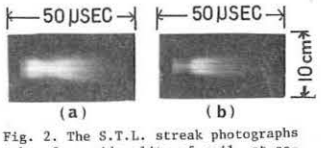

Fig. 2. The S.T.L. streak photographs taken from side slits of coil, at central bad region(a), and at good region (b).

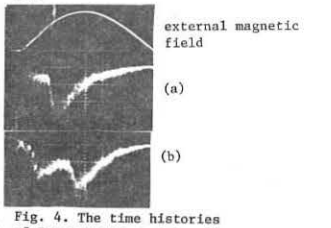

Fig. 4. The time histories of Bremsstrahlung intensity (6940 A) at good(a) and bad (b) regions without crowbarring.

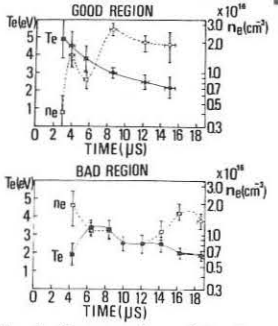

Fig. 3. The comparison of T_e, N_e at good and bad regions.

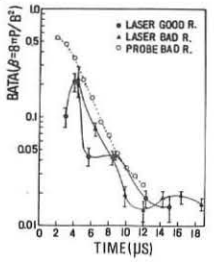

Fig. 5. The comparison of β values by Laser scattering (assuming T_i=T_e) at good and bad regions.

THETA-

RELAXATION PHENOMENA AND ENERGY LOSSES IN A LOW DENSITY Θ-PINCH

P. Bogen, K.J. Dietz, E. Hintz, K. Höthker, Y.T. Lie, and A. Pospieszczyk

Institut für Plasmaphysik der Kernforschungsanlage Jülich GmbH
Association EURATOM-KFA

Abstract: The temporal variation of n_e, T_e, B, $T_{i\perp}$ and $T_{i\parallel}$ have been measured to identify the relaxation processes and energy loss mechanisms which lead to a plasma diameter and temperature lower than expected from the usual adiabatic compression law.

Introduction: In a high-ß-stellarator a low compression ratio of the plasma is needed to achieve wall stabilization, e.g. /1/. The compression ratio depends on the time dependence of the magnetic field pulse and the energy transfered to and lost by the plasma. If the quarter cycle is short enough, the energy is supplied only during the fast compression. The main relaxation and loss processes which determine the plasma diameter seem to be the relaxation of the initially anisotropic ion velocity distribution, the electron thermal conduction to the coil ends and cooling by charge exchange neutrals. Measurements which will indicate the relative significance of these processes will be presented here.

Experimental arrangement and diagnostics: For the investigation of the thermalization phase following the fast compression, a short Θ-pinch /2/ has been used (electric field at the discharge tube E = 500 V/cm, tube diameter d = 40 cm, coil length l = 80 cm, $n_{e1} = 5.10^{12}cm^{-3}$), whereas the long time behaviour of the plasma has been studied in a long Θ-pinch /2/ (E=350 V/cm, d = 30 cm, $p_o = 10^{-3}$ Torr D_2, n_{e1} = 1.5 or $3.10^{13}cm^{-3}$, l = 7 m, $\tau/4$ = 1.3/us, 1/e decay of the magnetic field 60/us).
A laser was focussed to a point 170 cm away from the coil end to determine n_e and T_e on the axis by Thomson scattering. The observation was made at 90° to the beam through a slit of 1 cm width. The ion temperatures $T_{i\perp}$ and $T_{i\parallel}$ have been deduced from D_α profiles obtained with a multichannel spectrometer in axial and radial direction. The radiation in the wing of this line is emitted by charge exchange neutrals which reflect the velocity distribution of the ions. The centre of the line is partly due to cold neutrals in the plasma boundary and is neglected in the evaluation as usual in the interpretation of the charge exchange spectra (c.f. Fig. 2). $T_{i\perp}$ determined from the pressure balance and from D_α agree within the error limits of about 30% (c.f. Fig. 3).

Results: During the fast compression most of the plasma energy is stored as flow energy of the ions. The thermal energy of the ions (c.f. Fig. 1 at 300 nsec) $kT_{i\perp}$ as well as $kT_{i\parallel}$ is relatively low, that of the electrons is much higher for a short time, but it is lost very fast due to thermal conduction to the ends. When the shock reaches the axis, the flow energy is converted into thermal energy perpendicular to the magnetic field. The maximum value of 2.4 keV expected from the piston velocity of 4.10^7 cm/sec and ratio of 1:4 of the reflected particles to the particles trapped in the piston is near to the observed value of 2.0 keV. The energy parallel to B is considerably lower (Fig. 1). After the first compression $T_{i\perp}$ decreases since the plasma loses energy due to expansion.
Fig. 2 shows the distribution function f(v) perpendicular to B at 800 nsec derived from the blue wing of D_α (the red one shows some perturbation by other lines). It can be approximated by a Maxwellian distribution. The peaks corresponding to the piston velocity and twice this velocity have nearly disappeared, probably as a result of a diffuse reflection at the current sheath.

With the small experiment pressure isotropy is not reached. The results of similar measurements in the 7 m experiment are shown in Fig. 3. Here isotropy is reached after a time of about 5/us which is much shorter than the calculated selfcollision time. Little energy is transfered to the axial degree of freedom indicating that the relaxation of pressure anisotropy due to mirror instabilities does not proceed as fast as predicted by numerical computations /3/.
Most of the perpendicular ion energy is lost by other processes. Energy transfer from the ions to the electrons is of minor importance. The electron-ion equipartition times are longer than 30/us (T_e > 30 eV), so that less than 20% of the ion energy is lost due to collisions with electrons.
Loss rates can be explained by charge exchange neutrals. This hypothesis is strengthened by the observation that the plasma cools much faster at lower initial degrees of ionization. For the case $n_{e1} = 3.10^{13}cm^{-3}$ a flux density of less than 5.10^{19} neutral atoms/cm^2s at the periphery would be sufficient to explain the observed cooling rate. This corresponds e.g. to $n_o = 3.10^{13}cm^{-3}$ and $v = 1.5 \cdot 10^6$cm/s.

Conclusions: Plasma compression ratio and ion temperature seem to be strongly influenced by energy losses due to charge exchange. If these could be avoided, the present compression ratio of about 3 might be considerably decreased. The establishment of an isotropic velocity distribution occurs faster than expected from binary collisisions but seems to be caused mainly by energy losses.

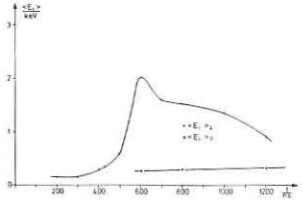

Fig. 1 Ion energies as function of time

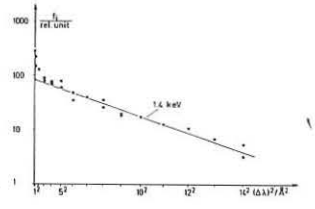

Fig. 2 f(v) from side on observations

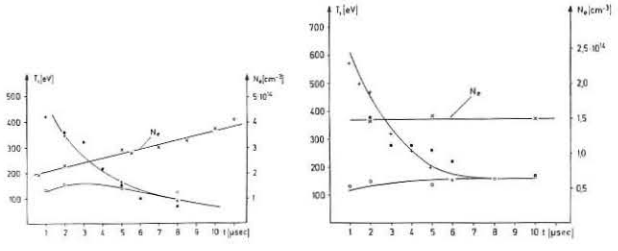

Fig. 3 $T_{i\perp}$, $T_{i\parallel}$ and n_e as function of time
a) $n_{e1} = 1.5 \cdot 10^{13}cm^{-3}$ b) $n_{e1} = 3 \cdot 10^{13}cm^{-3}$
(+)$T_{i\perp}$, (o)$T_{i\parallel}$, (•)T_i from pressure balance

References:

/1/ M.N. Rosenbluth et al., Phys. Fluids 12 (1969) 726

/2/ P. Bogen et al., Proc. V. Conf. on Plasma Physics and Controlled Nuclear Fusion Research, IAEA-CN-33-E8-1

/3/ R.L. Morse, Proc. APS Topical Conf. on Pulsed High Density Plasmas, Los Alamos, LA-3770, paper F3.

EXPERIMENTAL STUDY OF THE MICROTURBULENCE IN THE COLLISIONFREE SHEATH OF A Θ-PINCH

K. Höthker

Institut für Plasmaphysik der Kernforschungsanlage Jülich GmbH
Association EURATOM-KFA

Abstract: Characteristic properties of the microturbulence in the magnetic piston of a Θ-pinch are measured and compared with theory. Several instabilities may be excited in the sheath. All experimental results can be explained by a theory on ion acoustic turbulence. This theory predicts that the unstable ion acoustic waves are saturated by quasilinear ion Landau damping.

I. Introduction: Previous experimental investigations at this laboratory were concerned with the magnetic field diffusion and the piston induced radial plasma flow in a collisionless Θ-pinch of 40 cm diameter at densities between 10^{12} and $10^{13}cm^{-3}$ /1/,/2/. Laser scattering measurements showed for a magnetic-field-free deuterium plasma with $n_1 = 5.10^{12}cm^{-3}$, $T_{e1}=T_{i1}=2.5$ eV that the properties of the sheath are strongly time dependent. On the first few cm of its way the piston reflects the plasma elastically, generating a plasma flow with twice the piston velocity. The sheath properties then suddenly change, and for the rest of the implosion the plasma is trapped in the sheath. The plasma trapping by the piston and the observed anomalously fast diffusion of the magnetic field is attributed to the excitation of microturbulence in the sheath. The observed diffusion can be described by an effective collision frequency ν_{eff} of the order of the ion plasma frequency ω_{pi}. This value is an average across the sheath and should give only the order of magnitude of ν_{eff}. The experimental studies on which are reported here were concerned with a more detailed investigation of the microturbulence during the period, when the imploding magnetic piston reflects the plasma inelastically.

II. Apparatus: The expermimental set up is described in /1/. The magnetic field was measured along the radius by means of probes. The electron density and temperature were determined by Thomson scattering. The ion velocity distribution was measured by D_α and D_β spectroscopy. The amplitude and an upper bounds for the frequency of the fluctuating electric fields were determined by spectroscopy on forbidden HeI lines /3/,/4/.

III. Results: When the plasma is swept up by the piston, the electrons are heated at a rate 10^{10} eV/s to about 1 keV. This rate corresponds to an effective collision frequency $\nu_{eff}=10^9$ Hz= 0.3 ω_{pi} which is an avarage across the density pulse. This value is 4 orders of magnitude larger than the binary collision frequency. This anomalous heating as well as the observed inelastic reflection by the piston and the anomalous magnetic field diffusion indicate that suprathermal electric field fluctuations are excited in the sheath. To measure the amplitude and frequency of the fluctuating electric fields, a small amount of He was added to the deuterium gas, and spectroscopy on forbidden HeI lines have been performed. Fig. 1 shows the HeI 4922 (2^1D-4^1P, 4^1F) lines obtained from axial measurements, when the density pulse passes the line of sight at R = 8 cm. Instead of two satellites at a distance $\pm\omega$ from the forbidden line which theory predicts to be generated by electric fields of frequency ω, we observe one relatively weak intensity peak at the position of the forbidden line. Because of the weak line intensity, it was not possible to increase the resolution in order to detect satellites. But the resolution was sufficient to state that the mean frequency of the fluctuating electric fields is smaller than ω_{pe}. From the relative intensity of the allowed and forbidden lines we get for the mean amplitude of the electric fields $\sqrt{\langle E^2\rangle} = (5.5\pm1.1)$kV/cm which is an average across the trapped density pulse. The corresponding turbulence level W has the value $W = \langle E^2\rangle/8\pi n k T_e = 2.10^{-3}$. Comparing this value of W with the W for a thermal plasma W_{th} $1/(n\lambda_D^3)$, we get $W/W_{th}=3.10^3$ which means that indeed large suprathermal electric field fluctuations are excited in the sheath.

In order to examine from which type of unstable waves these fluctuations develop and which saturation mechanism is responsible for the observed level of turbulence, we have compared $c_s=\sqrt{\kappa T_e/m_i}$ with the azimuthal drift velocity v_d of the electrons which presumable drives the instability, Fig. 2. In the region of turbulent electron heating v_d/c_s is roughly const = 2. This means that Buneman instability should be unimportant which is consistent with the result $\omega<\omega_{pe}$. To determine the ion velocity distribution $f_i(v)$, spectroscopic measurements on D_α and D_β have been performed. These lines are predominantly Doppler broadened. Fig. 3 shows $f_i(v)$ from axial measurements on D_α at R=8cm. $f_i(v)$ from the radial measurements is essentially the same. The distribution is not a Maxwellian but has an enhanced tail at $v\approx c_s$. The ratio of the total number of ions to the number in this tail is about 20. The "temperature" of the ions in this tail $T_{i,tail}$ is of the same order as T_e. The mean electron energy is by a factor of 5 larger than the mean ion energy in the piston frame at R = 8 cm.

IV. Discussion: The plasma trapped in the magnetic piston is dominated by turbulent electric field fluctuations of mean frequency $<\omega_{pe}$. Anomalously fast electron heating is observed. The observations on v_d/c_s and $f_i(v)$ are in good agreement with theoretical results on ion acoustic turbulence /5/,/6/. This theory predicts that v_d/c_s should tend to a value of the order of $(m_i/m_e)^{1/4}\approx 8$, that $f_i(v)$ should have an enhanced high energy tail at $v\approx c_s$, that $T_{i,tail}\approx T_e$, and that the ratio of the total number of ions to the number of ions in this tail should be of the order of $(m_i/m_e)^{1/4}$. This agreement suggests that the measured turbulent fields develop from unstable ion acoustic waves which saturate by quasilinear ion Landau damping. A number of other modes /7/,/8/,/9/ is, too, predicted to be unstable in the sheath. Quasilinear ion Landau damping and ion trapping have been proposed to act in the saturation phase of these modes, too, and should therefore produce ion velocity distributions similar to those observed. But since the predicted W for these modes are at least one order of magnitude smaller than the measured W and since the growth of these modes is essentially restricted to the plane perpendicular to the magnetic field B, while the experimental $f_i(v)$ is roughly the same perpendicular and parallel to B, it seems that the turbulent electric field develop predominantly from unstable ion acoustic waves.

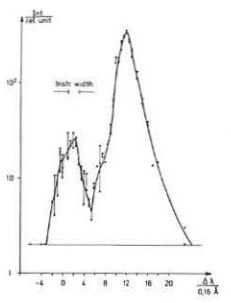

Fig. 1

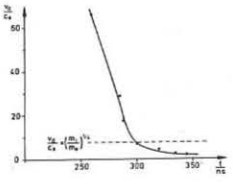

Fig. 2

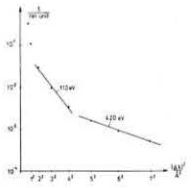

Fig. 3

Fig. 1 HeI 4922 line at R = 8 cm, end-on
Fig. 2 v_d/c_s as function of time at R = 8 cm
Fig. 3 Ion velocity distribution at R = 8 cm, end-on

References

/1/ K.J. Dietz et al, 2nd Top. Conf. on Pulsed High-ß-Plasmas, IPP Report 1/127, Garching 1972;
/2/ K. Höthker et al, Proc. 6th Europ. Conf. on Contr. Fusion and Plasma Physics, Moscow (1973) 299;
/3/ M. Baranger, B. Mozer, Phys. Rev. 123 (1961) 25;
/4/ H.J. Kunze, H.R. Griem, Phys. Rev. Lett. 21 (1968) 1048;
/5/ G.E. Bekshtein, R.Z. Sagdeev, JETP Lett. 11 (1970) 195;
/6/ C.T. Dum et al, Phys. Rev. Lett. 32 (1974) 1231;
/7/ M. Lampe et al, Phys. Rev. Lett. 26 (1971) 1221;
/8/ P.C. Liewer, N.A. Krall, Phys. Fluids 16 (1973) 1953;
/9/ E. Ott et al, Phys. Rev. Lett. 28 (1972) 88.

PLASMA CONFINEMENT IN A PULSED SYSTEM WITH A COMPACT TOROIDAL CONFIGURATION

A.G.Es'kov, O.A.Zolotovsky, A.G.Kalygin, R.Kh.Kurtmullaev, Ya.N.Laukhin, A.I.Malyutin, A.I.Markin, A.P.Proshletsov, V.N.Semenov
Kurchatov Institute of Atomic Energy, Moscov,USSR

Some hopeful results of shock heating and stable confinement by a purely poloidal field were obtained with times being substantially longer than rise times of characteristic MHD-instabilities [1]. Further development of these experiments is presented in this work.

The experiments were carried out with a Θ-pinch device (B =4,5kG, D=19 cm) with a reversed bias field B_o=0,5÷2kGs. It is wellknown, that plasma expantion to walls at the initial stage of discharge results in a number of unwanted effects [2] . Pulsed plasma pressing out from the wall by means of a barrier field during this stage seems to be the most drastic way to remove this disadvantage. Such barrier field is provided by longitudinal bars,placed on the surface of the cylindrical plasma volime (Fig 1). In the same figure an end coil is shown, designed for fluxes $B_\sim$ and B_o reconnection controlling and longitudinal plasma contraction programming(similar to [3]).

The same aims can be reached by use of a quasi-stationary (here octupole) barrier field: on the first half-cycle of the main discharge plasma compression and heating take place at parallel fields $B_\sim$ and B_o, while at the beginning of the second half-cycle, at the expansion stage, hot plasma is effectively retarded near the wall by a stationary barrier field. A crowbar on the second halfcycle provides confinement of the toroidal plasma obtained.

In all cases studied it is possible to distinguish two main stages of the process as follows:I-formation, heating and onset of a toroidal equilibrium structure, and II-confinement, accompanied by longitudinal and radial plasma pulsations due to residual occilations in an external shock field (Fig 2,a,b,). Note that known limitations, associated with the use of probes at relatively large confinement times are likely to be reduced by the large skin width (δ >1 cm) and permanent plasma motions, which are typical for given experiments. At operating density $n_o \sim (1\div5)\cdot10^{14}$cm^{-3} an elongated plasma toroid with peak pressure of $nT\sim(2\div3)\cdot10^{17}$eV/cm^3 and radius of 2÷3 cm was formed at the first stage (t<5 μsec). Measured ion temperature T_i (atomic analyzer) is shown in Fig 3. Similar behavior shows the electron temperature T_e (X-ray measurements), which at its maximum (at t≃5 μsec) amounts to 0,5÷1 keV. In framing pictures taken end on by electronic image converter, in a relatively wide range of conditions the formation of an azimuthally symmetric plasma cylinder with an annular current sheath of regular form was observed (Fig 4,a).

In the presence of a barrier field framing photographs show strong plasma column compression on the first half-cycle (0÷3 μsec) and successive radially-divergent plasma retardation by the barrier field (Fig 4,b). When the external field passes zero, the probes on the axis show a relatively large trapped field (Fig 2,b).

The second stage is rather sensitive to initial conditions, plasma configuration and size; this greatly affects the life-time of the closed magnetic structure.

Intensive radial compression of plasma (as a rule at $B_\sim \gg B_o$ or at relatively high density $n_o \geq (0,5\div1)\cdot10^{15}$cm^{-3}) affects adversely, leading to rapid disapearance of an antiparallel field geometry ($\tau \leq 10$ μsec)

The confinement time of the closed magnetic structure (up to t ~50 μsec) is observed when plasma column diameter is relatively large ($D_p/D \simeq 0,5\div0,8$) and current sheath is greately diffused being of the order of plasma radius. In conventional experimental scheme these requirements led to the necessity of shifting the crowbar to the point, lying substantially below the maximum of the pulsed magnetic field $B_\sim$. This resulted in a plasma pressure decrease by an order of magnitude. Use of a passive (stationary) barrier field didn't allow to avoid this difficulty, since the crowbar on the second half-cycle reduced, to large extent, a confining field. A pulsed barrier field ($B_b \sim 6$ kG,T/2≈3 μsec)is to solve the problem of stable confinement simultaneously providing substantial increase of energy content in a plasma.

Measurements of the azimuthal component B_θ indicates at the absence of a force-free configuration, so that in current sheath β=1.

It should be noted, that the closed magnetic structure lifetime observed is rather hopeful for a "Θ-pinch with liner" application in a quasi-spherical case [4] where required time is $\sim10^{-4}$sec.

The authors express their gratitude to E.P.Velikhov for fruitful discussions."

References

1. A.G.Es'kov et al. 6 European Conf.on Controlled Fusion and Plasma Phys.,Moscow, 1973,p.599. A.G.Es'kov et al.Y Intern. Conf.on Plasma Phys.,Tokio,1974, CN-33/E5
2. M.A.B.Bodin,Nucl.Fusion,3,215, 1963
A.Eberhagen and W.Grossmann,Z.Physik, 248?, 130, 1971
3. A.G.Es'kov et al. 6 European Conf.on Controlled Fusion and Plasma Phys., Moscow, 1973, p. 595
4. E.P.Velikhov. Comments on Modern Phys., E,1, n6, 171, 1972
R.Kh.Kurtmullaev and A.I.Malyutin. All-Union Symp.on Engineering Probl.of CTR.,Leningrad, 1974, p. 48.

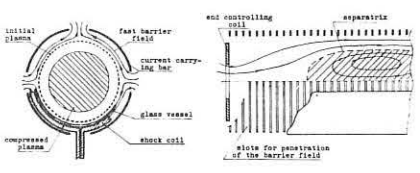

Fig1. Schematic diagram of installation

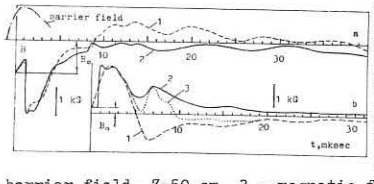

Fig2. Magnetic probes signals; a) antiparallel fields $B_\sim$ and B_o. n_o= 3.10^{14}cm^{-3}. 1 - probe is on the axis outside the toroid, Z=20 cm; 2 - probe is on the axis inside the toroid, Z=50 cm; b)crowbar is on the 2nd halfcycle. 1,2 - magnetic field at the wall and on the axis with stationary barrier field, Z=50 cm, 3 - magnetic field on the axis without barrier field.

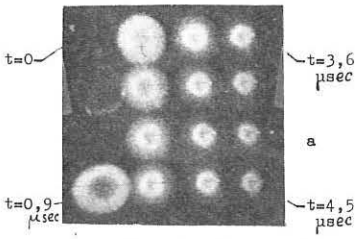

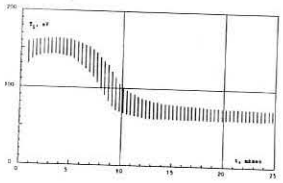

Fig3. Time variation of ion temperature, $n_o \sim 2.10^{14}$ cm^{-3}.

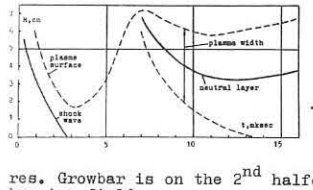

Fig4. a) End view of discharge. Interval between frames t=0,3μs. Antiparallel fields $B_\sim$ and B_o=-1kG. B) Radial plasma and current sheath position, obtained from end pictures. Growbar is on the 2nd halfcycle, B_o=1 kG, with stationary barrier field.

NONADIABATIC EFFECTS IN LOW PRESSURE THETA - PINCHES

K.B.Abramova, V.B.Boshnyak, V.P.Krivets, B.P.Peregood
A.F.Ioffe Physico - Technical Institute, Leningrad, USSR.

Effects observed in low pressure theta-pinches are considered. The effects can be explained by means of nonadiabatic motion of particles analysis. General theoretical results and first experimental observations under pure conditions of two main nonadiabatic effects, particles' energy square dependence on the magnetic field and particles' collapse, are adduced.

In experimental works on fast theta-pinches of initial density $n_0 \leqslant 10^{18} m^{-3}$ (collisionless and skinless regime) there were observed phenomena [I-5] which would naturally be associated with single-particle processes resulting from a nonadiabatic part of magnetic field change [I]. Some of them remain inexplicable from other standpoints (see for inst. [6]).

Particles' motion in nonadiabatic conditions was studied in some theoretical works [7 - I2], mostly on the basis of exact solution of motion equations for special laws of a field change, or in a "top nonadiabatic case" [II,I2], i.e. when nonadiabaticity parameter ε grows with the magnetic field growth:

$$\varepsilon = \frac{1}{\omega^2}\frac{d\omega}{dt} \xrightarrow[\omega\to\infty]{} \infty , \quad \omega = \frac{eB}{mc}$$

Most general conclusions can be made when the particle's orbit magnetic moment $\mu = \frac{W_\perp}{B}$ is analysed as a function of ε. Equations for the μ behaviour in the homogeneous axis-symmetric magnetic field can be reduced to the form

$$\frac{dJ}{d\theta} = \sqrt{J(J+P_\varphi)}\,\varepsilon\cos\psi$$

$$\frac{d\psi}{d\theta} = 1 - \varepsilon\frac{2J+P_\varphi}{2\sqrt{J(J+P_\varphi)}}\sin\psi \quad ; \text{ where}$$

$$d\theta = \omega dt , \; P_\varphi = mr^2(\dot\varphi + \frac{\omega}{2}) = \text{const} , \; J = \frac{mc}{e}\mu$$

Analysis of these equations shows that when the field increases monotonously from zero (provided that $\frac{d^2B}{dt^2} \leqslant 0$) all particles with the initial energies $W_0 \ll W^*$ (where W^* is a particle's energy in the moment $\varepsilon = 1/2$) move up to the moment when $\varepsilon = 1/2$ so, that μ increases almost linearly with the field; thus W is proportional to B^2.

With further growth of the field and decrease of ε (adiabatic part of motion) magnetic moment tends quickly to a constant value. The Larmor radius S, calculated from this value, equals to the distance A from the center of the Larmor circle of each particle to the axis, besides the phases of particles' Larmor rotation are synchronized during the nonadiabatic part of motion, thus making the whole set of particles with the same e/m to constrict to the axis periodically, with the period of collapses $T \simeq \frac{2\pi}{\omega}$ as in the "top nonadiabatic case" [II,I2], but now in the case of continuous field growth as well.

From now on particles' energy increases from compression to compression linearly with the field. The value of total energy gained is proportional to $B_{max}^{3/2}$. The contractions will last untill the motion is upset with collisions.

Phenomena observed in low pressure theta-pinches correlate qualitatively with the given picture of particles' motion. Quantative estimations of permissible plasma density and energy gain coincide well with experimental data.

In order to observe effects mentioned an experiment was set [I3], in which K^+ ions moved in a homogeneous axis-symmetric magnetic field. Scheme of the experiment is shown. K^+ ions were extracted from hot filament covered with a potassium salt and placed along the field axis. Magnetic field rose from zero up to 0.5 tl during 4 μsec providing highly nonadiabatic regime for the ions' acceleration. Periodical compressions of accelerated particles' set taking place after the field growth had been stopped induced an oscillatory component of the external circuit current, which was oscillographed. Ions' energy dependence on the acquired magnetic field strength had been measured by means of the retarding potential method. There was found out that I) Current oscillation frequency (frequences of collapses) equals to the ions' cyclotron frequency in the acquired field. 2) Energy ions gained depends on the field as B^2, 3) Oscillations damping rate coincides with an estimation proceeded from the effect of the collisions with the residual gas molecules.

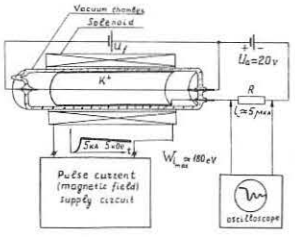

Nonadiabatic effects in our opinion are interesting themselves as a physical phenomena. Besides, collapse can be utilized for the energy compression as high values of power flux can be produced with its help: when $R_0 = 3\times10^{-2}$ m, $n_0 = 5\times10^{14} m^{-3}$; $\dot B = 10^9$ tl/sec, $B_m = 0.03$ tl, the set of electrons will be compressed: the density will increase 5.6×10^4 times, power flux will be 6.3×10^{16} J/m²sec.

Described picture of nonadiabatic effects can apparently be applied to some of the astrophysical phenomena interpretation.

References:

I) T.A.El Halafavi, V.A.Suprunenko, A.M.Ternopol, L.Hafis, A.Burgam "Plasma Phys.Prob.Fusion" v.I p.I37 Kiev I97I. 2) E.M.Little, W.E.Quinn, F.L.Ribe Phys.Fluids 4,7II, (I96I). 3) Dushin L.A., V.I.Kononenko, I.K.Nikolski, O.S.Pavlichenko "High frequency properties of Plasma", Kiev I968. 4) E.Oktay, A.W.De Silva, Bull.Am.Phys.Soc. I7,I047 (I972). 5) W.Davis, A.W.De Silva, W.Dove, U.R.Griem, N.A.Krall, P.C.Liewer, "Plasma Phys.Fus.Res. v.III p.289, Vienna I97I. 6) Paulette C.Liewer, N.A.Krall Phys.Fl. I6, N II, I953 (I973). 7) M,Sato Nuovo Cimento 23, 22, (I962). 8) V.A.Ankudinov, V.M.Kelman, O.M.Kresin, L.N.Sysoeva, Soviet Phys.-Techn.Phys. 32, 22, (I962). 9) L.G.Glikman, V.M.Kelman Sov.Phys.-Techn.Phys. 39, I534, (I969). I0) L.Dupas, J.Leroy, T.Consoli, Nuclear Fusion, 3, I60, I963. II) V.P.Krivets, B.P.Peregood Phys.Letters, 3I^A, 77, (I970). I2) V.P.Krivets, B.P.Peregood Sov.Phys.-Techn.Phys. 4I, 6, II74 (I97I). I3) K.B.Abramova, V.B.Boshnyak, B.P.Peregood Pisma Zh.Techn.Fiz. I, I, I8, (I975)

Time and Space Resolved Measurements of Density and X-Ray Emission of the NESSI Plasma Focus

H. Schmidt, B. Nahrath and B. Rückle

Institut für Plasmaforschung der Universität Stuttgart
Federal Republic of Germany

Abstract: Density profiles of the plasma focus with 450 psec time resolution were obtained by interferometry, the maximum electron density on the focus axis by a beam deviation method. X-ray pinhole pictures were registered with a channel plate with 3 nsec exposure and the chronology of the various plasma focus parameters was determined.

Introduction

Neutron spectra taken of the NESSI plasma focus (E_o = 30 to 60 kJ, $U_o \leq 20$ kV) indicate that different reaction mechanisms occur, depending on the operating conditions of the plasma focus (high- or low-pressure regime, hollow or solid inner electrode) resulting in different velocity distribution functions for the accelerated deuterons. Therefore it was attempted to correlate the macroscopic development of the plasma focus - i.e. space and time behaviour of density, formation of instabilities - to the observed emission of neutrons and X-radiation. To study the exact chronology of the very fast events in the plasma focus, diagnostics with time resolution of about and less than 1 nsec have to be applied. Though the development of the plasma focus is rather reproducible on a 10 nsec time scale and 1 cm spatial scale, the events on shorter time and spatial scales may develop differently from shot to shot for the same initial conditions. This requires simultaneous measurements of the various parameters in order to derive their correlations from these measurements.

Density measurements

Two methods were used to determine the density: interferometry and beam deviation. The method of beam deviation is simple to arrange and yields (by registration of the deviation angle of a laser beam with an electronic streak camera) the time-dependent value of the maximum electron density n_e with an accuracy of better than 30 %. Interferometric methods require exposure times in the subnanosecond regime. A nitrogen laser with a half-width of 450 psec was used as light source for the interferograms resulting in sharp fringes in spite of the large plasma velocities at the end of the compression phase and the subsequent break-up of the pinch. By incorporating an optical delay line, two interferograms with a fixed time difference could be taken for the same shot, thus allowing to observe the formation of instabilities. A sequence of 4 interferograms is shown in Fig. 1. The time scale is based on the onset of hard X-radiation X_h (at t = 0; see also Fig. 4).

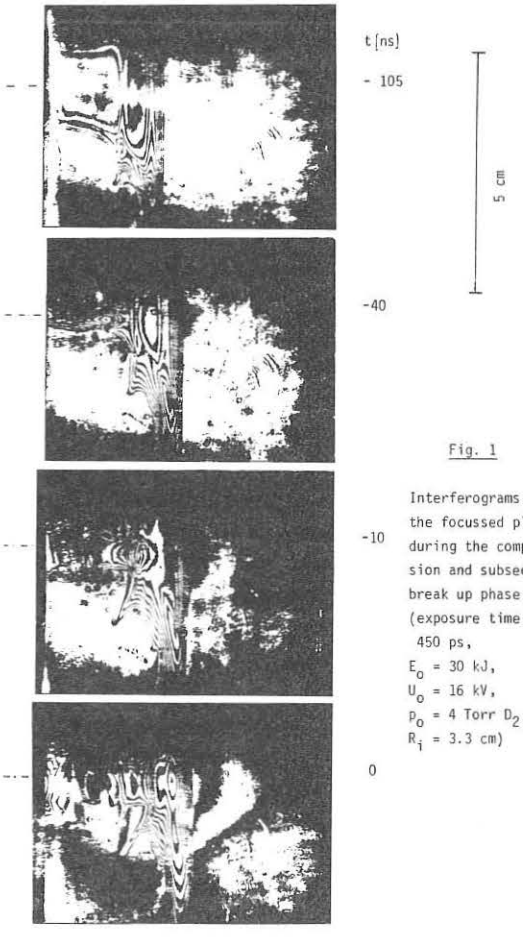

Fig. 1

Interferograms of the focussed plasma during the compression and subsequent break up phase (exposure time 450 ps, E_o = 30 kJ, U_o = 16 kV, p_o = 4 Torr D_2, R_i = 3.3 cm)

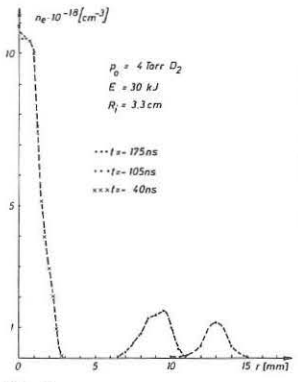

Fig. 2

Electron density profiles during the compression phase

Fig. 2 shows the electron density profiles at a distance of z = 0.75 cm from the hollow anode. Maximum electron densities of up to $3 \cdot 10^{19}$ cm^{-3} were measured locally on the axis.

X-radiation

X-ray diagnostics is important for the chronology of the dense, hot focus plasma. The focus plasma was imaged onto a channel plate by a pinhole camera. By pulsing the channel plate a time resolution of about 3 nsec could be realized. In Fig. 3 two typical pinhole pictures are shown. Comparison of the X-ray pictures with pictures taken in the visible shows the spatial coincidence of the X-ray and visible light emission as expected. It is not possible to determine a temperature from measured space-integrated X-radiation with foil absorption methods. A typical soft X-ray signal X_s is shown in Fig. 4. Evidently there is no Bremsstrahlung originating only from electrons with a Maxwellian velocity distribution.

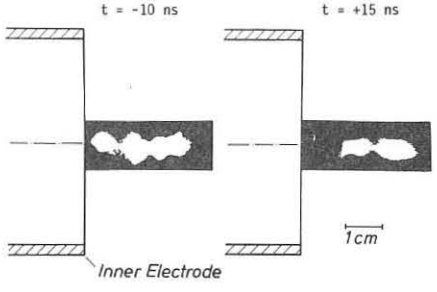

Fig. 3

X-ray structures of the dense plasma focus at two different times; exposure time 3 ns.

Discussion

From the interferograms and pinhole pictures the following can be derived: The current sheath, the thickness of which is about 0.2 cm, is accelerated towards the axis from a velocity of $5 \cdot 10^6$ cm/sec at r = 1.2 cm to $1.5 \cdot 10^7$ cm/s at r = 0.5 cm and subsequently decelerated until the minimum plasma radius of about 0.2 cm is reached. The dense pinch lasts less than 10 ns (see Fig. 1b and Fig. 4) and is followed by m = 0 instabilities of the plasma column (see Fig. 1c and Fig. 3a). The line density of the dense column is only 15 to 20 % of the line density corresponding to the number of particles within a cylinder with the radius of the inner electrode, i.e. the compression efficiency is less than 20 %. Still lower line densities occur at certain axial positions because of the axial plasma motion caused by the m = 0 instabilities, which initiate the breakup of the dense pinch (Fig. 1d, Fig. 3b). At this time the neutron and hard X-ray emission begins (see Fig. 4).

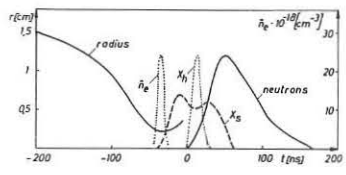

Fig. 4

Chronology of characteristic plasma focus parameters

An important feature is the formation of a density wave, which can be seen first at t = -10 ns and which then precedes the axial shock wave (Fig. 1d) and is accelerated up to $1.2 \cdot 10^8$ cm/sec. This wave is caused by fast deuterons ionizing the filling gas on their path. The measured maximum velocity of this ionization wave corresponds to deuteron energies of 14 keV.

TIME AND SPACE RESOLVED STUDY OF X-RAY EMITTING ZONES IN A 24 kJ-MATHER TYPE PLASMA FOCUS

J.P. Rager

Associazione EURATOM-CNEN sulla Fusione, Centro Gas Ionizzati, Frascati, Rome, Italy.

ABSTRACT

Using a 10 ns-gated soft X-ray image intensifier /1/, it is observed that during the neutron production phase of a 24 kJ Mather type plasma focus, there exists a well defined, stationary, low density, high temperature plasma of $\lesssim$ 1 cm overall dimension.

1. PLASMA DYNAMICS AS DEDUCED FROM SOFT X RAY FRAMING PICTURES

The instrument used in this work is described in full technical details in /1/, and its performances have been reported in /2/. Under this form, one 10 ns-soft X-ray frame per shot is obtained, using a 200 μm diameter pinhole covered by a 15 μm Be window. Proper time marking allows the "a posteriori" reconstruction of the sequence (10 ns due to non detailed shot to shot reproducibility in voltage scope traces used as a monitor). The plasma focus here investigated is a Mather type device, fully described in /3/. Working conditions are: V_o = 32kV, W = 24 kJ, filling pressure is 6 torr, pure D_2.

A. The soft X-ray pictures during the MHD governed radial implosion (Fig. 1, part 1) show out striking similarities in dynamics and shapes of plasma column to that revealed using many different techniques of optical imaging /4/, /5/, /6/. The first necking off of the plasma column, due to strong m = 0 instabilities, coincides with the start of the neutron and γ pulses (taken as t = 0). The implosion phase and maximum compression is reproducible and axisymmetric.

B. For 30 $\lesssim t \lesssim$ 130 nsec there exists a well defined plasma structure of 0.5 to 1 cm overall dimensions, standing underneath the z coordinate of previous necking off and either inclined with respect to the anode axis or off axis. This is the main neutron production phase. This so to speak confined structure then degenerates into a diffuse expanding sphere of plasma, marking the ends of both the neutron and first soft x-ray bursts.

C. From 150 $\lesssim t \lesssim$ 400 time resolved mica crystal spectroscopy (de Broglie geometry) shows out definite spectral features in the vicinity of the $k_{\alpha,\beta}$ lines (strong source braodening effect) of anode material, not observed during preceding phases. They correspond to a second large soft X-ray burst. The use of a hollow electrode delays the appearance of the burst and cancels the spectral features which therefore trace an electron beam--anode interaction.

D. Time integrated soft x-ray pictures (Fig. 2) show a m=0 MHD instable filament-like structure bearing no relationship with the filament phase reported in A because of smaller overall dimensions, different m=0 wave length, and probable relationship with the neutron production phase because of systematic inclination with respect to z axis. An artificially compounded picture is seen in Fig. 3 in which a filament is shown superimposed on the plasma bubble of Fig. 1 (t = 55 ns). The differences in shape between time integrated and time resolved pictures is to be attributed to the spectral sensitivities of the respective detecting devices.

2. CONCLUSIONS

Plasma pictures obtained using a gated soft X-ray image converters and that obtained using interferometry /5/ reveal similar dynamics up to the necking off of the plasma column. The reason for which the former techniques does not show "confined" plasma structures during the neutron production phase while the latter does, can be attributed to strong plasma heating. The reconstructed plasma picture of Fig. 3 would support the idea of anomalous phenomena triggered by the generation of unstable run-away electron beam, eventually transferring their energy to the underlaying plasma, which agree with anomalous spectra of scattered laser light found in this region for t $\sim$ 50 ns /6/.

Any attempt to determine the neutron source distribution in space has confirmed the existence of neutron emitting phenomena in the vicinity of the anode /6/, /9/.

REFERENCES

/1/ L. Bettinali, F. Pecorella, J.P. Rager: Rev.Sci.Instr. 46, 322 (1975)

/2/ M.G. Hobby, J.P.Rager, N.J. Peacock: Culham Report, CLM-R-138 (1974), unpublished.

/3/ C. Gourlan, J.P. Rager, M. Samuelli, C. Strangio: Report LGI/R/PLAD/74 (1974), unpublished.

/4/ P.D. Morgan; PhD Thesis, University of London (1974)

/5/ A. Bernard, A. Coudeville, A. Jolas, J. Launspach, J. de Mascureau: Phys.Fluids 18, 180 (1975)

/6/ A. Bernard, A. Coudeville, J.P. Garçonnet et al.: Proc. 5th Conf.Plasma Phys and Controlled Fusion Research, Tokyo 1974, Paper CN-33/E6, IAEA, Vienna.

/7/ C. Patou: Le Journal de Physique 31, 339 (1970)

/8/ E.H. Beckner, E.J. Clothiaux, D.R. Smith: Phys.Fluids 12, 253 (1969)

/9/ M.J. Bernstein: Rev.Sci.Instr. 40, 1415 (1969).

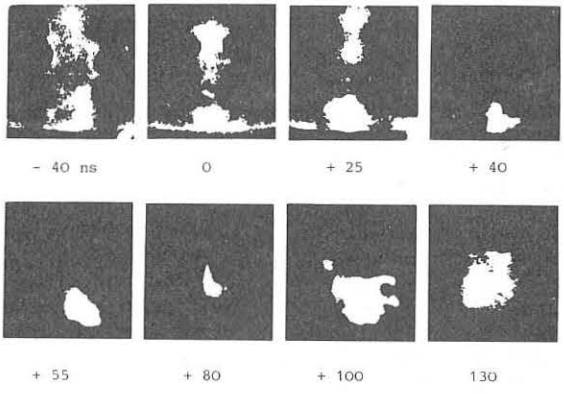

Fig. 1 Sequence of time resolved soft X-ray framings.

Fig. 2 Time integrated X-ray framing

Fig. 3 Artificially compound X-ray framing

CALCULATIONS OF THE ACCELERATOR AND MEASUREMENTS OF PARAMETERS OF THE DEUTERIUM PLASMA FLOW WITH STAGNATION TEMPERATURE ABOUT 1 KeV AND TOTAL DIRECTED KINETIC ENERGY ABOUT 100Kj

Vasiljev V.J., Gavrilov V.V., Zhitlukhin A.M., Kiskin A.D., Lototsky A.P.,Skvortsov Yu.V., Solovjova V.G.,Umrikhin N.M., Yaroslavsky A.J.

I.V.Kurchatov Institute of Atomic Energy, Moscow,USSR

Abstract.Using model of thin current sheet the configuration of electrodes of coaxial plasma gun was calculated. The deuterium plasma clusters generated with this gun were investigated. It is found that the total amount of deuterium ions in the cluster is $\sim 3\cdot10^{20}$ its mean velocity is $\sim 5\cdot10^{7}$ cm/sec.

To obtain thermonuclear temperature using θ-pinch the preheating of plasma is necessary. The parameters of this plasma (density, temperature, total amount of particles) must be varied widely. Some methods are considered now: the shock wave or laser heating of gas, filling θ-pinch chamber volume, and the external injection of plasma.

In this work the source for plasma injection in θ-pinch is discussed. The pulse electrodynamic coaxial plasma gun was used as the plasma source. An advantage of such a source was experimentally shown [1] and was due to its high efficiency of transition of energy stored in capacitor bank to kinetic energy of plasma flow, small contamination and possibility to vary widely the plasma cluster parameters.

To obtain plasma clusters with total amount of particles about 10^{22} and kinetic energy of the order of hundreds kilojoules the accelerator device has the capacity battery with $C_0 = 5.5\cdot10^{-4}$ F, $U_0 \leq 50$ kV, $T/4 = 7.5$ μsec the peak current is ~ 5 MA. The initial vacuum is about 10^{-6} mm Hg. The device operates with pulse inlet of hydrogen or deuterium.

The operation order is following: at first the pulse electromagnet high pressure value (~ 100 atm) is opened and in the interelectrode gap the neutral gas cloud is formed. Then the voltage of the capacitor battery is applied to electrodes. Electrical breakdown and ionization of gas occurs and the plasma is accelerated by electrodynamic forces along electrodes. When the accelerated plasma reaches the tip of the inner electrode, the formation of the plasma focus on the axis of the accelerator takes place. Then current loops in the space between the electrodes are formed. The plasma cluster brakes away from electrodes. All experimental data previously achieved indicate that such process of acceleration is described quite correctly by the current sheet model. In these initial experiments the plasma clusters with total amount of particles $\sim 5\cdot10^{21}$ had the velocity $\sim 2\cdot10^{7}$ cm/sec. These clusters themselves are of considerable interest as a hot plasma source. However, it is clear that possibilities of this device were not exhausted and it is interesting to obtain plasma flows with considerable higher velocities without decreasing its total energy. For this purpose the calculation of accelerator based on the model of electrodynamic acceleration of current sheet was performed. Ohmic losses in electrical circuit, ionization losses and real gas distribution took into account in this calculation. In Fig.1 the computer inductance and configuration of electrodes corresponding to this inductance are shown. In Fig.2 the computer efficiency versus the voltage of the capacity bank for clusters with velocities $4\text{-}6\cdot10^{7}$ cm/sec and total amount of particles $\sim 5\cdot10^{21}$ are shown.

Experimental verification of the computer results was performed with copper electrodes. The external electrode is a system of 0.5 cm dia rods, arranged uniformly on 0.5 cm dia circle. The distance between neighbouring rods is 2 cm. Plasma cluster parameters(density and velocity) were measured with Mach-Zender interferometer. The shift of interference fringer was detected with the streak-camera. The typical interferogram is shown in Fig.3. The cluster front velocity obtained from these measurements is about $8\cdot10^{7}$ cm/sec, its mean velocity is $5\cdot10^{7}$ cm/sec The main part of cluster kinetic energy is in its frontal region. The density measured at the distance 50 cm from the inner electrode end is in the range 10^{16} - 10^{17} cm^{-3} for various modes of acceleration. The total amount of particles in the plasma cluster is approximately $(1\text{-}5)\cdot10^{20}$, its directed kinetic energy at $U_0 \geq 30$ kV is more than 100 kJ. This value is in a good agreement with energy calculated from the current and voltage oscillograms (see Fig.4). The impurity presence in plasma was detected using the monochromator with photomultiplier. The velocity of carbon impurity was measured with two monochromators placed along the plasma flow. It is less than $2\cdot10^{7}$ cm/sec. Therefore the impurities retard the plasma front.

As it is known from [2] the plasma focus is formed at the output of electrodynamic accelerators. In presented work electron temperature of plasma focus was measured using the soft x-ray pinhole-camera with various filters. One of the pinhole photograph is shown in Fig.5. The temperature of plasma focus obtained from these measurements is not more than 200 kV and is ~ 100 eV as a rule. Measurements of integral neutron yield have shown that it depends considerably on mass of accelerated gas and is about 10^{10} neutrons per discharge for the initial stored energy $W_0 \approx 150$ kJ. It should be noted that any special efforts were not made in order to increase the neutron yield.

Thus, as result of these investigations the deuterium plasma clusters with mean velocity $\sim 5\cdot10^{7}$ cm/sec, total kinetic energy ~ 100 kJ and length of 3 m were obtained. A good agreement of computer and experimental data allows to hope for subsequent progress in this field.

Acknowledgement

The authors wish to thank N.V.Gorjacheva, A.M.Tikhonov, S.S.Tserevitinov, A.J.Kolchenko, S.A.Sergeev, for assistance in the construction and adjustment of the experimental device and also D.A.Akhmerova, M.V.Zolnikov, M.B.Kirpa, T.M.Kurnukhin, V.D.Strizhanova for assistance in the performance of experiment.

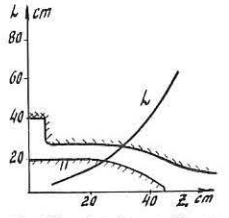

Fig.1. Electrode configuration and corresponding inductance plotted against distance from electrode base.

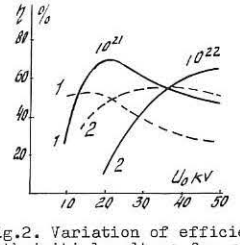

Fig.2. Variation of efficiency with initial voltage for various values of total amount particles N. Dotted lines correspond to real electrodes. Unbroken lines correspond to optimum electrodes.

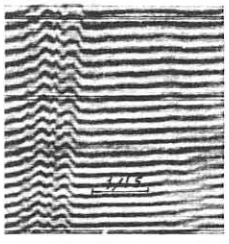

Fig.3. Interferogram of cluster front motion. $U_0 = 25$ kV

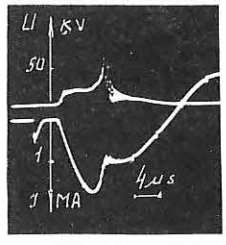

Fig.4. Current and voltage oscillograms.

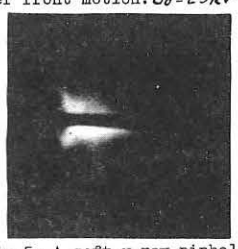

Fig.5. A soft x-ray pinhole photograph of the focus region. Filter 3 mem Al.

References

1 Aretov G.N. et al. Proc. Second Top.Conf. Pulsed High-Beta Plasmas (1972).

2 Burdonsky J.N. et al. Plasma Phys. Contr.Nucl. Fusion Research. Vienna (1971), v.I, 601.

MICROINSTABILITIES CONNECTED WITH NEUTRON EMISSION AND ELECTROMAGNETIC RADIATION IN THE PLASMA FOCUS

A. BERNARD, A. COUDEVILLE, J.P. GARÇONNET, P. GENTA, A. JOLAS
Y. LANDURE, J. de MASCUREAU, M. NAIL and R. VEZIN

Commissariat à l'Energie Atomique, Centre d'Etudes de Limeil
B.P. n° 27 - 94190-VILLENEUVE SAINT-GEORGES - FRANCE

Abstract : Maximum yield of 10^{12} neutrons has been observed with a 340 kJ bank, confirming the increase with energy of the turbulence efficiency. Neutrons are emitted predominantly by bombardment but other mechanisms could explain a smaller part of the neutrons, coming close from the anode. Hard x rays may have fast risetime and short duration.

Previous measurements /1,2/ have shown that microinstabilities occur at the end of the compression stage of the plasma and that high energy deuterons are accelerated from 700 eV to tens of keV and cause ionization of the cold gas leading to the development of a bubble.

To know whether the neutrons also could be created by bombardment of high energy deuterons onto a target we have made a careful analysis of their energy by the time-of-flight technique. Three detectors placed at more than 200 meters measure the spectra simultaneously in 3 directions (energy resolution better than 50 keV). The photomultipliers have been calibrated to know the neutron relative fluxes. It is necessary to account for the variation with energy of the neutron mean free path in atmospheric nitrogen. These corrected energy spectra are compared by a least square fit with the spectra computed from the generalized beam target model presented in /2/. Figure 1 shows for the 3 directions, both the experimental oscillogram (redrawn and enlarged) and the computed spectrum (dots) transformed in time and corrected back for the air neutron attenuation (this time scale is graduated in MeV). The deuteron distribution is chosen to be the product : function (E_d) × function (θ_d), E_d is the energy and θ_d the angle to the axis. In the discharge of Fig. 1 the incident deuteron energy distribution is proportional to E_d^{-3} with $30 < E_d < 350$ keV and to the angular distribution shown in Fig. 2. The target is at rest. The computation that yields $f^1(E_d, \theta_d)$ incorporates all experimental points of the 3 spectra with their relative calibration.

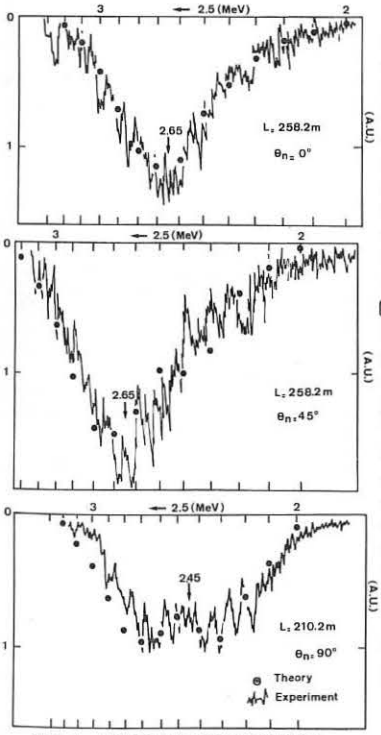

Fig. 1 - Comparison between computed and experimental spectra (see also Fig. 2).

To support these results we have studied the location of the neutron source with the equipment described in Ref. /2/. At every discharge two photomultipliers measure the total neutron yield and that coming from the part of the plasma limited by a straight cylinder whose section is a square with a 24 mm side. In Fig.3 (upper) one is interested in the ratio of the collimated neutrons to the total neutrons during the first 100 nsec of the pulse. 50 % of the neutrons are emitted in the bubble region (numbers in the squares are averages for 10 shots, before the collimator is moved to observe another region of the plasma). The study, however, with a smaller collimator (Fig. 3, lower) indicates that many neutrons come from the vicinity of the anode more than 100 nsec after the beginning of the neutron pulse at a time when the high density plasma is no longer present.

The relationship observed between the instabilities and the x rays has induced us to develop an experimental setup (Fig. 4) in which the electromagnetic spectrum could be analysed. By Ross filters 7 points (14 detectors), between 1.5 and 115 keV, can be measured at the same discharge and with a 2 nsec time accuracy. The study is possible at 20°, 55° and 90° to the axis.

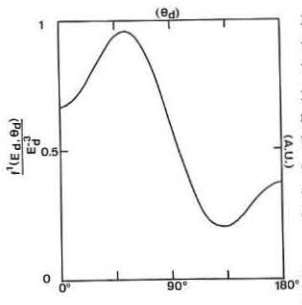

Fig. 2 - Deuteron angular distribution yielding the 3 computed spectra of Fig. 1

Preliminary results at 90° have shown the x-ray emission (above 3 keV) to be axisymmetric at high filling pressures. In the low pressure régime hard x-ray pulses (through 200 μm Uranium) have fast risetime and short duration width : lower than 1.5 nsec and 2.5 nsec respectively in the discharge of Fig. 5.

The scaling of the neutron yield with W^α and α larger than 1 (1.5 to 1.7) has been confirmed /3/ up to W = 340 kJ in a Mather-type configuration. Maximum yield of 10^{12} neutrons has been measured. The data are the following : bank voltage 40 kV, maximum current 2.7 MA reached in 5.5 μs, inner electrode diameter 230 mm, length 350 mm, outer diameter 310 mm.

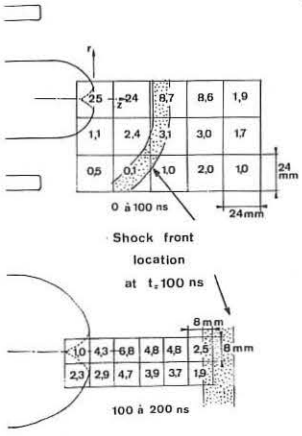

Fig. 3 - Location of the neutron source
Upper : numbers in squares are the percentage of the collimated neutrons to the total number of neutrons between 0 and 100 ns.
Lower : study of the neutrons coming from the vicinity of the anode with greater resolution between 100 and 200 ns.

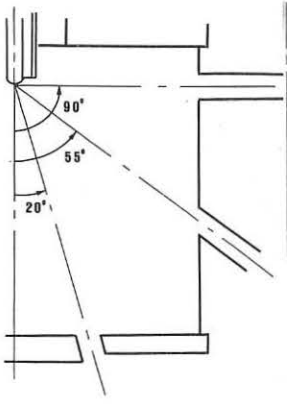

Fig. 4 - X-ray observation chamber showing 1 out of 14 ports in the 3 directions

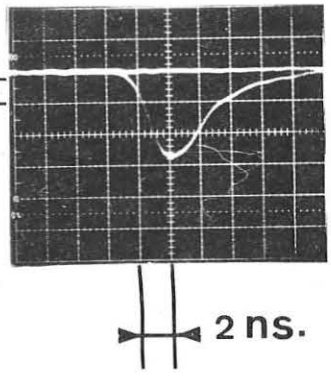

Fig. 5 - X-ray pulse behind 200 μm Uranium at low H_2 filling pressure

REFERENCES

/1/ A. BERNARD et al., Phys. Fluids 18, 180 (1975).-

/2/ A. BERNARD et al., in Plasma Physics and Controlled Nuclear Fusion Research (I A E A), Tokyo Conference, Nov. 1974.-

/3/ J.N. DOWNING, D.A. FREIWALD and J.W. MATHER, Bull. Am. Phys. Soc. 18, 1363 (1973).-

INVESTIGATIONS OF THE F-20 PLASMA-FOCUS MACHINE
BY MEANS OF LASER INTERFEROMETRY

J.Appelt, J.Nowikowski, M.Sadowski, and S.Ugniewski
Institute of Nuclear Research,
05-400 Otwock-Świerk, Poland

Abstract: Electrical characteristics of the F-20 Mather-type plasma-focus machine and the results of interferometric measurements are presented. Particular attention is paid to the effect of a hollow in the inner electrode. The results of X-ray and neutron measurements are also given.

Some plasma-focus experiments are carried out with Mather-type coaxial injectors having a cavity or a hole in the front surface of the center electrode. Such a cavity enables the distance between the electrode and the region occupied by a high-temperature plasma to be increased. A hole in the center electrode can also be used for diagnostics or other purposes, e.g., to lead a laser beam along the axis of symmetry.

The main purpose of the studies presented in this paper was to investigate the effect of a hollow in the center electrode on the operating conditions and parameters of a plasma. Experimental studies were performed with the F-20 machine [1,2] equipped with a Mather-type injector having electrodes of 30 cm in length. The outer dia. of the interelectrode gap was 10 cm, and the inner dia. - 5 cm. The injector was supplied from a 21-μF, 50-kV, current pulse generator charged to the voltage U_o = 36 kV. When the initial deuterium pressure was changed from 0.5 to 2.0 torr, the amplitude of the discharge current varried from 330 to 360kA. Appropriately, the time delay from the beginning of discharge to the current singularity varried from 2.5 to 2.8 μs. Some current- and voltage-traces have demostrated double singularities /Fig.1/. Contrary to Ref.[3], such singularities have also been observed for hollow inner electrodes. With an increase in a hole dia. a percentage of such discharges has however decreased. For the solid inner electrode it reached 15%, and for electrodes with a 2-, 8-,and 25-mm-dia. hole it was equal to 12%, 10%, and 4%,respectively.

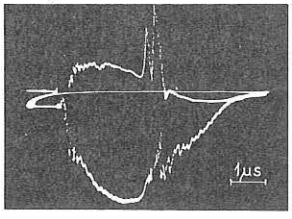

Fig.1.Oscillogram of voltage and current traces showing the double singularity.

To investigate dynamics of discharges, especially during the breakup of plasma-focus [4-5], use was made of a Mach-Zehnder interferometer equipped with a pulsed ruby laser[7]. Interferometric investigations were performed for various inner electrodes and at various initial pressures. Interferograms obtained showed that with an increase in the hole dia. the region occupied by a high-density plasma is shifted towards the electrode surface, and plasma fills up the hollow. Differences in the interferograms taken during the breakup of plasma-focus, were however small /Fig.2/. This observation was consistent with the fact that there was no difference in the average neutron yield for the solid inner electrode /Fig.3/ and for the hollow electrodes investigated. Those neutron measurements were performed with a silver activation counter calibrated with a Pu-Be source.

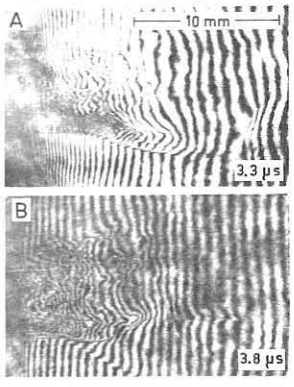

Fig.2. Interferograms of the plasma-focus breakup for an inner electrode with an 8-mm-dia./A/ and 25-mm-dia./B/hole.

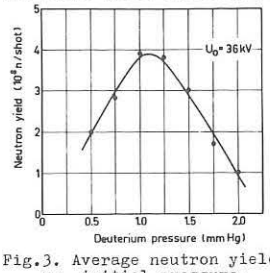

Fig.3. Average neutron yield vs. initial pressure.

Independently on the type of the electrode, the optimum operating pressure was found to be some 1 torr. The maximum neutron yield amounted then to 2×10^9. That value corresponded the point situated somewhat above the neutron yield curve given in Ref.[6].

In interferometric investigations performed particular attention was paid to the late-time stages of plasma discharges. During these late stages remarkable differences in the interference patterns were observed for various inner electrodes.

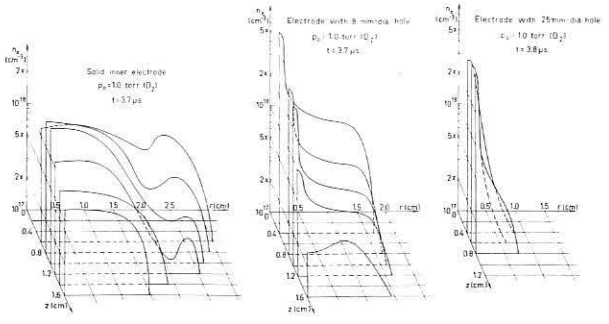
Fig.4. Electron concentration distributions as determined for various inner electrodes.

For the solid inner electrode a broad radial density distribution, of 2.5 cm in radius at the moment t = 3.7 μs /from the beginning of current/ was found /Fig.4/. For the hollow inner electrodes plasma columns had smaller dia. at that time. The measurements performed at various initial pressures showed that with an increase in pressure the dia. of the plasma column decreases, but the average electron concentration does not change very much /Fig.5/.

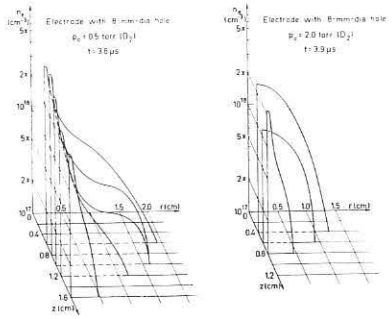
Fig.5. Electron concentration distributions at various initial pressures.

The frame interferograms /Fig.2/, as well as those taken by a streak method[8], demonstrated the disappearance of interferometric fringes in the vicinity of the inner electrode during the later stages of the discharge. This effect cannot be explained by refraction only, and it is probably connected with light absorption by metal ions evaporated from the electrode. This hypothesis has however to be verified.

The interferometric investigations described above were accompanied by X-ray measurements performed by means of a pinhole camera equipped with 15-, 45-, and 90-μ Al-filters. The measurements carried out for various inner electrodes showed that X-rays were emitted from a zone of ab. 1 cm in dia./Fig.6/.

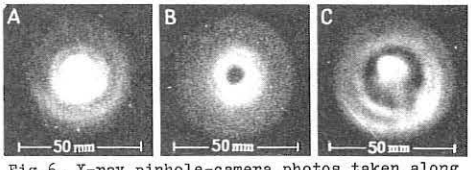

Fig.6. X-ray pinhole-camera photos taken along the symmetry axis for a solid inner electrode /A/, and for the electrodes with 8-mm /B/ and 25-mm /C/ hole; p_o = 1 torr/D_2/, 15-μ Al-filter.

For the hollow inner electrodes the maximum X-rays intensity, as registered with a standard ionization chamber, was smaller than that for the solid electrode. Independently on the type of the inner electrode, the average- and maximum-intensity of X-rays increased with a decrease in the initial pressure within the range investigated. Besides, some correlations between hard X-rays yield and voltage spikes have been often observed. These correlations are the object of further investigations[9]. Also investigated is neutron production.

1. World Survey of Major Fac. in CFR: Nucl.Fusion Suppl.1974.
2. J.Nowikowski: Nukleonika 19, 1081/1974/.
3. H.Rapp, M.Trunk: Proc. 6th European Conf./Moscow 1973/,371.
4. Ch.Maisonnier et al.: Proc. 5th European Conf. /1972/,183.
5. P.D.Morgan et al.: Proc. 6th European Conf. /1973/,359.
6. L.Michel et al.: Appl. Phys. Lett. 24, 57/1974/.
7. J.Appelt et al.: Nukleonika 19, 1/1974/.
8. M.Sadowski et al.: Proc. VI EKON Conf./1974/, Vol.B, p.28.
9. J.Nowikowski: Ph.D. Thesis /to be published/.

On $D(d,n)He^3$ and Secondary $T(d,n)He^4$ Reactions in Focused Plasmas

W. H. Bostick*, V. Nardi*†, W. Prior*†

*Stevens Institute of Technology, Hoboken, N. J., U.S.A.
†Istituto Elettrotecnico Nazionale Galileo Ferraris, Torino, Italy

Abstract: We present evidence that secondary reactions $T(d,n)He^4$ occur in a plasma focus experiment where the reacting tritium is produced by primary reactions only. Our data also show that the total D-D-neutron yield is an increasing function of the maximum energy E_{max} we observe for D-D neutrons.

1 We have observed in a plasma focus experiment - with pure-deuterium filling of the plasma accelerator chamber - the typical 14.1 MeV neutrons which are generated by secondary $T(d,n)He^4$ reactions. No tritium was introduced with the initial filling so that the reacting tritium can only be produced by primary reactions D(d,p)T. A description of the apparatus and of the methods of observation have been recently published[1] with the first group of data from these observations.

Additional data - from a 4.7 kJ (at 14.5 kV, 5.6 Torr of D_2) plasma focus at Stevens - are presented here with an analysis of the total neutron yield (n) from D-D reactions as a function of the maximum energy E_{max} for the D-D neutrons that we observe in each discharge. Our mean value $\bar{n}$ (by several hundred discharges) of the neutron yield n in a discharge is $\bar{n}\simeq 2\times10^8$ and the T-D neutron yield is $n_{T-D}\simeq10^{-4}\ n$ [1]. A remarkable fact that is consistently confirmed by our data is that $T(d,n)He^4$ reactions occur mainly within a $\sim$ 10 ns time interval, even though several independent diagnostic methods indicate that the time of strong activity in the discharge (e.g. disruption of the focused plasma column, emission intensity of soft x-rays, etc.) is longer by at least an order of magnitude[2,3]. Since according to our data the most favorable conditions for T-D neutrons productions occur in the plasma within a short time interval ($\sim$ 10 ns width), we intend to check whether or not the total D-D neutron yield in a single discharge can be correlated with the conditions (specifically those causing the hard x-ray emission) which characterize the plasma during this time interval of T-D-neutron high yield.

2 D-T neutrons are recognized by time-of-flight delay with respect to a typical burst of hard x-ray (with energy $\varepsilon \gtrsim 1$ MeV) which is emitted from the plasma at the onset of D-D neutron production. The scintillation detector we use for these hard x-rays (HXR) and for neutrons is a NE-102 disc, 28 cm dia., 5 cm thick, coupled with a 12 cm dia. photomultiplier (for a δ input the width of the output signal - including oscilloscope - is $\sim$ 10 ns) and both are sealed inside a box with lead walls 6 cm thick on all sides. Scattered x-ray with relatively smaller energy are screened out. We have observed this burst of HXR also by filling with hydrogen instead of D_2 the accelerator chamber and it is typical of the focused discharge in our operation regime, not depending on neutron-producing reactions. The signal from HXR burst has a FWHM of 30 ± 20 ns and it is usually resolved in two typical peaks 30 ± 10 ns apart on the scope trace (Tektronix 7704 display). Frequently a third (smaller) peak can be resolved within this burst. The position of the leading x-ray peak within the HXR burst is used as a time mark for our time-of-flight measurements because of peak sharpness and reproducibility in most of the discharges[1]. In order to identify the nature of a radiation pulse giving a signal after HXR we have to disentangle signal delays due to a difference Δt in the time of production (which is a priori not known) and delays $\Delta\tau$ due to time-of-flight on a chosen distance D between the source (focus) and detector system. D cannot be sufficiently increased to make $\Delta\tau \gg \Delta t$ because the radiation intensity ($\sim 1/D^2$) on the detector can decrease below significant values for observation. We can expect that only a few D-T neutrons for each discharge (or none, in some discharges) can reach a detector at $D \sim 10^3$ cm. The corresponding signal can appear at some intermediate position between the leading peak of the HXR burst (at $\Delta\tau = 0$, by definition; we evaluate all delays with respect to this leading peak of HXR) and the location $\Delta\tau_o$, say, of the leading edge of the D-D neutron signal (we define

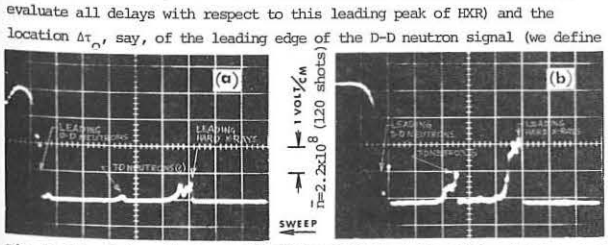

Fig. 1: Signal from discharge with (a) low neutron yield $n \lesssim 0.5\bar{n}$; (b) high yield $n \simeq 4.2\bar{n}$. Detector at 90° from electrode axis, D=1486 cm, sweep speed 100 ns/cm.

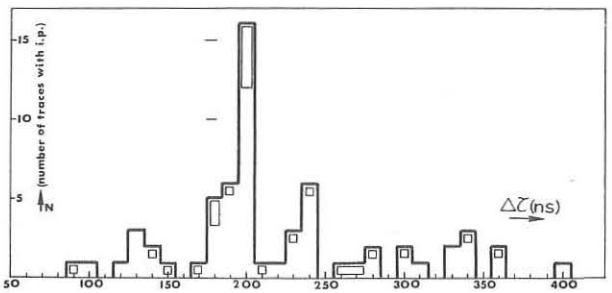

Fig. 2: The number N of scope traces (among $\sim$ 500 discharges) with only one single intermediate peak (i.p.) at $\Delta\tau$ is reported for each value of $\Delta\tau$. The double-bordered data came from 120 discharges with detector at 90° from electrode axis and D=1486 cm; other data all from 30° with different values of D; i.p. of Fig. 1a (time increases at left) is at $\Delta\tau(D')D/D' \sim 210$ ns. T-D-neutron velocity $\simeq$ 5.2 cm/ns.

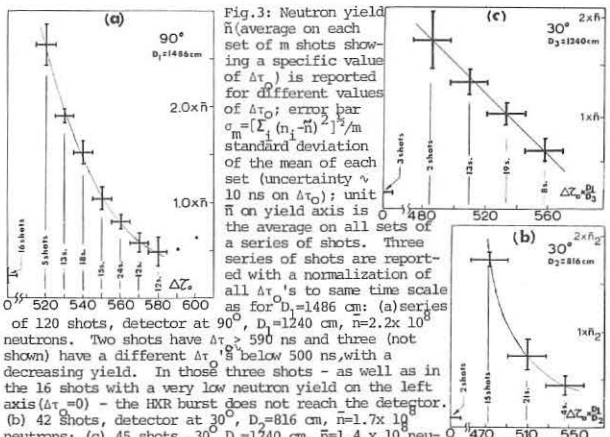

Fig. 3: Neutron yield $\tilde{n}$ (average on each set of m shots showing a specific value of $\Delta\tau_o$) is reported for different values of $\Delta\tau_o$; error bar $\sigma_m=[\Sigma_i(n_i-\tilde{n})^2]^{1/2}/m$ standard deviation of the mean of each set (uncertainty $\sim$ 10 ns on $\Delta\tau_o$); unit $\bar{n}$ on y axis is the average on all sets of a series of shots. Three series of shots are reported with a normalization of all $\Delta\tau_o$'s to same time scale as for D_1=1486 cm: (a) series of 120 shots, detector at 90°, D_1=1240 cm, $\bar{n}=2.2\times10^8$ neutrons. Two shots have $\Delta\tau_o > 590$ ns and three (not shown) have a different $\Delta\tau_o$'s below 500 ns, with a decreasing yield. In those three shots - as well as in the 16 shots with a very low neutron yield on the left axis ($\Delta\tau_o=0$) - the HXR burst does not reach the detector. (b) 42 shots, detector at 30°, D_2=816 cm, $\bar{n}=1.7\times10^8$ neutrons; (c) 45 shots, 30° D_3=1240 cm, $\bar{n}=1.4\times10^8$ neutrons. Values of E_{max} which correspond to the leading edge of the D-D neutrons signal are $\tilde{E}_{max}$ =4.1, 3.6, 3.1 MeV for $\Delta\tau_o$ = 480, 520, 560 ns respectively (D=1486 cm). Number of shots, m, in each set is marked below $\tilde{n}$.

$\Delta\tau_o$ as the time at which the amplitude of the D-D neutron signal reaches 1 volt before saturation; see Fig. 1). About 70% of our discharges show at least one (or several, if $n > \bar{n}$) of those intermediate peaks (i.p.). Scattering of HXR, delayed emission of x-rays and, possibly, γ from excited nuclei by neutron bombardment can also contribute to i.p. in addition to T-D neutrons. By using simultaneously two detectors at two different values of D we have verified that: (A) the time of production of both the HXR leading peak and of fast D-D neutrons is the same, i.e. $\Delta t=0$ (Δt and the fast D-D-neutron velocity $v=v_{max}$ are determined by $\Delta\tau=D/v - D/c + \Delta t$ with two values for both $\Delta\tau_o$, D; $c=3\times10^{10}$ cm/s); (B) several discharges show one single i.p. in both detector signals with the typical delay of a T-D (14.1 MeV) neutron which is produced at the same time of the HXR leading peak; (C) in some discharges one i.p., or a group of i.p.'s, is shown only by one detector signal and not by the other. Our analysis on $\sim$ 500 discharges indicates an accumulation of i.p. on the value of $\Delta\tau$ which is typical of a T-D neutron (with a $\Delta t=0$). The result is shown quantitatively in the histogram of Fig. 2 where all, and only the scope traces with one single i.p. are reported. Data from seven different values of D (594, 711, 816, 1216, 1240, 1428, 1486 cm) have been used with a telescopic normalization $\Delta\tau(D') \to \Delta\tau(D')\ D/D'$ to the same time scale of the detector distance D = 1240 cm. The accumulation of data points at $\Delta\tau \simeq 1240 \times [1/5.2 - 1/30]$ ns $\simeq$ 200 ns is above statistical fluctuations. The use of different values of D rules out the possibility of spurious effects due to, e.g., scattering or to an emission-delay Δt which might, accidentally, fit the time-of-flight delay of a T-D neutron for one specific value of D. The two traces in Fig. 1 illustrate borderline cases of our analysis: the traces we have reported in Fig. 2 have an amplitude (of i.p.) larger, or at least not smaller than the value 0.2 V of Fig. 1(a) and a definition of the i.p. position better than, or at least as clear as in Fig. 1(b). Data which relate the total yield $\tilde{n}$ of D-D neutrons with $\Delta\tau_o$ are presented in Fig. 3. $\tilde{n}$ is generally increasing for smaller values of $\Delta\tau_o$ and reaches a maximum value $\tilde{n}_{max} \gtrsim 2 \times \bar{n}$ for some $\Delta\tau_{o\ min}$ which depends on the direction of observation and somewhat by the performance of the focus as it is characterized by $\bar{n}$ during a series of discharges [defin. of $\tilde{n}, \bar{n}$ in caption of Fig. 3; note $E_{max}(\Delta\tau_o)$ anistropy].

3. The emission pulse of HXR, fast D-D neutrons and T-D neutron peak can be consistently explained by electron and ion inductive acceleration[1,3].

Work supported by AFOSR(U.S.); CNR(Italy); I.Avogadro Tec., c.p.10757, Roma(I).

1) Bostick, Nardi, Prior: Proc. V Conf. Plasma Phys. Contr. Nucl. Fusion (Tokyo, 1974).
2) Bernard, Coudeville, Jolas, Launspach, deMascureau: Phys. Fl. 18, 180 (1975).
3) IEN-SIT Contrib.: Proc. I. Conf. Energy Stor. Compr. Switch. Asti 1974, Plenum, N.Y.

A Theoretical Model for the Mather-type Plasma Focus

by

H.J. Kaeppeler, N. Ruhs, M. Trunk and G. Decker

Institut für Plasmaforschung der Universität Stuttgart
Federal Republic of Germany

Abstract: For developing a theoretical description of physical phenomena in the plasma focus, MHD and PIC calculations and analytical solutions were carried out. A comparison of these shows that m = 0 instabilities are the macroscopic reason for electron and ion beams producing microinstabilities, the ion beam-beam interaction also producing the majority of neutrons.

The purpose of this paper is an attempt at establishing a consistent model of the compressed phase in a Mather-type plasma focus device. According to Bernard et al. /1/, the plasma sheath forming behind the anode collapses into a very dense and quiescent column of about 1 mm minimum radius. The plasma (ion) temperature in this very dense phase is approximately 500 to 700 e.V. and agrees with the value calculated from a thermalisation of the compression kinetic energy. From snow-plough theory and consideration of diffusion of the magnetic field into the plasma, Kaeppeler /2, 3/ derived an equation for the minimum plasma radius r_m

$$\left(\frac{r_m}{R_0}\right) = \frac{z_{pf}\sqrt{8\pi\rho_0}\;c^3}{I_0\cos\left(2\pi\frac{t_0}{t_c}\right)4\pi\sigma_m}\;\frac{L_m/L_0}{\Delta L}\quad , \qquad (1)$$

where R_0 ist the anode radius, I_0 the maximum current, $t_0 = v_r/R_0$ the plasma compression time (v_r = compression velocity), $t_c \sim \sqrt{L_0 C_0}$ the "circuit time" (C_0 = capacitance of the condensor bank), L_0 the inductivity of the circuit. L_m the total inductivity of the system at $r = r_m$, and $\Delta L = L_m - L_0$ the gain in inductivity due to compression. σ_m is the electrical conductivity, determined by the electron temperature which, from scattering experiments, Bernard /1/ estimates at $T_e \approx 100$ e.V.. From infrared measurements, H. Schmidt /6/ also obtains values for T_e lower than T_i. Furthermore, soft component x-ray measurements /7, 8/ indicate T_e values between 200 and 400 e.V.. Using a value of $T_e \approx 100$ to 300 e.V., Eq. (1) for r_m, and

$$\left(|\vec{E}|\right)_{max} = \left|\frac{I_m}{c}\left(\frac{dL_z}{dt}\right)_{max}\right| = \frac{I_m^2}{c^2 R_c^2}\left(\frac{R_c}{r_m}\right)\sqrt{\frac{2}{\pi\rho_0}} \qquad (2)$$

cf. /4/, the maximum average field strength $\left(|\vec{E}|\right)_{max}$ on the axis of the focus can be calculated. For a current of 1 MA, anode radius R_0 = 5 cm, plasma radius 0.1 cm, there result fields in the order of 20 kV/cm, in agreement with MHD-calculations /5/, used with PIC-calculations /9/ of the compressed stage of the plasma focus. According to Bernard /1/, this very dense and quiescent stage lasts for approximately $8\cdot10^{-9}$ sec.

One of the mechanisms, disrupting the very dense phase, are m = 0 instabilities, experimentally observed by H. Schmidt /10/ among others. Analytical theory shows /4/ that ion viscosity does not essentially damp the growth of the instabilities but acts selectively on the wavelength for which maximum growth rate occurs. It turns out that $\lambda_m \approx r_m$, if the m = 0 instabilities set in when the minimum plasma radius is reached. Recent MHD calculations /8/ also show the appearance of m = 0 instabilities, though with an inappropriate time scale due to a too high von Neumann viscosity in the calculation. It can be shown /4/ that due to these m = 0 instabilities, the local electric field strength $|E|_z$ can rise from the average 20 kV/cm to 200 kV/cm in approximately 10^{-8} sec or slightly less.

As the critical field for electron runaway under plasma focus conditions ($T \approx 700$ e.V., $n \approx 3\cdot10^{19}$ cm^{-3}) is approximately 30 kV/cm /4/, the m = 0 instabilities cause a local breakup of the dense column and simultaneously cause the onset of electron runaway. This results in beam-plasma instabilities (cf. Fig. 1) of the Bunemann type with a growth rate of $\omega_i \approx 10^{10}\,sec^{-1}$. Fig. 1 shows that because of $T_i/T_e > 1$ in the dense phase of plasma focus, also kinetic instabilities due to hot ions may occur.

From his PIC calculations, Ruhs /9/ has established a beam-beam collision model for the neutron production. It turns out that the deuterium ions accelerated by the electric field of Eq. (2) and crossing the focus axis repeatedly form beams [cf. also Fig. 2] which upon collision whith each other produce more neutrons then those from beam-target interaction. The total of the accelerated ions form a disperging beam observed by Bernard /1/ and by Schmidt /10/. This ion beam also gives rise to kinetic instability /12 - 15/.

In order to determine the regime for the appearance of these kinetic ion instabilities, the values of n_1/n_0, $\Delta v_b/v_b$ and v_b were determined from the PIC calculations /9/. The subscript 1 denotes beam values, 0 plasma values, v_b is the beam velocity, Δv_b the beam velocity spread. It is seen from Fig.3 that, locally, n_1/n_0 can exceed unity and, taken over the entire plasma column, n_1/n_0 is relatively large. Figs. 4 and 5 show that the ion beam has to be considered as "hot". The condition $v_b > (T_e/m_i)^{1/2}$ prevails, as v_b is in the order of 10^8 cm/sec and $(T_e/m_i)^{1/2}$ in the order of 10^7 cm/sec. For waves propagating parallel to the electric field ($E \perp B$), the cold-plasma condition prevails bacause $\Delta v_b/v_b < (n_1/n_0)^{1/3}$ and the growth rate of the instability is, because of $\omega_{p_e} \gg \omega_{c_e}$ near the axis,

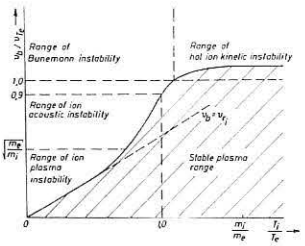

Fig. 1: Ranges of stability and instability of hot electron-ion plasma with electron and ion beam formation

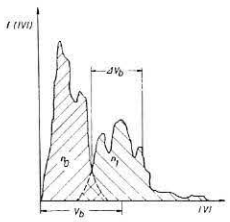

Fig. 2: Typical ion velocity distribution in plasma focus from PIC calculations

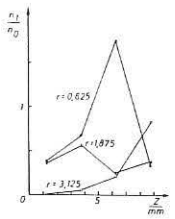

Fig. 3

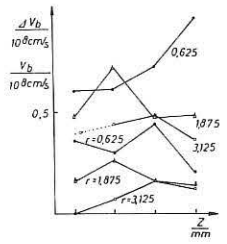

Fig. 4

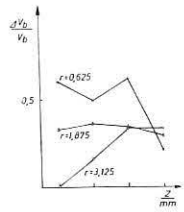

Fig. 5

Fig. 3: Ratio of ion beam and plasma densities n_1/n_0 for various radii along z-axis

Fig. 4: Velocity spread Δv_b and velocity v_b of ion beam in plasma focus from PIC calculations

Fig. 5: $\Delta v_b/v_b$ – ratio for various radii and axial positions z from PIC calculations

$$\widetilde{\omega_i} \approx \left(\frac{n_1}{n_0}\right)^{1/3}\left|\omega_{c_e}\omega_{c_i}\right|^{1/2} \quad , \qquad (3)$$

where $|\omega_{ci}\,\omega_{ce}|^{1/2}$ is the hybrid frequency. In the range of highest v_b, n_1/n_0 is practically unity, so that the hybrid frequency actually determines the growth rate of the kinetic instability. In this same range, the magnetic field is of the order of 10^5 Gauss according to PIC calculations, so that the hybrid frequency and with it the growth rate is of the order of $10^{10}\,s^{-1}$, just as in the case of the electron runaway instability.

It is thus shown that a theoretical model for the Mather-type plasma focus will have to incorporate electron runaway as well as a kinetic instability due to the ion beam which is responsible for neutron production. Both fast components, electrons and ions, result from acceleration in locally enhanced fields produced by m = 0 instabilities.

References

1. A. Bernard, A. Coudeville, J. Durantet, A. Jolas, J. Launspach J. de Mascureau, and J.P. Watteau, Phys. Fluids, 18, 180-194 (1975)
2. H.J. Kaeppeler, Institut für Plasmaforschung der Universität Stuttgart, Report IPF-74-7, 1974
3. H.J. Kaeppeler and N. Ruhs, Physics Letters 49A, 383-385, 1974
4. H.J. Kaeppeler, Instabilities in the Plasma Focus. Invited Paper presented at the 2 nd International Congress on Waves and Instabilities in Plasmas, Innsbruck (Austria) 1975. Report IPF 75-1
5. M. Trunk, Institut für Plasmaforschung der Universität Stuttgart, Report IPF-73-2, 1973
6. H. Schmidt, Verhandlungen der DPG 7/1974, p. 508
7. R. Schön, Institut für Plasmaforschung der Universität Stuttgart, Report IPF-INT-74-1, 1974
8. B. Nahrath, Thesis, Institut für Plasmaforschung der Universität Stuttgart, Oct. 1974
9. N. Ruhs, Ein Vielteilchenmodell zur Beschreibung der Neutronenproduktion im Plasmafokus. Diss. Univ. Stuttgart, 1975
10. H. Schmidt, Verhandlungen der DPG 4/1975, p. 297
11. N. Ruhs, Verhandlungen der DPG 4/1975, p. 298
12. O. Bunemann, J. Nucl. Energy, C, 4, 111 (1962)
13. R.Z. Sagdeev, Sov. Physics - Tech. Physics 6, 867 (1962)
14. A.A. Vedenov, E.P. Velikhov, and R.Z. Sagdeev, Sov. Physics-Uspekhi 4, 332 (1961)
15. V.L. Sizonenko and K.N. Stepanov, Nucl. Fusion 7, 131 (1967)

ANALYTIC SOLUTIONS FOR THE MOTION OF THE AXIAL SYMMETRIC CURRENT SHEATH IN A PLASMA FOCUS

F.Gratton and M.Vargas
Laboratorio de Fisica del Plasma, Facultad de Ciencias Exactas y Naturales, UNBA, Buenos Aires, Argentina.

Abstract: The motion of the current sheath (CS) is approximated by a partial differential equation whose solutions are given by simple analytic formulae. The shape of the CS can be obtained graphically for general initial and boundary conditions by means of a nomograph. An example shows the "rolling-off" and the formation of the "bubble" in the plasma focus.

The motion of the CS in the plasma focus has been thoroughly studied numerically by Potter[1]. However,considering the complexities of the computation and its results,we felt that there is still a need for a simpler, albeit only approximate, way to describe the CS evolution which can provide analytic formulae. For many purposes like project design or estimations of self inductance variations our graphical construction of the solution may be useful. We have been preceded by Basque, Jolas and Watteau in the attempt to obtain the CS motion from simple "snow-plow" models[2]; however they could only study the coaxial stage. Differing from them,our treatment starts anew from a partial differential equation for the CS surface and allows for a large set of initial and boundary conditions which include the ordinary plasma focus disposition of electrodes and also many other variations around this theme.

Assuming axial symmetry and cylindrical coordinates (z along the axis of the apparatus) the magnetic field between the electrodes and the CS is $B_\theta = 2I(t)/cr$. Neglecting the acceleration effects and the width of the CS, the linear momentum balance equation along the normal to the CS is given by $\rho_0 v_n^2 = B_\theta^2/8\pi$ (ρ_0: initial density of gas in front of CS). Let $z = f(r,t)$ be the equation for the CS surface. The normal velocity of advancement is given by $v_n = \pm f_t/(1+f_r^2)^{1/2}$. Hence we obtain the following non linear partial differential equation for f

$$\frac{\partial f}{\partial t} = \pm \frac{a(t)}{r}\sqrt{1+\left(\frac{\partial f}{\partial r}\right)^2} \qquad (1)$$

where $a(t) = I(t)/\sqrt{2\pi\rho_0}c$ (here I(t) is the total current in CS; c: velocity of light, cgs units throughout) Equation 1 can be transformed in a quasilinear one introducing the new variable $N = r\cos\phi$, where ϕ is the angle between the normal to CS and the z axis. We have then

$$\frac{\partial f}{\partial t} = a(t)\,N \quad , \quad \frac{\partial f}{\partial r} = s\sqrt{\frac{r^2-N^2}{N^2}} \quad , \qquad (2)$$

and

$$\frac{\partial N}{\partial t} - s\,\frac{a(t)}{r^2}\sqrt{r^2-N^2}\,\frac{\partial N}{\partial r} = 0 \quad , \qquad (3)$$

where $s = \text{sign}(f_r)$ ($s^2 = 1$). Equation 3 can be solved by the method of the characteristics[3]. The 'characteristic base curves' $C_i(r,t)$ of eq.3 in the r,t plane are given by

$$\frac{dr}{dt} = -s\,\frac{a(t)}{r^2}\sqrt{r^2-N^2} \quad , \qquad (4)$$

and along each one of them N is a constant ($N = N_i$ say, where the i means initial value). The $C_i(r,t)$ determines cylinders in the z,r,t space that intersect the $z = f$ surface along the true characteristic lines which generate the solution. It is found more convenient to work with the projections $C_i(z,r)$ of the z,r,t characteristic lines on the z,r plane, instead of eq.4. From the previous equations one can easily find that

$$\frac{dz}{dr} = -s\,N_i/\sqrt{r^2-N_i} \qquad (5)$$

holds for the $C_i(z,r)$, which gives

$$x/|N_i| = \text{Ch}\,\eta \quad , \quad \eta = \text{Arg Ch}\,r_i/|N_i| - s(z-z_i)/N_i \qquad (6)$$

Furthermore, along the $C_i(r,t)$ we have $dz/dt = a(t)N_i/r^2$ and substituting eq.6 in here we can integrate to obtain the relationship between z and t:

$$\text{Sh}\,\eta\,\text{Ch}\,\eta - s\,\frac{(z-z_i)}{N_i} - \frac{r_i}{N_i}\sqrt{\left(\frac{r_i}{N_i}\right)^2-1} = -s\tau \quad , \quad \tau = \frac{2}{N_i^2}\int_0^t a(t')\,dt' \quad . \qquad (7)$$

If we know the initial shape $z_i = z_i(r_i)$ and consequently $N_i = N_i(r_i)$, then we can eliminate r_i between eq.6 and eq.7 and obtain the solution $z = f(r,t)$ which satisfies the initial data.

From eqs. 2 and 5 it follows that the $C_i(r,z)$ are always orthogonal to the projection of the solution on the r,z plane. Hence from a practical point of view it is convenient to draw a nomograph with the C_i curves which start at a single point for all values of $\cos\phi$ (see fig.1 where $\cos\phi_i = 1$, $r_i = 1$ at $z_i = 0$). For $r_i = 1$ we have curves for all possible values of $\cos\phi$; for $r_i \neq 1$ making shifts in the z direction (shape of C_i is invariant for z translation) we have at our disposition a fairly large choice of curves with different values of N_i. It is not necessary to compute $z = z(\tau)$ for all the r_i values. It is sufficient to consider the case $N_i = 1$, $r_i = 1$, $z_i = 0$ which corresponds to $\tau = z + \text{Shz Chz}$ and $r = \text{Chz}$. Then we can mark the time scale on this particular C_i easily. After completing the orthogonal lines of the $z = f$ solution we will assign the corresponding τ value which follows from their intersection with $r = \text{Chz}$. An example of the application of this procedure to the plasma focus with hollow center electrode is shown in fig.2 (which was obtained graphically by working with transparent paper on the nomograph). Clearly this method is also applicable to a variety of similar problems with different electrode shapes and different initial conditions for CS giving the solutions in a very short time.

We will clarify some aspects of this method, referring to fig.2 as an illustration. The C_i given by eq.6 have a minimun for $r = r_- = N_i$ which happens when $r_i/r_- = \text{Ch}[(z_- - z_i)/r_-]$. This fact allows us to know the sign s; for instance if $z > z_-$ then $r > r_-$ and $(dz/dr)_{C_i} > 0$, that is $\partial z/\partial r < 0$ for the solution. The line which joins the r_-, z_- points separates the CS in two parts with different s sign (this is the dotted line in fig.1). We can also impose boundary conditions to extend the solution beyond the domain of dependence of the initial data. We can give a condition on the central electrode like asking that $\phi = \phi_e(r)$ at $z_e = z_e(r)$. In particular we imposed that CS is normal to the upper face of the central electrode in fig2 because this condition seems to fit the available evidence from photographs of CS. The CS profile in the domain of dependence of the electrode is given by $z - z_0 = -\frac{1}{2}[\, r - \sqrt{r^2-1} - \text{ArgChr}\,]$ (taking $r_i = 1$) and does not change during the motion along z . We call this solution the "traveling wave". At the electrode edges we assumed that the CS immediately gives rise to a set of N_i values,much like a point source of characteristics. It is apparent from figs.1 and 2 that an envelope of the C_i forms as the CS rolls-off toward the axis. The CS is normal to the envelope which has a finite angle at the point of contact with the axis. We can extend the solution beyond the envelope (singular solution of eq.5) assuming that along the axis, at r=0, the new characteristics are given by the envelope itself. The "singular profile" which is so determined is also a 'traveling profile' which has the form of a'bubble'(see fig2). This is a well know feature of the later stages of the focus (see fig.3).

We are grateful to the Stevens group for the photograph fig.3. This work have been supported in part by the Argentine CNEGH (Comisión Nacional de Estudios Geo-Helio-Físicos) and the CONICET (Consejo Nacional de Investigaciones Científicas y Técnicas).

Fig.3

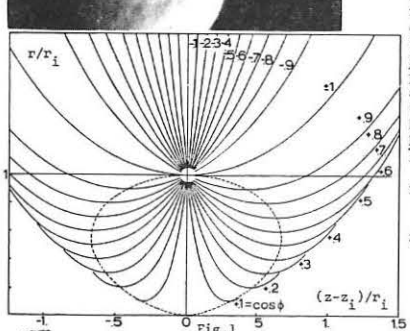

Fig.1

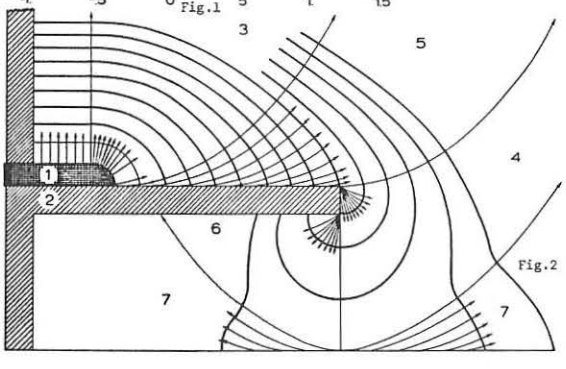

Fig.2

Fig.1: Nomograph from eq.6
Fig.2: Example of CS motion for a plasma focus (hollow central elect.; external elect. not shown) Initial CS is assumed to follow the insulator shape (arbitrary scales for r and τ). 1 insulator; 2 elect.; domain of dependence of: 3 insulator, 4 borders of elect.; external 5 and internal 6 domains of dep. of elect; 7 singular solution (bubble).
Fig.3: Image converter photograph of the later stage in the plasma focus (side view; deuterium, 11 Kv, 5.6 torr).

References:
1. D.E.Potter,Phys.Fluids 14 (1971) 1911.
2. G.Basque,A.Jolas,T.P. Watteau, Phys.Fluids 11 (1968) 1384.
3. R.Courant and D.Hilbert Methods of Mathematical Physics, VolII, NY,1966.

DEPENDENCE OF FOCUS INTENSITY ON MASS AND FIELD DISTRIBUTION

S. Lee[+], T.H. Tan.
Physics Department, Universiti Malaya, K.L.,Malaysia.
[+]Presently: Institut für Plasmaphysik, KFA, Jülich, BRD.

Abstract: Using piezoelectric probes we estimate that at the end of the axial run-down region 4-7% of the ambient mass encountered arrive in time to participate in the focusing action. Focusing intensity appears to depend more on the magnetic field distribution than on the mass distribution.

In theoretical computations of focus trajectories it is necessary to include in the radial equation of motion a quantity (m_o) representing the amount of mass that is swept from the axial run-down region into the radial focusing region. In the present work measurements are made at the end of the axial run-down region which enable an upper limit to be placed on this m_o.The measurements also throw light on an important associated problem; namely the dependence of focusing intensity on the mass and magnetic field distributions. A knowledge of this dependence could be useful in the design of a fusion machine based on the focus principle.

We use a calibrated PZT piezoelectric probe (1) and a magnetic field coil for these measurements. The calibration pressure signals were carefully studied so that the probe response time and inherent noise harmonics were known. In the actual measurements the pressure signals were processed to eliminate these noise harmonics.

The focus device in which these measurements were made (2,3) was operated with deuterium at o.2 torr with 8 kJ. For these operating conditions it was noticed that the focusing intensity was not reproducible as judged from voltage and current oscillograms. Indeed for some shots, the characteristic focusing voltage spike and current dip were absent.

A comparison is made of the pressure (P) and magnetic field (B) oscillograms for focusing (F) and non-focusing (NF) shots. In Fig. 1 the B oscillograms have been transformed into B as distance coordinates. A distinct difference (very reproducible) can be observed between the B distributions of a F and a NF shot. The F shot has a high current density in the first1 to 2 cm of the current sheet with B rising typically to o.8 T in the first 1 1/2 cm. The NF shot has a much lower current density with B rising to only o.4 T over 7 cm. For the P pulses, a somewhat typical distribution (for example Fig.2) for the F shot shows a sharp narrow pulse in the first part of the P signal. For the NF shot, this frontal pulse is not so sharp or distinct.

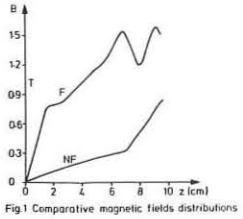

Fig.1 Comparative magnetic fields distributions

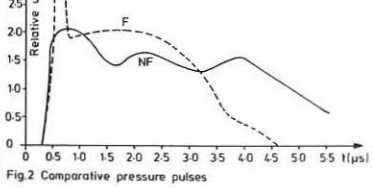

Fig.2 Comparative pressure pulses

In order to quantify the P measurements, an empirical model is used in which the frontal part of the P pulse is taken to be a shock in which there is a post shock magnetic field. This is to conform with experimental observations , and has the correct effect of lowering the post shock kinetic pressure (when compared to a gas shock model) for each given shock speed. By empirically taking the ratio of specific heats to be x = 2 the pressure measured at the probe face could be related to the free-stream Newtonian pressure (4). The density ratio Γ is then computed from the measured pressure.

The P pulse is divided into 2 regions for study namely (i) the first o.o5 μs and (ii) the first o.3 μs. The mass arriving in the first o.o5 μs is here called the"initial"mass. The mass arriving after this o.o5 μs could not participate in the focus since the focus action occurs in o.o5 μs. The time of o.3 μs corresponds to the e^{-1} diffusion time of the probe. Beyond this time the diffusion of the B field behind the probe face would make the estimate $q\Gamma$ and hence of mass an underestimate.

The results show that the "initial mass" is 4-7% of the ambient mass with F shots having a slightly greater initial mass than NF shots. Due to the continual axial motion of the imploding plasma, it is expected that "m_o" is only a small fraction of this initial mass. This is in agreement with a recent radial trajectory computation (5). Also F shots have a slightly greater quantity of mass (3o % of ambient mass) in the first o.3 μs than NF shots.

The most important factor in deciding the intensity of a focus appears to be the magnetic field distribution associated with the current sheet; although it is also observed that the structure of the current sheet has some points of correlation with the structure of the pressure pulse.

1. Lee S., Ph. D. Thesis A.N.U. (1969)
2. Lee S., Chen Y.H., Mal. J. Sci. 3 (1975)
3. Chen Y.H., Lee S., Int. J.Elec. 35 (1973) 341.
4. Lee S., Sandeman R.J., J. App. Phys. 43 (1972) 3980.
5. Lee S., Chen Y.H., XII ICPIG Eindhoven (1975) submitted.

KMS FUSION HIGH POWERED LASER FOR FUSION EXPERIMENTS,
ITS PERFORMANCE AND EXPERIMENTAL APPLICATION (1)

B. R. Guscott, G. Charatis, J. S. Hildum, R. R. Johnson,
F. J. Mayer, N. K. Moncur, D. E. Solomon, C. E. Thomas
KMS Fusion, Inc., Ann Arbor, Michigan, United States of America

Abstract: The performance of a high power Nd:glass laser system for laser fusion experiments will be discussed. A series of well characterized target shots will be presented, showing the effects of laser power on neutron scaling. The microsphere targets used in these experiments will be discussed, along with techniques for their characterization.

In the KMS Fusion laser system the laser pulse originates in a mode locked Nd:YAG oscillator and is then shaped temporally by a KMSF designed and constructed pulse stacker. Laser pulse shaping is essential to successful experiment performance. It has been found both experimentally and theoretically that the laser pulse shape has a great influence on compression and on the symmetry of an implosion.

The pulse stacker acts upon a single selected laser pulse from the oscillator by means of reflections and optical delays to generate a shaped pulse. As many as 22 individual reflection pulses have been used to form the stacked pulse train, with a minimum separation of 40 psecs between adjacent reflected pulses. The width of the stacked pulse is adjustable from 30 psecs to greater than 1 nsec with a rise and fall time of 15 to 20 psecs.

After the stacked pulse is formed it is amplified by a series of conventional Nd:glass rod amplifiers (fabricated by CILAS). The output of this rod amplifier train is 20 joules in 250 psecs with a beam diameter of almost 8 cm. The laser energy is further increased by a series of slab amplifiers (fabricated by General Electric) each with a 10 cm clear aperture. The KMSF laser system configuration used for the experiments to be detailed later is shown in Figure 1.

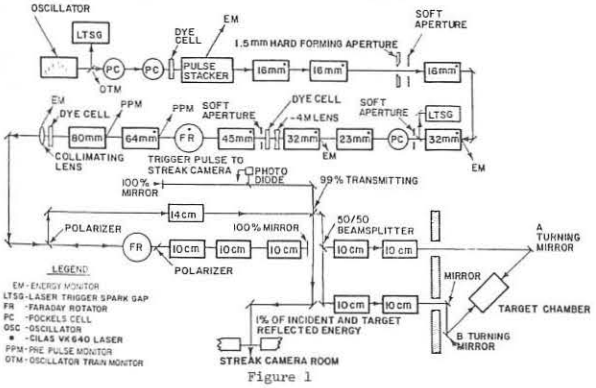

Figure 1

Control of the laser beam's spatial intensity variations is paramount to the successful repetitive operation of a large high power laser system. To achieve this KMSF designed and constructed a series of apodised apertures and a high power spatial filter. The apodisers use a unique absorbing fluid that is index matched to the glass windows by careful thermal control of the unit. The liquid glass combination presents a pre-calculated absorption profile to the incident 1.06 μ laser beam, resulting in a reshaping of the beam's spatial profile without the addition of further noise components. The high powered spatial filters currently placed between the 80 mm rod amplifier and the first disc amplifier serve to reduce considerably the beam's high frequency spatial noise, thus spatially preparing the beam for amplification by the disc amplifiers.

The KMSF laser system has been used to produce implosions in DT gas-filled glass micro-spheres. There have been approximately 500 experiments performed during the past year which have resulted in neutron production from the compressed deuterium-tritium fuel. Neutron yields of the order of 10^7 have been measured as well as volumetric reductions of the order of 1000.

A series of well-characterized target shots were performed to study the effect of laser power on neutron scaling. The targets were approximately 55 μ in diameter with aspect ratios ($R/\Delta R$) of 20:1 and 40:1, and with gas fill pressures of 10 or 100 atmospheres. It was found from the four different target characterisitcs that the neutron production increased as the pulse length was decreased from 480 psec to 240 psec maintaining 60 joules on target. The largest neutron yields were achieved at the lower pressure and 40:1 aspect ratio. The diagnostics used for these measurements consisted of X-ray pinhole cameras to determine the volumetric conpression, neutron and X-ray detectors to determine the yields and spectral distribution. The results from a typical X-ray pinhole camera photograph including the micro-densitometer trace are given in Figure 2.

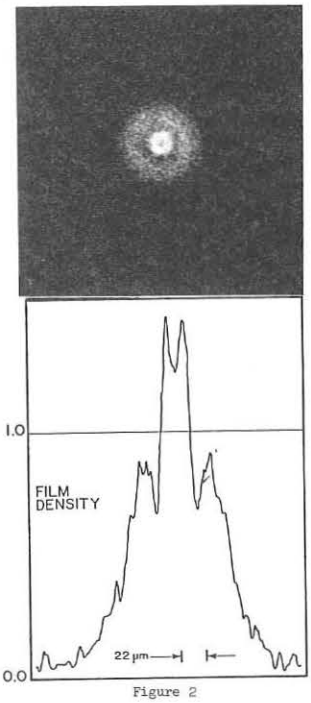

Figure 2

Figure 2. The energy balance of the laser-plasma interaction was made using photodiodes, charge collectors, time-of flight mass spectrometer, X-ray thermo-luminescent dosimeters (TLD's) and calorimeters.

During these experiments the fluorescent and prepulse energies were monitored and it was observed experimentally that prepulse energies in excess of 0.17 millijoules degraded the implosion characteristics. The fluorescence measurements indicated that energies in excess of 20 millijoules were sufficient to significantly alter the target plasma properites.

The neutron yields of the order to 10^6 were achieved in these experiments with 0.24 TW of laser energy on target and are expected to increase rapidly as the KMSF laser output energy is expanded.

(1) A portion of this work was supported by a contract with the Energy Research and Development Administration.

LASER FUSION, THEORY, EXPERIMENTS AND LASERS AT LLL*

J. L. Emmett, J. H. Nuckolls, H. G. Ahlstrom, C. D. Hendricks, L. W. Coleman, J. A. Glaze, J. H. Holzrichter, G. H. Dahlbacka

University of California/Lawrence Livermore Laboratory
Livermore, California 94550

ABSTRACT

The realization of laser fusion requires advanced developments of many disciplines: high power lasers, optics, 2-D magneto fluid dynamic codes, microscopic fast time diagnostics and target fabrication. The laser fusion program at LLL which involves 230 scientists, engineers and technicians has made significant advances in all of the above areas. Nd glass lasers are now irradiating targets with laser powers of 0.4 - 1.0 terrawatts. Laser fusion targets of the exploding pusher genre have produced up to 10^7 14.1 MeV neutrons from the D + T reaction. By measuring the energy spreading of the 3.5 MeV He^4 reaction product it has been demonstrated that the results are consistent with an ion temperature of 1.7 - 1.9 KeV. The 2-D code calculations are in good agreement with the experimental results which increases the confidence in extrapolations to break even and net gain targets. Significant advances are also described in the fabrication of the microscopic targets and in picosecond, micron scale diagnostics.

*Work performed under the auspices of the U.S. Energy Research and Development Administration.

EXPERIMENTAL STUDY OF THE LASER DRIVEN SHOCK WAVE PROPAGATION INTO SOLID TARGETS

D. BILLON, D. COGNARD, J. LAUNSPACH, C. PATOU, D. SCHIRMANN

Commissariat à l'Energie Atomique, Centre d'Etudes de Limeil
B.P. n° 27, 94190-VILLENEUVE-SAINT-GEORGES, FRANCE

Abstract : Plane and cylindrical shock wave propagation through solid targets is studied in one beam and four beam experiments. Density and pressure behind the shock as functions of the absorbed laser flux are deduced from the shock velocity using the state equation of the material.

The illumination of a solid target by the focussed beam of a powerful pulsed laser leads to the formation of a dense and hot plasma. Under the considerable pressure exerted on the solid material, this one is set in motion and may be compressed to densities well above solid state density according to theoretical models /1,2,3/. The first experimental observation of this prediction is relatively recent and was made in Garching /4,5/. In this paper, we present experimental results concerning the propagation of a laser driven shock wave firstly in plane geometry where a single laser beam is focussed onto a plane target and secondly in cylindrical geometry where four coplanar and orthogonal laser beams are focussed onto a hollow cylindrical target.

In plane geometry, the experiments are performed with one of the four beams emitted by our neodymium glass laser C_6 device. The maximum energy which can fall on the target is 30 J. The rise time and the half width of the laser pulse are respectively 1 ns and 3 ns. The contrast ratio between the maximum power and the power before the laser pulse is greater than 600. The laser light is focussed by a $\frac{f}{1.5}$ (f = 117 mm) aspherical lens down to a spot size of 60 μm. For the experiments described here the target consists of a thin polyethylene foil of 30 μm thickness ΔX .

The dense and hot plasma created on the front surface of the target and the emergence of the shock front from the free surface of the foil is observed with a JAMIN interferometer illuminated by a diagnostic laser beam at 0.53 μm. The direction of analysis is perpendicular to the target normal. The interferograms are photographed by three framing cameras which can be opened during one nanosecond at different times during the shock wave propagation and by an ultra fast streak camera TSN 504 /6/. Transit time Δt of the shock front through the foil is deduced from the instant at which the free surface is set in motion. The mean velocity D of the shock front is calculated by the relation :

$$D = \frac{\Delta X}{\Delta t}$$

The value of D allows us to determine the pressure P and the density $\frac{\rho}{\rho_o}$ behind the shock front by using Hugoniot's equation :

$$P = \rho_o D u \qquad \text{and} \qquad \frac{\rho}{\rho_o} = \frac{D}{D - u}$$

where ρ and ρ_o represent the density behind the shock and the initial solid density. Moreover we assume that the material velocity u is related to D by the empirical relation

$$D = C_o + \lambda u$$

where C_o and λ are constants which we taken respectively equal to 2.9 10^5 cm/s and 1.48 according to /7/.

The shock area S_s is deduced from the dimension of the shock at the time of its emergence. The comparison of the value of S_s to the area S_f of the laser energy deposition shows an effective enlargement of the shock wave due to lateral heat conduction according to /5/.

For this reason the absorbed laser flux ϕ_a is evaluated by the relation

$$\phi_a = \frac{E_a}{t \cdot S_s}$$

where E_a is the absorbed laser energy at the emergence time of the shock wave and S_s is the effective area of the shock front at the time of its emergence in order to take into account the two dimensional effect due to lateral heat conduction. The value of E_a is obtained by subtracting the reflected energy measured by calorimeters into the half space from the incident energy.

At increasing absorbed laser fluxes ϕ_a from 5.10^{12} W/cm^2 to 8.10^{13} W/cm^2, we have measured decreasing transit times from 5ns to 1.5ns. Corresponding pressure P and density $\frac{\rho}{\rho_o}$ increase respectively from 90 kbar to 2 Mbar and from 1.4 to 2.3 as we can see in figure 1.

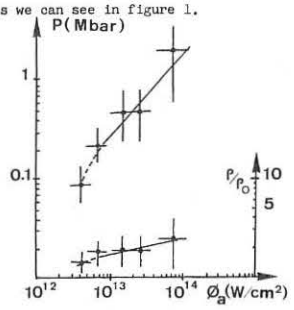

figure 1

Measurements made with a thicker foil ΔX = 100 μm in this laser flux range show that the transit time is greater than the laser pulse duration.

In cylindrical geometry the experiments are performed with the four beams emitted by our neodymium glass laser C_6 device. The beams are focussed with similar $\frac{f}{1.5}$ (117 mm) focal lens length. The focusing conditions are chosen to favour the uniformity of the laser energy deposition on the outer surface of the target, i.e., according to /8,9/. The focal spot of each lens is placed at a distance d beyond the axis of the target equal to about $\frac{5}{2} R_e$ where R_e is the outer radius of the target. The target is a hollow cylinder made of aluminium. The first purpose of these studies is to explore the effects of asymmetry of the laser light deposition on the structure of the convergent laser driven shock wave. The second purpose is to measure its transit time through the target wall thickness and its convergence time.

The emergence of the shock front at the inner surface of the target is detected by observing the intensity of a probe laser beam transmitted along the axis of the target with a high velocity streak camera TSN 504 /6/. When the wave front emerges from the inner surface, the probe laser light is absorbed and/or refracted by the slightly ionized dense matter which is moving in towards the axis of the target. Typical results were obtained with an aluminium target of 245 μm outside diameter 2 R_e and of 67 μm wall thickness ΔR illuminated by an absorbed laser flux ϕ_a of 3.10^{13} W/cm^2. A transit time Δt of 5.1 ns is measured. The pressure P and the density $\frac{\rho}{\rho_o}$ behind the shock evaluated as in plane geometry are estimated respectively at 1.9 Mbar and 1.75. The light transmitted disappears entirely at the time t_f = 6.3 ns which can be considered as the convergence time of the shock wave on the axis of the target. The symmetrical disappearance of the laser light transmitted allows us to assume that the shock wave is moving symmetrically in towards the axis of the target in spite of residual asymmetries in the laser energy deposition. This fact can be explained by the effect of lateral thermal conduction which smoothes the peaks of laser flux.

In conclusion, these measurements confirm that a high power laser beam focussed onto a solid target is able to drive a strong shock wave inside it. Discrepancies exist, however, between the experimental values of the pressure and the values predicted by numerical calculations in agreement with /5/. These discrepancies can be interpreted first by the two dimensional aspect of the plasma expansion due to the lateral thermal conduction and second by the fact that the velocity D is not constant, as we assume it to be during the shock front propagation. It varies with the time as $\phi_a^{1/3}(t)$. In cylindrical geometry, the measurements show that several beams focussed onto a target are able to drive a convergent shock wave. Residual asymmetries in laser light energy deposition are smoothed by thermal conduction.

/1/ Fauquignon, C., Floux, F., Phys. of Fluids 13 (1970) 386
/2/ Bobin, J.L., Phys. of Fluids 14 (1971) 2341
/3/ Kidder, R.E., Nuclear Fusion 8 (1968) 3
/4/ Kessel, C.G.M., Sigel, R., 3rd Workshop on Las. Int. and Rel. Phen. Troy (1973)
/5/ Kessel, C.G.M., Sigel, R., Phys. Rev. Letters 33 (1974) 1020
/6/ Chancel, C., Fleurot, N., Gex, J.P., XI Congrès de Cinématographie Ultra Rapide, Londres (1974)
/7/ Mac Queen, R.G., et al., High Velocity Phenomena, New York, Ray Kinslow (1970).
/8/ Schirmann, D., Billon, D., Cognard, D., Launspach, J., Patou, C., VIII Int. Quant. El. Conf., San Francisco (1974)
/9/ Schirmann, D., Billon, D., Cognard, D., Launspach, J., Patou, C., 5th IAEA, Tokyo (1974)

LASER INTERACTION WITH ALUMINIUM TARGET

J.C. COUTURAUD, C. FAURE, J. MARTINEAU

Commissariat à l'Energie Atomique, Centre d'Etudes de Limeil
B.P. n° 27, 94190-VILLENEUVE-SAINT-GEORGES, FRANCE

Abstract : A study concerning the interaction of laser beam with Al target is presented. Investigations were made of charge state of ions, reflectivity and X-line emission. Experimental results were compared with a theoretical model.

INTRODUCTION

In the context of laser driven fusion, most of the works concern interaction studies of a laser beam with hydrogen or deuterium targets, i.e. with light elements. For the last three years many experiments have been carried out using multibeam laser systems to compress small spherical pellets. In the future these targets more complex may consist of thermonuclear fuel surrounded with high Z materials.

In order to understand and improve the laser coupling efficiency some single beam experiments involving interaction with high Z targets are required. In this paper we present some results concerning the interaction of a neodymium glass laser with an aluminium target.

EXPERIMENTAL SET UP

A Nd^{3+} glass laser with a power of about 1 GW was used. The pulse duration was 30 ns half width. The laser radiation was vertically polarized.

The laser beam was focussed in vacuum onto a plane massive aluminium target with a lens of 5 cm focal length and f/1 aperture. The flux density on the target reached 5.10^{12} W/cm^2. The focus size was determined from X-ray pinhole pictures. The experimental set up is represented in fig. 1.

An electrostatic analyzer and a Faraday cup were placed perpendicularly to the target surface. The analyzer gave energy spectrum and charge

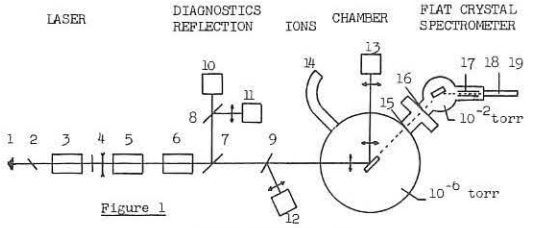

Figure 1

EXPERIMENTAL SET UP

1-6	: Laser system	14	: Electrostatic analyzer
7-8-9	: Glass plate	15-16	: Absorbing foils
10	: Calorimeter	17	: Soller slits
11-12-13	: Cells	18-19	: X-rays detectors

state of the ions. The Faraday cup allowed to measure the total number of charges.

Fast cells measured the specular reflected at 90° and the backscattered laser radiation through the angular aperture of the lenses (fig. 1).

A flat crystal spectrometer with a proportionnal flux gaseous counter was used to identify X-ray lines from highly stripped ions and measure the intensity of these lines.

EXPERIMENTAL RESULTS

In figure 2 is represented the average charge state of the ions in the plasma versus the incident laser flux. These values were deduced from experimental results obtained with the electrostatic analyzer, taking into account recombination phenomena which play an important role during plasma expansion /1/.

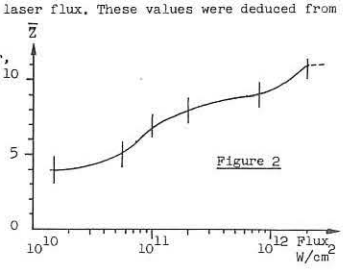

Figure 2

The reflectivity in the backscattered direction and in the 90° direction is represented in figure 3 as a function of laser flux ϕ / ϕ_o (where $\phi_o = 5.10^{12}$W/cm^2). The variation of the reflectivity during the laser pulse is shown in figure 4. We can see that the reflection at 90° is more important than the backscattered reflection, but its value is relatively low (10^{-2}).

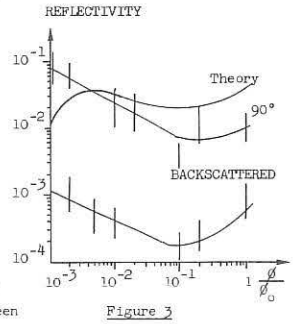

Figure 3

With a spectrometer we have identified Al XII X-ray line at $\lambda_1 = 7.75$ Å and $\lambda_2 = 6.63$ Å. No lines from Al XIII were observed. The energy in the Al XII X-ray line has been evaluated to 2.10^{-5} Joule in 4π steradians.

DISCUSSION

Electron temperature can be determined from the charge state of the plasma (fig. 2) assuming coronal equilibrium /3,4/. Values are shown in figure 5a.

The ions mean kinetic energy is related with the electron temperature by /5/ :

$$E_i = \frac{1}{2}\,\gamma\,\frac{\gamma+1}{\gamma-1}\left(\bar{Z}+1\right) R T_e$$

Knowing the mean kinetic energy and the mean state charge from analyzer and Faraday cups measurements, we can deduce T_e (figure 5b). These values are larger than these shown in figure 5a. This disagreement probably comes from the fact that in addition to free adiabatic expansion, ions are accelerated by a self-consistent electric field /6/.

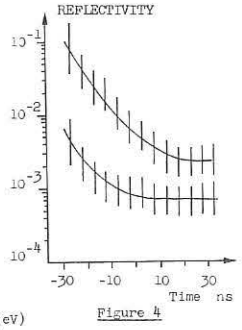

Figure 4

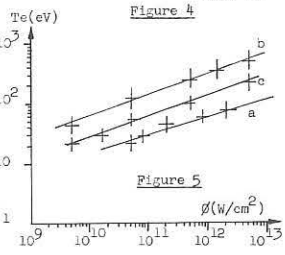

Figure 5

In the thin target model /7/ giving scaling laws, the temperature can be deduced by the relation :

$$T_{max} = 3.8\ 10^4\ \phi_a^{1/2}\ \ \lambda^{1/4}\ \ m^{1/5}\ \ Z^{-1/3}\ \ N^{-1/5}$$

ϕ_a in W/cm^2, λ in μm, m in kg, Te in eV. The temperature is represented in figure 5c.

As we see in figure 5, the three different methods of deducing Te give a dependance $Te \propto \phi^{1/3}$. This result is in good agreement with the thin target model and with results of reference /8/.

An absorption model of laser energy by electron-ion inverse bremsstrahlung has been carried out, which takes into account an absorption coefficient with a finite value at the critical density. Numerical results in figure 3 (Th) agree with the experimental results.

At the maximum flux density it is possible to present an energy balance : reflected energy laser 2 % ; kinetic energy of the ions 70-90% ; ionization energy of the ions 7-10 % ; X-ray energy (X > 1 keV) 0,1 %.

We thank B. AVENEAU, M. BRUEZIERE and J.L. LARCADE for their technical assistance.

/1/ Afanas'ev, Y.U., Rozanov, V.B., J.E.T.P. 35 (1972) 133
/2/ Mc Whirter, R.W.P., Plasma Diagnostic techniques, Acad. Press (1965)
/3/ House, L.L., Astrop. Journal 8 (1964) 307
/4/ Mosher, D., Report N.R.L. 2563 (1973)
/5/ Dick, K., Pepin, H., Martineau, J., Parbhakar, K., Thibaudeau, A., J. of Appl. Phys. 44 (1973) 3284
/6/ Bykovskii, Y.A., Sov. Phys. Tech. Phys. 18 (1974) 1597
/7/ Bonnier, A., Martineau, J., J. Appl. Phys. 44 (1973) 3626
/8/ Donalson, T.P., Hutcheon, R.J., Key, M.H., J. Phys. B. Atom. Mol. Phys. 6 (1973) 1525

ION TAIL FILLING IN LASER-FUSION TARGETS

Dale B. Henderson

Theoretical Division, Los Alamos Scientific Laboratory

Los Alamos, New Mexico 87544, U.S.A.

Abstract: Thermonuclear burn begins in laser-fusion targets with the collapse of the imploding fuel shell. At this instant the ion velocity distribution is non-Maxwellian, requiring correction to the commonly used computer simulation codes. This correction is computed and compared with that arising from the loss of fast ions.

Thermonuclear burn of laser-fusion targets is generally thought of as commencing when a shell of DT (deuterium-tritium) fuel collapses at the central point. This shell may either be present initially or it may be formed through accumulation and compression of an initially homogeneous fuel.[1] At the instant of collapse the velocity distribution of fuel ions may be thought of as a delta-function in speed: ions moving in all directions but with a common speed equal to that at which the shell moved inward.

In computer calculations of the implosion and burn,[2,3] however, the velocity distribution is not taken into proper account. Instead the ion fluid is taken to always have a Maxwellian distribution with the corresponding fusion reactivity $\langle\sigma v\rangle_M$. Because the fusion target may disassemble on a time scale comparable to that on which the ion distribution relaxes, it is important to study the relaxation and the corresponding values of fusion reactivity $\langle\sigma v\rangle$. In this paper we describe a multi-species Fokker-Planck computer code developed for this purpose. We present calculations of the magnitude of the result which may be used to post-correct the usual computer simulations. We also compare this effect with another related correction: the loss of ions from the tail of the distribution.[4]

The relaxation of $\langle\sigma v\rangle$ toward its asymptotic value $\langle\sigma v\rangle_M$, corresponding to a Maxwellian ion distribution, is shown in Figure 1 for a number of cases. In each case the temperature T is that of the Maxwellian; the initial beam speed is $v = (3kT/m)^{1/2}$. The horizontal lines are the asymptotic values $\langle\sigma v\rangle_M$. From the figure we see that the relaxation requires more collision times at the lower energies, because of the steepness of the cross section σ at lower energies. The T = 20 keV case is interesting in that it shows a small (5%) overshoot with the relaxation to the asymptotic value coming from above.

In figure 2 we plot the distribution function g(v) as it relaxes toward the Maxwellian. The plot is for the T = 6 keV case, but is really self-similar if scaled for different energies. We see that even after nearly 100 mean collision times the deviation from Maxwellian is appreciable at 10 times the thermal energy. Overlaid on the plot is a plot of the DT cross section σ, scaled in the energy coordinate as is appropriate.

Also plotted in figure 2 is the distribution for the T = 20 keV case initially, asymptotically, and at $\nu t = 12.38$ which corresponds to the maximum value of $\langle\sigma v\rangle$. From this figure it is clear that the relative over-population of g(v) adjacent to the initial delta-function is more important than the relative under-population in the far tail which lies largely beyond the maximum in σ. This explains the interesting overshoot.

The data[5] are intended to allow the post-correction of computed results which assume Maxwellian distributions. As an interesting application we apply these tail-filling corrections to the results of the initial condition burn-study[2] which we have also modified to estimate the effects of fast ion losses.[4] The two corrections overlaid on the (Maxwellian) computer simulations are shown in figure 3. We see that there is a linear region separating the bootstrap heating and central ignition regime at high $\rho R > 1$, gm cm^{-2} from the region of important corrections at low $\rho R < 0.01$ gm cm^{-2}. This separation justifies the neglect of non-linear processes in the present analysis. The values of $f \ll 1$ justify the neglect of fuel depletion.

From inspection of the two results it is clear that in most cases the fast ion loss is the more important effect. In those cases in which the finite tail-filling is more important it is only a 20 to 30% effect.

In the spirit of post-corrections to hydrodynamics calculations which assume Mazwellian distributions, we have performed some combined-ion loss and ion evolution-calculations. For the loss term we consider the loss of particles by diffusion from a uniform sphere, using well-known results from reactor theory.[5] The fractional burn-up values for the 3 keV case are shown in figure 4. For the very thin $\rho R = 10^{-4}$ case, the fractional burn-up becomes nearly constant as the $\langle\sigma v\rangle$ value drops. Such data may be used to post-correct hydrodynamics-burn calculations. Simple bare pellets are known to effectively disassemble in an expansion time[2]

$$\tau_e = R/4C_s, \quad C_s = \text{sound speed.}$$

For 1.0 μg DT spheres at 3 keV, this works out to approximately

$$n\tau_e = 1.4 \times 10^{15} \ (\rho R) \quad \text{(cgs units)}$$

In the $\rho R = 10^{-4}$ and 10^{-3} gm cm^{-2} cases the disassembly is so rapid as to occur before the fractional burn-up deviates significantly from the thick ($\rho R \geq 10^{-2}$ gm cm^{-2}) result. That is, in these problems the truncation of the distribution loss by ion loss will have no effect. In structured systems, however, the confinement times may be considerably longer and the deviations from the thick-case results may be important.

Having explored the ion loss effect;[4] the time evolution of the distributions, and the combined problem, we feel that we understand the observed yields which are below a priori (Maxwellian) estimates.[6] It is possible to construct hydrodynamics-burn computer codes which take proper account of these effects using the methods outlined here. However, in view of these effects becoming unimportant above $\rho R = 0.01$ gm cm^{-2}, the effort does not appear justified. It is important, however, to have resolved the question of why the initial experimental yields lie below the Maxwellian results.

*This work was performed under the auspices of the United States Energy Research and Development Administration.

References

[1] J. S. Clarke, H. N. Fisher, and R. J. Mason, Phys. Rev. Lett. 30, 89, 249 (1973).

[2] G. S. Fraley, E. J. Linnebur, R. J. Mason, and R. L. Morse, Phys. Fluids 17, 474 (1974).

[3] J. Nuckolls, L. Wood, A. Thiessen, and G. Zimmerman, Nature (London) 239, 139 (1972).

[4] D. B. Henderson, Phys. Rev. Lett. 33, 1142 (1974).

[5] D. B. Henderson, Los Alamos Scientific Laboratory Report, LA-5917-MS (1975).

[6] H. Brysk and P. Hammerling, Phys. Rev. Lett. 34, 502 (1975).

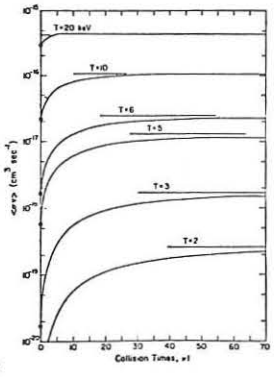

Fig. 1. Time evolution of the fusion reactivity $\langle\sigma v\rangle$.

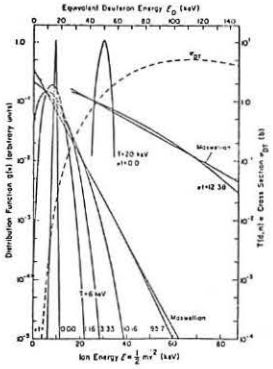

Fig. 2. Evolution of the distribution function g(v) vs. ion energy.

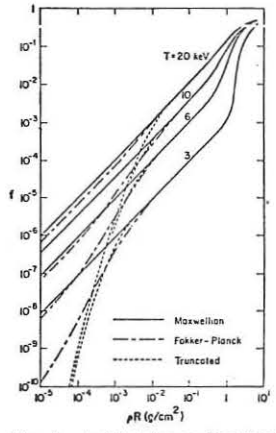

Fig. 3. Application to fractional burn-up from a burn study (Ref. 2).

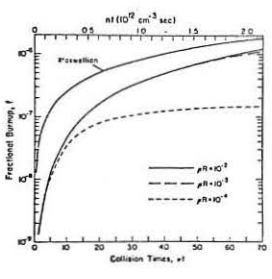

Fig. 4. Fractional burn-up for a combined problem.

X-RAY EMISSION FROM LASER-PRODUCED PLASMAS

J P Christiansen, N J Peacock and M Galanti

Culham Laboratory, Abingdon, Oxfordshire, England
(Euratom/UKAEA Fusion Association)

Abstract: Comparisons are made between experimental spectroscopic measurements and computer calculations of the soft X-ray spectrum emitted by a polyethylene target irradiated by an Nd laser. A 2-D MHD model depicts the behaviour of the plasma which is assumed optically thin in the X-ray regime. Effects from self-generated magnetic fields are discussed.

1. Introduction. There is considerable interest in the behaviour of plasmas produced by irradiation of solid targets with high intensity laser beams, e.g. laser fusion [1], X-ray sources [2], X-ray spectroscopy [3]. In this paper we study the production of X-rays from polyethylene targets irradiated by a 1.06 micron neodymium laser. We present results from calculations with a 2-D MHD model "CASTOR" [4] and compare our results with the measurements of Galanti, Peacock, Norton and Puric [5]. First we briefly describe the model CASTOR and the assumptions made to calculate the X-ray spectrum. The parameters of the experiments-calculations are given separately. The results from our calculations and the spectroscopic measurements [5] are in reasonable agreement and this is discussed at the end of the paper along with the validity of the assumptions made.

2. The Physical Model. Cylindrical geometry with rotational symmetry is assumed, i.e. only (r,z) dependence of any quantity is allowed. The laser light pulse travelling in the z-direction and characterized by an illumination profile $P_L(r,t)$ hits a cylindrical plasma target of dimensions R_o by Z_o. The target is assumed to consist of a moderate Z element, e.g. carbon, aluminium, iron etc. or a compound like polyethylene or nylon. The state of the target is described by a coronal steady-state model [6]. The model assumes equal ion and electron temperatures ($T_e = T_i$) and from T_e and the ion number density n_i all thermodynamic quantities of interest are calculated. The total power loss from continuum radiation (bremsstrahlung and recombination radiation) is [6]

$$P_c \propto n_i n_e \quad T_e^{\frac{1}{2}} \left(\overline{Z^2} + \frac{\overline{Z^2 E_{Z-1}}}{T_e} \right) \quad , \qquad (1)$$

where the bars denote a summation over different ionization stages and E_{Z-1} is the ionization energy at level Z. Similarly the power loss due to line radiation is [6] (g^Z oscillator strength).

$$P_L \propto n_i n_e \quad T_e^{-\frac{1}{2}} \overline{g^Z \exp \left(-E^Z_{N \to N+1} / T_e \right)} \quad , \qquad (2)$$

$E^Z_{N \to N+1}$ being the energy difference for the transition N→N+1 and the bar indicating a summation. The total radiation loss $P_c + P_L$ is black-body limited.

The plasma is described by a set of MHD equations as given by Braginskii [7]. The equation for the magnetic field includes the source term $\nabla \times \frac{\nabla p_e}{e n_e}$ responsible for the generation of the azimuthal component B_θ (Winsor and Tidman [8]), which affects the transport coefficients.

3. The Spectrum. The calculation of the spectrum of the emitted radiation is based on the following two simplifications:

(i) spatial transport of radiation and frequency diffusion are neglected;

(ii) only the continuum spectrum (Eq.1) is studied. However, line radiation (Eq.2) still counts as a loss to the plasma.

In terms of the radiation temperature $T_r = h\nu$ the spectral intensity distribution is given as

$$S(T_r)\, dT_r = P_c \frac{1}{T_e} e^{-T_r/T_e} dT_r \qquad (3)$$

The total spectral energy distribution is

$$E(T_r)\, dT_r = \int_o^{t_o} \int_v S(T_r > T_m)\, dv\, dt \qquad (4)$$

where $dv = 2\pi r\, dr\, dz$, $T_m = h\omega_p$ is a cut-off at the plasma frequency ω_p, and t_o is the time taken for the plasma to cool down. The calculation (4) predicts only that part of the spectrum originating from the thermal electron distribution and cannot accurately deal with the high-energy tail of the spectrum arising from supra-thermal electrons.

4. Laser-Target Parameters. A polyethylene target with $R_o = 250\,\mu m$, $Z_o = 400\,\mu m$, is given an initial temperature of 1 eV and an initial exponential density distribution in z with n_i varying from solid density n_o to $10^{-5} n_o$ over a distance d. The laser pulse [5] is assumed Gaussian in time, half-width 2.25 nsec, peak power 5×10^9 Watts, energy ~ 18 Joule. The illumination intensity has a Gaussian variation in r and the half-width f_R is varied from 75 μm to 150 μm.

5. Results. In Figure 1 we show the calculated energy spectra $E(T_r)$ (Eq.4) for $f_R = 75\,\mu m$ and 150 μm corresponding to average illumination intensities of 2.8×10^{13} Watts cm^{-2} and 7×10^{12} Watts cm^{-2} respectively. The experimentally-measured values [5] also shown in Figure 1 have been obtained at an illumination intensity of 7×10^{12} Watts cm^{-2}, and we observe a reasonable agreement between calculations and experiments. In our calculations we have varied the value of d from 30 μm to 375 μm and found little change in $E(T_r)$, although at a given instant in time $S(T_r)$ changes substantially. We have also studied the effects from the self-generated magnetic fields by performing calculations with and without B_θ. It is found that at $f_R = 150\,\mu m$ B_θ has little influence on the spectrum. However at $f_R \leq 75\,\mu m$ the spectrum of Figure 1 changes from a two-temperature spectrum (with B_θ) towards a one-temperature spectrum (no B_θ) like the one shown for $f_R = 150\,\mu m$. With increasing illumination intensity (f_R decreasing) a higher $\frac{\partial T_e}{\partial r}$ is established and this gives rise to a faster growth of B_θ [8]. The main influence from B_θ on a nanosecond timescale is the reduction in the electron thermal heat transfer across the field. At densities near the critical density $n_c (\sim 10^{21}\ cm^{-3})$, where most of the laser light is absorbed, the emitted radiation will hence be characterized by a temperature higher than those which characterize other emitting regions of the plasma. Our results indicate that a two-temperature spectrum as shown in Figure 1 results from illumination intensities above 10^{13} Watts cm^{-2}, when the generated B_θ is sufficiently strong to prevent isothermalization on a nanosecond timescale.

To reproduce the experimental values shown, it has been found necessary to increase the intensity by a factor 3-4 and even then the second temperature of 680 eV is still below the experimentally determined value of 1300 eV. This discrepancy is caused by the simplifications to the model: trapping of line and continuum radiation would give rise to higher energy densities; a finite ion-electron energy equipartition rate ($T_e \neq T_i$) would produce a higher T_e, particularly in the corona.

In conclusion our results demonstrate that the model used in the calculations is sufficiently realistic to reproduce experimental laser-target situations and explain the behaviour of the produced plasmas.

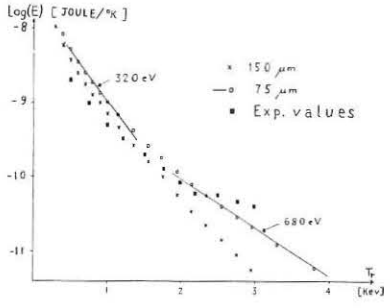

Fig.1. X-ray spectra calculated at two values of the laser beam radius f_R (x and o). The experimental values shown are those obtained by Galanti et al. [5].

References

[1] Nuckolls J, Wood L, Thiessen A and Zimmerman G (1972). Nature 239, 139.

[2] Stamper J and Tidman D A (1973). Phys.Fluids 16, 2024.

[3] Galanti M and Peacock N J (1974). Culham Laboratory Preprint CLM-P401. Submitted to J.Phys.B, Atom.Molec.Phys.

[4] Christiansen J P, Winsor N K and Magill J (1975). CASTOR, a two-dimensional laser target model. To be published.

[5] Galanti M, Peacock N J, Norton B A and Puric J (1974). Proc.Int.Conf. on Plasma Physics and Controlled Thermonuclear Fusion, Tokyo. Paper CN-33/F3-4.

[6] Mosher D (1973). NRL Memorandum Report 2563.

[7] Braginskii S I (1965). Reviews of Plasma Physics. Edited by M A Leontovich. (Consultants Bureau, New York).

[8] Winsor N K and Tidman D A (1973). Phys.Rev.Letters 31, 1044.

MAGNETIC FIELDS IN A LASER-PLASMA INTERACTION

R.S. Craxton and M.G. Haines
Imperial College, London

Abstract: Spontaneously generated magnetic fields can substantially reduce the thermal conductivity in pellet atmospheres and give rise to localized hot-spots, which may lead to the ablation of anomalously fast ions.

Origin and role of magnetic fields: Magnetic fields have been observed in laser-target experiments and are believed to be thermo-electrically generated as a result of non-parallel density and temperature gradients in the absorption region[1]. In laser-fusion experiments they may grow through non-uniformities in the laser beam or from instabilities[2].

The electron thermal conductivity, essential for the efficient transfer of heat into the compression region, may be drastically reduced by the large value of $\Omega\tau$ generated; a related effect is the production of "hot-spots" - regions where heat is deposited by the laser but prevented from escaping by large confining magnetic fields. These hot-spots may be the origin of the suprathermal fast ions observed to carry away an anomalous proportion of the absorbed energy in ablative kinetic energy[3].

Alternatively, $\underline{J} \wedge \underline{B}$ forces in the low density atmosphere may be a source of acceleration, although according to our computations this is a less important effect.

Computer Model: These phenomena have been studied computationally using a 2-D cylindrically-symmetric Eulerian code. Fluid equations describe the density (ρ), radial and axial velocities (V_r, V_z), azimuthal magnetic field (B_θ) and electron and ion temperatures (T_e, T_i). The equation for B_θ is

$$\frac{\partial B_\theta}{\partial t} = -\nabla \wedge \left[-\underline{V}_e \wedge \underline{B} - \frac{1}{ne} \nabla n k T_e \right]_\theta$$

$$= -\frac{k}{ne} \frac{\partial T_e}{\partial r} \frac{\partial n}{\partial z} + \text{smaller terms},$$

the source term largely determined by $\partial T_e / \partial r$.

In Diag. 1 the (1.06μm) laser impinges on a deuterium plasma along the z-axis from the low density region on the right, and dumps its energy at the critical density. The beam has a Gaussian radial profile of half-width 75μm, one quarter the width of the simulation region, and its intensity increases linearly with time to a peak of 2×10^{12} Watts at 40ps, and thereafter remains constant. Typically, at about 100ps, 10-20% of the energy is transferred to ion thermal energy via equipartition and 5-15% to kinetic energy via the electric field.

Diag. 1 shows T_e at successive times. The diagrams are scaled to the maxima (respectively 1.6, 4.5, 9.4 and 29KeV) and illustrate the thermal front advancing towards the solid (on the left) and the development of the hot-spot.

Diag. 2 (A,B) shows the maximum B and $\Omega\tau$ as functions of time, attaining the typical values of 1MG and 600 respectively. Diag. 2(C) shows the distribution of T_i with a peak of only 420eV, compared with ablative velocities (Diag.2D) of 3×10^8 cm/s.

References: 1. J.A.Stamper et.al.,Phys.Rev.Lett.26,1012 (1971).
2. D.A.Tidman and R.A.Shanny, Phys.Fluids 17,1207 (1974).
3. R.C.Malone et.al., Phys.Rev.Lett.34,721 (1975).

DIAGRAM 1

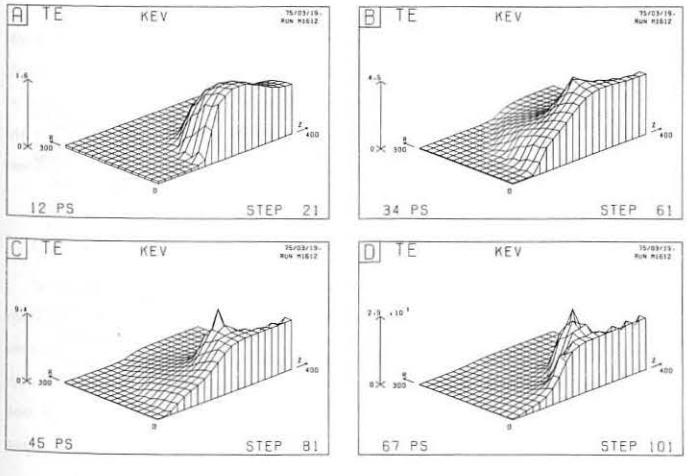

DIAGRAM 2

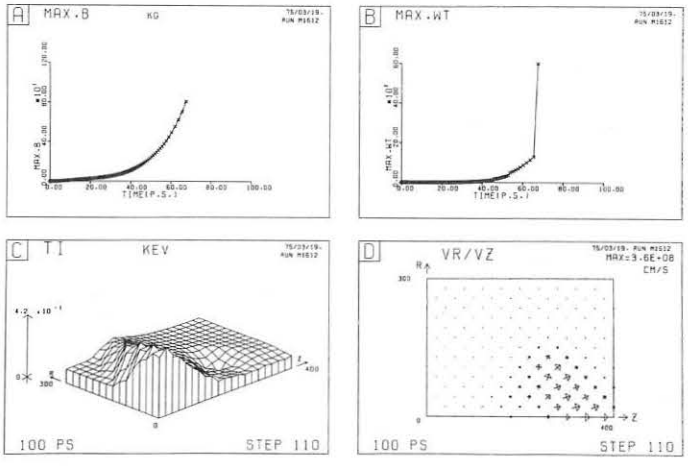

HARMONIC STUDIES IN A NEODYMIUM LASER CREATED PLASMA

A. SALERES, M. DECROISETTE

Commissariat à l'Energie Atomique, Centre d'Etudes de Limeil
B.P. n° 27, 94190-VILLENEUVE-SAINT-GEORGES, FRANCE

Abstract : New experiments concerning ω_0, $2\omega_0$, $\frac{3\omega_0}{2}$ backscattered radiations, from a Nd^+ laser created D_2 plasma, have been performed. The $2\omega_0$ and $\frac{3\omega_0}{2}$ harmonics afford the laser radiation flux in the critical absorbing region, and the density scale length of the expanding plasma.

When focusing a powerful neodymium laser beam onto a solid deuterium stick, a hot plasma is continuously created on the surface of the ice. Moreover, according as heating of the plasma is dominated by hydrodynamic or thermal conduction /1/, the critical density may be located inside or outside the target. Harmonic and subharmonic occuring during the interaction have been previously reported /2,3/. They provide emissions increasing with radiation flux inside the plasma.

We present here an experiment where spatial investigations on $2\omega_0$ and $\frac{3\omega_0}{2}$ generation leads to the location of the plasma density where $n_e \simeq n_c$ and $n_e \simeq n_c/4$.

Two main mechanisms give well account for second harmonic generation in an inhomogeneous plasma in the vicinity of n_c.

First, the component of the electric field along the density gradient can drive electronic plasma waves at $\omega_p \simeq \omega_0$; ($\omega_p^2 = \frac{n_e e^2}{\varepsilon_0 m_e}$). Coupling between longitudinal waves and transverse ones leads to the $2\omega_0$ generation. For a one dimensional plane plasma expansion, the second harmonic field components propagating backward, outside the plasma, are symmetrical of the incident ones. For experiments of interest, a plane expansion is expected for a spot diameter greater than 120 μm, obtained by slightly moving the target with respect to the focal point of the lens /3/.

The angle θ_0 between the incident wave vector and the density gradient along the axis of the lens increases from 3 degrees to 16 degrees, the focal distance of the lens being 75 mm or 95 mm, and beam diameter about 50 mm. The radiation flux in vacuum being less than 7.10^{13} W/cm^2, the structure of the field near n_c is determined by weak spatial dispersion /5/. The density scale length $\frac{1}{n_e}\frac{\partial n_e}{\partial z} = H$ is greater than 100 μm and implies $\frac{\omega_0 H}{c}\sin^3\theta_0 \gg 1$. Then if I_i is the incident radiation flux, power emitted at $2\omega_0$ is of the form :

$$P_{2\omega_0} \simeq A I_i^2 \int_{\theta} \exp -\frac{8}{3}\frac{\omega_0 H}{c}\sin^3\theta_0 \; f(\theta, H, T_e)\, d\theta_0$$

The second convenient mechanism involves the plasmon phonon decay instability, which causes the ion density to oscillate at Ω_s ; the non linear response of the plasma lead to light emission with frequencies $2\omega_0 - \Omega_s$ or $2(\omega_0 - \Omega_s)$. This process takes place near $\omega_0 \simeq \omega_p$ and the emitted intensity is a function of I_i^2. Such a mechanism threshold is ranging about 10^{14} W/cm^2.

Plane aspherical focusing lenses are not achromatic and their focal distances increase with wavelength (for instance λ_0 = 10 600 Å, f_0 = 75,20 mm ; for λ_1 = 5 300 Å, f_1 = 73,18 mm). But the dense point of the plasma and its critical density lie in the vicinity of the focus of the lens for 10 600 Å. Thus the $2\omega_0$ backscattered beam will converge ; a prismatic beam splitter, inserted on the laser beam, allows us to obtain a $2\omega_0$ picture of the critical density region on a photographic plate and the $2\omega_0$ time evolution by means of a photocell. According to the focusing conditions, the $2\omega_0$ pulse half width varies from 0.8 ns to 1.5 ns ; these values are the exposure time of the plates from which location and size of the critical density region are inferred. This exposure time was reduced down to 0.4 ns by using a 400 ps opening framing LEP camera. It was shown that the interaction spot dimension is constant during the top of the incident pulse. Keeping incident power fixed at 16 GW, we have performed a study of size and location of the cut off region, the surface of the target being moved with respect to the focus of the lens (see fig. 1). The radiation intensity ranged from 10^{13} W/cm^2 to 5.10^{14} W/cm^2 in the critical spot.

For a constant value of d (accuracy $\simeq$ 10 μm) the radiation flux is varied with neutral filters. For d > 100 μm we have shown that the reflected energy at ω_0 increases with I_i, the law $P_{2\omega_0} \simeq I_i^2$ is well

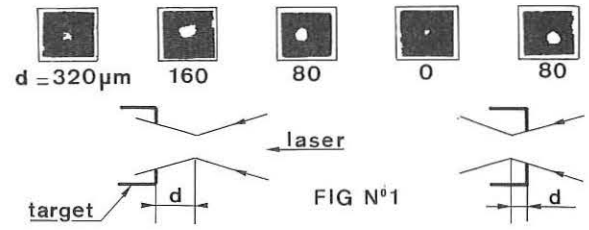

FIG N°1

accounted and the $2\omega_0$ emitting zone is slightly inside the target. For d = 0, ω_0 reflection increases up to laser radiation fluxes of 3.10^{14} W/cm^2 and then decreases. It seems well accounted by stimulated Brillouin backscattering. The square law for second harmonic backscattering is well verified up to 8 GW. Above this value, $P_{2\omega_0}$ increases more quickly. Moreover the $2\omega_0$ emitting zone is located inside the stick. Parametric effects arise correlated with hard X ray emission with energy up to 300 keV, and with shift and broadening for the second harmonic line.

At right angle the $2\omega_0$ pulses have the same duration as the backscattered ones and the photographs of the plasma give the same results as in axial experiments. Moreover, it is observed that the plasma expansion becomes more and more plane with increasing defocusing.

As the $2\omega_0$ beam, the $\frac{3\omega_0}{2}$ backscattered beam converges (focal distance = 74,25mm at 7060 Å) and gives a picture of its emitting region as can be seen on fig. 2. It appears that the $\frac{3\omega_0}{2}$ line is generated in a region closer to the lens than the $2\omega_0$ one. For d = 0, $\frac{3\omega_0}{2}$ is issued from a region located slightly inside the target, and for d $\gtrsim$ 80 μm, outside of it. This result agrees with theoretical and computer works /8,9/ where the $\frac{3\omega_0}{2}$ line is produced in the underdense region of the plasma. It probably arises from $n_c/4$ and may be due to a parametric plasmon-phonon or stimulated Raman instability.

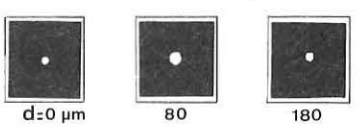

FIG N°2

The reflected light at ω_0 and the intensity of $\frac{3\omega_0}{2}$ line peaks at the same point for d = 0 and decreases when d increases. At right angle $\frac{3\omega_0}{2}$ line intensity increases with d and peaks for d $\simeq$ 180 μm, inside or outside the target ; this seems to be due to a partial reabsorption by the target itself. These results agrees with $\frac{3\omega_0}{2}$ perpendicular photographs. Fig. 3 shows the relative position of n_c and $n_c/4$ in the plasma ; the

FIG N°3

	d(µm)	0	80	160
θ=0	$S'_1S'_2$	60	70	140±10
θ=90	S_1S_2	?	60	120

insert gives the averaged plasma density scale length (in μm) measured (S'_1 , S'_2) and corrected taking into account plasma refraction (S_1 , S_2).

Such pictures provide an easy method to measure spot irradiation of the stationnary plasma. It will be useful to compare it with X ray photograph /10/ giving the spot diameter of the energy distribution due to thermal conduction. Such experiments allow us to classify absorption phenomena according to radiation flux inside the plasma and to measure threshold for instabilities occuring at n_c and $n_c/4$.

The authors are indebted to J.P. BABUEL-PEYRISSAC, P. GUILLANEUX and C. PATOU for useful discussions and to H. CROSO and A. QUEFFELEC for technical assistance.

/1/ Bobin, J.L., Thesis of Doctorat, University of Paris XI (1974)
/2/ Bobin, J.L. et al., Phys. Rev. Lett. 30, 13 (1973) 594
/3/ Salères, A. et al., Phys. Lett. 45A, n° 6 (1973) 451
/4/ Vinogradov, A.V. et al., Soviet JETP 36 (1973) 492
/5/ Piliya, A.D., Sov. Phys. Tech. Phys. 11 (1966) 609
/6/ Erokhin, N.S. et al., Nucl. Fusion 14 (1974) 333
/7/ Salères, A. et al., Optics Communications, to be published
/8/ Martineau, J. et al., Phys. Lett. 47A, n° 1 (1974) 43
/9/ Biskamp, A. et al., P.R.L. 34 n° 6 (1975) 312
/10/ Key, M.H. et al., Phys. Lett. 48A (1974) 121

HARMONIC GENERATION BY A FOUR-WAVE PROCESS*

Nguyen Duc Long, K.J. Parbhakar and T.W. Johnston

Centre de l'Energie, Institut National de la Recherche Scientifique

Université du Québec, Varennes, Canada

Abstract: The superelastic scattering of the incident radiation from decay instability plasmons or from two plasmon instability plasmons is considered as a possible mechanism for the emission of the second and three-half harmonics. The instability thresholds and the growth rates are given for the harmonics.

Several laboratories have reported emission of the second and three-half harmonic of powerful lasers due to the interaction of laser light with the plasma created by the laser pulse using various targets. Attempts to explain these emissions have been made by Bobin et al [1], Mascheroni [2] and Chambers and Bers [3]. Whereas any non-linear mechanism can produce second harmonic the theoretical explanations for the three-half harmonic are rather limited. The authors [3] consider the two plasmon instability followed by three wave Raman up conversion while the mechanism discussed in [1] is rather obscure. We consider here another possibility for the emission of second and three half harmonics, namely the superelastic scattering from the decay instability plasmons and from two-plasmon instability plasmons respectively, (see Fig. 1). The typical plasmon has a wave number $\vec{K}_L$ which is too large for three wave Raman up conversion, the introduction of the decay phonon S makes the momentum conservation condition easy to satisfy and since a large range of initial plasmon wave numbers are possible one can nearly use all plasmons.

Evidently one must weigh the lower cross section for this four wave process which uses most plasmons against the larger cross section for

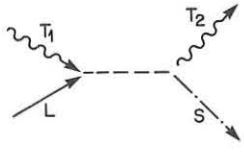

Fig. 1 Four wave superelastic scattering

three wave Raman up conversion which can use only those plasmons with electromagnetically small wave numbers. The simple plasma model used here is characterized by the fluid equations for electrons and ions with adiabatic state law. The equilibrium state in the presence of an ensemble of waves in a plasma is then described by

$$\begin{aligned} E &= \sum_A \vec{E}_A \\ n_o &= \sum_A n_A + 1/2 \sum_{A,B} n_{AB} \\ \vec{v}_o &= \sum_A \vec{v}_A + 1/2 \sum_{A,B} \vec{v}_{AB} \end{aligned} \tag{1}$$

where A,B $\varepsilon\{T_1, T_2, L, S, T_1^*, T_2^*, L^*, S^*\}$ and the * indicates the complex conjugate. Here n_A and $\vec{v}_A$ are the first order induced density and velocity by a wave. Similarly n_{AB} and $\vec{v}_{AB}$ are the second order induced quantities. Both n_{AB} and $\vec{v}_{AB}$ can be easily expressed [4] in terms of the first order quantities n_A and $\vec{v}_A$.

Combining the fluid equations with Maxwell's equation we get

$$\frac{\partial}{\partial t^2}\left[\frac{\partial}{\partial t^2} + c^2\,\nabla x\nabla x + \omega_{pe}^2 - \gamma v_{th}^2\,\nabla\nabla\,.\right]\vec{E} - \gamma v_{th}^2\,\omega_{pi}^2\,\nabla\nabla\,.\,\vec{E} = \vec{F} \tag{2}$$

where the second order non-linear source term F is given by

$$\vec{F} = -\frac{m_e}{q_e}\frac{\omega_{pe}^2}{2}\left[\sum_{A,B} i\omega_{AB}^3 \frac{\vec{K}_{AB}}{\omega_{AB}} f_{A,B} + \vec{J}_{A,B} + \sum_{A,B,C} i\omega_{ABC}^3 \frac{\vec{K}_{ABC}}{\omega_{ABC}} f_{AB,C} + \vec{J}_{AB,C}\right] \tag{3}$$

where $K_{ABC} = K_A + K_B + K_C$, $\omega_{ABC} = \omega_A + \omega_B + \omega_C$ and

$$f_{AB,C} = \gamma(\gamma-2)\, v_{th}^2 \frac{n_{AB} n_C}{N^2} + \vec{v}_{AB}\,.\,\vec{v}_C$$

$$\vec{J}_{AB,C} = \frac{n_{AB}}{N}\vec{v}_C + \frac{n_C}{N}\vec{v}_{AB} \tag{4}$$

N being the equilibrium density in the absence of waves

To derive the coupled mode equations $\partial/\partial t$ in Eq.(2) is replaced by $(-i\omega + \frac{\partial}{\partial t})$ where $\partial/\partial t$ acts on the amplitude only [5]. Substituting in Eq. (2) and using linear dispersion relation for mode A we get to first order in $\partial/\partial t$

$$\sum_A a_A \frac{d\vec{E}_A}{dt} = \vec{F} \tag{5}$$

where $a_A = 2i\omega_A^3$ if A is a plasmon or a photon and $a_A = -2i\omega_{pe}^2\omega_A$ for a phonon. By identifying terms satisfying the resonant condition $\{(\omega_{T1} + \omega_L, \vec{K}_{T1} + \vec{K}_L) = (\omega_{T2} + \omega_s, \vec{K}_{T2} + \vec{K}_s)\}$ Eq. (5) reduce to a system of equations describing coupling between T_2 and S in the presence of T_1 and L. The coupled equations are

$$\begin{aligned} \frac{dE_{T2}}{dt} + \nu_{T2}E_{T2} &= iC_{T2}E_{T1}E_L E_S^* \\ \frac{dE_S}{dt} + \nu_s E_s &= iC_s E_{T1} E_L E_{T2}^* \end{aligned} \tag{6}$$

where we have phenomenologically introduced the damping of E_{T2} and E_s by the appropriate collision frequencies. The coupling coefficients are given by

$$C_s = -\frac{1}{2}\left(\frac{q_e}{m_e}\right)^2 \frac{1}{v_{th}^2}\frac{\omega_s}{\omega_{pi}^2}\frac{\omega_s}{\omega_{T2}}\frac{\omega_L}{\omega_{T1}}\frac{(\omega_L + \omega_s)(\hat{E}_{T1}\,.\,\hat{E}_L)(\hat{E}_s\,.\,\hat{E}_{T2})}{(\omega_{T1} - \omega_s)(\omega_{T1} + \omega_L)}$$

$$C_{T2} = -\frac{1}{2}\left(\frac{q_e}{m_e}\right)^2 \frac{1}{v_{th}^2}\frac{\omega_L}{\omega_{T1}}\frac{(\omega_L + \omega_s)(\hat{E}_{T1}\,.\,\hat{E}_L)(\hat{E}_s\,.\,\hat{E}_{T2})}{(\omega_{T1} - \omega_s)(\omega_{T1} + \omega_L)}$$

where $\hat{E}$ refer to a unit vector. In what follows we assume that $\hat{K}_{T2} = -\hat{K}_{T1}$ (i.e. back scattering). The instability threshold is given by

$$|E_{T1}|\,|E_L| = \frac{\nu_{T2}\nu_s}{C_s C_{T2}}$$

and the growth is

$$\gamma = \frac{1}{2}\{-(\nu_{T2} + \nu_s) + [(\nu_{T2} - \nu_s)^2 + C_s C_{T2} E_{T1}^2 E_L^2]^{1/2}\}$$

Far above the instability threshold we have for

a) Second harmonic $(\omega_{T1} \simeq \omega_L)$

$$\gamma_2 = \frac{1}{4\sqrt{2}}\frac{q_e^2}{m_e^2}\frac{1}{v_{th}^2}\frac{1}{\omega_{T1}}\left(\frac{\omega_s}{\omega_{T1}}\frac{\omega_s}{\omega_{pi}^2}\right)^{1/2}|E_{T1}||E_{L2}|$$

b) Three-half harmonic $(\omega_{T1} \simeq 2\omega_L)$

$$\gamma_2 = \frac{1}{12\sqrt{6}}\frac{q_e^2}{m_e^2}\frac{1}{v_{th}^2}\frac{1}{\omega_{T1}}\left(\frac{\omega_s}{\omega_{T1}}\frac{\omega_s}{\omega_{pi}^2}\right)^{1/2}|E_{T1}||E_{L2}|$$

These are the maximum growth rates which occur when the incident radiation and the emitted light have the same polarisation. Note that the second harmonic is produced at critical density while the 3/2 harmonic at the 1/4 critical density.

References

1) J.L. Bobin, M. Decroisette, B. Meyer and Y. Vittel, Phys. Rev. Lett. 30, 594 (1973).

2) P.L. Mascheroni, Phys. Rev. Lett. 34, 141 (1975).

3) F.W. Chambers and A. Bers, Bull. Am. Phys. Society 19, 881 paper 2H3 (1974).

4) D.C. Watson and A. Bers QPR No. 111, p. 84 (1973).

5) V.N. Tsytovitch "Nonlinear Effects in plasmas Plenum Press, New York (1970).

* This work is partially supported by National Research Council of Canada grants A6764 and A9613.

ENHANCED REFLECTION DUE TO BRILLOUIN SCATTERING FROM AN EXPANDING PLASMA

I. M. BEGG and R. A. CAIRNS

University of St. Andrews, St. Andrews, Scotland.

Abstract: If the expansion velocity of a laser-produced plasma is around the ion-sound speed then in the laboratory frame we can have standing ion-sound waves with pump and backscattered waves of equal frequency. Partial reflection of the pump wave from the high-density regions of the plasma can then lead, via Stimulated Brillouin Scattering, to enhanced reflection.

Consider three waves (ω_i, k_i), with subscript 0 denoting the pump wave, subscript 1 the backscattered wave and subscript 2 the ion-sound wave. For strong interaction to occur these waves must satisfy the resonance conditions $\omega_0 = \omega_1 + \omega_2$, $\underset{\sim}{k}_0 = \underset{\sim}{k}_1 + \underset{\sim}{k}_2$. In the rest frame of the plasma $\omega_2 \sim k_2 c_s$, where c_s is the ion-sound speed, and $\omega_1 = \omega_0 - k_2 c_s$. If, however, the plasma is, in the laboratory frame, expanding with speed $\sim c_s$, the frequency of the ion sound wave is Döppler-shifted to around zero, the pump and backscattered waves then having equal frequencies. So, consider a laser beam incident upon a pellet surrounded by a spherically expanding plasma. This beam travels through an underdense region before reaching the critical surface (where $\omega_0 = \omega_{pe}$) and there being strongly absorbed. In general, absorbtion at this surface is expected to be incomplete and partial reflection will then occur. If the expansion valocity is around c_s, then the incident and reflected waves (which, of course, have the same frequency) can interact resonantly with ion-sound waves via Brillouin Scattering, as described above. This behaviour is analysed below and it is shown that it may lead to strong enhancement of reflection and reduction of the energy reaching the critical surface.

Consider, now, these ideas in 1-D, representing the plasma by a slab $0 \leq x \leq L$ with linear density profile $n_0(x) = n_0 x/L$, onto which the pump impinges for $x < 0$. We use the equations of Forslund et at. [1], but transforming to a frame moving with velocity u. In the stationary case, these are,

$$\left[(u^2 - c^2)\frac{\partial^2}{\partial x^2} + \omega_{pe}^2\right] A_{0,1} = -\omega_{pe}^2 \frac{n_e}{n_0} A_{1,0} \qquad (1)$$

$$(u^2 - c_s^2)\frac{\partial^2 n_e}{\partial x^2} + u\gamma_D \frac{\partial n_e}{\partial x} + \omega_{pe}^2(n_e - n_i) = \frac{e^2 n_0}{m_e M_i c^4}\frac{\partial^2}{\partial x^2}(A_0 A_1) \qquad (2)$$

$$u^2 \frac{\partial^2 n_i}{\partial x^2} + \omega_{pi}^2(n_e - n_i) = 0 \qquad (3)$$

where γ_D is a collisional damping coefficient for ion-sound waves. We now carry out a standard analysis with small amplitude variations over a wavelength to obtain

$$\frac{\partial k_{0,1}}{\partial x} + 2k_{0,1}\frac{\partial \alpha_{0,1}}{\partial x} = -\omega_{pe}^2 \frac{n_e}{n_0}\alpha_{1,0} \qquad (4)$$

$$\frac{n_e}{n_0} = \frac{2k_0 c^2}{u\gamma_D}\alpha_0\alpha_1 \qquad (5)$$

where $\alpha_{0,1} = \dfrac{eA_{0,1}}{(m_e M_i c^4)^{\frac{1}{2}}}$, and we have neglected u with respect to c in (1). There is no derivative in eqn (5) because the group velocity of the ion-sound wave is zero. These non-propagating ion-sound waves are assumed to be driven until they reach a level at which damping prevents further growth. This saturation is assumed to take place in an initial period short compared with the duration of the laser pulse, after which time the amplitudes are stationary. If we measure distance in units of K_0^{-1}, where $K_0 = \dfrac{\omega_0}{c}$, then equations (4) have the solutions

$$(k_0^{\frac{1}{2}}\alpha_0)^2 = K_0 c_1^2\left\{1 - \frac{\alpha_0^2(0) - c_1^2}{\alpha_0^2(0)}\exp\left[-2c_1^2\int^x \frac{\omega_{pe}^2}{k_0 u \gamma_D}\,dx\right]\right\}^{-1}$$

$$(k_1^{\frac{1}{2}}\alpha_1)^2 = (k_0^{\frac{1}{2}}\alpha_0)^2 - K_0 c_1^2$$

where $c_1^2 = \alpha_0^2(0) - \alpha_1^2(0)$ is a constant. In the case of 10.6μm CO_2 laser radiation with the following parameter values: $u = c_s = 10^8$ cm/s, L = 300 [corresponding to a plasma of depth 0·5 mm [2]] and $\gamma_D/\omega_0 = 0{\cdot}4075$ [collision frequency due to damping at wave number K_0 [3]] and incorporating a linear density profile, these solutions are shown in Figure 1.

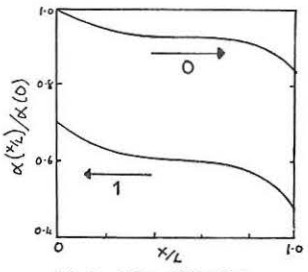

FIG. 1 WAVE AMPLITUDES

We note the relatively large value of the backscattered wave at x = L. This is due mainly to the partial reflection of the pump at the critical surface, which, as we said before, arises because the pump and backscattered waves have the same frequency. Thus, the pump and reflected waves can interact resonantly with a stationary ion-sound wave to increase the amount of backscatter. In other words, we can get a strong enhancement of reflection due to this intersction. Note that if the plasma is at rest the pump and backscattered waves do not have the same frequency and this mechanism is not feasible - the level of backscatter at the critical surface is then the thermal level of wave 1. We now define the reflection coefficient at x = 0 to be $RO = \left[\dfrac{(k_1^{\frac{1}{2}}\alpha_1)^2}{(k_0^{\frac{1}{2}}\alpha_0)^2}\right]_{x=0}$ and that at the critical surface to be $RC = \left[\dfrac{(k_1^{\frac{1}{2}}\alpha_1)^2}{(k_0^{\frac{1}{2}}\alpha_0)^2}\right]_{x=L}$. They are related by

$$RO = RC\exp\left\{2c_1^2\int_0^L \frac{\omega_{pe}^2}{k_0 u_D}\,dx\right\}.$$

In Figure 2 the extent of the backscatter, i.e. RO, is shown as a function of incident power, for the cases RC = 0·1 and RC = 0·2.

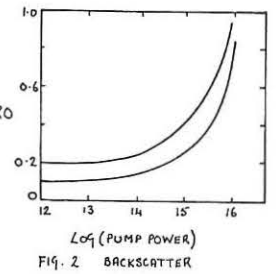

FIG. 2 BACKSCATTER

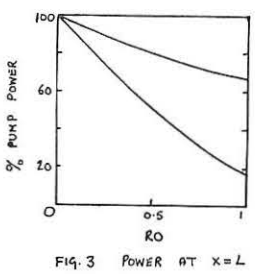

FIG. 3 POWER AT x = L

For low pump powers, there is little effect and the backscatter is merely due to the partial reflection of the pump at the critical surface. However, around 10^{15} W cm^{-2}, the resonant interaction already described becomes dominant and the reflection is strongly enhanced. This reduces, considerably, the power reaching the critical surface as shown in Figure 3. For pump powers between 10^{15} and 10^{16} W cm^{-2}, the effect is very marked, increasing rapidly in this range. This is the sort of range mentioned in laser fusion situations. These results are for the case $u = c_s$. However, calculations indicate that this effect is fairly insensitive to an off-resonance situation where $u \neq c_s$. We would like to add that this backscatter is dependent on L and so, for larger values of L, the effect will be somewhat greater.

Thus, when we include the partial reflection at the critical surface of a pump wave into a backscattered wave of the same frequency, the subsequent resonant interaction with an ion-sound wave leads to enhancement of the backscatter. Because of the high pump powers involved, the reduction of energy reaching the critical surface can be quite considerable and thus provide a possible barrier to laser fusion applications.

References

[1] D. W. Forslund, J. M. Kindel & E. L. Lindman; Phys. Rev. Lett. 30, 739.
[2] K. A. Bruekner and S. Jorna; Rev. Mod. Phys. 46, 325.
[3] B. D. Fried and R. W. Gould; Phys. Fluids 4, 139.

TWO-DIMENSIONAL INTERFEROMETRIC MEASUREMENTS

OF A LASER-PRODUCED PLASMA IN A STRONG MAGNETIC FIELD†

L.C. Johnson and T.K. Chu

Plasma Physics Laboratory, Princeton University

Princeton, New Jersey 08540, USA

Abstract. Interferometric measurements on CO_2-laser-produced plasmas in a 250 kilogauss magnetic field show the development of a slender, well-behaved plasma column with an on-axis minimum, suitable for refractive trapping of the laser beam.

High resolution interferometric techniques have been used to observe laser-induced gas breakdown plasmas immersed in a strong magnetic field. The object of the experiment was to investigate self-trapping of a laser beam in a magnetically confined plasma, with possible application to the development of a fusion reactor of the type proposed by Dawson, et al. [1].

The magnetic field was provided by a twelve turn, helical, beryllium-copper coil, energized by a 260 kilojoule capacitor bank. The magnet had a bore of 5 cm diameter and a length of 20 cm. The field strength was variable up to 270 kilogauss.

Plasmas were produced by gas breakdown at the focal spot of a CO_2 laser beam. Pulse energy was 30 joules, with a half-intensity pulse duration of 150 nsec.

The CO_2 laser beam was focused onto a free-expansion gas jet in the bore of the magnet. The jet was arranged to exhaust toward the incident laser beam so that gas pressure on the laser side of the focal plane could be kept low while the initial pressure on the other side of the focal plane was set at some pre-selected value.

By this means it was possible to eliminate the laser-driven shock wave which otherwise would propagate backward, toward the laser, and shield the plasma from the incident beam. [2]

Two types of laser interferometry were used to observe the evolution of plasma density in space and time. A Mach-Zehnder interferometer, illuminated by a focused He-Ne laser beam and detected with a photomultiplier tube [3], viewed the plasma side-on through small holes drilled in the magnet coil. This gave a continuous measurement of fringe shift along a pre-selected chord through the plasma with spatial resolution of about 50 μm and temporal resolution of less than 5 nsec. The same interferometer measured initial gas pressure on the high pressure side of the gas jet by the phase shift caused by neutral gas along the line of sight.

Conventional two-dimensional interferograms were made at pre-selected times after gas breakdown, using a ruby laser with a 3 nsec pulse duration. Mirrors in the bore of the magnet allowed the plasma to be viewed side-on with a field of view about 1.5 cm in diameter.

Figure 1 shows side-on interferograms of the plasma produced in helium at an initial pressure of 50 Torr, and with an applied field of 50 kilogauss. The plane of the jet orifice is at the left edge in each picture. The laser is incident from the left, with the focal plane coincident with the plane of the jet. The interferograms show that the plasma grows in time, both along the beam (and magnetic field) and in the transverse direction.

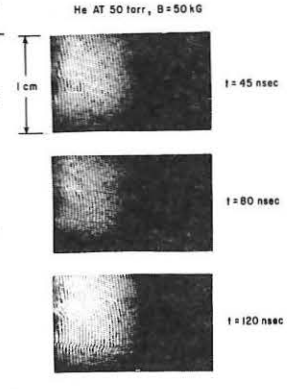

Fig. 1

Figure 2 is an analysis of the first interferogram of Fig. 1, at 45 nsec after gas breakdown. Clearly, there is a build-up of electron density at the periphery of the expanding plasma, particularly in the direction of beam propogation, where the density rises to more than half the critical density for 10.6 μm radiation (10^{19} cm^{-3}). We note that refraction of the incident beam, caused by such density profiles, was also directly observed, as in Ref. [3].

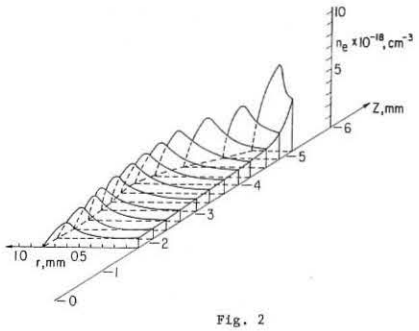

Fig. 2

Figure 3 shows interferograms at seven times after gas breakdown, with an applied field of 250 kilogauss. The focal plane was moved 7.5 mm into the high pressure side of the chamber to illustrate the beam-shielding effect of the backward-going laser-driven shock wave. After gas breakdown, the plasma grows rapidly in the backward direction (toward the laser) but slowly in the forward and transverse directions. Only after the backward expansion reaches the low pressure gas on laser side of the jet does the plasma become sufficiently transparent to drive plasma expansion in the opposite direction.

Figure 4 is an analysis of the last interferogram of Fig. 3. Again there is a pronounced density minimum on the plasma axis. Radial expansion is considerably reduced by the strong magnetic field. At this high field, the on-axis density minimum was clearly observable for at least half a microsecond.

In conclusion, our results show that (1) the on-axis density minimum, required for laser beam self-focusing, is preserved in the presence of a strong magnetic field, (2) the expected beam self-focusing is also observed, (3) the lateral expansion of plasma boundary into the ambient gas is slowed down as the magnetic field is increased, and (4) the higher the magnetic field, the longer the on-axis density minimum persists after the termination of the laser pulse, demonstrating the stronger confining effect of the magnetic field on both particles and (particle) energy.

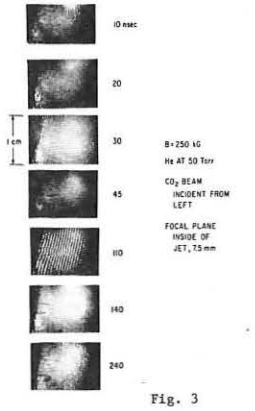

Fig. 3

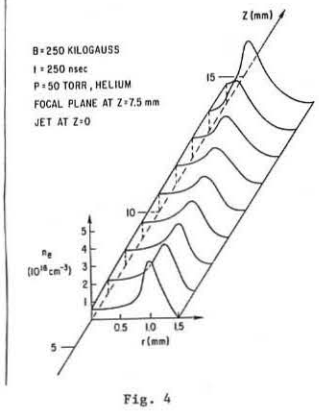

Fig. 4

References

[1] J.M. Dawson et al, in Fourth Conference on Plasma Physics and Controlled Fusion Research, (IAEA, Vienna, 1971) Vol. 1, p. 673.

[2] T.K. Chu and L.C. Johnson, Bull. Am. Phys. Soc. 19, 642 (1974); also Princeton Plasma Physics Laboratory Report Matt-1085 (1974).

[3] L.C. Johnson and T.K. Chu, Phys. Rev. Lett. 32, 517 (1974).

†This work was supported under Contract AT(11-1)-3073 with the U.S. Energy Research & Development Administration.

SCATTERING MEASUREMENTS ON THE HEATING OF AN UNDERDENSE PLASMA BY AN INTENSE CO_2 LASER BEAM.

M.S. White, J.D. Kilkenny and A.E. Dangor
Imperial College, London, England.

Abstract: Using ruby laser scattering we have measured the heating of a plasma at density $8.10^{16}cm^{-3}$ by CO_2 laser radiation at $10^{10}W/cm^{-2}$. Comparison with a numerical simulation yielded a thermal conductivity about half the theoretical value. An extension of the experiment to the flux-limited regime is proposed.

We report an experiment in which a plasma of sub-critical density was heated by CO_2 laser radiation under conditions where classical thermal conduction theory should apply. Ruby laser scattering was used to measure the heating and rarefaction. The observed time histories (at various positions) of perturbed density and temperature were fitted to the results of a numerical simulation of the experiment, using the absorption and conduction coefficients as parameters.

The plasma was a Z-pinch discharge in 200mTorr of hydrogen, giving an electron density $n_e \simeq 8.10^{16}cm^{-3}$ and an electron temperature, $T_e = 5$ ev. This was heated by a T.E.A. CO_2 laser, which gave a 20MW, 70ns pulse. Both the CO_2 laser and the diagnostic ruby laser were incident radially on the pinch column centre, the radii being 45^o apart. Light scattered at 90^o from the ruby laser beam was imaged onto the polychromator entrance slit. The relative displacement δ of the two lasers was adjusted along the pinch axis by a tilting KCl plate in the CO_2 laser beam.

On the length scale (1mm) and timescale (100ns) of the heating experiment, the Z-pinch was essentially homogeneous, constant and unmagnetised.

Results were taken for four relative displacements between the laser beams; δ = 0, 700μm, 2.4mm and 4mm. There was no change observed at δ = 2.4mm and 4mm. The results at δ = 0 and 700μm, which are on Fig. 1, show conduction and a rarefaction.

A one dimensional cylindrical two fluid simulation was performed to compare with the experiment. The absorption of CO_2 radiation was taken as being by inverse bremsstrahlung, and Spitzer's thermal conductivity was used. The multiples k (absorption) and s (conductivity) were introduced to allow computational variation. Thus s = 1, k = 1 is the purely classical situation. The effect of photoionisation should be less than 4%, and that of stimulated Compton scattering less than 2%.

As shown in Fig. 1(a) the values of s = 1, k = 1 do not give good agreement. But excellent fits can be produced by variation of s and k, as shown in Fig. 1(b-d).

The fact that these results show roughly classical heating and conduction is expected. At a density of 10^{17} cm^{-3} the only parametric instabilities with a threshold less than 10^{10} Wcm^{-2} are the backscatter instabilities[2]. A negligible amount of radiation would be absorbed. Langmuir waves excited would have a wave number $k \simeq 1.2\mu m^{-1}$, and so would not be detected by the ruby scattering where $k = 12.9\mu m^{-1}$. The heat flux in the experiment should be much less than the flux limited value. From the simulation $0.06 < R < 0.1$ where R is the ratio of the heat flux to the free streaming limit. The further possibility of heat flux limitation by an ion acoustic instability can be ruled out because of the low value of $T_e/T_i \sim 1.2$ here[3].

However, the simulation does show that a short (2ns) intense (1GW) CO_2 laser pulse will both drive the heat flux up to its flux limited value and produce ion acoustic instability limited flow.

The question arises as to whether the theoretical absorption, or theoretical conduction, or both are incorrect; our data alone cannot entirely discriminate. A measurement of the amount of 10.6μm radiation transmitted did not give accurate information on the absorptivity because of the variation of plasma properties along the beam. However, good theoretical agreement (e.g. 1,4) and an accurate experiment[4] establish the absorption at $k = 1.0 \pm .15$. In contrast there is little experimental work on thermal conduction, and a variety of theoretical values of the conductivity. We therefore regard the theoretical absorption as correct at k = 1.0 and use our results to deduce the thermal conductivity, giving $s = 0.4 \pm .2$,or $40\% \pm 20\%$ of Spitzer's theoretical value.

References

1. L.Spitzer, Physics of Fully Ionised Gases (Wiley, 1962).
2. C.Lashmore-Davies, Plasma Phys. 17, 281 (1975).
3. E.Jackson, Phys. Fluids 3, 786 (1960).
4. K.W.Billman et al., Phys. Fluids 17, 751 and 759 (1974).

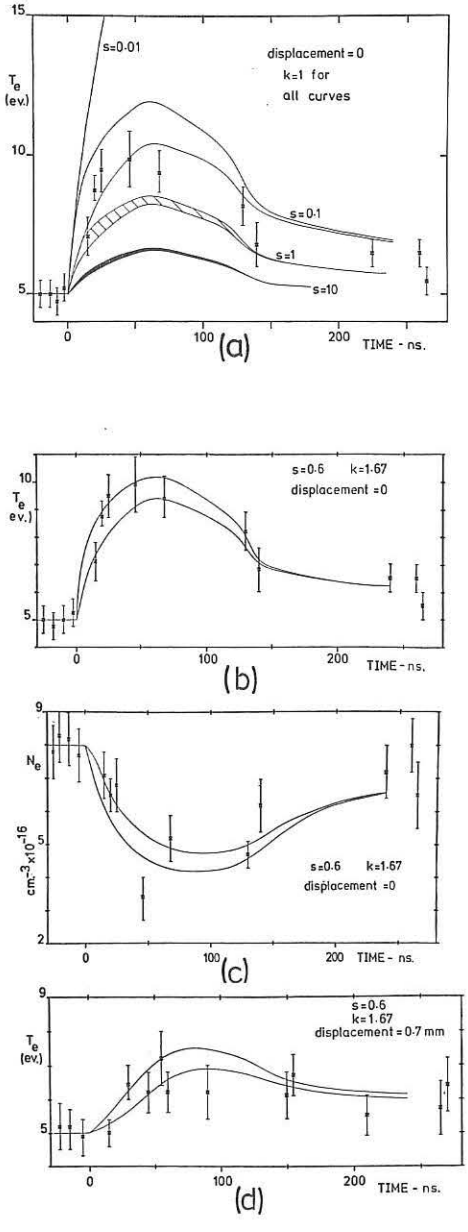

Fig.1. Examples of experimental data (X) and some numerical fits. The band represents the simulated variation across the spatial resolution. 1(a) shows a coarse fit to the observed temperature history at zero displacement, to illustrate the sensitivity of the method. 1(b to d) show good fits for the temperature histories at 0 and 0.7mm, and density history at 0mm. The simulated laser pulse rises linearly from zero to 15 MW at 60ns, then falls to zero at 140ns. It decreases spatially in an Airey pattern to 0.25mm.

LASER-PLASMA INTERACTIONS IN INTENSE MAGNETIC FIELDS*

W. Halverson, D. R. Cohn and B. Lax†

Francis Bitter National Magnet Laboratory‡
Massachusetts Institute of Technology
Cambridge, Massachusetts 02139 USA

Abstract: Interactions of high-power CO_2 laser radiation with magnetically confined plasma are characterized by strong beam-channeling, a "bleaching wave" in the plasma, and an undercompressed detonation wave in the unionized gas. Powerful submillimeter lasers are being developed to study laser-plasma interactions and for diagnostics of Tokamak plasmas.

I. CO_2 Laser Heating of Magnetoplasmas

In order for a laser to heat efficiently a plasma column of length much greater than its diameter, the plasma must stably trap the beam by the formation of an effective dielectric waveguide throughout its length. We have shown experimentally and theoretically that beam-trapping can be produced in plasmas created by laser-induced breakdown of low pressure gases in a strong longitudinal magnetic field.

In our experiments[1,2] we used a pulsed CO_2 laser which was operated with an unstable resonator cavity and produced an annular beam with about 15 joules in a 75 nsec pulse. The beam was focused by a 40 cm FL germanium lens into a low pressure gas-filled cell located in the bore of a Bitter solenoid capable of producing axial magnetic fields up to 110 kG. The transmitted laser radiation passed through a NaCl window mounted at the opposite end of the cell and was monitored with small moveable germanium photon-drag detectors.

The temporal and spatial evolution of laser-heated helium plasmas was determined using an optical detection system which measures locally the optical emission from the 4686 Å He II line and nearby continuum at 5210 Å. Abel-inverted radial scans of the plasma were used to calculate the radial distribution of plasma density and temperature. Soft x-ray diagnostics using gas x-ray absorbers instead of metallic foils were used to check the optical temperature measurements above ~ 35 eV.

We found for plasmas formed by laser-induced breakdown of hydrogen and helium from 5 to 40 torr, that a longitudinal magnetic field caused a strong concentration of the transmitted laser beam along the axis of the plasma region. Figure 1 shows the transmitted laser intensity at various times after the beginning of the laser pulse for (a) no plasma and (b, c) breakdowns in 20 torr of helium. The intensity of the central peak increased at higher magnetic field and lower initial gas pressure. The transmitted central peak was quite narrow; its FWHM divergence angle was 0.9°.

Channeling of the transmitted beam is caused by the formation of a plasma density minimum on the column axis due to plasma expansion during the laser heating. The radial decrease of the index of refraction can cause total internal reflection of the laser radiation. Figure 2 shows radial density profiles in helium plasma in a field of 19.4 kG. The ~ 30% axial density minimum is much more than

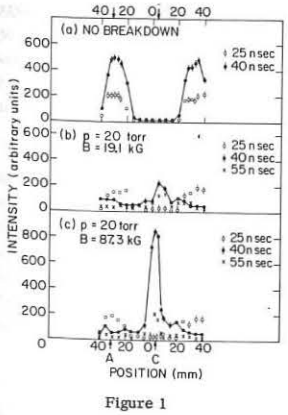

Figure 1

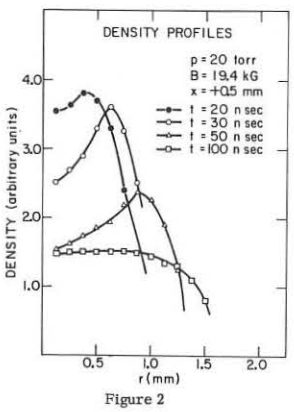

Figure 2

necessary to trap the incident laser beam. For this case, $n_e \approx 5 \times 10^{17} cm^{-3}$ and $T_e \approx 25$ eV so that $\beta \approx 3$. As the magnetic field was increased, the radial dimensions of the plasma were reduced to about 0.5 mm at a magnetic field of 88 kG and the plasma β decreased to about 0.3. For cases where $\beta \approx 0.3$ to ~ 1, no clear density minimum was observed, although the collimated transmitted beam intensity increased with magnetic field. For these cases the radial dimensions of the plasma were of the same order as the resolution of the optical diagnostics.

The presence of a beam-trapping minimum has been predicted for plasmas with $\beta < 1$ using a quasi-static (QS) model of the radial flow. The total magnetic and kinetic pressure is equated to the initial magnetic field pressure and the field is assumed to be "frozen" into the plasma.[3] Using Snell's law, the density minimum required for total internal reflection is then calculated in terms of the plasma temperature, angle of incidence of the laser beam, and initial plasma conditions. The temperature required for total internal reflection of an incident laser beam of convergence half-angle α can be expressed approximately by

$$kT = \frac{B_o \alpha^2}{8\pi N_{eo}} \left[\frac{N_c}{N_{eo}} + \frac{\alpha^2}{2} \left(\frac{N_c}{N_{eo}} \right)^2 - 1 \right] \qquad (1)$$

In Eq. (1) we have assumed that the plasma density for cutoff, N_c, is much greater than the initial electron density N_{eo}; $\alpha^2 \ll 1$; and that $T_e = T_i = T$.

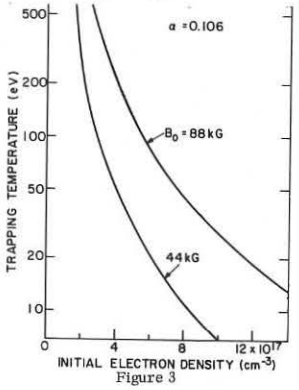

Figure 3

The termperature required for beam-trapping was calculated from the QS model for the conditions of our experiment, Fig. 3. It can be seen that electron temperatures of only 20-30 eV are required to trap the incident laser beam. Electron temperatures in the range of 20-35 eV were measured for the 20 torr He plasmas by the optical and x-ray diagnostics.

We have also studied the axial propagation of the laser-driven plasma fronts both toward and away from the laser. Observations of the front velocities and measurements of the plasma density and temperature indicate that the fronts propagate as under-compressed detonation waves.

In theoretical studies of CO_2 laser heating of a long plasma column, we have included the effects of electron-ion energy transfer and radial plasma expansion in the propagation of the longitudinal "bleaching wave" of laser radiation. Ion heating rates are increased when radial plasma expansion is included in the model and when the CO_2 laser power is programmed[4] as $P \propto t^{\frac{3}{2}}$.

II. Submillimeter Laser-Plasma Interactions

Powerful sources of submillimeter laser radiation have been developed recently which are being used for studies of laser-plasma interactions. A 496 μm CH_3F laser, which is optically pumped with CO_2 laser radiation, is now operating as a dominant single mode oscillator with rather high efficiency. This laser appears to be scalable to the 1 MW level required for ion temperature measurements by Thomson scattering and other diagnostics of Tokamak plasmas.[5]

Using lower power CH_3F lasers we are presently studying cyclotron resonance breakdown of gases in a DC magnetic field of 216 kG and plasma heating at harmonics of the cyclotron frequency. The laser will also be used to study parametric decay instabilities in arc plasmas.

*Work supported in part by U.S. Air Force Office of Scientific Research
†Also Physics Department, Massachusetts Institute of Technology
‡Supported by National Science Foundation

References

1. D.R. Cohn, G.J. Raff, R.L. Brooks, N.G. Loter and W. Halverson, Phys. Lett. 49A, 95 (1974).
2. N.G. Loter, D.R. Cohn, W. Halverson and B. Lax, J. Appl. Phys. (1975).
3. W. Halverson, J. Appl. Phys. 45, 5209 (1974).
4. S.Y. Yuen, B. Lax and D.R. Cohn, Phys. Fluids (1975).
5. D.L. Jassby, D.R. Cohn, B. Lax and W. Halverson, Nuc. Fusion 14, 745 (1974).

Experimental Investigation of Laser Heated Plasma
in a Solenoidal Magnetic Field

Z.A. Pietrzyk, H. Rutkowski, G.C. Vlases

University of Washington, Seattle, Washington USA

Abstract: Plasma columns 20 cm x 6 mm have been produced in a 100 kG steady solenoidal field by CO_2 laser irradiation. Measured densities and temperatures are $n_e \simeq 5 \times 10^{17}$ and $T_e \simeq 150$ eV, for filling pressures of 19 torr and laser energies of about 250 joules.

Following a suggestion by Dawson, et.al.,[1] that CO_2 lasers could be used to heat long, magnetically confined plasma columns to thermonuclear temperatures, an experimental program to explore this concept was initiated at the University of Washington. This paper presents our most recent results on the "laser heated solenoid," one of several experiments in progress. An e-beam stabilized CO_2 laser is used to irradiate a plasma tube 20 cm long x 1.7 cm in diameter, which is immersed in a quasi-steady field of up to 100 kG. The tube was puff-filled with neutral hydrogen from one end. An orifice plate with a 5 mm hole was placed at the other end, nearest the incoming laser beam. A pressure ratio of greater than 10 was measured across the orifice, with good uniformity along the tube. The laser beam was focused at the orifice location, producing a wave propagating along the tube (away from the laser), and eliminating the backward-going wave normally present in breakdown experiments.[2]

It was previously reported[2] that, with this arrangement, a density minimum is created on axis by the heating action of the laser beam, and that the "heating wave" propagates along the axis, creating a long, slender plasma. Most data were taken at fields of 0 or 100 kG, filling pressures on the order of 20 torr, and laser energies up to 300 joules in a 1 μsec pulse.

In more recent work, the evolution of the plasma column has been more thoroughly studied by streak photography and interferometry. Streak pictures with the slit parallel to the axis were taken through plexiglass spacers between the turns of the solenoid, and through holes in the turns. For B=0 the breakdown front velocity is about twice that for B = 100 kG, and is nearly constant along the 20 cm of tube length. For 100 kG magnetic field and low laser energies (50-150 joules), the breakdown velocity is constant for 8-12 cm and then decays quickly, as the laser pulse has terminated by then. When the laser energy is increased the constant velocity segment increases, and for energies of about 240 joules the front accelerates for some distance and then travels at constant speed to the end of the tube (Figure 1). The length of the column in our experiments is limited by the magnet length.

The shape of the propagating front has also been examined. Streak pictures with the slit perpendicular to the axis were taken at several locations, using an H_β filter to accentuate the (cooler) interface between the plasma and the neutral gas. When observed in this manner, the advancing front is not flat, as is usually assumed in theoretical models, but rather is pointed. The full angle of the front is approximately 20°, and the length of the conical section is about 3 cm, after which the diameter is nearly constant. This observation suggests that the presence of a strong field is important not only for radial containment, but also, due to refraction, in determining the properties of the advancing front. It appears that this effect is advantageous for beam trapping near the front and deepens the laser induced density minima reported earlier.[2]

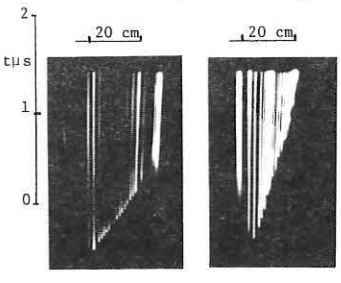

Fig. 1. Streak pictures of breakdown front propagation. Laser energy = 240 J.

Particle loss rates were estimated from measurements of radially averaged densities as a function of time at a given axial location. A single-ray Mach-Zehnder interferometer, illuminated by an argon ion laser was used, which provided spatial resolution of approximately 1 mm. Figure 2 shows comparison of these data with a simple one-dimensional rarefaction wave model, with detonation wave at the front, shows fair agreement except for later times for B = 100 kG. The lack of agreement for later times may be due either to the neglect of the effect of laser heating on the expanding gas, or to the failure to undergo transition from a bleaching wave[3] to a detonation wave[4] within the duration of the experiment. More complete models of the laser-plasma interaction[4,5] cannot be compared quantitatively due to their failure to incorporate end effects, but qualitative agreement is good. For B=0, the measured densities are much lower and the one-dimensional model with the rarefaction wave does not agree well with the data due to radial motion and heat conduction.

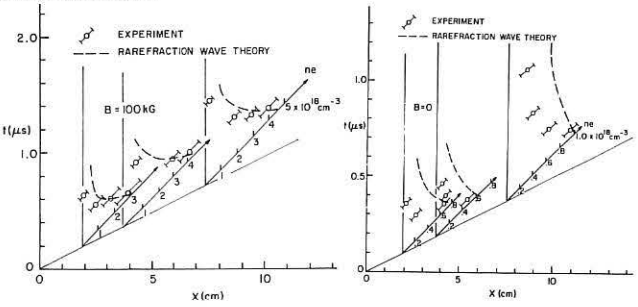

Fig. 2. Densities versus time for various position in the tube. Laser energy = 150 J.

The electron temperature was measured, at several axial locations, by using the carbon V method of Kunze, et.al.[6] to be in the range of 130-150 eV.

Finally, measurements were made of the radiation backscattered from the underdense plasma[7] by the use of time resolved infrared spectroscopy. The backscatter, which appears to saturate at about 5% of the initial laser energy, was identified as stimulated Brillouin scattering.

This work was supported by the U.S. Energy Resource Development Agency and the National Science Foundation. The authors wish to thank K. Berggren, R. Massey, and D. Scudder for their help in performing the experiments.

References:

1. J.M. Dawson, A. Hertzberg, R. Kidder, G.C. Vlases, H.G. Ahlstrom, L. Steinhauer, Proc. IAEA Conference on Plasma Physics and Controlled Fusion Research, Madision I(IAEA Vienna 1971), p. 693.
2. H. Rutkowski, D.W. Schudder, Z.A. Pietrzyk, G.C. Vlases, Appl. Phys. Lett. 26, April 15, 1975.
3. L.C. Steinhauer and H.G. Ahlstrom, Phys. Fluid 14, 1109 (1971).
4. Iu.V. Afanase'ev, V.M. Krol', O.N. Krokhin, I.V. Nemchinov, PMM 30, #6, pp. 1022-1018 (1966).
5. R.G. Rehm, Phys. Fluid 13, 919 (1970).
6. H.J. Kunze, A.H. Gabriel, H.R. Griem, Phys. Fluids 11 (1968) p. 662.
7. R. Massey, K. Berggren, Z.A. Pietrzyk, Phys. Rev. Lett. (1975). To be published.

NANOSECOND CO_2 LASER INTERACTION WITH SOLID TARGET

J. MARTINEAU, P. PARANTHOEN and M. RABEAU

Commissariat à l'Energie Atomique, Centre d'Etudes de Limeil
B.P. n° 27, 94190-VILLENEUVE-SAINT-GEORGES, FRANCE

Abstract : At fluxes of 10^{12} W/cm^2, the nanosecond CO_2 laser interaction with a solid deuterium target has been studied. Reflection, X ray and ion measurements were performed. Energy balance led to a total reflectance of 60 to 90 %. Fast D^+ ions with kinetic energy of 40 keV were detected. X rays were observed up to 10 keV.

The interest in lasers as a possible source of energy has been growing considerably for the last three years. New experiments based on the concept of compression /1/ have been carried out using neodymium glass lasers (λ = 1.06 μm) as well as carbon dioxyde lasers (λ = 10.6 μm). Thus single beam experiments contribute to a better knowledge of the phenomena involved in the interaction. The coupling efficiency of the laser radiation with the plasma which remains one of the most important problems, can be improved. On the other hand, as predicted by theory, most of the parametric instabilities, can be observed and studied at lower incident laser fluxes using a CO_2 laser /2,3,4/.

The purpose of this paper is to describe the interaction of a nanosecond CO_2 laser with a solid deuterium target. With incident fluxes of about 10^{12} W/cm^2, the interaction makes the observation of fast ions and hard X rays possible.

The nanosecond 1 GW CO_2 TEA laser consisted of an oscillator delivering 200-300 mJ in 40 ns. This pulse was preamplified up to 600 to 800 mJ. Then the 1.5 ns short pulse was cut out of the 40 ns pulse. For this purpose we used a double pockells cell composed by two As-Ga placed between crossed polarizers. After amplification through a double discharge C.G.E. system the laser output energy was about 2 to 3 J. The beam was focussed onto a solid deuterium target using a 20 cm focal length Na Cl lens which corresponded to an aperture of f/3. Maximum incident flux in a vacuum did not exceed several times 10^{12}W/cm^2. The target was a solid deuterium prism with a one millimeter square section.

Energy and pulse shape measurements were recorded at 0°, 45° and 90°. In any direction of observation the reflectance presents an important scatter (fig. 1). On the other hand a plot of the measured reflectance vs the focal position indicates that the reflectance does not correlate with the focus. At 0° the reflection coefficient ranges from 1 to 10 %, while at 45° and 90° from 0.5 to 2 % and 0.1 to 1 % respectively. This behavior shows a directional reflectance which can reach 42 % per steradian. On integrating the reflectance over the relevant half space about 60 to 90 % of the incident laser energy is lost out to reflection (fig. 2).

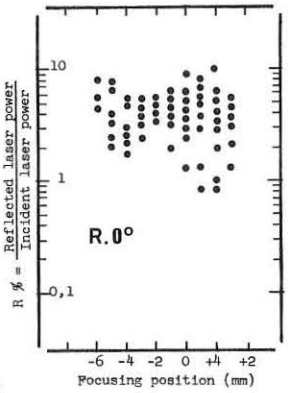

Figure 1

X ray spectrum from the continuum bremsstrahlung emission is analyzed at 45° by using absorbing beryllium foils of different thicknesses (6.05, 30, 52.2 and 105 mg.cm^{-2}), combined with two X ray scintillator detectors. For focusing on the surface or slightly inside X ray emission is maximum.

The transmitted X ray signal decreases slowly when increasing the thickness of the absorber (fig. 3). This is characteristic of the presence of hard X ray emission which corresponds to a non maxwellian electron distribution function. X rays with high energy up to 10 keV were observed.

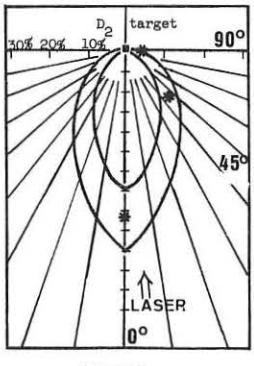

Figure 2

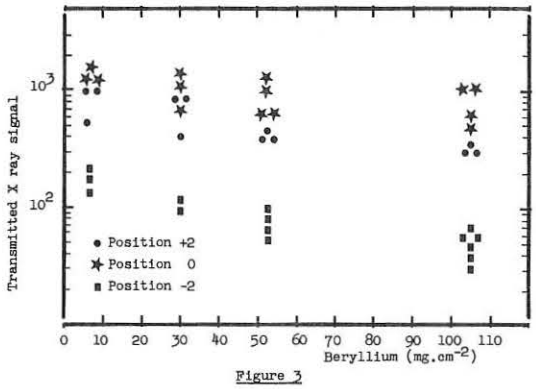

Figure 3

Ion collectors (at 45° and 25°) and an electrostatic charged particle analyzer (at 45°) were used to measure ion kinetic energy and identify ion species. The results show clearly the presence of high energy ions belonging to a hot plasma (0.5 to 1keV) followed by ions corresponding to a cold plasma (100 eV). In addition from time to time some fast ions are evidenced before the ion current corresponding to the main plasma described previously. Then the ion energy spectrum expands continuously from high energy (up to 40 keV) to low energy (down to 0.1 keV). The number of high energy ions ($\sim 5.10^{12}$/sterad at 45°) is less important than the one of ions coming from the main plasma ($\sim 10^{14}$/sterad at 45°). With an electrostatic charged particles analyzer D^+ ions were observed with energies as high as 40 keV. Typically most of the fast ions are with energies between 10 to 25 keV. They can take out up to 40 % of the total absorbed energy. Comparable results presented in table I have been obtained at Los Alamos /5,6/ and Osaka /7/ in similar nanosecond experiments using polyethylene and aluminium targets.

The hard X rays and the fast ions are probably significant of non linear phenomena present during the interaction. If it is difficult at present to give a certain interpretation, nevertheless it appears that too much energy taken out by the fast ions is a problem for laser driven shocks.

We thank G. NIERAT, E. GOESTCHY, M. ROSTAING for their technical assistance.

Location	Target	Intensity W/cm^2	Pulse Width	% Absorption	Fast ions	
					Observed	% Total Absorbed Energy
LOS ALAMOS	SLAB CH_2	$5x10^{14}$	1.5 ns	50	YES	80
OSAKA	SLAB	$5x10^{14}$	2 ns	50	YES	-
LIMEIL	D_2	10^{12}	1.5 ns	10-30	YES	5 - 40

TABLE I

/1/ Nuckolls, J., Wood, L., Thiessen, A., Zimmermann, G., Nature 239 (1972) 139

/2/ Fabre, E., Stenz, Phys. Rev. Lett. 32 (1974) 823

/3/ Martineau, J., Repoux, S., Rabeau, M., Patou, C., J. of Appl. Phys. (1975), to be published

/4/ Baldis, H., Pepin, H., Parbhakar, K., Johnston, T.W., Bull. Am. Phys. Soc. 19 (1974) 922

/5/ Kephart, J.P., Godwin, R.P., Mc Call, G.H., Appl. phys. Lett. 25 (1974) 108

/6/ Ehler, A.W., J. of Appl. Phys. (1975), to be published

/7/ Yamanaka, C., Proc. of the Fuji Seminar on Laser Interaction with Plasma, Osaka (1975) 186

Experiments on CO_2 laser interaction with polyethylene slabs

E. FABRE - C. POPOVICS - C. STENZ

Ecole Polytechnique
Laboratoire P.M.I. - 91120 Palaiseau France

Abstract : In CO_2 Laser produced plasma, we study the dependancy with light intensity of electron temperatures, ion velocity, plasma reflectivity and spectrum of back reflected light at 10.59 μ and 2nd harmonic. Results show some evidence for anomalous processes of interaction.

Several publications have reported experimental results obtained on plasmas produced by CO_2 laser irradiation of plane targets. In order to have a better understanding of the processes involved in the interaction of CO_2 laser radiation with a target, we have made an extensive study of the dependancy of some of the plasma parameters with the laser fluxes. This shows[4,8] that, at moderate light intensities, anomalous processes of absorption occur, which can be attributed to the onset of parametric instabilities. We have also analysed the spectrum of backscattered light at 10.59 microns and at 5.3. microns.

The experimental set up is the following : we focus, onto a polyethylene slab, with a spherical mirror of 30 cm of focal length and a f : 2.5 aperture, the output beam of a Lumonics TEA laser. The pulse duration is 40 ns FWHM and the peak power on the target 1 Gigawatt. The resulting maximum intensity on the focal region is 2 10^{12}W/cm². Variations of light fluxes on the target are obtained by beam attenuation with thin film. The electron temperature Te is determined by the absorber foil method using five different thickness of Aluminium foils. Charge collectors located at 40 and 90cm from the plasma provide the ion energy by time of flight method. The incident pulse and the back reflected pulse in the aperture of the collimating optical system are monitored by photon drag detectors and give the reflection coefficient of the plasma. Finally the back reflected light at 10.59 micron, the emission at 5.3 micron and the reflection at 10.57 micron, which is an auxiliary line emitted by the laser, are monitored in relative intensity and in spectral shape with a 2 meter focal length monocromator. The resolution of the spectrograph is of the order of $2.8 10^4$ at 10.6 micron. The measured spectral width of the incident laser lines is 3.8 Å which corresponds to the instrumental width.

The experimental results are the following

- The reflection coefficient of the plasma R (figure 1), at 10.59 μ increases with laser intensity I at low fluxes, saturates at a value of 9 to 13 % for intensities in the range of 4 10^{10}W/cm² and decreases to a value of 4 to 6 % from 5 10^{11} to 2 10^{12}W/cm² laser intensity.
- The second harmonic emission already observed in previous works[4,9] increases rapidly at low fluxes and shows a dependancy as $I^{3/2}$ for high intensities (fig.1).
- The electron temperature Te measured by the absorber foil method has two features (fig.2) : a thermal component which varies as $\sim I^{.3}$ and a suprathermal component which varies as $\sim I^{.6}$ and which is detectable only for intensities above 10^{11}W/cm².
- The ion energy (fig.2) in the leading edge of the expanding plasma depends upon intensity as $I^{2/3}$; a small number of ions with energy up to 15 kev are detected.

These results show that for laser intensities in the range of 4 10^{10}W/cm² interaction processes involve the onset of parametric instability mechanism which can explain the saturation of plasma reflectivity, and the occurance of suprathermal electrons, which determine then the energy of the ion at the frontier of the expanding plasma plume. These results are also consistent with previous experiments (10) that we have done on light absorption by a dense plasma which had shown the occurance of anomalous absorption at laser intensities of the order of 2 to 4 10^{10}W/6m² in agreement with the computed threshold for parametric decay instability. The dependancy of ion energy with flux is in agreement with the results at higher intensities (11-12).

Asecond set of experiments deals with spectroscopic studies. The spectrum of the back reflected light (fig.3) at 10.59μ shows a large broadening of the line which presents also a strong assymetry toward the red at high laser intensities. At lower intensities there is still a broadening of the line but then line profile is symmetric around the origin λ_o. The emission of the second harmonic (fig.4) at 5.3 micron present a contribution at the origin $\lambda_o/2$ and a strong satellite in the red wing with a shift of the order of 20 to 25Å. The spectrum of backscattered auxiliary line (fig.4) 10.57μ which intensity is 5 to 8 % of the main laser line at 10.59, presents also two components : a narrow line at the origin 10.57 and a component with a red shift of 20 Å. This corresponds in frequency to half of the frequency shift of the satellite of the 10.59 second harmonic. The interpretation of these results is not complete at present time. However some of these results agree with observations made in experiments with Neodymium laser for light intensities two order of magnitude higher.[13-15]

The red shifted contribution of the main laser line at 10.59 may be interpreted as brillouin back scattering, the frequency shift being close to the ion acoustic frequency. It has to be mentionned that in the case of short pulse experiments similar results has been observed with a red shifted component.[16] However other experiments[17] show a blue shifted satellite which is explained as reflection on the critical density surface moving away from the target. The second harmonic generation has two contributions : the line centered around the origine $\lambda_o/2$ is probably generated by non linear interaction at oblique incidence in the density gradient near critical density. The red shifted satellite can be interpreted as being generated in a four wave mechanism as suggested by Yamanaka[13]. The observation of a red satellite with the probe beam at 10.57, which has a frequency shift half of the shift of the second harmonic can be a confirmation of this interpretation.

REFERENCES

1. P.E. DYER and al. Phys. Lett. 48A, (1974), 311
2. R.E. BEVERLY Phys. Lett. 44A, (1973), 321
3. K. DICK, H. PEPIN Opt. Comm. 13, (1975), 289
4. E. FABRE and al. 5th IAAE conference. Tokyo Nov. 1974
5. J. MARTINEAU Opt. Comm. 12, (1974), 307
6. J.F. KEPHART and al. Appl. Phys. Lett. 25, (1974), 108
7. C. YAMABE and al. Phys. Lett. 50A, (1974), 349
8. E. FABRE and al. 5th Conference on Anomalous Absorption, UCLA, April 1975, Paper E2.
9. H.A. BALDIS and al. INRS Int. Report 044-Dec. 1974
10. E. FABRE, C. STENZ Phys. Rev. Lett. 32 (1974) 823
11. G.H. Mc CALL Mt Fuji Seminar on Laser Fusion - Nov. 1974
12. A.W. EHLER to be published in J. Appl. Phys.
13. C. YAMANAKA and al. Phys. Rev. Lett. 32, (1974), 1038
14. K. EIDMANN, R. SIEGEL, Phys. Rev. Lett. 34, (1975), 799
15. GOLDMAN and al. Phys. Rev. Lett. 31, (1973), 1184
16. B. MITCHELL and al. to be published in App. Phys. Lett.
17. H.A. BALDIS and al. 5th Anomalous Absorption Conf. UCLA April 1975, B. Grek paper E4 and E5

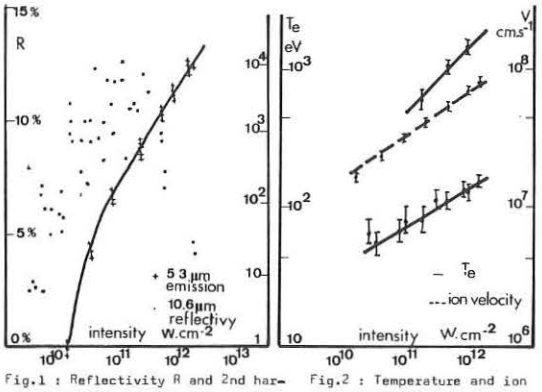

Fig.1 : Reflectivity R and 2nd harmonic relative intensity dependance with incident flux.

Fig.2 : Temperature and ion energy variations with laser intensity.

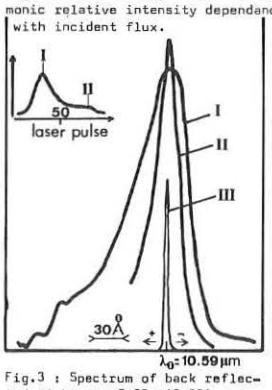

Fig.3 : Spectrum of back reflected light at 10.59μm(I,II) and incident (III).

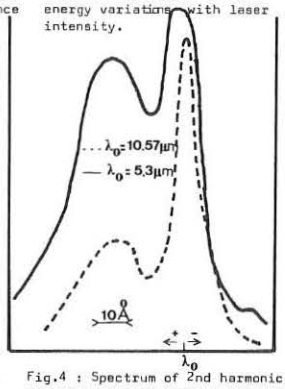

Fig.4 : Spectrum of 2nd harmonic and of reflected light at 10.57μm.

EXPERIMENTAL STUDIES OF CO_2 LASER PRODUCED PLASMAS

by

T.A. Hall and Y.Z. Negm

University of Essex, Colchester, England

Abstract Experimental results of X-ray temperatures, ion energies and plasma reflectivities are presented for a CO_2 laser produced plasma. A clear indication of anomalous absorption is shown with a threshold irradiance of 4×10^{10} W cm^{-3} and at high irradiances a discrepancy in the energy balance is reported.

Introduction Several papers [1] [2] [3] [4] have recently reported reflectivity and other diagnostics on CO_2 laser produced plasmas. The results to some extent have been conflicting. In [2] no obvious threshold for anomalous absorption is observed whereas in [1] [3] and [4] clear indications of this are shown, but with different degrees of agreement between theory and experiment.

Experiment The CO_2 TEA laser used in these experiments gave peak power outputs ~ 200MW in a pulse of FWHM ~ 40-50nsec. The laser is described more fully in [1] . Light from the laser is focussed onto targets of carbon and the light reflected back from the plasma is collected by the same lens. Both the reflected and incident light intensities are monitored by photon drag detectors. The laser is run under constant conditions and the irradiance is altered by introducing calibrated filters in the beam. Other diagnostics include two X-ray scintillators using 6μm and 12μm thickness aluminium foil absorbers to measure X-ray temperatures and a retarding potential probe to measure ion fluxes.

Results and Discussions The open circles in Fig. 1 show plasma reflectivities as a function of irradiance. As the irradiance is increased from the lowest detectable levels, the reflectivity increases up to a maximum of about 23% at an irradiance of 4×10^{10} W cm^{-2}. Above this value the reflectivity falls steadily with increasing irradiance to about 5% at 2×10 W cm^{-2}.

If we assume inverse bremsstrahlung absorption and a linear density profile then an expression for the plasma reflectivity, R, can be obtained [5]

$$R = \exp\left(-a\bar{Z}\ \ln\Lambda H_L/\lambda^2 T^{3/2}\right) \qquad (1)$$

where $\bar{Z}$ is the mean ion charge and H_L is the density scale length, T is the electron temperature and a is a constant.

The broken line plotted in Fig. 1 obeys the relation

$$R \propto \exp(-b\phi^{-\frac{1}{4}}) \qquad (2)$$

where ϕ is the flux. Fig. 1 also shows X-ray temperatures plotted against incident flux and we see that at the lower powers the experimental values fit the relation

$$T \propto \phi^{\frac{1}{4}} \qquad (3)$$

which is in agreement with the model of Caruso et al. [6] .

Substituting expressions (2) and (3) into (1) we find that:

$$\bar{Z} H_L \propto T \qquad (4)$$

The temperature dependence of $\bar{Z}$ is difficult to determine since neither LTE nor the coronal model are strictly applicable under the conditions described here. However, for the purposes of obtaining simple scaling laws the coronal model more nearly describes the plasma conditions here and we find that in the region of T = 100-200eV, for carbon, the relation

$$Z \propto T^{\frac{1}{4}} \qquad (5)$$

holds approximately [7] . Thus this implies that the scale length has a temperature dependence of the form

$$H_L \propto T^{\frac{3}{4}} \qquad (6)$$

Above 4×10^{10} W cm^{-2} the reflectivity falls with increasing irradiance and it is assumed that some non-collisional absorption mechanism is responsible. A possible mechanism is the parametric instability which for a temperature of 300eV observed in these experiments, predicts a threshold irradiance, given by [3] of:

$$I_{th} = 10^{11} \text{ W cm}^{-2}$$

which is somewhat higher than the value found here. This discrepancy may be a result of the plasma refractive index which has been neglected in the above calculations.

Above threshold the plasma reflectivity falls rapidly and at the same time a change in the temperature scaling law is observed. In this region however there seems some evidence that the plasma electron distribution function has become non-Maxwellian and consequently the results must be interpreted with care.

A retarding potential probe has been used to measure ion fluxes and estimates have been obtained for the total energy emitted by the plasma in the form of ions. These are shown in Fig. 2.together with the ratio of total ion energy to incident laser energy. Below the threshold for anomalous absorption we can see that the energy which is not reflected is carried away in the form of ion motion. Above the threshold however both the reflectivity and the relative energy carried away by the ions fall. The increased X-ray emission at these high irradiances does not nearly compensate for this.

References

[1] T.A. Hall, Y.Z. Negm, submitted to Optics Communications

[2] P.E. Dyer, et al. Phys.Lett. 48A, 4, 311, 1974.

[3] C. Yamanaka et al. V Int. Conf. on Plasma Physics and Controlled Nuclear Fusion, 1974.

[4] K. Dick, H. Pepin, Optics Communications 13, 3, 289, 1975.

[5] J.W. Shearer, J.J. Duderstadt. Nuclear Fusion, 13, 401, 1973.

[6] A. Caruso, B. Bertotti, P. Guipponi, Nuovo Cimento 45B, 176, 1966.

[7] T.P. Donaldson, R.J. Hutcheon, M.H. Key. J. Phys. B. 6, 1525, 1973.

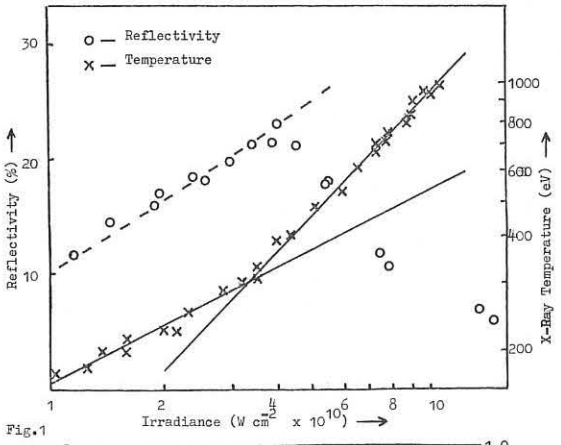

Fig.1

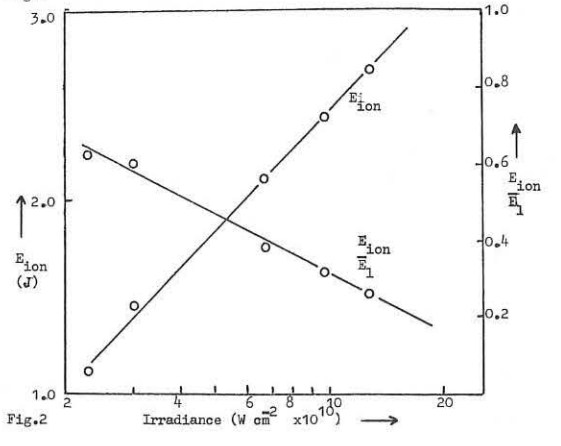

Fig.2

CO_2 LASER-HEATING EXPERIMENTS

T.P. Donaldson*, J.W. van Dijk+, A.C. Elkerbout+, and I.J. Spalding†
Queen's University*, Belfast, Hogere Technische School+, Rijswijk, The Netherlands, and UKAEA Culham Laboratory†, United Kingdom.

Abstract: The interaction of 75J CO_2 laser pulses with plane SiO_2 and C targets at intensities ~ 9 x 10^{12} W/cm^2 is described. The resulting flow has been measured with framing photography, holographic interferometry and X-ray techniques (using a fast photodiode, a 13 μm resolution pinhole camera and 2-channel absorption spectrometers); finite λee should be included in MHD models of such interactions.

1. INTRODUCTION

Subkilojoule CO_2 laser-produced plasmas are of potential interest for filling present-generation magnetic-confinement devices.[1] As part of a cooperative Euratom programme, a 160 litre-atmosphere electron-beam pre-ionized CO_2 laser is now being commissioned for laser-heating experiments at Culham; this device has an active volume of 200 x 20 x 20 cm, and will be described elsewhere. However, laser-plasma interaction measurements have already been made with a 75J driving oscillator stage for the system and some of these preliminary measurements form the basis of the present paper. Experimental and diagnostic techniques are outlined in para.2; the experimental results are summarised in para.3 and discussed in para.4.

2. EXPERIMENTAL AND DIAGNOSTIC TECHNIQUES

The experimental arrangement is illustrated in Fig.1. Although small, low z, targets will be used in later (confinement) experiments, it proved more convenient to use carbon or fused silica rods of 5 mm diameter for these initial diagnostic tests. The output from a gain-switched double-discharge TEA laser of cross section 5 x 10 cm was focused by a 12 cm diameter (rear) mirror on to targets located at its 30 cm focus; with an incident energy of 75J, a focal diameter of 150 μm was measured by a grating technique.[2] Although a stable optical resonator was used in this particular laser, relatively little fine-structure was observed in the far-field pattern, which was consistent with a beam divergence of ~ ½ milliradian. (The target geometry thus approximates to normal cylindrical illumination of a semi-infinite plane.)

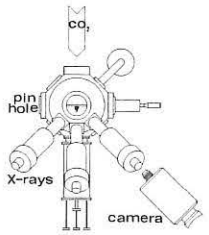

Fig.1 Plan-view of target chamber.

Simultaneous X-ray emission measurements were made with a 2-channel foil (scintillator) spectrometer,[3] a (time-integrated) pinhole camera and a photodiode of novel design. The pinhole camera had a hole of 5 μm diameter and a geometrical magnification of 1.5; it was used with a Kodak-Pathe SC7 emulsion having a measured mean grain size of 14 μm, giving an effective spatial resolution of ~ 13 μm. The X-ray photodiode was a gold-coated diode of the general type developed by Key;[4] however, the surface of our diode was contoured to give an angle of incidence of ~ 3.5°, thus ensuring maximum photoelectric sensitivity to 1.4 keV X-rays. (The diode has a calculated time-response of 0.6 ns when used with a 1 GHz band-width oscilloscope, and a high sensitivity to the soft X-rays characteristic of present plasmas.) (Visible) streak and framing photographs were taken with streak speeds and exposures of 4 ns/cm and 5 ns respectively. The layout of the λ = 6943 Å ruby-laser holographic interferometer is illustrated schematically in Fig.2. Holograms were taken[5] on Agfa 10E75 and Kodak 649F emulsions with exposure times of 20 ns (Q-switched) or 2 ns (gated). Straight-line reference fringes are obtained by calibrated displacement of a reference mirror (R) in between the two exposures. (λ = 3471 Å, frequency-doubled, holograms have also been produced with this equipment, but were not analysed in the present experiment.)

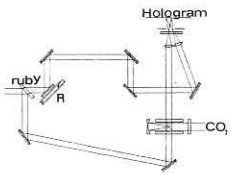

Fig.2 Holographic Interferometer.

3. EXPERIMENTAL RESULTS

3.1 Pinhole Camera

Microdensitometer traces across a single-shot exposure, (taken with a 0.22 mg/cm^2 Al filter, having a bandpass of 9 Å centred at 15 Å, for 200 eV thermal plasmas) are shown in Fig.3, at various positions above the target surface. The 13 μm spatial resolution of the camera is extremely good, and the dip in photographic density across the laser axis is therefore thought to be experimentally significant. (In Fig.3, the γ of the film is linear, and the FWHM of the X-ray intensity unfolded from curve (a) is 420 μm.)

3.2 Holographic Interferometry

Fig.4 illustrates density profiles obtained by Abel Inversion of a holographic reconstruction. Note that the transverse dimensions of the plasma are ~ 1 mm, i.e. comparable to the diameter of the X-ray region, and very much greater than the focal spot diameter of the incident laser beam.

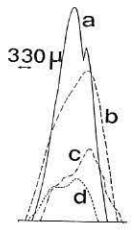

Fig.3 X-ray pinhole pictures at distances (a) 0.33 (b) 0.7 (c) 1.0 (d) 0.17 mm above a silica target.

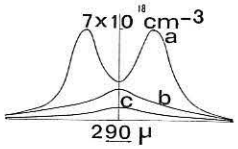

Fig.4 Density profiles at (a) 0, (b) 200 and (c) 500 μm above a carbon target, 30 ns after firing CO_2 laser (exposure 20ns)

3.3 Time-resolved X-ray Measurements, and Supporting Diagnostics

X-ray signals detected by the fast photodiode followed, within the experimental errors, the incident CO_2 laser pulse - which was measured with a 2 ns response-time photon drag detector. The foil-absorption spectrometers had a response of 4 ns, and indicated a 'temperature' of 400 ($^{+400}_{-200}$) eV for SiO_2 and 1.3 ($^{+0.15}_{-0.20}$) keV for carbon targets at the time of maximum emission (i.e. 25 ns after initiation of the heating pulse). As has been previously noted in θ-pinch and laser-plasma spectroscopy, the apparent temperature of the X-ray source is a function of foil-absorber thickness, indicating a non-Maxwellian electron distribution. We used sufficiently thin foils to weight the measurements towards the (low energy) bulk of the velocity distribution, and checked for self-consistency against the absolute intensity of the X-ray signals. Visible streak and framing photographs suggest that the target is heated very rapidly in the radial direction, far beyond the 150 μm (FWHM) diameter of the 1.5 GW (50ns) focused beam. Ruby laser shadowgrams also qualitatively confirm the wide radial extent of the plasma.

4. DISCUSSION

Some measurements of density scale length (L) and electron 'temperature' taken near the time of peak CO_2 laser intensity are summarised below. Also tabulated are binary electron-electron (λee) and ion-ion (λii) mean free paths, evaluated at half the critical density (i.e. at $n_c/2 = 5 \times 10^{18}$ cm^{-3}).

Target (Focal intensity ~ 9x10^{12}W/cm^2)	Carbon	SiO_2
Density scale length (L)		
⊥ to target	~ 0.3 mm[a]	~ 0.3 mm
∥ to target	0.6 mm[a]	~ 0.7 mm
'Te'	1.3 keV[b]	400 eV[c]
λee[d]	7.0 mm	0.7 mm
λii[d]	≤ 5 μm[e]	0.18 μm[f]
Classical Reflection Coefficient for λ = 10.6 μm	~ 92% [e]	~ 51% [f]

NB (a) Measured at 30 ns, interferometrically
(b) Measured with foil masses (mg/cm^2) of 4.02 Al + 1.55 Mylar/ 2.68 Al + 3.1 Mylar
(c) Measured with foil masses (mg/cm^2) of 4.0 Al/3.5, 3.0 and 2.5 Al
(d) Calculated, at $n_c/2$
(e) Calculated, $\bar{z} \sim 6$
(f) Calculated, $\bar{z} \sim 8$

The experiments clearly demonstrate the following ordering: λee $\gtrsim$ L $\gg$ λii. It follows that the coronal ions are well described in a fluid approximation, but that the electrons are not. However, absorption by inverse bremmstrahlung is still significant and linear, since the ratio of electron drift to thermal speed is of order 0.3 at the applied laser intensity. (The classical reflectivity is listed in Column 6; the actual reflectivity has still to be measured, but is expected to be lower.) Although instabilities, and thermo-electric magnetic fields[6] may reduce λee and particle gyroradii respectively, we conclude that the effects of finite λee must be included in two-fluid magnetohydrodynamic codes to provide adequate modelling of such plasmas. (This conclusion may also be of some significance in experiments where density gradients are inferred, rather than measured.[7])

REFERENCES

1. Euratom Report EUR FU74/AGHI 10/R1, Section B5(c)
2. MARQUET, L.C. - Appl.Optics 10, 960 (971)
3. DONALDSON, T.P. et al - J.Phys.B, 6, 1525 (1973)
4. KEY, M.H. et al - Appl.Phys.Letts. 25, 335 (1974)
5. ELKERBOUT, A.C. et al - Culham Report (unpublished 1975)
6. STAMPER, J.A. et al - Phys.Rev.Lett. 34, 138 (1975)
7. DYER, P.E. et al - Phys.Letts. 48A, 311 (1974)

INTERACTION OF AN INTENSE LASER FIELD WITH A PLASMA : A KINETIC APPROACH.

by R. Balescu
Université Libre de Bruxelles, Association Euratom-Etat Belge
and I. Paiva-Veretennicoff
Vrije Universiteit Brussel, Fakulteit van de Wetenschappen,
Brussels, Belgium.

Abstract : The kinetic equations for the evolution of a plasma in a strong external field, is shown to reduce, under certain conditions, to a set of 14 differential equations describing mode-mode coupling, parametric effects as well as spontaneous processes.

Introduction : We consider a fully ionized hydrogen plasma in presence of an intense, homogeneous, time-dependent external electrical field. In former works dealing with this problem, the dissipation mechanisms are not treated adequately. It is well-known, however, that the damping constants - hence the transport coefficients - play a crucial role in determining the threshold intensity for the onset of parametric instabilities. Futhermore, the heat conduction and the viscosity are essential factors in the transport mechanism of the energy deposited at the critical surface towards the center of the pellet.
The purpose of the present work is the elaboration of a consistent kinetic theory of a plasma submitted to a strong homogeneous electrical field, with an emphasis on the dissipative mechanisms at work. It appears as a natural continuation of our former work [1].

The construction of the theory requires three steps.
1. The establishment of the fourteen complex eigenfrequencies of the set of linearized macroscopic plasmadynamical equations, (including the balance equations for the two temperatures), in absence of external field. For lack of space, we cannot list them all. As an example, we give the expressions for the eight eigenfrequencies of the transverse modes.

$$\omega_e^{-1}\omega_{7,8} = \omega_e^{-1}\omega_{11,12} = \pm\omega_T/\omega_e - \frac{i}{2}\frac{(1+\mu)^2\zeta}{(\omega_T/\omega_e)^2} - \frac{i}{2}\frac{\eta_e+\mu\eta_i}{1+\mu}(c_e k/\omega_e)^2$$

$$\omega_e^{-1}\omega_9 = \omega_e^{-1}\omega_{13} = -i\zeta(ck/\omega_e)^2 - i\frac{\mu}{1+\mu}(\eta_e+\eta_i)(c_e k/\omega_e)^2$$

$$\omega_{10} = \omega_{14} = 0 \qquad (1)$$

where ω_e is the electron plasma frequency, c_e the electron thermal speed, c the speed of light in vacuum, μ is the mass ratio m_e/m_i, ζ is the electron-ion friction coefficient and η_e (η_i) are the electron (ion) viscosity (in suitably reduced dimensionless form). ω_T is the well-known frequency of the transverse plasma mode :

$$\omega_T = \left|(1+\mu)\omega_e^2 + c^2k^2\right|^{1/2} \qquad (2)$$

To our knowledge, two features are new in this result.
(a) The inclusion of the purely damped viscous and thermal modes, along with the plasma and ion-sound waves, in the description of the "plasmadynamical state".
(b) The explicit expressions of the dampings in terms of the transport coefficients.

2. The microscopic foundation of the structure of these modes can be established along the lines of ref. (1). The eigenvalue problem for the linearized kinetic equations for the one-particle electron and ion distribution functions f^α (α=e,i), is solved by a perturbation method. It is shown that the lowest eigenvalues are identical with the macroscopic eigenfrequencies. As a bonus, this procedure provides explicit microscopic expressions for the transport coefficients.
The distribution functions of the two components being written in the form $f^\alpha = f_o^\alpha(1+\chi^\alpha)$, where f_o^α is maxwellian, the deviations χ^α can now be represented, in the Fourier picture, as

$$\chi_k^\alpha(v) = \sum_{n=1}^{14} a_{n,k}\, e^{-i\omega_{n,k}t}\, \psi_{n,k}^\alpha(v) + \delta\chi_k^\alpha(v,t) \qquad (3)$$

$\psi_{n,k}^\alpha(v)$ is the α-component of the n^{th} plasmadynamical eigenvector. $\delta\chi_k^\alpha$, the "non-plasmadynamical" part, is damped by the collisions in a time much shorter than $(\mathrm{Im}\,\omega_n)^{-1}$ ($\forall n$).

3. Action of the external field. We assume that, prior to the switching on of the field, the system has reached a "plasmadynamical state" in which $\delta\chi^\alpha=0$. Further, we suppose that in presence of the field, none of the modes contained in $\delta\chi^\alpha$ can be systematically amplified. Therefore, the state of the system is fully described by the coefficients $a_{n,k}$ which now become time dependent. Their evolution law is obtained upon substitution of eq. (3) into the full kinetic equation :

$$\dot{a}_{n,k}(t) = \sum_{m=1}^{14} e^{i(\omega_{n,k}-\omega_{m,k})t}\left[E_{n,k;m,k}(t)+\Lambda^E_{n,k;m,k}(t)\right]a_{m,k}$$

$$+\sum_{m,l=1}^{14}\int d^3k'\, e^{i(\omega_{n,k}-\omega_{m,k'}-\omega_{l,k-k'})t}\left[\Gamma^E(t)+\Delta\right]_{n,k;m,k';l,k-k'} \cdot a_{m,k'}a_{l,k-k'}$$

$$+\Sigma^E_{n,k}(t) \qquad (4)$$

$E_{n,k;m,k}(t)$ is a matrixelement of the one-particle Liouvillian, proportional to the amplitude of the external field.

$\Lambda^E_{n,k;m,k}(t)$ results from the influence of the electric field on the linearized collision operator.

$\Delta_{n,k;m,k';l,k-k'}$ contains the Vlassov non linearities, as well as the collisional non linearities existing even in the absence of the field. $\Gamma^E_{n,k;m,k;l,k-k'}(t)$ is a field correction to this non linear term.

$\Sigma^E_{n,k}(t)$ is a source term describing "spontaneous processes". This novel feature can only be found through a kinetic theory, taking due account of the action of the field on the particles, during the collision process. In the Landau approximation, all these quantities have been calculated explicitly. Eq.(4) is the starting point for the analysis of the mode-mode couplings and of the parametric effects, some results of which will be presented at the Conference. The details of this work will be published separately.

Reference :

(1). R. Balescu, I. Paiva-Veretennicoff and L. Brenig, two papers to appear in Physica.

LOW FREQUENCY INSTABILITIES IN STREAMING PLASMAS WITH ANISOTROPIC PRESSURES

Frank Verheest

Instituut voor theoretische mechanika, Rijksuniversiteit Gent
Krijgslaan 271 - S9, B-9000 Gent, Belgium

Low frequency waves in streaming plasmas can become unstable, broadly speaking, when the square of the Alfvén velocity is smaller than the mean quadratic drift of the plasma. For these new Alfvén instabilities the streaming effects can be enhanced or diminished, even wiped out, by a suitably biased pressure anisotropy. Perpendicular pressure effects are stabilizing, parallel pressure effects are destabilizing, as in the usual fire-hose instability.

With the current interest in laser produced plasmas, attention has been focussed again on instabilities which are possible in beam-plasma systems or in streaming plasmas [1,2]. A multicomponent treatment is called for, since the number of constituents of such a system is higher than in a usual electron-hydrogen plasma at rest. Indeed, groups of electrons or other particles with different streaming velocities have to be treated as different components of the system. The collisionless coupling between the plasma components occurs via the electromagnetic fields created by the perturbation. The evolution of these fields is described by Maxwell's equations [3].

In equilibrium every plasmaconstituent is characterized by a density n_{0s} , a streaming velocity $\underset{\sim}{u}_{0s}$ (possibly zero for some parts of the plasma) and a pressure in tensor form $\underset{\approx}{P}_{0s} = p_{\perp s}\underset{\approx}{1} + (p_{\parallel s}-p_{\perp s})\underset{\sim}{e}_B\underset{\sim}{e}_B$. The index s refers to the species under consideration, and the labels $\perp$ and $\parallel$ are with respect to the externally imposed equilibrium magnetic field $\underset{\sim}{B}_0$, such that $\underset{\sim}{e}_B = \underset{\sim}{B}_0/|\underset{\sim}{B}_0|$.

The treatment starts from the fluid equations per component, which include suitable equations for the pressure tensor:

$$\partial_t n_s + \underset{\sim}{\nabla}\cdot(n_s\underset{\sim}{u}_s) = 0,$$

$$\partial_t \underset{\sim}{u}_s + \underset{\sim}{u}_s\cdot\underset{\sim}{\nabla}\underset{\sim}{u}_s + (m_s n_s)^{-1}\underset{\sim}{\nabla}\cdot\underset{\approx}{P}_s = q_s(\underset{\sim}{E} + \underset{\sim}{u}_s\times\underset{\sim}{B})/m_s \ , \tag{1}$$

$$\partial_t \underset{\approx}{P}_s + \underset{\sim}{\nabla}\cdot(\underset{\sim}{u}_s\underset{\approx}{P}_s) + \underset{\approx}{P}_s\cdot\underset{\sim\sim}{\nabla}\underset{\sim}{u}_s + (\underset{\approx}{P}_s\cdot\underset{\sim\sim}{\nabla}\underset{\sim}{u}_s)^T = q_s(\underset{\approx}{P}_s\times\underset{\sim}{B}-\underset{\sim}{B}\times\underset{\approx}{P}_s)/m_s \ .$$

Using the small signal linearization and restricting oneself to the low frequency or Alfvén regime, where ω and $k_\parallel u_{0s}$ are for each constituent much smaller than the gyrofrequency $\Omega_s = q_s B_0/m_s$, one gets two parts of the dispersion law, written as

$$N^2 = \frac{v_A^2 + c^2}{v_A^2 - \langle u_0^2+c_\parallel^2-c_\perp^2\rangle\cos^2\theta + 2\langle c_\perp^2\rangle\sin^2\theta} \ ,$$

$$N^2 = \frac{v_A^2\ S\ P}{(v_A^2 - \langle u_0^2+c_\parallel^2-c_\perp^2\rangle)(S\sin^2\theta + P\cos^2\theta)} \ . \tag{2}$$

The following abbreviations and symbols have been used:

$$P = 1 - \sum_s \frac{\omega_{ps}^2}{\omega_s'^2}\left(1 + 3\frac{k_\parallel^2 c_\parallel^2}{\omega_s'^2} - \frac{k_\perp^2 c_\perp^2}{\Omega_s^2}\right) , \qquad S = 1 + \frac{c^2}{v_A^2} \ ,$$

$$N = ck/\omega \ , \quad \omega_s' = \omega - k_\parallel u_{0s} \ , \quad v_A^2 = B_0^2/(\mu_0\sum_s n_{0s}m_s) \ ,$$

$$\langle u_0^2\rangle = \sum_s n_{0s}m_s u_{0s}^2/\sum_s n_{0s}m_s \ , \quad \theta = \text{angle}\ (\underset{\sim}{k},\underset{\sim}{B}_0) \ , \tag{3}$$

$$\langle c_{\perp,\parallel}^2\rangle = \sum_s p_{\perp,\parallel s}/\sum_s n_{0s}m_s \equiv \sum_s n_{0s}m_s c_{\perp,\parallel s}^2/\sum_s n_{0s}m_s \ .$$

For not too tenuous plasmas and for *wave propagation not perpendicular or nearly perpendicular to* $\underset{\sim}{B}_0$, (2) yields two modified Alfvén waves with phase velocity given by

$$\left(\frac{\omega}{k}\right)^2 = (v_A^2 - \langle u_0^2+c_\parallel^2-c_\perp^2\rangle)\cos^2\theta \ ,$$

$$\left(\frac{\omega}{k}\right)^2 = v_A^2 - \langle u_0^2+c_\parallel^2-c_\perp^2\rangle\cos^2\theta + 2\langle c_\perp^2\rangle\sin^2\theta \ , \tag{4}$$

if $v_A \ll c$, as is usually the case. For the first of these waves the necessary criterion for instability is that

$$v_A^2 < \langle u_0^2+c_\parallel^2-c_\perp^2\rangle \qquad \text{(all angles } \theta) \ . \tag{5}$$

If this is fulfilled, the other wave can also be unstable, but only for angles of wave propagation between 0 and θ_{max} , where θ_{max} obeys

$$v_A^2 + 2\langle c_\perp^2\rangle = \langle u_0^2+c_\parallel^2+c_\perp^2\rangle\cos^2\theta_{max} \ . \tag{6}$$

Above that angle, only one of the two Alfvén waves can be unstable.

In addition to the above mentioned waves, one also finds for *parallel propagation* the modified longitudinal waves which can give rise to the so-called streaming instabilities, with the dispersion law:

$$1 = \sum_s \frac{\omega_{ps}^2}{\omega_s'^2}\left(1+3\frac{k_\parallel^2 c_{\parallel s}^2}{\omega_s'^2}\right) \ . \tag{7}$$

In the case of *perpendicular propagation*, on the other hand, (2) yields

$$\left(\frac{\omega}{k}\right)^2 = v_A^2 + 2\langle c_\perp^2\rangle \ ,$$

$$\omega^2 = c^2k^2 + \sum_s \omega_{ps}^2 - c^2k^2\langle u_0^2+c_\parallel^2\rangle/v_A^2 \ . \tag{8}$$

One of these waves is stable, the other one can become unstable if

$$v_A^2\left(1+\sum_s\omega_{ps}^2/c^2k^2\right) < \langle u_0^2+c_\parallel^2\rangle \ . \tag{9}$$

As a conclusion and in general terms, the mean quadratic drift of the plasma has to exceed the Alfvén velocity squared for the waves to become unstable. The instabilities are further influenced by a pressure anisotropy biased in the direction of $\underset{\sim}{B}_0$. For streaming plasmas these Alfvén instabilities generalize the well-known concept of a fire-hose instability, see eg [4].

[1] A Y Cheung, R R Goforth and D W Koopman *Physical Review Letters* 31 (1973) 429-432.

[2] K F Lee *Journal of Applied Physics* 41 (1970) 3045-3047.

[3] J A Stratton *Electromagnetic Theory* (McGraw-Hill: New York 1941) 23.

[4] N A Krall and A W Trivelpiece *Principles of Plasma Physics* (McGraw-Hill: New York 1973) 228-229.

TARGET IRRADIATION STUDIES USING RELATIVISTIC ELECTRON BEAMS*

M.J.Clauser, J.R.Freeman, S.A.Goldstein, G.R.Hadley, J.A.Halbleib, J.G.Kelly, G.W.Kuswa†, C.W.Mendel, P.A.Miller, L.P.Mix, F.C.Perry, J.W.Poukey, S.L.Shope, D.W.Swain, M.A.Sweeney, A.J.Toepfer, W.H.VanDevender, M.M.Widner, T.P.Wright, G.Yonas, K.D.Bergeron, and J.Chang

Sandia Laboratories, Albuquerque, New Mexico, USA

Abstract: Recent experiments are discussed in which hemispherical and spherical, high density targets were irradiated using a single relativistic electron beam (REB). It is found that a substantial portion of the beam energy is incident on the target and that the deposition symmetry is, in some cases, quite uniform.

Introduction: The ablation driven implosion of DT filled, high density spherical targets using intense REB's, as an approach to inertial confinement fusion, has been previously described [1,2]. For this approach to be successful, it is important to efficiently focus the beam on target as well as to symmetrically load the target so as to obtain compression ratios ~ 1000 as needed for high fusion yields. We report here on target irradiation studies done on the HYDRA accelerator, which nominally produces a 700 kev, 300 kA, 100 nsec beam, and on other related experiments and calculations. We examine both beam focusing and deposition symmetry.

Beam Focusing: The focusing efficiency (i.e., the fraction of the total beam energy contained within the beam pinch) has been determined with no target present by assessment of anode witness plate damage, diode simulation, and x-ray PIN array measurements [1]. These all indicate that about 1/2 of the total beam energy is contained within the pinch after the pinch is fully developed for beams produced on the HYDRA accelerator.

Recent experiments and calculations go a step further and examine the energy incident on a high density target. These consist of holographic studies of plasma blowoff, implosion time measurements, and time and space resolved x-ray measurements with a target present. We will discuss the latter two in more detail.

The implosion time of a gold hemishell of outside diameter .4 cm and shell thickness .0254 cm was measured using laser reflection techniques as shown in Fig. 1. A laser beam is reflected from an aluminized mylar membrane of thickness .00254 cm at the base of the hemishell and onto a photomultiplier tube. The implosion time, defined here as the time from the beginning of the x-ray pulse to the time of loss of laser signal, is measured to be from 360 nsec to 385 nsec for several shots. These results are then compared with computed implosion times from a hydrodynamic code. From this it is concluded that approximately 5 kJ of energy is absorbed on target which is in qualitative agreement with previous work.

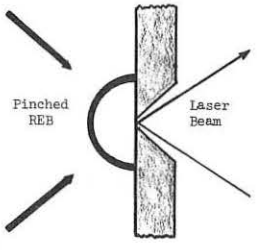

Fig. 1 Implosion Time Measurement

Time and spatially resolved x-ray measurements of bremsstrahlung emission from the anode face were made using a collimated PIN array. This array samples x-ray emission from the focus to a radius of about 6 cm. Comparisons were then made of data from shots which had a .4 cm diameter, gold spherical target mounted on the anode plate with shots which had no target. The measurements indicate that during and following the pinch formation that the current outside a radius of .4 cm was different by only 10%. The pinch radius for these shots is .2 cm which is approaching the spatial resolution of the PIN array. We therefore feel that much of the previously gained knowledge of focusing can be applied to diodes with targets.

Other work on focusing has concentrated on the effects of plasmas and ions in diodes. Diode simulations indicate that beam pinching is facilitated and improved by thick anode plasmas and by space charge limited ion flow. A number of recent experiments, in which a preformed plasma with $n_e \sim 10^{13}$ cm^{-3} is injected into a REB diode prior to the REB pulse, also indicate this. As the REB pulse begins, an expanding space charge sheath evolves from the cathode, with a sheath thickness which is less than the diode gap. The impedance is lowered by both the ion current flow across the gap as well as the effective reduced gap thickness. Pinching is facilitated because there is more current and also since there is a larger charge neutral region for electrons to orbit before striking the anode.

Symmetry: A series of experiments and calculations of single REB irradiation of spherical targets was conducted to examine deposition symmetry over the target surface. Diagnostics consisting of x-ray pinhole photography, flash radiography, and evaluation of anode backing plate damage were used to infer a degree of symmetry much better than 2:1.

Shown in Fig. 2 are time integrated x-ray pinhole photographs of a .4 cm diameter, solid brass sphere which is mounted on an anode backing plate with a .1 cm long aluminum stem. Shown are: (a) the rear view taken along the diode axis, (b) a side view taken along the anode plane, and relative optical densities around each circumference. There is clearly substantial bremsstrahlung emission from the rear portion of the sphere and very uniform emission over most of the surface. Similar results are observed for hollow gold targets.

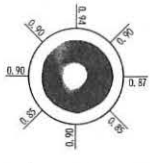

a) Back View

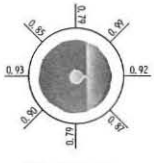

b) Side View

Fig. 2 X-ray Image

Flash radiograph snapshots were taken during the implosion phase and shortly thereafter, of a .4 cm diameter, gold, spherical shell of thickness .03 cm. Comparisons between this data and radiograph predictions, obtained from two-dimensional hydrodynamic calculations, were then made with different surface loadings considered in the calculations. Despite resolution and intensity limitations, no gross asymmetry was indicated.

The most striking evidence of deposition symmetry is the backing plate damage. In previous experiments, it was observed that irradiation of a hemispherical shell produces a cylindrical hole in an anode backing plate due to an implosion produced, high velocity jet of material which acts as a projectile. When a spherical shell target is irradiated, however, the damage is considerably reduced and consists of a shallow crater with a small pedestal in the center. Hydrodynamic calculations of anode plate damage indicate qualitative agreement with the experimental damage for uniform loading over the exposed portion of the target. On the other hand, if only portions of the front and side surfaces are loaded the axial momentum of the implosion was not balanced and a deep crater was produced on axis.

We feel there are several possibilities for the observed symmetry: (1) scattering in the target blowoff or surface, (2) scattering in the anode blowoff or surface, and (3) the presence of a stagnated or "hot beam." A "hot beam" is predicted by recent relativistic fluid calculations of pinched beam equilibria which are characterized by a uniform density, stagnated central region which is surrounded by a cylindrical current density shell. Work is also in progress to assess the effect of scattering using electron transport calculations.

*Work supported by the U. S. Energy Research and Development Administration.

†Present address: U. S. ERDA, Division of Military Applications, Laser Branch, Washington, D. C. 20545

References: (1) J. Chang, et al., Fifth Conf. on Plasma Physics and Controlled Nuclear Fusion Research (Tokyo, Japan, 1974). (2) M. J. Clauser, Phys. Rev. Lett. 34, 570 (1975).

HEATING OF LINEAR AND TOROIDAL FUSION DEVICES BY HIGH INTENSITY ELECTRON BEAMS

S. Putnam, V. Bailey, J. Benford, and T.S.T. Young

Physics International Company
San Leandro, California, U.S.A.

Abstract: Return current heating by non-linear electron-electron two stream instability modes is used to give effective interaction lengths. Criteria for linear and toroidal reactor parameters are given.

The high energy/power technology of intense electron beams can potentially have a major impact upon fusion systems. High density pulsed reactors such as a linear solenoid intrinsically require $\gtrsim 10^9$-10^{10} W and 10-100 MJ of energy; larger toroidal devices project 10^8-10^9 W and hundreds of megajoules for ignition, with the energy requirement reduced with higher power heating. In both of these magnetically confined plasmas, microsecond or longer beam pulse widths are acceptable for heating, thereby eliminating the pulse forming lines of conventional ~ 100 nsec generators, and resulting in an increase of the electrical efficiency of the beam to 75-80%. Experimental work on a 100 kJ, 2 MeV, 1.5 μsec generator is now underway at Physics International.

Quasi-steady-state operation is in principle possible with both devices. According to theory beam-plasma energy coupling in the solenoidal reactor can be achieved at densities where superconducting magnets can be used (10^{16}-10^{17}/cm^3). Net toroidal current for confinement can be supplied by the beam in a toroidal reactor. Thus, the high electrical efficiency, together with the use of steady state superconducting magnets, offer a minimum circulating power capability.

Recent theoretical and experimental work (1,2) has resulted in detailed heating scenarios for reactor applications, and confirmation of these coupling predictions over a wider parameter space is the main experimental priority. In order to heat a plasma to fusion temperatures, a two-stage process is envisioned. Return current heating via electron-ion turbulent modes (Buneman, Ion Acoustic) heats initially cold plasma to ignition regions for electron-electron two-stream instability in the warm beam or kinetic phase (3). Most of the energy transfer in kinetic two-stream heating is also predicted to be via resistive dissipation of the return current by parametrically induced density fluctuations in the non-linear regime. Recent work by T.S.T. Young suggests an effective interaction length L_Y:

$$L_Y(\text{cm}) \approx 3.5 \times 10^{-13} [(\gamma-1)\theta_b/j_b]^2 n_p^{3/2} \qquad (1)$$

with θ_b the rms beam angular spread in radius, j_b the beam current density in A/cm^2, and n_p the plasma density (cm^{-3}). Figure 1 shows linear reactor lengths using Eq. 1. The dashed lines indicate Q=1 (breakeven) conditions with end loss determined by free streaming, end plugs, or multiple mirrors with mirror ratio of 2. Reactors with a few hundred meter lengths are realizable, requiring, e.g., ~150 kG at $n_p \sim 5\times10^{16}$/cm^3 and β=1.

Recent experimental work at PI has demonstrated the concept of multi-turn drift injection for toroidal systems (4), and numerical calculations by one of us (V.B.) have demonstrated energy loss trapping of beams in the presence of pre-existing toroidal current channels (5). We now outline necessary conditions to (a) satisfy plasma heating requirements, (b) satisfy field energy requirements, and (c) maintain MHD instability. The beam is injected parallel to pre-existing plasma current over a duration t_1, at which time the net toroidal current $I_n = f_1 I_B$ and $q \equiv (B_z/B_\theta)(a/R) = q_1$. We next assume that heating occurs via return current dissipation according to Eq. 1 over an interval $t_h \ll t_{Lawson}$ at which time $I_n = f_2 I_B$, and $q = q_2$ which is large enough to still maintain MHD stability. Then the diode current I_B° which is needed to heat the plasma to thermonuclear temperatures is:

$$I_B^\circ \text{ (A)} \; 4.19\times10^{-6} \; a^2 \; t_t/t_L t_I \; \sqrt{\sigma/\epsilon}$$

where t_t is the transit time about the torus, a is the plasma radius (cm), $\epsilon \equiv t_h/t_{Lawson}$ and σ is the effective conductivity determined from Eq. 1. After the heating occurs, the injected beam energy, $I_B^\circ V_B t_I$, has been converted to plasma kinetic energy, W_p, and magnetic field energy, W_m, and is given by

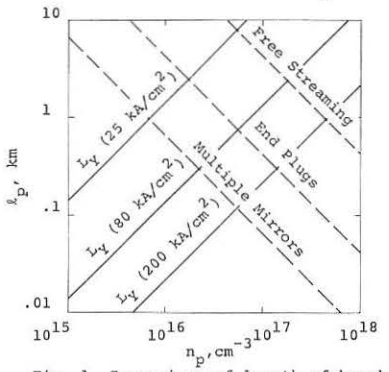

Fig. 1 Comparison of length of breakeven reactor with beam deposition length by non-linear e-e instability mode.

$$I_B^\circ V_B t_I = W_p + W_m \int I_B \frac{dLI_n}{dt}\, dt \approx L(I_B^\circ)^2 \left(\frac{t_i}{t_t}\right)^2 F_1 \left(\frac{q_1}{q_2} - 1\right)$$

where V_B is diode voltage and L the plasma-chamber inductance. The above equations relate the required beam parameters to specific reactor parameters. In order to reduce the beam energy requirements, q_2 is chosen to be the minimum q which will maintain MHD stability (≈ 2 or less for relativistic beams). Choosing ϵ and q_1 (F_1) then defines the necessary beam parameters. These equations require tens of megajoule beam energy for tokamak feasibility reactor parameters.

1. T.S.T. Young, Sherwood Theory Meeting, Washington, D.C., U.S.A., April (1975).
2. K. Papadopoulos, NRL Report 3002, Naval Research Laboratory, Washington, D.C., U.S.A., March (1975).
3. H. Singhaus, Phys. Fluids 7, 1534 (1964).
4. J. Benford, B. Ecker and V. Bailey, Phys. Rev. Letters 33, 574 (1974).
5. V. Bailey and J. Benford, Bull. APS 19, 935 (1974).

LASER SCATTERING MEASUREMENTS OF THE HEATING OF A PLASMA BY AN INTENSE ELECTRON BEAM.

A.E. Dangor, A. Dymoke-Bradshaw, J.D. Kilkenny, J.P. VanDevender*

Imperial College, London, U.K.

Abstract: Ruby laser scattering measurements are made of the heating of a plasma by an intense relativistic electron beam. In a preformed plasma the heating indicates an ion acoustic instability. For a neutral gas there is appreciable plasma motion, and a non-Maxwellian electron velocity distribution. Comparison is made with a numerical simulation.

We report on experiments investigating the interaction between an intense relativistic electron beam and a plasma. Different effects dominate the interaction depending on whether the initial background is a plasma or a gas. For injection into a preformed plasma the low net current results in Ohmic heating dominating and the observed heating indicates an ion acoustic instability. In contrast injection into a neutral gas results in a large net current, and a large Hall electric field which transfers significant energy into mass motion. This motion is modelled by a one dimensional simulation. Under some conditions the laser scattering shows a markedly non-Maxwellian electron velocity distribution and the origin of this is discussed.

For these experiments an electron beam was passed through a focussing cone giving a 36kA, 350keV, 100ns electron beam of diameter 18mm, with a half angle of 20°. This beam was passed through a window into a test chamber. Ruby laser light was scattered at 90° from a volume 8mm from the entry window with the scattering k vector normal to the beam. The scattering parameter $\alpha = 1/k\lambda_D$ was always less than one, and so the scattered light was interpreted directly as the electron velocity distribution.

In the first set of experiments the test chamber was filled with a plasma by using it as one of the electrodes of a z pinch. The e-beam was injected into the afterglow of this z pinch. The net current of the e-beam was always less than 2kA and the beam expanded quite freely. The spectra of the scattered light were Maxwellian. The measured electron densities (N_{ef}) and energy densities (W_{exp}) at the end of the beam are shown in the table for several initial densities (N_{eo}).

	N_{eo} cm^{-3}	N_{ef} cm^{-3}	W_{exp} $10^{16}eVcm^{-3}$	W_c $10^{16}eVcm^{-3}$	W_{IA+c} $10^{16}eVcm^{-3}$
I	310^{13}	210^{15}	4 ± 1.4	.9	3.4-4.9
II	710^{14}	$1.8\ 10^{15}$	$2.9 \pm .8$	1.2	2.3-2.4
III	810^{13}	510^{14}	$.8 \pm .2$	.6	3.6-4.

This data is interpreted by a simple energy equation,

$$\frac{\partial W}{\partial t} = \mathfrak{J} j_p^2 - W_{ion} \frac{\partial N_e}{\partial t}$$

The resistivity is taken as either classical or classical plus ion acoustic (2). The ion acoustic instability will be excited only in cases I and II where $T_e > T_i$ is expected. The resultant plasma energy densities are shown above. A two stream instability between the beam and plasma electrons is also expected (from the Singhaus criterion) but only in case III. The plasma energy density should saturate (3) at

$$W_{e-e} \sim .2\ W_{beam} = 3.4\ 10^{17}\ eV\ cm^{-3}.$$

From the data in the table the heating by this mode is not observed. Possibly this is because the high energy plasma electrons affected cannot thermalise in time. However the ion acoustic instability is necessary to explain the heating observed in cases I and II.

In the second set of experiments the e-beam was injected into initially neutral hydrogen, in the pressure range 60-1000 mTorr. Because of the time required to ionise the gas there was a large net electron beam current. The electron beam transported with a constant radius of about 9mm. The plasma is seen to expand during the e-beam pulse and then repinch at the end of the beam (1). This is because the $j_{plasma} \times B$ force on the plasma is outward during the beam, and reverses when the beam switches off.

This experiment has been modelled by a one dimensional code. A rigid e-beam is assumed, and initial conditions appropriate to the time when $\partial I_{beam}/\partial t = 0$. The effects of ionisation, plasma and neutral motion and electron heating are included. Ionisation expansion and plasma deceleration at the edge of the beam are seen. Some results are shown on Fig. 1 for 100 mTorr hydrogen.

The increase in the electron density by ionisation, the subsequent drop because of plasma motion, the radius of the plasma at 100 ns and the expansion velocity all agree with experimental measurements. When the beam switches off at 100 ns the plasma current changes direction and a pinch forms. The simulations shows a peak density of 2 $10^{16}cm^{-3}$ at 180 nsec, of diameter 4mm. Scattering measurements show a similar increase in the density at 200 ns, but the density only increases to 9 $10^{15}cm^{-3}$. The discrepancy is probably a result of the 8mm length of the scattering volume.

At low pressures the scattering spectra are non-Maxwellian. Fig.2 is an extreme exemple. An explanation of this involves the lack of azimuthal symmetry of the e-beam. This is a reproducible feature of the e-beam. The azimuthal variation of the Hall electric field can induce current loops in the r-θ plane, and these could produce a drifted Maxwellian. Alternatively this feature might be a manifestation of runaway electrons. Laser scattering is currently being performed with the k vector parallel to the beam current, to investigate this.

References

(1) J.P. VanDevender, J.D. Kilkenny and A.E. Dangor, Phys. Rev. Lett., 33, 689 (1974).

(2) M.Z. Caponi and R.C. Davidson, Phys. Rev. Lett., 31, 86 (1973).

(3) L.E. Thode and R.N. Sudan, Phys. Rev. Lett., 30, 732 (1973).

* Present address: Sandia Laboratory, N.M., U.S.A.

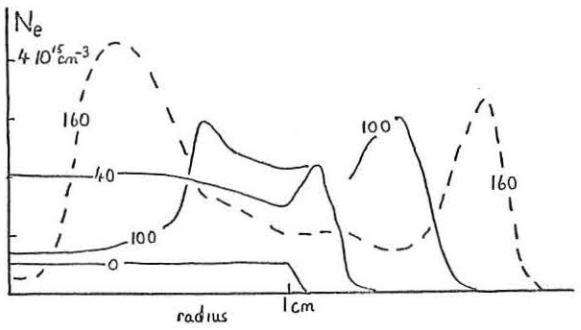

Fig. 1. Radial profiles of electron density from the simulation for 100 mTorr H_2. Times are written in ns on the profiles.

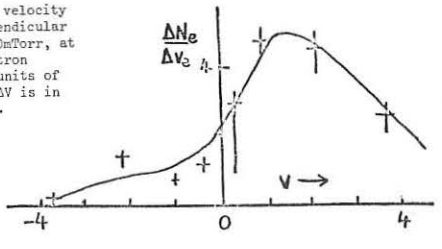

Fig. 2. Electron velocity distribution perpendicular to the beam for 60mTorr, at 200ns. The electron velocity V is in units of $10^8 cms^{-1}$, and $\Delta N/\Delta V$ is in units of $10^6 cm^{-4}s$.

INJECTION OF A 500 AMP. R.E.B. IN A PLASMA

B. Jurgens, A. Sinman, H.J. Hopman, P.C. de Jagher

FOM-Instituut voor Atoom- en Molecuulfysica, Kruislaan 407, Amsterdam, The Netherlands

Abstract: The response of an independently created plasma to REB-injection is investigated in the interval $5 \lesssim (n_p/n_b) \lesssim 50$. For $n_p/n_b \approx 50$ full charge neutralisation and 60% current compensation is found. At $n_p/n_b \approx 10$ a large positive space charge is observed after the beam pulse is over due to loss of return-current electrons to the anode foil.

Description of the experiment: The experiment (see fig. 1) consists essentially of a conducting tube, total length 260 cm with an innerdiameter of 13 cm, tapered on both ends to an innerdiameter of 3 cm. Gas is pumped out through slits in the tubewall to a base pressure of 10^{-7} Torr. At one end of the tube the beam is injected, at the other end the plasma is produced. Plasma production occurs by means of a helical coil (16) of 3 cm i.d. fed with microwaves at 2.45 GHz, pulsed from 400 W to 1200 W before injection of the beam. The pressure is about 5×10^{-4} Torr Argon. The plasma is confined in a magnetic mirror field of 0.16 T in the homogeneous part (length 180 cm) and a mirror ratio of 1.5. The position of the mirrors is indicated by (M) in fig. 1. The plasma density can be varied from 10^{11} cm^{-3} to 10^{12} cm^{-3} by changing the phase of beam injection with respect to the microwave pulse. To overcome plasma density fluctuations the beam is triggered at a preset level of the ion saturation current measured with a Langmuir probe (13). The plasma density is obtained from Langmuir probe characteristics. This method will result in a large error in the indicated densities which can differ by a factor of 2 or 3 from the actual values. The relativistic electron beam of 500 keV energy, 500 A peak current and 20 ns pulse duration (FWHM) is produced by a field emission diode (1,10) fed from a Marx generator. The beam is injected into the plasmacolumn through a 30 μm thick Ti foil (11) and an Al tube (12) of 12 cm length and 3 cm i.d. Assuming a constant beam density over its cross section, we find $n_b \approx 2 \times 10^{10}$ cm^{-3} for a beam of 500 A, a radius of 1.5 cm and a velocity of 0.87 c. Varying plasma density $10^{11} < n_p < 10^{12}$ cm^{-3}, the ratio n_p/n_b is increased from 5 to 50.
Diagnostics are selfintegrating Rogowski coils (3,4,6) and Langmuir probes (5,13,15), consisting of a 0.2 mm Tungsten wire covered with alumina except for a tip of 4 mm. The probes reach to the axis of the column.

Experimental results: Measurements of the beam current (I_b) in vacuum (10^{-7} Torr) at a distance of z = 220 cm from the gun with Rogowski coil (6) show that the beam current increases with increasing magnetic field strength up to 0.16 T, at which value R-coils (3) and (6) record the same maximum current with a time difference of 8 ns over a distance of 2 m. At the pressure of 5×10^{-4} Torr Argon, needed for plasma production, we see no difference in the signals with respect to a pressure of 10^{-7} Torr, from which fact we conclude that ionisation by the beam is negligible. Injecting the beam into a plasma the current measured by the R-coils (3) and (6) decreases with increasing plasma density. Fig. 2 shows the oscilloscope traces of R-coil (6) with and without plasma.
Subtracting the current measured with plasma at subsequent times from the beam current in vacuum (I_b) at corresponding times we find the time dependence of the return current (I_R) carried by the plasma [1]. This return current measured by R-coil (6) is plotted against plasma density for the moment of maximum beam current in fig. 3 (solid-line). We notice that at a density of about 2×10^{11} cm^{-3} the plasma return current starts to flow and that it rises to 0.6 I_b at a density of 10^{12} cm^{-3}. The R-coil (3) gives a similar result but shows a larger return-current of 0.75 I_b at 10^{12} cm^{-3}. At the same time we see a corresponding decrease in the signal of R-coil (4) which measures part of the current flowing through the wall. Simultaneously we record the signal of a Langmuir probe (15) during the beam pulse. For increasing density fig. 4 shows the probe response with the probe positioned at z = 85 cm. The maximum positive value (averaged over 6 pulses) taken from the probe signal is plotted against density in fig. 3 (broken line). We see that where the plasma return current starts to flow the probe records the largest positive signal. If we plot the positive maxima at a fixed density (6×10^{11} cm^{-3}) as a function of distance we see that the positive signal decreases with distance from the gun, see fig. 5; the broken line here indicates the average.

Discussion: At increasing plasma density starting from $n_p/n_b = 10$ we see that both charge and current neutralisation increase; at $n_p/n_b = 50$ we see full charge neutralisation after 20 ns and 60% current neutralisation after 12 ns, measured for a beam current far below the Alfvèn current of 28 kA [1]. The occurrence of positive probe signals after approximately 30 ns at lower densities can be explained by the loss of plasma electrons to the anode foil (11) due to the return current. If we calculate

$$Q(t) = \int^{t'} \{I_{RC3}(t') - I_{RC6}(t')\}\, dt'$$

as being the charge present in the system between R-coil (3) and R-coil (6), we find that in the case of $n_e = 10^{12}$ cm^{-3}, Q(t) is small and always negative, whereas for $n_e = 3 \times 10^{11}$ cm^{-3}, Q(t) is first negative but after t = 30 ns, Q(t) becomes positive. Apparently Q(t) and $V_{probe}(t)$ show similar time dependence, hence we can conclude that the probe signals are proportional to the space charge in the beam-plasma column. The appearance of a positive space charge decreasing with distance, fig. 5, in an initially homogeneous plasma column, indicates that plasma electrons drift back into the direction of the collector. As long as $dI_b/dt > 0$ the return current is flowing towards the diode. When dI_b/dt reverses sign the induced axial electric field belonging to the tail of the REB just stops the return current. But in this experiment, and also recorded by [2], the return current is found to reverse sign after ≈ 30 ns when the main beam pulse is over. The reversed plasma current amounts to about 25% of the initial return current.

References:

[1] Hammer & Rostoker, Phys.Fluids 13 (1970) 1831.
[2] Van Devender, Kilkenny & Dangor, Phys.Rev. Lett. 33 (1974) 689.

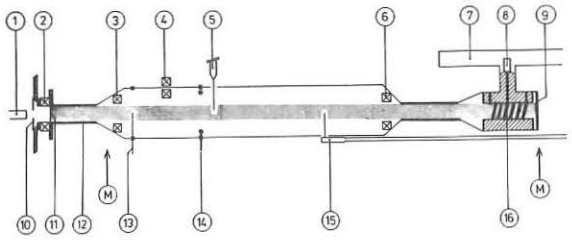

Fig. 1: Schematic experimental setup. (1,10) – field emission diode, (2,3,4,6) – Rogowski coils, (5,13,15) – probes, (7,8,16) – plasma source, (9) – collector, (11) – anode foil, (12) – diaphragm, (M) – mirror point.

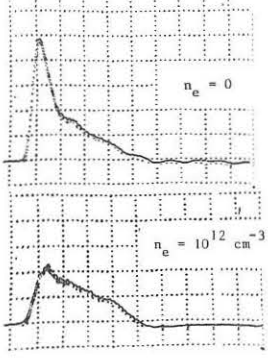

Fig. 2 – Horz. 20 ns/div.
Vert. 100 Amp/div.

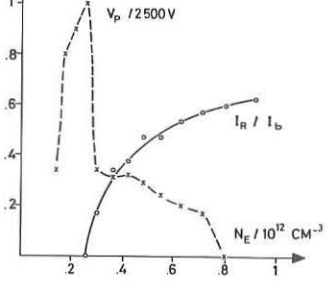

Fig. 3.

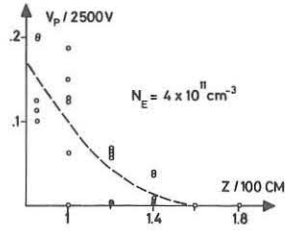

Fig. 5.

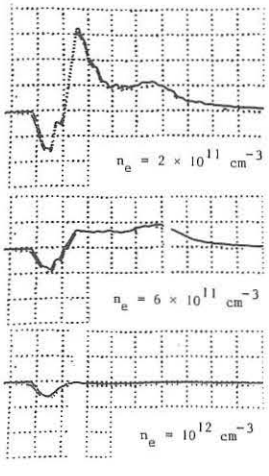

Fig. 4 – Horz. 20 ns/div.
Vert. 1 kV/div.

EXPERIMENTS ON THE GROSS STABILITY OF FIELD-REVERSING E-LAYERS

H. A. Davis, H. H. Fleischmann*, S. Luckhardt, R. A. Meger, A. C. Smith,Jr. and D. M. Woodall

Laboratory for Plasma Studies and School of Applied & Engineering Physics
Cornell University, Ithaca, N.Y. 14853, U.S.A.

Abstract: The gross behavior of field-reversing electron rings trapped in RECE-Berta was investigated. Apart from the undangerous precessional mode, and very occasional "fissioning", no instability was observed. Additional experimental indication for a gross stability are presented. Field-reversing electron rings have been generated also in two other machines.

The Astron scheme of Christofilos[1,2] proposed to confine a thermonuclear plasma in the magnetic minimum-B geometry generated by a strong, "field-reversing" ring of near-relativistic protons (p-layer) trapped in an externally applied magnetic mirror field. The "Ion Ring Compressor",[3,4] a recent modification of that scheme, expects to generate such rings by adiabatic compression of low-energy ion rings. That procedure is to alleviate two basic problems of the original scheme, the marginal overall energy gain resulting from the poor efficiency of high-energy accelerators, and the rather high cost of such accelerators. Our recent studies[3] indicated a number of potentially attractive features of such a scheme, mainly resulting from the good high-β confinement characteristics expected for such minimum-B systems. The present paper is to report and summarize recently obtained favorable experimental evidence concerning the gross stability of such rings.

The experiments were performed with relativistic electron rings (E-layers). According to a recent analysis of Lovelace,[5] the gross stability of strong p-layers is to be equal to that of strong E-layers of the same relative strength so that it becomes possible to test this important question using the much cheaper and more flexible electron ring technology.

The experimental facility, RECE-Berta, shown in Fig. 1 has been described earlier.[6,7] In brief, electron pulses (10-20 kA, 3-500 keV, 60 nsec) were injected into a confinement tank filled with several hundred mTorr of hydrogen and an axial magnetic field of about 200 Gauss. With this arrangement, strongly field-reversing E-layers producing axial field changes of up to 360 Gauss were generated. These rings as supported by detailed measurements of the pressure and gas dependence of the decay, of the energy changes of the fast electrons, and by a detailed theoretical analysis, generally exhibit a smooth purely collisional decay over most of their lifetime of up to 20 μsec. Magnetic probe measurements indicate a "fat" geometry with the minor ring diameters approximately equal to the major ring radius.

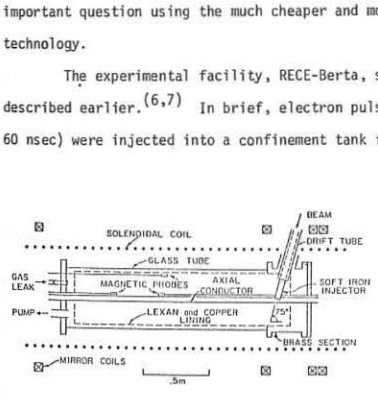

Fig. 1 - Experimental Arrangement RECE-Berta.

Only after the rings decay to small strength values, a more rapid "dump" sets in. This feature is clearly identified (by the good agreement of the dump strength with theoretical predictions, by the precession of remaining ring parts after the dump, and by the correct stabilization by additional small toroidal fields) as due to the precessional mode predicted by Furth[8] and observed in the Astron experiment.[9] No other instabilities are observed with the exception of an occasional axial "fissioning" of the layers during which some ring parts are expelled.

Additional experiments showed that the precessional mode can be stabilized also by the addition of a quadrupole Ioffe field, again in good quantitative agreement with theoretical predictions. Most recent experiments indicate that the electron rings can be generated and confined in this case also without stabilizing metal wall present.

To provide a further test on the basic gross stability of the rings, the ring decay was investigated with various perturbations added to the basic mirror field. A canting of the downstream mirrors by up to 15 deg and the application of a strongly asymmetric toroidal field, B_o, did not significantly change the ring decay. Similarly, perpendicular magnetic fields and gradient fields of up to 2% of the base field again did not change the ring decay significantly. Detailed studies of the ring behavior in a field gradient showed again a theoretically predictable behavior.

Field-reversing electron rings also were generated in two other machines. Using a steady-state gas filling, field-reversing rings with lifetimes of up to 10 μsec were observed in a small cusp-injection device. The use of a pulsed gas feed led to the generation of strong rings with lifetimes of up to 80 μsec. In the larger RECE-Christa facility, using a 5-MeV electron beam for injection, again field reversal was achieved, with ring lifetimes ranging up to 250 μsec. Again, the lifetimes are in rough agreement with the earlier theoretical predictions.

* This work was supported by Empire State Electric Energy Research Corporation and the U. S. Energy Research and Development Administration under Contract AT(11-1)2319.

1. N. C. Christofilos, Proc. of the 2nd. Intern. Conf. on Peaceful Uses of Atomic Energy, IAEA, Geneva, 1958, Vol. 32, p. 279.
2. N. C. Christofilos, UCRL 72369, Sept. 1970.
3. H. H. Fleischmann, and T. Kammash, to be published.
4. H. H. Fleischmann, Conference on the Electrostatic and Electromagnetic Confinement of Plasmas and the Phenomenology of High-Current Electron Beams, New York Academy of Sciences, March 1974.
5. M. V. Lovelace, Cornell Report LPS 163 (March 1975).
6. J. J. Bzura et al., Phys. Rev. Letters 29, 256 (1972), and 5th. Europ. Conference on Controlled Fusion and Plasma Physics, Grenoble, Aug., 1972.
7. D. A. Phelps et al., Phys. Fluids 17, 2226 (1974).
8. H. P. Furth, Phys. Fluids 8, 2020 (1965).
9. J. W. Beal et al., 3rd Intern. Conf. on Plasma Physics and Controlled Nuclear Fusion Research, IAEA, Vienna, Vol. 1, p. 967.

A DIFFUSION THEORY FOR THE INTERACTION OF RELATIVISTIC ELECTRON BEAMS WITH FUSION TARGET BLOW-OFF PLASMAS

D. Mosher and I. B. Bernstein *

Naval Research Laboratory, Washington, D.C., U.S.A.

Abstract: The interaction of a relativistic electron beam with high-atomic-number plasmas blown off of fusion targets is modeled. The relativistic Boltzmann equation with a Fokker-Planck collision term is solved by assuming that elastic scattering characterizes the shortest time scale of the beam-plasma system. The solution $f(\vec{p}, \vec{x}, t)$ incorporates arbitrary beam-plasma configurations and electromagnetic fields, and dynamic friction.

The development of high-power pulse generators has created interest in the use of relativistic electron beams to compress and heat small masses of deuterium and tritium to fusion [1]. Fusion-pellet designs usually employ thin shells of high-atomic-number material in which the beam deposits energy [2,3]. To date, modeling of pellet implosion has neglected the effects of the electromagnetic field and scattering collisions in the beam-heated plasma blown off of the shell [1-3]. This work presents a formalism which allows one to determine the character of beam deposition in the high-atomic-number plasma and shell when these effects are included. The relativistic Boltzmann equation with a Fokker-Planck collision term is solved by assuming that the elastic-scattering time is the shortest characterizing the system. (This approximation is valid for cases of interest: the interaction of a 1-3 MeV electron beam of about 10 nsec duration with initially-solid shells of heavy material.) Solutions yield current distributions and energy-deposition profiles directly and can be used to close a system of beam fluid equations [4] self-consistently. The procedure employed here also compares favorably with Monte-Carlo techniques applied to electron deposition [5] in that computational costs are much less and the effects of electric and magnetic fields are included.

The equation describing the momentum distribution function of relativistic electrons interacting with a cold, high-atomic-number plasma may be written [4]

$$\frac{\partial f}{\partial t} + \frac{\vec{p}}{m\gamma}\cdot\nabla f - e\left(\vec{E} + \frac{\vec{p}\times\vec{B}}{m\gamma}\right)\cdot\nabla_p f = \nabla_p\cdot[\nu_S(p)(p^2\vec{I} - \vec{p}\vec{p})\cdot\nabla_p f] + \nabla_p\cdot[\nu_E(p)\vec{p}f] \tag{1}$$

where $\gamma^2 = 1 + p^2/(mc)^2$. The quantities ν_S and ν_E are scattering and energy-loss frequencies

$$\nu_S = \Omega_S\gamma/(\gamma^2-1)^{3/2} \quad ; \qquad \nu_E = \epsilon\gamma\nu_S \tag{2}$$

where $\Omega_S = 2\pi n_i r_o^2 c(Z^2 + Z)\ln\Lambda$, and $\epsilon = 2/(Z+1)$. Here n_i is the plasma ion density, r_o is the classical electron radius, c is the velocity of light, Z is the plasma atomic number, and $\ln\Lambda$ is in the range 10-20.

Treating ϵ as second order in ν_S^{-1}, the term of Eq. (1) are ordered according to $0(\nu_S^{-2}):0(\nu_S^{-1}):0(\nu_S^{-1}) = 0(1):0(\nu_S^{-2})$. When f is expanded in powers of ν_S^{-1}, $f = f_o + f_1 + \ldots$, Eq. (1) can be iteratively solved. The solution correct to second order is given by

$$f_o = f_o(p, \vec{x}, t) \tag{3}$$

that is, f_o is isotropic in momentum space and

$$f_1 = \vec{A}\cdot\vec{p} \tag{4}$$

$$f_2 = \frac{1}{6\nu_S}\left(\frac{e\vec{E}}{p}\frac{\partial\vec{A}}{\partial p} - \frac{1}{m\gamma}\nabla\vec{A}\right) : \vec{p}\vec{p} + \frac{e}{2\nu_S m\gamma}(\vec{B}\times\vec{A})\cdot\vec{p} \tag{5}$$

where

$$\vec{A} = \frac{1}{2\nu_S}\left(\frac{e\vec{E}}{p}\frac{\partial f_o}{\partial p} - \frac{1}{m\gamma}\nabla f_o\right) \tag{6}$$

Setting secular terms in the second-order equation equal to zero yields

$$\frac{\partial f_o}{\partial t} + \frac{p^2}{3m\gamma}\nabla\cdot\vec{A} = \frac{1}{p^2}\frac{\partial}{\partial p}\left[p^3(\nu_E f_o + \frac{1}{5}e\vec{E}\cdot\vec{A})\right] . \tag{7}$$

Moments of f which yield the beam-electron and energy fluxes are of primary interest. To lowest order, these quantities are

$$\vec{\Phi} = \int\frac{\vec{p}}{m\gamma}f_1 d^3p = \int\frac{\vec{p}\vec{p}}{m\gamma}\cdot\vec{A}\, d^3p \tag{8}$$

$$\vec{q} = \int mc^2(\gamma-1)\frac{\vec{p}}{m\gamma}f_1 d^3p = mc^2\int(\gamma-1)\frac{\vec{p}\vec{p}}{m\gamma}\cdot\vec{A}\, d^3p. \tag{9}$$

Taking $\nabla\cdot\vec{\Phi}$, substituting for $\nabla\cdot\vec{A}$, and integrating by parts yields

$$\nabla\cdot\vec{\Phi} = -4\pi\left(p^3\nu_E f_o\right)_{p=0} \tag{10}$$

Lack of particle conservation is due to beam electrons, slowed by dynamic friction to very low energies, merging with the thermal-electron background.

The rate at which energy is transferred from the beam to a unit volume of plasma is obtained by taking the divergence of Eq. (9). In the steady state,

$$Q = -\nabla\cdot\vec{q} = e\vec{E}\cdot\vec{\Phi} + 4\pi\int_o^\infty\frac{p^4\nu_E}{m\gamma}f_o dp. \tag{11}$$

Solutions of the steady-state equations in 1 and 2 dimensions have been obtained. The effect of self-consistent electric fields in the plasma on beam deposition will be discussed.

The authors are grateful to Dr. David L. Book for many useful discussions. This work was supported by the U. S. Defense Nuclear Agency.

* Permanent address: Yale University, New Haven, CT

[1] G. Yonas, J. W. Poukey, K. R. Prestwich, J. R. Freeman, A. J. Toepfer and M. J. Clauser, Nucl. Fusion 14, 731 (1974).

[2] L. I. Rudakov and A. A. Samarsky in Proc. 6th Europ. Conf. on Controlled Fusion and Plasma Physics (Moscow 1973), p. 487.

[3] M. J. Clauser, Phys. Rev. Letter. 34, 570 (1975).

[4] D. Mosher, Naval Research Lab. Memo Report 2959 (1974), to be published in Phys. Fl.

[5] Z. Zinamon, E. Nardi, and E. Peleg, Weizmann Institute Rep. WIS-74/54 Ph (1974).

GENERATION OF LONG ION PULSES AND PROTON LAYERS

J. Golden* and C. A. Kapetanakos

Naval Research Laboratory, Washington, D.C. 20375, U.S.A.

and

S. A. Goldstein†

University of Maryland, College Park, MD 29742, U.S.A

Abstract: Experimental results are reported on the formation, propagation, size, degree of current and charge neutralization of a 400 keV, 50 nsec duration proton layer and the generation of 600 nsec long ion pulses.

Several important applications are presently foreseen for high current (1-100 kA) pulsed ion beams in the energy range of 0.1-1 MeV, including (a) plasma heating, (b) generation of intense neutron fluxes, (c) production of UV [$H^+ + C_s \rightarrow H + C_s^+$, at 1215 Å] and soft x-ray [$H_e^{++} + H \rightarrow H_e^+ + H^+$, at 304 Å] lasers, and (d) formation of field reversing ion layers and ion rings for stable plasma confinement.

In this paper we report a summary of experimental results on the formation and various properties of a 50 nsec long proton layer and preliminary results on the production of long ion pulses. Finally, we discuss briefly theoretical results concerning the reflex triode.

PROTON LAYER--The 400 keV ion beam is produced by a reflex triode similar to that described by Humphries et al[1]. The electrons are emitted from an 11-cm OD, 4.4-cm thick annular carbon cathode that is held at ground potential. Accelerated by the 50 nsec duration positive voltage pulse that is applied to the anode, these electrons pass through the 6.25 micron thick aluminized mylar anode and form a virtual cathode. As the electrons oscillate between the real and virtual cathodes, plasma is produced from about 20 polyethylene filaments (0.25 mm diam.) mounted on the side of the aluminized mylar that is away from the carbon cathode. The protons accelerate toward and through the virtual cathode and form a drifting beam. After crossing the virtual cathode, the proton beam travels for a few cm in a uniform magnetic field and enters the magnetic cusp, which has a linear extrapolated transition width of about 12 cm. The magnitude of the uniform field preceding and following the cusp can be varied from 0 to 23 kG. All the results reported here were obtained at a background pressure below 0.4 mTorr.

A variety of diagnostics are used to study the properties of the ion beam. The number of protons is measured by nuclear techniques, the total energy by calorimetry, the current density by biased collectors and Faraday cups, the time of the flight with scintillators, the shape of the beam with frame photography and the diamagnetism of the beam with mangetic probes.

The nuclear physics technique allows an unambiguous measurement of the energetic protons and consists of measuring the γ-rays associated with the annihilation of positrons produced from the decay of O^{15}, which has been generated by the reaction $N^{14}(p,\gamma)O^{15}$ when protons of energy greater than 279 keV strike a nitrogen-bearing target. The number of protons in a pulse measured by this technique is about 3×10^{14}, corresponding to a current of more than 1 kA. From the above diagnostics the following information were obtained about the p-layer:

(a) The number of protons transmitted through the cusp is drastically reduced for values of magnetic field B_o greater than 6 kG [Fig. 1], even though this field is about three times smaller than the minimum critical magnetic field [$(B_{cr})_m \approx 16$ kG] corresponding to 400 keV protons born at a radius equal to the maximum radius of the cathode;

(b) at $B_o \approx 15$ kG, the rotation velocity of protons is about twice their axial velocity;

(c) the p-layer is initially thin and has a radius comparable to the maximum radius of the cathode, but its thickness progressively increases in time and becomes equal to the thickness of the cathode; and

(d) the azimuthal current density of the p-layer is about 2.6 A/cm^2 and at $B_o \approx 14$ kG is current neutralized by about 20-30%. The space charge neutralization, i.e., n_e/n_i, is ≈ 0.1.

LONG ION PULSES--It appears presently that the most promising approach to produce field reversing ion ring is by using ion pulses 1 μsec or longer with subsequent confinement of these ions in a time varying magnetic field [2]. The short circuit of the anode-cathode gap can be considerably delayed by immersing the triode in a magnetic field with a radial component, e.g., by placing the anode inside a nonsymmetric cusped magnetic field.

In order to obtain a better understanding of the short-circuit effect in the anode-cathode gap we are presently performing experiments with a 600 nsec long positive pulse. This pulse is produced by connecting directly the triode to the Marx generator. The magnetic field is uniform except in the vicinity of the triode, where it is suitably shaped by inserting a 11-cm long, 11cm-ID, 2-cm thick soft iron collar around the cathode stalk. The radial component of magnetic field produced by the soft iron serves to delay the short circuit effect in the diode as is demonstrated in Fig. 2. The proton pulse is of the same duration as the voltage pulse, i.e., ~ 600 nsec as is shown in Fig. 2c.

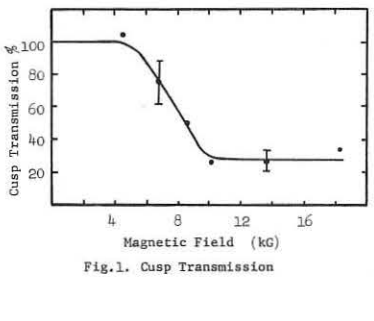

Fig.1. Cusp Transmission

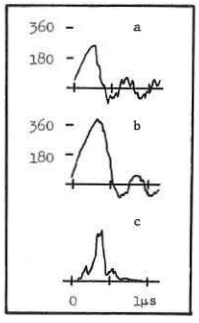

Fig.2. Diode voltage in kV, (a)without and (b) with iron collar; (c) ion pulse.

TRIODE--Due to the energy loss of the electrons in the anode as these electrons oscillate between the real and virtual cathode, the space change distribution in the triode is drastically different than that in the simple planar diode. Thus, both the electron and ion current have a different relationship upon the applied voltage than in the case of the planar diode. Assuming that the scattering in angle of the oscillating electrons at the anode can be neglected, it can be shown that the ratio of the ion to electron current depends upon the number of passes of these electrons through the anode and the square root of the mass ratio. The electron dynamics are treated relativistically, and the electron contribution to the spatially dependent charge density is computed after each reflection. Boundary conditions are treated with cathode and anode plasmas present. The formalism allows inclusion of time dependent phenomena such as ion motion.

REFERENCES

*National Research Council Research Associate at NRL
†Supported by NRL

1. S. Humphries et al., Appl. Phys. Lett. 25, 20 (1974); also J. Appl. Phys. 46, 187 (1975).

2. C.A. Kapetanakos, et al., Appl. Phys. Lett. 26, 284 (1975).

GENERATION OF MULTIKILOAMPERE PROTON BEAMS AND APPLICATION TO REVERSED FIELD P-LAYERS

R. N. Sudan[‡]
Naval Research Laboratory, Washington, D.C. 20375, U.S.A.
and
S. Humphries Jr.
Laboratory of Plasma Studies
Cornell University, Ithaca, N. Y. 14850, U.S.A.

Abstract: Possible application of recently achieved pulsed proton beams in the several kiloampere range at energies from 100 keV to 1.8 MeV to the formation and compression of field reversed proton layers is discussed.

HIGH POWER ION ACCELERATORS--Quite recently high power, high voltage electrical technology, which is the basis of the development of relativistic electron beams, has been applied to create pulsed multikiloampere ion beams at energies ranging from 0.1 - 2.0 MeV by Humphries et al. [1]. In a diode in which both cathode and anode are capable of emitting electrons and ions the electrons carry away almost all of the power delivered to the anode and the plain diode is quite inefficient for ion-beam production.

A simple device alleviates this problem. Two cathodes are located symmetrically on each side of an anode made of a highly transparent mesh. A fraction T of the electrons arriving at the anode pass through and are reflected by the opposite cathode. Thus, a large fraction of the emitted electrons circulate in the device and only a fraction $2(1 - T)/(1 + T)$ of the equivalent current for a solid anode constitutes the drain on the external power supply. The fraction of the electrons that actually collide with the anode deposit their energy to produce a plasma for ion emission. Successful results have been obtained from (i) coating metal anode meshes with hydrocarbons, (ii) nonconducting nylon meshes and (iii) aluminized mylar sheets of appropriate thickness for high energy $\gtrsim$ 1 MeV. Electrons produced at the cathode edge are affected strongly by the fringing electric field and follow an orbit that quickly takes them to the opaque anode holder. A magnetic field of sufficient strength parallel to the triode axis helps to prevent these electrons from drifting outwards and improves the device performance significantly. If one of the cathodes is removed to infinity the reflecting electrons form a virtual cathode at approximately the same distance as the actual cathode anode gap. Eliminating one of the cathodes allows for easy ion extraction. At the high achieved ion-current densities ~ 10 A/cm^2 the propagation of unneutralized ion beams over any distance is not possible because of strong space charge repulsion. However, the ion beams in this device emerge automatically neutralized because they pick up an equal number of electrons from the surfeit of electrons around the cathode. These electrons need only a small fraction (m_e/m_i) of the ion energy to follow the beam. Thus, the beam is able to propagate in a good vacuum, unlike E-beams, with divergence properties determined by the initial emittance. Proton currents in excess of 3 kA at current density ~ 10 A/cm^2, and total protons per pulse in excess of 10^{14} have been achieved. The best device efficiency, at 100 keV, achieved is 42% which is pretty close to the maximum possible of 50%. The current density is also close to the space charge limit. Table I summarizes the experimental data.

PULSED PROTON-LAYER--The earliest application of relativistic electrons to a fusion device was suggested by Christofilos [2]. This "Astron" concept ran into two difficulties: (i) prohibitive energy loss by synchrotron radiation and (ii) inability of the E-layer current density to reach field reversal by stacking of successive injection of pulses. Fortunately

Machine	100 kV Marx	500 kV, 7 Ω Blumlein	150 kV Blumlein	5 MV CREB
Ion Energy	~ 100 keV	300 keV	130 keV	2 MeV
Ion Current	2 x 250 A	2 x 2,050 A	2 x 3,300 A	~ 5,000 A
Pulse Width	~ 50 nsec	~ 50 nsec	~ 50 nsec	⩽ 50 nsec
Current Density	~ 10 A/cm^2	8.3 A/cm^2	~ 20 A/cm^2	~ 30 A/cm^2
Efficiency η		9%	42%	
Type of Ions	proton	proton	proton	proton & Al^{++}

TABLE I - η = Proton Energy/Total Energy Input $\int VIdt$

Fleischmann and coworkers [3] were successful in producing field reversal in single pulse injection using a 500 kV, ~ 40 kA, ⩽ 100 nsec E-beam. Christofilos suggested the use of ~ GeV protons to overcome the first difficulty.

P-LAYER COMPRESSION--Since the proton energy required for a "breakeven" situation is still very much in excess of what is possible from diode technology, Sudan and Ott [4] suggested the adiabatic magnetic compression of a P-layer, formed by single pulse injection, to the required energy. Let the proton layer be of thickness Δ, mean radius R and length L such that $\Delta/L \ll 1$ and $\Delta/R \ll 1$ with $L \gg R$ and neutralized electrostatically. The compression time is assumed much smaller than the time taken by the flux to diffuse through the layer $4\pi\sigma\Delta^2/c^2$. In this limit both the axial flux Φ_a through the layer and the poloidal flux trapped within the layer Φ_p are conserved i.e., $\Phi_a = \pi R^2(B_{ex} + 4\pi I/L) = \text{const.}$, $\Phi_p = 2\pi R(2\pi I\Delta/L) = \text{const.}$, where $I = I_B + I_e$ is the net azimuthal current composed of the beam current I_B and the electron current I_e and B_{ex} is the external magnetic field. From the conservation of canonical angular momentum and Φ_a we obtain $Ru_\varphi = \text{const.}$, where u_φ is the mean azimuthal beam velocity. Thus the beam current $I_B = Neu_\varphi/2\pi R$ scales as $R^2 I_B = \text{const.}$, where N the total number of beam ions is assumed to be conserved. The variation of Δ with compression is obtained from the constancy of the radial invariant $J_r \approx u_\perp^2/\omega_\beta$ where $\omega_\beta = \Omega\,[1 + \zeta u_\varphi/\Omega\Delta]^{1/2}$ is the betatron frequency and the transverse beam pressure $\approx n_b m_i u_\perp^2$; $\zeta = 4\pi I/LB_{ex}$ is the field reversal factor, $\Omega = eB_{ex}/m_i c$ is the cyclotron frequency in the external field. Furthermore, it is easy to establish the constancy of IR^2, $B_{ex}R^2$, Δ/R, ζ. Defining C to be ratio of final to initial external magnetic field, the ion energy increases as C, I_B increases as C and the current density as $C^{3/2}$. It is, in principle, possible to achieve breakeven conditions by compression to high magnetic fields of a few hundred kilogauss. For field reversal the number of injected ions required is $\geq 10^{17}$; and the injected energy ~ 1 MeV. Such a layer can be formed by injection through a magnetic cusp [5] or by alternative techniques. Initial experiments already indicate that such injection is feasible [6]. The topology of the magnetic field creates a natural divertor for the impurities from the walls which are swept along the open lines of force.

‡ Permanent Address: Laboratory of Plasma Studies, Cornell University, Ithaca, N.Y., U.S.A.

REFERENCES

1. S. Humphries, et al., Appl. Phys. Lett. 25, 20 (1974); J. Appl. Phys. 46, 187 (1975); LPS Report 161, Laboratory of Plasma Studies, Cornell University, N.Y.
2. N. Christofilos, Proc. 2nd U.N. Int. Conf. on Peaceful Uses of Atomic Energy, Geneva, 1958, Vol. 32, p. 279.
3. M. Andrews, et al., Proc. Fourth IAEA Conf. on Plasma Phys. and Controlled Fusion Research, Vol. 1, p. 169, Madison, Wis. (1971).
4. R. N. Sudan and E. Ott, Phys. Rev. Lett. 33, 355 (1974).
5. S. Humphries, LPS Report 156, Lab. of Plasma Studies, Cornell Univ.
6. C. Kapetanakos, J. Golden and F.C. Young, Pvt. Communication.

THE MEASUREMENT OF IONISATION RATES IN ION SOURCES

T.S. GREEN, C. GOBLE, M. INMAN and A.R. MARTIN

Euratom UKAEA, Association for Fusion Research, Culham Laboratory, Abingdon, Oxfordshire OX14 3DB, UK.

Abstract: A new diagnostic experiment for the evaluation of the performance of ion sources is described in this report. Comparisons of the measured rate of ion production with a simple theory of ionisation leads to estimates of the containment time of the ionising electrons.

1. Introduction: High current ion sources, for application to neutral particle injection into the next generation of fusion experiments, must meet more stringent requirements on performance than heretofore. In particular, the problems of uniformity, stability, gas utilisation, component lifetime and species control are such as to necessitate a better understanding of the principles of source operation.

To this end we have investigated the factors which determine the rate of ion production in a source. Using a new diagnostic experiment we have been able to evaluate the ionisation efficiency of the current carrying electrons and its dependence on the electron containment time.

2. Experimental Arrangement: The studies to be discussed have been carried out on a development prototype for a 20 amp source. The source has a basic rectangular format (figure 1) built to allow flexibility in varying cathode, anode and magnetic field geometries. Six directly heated cathodes (1.5 mm ϕ, 12 cms long tantalum wire) are mounted in two rows of three, on an interchangeable back plate. The water cooled anodes are introduced through insulators in the source body, and their number and location can be altered easily. The magnetic field coils can be slid over the source body. (The results in this paper, however, are restricted to cases of zero magnetic field).

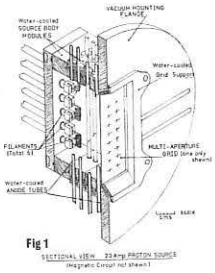

Fig 1

SECTIONAL VIEW - 20 Amp PROTON SOURCE (Magnetic Circuit not shown)

3. Measurement and Control of the Ion Production Rate: By utilising a source with the body isolated from anode and cathode, we can bias the body to collect ions only and thus measure the ion flux to the body. This measurement enables us to estimate the total ion production rate (in amps equivalent) to an accuracy of $\pm$ 10% by correcting for ions which impinge on the anode and cathode and so are not recorded.

It has been known, since the early studies of sources carried out in the Manhatten Project[1], that the ratio of the ion production rate (I_+) to the electron current (I_e) in an arc discharge source with a directly heated filament cathode is determined by the boundary conditions at the cathode. As a consequence, in source operation with spacecharge limited electron current I_+/I_e has a unique value for a given cathode area and source geometry. However, in the emission limited regime, I_+/I_e may be varied at will by varying the heater current, and operating in a narrow range near the emission limit (figure 2). When this happens the arc voltage, U , also varies to match the required changing ionisation rate. By measuring this variation of I_+/I_e and U at different gas densities in the source we can determine the variation of I_+/I_e with gas density for a range of values of arc voltage.

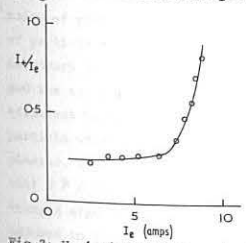

Fig.2: Variation of ion production per electron (I_+/I_e) with electron current I_e near emission limit.

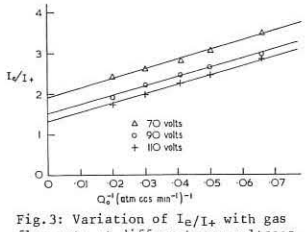

Fig.3: Variation of I_e/I_+ with gas flow rate at different arc voltages.

4. Model of Ionisation in the Source: The rate of production of ions in the source volume (in amps equivalent) is given by the equation

$$I_+ = e\, n_o\, n_e\, \langle\sigma v\rangle_{ION}\, V \qquad (1)$$

where n_o is the neutral gas density, n_e is the average electron density, $\langle\sigma v\rangle_{ION}$ the average ionisation rate coefficient, and V the source volume. The value of n_e is related to the electron current:-

$$I_e = e\, n_e \left[n_o \langle\sigma v\rangle_{IN} + \frac{1}{\tau_e} \right] . V \qquad (2)$$

where $\langle\sigma v\rangle_{IN}$ is the average rate coefficient for inelastic scattering of electrons to energies below the ionisation threshold, and τ_e is the average electron containment time. [This expression is only approximate in that it neglects the effect of inelastic scattering on the energy spectrum of the electrons and also slowing down by cool thermal plasma electrons. Further it is only strictly applicable to monatomic gases, though it can be used for hydrogen at low arc currents where ionisation following dissociation can be neglected. These approximations will be considered in a more detailed discussion]. From equations 1 and 2 we derive the relation

$$\frac{I_e}{I_+} = \frac{\langle\sigma v\rangle_{IN}}{\langle\sigma v\rangle_{ION}} + \frac{1}{n_o \langle\sigma v\rangle_{ION} \tau_e} .$$

5. Comparison of Experimental Data with Theoretical Predictions: The first prediction of equation 3 which is amenable to experimental test is that measured values of I_e/I_+ should vary linearly with the inverse of gas density. In these experiments we measure and control not the density, but the gas flow rate Q_o; however the two are proportional at low arc currents. Thus to test the validity of equation 3 we have plotted I_e/I_+ versus Q_o^{-1} for various arc voltages (figure 3). The data fit the linear plots well indicating that the density scaling is correct.

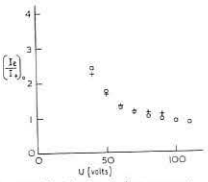

Fig.4: Variation of intercept $(I_e/I_+)_o$ with arc voltage, prototype 20A source (o) and cylindrical source (+).

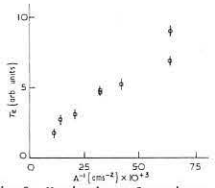

Fig.5: Variation of estimated electron containment time, τ_e, with anode area, A.

Having established this we can now test the second prediction, namely that the intercept $(I_e/I_+)_o$ depends on arc voltage only and not on details of the source design. For this we determined $(I_e/I_+)_o$ (U) for the source described above and for a source of cylindrical geometry with a single cathode and anode ring. Data are shown in figure 4: they show excellent agreement between the values of $(I_e/I_+)_o$ from the two sources.

Finally, the theory indicates that the slopes of the lines in figure 3 vary as the inverse of the electron containment time. To test this prediction we varied the area A of the anodes by varying their number, since in a magnetic field free source the containment time is given by $4V/A.v_e$ (v_e is the electron velocity). The data in figure 5 show that τ_e derived from the slope of the line varies approximately linearly with the inverse of the anode area, in agreement with the theoretical prediction.

6. Conclusion: The diagnostic experiment we have developed to study ion production rates in ion sources has allowed us to test a model for ionisation in a source in the simple case of a magnetic field free source. The model predicts, in agreement with experiment, that there is an ultimate efficiency of ionisation (I_+/I_e) which depends on atomic cross-sections only: the degree to which one approaches this limit in a given source depends on the gas density and the containment time of electrons. This experiment provides a method for measuring the containment time for a given source and thus of evaluating the comparative performance of different sources, and the influence of magnetic fields.

Reference: (1). GUTHRIE, A. and WAKERLING, R.K., Characteristics of Electrical Discharges in Magnetic Fields (McGraw-Hill New York) 1949.

NON CIRCULAR CROSS-SECTION TOKAMAKS :
EXACT SOLUTIONS OF MHD EQUILIBRIUM AND STABILITY LIMIT NEAR THE AXIS.

R. Aymar, J. Jacquinot.

ASSOCIATION EURATOM-CEA SUR LA FUSION
Département de Physique du Plasma et de la Fusion Contrôlée
Centre d'Etudes Nucléaires
Boîte Postale n° 6. 92260 FONTENAY-AUX-ROSES (FRANCE)

Abstract : A method of deriving solutions, expressed in closed form of toroidal MHD equilibrium is presented. The method is applied to the stability analysis of a fat torus with non circular cross-section in the case of a peaked current distribution.

Fat tori with non circular cross-section are increasingly being considered in Tokamak research programmes. This tendancy has induced a search for new classes of ideal MHD equilibria. Exact solutions, in the peaked current case, have been reported to treat deviation from circular shape [1] or the effects of finite inverse aspect ratios [2]. The methods used involve a linear superposition of a finite number of exact solutions expressed in term of hypergeometric functions. We show here that an integral representation with simple kernel may be used to generalize the preceeding results to fat non circular geometry.

Treating the "parabolic" case with no pressure (P) and no current at the plasma boundary (surface $\Psi = 0$) we assume (cylindrical coordinates) that $P = \mu\gamma\Psi^2/2r_0^4$ and $r^2B_\varphi^2 = r_0^2 B_{\varphi_0}^2 + \mu\Psi^2/r_0^2$; the partial differential equation resulting from ideal MHD becomes :

$$\frac{\partial^2\Psi}{\partial r^2} + \frac{\partial^2\Psi}{\partial z^2} - \frac{1}{r}\cdot\frac{\partial\Psi}{\partial r} + \mu(1+\gamma r^2)\Psi = 0$$

All solutions of this equation which are symmetric with respect to the equatorial plane may be written as :

$$\Psi = \int_0^\infty \left[\alpha(k)R_1(r,k) + \beta(k)R_2(r,k)\right]\cos(kz)\,dk \quad (1)$$

R_1 and R_2 are two independant solutions of the radial differential equation. They can be expressed in terms of a combination of the 2 Coulomb wave functions [1] but in order to perform analytical integration of (1) they may more conveniently be written as polynomials of $x = (r - r_0)/r_0$:

$R_1 = x + a_{12}x^2 + \ldots + a_{1n}x^n + \ldots$; $R_2 = 1 + a_{22}x^2 + \ldots + a_{2n}x^4 + \ldots$

where the a_{in} are given by the recurrent relation :

$$(n+2)(n+1)a_{i,n+2} = \left\{k^2 - \mu(1+\gamma)\right\}a_{i,n} - 2\mu\gamma a_{i,n-1} - \mu\gamma a_{i,n-2} + \sum_{j=1}^{n+1}(-1)^{j+1}(n+2-j)a_{i,n+2-j}$$

At this point we are left with the problem of finding the functions α and β corresponding to a prescribed $\Psi = 0$ surface. The condition that the line $z = x = 0$ is a magnetic axis imposes $\int_0^\infty \alpha\,dk = 0$. Single magnetic axis Tokamak correspond to $\int_0^\infty \beta k^2 dk > 0$ (opposite signe for doublet). Furthermore β fixes the ellipticity near the axis : $(\varepsilon^2+1) = \mu(1+\gamma)\int_0^\infty \beta k^2 dk$ (where ε is the ratio of the vertical and horizontal axis) and α is connected to the triangular deformation of the surfaces. Consequently "Horsetrack" or elliptic $\Psi = 0$ surfaces are produced with $\alpha = 0$ and $\beta > 0$; "D" or "kidney" shapes correspond to both α and $\beta \neq 0$. The rapid divergence of R_1 and R_2 with k (Fig.1.2) and the requirement that a closed $\Psi = 0$ surface exists limit the range of k where α and β are different from 0 to approximately $0 \leq k \lesssim \left[\mu(1+\gamma)\right]^{1/2}$.

A large variety of aspect ratio and shape has been obtained with the same simple forms : $\beta(k) \propto k^n e^{-ak} H(k_T - k)$ (where H is the Heaviside function) (Fig.3) and $\alpha(k)$ is the algebraic sum of a positive and a negative half period of 2 cosine functions each adjustable in position and width (Fig.4). In particular these functions can generate the cases of a fat torus with non circular cross-section (Fig. 5 and 6). The small difference between cases 1 and 2 (Fig. 5) despite the large change of shape of β (Fig. 3) illustrates the fact that the integral representation is not very sensitive to the detailed shape of the Kernel. This suggests that even more elementary forms of α and β could have been choosen in order to simplify analytical integration of (1).

This method has specific advantages over purely numerical treatment already existing [5]. For instance high order partial derivation $\Psi^{(i)}$ which are needed to calculate various quantities in the vicinity of the magnetic axis are not, in general, accurately calculated by numerical method. In our case these quantities are directly expressed in terms of α and β . Consequently poloidal field (involving Ψ^I) and the Mercier stability criteria (involving Ψ^{II} and Ψ^{III}) can be accurately determined. For instance the Mercier stability limit takes the form : $q_c^2 = f(\int_0^\infty \alpha k^2 dk, \int_0^\infty \beta k^2 dk)$, where f is an algebraic function.

In the limit of large aspect ratio, it has been shown [3] that vertical elongation of the plasma had a defavourable effect on the limiting safety factor (q_c) for stability against localized modes near the magnetic axis [4]. However triangular deformation in the proper direction could overcome this effect and even decrease q_c well below 1. Unfortunately our calculations show that the triangular effect is much less effective in the case of small R/a. For instance in case 3, 1, 4 (Fig. 6) q_c takes respectively the values 1.5, 1.25, 1.17 . Most of the decrease in q_c occurs when the shape changes from the ellipse to the D shape. Further triangular deformation to a kidney shape (case 4) only produces a modest improvement of q_c. Ultimately if $\alpha(k)$ is made too large a singularity appears on the plasma boundary which becomes a separatix.

References.

[1] Maschke,E.K.. Plasma Phys. 15, (1973) 535.
[2] Mazzucato, E. MATT-1044 (1974).
[3] Laval, G.; Luc, H.; Maschke, E.K.; Mercier, C.; Pellat, R.; Plasma Phys. and Controlled Nuclear Fusion Research II, AIEA, Madison (1971) 507.
[4] Mercier, C., Nucl. Fusion 4 (1964) 213.
[5] P. Grelot, J. Weisse, Proceedings of 5th Eur. Conf. on Controlled Fusion and Plasma Phys. Vol. I p. 24 (1972).
D. Edery, Internal rep. CISI Saclay AST n° 73-22 (1973).

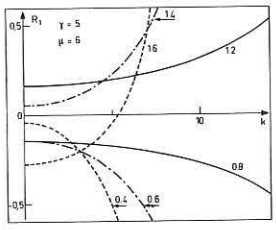

FIG.1 - R_1 versus k for various values of r/r_0 .

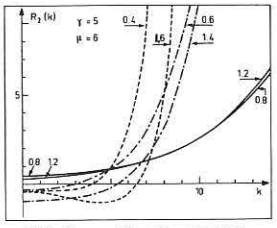

FIG.2 - R_2 versus k for various values of r/r_0.

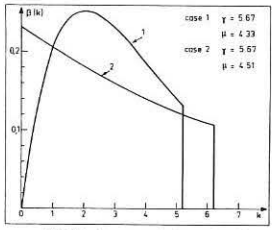

FIG.3 - β function corresponding to cases 1 and 2

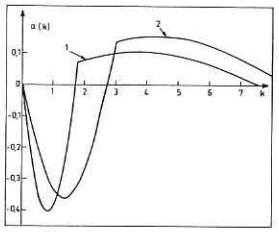

FIG.4 - α function for cases 1 and 2

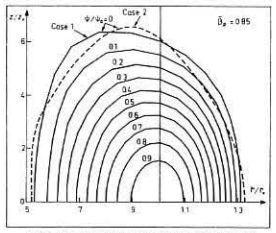

FIG.5 - Flux surfaces for case 1, $\psi = 0$ surface for case 2

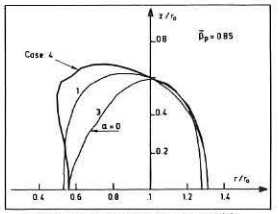

FIG.6 - $\psi = 0$ surfaces corresponding to $q_c = 1.5$ (3), 1.25 (1) and 1.17(4) .

RESISTIVE TOROIDAL EQUILIBRIA

R. J. Bickerton, L. C. Woods* and M. Woodward*
(Euratom. UKAEA Association for Fusion Research, Culham Laboratory, Oxfordshire, England)
*Department of Mathematics, University of Oxford

ABSTRACT

The starting point is a given toroidal plasma equilibrium of the tokamak type. Then assuming a steady state and specifying the plasma resistivity on the magnetic axis the corresponding self-consistent distributions of particle sources, electron density, temperature, and plasma convective velocity are calculated. Problems at the boundary are discussed but not resolved.

INTRODUCTION

We study resistive toroidal equilibria in order to understand toroidal effects which are masked when "toroidal transport" equations are used in cylindrical geometry. A one-fluid resistive model for the plasma is used, a steady state is assumed and inertial terms are neglected. Similar work has been reported by Green, von Hagenow and Zehrfeld[1].

BASIC EQUATIONS

The starting point is a given infinite conductivity toroidal equilibrium, that is a solution of the equation[2]

$$R\frac{\partial}{\partial R}\left(\frac{1}{R}\frac{\partial\Psi}{\partial R}\right)+\frac{\partial^2\Psi}{\partial z^2} = -f f'(\Psi) - R^2 g'(\Psi)$$

where $f(\Psi) = \frac{B_\varphi R}{B_o R_o}$ and $g(\Psi) = \frac{4\pi p}{B_o^2}$

using R, φ and z as cylindrical cordinates based on the axis of symmetry, Ψ is the poloidal flux, f and g are arbitrary functions of Ψ, p is the plasma pressure, B_o a reference magnetic field and R_o the radius of the magnetic axis.

Next we specify the plasma resistivity on the magnetic axis η_o ; we then know the applied electric field everywhere since

$$(E_\varphi)_o = \eta_o (j_\varphi)_o$$

and $E_\varphi = \frac{(E_\varphi)_o R_o}{R}$

assuming a perfect transformer with no leakage flux. Then using a series of integral relations given for example by Maschke[3] we can calculate the various plasma parameters corresponding to this finite resistivity equilibrium

$$\eta(\Psi) = \frac{\oint_\Psi \left|\frac{d\ell}{\nabla\varepsilon}\right| R\,\underline{B}\cdot\underline{B}_p}{\oint_\Psi \left|\frac{d\ell}{\nabla\varepsilon}\right| R\,\underline{B}\cdot\underline{j}}$$

The temperature variation is then calculated assuming $\eta \propto T^{-\frac{3}{2}}$,

$$T(\Psi) = (\eta(\Psi))^{\frac{2}{3}}$$

and then since the pressure is known,

$$n(\Psi) = g(\Psi)/T(\Psi)$$

The volume integral of the particle source function S is

$$\int_{V(\varepsilon)} d\tau S = n \int \left|\frac{d\sigma}{\nabla\varepsilon}\right| (j^2\eta - j\cdot E_\varphi)$$

then assuming S is only a function of Ψ,

$$S(\Psi) = \frac{d}{d\Psi}\int_{V(\Psi)} d\tau S / \frac{dV}{d\Psi}$$

where V is the volume of a magnetic surface.

The component of plasma velocity normal to the magnetic surface is calculated as a function of position,

$$V_n = \frac{1}{|\nabla\varepsilon||B|^2}\left[\eta|\nabla\varepsilon|^2 - |B|^2(E_\varphi j_\varphi)+(\underline{B}\cdot\underline{j})(B_\varphi E_\varphi) + |\nabla\varepsilon|\left(\frac{B_\varphi}{B_{pol}}\right)(B_\varphi E_\varphi - \eta\,\underline{B}\cdot\underline{j})\right]$$

RESULTS

Cases have been computed for the following forms for g and f,

$$g(\Psi) = \frac{A}{2}(1-\Psi^2)$$

$$f(\Psi) = (B^2 + CA(1-\Psi^2))^{\frac{1}{2}}$$

where A, B and C are constants and $\Psi = 1$ on the boundary.

Figures 1-4 show the results for the particular case A=B=5, C=0. Since C=0 the toroidal field is a vacuum field so there are no poloidal components of plasma current. The results show that there is a relatively small variation of plasma temperature from the axis to the wall and that a combination of particle sources near the axis and sinks (S-ve) in the outer regions is necessary to maintain the equilibrium. Because of the boundary condition p=0 the net particle flux from the plasma is zero since the diffusion coefficient being proportional to p also vanishes on the boundary. Since particle sinks (recombination) are not expected on any scale in tokamak plasmas, it would be more realistic to move the boundary to a radius such that $S \gtrless 0$ everywhere. There is then the problem that the normal velocity changeq sign round the surface and this is not realistic if the wall is assumed to absorb but not to emit plasma. That is the constraint $v_n \gtrless 0$ has to be applied at the boundary. It would seem that the matching of an interior solution to such a constraint is only possible if an additional physical effect is included near the boundary; for example the plasma inertia, since the convective velocities increase towards the boundary while the sound speed decreases. We have not yet carried out this matching and can only assume that merely a thin boundary layer will be affected.

It is interesting to note that in the case of a vacuum toroidal field and a scalar resistivity the plasma loss rate is unaffected by the toroidal field. The convective motion required to match the current distribution and the applied electric field is such as to lead to a net plasma flow corresponding to a diffusion coefficient $D \sim (r/R)^2 \frac{B_p}{B_\varphi}\eta$, i.e. the Pfirsch-Schluter correction applies equally to a toroidal pinch with no toroidal magnetic field.

Another aspect of the same point is that due to the convective plasma motion there is no correspondence between the current density and the plasma conductivity, contrary to what is often assumed in the interpretation of experiments. The difference is usually small but can be extreme in the case of tight aspect ratio.

The variations of $\eta(\Psi)$ and $S(\Psi)$ have been calculated for a variety of cases with A = B = 5, C ≠ 0, corresponding to a range of poloidal beta values and to non-vacuum toroidal fields. In some cases the plasma is required to be hotter at the wall than on the axis (lower η) and a complex system of sources and sinks is also needed. This is the result of taking arbitrary g and f so that it is not surprising that we find the corresponding $\eta(\Psi)$ and $S(\Psi)$ non-physical. Green et al[1] specify S and η and then calculate the corresponding g and f. This is more difficult but also clearly more satisfactory. However few results have been presented. It is also desirable to extend the present calculations to include the energy equation.

UNITS

In the diagrams all the parameters are presented in dimensionless units. To convert to real units use the following

Length = R_o = radius of magnetic axis; Resistivity = η_o = resistivity on magnetic axis; Velocity = $\eta_o/4\pi R_o$; Density = n_o = density on axis; Temperature = T_o = temperature on axis; Magnetic field $B_o = (B_\varphi)_o/f(\Psi))_o$; Pressure = $B_o^2/4\pi$; Current Density = $B_o/4\pi R_o$; Source $S = \left(\frac{n_o\eta_o}{4\pi R_o^2}\right)$

ACKNOWLEDGEMENT

We thank C. Ll. Thomas and F. A. Haas for the use of the computer programme[4] they developed to solve the infinite conductivity equilibrium equation.

REFERENCES

1. GREEN B. J., VON HAGENOW K. U., and ZEHRFELD H. P. Proceedings 6th European Conference on Controlled Fusion and Plasma Physics, Moscow, 1, 225, (1973).
2. LAING E. W., ROBERTS R. J., and WHIPPLE R. T. P. Plasma Physics, J.N.E. Pt. C, 1, 49, (1959).
3. MASCHKE E. K. Plasma Physics, 13, 905, (1971).
4. THOMAS C. Ll., and HAAS F. A., Culham Report CLM-R133 (1974).

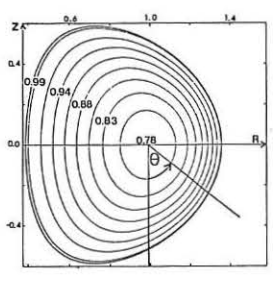

Fig.1 Contours of flux, Ψ

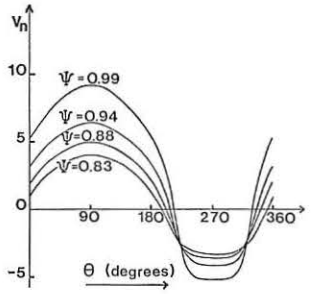

Fig.2 Normal velocity V_n around selected contours.

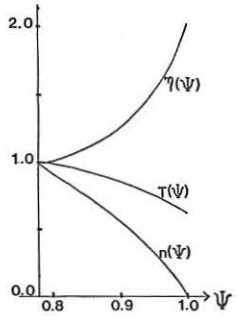

Fig.3 η, T, n as functions of Ψ

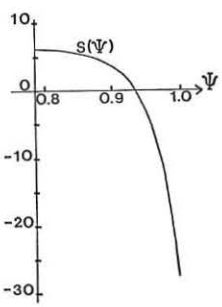

Fig.4 S as a function of Ψ

THE INFLUENCE OF DISSIPATIVE MECHANISMS AND THE EFFECT OF SHEAR ON STATIONARY CONVECTION IN A PLASMA

R.Y.Dagazian, E.K.Maschke and R.B.Paris
ASSOCIATION EURATOM-CEA SUR LA FUSION
Département de Physique du Plasma et de la Fusion Contrôlée
Centre d'Etudes Nucléaires
Boite Postale n° 6. 92260 FONTENAY-AUX-ROSES (FRANCE)

Abstract: Stationary convective solutions of the MHD equations with resistivity, heat conductivity, and viscosity are studied for a plasma slab in a sheared magnetic field.

Convective motion of plasma across a magnetic field has been proposed by several authors as a possible mechanism for anomalous transport [1,2]. In contrast to ref. 1,2, where the resistivity leads to instability, we consider convective motion in situations where the plasma is slightly unstable in ideal MHD theory and the dissipative mechanisms play a stabilising role. For a plane slab without magnetic shear in the presence of gravity or weak curvature of the field lines, the inclusion of resistivity and viscosity [3,4] leads to the existence of a marginal state ($\omega = 0$), characterised by a critical "Rayleigh number" $\mathcal{R} = \mathcal{R}_{crit}$, which in linear theory separates damped and exponentially growing modes. Nonlinear analysis, analogous to the theory of Bénard convection, shows that even for values of $\mathcal{R}$ beyond the critical Rayleigh number, stationary convective states exist resulting from the balance between the driving forces and dissipation [3,4].

In the present paper we limit our discussion to the linear theory of a plane plasma slab, which is interchange unstable in the ideal MHD limit, and consider the influence of dissipative mechanisms and magnetic shear on the onset of convection.

We use the MHD equations with constant resistivity η, heat conductivity $\mathcal{K}$, and viscosity coefficients μ_0(parallel), μ_L(diamagnetic), $\mu_\perp$(perpendicular). We write these equations in dimensionless form:

$$\rho\frac{\partial\vec{v}}{\partial t} + \frac{1}{\mathcal{P}_D}\rho(\vec{v}.\nabla)\vec{v} = Q\left[\vec{j}\times\vec{B} - \nabla p + \rho g\vec{e}_x\right] + \vec{F}_{visc} \qquad (1)$$

$$\mathcal{P}_D\frac{\partial\rho}{\partial t} + \nabla.\rho\vec{v} = 0 \qquad (2)$$

$$-\nabla\Phi + \vec{v}\times\vec{B} = \vec{j} \qquad (3)$$

$$\frac{3}{2}\mathcal{P}_T\rho\frac{\partial T}{\partial t} + \frac{3}{2}\rho\vec{v}.\nabla T + p^T\nabla.\vec{v} = \frac{\nu_{hc}}{\nu_{diff}}\nabla^2 T \qquad (4)$$

where we have normalised as follows: $\rho/\rho_0 \to \rho$, $p/(n_0T_0) \to p$, $\vec{B}/B_0 \to \vec{B}$, $x/L \to x$ with L the slab thickness; furthermore, introducing the classical diffusion coefficient $D_0 = n_0T_0/B_0^2$ and defining $\nu_{diff} = D_0/L$, $\nu_{hc} = \mathcal{K}/(n_0L)$, $\nu_{visc} = L/\tau_{visc} = \mu_\perp/(\rho_0 L)$ we have put $t/\tau_{visc} \to t$, $\eta\vec{j}/(B_0\nu_{diff}) \to \vec{j}$, $\Phi/(LB_0\nu_{diff}) \to \Phi$, $gL/v_{th}^2 \to g$ with $v_{th}^2 = T_0/m_i$. Also

$$\mathcal{P}_D = \frac{L/\nu_{diff}}{\tau_{visc}}, \quad \mathcal{P}_T = \frac{L/\nu_{hc}}{\tau_{visc}}, \quad Q = \frac{v_{th}^2}{\nu_{diff}\nu_{visc}} = \frac{L^2B_0^2}{\mu_\perp\eta} = \frac{\mu_0}{\mu_\perp}\frac{L^2}{a_i^2}\left(\frac{m_iT_e^3}{m_eT_i^3}\right)^{1/2} \gg 1$$

For classical resistivity and viscosity we have $\mathcal{P}_D \gg 1$, $\mathcal{P}_T \gg 1$. If the perturbations vary sufficiently slowly along the magnetic field and if $\vec{v}.\vec{B}$ is small, the viscosity term is

$$\vec{F}_{visc} = \left(\tfrac{1}{3}\mu_0 + 1\right)\nabla(\nabla.\vec{v}) + \frac{\mu_L}{\mu_\perp}\left[\nabla(\vec{B}.\nabla\times\vec{v}) - \vec{B}\times\nabla(\nabla.\vec{j})\right] - \nabla\times(\nabla\times\vec{v})$$

Quite generally we may write

$$\vec{v} = \vec{u} - \nabla\pi \qquad \vec{u} = \vec{B}\times\nabla\Phi, \quad \nabla.\vec{u} = 0 \qquad (5)$$

If the diffusion is purely classical, using $Q \gg 1$ we find from eqs. (1),(2) that $\pi = p$; if it is anomalous due to some microturbulence one may put $\pi = \rho$ and replace the classical D_0 by an anomalous coefficient D.

Let us first consider a magnetic field with weak curvature $1/R_0$ without shear and $g = 0$. Following the procedure of ref.3 we find that only the perpendicular viscosity appears in the final linearised equations which are

$$2ik(Q/R_0)p^{(1)} + \nabla^4\Phi = 0,$$

$$ik\Phi(\rho^{(0)})' + \nabla^2\pi^{(1)} = 0; \qquad \frac{3}{2}ik\Phi(T^{(0)})' + \nabla^2 p^{(1)} = -\frac{\nu_{hc}}{\nu_{diff}}\nabla^2 T^{(1)}$$

Imposing the boundary conditions $\Phi = \partial^2\Phi/\partial x^2 = \partial^4\Phi/\partial x^4 = 0$ at $x = \pm\frac{1}{2}$ we find onset of convection for $\mathcal{R} = \mathcal{R}_{crit}$ with $\mathcal{R}_{crit} = 27\pi^4/4$ for $k_{y,crit}^2 = \pi^2/2$ where $\mathcal{R}$ is the Rayleigh number defined by

$$\mathcal{R} = \begin{cases} (2/R_0)Q\left[(\rho^{(0)})'(\nu_{hc}/\nu_{diff}) + (3/2)(T^{(0)})'\right]\dfrac{1}{1+(\nu_{hc}/\nu_{diff})} & \text{if } \pi = \rho \\ (2/R_0)Q(\rho^{(0)})' & \text{if } \pi = p \end{cases} \qquad (6)$$

For $\nu_{hc}/\nu_{diff} \to \infty$ both expressions for $\mathcal{R}$ become identical.

We now consider a semi-infinite plane slab bounded between $x = \pm\frac{1}{2}$, with gravity simulating curvature and a sheared magnetic field $\vec{B}^{(0)} = \vec{e}_z + B_y^{(0)}(x)\vec{e}_y$, $B_y^{(0)}(x) = B_0x/L_s$. The shear is produced by a uniform weak current flowing in the z-direction such that $B_y^{(0)} \sim \varepsilon^2$, $\partial/\partial y = ik_y \sim \varepsilon^0$ and $\partial/\partial z = ik_z \sim \varepsilon^2$ with $\varepsilon \ll 1$. We assume a uniform $T^{(0)}$ and that $\nu_{hc}/\nu_{diff} \gg 1$ so that temperature perturbations may be neglected and $\pi = \rho$ in eqs. (5),(6). The equilibrium density profile is diffusional of the form $(\rho^{(0)})^2 = 1 - A(x+\frac{1}{2})$ where A is a positive constant $\ll 1$. We note that since η is assumed uniform and $(\vec{k}.\vec{B}^{(0)})'$ is constant rippling and tearing modes are excluded.

Linearising eqs. (1)-(3) and setting perturbed quantities proportional to $\exp(ik_yy + ik_zz + \omega t)$ we obtain the approximate marginal system ($\omega = 0$)

$$\nabla^4\Phi + Q\left[(\vec{k}.\vec{B}^{(0)})^2\Phi - ik_y\rho^{(1)}g\right] = 0; \qquad \nabla^2\rho^{(1)} + ik_y\Phi(\rho^{(0)})' = 0$$

in which it is seen that the shear term is multiplied by the parameter Q. Solving for Φ we find

$$\nabla^6\Phi + Qk_y^2\left[\nabla^2F^2\Phi + G\Phi\right] = 0, \qquad F = \vec{k}.\vec{B}^{(0)}/k_y, \quad G = -g(\rho^{(0)})'$$

which admits of the following variational principle for the previous boundary conditions

$$k_y^2\mathcal{R} = -\int_{-1/2}^{1/2}\psi\left[\nabla^6\Phi + Qk_y^2\nabla^2F^2\Phi\right]dx \Big/ \int_{-1/2}^{1/2}\psi\Phi\,dx \qquad (7)$$

where $\mathcal{R} = QG$ is the Rayleigh number and ψ is the adjoint of Φ satisfying the same boundary conditions as Φ and being a solution of the adjoint differential equation

$$\nabla^6\psi + Qk_y^2\left[F^2\nabla^2\psi + G\psi\right] = 0 \qquad (8)$$

An estimation of the Rayleigh number may be obtained by considering the trial functions $\psi = \Phi = \cos m\pi x$ where m is an odd integer. From eq. (7) we then find $\mathcal{R}$ as a function of m and k_y^2. For m = 1, the minimum value of $\mathcal{R}$ with respect to k_y^2 is

$$\mathcal{R}_{crit} = \frac{27}{4}\pi^4 + Q\left[3k_z^2 + \left(\frac{\pi^2-6}{8}\right)F'^2\right]; \quad k_{y,crit}^2 = \frac{\pi^2}{2} + \frac{2Q}{9\pi^2}\left[k_z^2 - \left(\frac{\pi^2-6}{48}\right)F'^2\right]$$

when ε^2Q/π^4 is small whereas for $Q \to \infty$, $k_{y\,crit}^2 \to \left(\frac{12\pi^4}{\pi^2-6}\right)^{1/3}\left|\frac{k_z}{F'}\right|$ independent of Q while $\mathcal{R} \sim Q$. Since Q is very large for hot plasmas it is seen that even weak shear ($F \sim \varepsilon^2$) has a very strong stabilising effect upon this type of convection.

For a strong uniform equilibrium current $j_z^{(0)}$ ($B_y^{(0)} \sim \varepsilon$, $k_z \sim \varepsilon$; $F \sim \varepsilon$) solution of our system (1)-(3) for isothermal perturbations becomes possible only if there exists a point $x = x_s$ in the slab where $F(x_s) = 0$. In this "strong shear" case we redefine our equilibrium to include the pinching term so that $\rho^{(0)}$ is now parabolic. The perturbed velocity includes a pinching term $\vec{v}^{(1)} = \vec{u} - \nabla\rho^{(1)} + \vec{j}^{(0)}\times\vec{B}^{(1)}$. The problem is more easily formulated in terms of the perturbed density to yield approximately

$$\nabla^6\rho^{(1)} + k^2QF^2\left[\nabla^2\rho^{(1)} + \rho^{(1)}G/F^2\right] = 0$$

We are interested in situations where the plasma is weakly MHD unstable; that is, where x_s falls in the upper half of the slab and where the Suydam criterion is violated, $G/F'^2 > \frac{1}{4}$. We distinguish two regions; the "singular" region about x_s and the outer region. Viscosity now becomes important only in the singular region of width $\delta \simeq \left\{gk^2Q(\rho^{(0)})'\right\}^{-1/6}$. We obtain the external solution in terms of Whittaker functions and the solution of the sixth order boundary layer equation in terms of generalised hypergeometric functions. Matching of this boundary layer solution to the external solutions then yields the eigenvalue $\mathcal{R}$ as a function of k^2. The minimum of $\mathcal{R}$ with respect to k^2 yields the critical Rayleigh number which, in the present linear theory, is equivalent to a modification of the Suydam criterion.

REFERENCES

/1/ Roberts, K.V., and J.B.Taylor, Phys. Fluids 8 (1965) 315.
/2/ Kadomtsev, B.B., and O.P.Pogutse, Reviews of Plasma Physics (M.A.Leontovich ed.), Vol.5, Consultants Bureau N.Y. 1965.
/3/ Wobig, H., Plasma Physics 14 (1972) 403.
/4/ Maschke, E.K., and R.B.Paris, Proc. V. Conf. Plasma Physics and Controlled Nuclear Fusion Research, Tokyo 1974, paper IAEA-CN-33/A14-2.

ASYMPTOTIC SOLUTIONS OF THE MAGNETOSTATIC EQUATIONS WITH TENSOR PRESSURE AND GENERALIZED PRESSURE SURFACES

C. Lo Surdo

Associazione EURATOM-CNEN sulla Fusione, Centro Gas Ionizzati C.P. 65, 00044 Frascati (Rome) Italy

Abstract: Asymptotic solutions of the magnetostatic equations with tensor pressure and generalized magnetic surfaces are constructed to all orders for a quasi-axisymmetric, quasi-toroidal field configuration with a vacuum dominant $\vec{\mathcal{B}}$.

Non axisymmetric asymptotic solutions of the magnetohydrostatic (MHS) equations have been recently obtained to all orders /1,2/ under assumptions which appear appropriate to deal with a Tokamak discharge. Precisely, such MHS asymptotic equilibria were sought in a toroidal axisymmetric domain $\mathcal{T}$ in the limit where: // i) scalar and vector fields are quasi-axisymmetric, or $\mathcal{F}=\mathcal{O}(\varepsilon)$, where $\mathcal{F}\equiv$ 1—the azimuth-averaging operator, and ε is small; ii) the axisymmetric vector fields are quasi-toroidal, or $\mathcal{M}(1-\mathcal{F})=\mathcal{O}(\varepsilon)$, where $\mathcal{M}\equiv$ the meridian-projection operator; iii) a vacuum $\vec{\mathcal{B}}$ dominates, so that $\nabla\times\vec{\mathcal{B}}=\mathcal{O}(1)$, with $\vec{\mathcal{B}}=\mathcal{O}(\varepsilon^{-1})$. Furthermore, iv) the normal component of $\vec{\mathcal{B}}$ on the $\mathcal{T}$-boundary $\partial\mathcal{T}$, $\mathcal{B}_\nu$, as well as the $\vec{\mathcal{B}}$-circulation along a prescribed non-reducible cycle ℓ of $\mathcal{T}$, were assumed as given under the condition $\oint_{\partial\mathcal{T}}d\ell\,\mathcal{B}_\nu=0$ //. Still with iv), the asymptotic scheme i)÷iii) has been also extended to magnetohydrodynamic stationary regimes with infinite conductivity and constant temperature along $\vec{\mathcal{B}}$ /3/. Aim of the present paper is to illustrate a different generalization of the MHS asymptotic formalism: namely, we shall be concerned with magnetostatic equilibria with tensor pressure, in the framework of the (lowest-order) guiding-center (GC) model of the plasma. The concerned equations are well known:

$$\nabla\times\vec{\mathcal{B}}\times\vec{\mathcal{B}}=\nabla\cdot\vec{\mathcal{P}} \qquad (1);\quad \nabla\cdot\vec{\mathcal{B}}=0 \qquad (2);\quad \vec{\mathcal{P}}=p_\perp\vec{\delta}+(p_\parallel-p_\perp)\frac{\vec{\mathcal{B}}\vec{\mathcal{B}}}{|\mathcal{B}|^2} \qquad (3).$$

These equations can be put in the equivalent form /4/:

$$\vec{\kappa}\times\vec{\mathcal{B}}=f\nabla\alpha+g\nabla\beta \qquad (4);\quad (p_\parallel-p_\perp)/|\mathcal{B}|^2=2f \qquad (5),$$

where $(\alpha,\beta)\equiv$ the Euler potentials of $\vec{\mathcal{B}}$; $(f,g,h)\equiv$ shorthand notations for $(\partial_\alpha p_\parallel,\partial_\beta p_\parallel,\partial_{|\mathcal{B}|^2}p_\parallel)$; $\vec{\kappa}\equiv\nabla\times\vec{\tau}$ and $\vec{\tau}\equiv[1-(p_\parallel-p_\perp)/|\mathcal{B}|^2]\vec{\mathcal{B}}\equiv\sigma\vec{\mathcal{B}}$. Due to the definition of $p_\parallel$ and $p_\perp$ in terms of a GC distribution function, the parallel-equilibrium eq. (5) is automatically fulfilled, so that, if $p_\parallel$ is thought as a (macroscopically) given function of α , β and $|\mathcal{B}|^2$, eq. (5) can be used to determine $p_\perp$ (or σ). In addition to i)÷iv), we shall assume that // v) $\vec{\kappa}$ and $\vec{\mathcal{B}}$ have joint ("generalized") flux surfaces, namely that such α and β exist for which g (say) is identically zero (we remember that α and β are determined only up to an incompressible mapping); and vi) that these surfaces (hence the surfaces $\alpha=const$) are closed, i.e. toroidal surfaces nested into each other//. Eq. (4) is thus written as: $\vec{\kappa}\cdot\nabla\alpha=0$ (6), $\vec{\kappa}\cdot\nabla\beta=f$ (7). These equations provide us with the contravariant components $\kappa^\alpha,\kappa^\beta$ of $\vec{\kappa}$ in a reference system having $\alpha=const$, $\beta=const$ as coordinate surfaces. This is enough to determine $\vec{\kappa}$ (through $\nabla\cdot\vec{\kappa}=0$) up to an arbitrary summand (depending on α) in the third contravariant component, say $\kappa^\gamma=\vec{\kappa}\cdot\nabla\gamma$ (where $\gamma=const$ are surfaces transverse to $\vec{\mathcal{B}}$). The vector $\vec{\tau}$ is then computed in a standard way as the sum of three (linear, weakly singular) integral transforms, respectively of $\vec{\kappa}$, of $\partial_{|\mathcal{B}|^2}h\,\vec{\mathcal{B}}\vec{\mathcal{B}}:\nabla\vec{\mathcal{B}}$, and of $(1-2h)\mathcal{B}_\nu$, plus a solenoidal, irrotational term with no normal component on $\partial\mathcal{T}$, which contributes a (given) $\vec{\tau}$-circulation along the non-reducible cycle ℓ in $\mathcal{T}$. In conclusion, we end up with $\tau^\alpha=0$ and $\tau^\beta=0$ as coupled equations for α and β . The solution procedure is made possible by exploiting the asymptotic assumptions i)÷iii). We shall limit ourselves to a condensed outline. We take α^{-1} (superscript figures denote the asymptotic order) equal to $\frac{A^{-1}}{2\pi}$ times the poloidal flux of $\vec{\mathcal{B}}^0$ (say $\mathcal{G}^0$), where A^{-1} is the constant $(R)^2\vec{\mathcal{B}}^{-1}\cdot\nabla\varphi$ (φ and R are the usual cylindrical coordinates with respect to the symmetry axis), so that $\nabla\varphi\times\nabla\mathcal{G}^0\cdot\nabla\beta^0\equiv\partial_{\eta^0}\beta^0=\frac{1}{(R)^2}$. As a consequence, it can be shown that $[\alpha^0]=0$ and $A^{-1}[\beta^1]=2\pi$, with $[\,]$ denoting increments the long way around. Hence $\beta^1=\beta^1_*+\Psi/A^{-1}$, with $[\beta^1_*]=0$. Each $\alpha^{n\geq-1}$ and $\beta^{n\geq2}$ can be assumed to be single-valued along φ-cycles without loss of generality. All the (single-valued along φ -cycles) fields are then projected into the orthogonal (functional) subspaces of the axisymmetric (bar) fields and of the zero-φ-average (tilde) fields. The (solenoidal) $\vec{\mathcal{B}}$ and $\vec{\kappa}$ are put in the form:

$$\vec{\mathcal{B}}=\nabla\mathcal{G}\times\nabla\varphi+\mathcal{T}\nabla\varphi \qquad (8)\qquad \vec{\kappa}=\nabla\mathcal{L}\times\nabla\varphi+\Lambda\nabla\varphi \qquad (9)$$

where $\mathcal{G},\mathcal{T},\mathcal{L},\Lambda$ are axisymmetric scalars. To the lowest orders, one easily finds: $\mathcal{T}^{-1}=A^{-1}$; $\mathcal{T}^0=0$; $\mathcal{L}^0=0$; $\Lambda^0=-\mathcal{L}\mathcal{G}^0$, where $\mathcal{L}\equiv\equiv\partial^2_{\mathcal{M}}-\frac{1}{R}\partial_R$ and $\partial^2_{\mathcal{M}}\equiv$ Laplace operator in the meridian plane. By use of eq. (6)-bar, order 0, we find also that $A^{-1}\partial_{\eta^0}\mathcal{L}^1=0$ $(\bar6^0)$; thus $\mathcal{L}^1$ is an arbitrary function of $\mathcal{G}^0$, say $c^1(\mathcal{G}^0)$. Eq. (7)-bar, order 1, then gives: $\mathcal{L}\mathcal{G}^0/A^{-1}+\dot c^1+(R)^2\bar f^{-1}=0$ $(\bar7^1)$, where a dot means $d/d\mathcal{G}^0$. If one puts $p_\parallel(\alpha,|\mathcal{B}|^2)\equiv p^*_\parallel(\alpha/A^{-1},|\mathcal{B}|^2/(A^{-1})^2)\equiv p^*_\parallel(x,y)$, it is clear that $A^{-1}\bar f^1$ is the unperturbed value of $\partial_x p^*_\parallel$. By solving the elliptic semilinear eq. $(\bar7^1)$ with the prescribed $\mathcal{G}^0$ on $\partial\mathcal{T}$ (from $\vec{\mathcal{B}}^0_\nu=\vec{\mathcal{B}}_\nu$) one finally gets the whole solution to the order 0 (included) since $\vec{\mathcal{B}}^0$ is the gradient of a harmonic function (in $\mathcal{T}$) with prescribed normal derivative $\vec{\mathcal{B}}_\nu$ on $\partial\mathcal{T}$. Going to higher orders is more complicated. We shall illustrate the order-1-calculations. From eq. (6)-tilde, order 0, and eq. (7)-tilde, order 1, we have (since $\tilde f^1=0$): $A^{-1}\vec{\tilde\kappa}^1_{\mathcal{M}}=-\mathcal{L}\mathcal{G}^0\vec{\tilde{\mathcal{B}}}^0_{\mathcal{M}}$ $(6^0,7^1)$, where $_{\mathcal{M}}$ means meridian component. The whole $\vec{\tilde\kappa}^1$ is then computed from $\nabla\cdot\vec{\tilde\kappa}^1=0$. Eq. (6)-bar, order 1, gives: $\mathcal{L}^2=\dot c^1\mathcal{G}^1+c^2+\mu^2$ $(\bar6^1)$, where $A^{-1}\mu^2\equiv\int d\eta^0(\dot c^1\vec{\tilde{\mathcal{B}}}^0-\vec{\tilde\kappa}^1)\cdot\nabla\tilde\alpha^0$ and c^2 is an arbitrary function of $\mathcal{G}^0$. Here $\tilde\alpha^0$ is computed by integration of $A^{-1}\partial_\varphi\tilde\alpha^0=-(R)^2\nabla\alpha^{-1}\cdot\vec{\tilde{\mathcal{B}}}^0$ (10α). The requirement $[\![\mu^2]\!]=0$ should be observed (where $[\![\;]\!]$ denotes increments the short way around), because $[\![\mathcal{G}^1]\!]=0$. Finally, we get from eq. (7)-bar, order 2: $\mathcal{L}\mathcal{G}^1/A^{-1}+\mathcal{G}^1\dot c^1+(R)^2\bar f^2=-\dot c^2-(R)^2\cdot(\dot c^1\vec{\tilde{\mathcal{B}}}^0-\vec{\tilde\kappa}^1)\cdot\nabla\vec{\beta}^1_*+(R)^2\nabla\varphi\times\nabla\beta^0\cdot\nabla\mu^2$ $(\bar7^2)$, where $\vec{\beta}^1_*$ is computed from the companion equation of eq. (10α): $A^{-1}\partial_\varphi\vec{\beta}^1_*=-(R)^2\nabla\beta^0\vec{\tilde{\mathcal{B}}}^0$ (10β). By solving eq. $(\bar7^2)$ for $\mathcal{G}^1$, with $\mathcal{G}^1=0$ on $\partial\mathcal{T}$, one eventually gets the whole solution to order 1 (included). In fact, $\bar f^2$ and $\bar\sigma^2$ (we need $\bar\sigma^2$ to compute $\mathcal{T}^1=L^1-A^{-1}\bar\sigma^2$) are known quantities, i.e. $A^{-1}\bar f^2=\partial_x f^*|_0\,\bar\alpha^0$ (since $\vec{\mathcal{B}}^0\cdot\nabla\varphi=0$) and $\bar\sigma^2=-2\mathcal{L}|_0$, with f^* being defined in terms of x and y similarly to $p^*_\parallel$; $|_0$ means unperturbed value. Note that f^* and f_0 are formally of order 1 and 2 respectively. As regards $\bar\alpha^0$, it is seen that $2\pi(\mathcal{G}^1-\bar\alpha^0/A^{-1})$ is the poloidal flux of the solenoidal axisymmetric field $(\overline{\nabla\tilde\alpha^0\times\nabla\tilde\beta^1_*})_{\mathcal{M}}$. Finally, $\vec{\tilde{\mathcal{B}}}^1$ is computed as a weakly singular integral transform of $\vec{\tilde\kappa}^1$ from $\vec{\tilde\kappa}^1=\nabla\times\vec{\tilde{\mathcal{B}}}^1$, because $\tilde{\mathcal{B}}^1_\nu=0$. It can be proved that the arbitrary summand depending on $\mathcal{G}^0$ wich is enbodied in β^0 does not affect the overall results obtained so far; in particular, $\bar\alpha^0$ does not depend on the above summand. The full stabilization of the asymptotic routine is reached only to the next order, which we do not describe here for brevity. Yet, the overall results to the order 2 are not affected by the arbitrary summands enbodied in β^0 and in $\vec{\beta}^1_*$. The asymptotic procedure can be continued to any desired order, though more and more laboriously, with a new arbitrary function c of $\mathcal{G}^0$ and a new single-valuedness requirement (the short way around) for each order. These single-valuedness requirements can be shown to be identically fulfilled by elementary means, in particular, in the so-called "favourable symmetry" configurations described in /1/, Sect. 4.

REFERENCES

/1/ C. Lo Surdo, A. Sestero: The Physics of Fluids, 18, 255 (1975).

/2/ C. Lo Surdo, A. Sestero: Annali di Matematica Pura ed Applicata, in press.

/3/ C. Lo Surdo, A. Sestero: Proc. Int. Conf. on the Plasma Theory, Kiev (1974), p. 154, and submitted to the Journal of Plasma Physics.

/4/ H. Grad: The Guiding Center Plasma, MF-48/NYO-1480-50, N.Y. University, Courant Institute Mathem. Sciences (1966),

STABILITY OF GENERAL MHD EQUILIBRIA

D. Lortz, J. Nührenberg
Max-Planck-Institut für Plasmaphysik, 8046 Garching bei München,
Federal Republic of Germany

Abstract: Exact expressions for the magnetic well evaluated on the magnetic axis are calculated in terms of prescribable quantities with simple geometrical meaning for helically symmetric equilibria with ohmic heating current and for $\ell = 2$ toroidal stellarators without ohmic heating current.

Introduction. Various stability analyses [1-6] have borne out the hypothesis that Mercier's criterion is a valuable tool for the stability assessment of MHD equilibria with a conducting wall at the plasma boundary (internal modes). A prerequisite of such an analysis for general equilibria is the evaluation of $\ddot{\psi}/\dot{\psi}$ on the magnetic axis (ψ is the longitudinal flux inside a magnetic surface of volume V, $\dot{} = d/dV$). Although this has in principle been accomplished by Mercier [1], his treatment is not satisfactory since it does not lead to explicit results in terms of geometrically simple quantities occurring in the description of the neighborhood of the magnetic axis to third order in the distance from it. This is however essential, because only then a β-estimate becomes possible in connection with a discussion of the position of separatrices [3,4]. Furthermore, there are physically interesting cases, e.g. helically symmetric equilibria with ohmic heating current, $\ell=2$ toroidal stellarators with and without ohmic heating current, for which the equilibrium relationship between third order quantities occurring in $\ddot{\psi}/\dot{\psi}$ can be obtained explicitly, so that it is possible to calculate exact expressions for $\ddot{\psi}/\dot{\psi}$ in terms of independent parameters in these cases.

Notation and formal expression for $\ddot{\psi}/\dot{\psi}$. Let the magnetic axis be described by its curvature $\varkappa$ and its torsion τ and the nonorthogonal coordinate system ϱ, φ, ℓ linked to it by $\sqrt{g} = \varrho(1 - \varkappa\varrho\cos\varphi)$, $ds^2 = d\varrho^2 + \varrho^2 d\varphi^2 - 2\tau\varrho^2 d\varphi d\ell + [(1-\varkappa\varrho\cos\varphi)^2 + \tau^2\varrho^2]\, d\ell^2$. Let the contravariant components B^ϱ, B^φ, B^ℓ of the magnetic field be given by $B^\varrho = a_1\varrho + a_2\varrho^2 + O(\varrho^3)$, $B^\varphi = b_0 + b_1\varrho + O(\varrho^2)$, $B^\ell = c_0 + c_1\varrho + c_2\varrho^2 + O(\varrho^3)$ and V be the volume inside a magnetic surface, $V = V_2\varrho^2 + V_3\varrho^3 + O(\varrho^4)$. Then a simple calculation shows that on the magnetic axis

$$\ddot{\psi}/\dot{\psi} = \oint \frac{1}{c_0 V_2^3}\left[\frac{1}{2} V_2\,(c_2 - \varkappa c_1\cos\varphi) - V_3 c_1\right] d\varphi\, d\ell. \qquad (1)$$

Description of magnetic surfaces and second order results.
Let the volume inside a magnetic surface be described by

$$V = c_0 \oint \frac{d\ell}{c_0}\left\{\pi\left[\varrho^2(e\cos^2 u + \tfrac{1}{e}\sin^2 u) - 2\varkappa\varrho^3(\delta\cos u \sin^2 u + \Delta\cos^2 u \sin u)\right]\right\} \qquad (2)$$

where $u = \varphi + \alpha$, $\varrho\cos u = x\cos\alpha - y\sin\alpha$,
$\varrho\sin u = x\sin\alpha + y\cos\alpha$, and

$$x = \varrho\cos\varphi + \varkappa\frac{S}{e}\varrho^2\,(e\cos^2 u + \frac{1}{e}\sin^2 u)$$

$$y = \varrho\sin\varphi + \varkappa\frac{s}{e}\varrho^2\,(e\cos^2 u + \frac{1}{e}\sin^2 u).$$

Then $e(>1)$ is the half-axes ratio b/a of the (in second order) elliptical cross-section of the magnetic surfaces where b is the half-axis at $\varphi = \pi/2 - \alpha$ and a the half-axis at $\varphi = -\alpha$, so that α is the angle of rotation of the ellipses with respect to the binormal of the magnetic axis. The nondimensional third order quantities δ and Δ describe symmetric and antisymmetric triangular deformations of the surface, where the symmetry holds with respect to $u = 0$. The quantities S and s describe shifts of the magnetic surfaces with respect to the magnetic axis in the directions normal and binormal to the magnetic axis. Although the representation (2) of V may look complicated, the quantities $e, \alpha, \delta, \Delta$, S, s have simple meanings. Note that the curly bracket in (2) is the area of the cross-section of the magnetic surfaces normal to the magnetic axis. In addition to V_2 and V_3, which are obtained from (2), the following first and second order equilibrium results have to be employed in the evaluation of (1):

$$c_1 = 2\varkappa c_0 \cdot \cos\varphi$$

$$b_0 = b_{00} + b_{0u}\sin u + b_{0g}\cos u$$

$$b_{00} = j/2 + \tau c_0\,,\quad b_{0u} = (c_0 e')/(2e),\quad b_{0g} = (b_{00} + c_0\alpha')\cdot(e^2-1)/(e^2+1)$$

$$c_0(c_2 - \varkappa c_1\cos\varphi) = c_0(2\tau b_0 + c_0\varkappa^2\cos^2\varphi - c_0\tau^2) - b_{00}b_0 - \tfrac{1}{4}c_0(\partial^2 b_0/\partial\varphi\partial\ell + c_0'') - \dot{p}\cdot V_2$$

Here, j is the current density on the magnetic axis, p the pressure, and the prime indicates the derivative with respect to ℓ. Denoting $q_0 = \oint \frac{d\ell}{c_0}$, we obtain

$$\ddot{\psi}/\dot{\psi} = \frac{1}{2\pi q_0^2}\oint\frac{d\ell}{c_0^2}\left\{(e+\tfrac{1}{e})\left[(2\tau - \tfrac{b_{0c}}{c_0})\tfrac{b_{00}}{c_0} + \tfrac{\varkappa^2}{2} - \tau^2 - \tfrac{c_0''}{4c_0}\right] - (e-\tfrac{1}{e})\left[(2\tau - \tfrac{b_{00}}{c_0})\tfrac{b_{0g}}{c_0} + \tfrac{\varkappa^2}{2}\cos 2\alpha - \tfrac{1}{2c_0}(b_{0u}' - 2\alpha' b_{0g})\right] - 2\pi\tfrac{q_0}{c_0}\dot{p} - 2\varkappa^2\left[\tfrac{1}{e}S - (\Delta\sin\alpha + \delta\cos\alpha)\right]\right\} \qquad (3)$$

Here, the three third order coefficients δ, Δ, and S occur. Since the equilibrium equations connect δ, Δ, S, and s, eq. (3) does not describe $\ddot{\psi}/\dot{\psi}$ in terms of prescribable parameters.

Description of third order equilibrium calculation. To obtain the relation between δ, Δ, and S the following third order equations are used: (A) $O(\varrho^2)$ of $\nabla\cdot\underline{B} = 0$, (B) $O(\varrho^3)$ of $\underline{B}\cdot\nabla V = 0$, (C) $O(\varrho^2)$ of $\dot{p}\frac{\partial V}{\partial\varrho} = (\underline{j}\times\underline{B})\cdot\frac{\partial\underline{r}}{\partial\varrho}$, (D) $O(\varrho^3)$ of $\dot{p}\frac{\partial V}{\partial\varphi} = (\underline{j}\times\underline{B})\cdot\frac{\partial\underline{r}}{\partial\varphi}$, where the latter two equations are used to eliminate c_3. The procedure is algebraically quite tedious; to obtain correct results we have found that it is essential to check the calculation step by step with the help of the algebraic programming system REDUCE [7]. Details of the calculation will be published elsewhere.

Results for special cases. We first checked the result obtained in the axisymmetric case (eq. 9c of [3])

$$\delta = \frac{1}{e} + \frac{3}{2}e - Q(e + \frac{1}{e}) + S(3e + \frac{1}{e}) \qquad (4)$$

where Δ, $s = 0$ (symmetry of the magnetic surfaces with respect to the equatorial plane) is assumed and Q is related to $\dot{p}$ by $\dot{p} = -\dot{J}\dot{\chi}(1 - Q)$.

In the case of a helically symmetric equilibrium with magnetic surfaces which are symmetric with respect to the osculating plane (Δ, $s = 0$) we obtain

$$\delta = (3e + \frac{1}{e})S + \frac{e}{2} - \frac{2\tau_h}{\iota_\pm} - \frac{L^3}{2\pi\iota_\pm^2}\frac{\dot{p}}{c_0^2} \qquad (5)$$

Here, L is the periodicity length of the magnetic axis, $\tau_h = L\tau/2\pi$, and

$$\iota_\pm = \frac{L}{\pi}\frac{e}{e^2+1}\left(\tau + \frac{j}{2c_0}\right) = \iota \pm 1$$

where ι is the rotational transform per period and $\pm$ refers to a lefthanded and a righthanded helical magnetic axis respectively ($\tau > 0$ for a lefthanded helix). Note that eq. (4) is obtained from eq. (5) with the substitution $\iota_\pm \to \iota$ and taking the limit $\tau \to 0$.

In the case of an $\ell = 2$ toroidal stellarator with $\alpha' = \text{const}$ the situation is more complicated because for the choice $s = 0$, $S = \text{const}$ which appears physically reasonable, δ and Δ are no longer constant. The third order equations can be solved with $\delta = \delta_c\cos\alpha$, $\Delta = \Delta_s\sin\alpha$. We have used the additional simplifying assumption $j = 0$ (no ohmic heating current). The result is

$$\delta_c + \Delta_s = -\frac{3}{2}(e + \frac{1}{e}) + \frac{(e^2-1)^2}{e^3}S - 4\frac{(3e^2+1)(e^2+3)(e^2+1)^2}{(e^2-1)^4}\frac{\pi L}{\alpha'^2 c_0^2}\dot{p} \qquad (6)$$

From Eqs. (5), (6) we obtain the results for

$$\ddot{\psi}/\dot{\psi} = \frac{2\pi}{L^3}\left[6\varkappa_h(e - \frac{1}{e})S - \frac{L^3\dot{p}}{2\pi c_0^2}(1 + \frac{2\varkappa_h^2}{\iota_\pm^2}) + 4\tau_h\iota_\pm(1 - \frac{\varkappa_h^2}{\iota_\pm^2}) + (1 - \iota_\pm^2 - 2\tau_h^2)(e + \frac{1}{e})\right] \quad \text{(helical equilibria)} \qquad (7)$$

where $\varkappa_h = L\varkappa/2\pi$, and

$$\ddot{\psi}/\dot{\psi} = \frac{1}{4\pi^2 R^3}\left\{-(e+\frac{1}{e}) - R^2\alpha'^2\frac{(e^2-1)^2}{e(e^2+1)} + \frac{e^4 - 10e^2 + 1}{e^3}S - \frac{4\pi^2R^3\dot{p}}{c_0^2}\left[1 + 2\frac{1}{R^2\alpha'^2}\frac{(3e^2+1)(e^2+3)(e^2+1)^2}{(e^2-1)^4}\right]\right\}$$
(toroidal $\ell = 2$ stellarator with $j = 0$) (8)

where R is the radius of the magnetic axis.

Status und programm. Currently we are calculating the generalization of eq. (6) for $j \neq 0$. We will then discuss the parameter dependencies of the critical ohmic heating currents on the magnetic axis (analogous to the treatment of the axisymmetric case in [3]). Finally we will obtain β-estimates (from equilibrium and stability) in connection with a separatrix discussion (analogous to Sec. V of [4]). Results will be presented at the conference.

References

[1] Mercier, C., Nucl. Fusion 4 (1964) 213.
[2] Lortz, D., Nucl. Fusion 13 (1973) 817.
[3] Lortz, D., Nührenberg J., Fusion 13 (1973) 821.
[4] Lortz, D., Nührenberg J., IAEA-CN-33/A12-2.
[5] Wesson, J.A., Sykes, A., Nucl. Fusion 14 (1974) 645.
[6] Freidberg, J.P., Berge, G., IAEA-CN-33/E1-1.
[7] Hearn, A.C., University of Utah Report (1973) UCP-19.

" This work was performed under the terms of the agreement on association between Max-Planck-Institut für Plasmaphysik and EURATOM."

ON LOCAL STABILITY OF A PLASMA WITH CLOSED MAGNETIC FIELD LINES

V.D. Shafranov, A.V. Frolenkov
I.V.Kurchatov Institute of Atomic Energy, Moscow, USSR

Abstract. The "radial" type of displacement is considered for plasma with the closed magnetic field lines. A new criterion of plasma stability is derived.

Introduction. The local criterion of plasma stability for closed line equilibria differs in two respects from that for systems with ergodic field lines. 1) The constancy of $div\,\vec{\xi}$ on a magnetic field line which follows from a stability analysis gives rise automatically to $div\,\vec{\xi}=0$ for local displacements in the ergodic systems, while $div\,\xi\neq 0$ for the closed line systems. 2) The local criterion is identical over the whole magnetic surface in the ergodic case while it depends on a choosen field line (for finite plasma pressure gradient) in the closed line systems, that is it depends on the radial and azimuthal coordinate as well.

The first difference leads to a less stringent criterion of the form $g(p'+\gamma p f)<0$, where $f\sim div\,\vec{\xi}$ for the closed line systems /1/ instead of $gp'<0$ for the ergodic ones.

The second difference is associated essentially with a different character of the most dangerous displacements in both types of the systems under consideration. In the systems with shear the most dangerous displacements are "azimuthal" ones which are strongly localized in the radial direction and have mainly an azimuthal component. The corresponding criterion derived by Mercier /2/ and specified by Green and Johnson /3/ being applied to zero rotation transform angle systems leads to paradoxical result /4/: it does not restrict plasma pressure gradient for those magnetic field lines which are in the plane of magnetic axes(!) We have solved that paradox using the Mikhailovskij results /5/ for a general type of local displacements. The "radial" displacements rather than azimuthal are found most dangerous for the equatorial plane magnetic field lines. These displacements have mainly the radial component, and they are strongly localized in the azimuthal direction (Fig.1).

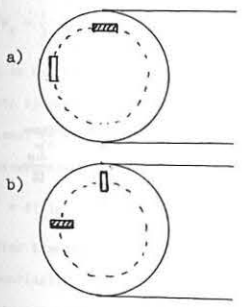

Fig.1. Region of localization a)"azimuthal", b)"radial" modes. Dashed displacements"sensitive" to the curvature of the magnetic field lines and restricting the plasma pressure.

Hence, it follows that the considerations of magnetohydrodynamic stability with closed magnetic field lines made recently by Spies /6/ are not comprehensive because they do not take into account radial displacement. The aim of our paper is to make up a gap in the magnetohydrodynamic stability theory with closed magnetic field lines.

Stability conditions. In deriving the stability criterions we use the solvability conditions for linearized equations of motion.

The displacement $\vec{\xi}$ may be written as

$$\vec{\xi} = \xi\,\vec{e} + \lambda\,\frac{\vec{B}\times\nabla V}{|\vec{B}|^2} + \mu\,\frac{\vec{B}}{|\vec{B}|^2}$$

where $\vec{e}=\nabla\theta\times\nabla\zeta$ is the covariant basis vector of the Hamada coordinates V,θ,ζ /7,8,9/, V is the volume of the pressure surface $p(V)$.

For the azimuthal modes, we assume as usually /2,3,6/, that $x=(V-V_0)/\varepsilon$, $\varepsilon\ll 1$,

$$\frac{\partial}{\partial V}=\frac{1}{\varepsilon}\frac{\partial}{\partial x};\qquad \xi=\varepsilon\xi_1+\varepsilon^2\xi_2+\cdots;\qquad \lambda=\lambda_0+\varepsilon\lambda_1+\cdots \quad (2)$$

In this case it turns out that $\vec{B}\nabla\lambda_0=\vec{B}\nabla\xi_1=0$. We assume for radial displacement

$$\frac{\vec{B}\times\nabla V\cdot\nabla}{|\vec{B}|^2}=\frac{1}{\varepsilon}\frac{\partial}{\partial u};\qquad \xi=\xi_0+\varepsilon\xi_1+\cdots;\qquad \lambda=\varepsilon\lambda_1+\cdots \quad (3)$$

Here $\vec{B}\nabla\xi_0\neq 0$, thus $\xi_0=\langle\xi_0\rangle+\tilde{\xi}_0$. It is possible to derive the general stability criterion for $|\tilde{\xi}_0|<|\langle\xi_0\rangle|$. Let us denote the quantities relating to the cases of azimuthal and radial displacements by A and R respectively. In both cases, after some algebra, the criterion of stability (necessary and sufficient for a given type of local displacements) can be written as $\left(\langle F\rangle\equiv\oint F\,d\ell/B\Big/\oint d\ell/B\right)$:

$$g_{A,R}\left(p'+\gamma p\,\frac{\langle div\,\vec{\xi}\rangle}{\langle\xi\rangle}_{A,R}\right)<0 \quad (4)$$

Here

$$g_{A,R}=\left(2p+\langle B^2\rangle\right)'+p'\,\delta^2_{A,R} \quad (5)$$

$$\frac{\langle div\,\vec{\xi}\rangle}{\langle\xi\rangle}_{A,R}=-\frac{g_{A,R}}{\langle B^2\rangle+\gamma p\,(1+\delta^2_{A,R})} \quad (6)$$

The coefficient $\delta^2_{A,R}$ results from the balooning effect ($\vec{B}\nabla\lambda_1\neq 0$; $\vec{B}\nabla\xi_0\neq 0$). In the case of $p'<0$, $g_{A,R}>0$ is sufficient for stability. However, there is a stable region even for $g_{A,R}<0$ when the expression in round brackets in (4) is negative. Substituting (5),(6) into(4) one can see that the sign of this expression does not depend on $\delta^2_{A,R}$:

$$g_{A,R}\left(p'-\gamma p\,\frac{(\langle B^2\rangle+2p)'}{\langle B^2\rangle+\gamma p}\right) \quad (4')$$

This result was derived by Spies /6/ for the azimuthal modes.

The explicit expressions for $\delta^2_{A,R}$ are as follows:

$$\delta^2_A=\langle B^2\rangle\langle\frac{1}{B^2}\rangle-1+\langle B^2\rangle\left[\langle\frac{\alpha_A^2B^2}{|\nabla V|^2}\rangle-\frac{\langle\alpha_A B^2/|\nabla V|^2\rangle^2}{\langle B^2/|\nabla V|^2\rangle}\right] \quad (7)$$

$$\delta^2_R=\langle B^2\rangle\langle\frac{1}{B^2}\rangle-1+\langle B^2\rangle\left[\langle\frac{\alpha_R^2B^2}{|\vec{B}\times\vec{e}|^2}\rangle-\frac{\langle\alpha_R B^2/|\vec{B}\times\vec{e}|^2\rangle^2}{\langle B^2/|\vec{B}\times\vec{e}|^2\rangle}\right] \quad (8)$$

where α_A is a solution of equation

$$\vec{B}\nabla\alpha_A=\frac{\vec{B}\times\nabla V\cdot\nabla B^2}{|B|^4} \quad (9)$$

and

$$\alpha_R=\frac{\vec{B}\vec{e}}{|\vec{B}|^2}-p'\frac{\varphi_1}{\langle B^2\rangle^2};\qquad \vec{B}\nabla\varphi_1=\langle B^2\rangle^2\left(\langle\frac{1}{B^2}\rangle-\frac{1}{B^2}\right) \quad (10)$$

(Note that $\vec{B}\vec{e}=\partial\varphi/\partial V$, where $\vec{B}\nabla\varphi=|B|^2-\langle B^2\rangle$).

It follows for $div\,\vec{\xi}=0$ that criterion $g_A p'<0$ derived from /4/ is the same criterion obtained by Mercier, Green, Johnson for systems without shear, while criterion $g_R p'<0$ with $\alpha_R=\vec{B}\vec{e}/|B|^2$ is similar to that derived by Mikhailovskij /5/ for radial displacements.

References.

1. B.B.Kadomtsev, in Plasma Physics and the Problem of Controlled Thermonuclear Reactions (Pergamon, London, 1960), v.4, p.450.
2. C.Mercier, Nucl. Fusion Suppl. 2, 801 (1962).
3. J.M.Greene and J.L.Johnson, Phys. Fluids, 5, 510 (1962).
4. V.D.Shafranov, E.T.Yurchenko, Nucl. Fusion, 9, 285 (1969).
5. A.B.Mikhailovskij, Zh. Ehksp. Teor. Fiz., 64, 536 (1973).
6. G.O.Spies, Phys. Fluids, 17, 400, (1974).
7. S.Hamada, Nucl.Fusion, 2, 23 (1962).
8. L.S.Solov'ev, Zh. Ehksp. Teor. Fiz., 26, 1167 (1968).
9. D.Lortz, E.Rebhan, G.Spies, Nucl. Fusion, 11, 583 (1971).

INTERNAL KINK INSTABILITY IN A CIRCULAR TOROIDAL PLASMA

M.N. Bussac*, D. Edery**, G. Laval*,
R. Pellat*, J.L. Soulé***,
* Ecole Polytechnique, Paris
** Compagnie Internationale
de Services en Informatique, Paris.
*** ASSOCIATION EURATOM-CEA SUR LA FUSION
Département de Physique du Plasma et de la Fusion Contrôlée
Centre d'Etudes Nucléaires
Boîte Postale n° 6. 92260 FONTENAY-AUX-ROSES (FRANCE)

Abstract : The stability criterion of the internal kink mode is given for a circular toroidal plasma. In contrast with the known cylindrical approximation, this mode may be stable if the pressure gradient is sufficiently low.

Recent experiments have shown that an m = 1, n = 1 unstable mode occurs in a Tokamak when the safety factor q falls below unity on the axis. This mode has been described as an internal kink mode in the frame of the ideal MHD approximation. Up till now, analytical calculations have employed the cylindrical approximation.[1,2] However, numerical simulations have shown that the toroidal geometry affects this mode very significantly.[3,4] In fact, in contrast with the usual kink, the energy reservoir is here of the same order as the toroidal terms.

The stability criterion and the linear growth rate are given here for a toroidal plasma with a circular cross-section and a large aspect ratio.

We consider an equilibrium depending on a small paramater $\varepsilon = \frac{a}{R_0 q}$, with $\frac{p}{B^2} \sim \varepsilon^2$. To study the stability of the internal perturbation, m = 1, arbitrary n, we use the energy principle, calculated with the equilibrium defined up to order ε^2. The guideline of the method is the remark that the perturbed toroidal magnetic field is of order ε compared to the perturbed poloidal field.[5]

To order ε, the mode contains an m = 2 component which comes from the coupling of the main term with the field modulation.

After minimization, we find :

$$\delta W = 2\pi^2 R_0 B_{\varphi}^2 \xi_0^2 \left(\frac{n r_0}{R_0}\right)^4 \delta\tilde{W} \qquad \delta\tilde{W} = \left(1 - \frac{1}{n^2}\right)\delta\tilde{W}_c + \frac{1}{n^2}\delta\tilde{W}_T$$

$$\delta\tilde{W}_c = -P - \int_0^{r_0} \frac{r^3 dr}{r_0^4}\left(\frac{1}{n^2 q^2} + \frac{2}{nq} - 3\right)$$

$$\delta\tilde{W}_T = \frac{\frac{9}{16} b(1-c) + \frac{s}{2}(1+b-c) - \frac{3}{2} bc\,(P+s) - (1+b)\,c\,(P+s)^2}{1+b-c}$$

$$s = \int_0^{r_0} \frac{r^3 dr}{r_0^4}\left(\frac{1}{n^2 q^2} - 1\right)$$

$$b = \frac{1}{4}\left[\frac{r}{u_1}\frac{du_1}{dr} - 2\right]_{r = r_0}$$

$$c = \frac{1}{4}\left[\frac{r}{u_2}\frac{du_2}{dr} + 2\right]_{r = r_0}$$

$$P = \frac{2R_0^2}{n^2 B_{\varphi}^2}\int_0^{r_0} \frac{r^2}{r_0^4}\left(-\frac{dp}{dr}\right) dr$$

where r_0 is the radius of the surface $nq(r_0) = 1$, $u_1(r)$ and $u_2(r)$ are respectively the regular solutions of :

$$\frac{1}{r}\frac{d}{dr} r \frac{du}{dr} - \frac{4u}{r^2} + 2\frac{Q'}{Q}\left(\frac{du}{dr} - \frac{u}{r}\right) = 0$$

within (o, r_0) and (r_0, r_1) with $Q = \frac{1}{nq} - \frac{1}{2}$, $Q(r_1) = 0$.

For n ∞, we recover the cylindrical approximation; since in general $\delta\tilde{W}_T$ is smaller than $\delta\tilde{W}_c$, it appears that this approximation is valid for $n \gg 2$; but for n = 1, the exact result is different at all.

$\delta\tilde{W}_T$ is a complicated function of q(r) in terms of s, b, c, but depends on the pressure only through P. For fixed q(r), $\delta\tilde{W}_T$ is a decreasing function of P, positive for P = 0 in the realistic cases. Therefore, the toroidal internal kink is stable, for sufficiently low P. For instance, for small $\Delta q = 1 - q(o)$, and a parabolic current profile, we obtain :

$$\delta\tilde{W}_T \sim 3\Delta q\left[\frac{13}{144} - P^2\right]$$

then the stability condition is $P < 0{,}30$.

In the figure the critical value of P is plotted as a function of r_0 for different shapes of the current profile.

The growth rate γ of the mode may be calculated by an extension of the method used in the cylindrical case. We find :

$$\gamma = \frac{\pi}{\sqrt{3}}\frac{v_A}{R_0^3} r_0 \left[q'(r_0)\right]^{-1}\left[-\delta\tilde{W}_T\right]$$

References.

1 V.D. Shafranov, Sov. Phys.-Tech. Phys., 15, 175 (1970).

2 M.N. Rosenbluth, R.Y. Dagazian, P.H. Rutherford, Phys. Fluids, 16, 1894 (1973).

3 A. Sykes, J.A. Wesson, Nucl. Fusion, 14, 645 (1974).

4 G. Bateman, W. Schneider, W. Grossmann, Nucl. Fusion 14 , 669 (1974).

5 G. Laval, R. Pellat, J.L. Soulé, Phys. Fluids, 17, 835 (1974).

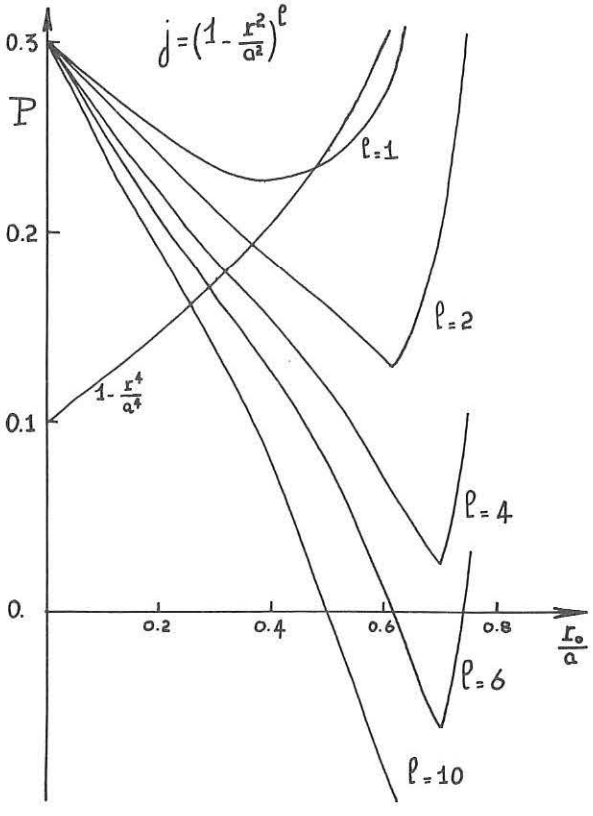

Critical pressure gradient for different shapes of the current profile, as a function of the radius where q = 1.

STABILITY OF TOKAMAKS WITH RESPECT TO 'SLIP' MOTIONS

E. Rebhan, A. Salat

Max-Planck-Institut für Plasmaphysik, 8046 Garching bei München,

Federal Republic of Germany

Abstract: Using the energy principle the stability of surface-current tokamaks is investigated with respect to perturbations which may not be stabilized by the toroidal main field. Wall effects are not included.

For given pressure profile and poloidal current distribution tokamak stability in general is a function of the external toroidal vacuum field $\Lambda_o \nabla\theta$ (coordinates are R,θ,z), the energy variation $\delta^2W=\delta W_{pl}+\delta W_s+\delta W_{vac}$ depends linearly and quadratically on Λ_o. The quadratic contribution in δW_{pl}: $\Lambda_o^2 \int \mathrm{curl}^2\ (\underline{\xi} \times \nabla\theta)\,d\tau$ is positive definite and hence most plasma motions may be stabilized (if unstable) by making Λ_o large enough. However, if curl $(\underline{\xi} \times \nabla\theta) = 0$ or

$$\underline{\xi} = R^2\ (\nabla\theta \times \nabla\phi) + \mu\ \nabla\theta, \qquad (1)$$

ϕ (R,z) and μ (R,θ,z) being arbitrary functions, all terms in δ^2W become independent of Λ_o. Perturbations given by (1) let the plasma 'slip' through the main field without any influence on it and may therefore not be stabilized by it. Minimization with respect to μ yields $\mu \not\equiv 0$. Further minimization with respect to ϕ is especially simple for the surface current model considered here.

Using dimensionless quantities we deal with equilibrium plasma surfaces given by

$$F\ (R,z) = a^2\ (R-1)^2 + (1+\tau_3{}^2)z^2 - 2A\tau_3\ (R-1)z^2 - A^2\tau_4\ \ (R-1)^2z^2 = \frac{e^2}{A^2} \qquad (2)$$

(A = aspect ratio, e = elongation in z-direction, τ_3, τ_4 = parameter for triangular, rectangular deformation.) Inside the plasma we have constant pressure $p = \frac{1}{2}\beta_p$ and vanishing poloidal magnetic field B_p. With $B_p = \frac{1}{R}\ (1+\beta_p\ (R^2-1)\ )^{1/2}$ on the surface and κ = curvature of the plasma boundary we get

$$\delta W_{pl} = \gamma\ \beta_p \int \phi_z^2\ d\tau, \qquad \delta W_{vac} = \frac{1}{2}\int (\underline{B}_p \cdot \delta\underline{B})\ \xi_n\ \ d\tau$$
$$\delta W_s = \frac{1}{2}\int \xi_n^2\ \left(\frac{1-\beta}{R^3}\ \frac{F_R}{\nabla F} - \kappa\ \frac{B^2}{p}\right) d\tau \qquad (3)$$

It is useful to split the normal component ξ_n of the displacement vector into symmetric and antimetric contributions with respect to the z = 0 plane: $\xi_n = \xi_n^s + \xi_n^a$. The minimizing perturbations inside the plasma corresponding to ξ_n^s and ξ_n^a have the form

$$\underline{\xi}^s = f(R)\underline{e}_z\ , \qquad \underline{\xi}^a = g\ (R)\ \underline{e}_R - R\ \left(\frac{\beta}{R}\right)' z\ \underline{e}_z\ , \qquad (4)$$

After transformation of δW_{pl} into a surface integral δ^2W is minimized numerically, the perturbational vacuum field $\delta\underline{B}$ being calculated from an integral equation, /1/. The numerical method closely follows /2/.

In Figs. 1-5 numerical results are shown. In Fig. 2, the marginal boundary $\delta^2W = 0$ is shown in an e, τ_3 and e, τ_4 plane for ξ_n^s (curve W_s), for ξ_n^a (W_a) and, for comparison, for rigid vertical displacements (W_r). Below the curve W_s and above the curves W_a and W_r we have instability. Thus, only a small region in the neighbourhood of circularity is stable, this region widing up for decreasing A. As $A \to \infty$ this region shrinks to the point $e = 1$, $\tau_3 = \tau_4 = 0$, in agreement with analytical calculations for straight cylindrical plasmas/3,4/. Fig. 3 shows these regions of stability in dependence of the aspect ratio. In Fig. 1 the minimizing perturbations (4) are shown for several unstable situations. Fig. 4 shows the dependence of the stability regions on β_p. The maximum values of β_p which may be reached are shown in Fig. 5 as a function of the aspect ratio, together with the limiting values of β_p from equilibrium considerations.

/1/ REBHAN E., Nuclear Fusion, (1975) to be published

/2/ MARTENSEN E., Acta Mathematica, 109 (1963) 75

/3/ RUTHERFORD P., Princeton, MATT-976, April 1973

/4/ LAVAL G., PELLAT R., SOULE J.L., Phys. Fluids, 17 (1974) 835

"This work was performed under the terms of the agreement on association between the Max-Planck-Institut für Plasmaphysik and EURATOM".

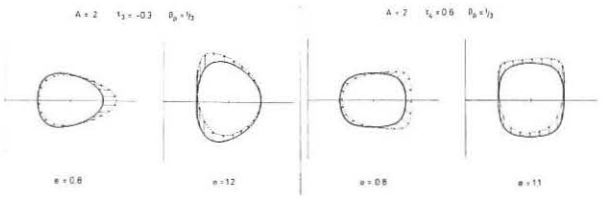

Fig. 1

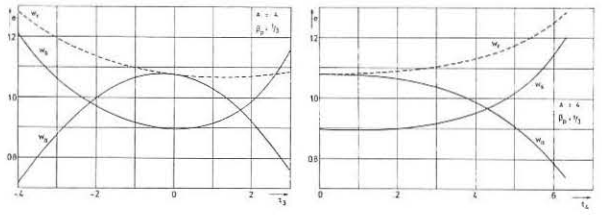

Fig. 2

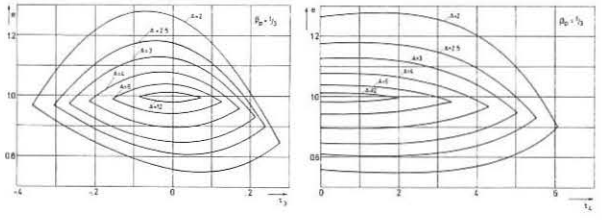

Fig. 3

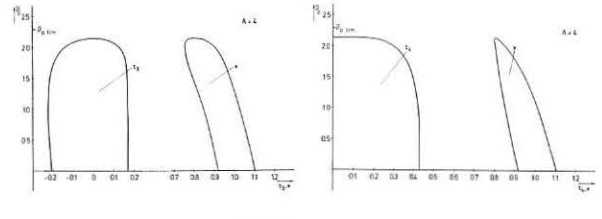

Fig. 4

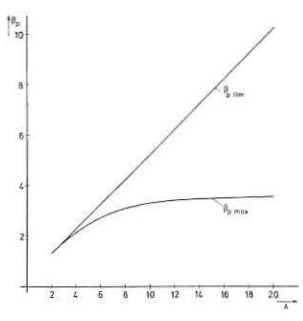

Fig. 5

STABILITY OF AN AXISYMMETRIC TOROIDAL PLASMA WITH PRESSURE ANISOTROPY

J W Connor and R J Hastie

Euratom-UKAEA Association for Fusion Research
Culham Laboratory, Abingdon, Oxon, OX14 3DB, UK

Abstract: The stability of a general axisymmetric toroidal plasma to localised perturbations is analysed when the pressure is anisotropic. Two limiting cases, corresponding to parallel and perpendicular injection of a neutral beam, are examined in detail for a large aspect ratio ($\epsilon \ll 1$) $\beta \sim \epsilon^2$ equilibrium with circular magnetic surfaces.

I. Introduction

The application of neutral injection heating to Tokamak plasmas will inevitably introduce some pressure anisotropy, and in the TCT scheme with $\Gamma \sim 1$ (where Γ is the ratio (beam energy density)/(plasma energy density)) this effect may be strong. In addition sufficiently high fluxes of high energy runaway electrons also produce significant pressure anisotropy. In this paper we examine the effect of unequal pressure components $(p_\parallel, p_\perp)$ on the localised interchange modes[1-4] in Tokamak plasmas. The starting point is the Kinetic Energy Principle[5-6], suitably modified to take account of trapped particles[7].

We use the ψ, χ, φ coordinates,

$$\nabla = \underset{\sim}{e}_\psi \, RB_\chi \frac{\partial}{\partial \psi} + \frac{\underset{\sim}{e}_\chi}{JB_\chi} \frac{\partial}{\partial \chi} + \frac{\underset{\sim}{e}_\varphi}{R} \frac{\partial}{\partial \varphi} \tag{1}$$

used by Mercier[1] for the original axisymmetric ideal MHD calculation, and by Mercier and Cotsaftis[8] in their anisotropic calculation using the CGL equations.

We avoid the CGL equations here because the collisionless kinetic equations provide a more correct description of Tokamak plasmas, and permit a description including trapped particle effects. In addition they are simpler to use and in fact all the minimisations which appear in the general isotropic case can be performed in the Kinetic Energy Principle, so that the final criterion obtained below is an analogue of the Mercier criterion and reduces to it (apart from a trapped particle correction) in the isotropic limit.

In practice two extremes of pressure anisotropy are likely to be encountered:

(1) An excess of longitudinal pressure $p_\parallel$, due either to parallel injection of a neutral beam, or to runaway electrons.

(2) An excess of perpendicular presure $p_\perp$, resulting from perpendicular injection.

In case (1) the additional pressure will be almost constant along magnetic field lines, and will not weigh in favour of either good or bad curvature. In this case we would expect the Mercier-Shafranov criterion ($q^2 > 1$) to be little modified.

In case (2), injection of a sufficiently narrow (in angle) beam into the trapped region of velocity space can create a $p_\perp$ component which is likely to weigh in favour of weak field regions, and therefore bad curvature. More detailed calculations confirm these intuitive conclusions.

II. Method and General Result

The method adopted is that first described by Greene and Johnson[4], in which a small parameter, δ, is introduced to describe the degree of localisation of the perturbations, so that

$$\underset{\sim}{\xi} = \underset{\sim}{\xi}\left(\frac{\psi - \psi_0}{\delta}, \chi, \varphi\right) \tag{2}$$

and expanding $\underset{\sim}{\xi}$ in powers of δ, a systematic expansion of δW permits a complete minimisation to be performed.

Omitting all details we give the final stability criterion below.

$$\frac{\frac{1}{4}\left[q' + 2\oint \frac{j_\parallel JB}{R^2 B_\chi^2} d\chi\right]^2}{\oint \frac{JB^2 d\chi}{R^2 B_\chi^2 (1 - \sigma_-)}} - \oint \frac{j_\parallel^2 (1 - \sigma_-)}{R^2 B_\chi^2} Jd\chi - \oint \nu' \frac{j_\parallel (1 - \sigma_-)}{B} d\chi$$

$$- \oint \frac{\partial}{\partial \psi}(p_\perp + \tfrac{1}{2} B^2) \left\{ \frac{\frac{\partial p_\parallel}{\partial \psi} + \frac{p_\perp - p_\parallel}{B} \frac{\partial B}{\partial \psi}}{1 - \sigma_-} + \frac{\frac{\partial p_\perp}{\partial \psi} - \frac{2p_\perp + c}{B} \frac{\partial B}{\partial \psi}}{1 + \sigma_\perp} \right\} \frac{Jd\chi}{B^2} + T^2 > 0 \tag{3}$$

where the magnetic field is given by

$$\underset{\sim}{B} = B_\chi \hat{\underset{\sim}{e}}_\chi + \frac{I}{R} \hat{\underset{\sim}{e}}_\varphi ,$$

$$\nu = \frac{IJ}{R^2} , \quad \sigma_- = \frac{(p_\parallel - p_\perp)}{B^2} , \quad \sigma_\perp = \frac{(2p_\perp + c)}{B^2}$$

$c = \sum_\sigma m \iint \frac{B}{|v_\parallel|} (\mu B)^2 \frac{\partial F}{\partial \epsilon} d\mu d\epsilon$. Prime denotes differentiation with respect to ψ, and T^2 is a complicated expression involving only the trapped particles.

III. Application to a large aspect ratio Tokamak

In this section we examine the form taken by criterion (3) for a Tokamak equilibrium with circular magnetic surfaces and $\beta \sim \epsilon^2$, where ϵ is the inverse aspect ratio. Expanding the equilibrium quantities in ϵ we find that the shift $\Delta(r)$ of the magnetic surfaces can be shown to satisfy the equation

$$\frac{d}{dr}\left(rB_\theta^2 \frac{d\Delta}{dr}\right) + \frac{r}{R} B_\theta^2 - \frac{r^2}{R} \frac{d}{dr}(p_\parallel + p_\perp) = 0 \tag{4}$$

while the stability criterion becomes:

$$\frac{1}{4}\left(\frac{q'}{q}\right)^2 + \frac{2}{rB_0} \bar{p}'\left(1 - \frac{3}{2} q^2\right) - \frac{1}{2} \frac{c'}{rB_0^2} q^2 > 0 \tag{5}$$

where $\bar{p} = \frac{1}{2}(p_\parallel + p_\perp)$ and the prime now denotes differentiation with respect to r.

(a) Longitudinal Injection

To simulate the effect of longitudinal injection or runaways we take $p_\perp = p_0(r)$, $c = -2p_0'$, $p_\parallel = p_0 + \hat{p}_\parallel$, so that p_0 is the scalar background pressure and $\hat{p}_\parallel$ the additional longitudinal component. Inequality (5) now becomes

$$\frac{1}{4}\left(\frac{q'}{q}\right)^2 + \frac{2p_0'}{rB_0^2}(1 - q^2) + \frac{\hat{p}_\parallel'}{rB_0^2}(1 - \tfrac{3}{2}q^2) > 0 \tag{6}$$

(b) Perpendicular Injection

To simulate the effect of perpendicular injection we choose a distribution of the form,

$$F = F_0(v^2) + y^n f(v^2) \tag{7}$$

where $y = \frac{v_\perp^2}{v^2}$, and F_0 represents the background plasma distribution function. With this choice

$$p_\perp = p_0 + \hat{p}_\perp , \quad p_\parallel = p_0 + \frac{\hat{p}_\perp}{(n+1)} ; \quad c = -2p_0 - (n+2)\hat{p}_\perp ,$$

and criterion (5) becomes

$$\frac{1}{4}\left(\frac{q'}{q}\right)^2 + \frac{2p_0'}{rB_0^2}(1 - q^2) + \frac{\hat{p}_\perp'}{rB_0^2} \frac{n+2}{n+1} \left[1 + \left(\frac{n-2}{2}\right) q^2\right] > 0 \tag{8}$$

Conclusions

It is clear from equation (6) that, provided the density gradient of the injected beam is in the same sense as that of the plasma, longitudinal injection has a stabilising influence for $q \gtrsim 0.8$. However for perpendicular injection, assuming $\Gamma = 1$, and $(\partial \ell n \hat{p}_\perp)/(\partial \ell n p_0) = 1$ the pressure gradient terms in (8) are only stabilising if

$$q^2 \left[12 + 4n - \frac{3}{2} n^2\right] > 7n + 12 \tag{9}$$

which requires $q \gtrsim 3$ for $n = 4$, and is impossible to satisfy for larger values of n.

Recalling that the effect of resistivity is to remove the shear stabilisation of interchange modes, we conclude that perpendicular injection might make a tokamak plasma prone to the resistive interchange mode.

References

1. Mercier, C. Nuclear Fusion 1, 1, 47 (1960).
2. Bineau, M. Nuclear Fusion Supplement Part 2, 809 (1962).
3. Mercier, C. Nuclear Fusion Supplement Part 2, 801 (1962).
4. Greene, J.M. and Johnson, J.L. Physical Fluids 5, 5, 510 (1962).
5. Rosenbluth, M.N. and Rostoker, N. Physics of Fluids 2, 23 (1959).
6. Kruskal, M.D. and Oberman, C.R. Physics of Fluids 1, 275 (1958).
7. Connor, J.W. and Hastie, R.J. Phys Rev Letts 33, 202 (1974).
8. Mercier, C. and Cotsaftis, M. Nuclear Fusion, 1, 121 (1961).

MHD TURBULENCE THEORY AND ITS IMPLICATIONS FOR THE REVERSED FIELD PINCH

C G Gimblett and M L Watkins

Culham Laboratory, Abingdon, Oxfordshire, England
(Euratom/UKAEA Fusion Association)

Abstract: Developments in MHD turbulence theory have identified two primary phenomena [1]. First, an electromotive force aligned with the mean magnetic field can be produced; second, a turbulent diffusivity is created. We apply a model of these effects to the 'self-reversal' of magnetic field observed in a number of plasma pinch experiments [2].

1. Derivation of the Mean Field Model. If the magnetic, $\underline{B}$, and velocity, $\underline{v}$, fields are expressed as the sum of a mean and fluctuating component, we derive eqs.(1) from Faraday's induction equation coupled with a simple Ohm's law

$$\frac{\partial \bar{\underline{B}}}{\partial t} = \nabla \times (\bar{\underline{v}} \times \bar{\underline{B}}) + \nabla \times \overline{(\underline{v}' \times \underline{b}')} + \eta \nabla^2 \bar{\underline{B}} \quad , \quad \nabla . \bar{\underline{B}} = 0 \qquad (1a)$$

$$\frac{\partial \underline{b}'}{\partial t} = \nabla \times (\bar{\underline{v}} \times \underline{b}') + \nabla \times (\underline{v}' \times \bar{\underline{B}}) + \nabla \times (\underline{v}' \times \underline{b}') - \nabla \times \overline{(\underline{v}' \times \underline{b}')} + \eta \nabla^2 \underline{b}' \quad , \quad \nabla . \underline{b}' = 0 \quad . \qquad (1b)$$

An overbar represents an ensemble average [3]. We assume the plasma to be incompressible ($\nabla . \underline{v} = 0$) with zero mean velocity, $\bar{\underline{v}} = \underline{0}$, and the magnetic Reynolds number of the turbulence to be large ($R_m^T = \frac{|\underline{v}'|\ell}{\eta} \gg 1$, where η is the magnetic diffusivity and ℓ is a length characteristic of the turbulence). We integrate (1b) with respect to time and form an expression for $\overline{\underline{v}' \times \underline{b}'}$. This expression simplifies if we assume that $\bar{\underline{B}}(\underline{x},t)$ does not change significantly over the correlation time of the turbulence, and that third order correlations between fluctuating components may be neglected. We obtain

$$\overline{(\underline{v}' \times \underline{b}')}_i = a_{ij} \bar{B}_j + b_{ijk} \frac{\partial \bar{B}_j}{\partial x_k} \quad , \qquad (2a)$$

where

$$a_{ij} = \epsilon_{ipm} \int_0^\infty \overline{v_p'(\underline{x},t) \frac{\partial}{\partial x_j} v_m'(\underline{x},t-T)} dT \quad ; \quad b_{ijk} = \epsilon_{ijp} \int_0^\infty \overline{v_p'(\underline{x},t) v_k'(\underline{x},t-T)} dT \quad . \qquad (2b,2c)$$

For isotropic turbulence the correlation tensors appearing in eqs.(2b, 2c) must be isotropic with the result that the eq.(1a) may be expressed as

$$\frac{\partial \bar{\underline{B}}}{\partial t} = -\nabla \times \bar{\underline{E}} \quad , \quad \bar{\underline{E}} = -\alpha \bar{\underline{B}} + \eta_T \nabla \times \bar{\underline{B}} \quad , \quad \eta_T = \eta + \beta \quad . \qquad (3a,3b,3c)$$

where

$$\alpha = -\frac{1}{3} \int_0^\infty \overline{\underline{v}'(\underline{x},b) . \nabla \times \underline{v}'(\underline{x},t-T)} dT \quad ; \quad \beta = +\frac{1}{3} \int_0^\infty \overline{\underline{v}'(\underline{x},t) . \underline{v}'(\underline{x},t-T)} dT \quad . \qquad (3c,3d)$$

A schematic illustration of the 'α effect' is given in Fig.(1). The above derivation follows an account given by P H Roberts [4].

2. Application of the Model to the Reversed Field Pinch. We solve eqs. (3a,3b) in an infinitely long circular cylinder in which the magnetic field is represented by $\bar{\underline{B}}(r,t) \equiv (0, \bar{B}_\theta(r,t), \bar{B}_z(r,t))$ and satisfies : (i) $\bar{\underline{B}}(r,o) \equiv (0, I_o r, B_o)$; (ii) $\bar{B}_\theta$ constant at plasma surface, r = a ; (iii) $\bar{B}_z$ flux conserved. The solutions required are

$$\frac{\bar{B}_z(x,\tau)}{B_o} = 1 - \frac{2\theta}{s} + \frac{\theta J_o(sx)}{J_1(s)} + \sum_{n=1}^{\infty} C_n^+ J_o(\gamma_n x) \quad , \qquad (4a)$$

$$\frac{\bar{B}_\theta(x,\tau)}{B_o} = \frac{\theta J_1(sx)}{J_1(s)} + \sum_{n=1}^{\infty} C_n^- J_1(\gamma_n x) \quad , \qquad (4b)$$

where

$$C_n^\pm = \frac{s\theta}{\gamma_n J_o(\gamma_n)} \left\{ \frac{\exp[-\gamma_n(\gamma_n - s)\tau]}{(\gamma_n - s)} \pm \frac{\exp[-\gamma_n(\gamma_n + s)\tau]}{(\gamma_n + s)} \right\} . \qquad (4c)$$

J_o, J_1 are respectively the zero and first-order Bessel functions of the first kind and γ_n satisfies $J_1(\gamma_n) = 0$, n = 1,2,3,... We have introduced the normalized variables, x and τ, the 'pinch ratio' θ [5], and the 'structure parameter', s, defined as

$$x = r/a, \quad \tau = \eta_T t/a^2, \quad \theta = \bar{B}_\theta(1,\tau)/B_o = I_o a/B_o \quad , \quad s = a\alpha/\eta_T \quad . \qquad (5a,b,c,d)$$

If $\beta \gg \eta$, eqs.(3c,3d,5d) show that s is a measure of the inverse correlation length, $s \sim a/\ell_c$. If

$$s < \gamma_1 = 3.83 \quad , \qquad (6)$$

the field relaxes to a steady state configuration on the timescale a^2/η_T. Fig.2 illustrates the temporal development of the mean magnetic field. The value chosen for θ gives a final configuration in which the 'field reversal' parameter, $F_\infty = \bar{B}_z(1,\infty)/B_o$, can be negative.

The case $2\theta = s$ gives the force-free Bessel function model [6]. If we assume that the final states satisfy the pressure balance equations: $\underline{J} \times \bar{\underline{B}} = \nabla \bar{p}$, $\bar{p}(a) = 0$, a measure of the deviation of the configuration from the force-free state may be represented by the β_θ^* value defined as

$$\beta_\theta^* = \frac{4\mu}{a^4 I_o^2} \int_0^a r\bar{p}\, dr = \frac{2 J_2(s)}{J_1(s)} \left(\frac{2\theta - s}{s\theta} \right) \quad . \qquad (7)$$

In Fig.3, states in regime I violate eq.(6), while those in regime II correspond to $\bar{p}(r) < 0$, $0 \le r \le a$. States in regime III exhibit field reversal, while those in regime IV do not. We note that a steady-state, reversed-field configuration can exist for $\theta \gtrsim 1.2$, $s < 3.83$. As β_θ^* increases, so does the value of θ at which reversal can first occur. Fig.4 shows loci of β_θ^* and total mean magnetic energy in the $\{F_\infty, \theta\}$ plane.

3. Summary. The kinematic effect of turbulence which is isotropic but lacks mirror symmetry is to modify the Ohm's law applicable in a plasma. The total power input to the plasma is modified as a result of both the increase in the effective resistivity (the 'β-effect') and the generation of an electric field aligned with the mean magnetic field (the 'α-effect'). Application of this model to the reversed field pinch indicates that a steady-state solution can exist and is represented uniquely by the pinch ratio, θ, and the structure parameter, s. In the case of infinite conductivity and zero β_θ^*, the pinch ratio may be linked to the structure of the turbulence through $\theta \sim a/2\ell_c$.

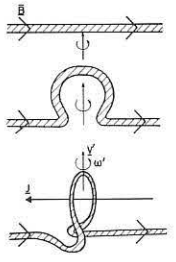

Fig.1. A schematic illustration of the 'α-effect'. Fluid motions with $\underline{v}'$ and $\underline{\omega}' = \nabla \times \underline{v}'$ correlated (that is, with helicity [7]) deform a slab of magnetic field to produce a loop with an associated current aligned with the mean magnetic field (after E.N.Parker [8]).

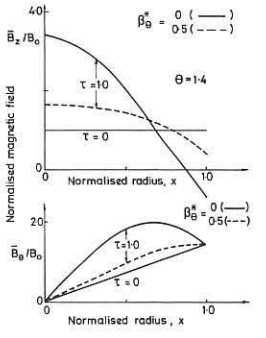

Fig.2. The temporal development of the mean magnetic field $\bar{\underline{B}} = (0, \bar{B}_\theta, \bar{B}_z)$.

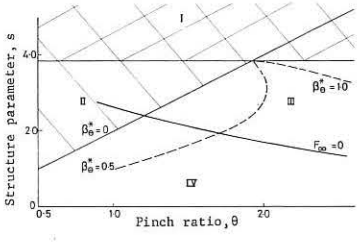

Fig.3. Operational regimes in the $\{s,\theta\}$ plane.

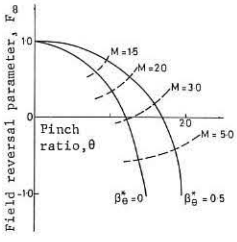

Fig.4. Loci in the $\{F_\infty, \theta\}$ plane of β_θ^* and normalized magnetic energy, M.

References

[1] Krause, F., Rädler, K H., and Steenbeck, M. (1971). 'The Turbulent Dynamo'. (Translated by P H Roberts and M Stix). Technical Note NCAR-TN/IA-60, National Centre for Atmospheric Research, Boulder.

Moffatt, H K. (1970). J.Fluid Mech. 41, 435.

[2] Butt, E P et al. (1958). Proc.2nd Int.Conf.on the Peaceful Uses of Atomic Energy, Geneva 32, 42.

Butt, E P et al. (1974). Proc.5th Int.Conf.on Plasma Physics and Controlled Nuclear Fusion Research, Tokyo, IAEA/CN33 E9-2.

[3] Batchelor, G K. (1953). 'The Theory of Homogeneous Turbulence'. Cambridge University Press, Cambridge.

[4] Roberts, P H (1971). 'Dynamo Theory'. In 'Mathematical Problems in Geophysical Sciences'. (Ed. W H Reid), Am.Math.Soc.

[5] Bodin, H A B et al. (1971). Proc.4th Int.Conf.on Plasma Physics and Controlled Nuclear Fusion Research, Madison 1, 225.

[6] Taylor, J B. (1974). Phys.Rev.Lett. 33, 1139.

[7] Moffatt, H K. (1969). J.Fluid Mech. 35, 117.

[8] Parker, E N. (1955. Astrophys.J. 122, 293.

THE EFFECT OF F.L.R. ON A ROTATING DIFFUSE PINCH

R.J. Wright, D.F.R. Pott, M.G. Haines
Imperial College, London, U.K.

Abstract: This article summarises a stability analysis based upon a dispersion equation derived initially from the Vlasov equation. Numerical solution of the equation indicates the influences of F.L.R. anisotropic pressures, sheared axial velocity, heat flow and rotation.

The Dispersion Equation: Defining ε as the ratio of the ion Larmor radius to plasma radius, the fluid modes which arise in the stability of a diffuse pinch in which $B_\theta \sim \varepsilon\sqrt{\beta}\, B_z$ [1] can be shown [2] to obey the equation:

$$\frac{d}{dr}\left(\frac{Fd\xi}{dr}\right) + G\xi = 0 \qquad \text{where:}$$

$$F = \rho r^3 \omega_1^2 + r^3\left(k + \frac{mB_\theta}{rB_z}\right)^2 \left(\sum_{\text{species}}(P_{//} - P_\perp) - \frac{B_z^2}{\mu_o}\right)$$

$$- m\omega_1 r^2 \frac{d}{dr}\left(\frac{P_\perp^i}{\Omega^i}\right) + \frac{mr^2}{\Omega^i}\left(k + \frac{mB_\theta}{rB_z}\right)\left(P_\perp^i \frac{du_z}{dr} + \frac{d}{dr} q_z^{\perp i}\right)$$

$$+ \frac{mr^2}{\Omega^i B_z}\frac{dB_z}{dr}\left(k q_z^{\perp i} + \frac{m}{2r} q_\theta^{\perp i}\right)$$

$$G = -\frac{(m^2-1)}{r^2} F + r^2 \frac{d\rho}{dr}\left(\omega_1 - \frac{mu_\theta}{r}\right)^2$$

$$+ k^2 r^2 \frac{d}{dr}\left(\sum_{\text{species}}(P_{//} - P_\perp) - \frac{B_z^2}{\mu_o}\right)$$

The Case of Anisotropic Pressure: It can be shown from the dispersion equation with only anisotropic pressure unsuppressed that the Suydam criterion at a resonant surface becomes:

$$\left(\frac{d\mu/dr}{\mu}\right)^2 + \frac{4}{r}\,\frac{\frac{d}{dr}\left(\sum_{\text{species}}(P_{//} + P_\perp)\right)}{\frac{B_z^2}{\mu_o} - \sum_{\text{species}}(P_{//} - P_\perp)} > 0$$

where $\mu = r_x B/rB_z$ with r_x conveniently being the wall radius. In Fig. 1 the influence of F.L.R. on the growth rate spectrum of modes now including m = 1, is shown for anisotropic pressure driven instabilities with $P_{//}/P_\perp = 10$ and $\beta = .5$.

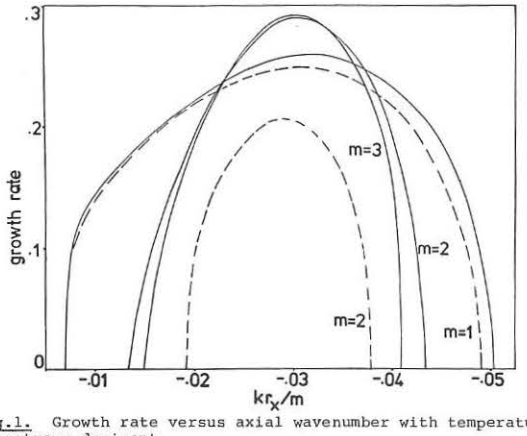

Fig.1. Growth rate versus axial wavenumber with temperature anisotropy dominant.
Solid Lines: $T_\perp^i = 0$. Broken Lines: $KT_\perp^i/(eBr_x^2) = .03$.
$\frac{nK\Sigma T_\perp}{B^2/2\mu_o} = .5$, $\frac{K\Sigma(T_{//} - T_\perp)^{\frac{1}{2}}}{M^i r_x^2} = 15$, $n = \exp(-.5(r/.3r_x)^2)$
$\mu = .01/(.25 + (r/r_x)^2)$, relative to $B/(\sqrt{\rho_x \mu_o}\, r_x) = 10$.

E x B Rotation on Suydam Modes: In Fig. 2 we show the influence of varying F.L.R. on the growth rate for a plasma rotating parallel and anti-parallel to the diamagnetic rotation. We note in the former case that there is a maximum growth rate due to the increase in total rotation, but larger F.L.R. stabilies both cases. In this, k was chosen so as to approximately maximise the growth rate.

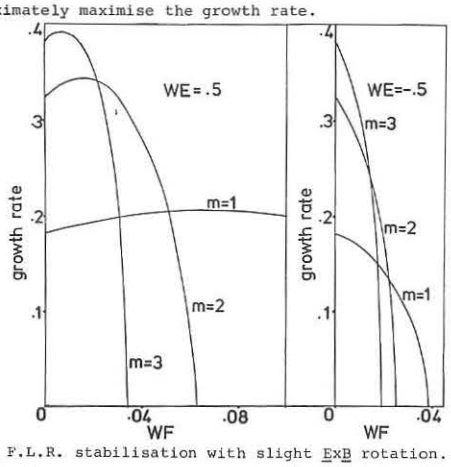

Fig.2. F.L.R. stabilisation with slight ExB rotation. $kr_x/m = -.028$. $n_x K\Sigma T_\perp/(B^2/2\mu_o) = .5$, $n = \exp(-.5(r/r_x)^2)$, $\mu = .01/(.25 + (r/r_x)^2)$, relative to $B/(r_x\sqrt{\rho_x\mu_o}) = 10$.

Radial Dependence of Eigenfunctions: In the context of analytic results, it is pertinent to investigate the radial structure of Suydam modes. Fig. 3 illustrates the progressive localisation of the eigenfunctions with increasing m. The real and imaginary parts are shown for a case with small F.L.R. present. Evidently the important m = 1 mode violates localised approximations [3] thus requiring complete integration between the boundaries.

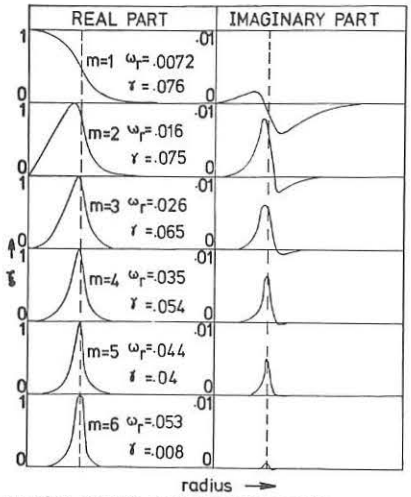

Fig. 3. Complex Suydam Eigenfunctions with

$$\left(\frac{KT_\perp^i}{eBr_x^2}\right)\Big/\left(\frac{B}{r_x\sqrt{\rho_x\mu_o}}\right) = .0002.$$

References:

(1) E.C. Bowers, Journal of Plasma Physics. 6, 80, (1971).

(2) R.J. Wright, D.F.R. Pott, M.G. Haines. (To be published).

(3) T.E. Stringer, Nuclear Fusion. 15 125 (1975).

CURRENT FILAMENTATION IN THE DIFFUSE PINCH

M.G. Haines and A. Tomimura
Physics Department, Imperial College, London, England

Abstract: Numerical solutions of the momentum and energy equilibria in a two temperature diffuse pinch show that it is possible for the electron temperature to have a radially oscillating component with a wavelength of the order of $a_e(m_i/m_e)^{\frac{1}{2}}$ where a_e is the electron Larmor radius. The necessary condition is that $T_e > 1.32T_i$ which is also the condition for the onset of an electrothermal instability in a spatially homogeneous plasma with the same optimum wavelength for growth.

Energy and Momentum Equilibria: We consider a steady state cylindrical equilibrium of a magnetically confined plasma with only radial dependence of parameters. Most of the calculations have been carried out with classical transport coefficients, but some have been made with neoclassical coefficients. The former may be written as follows:

(1) Electron energy: $\frac{j^2}{\sigma} = \frac{3n^2e^2K}{m_i\sigma}(T_e-T_i) - \frac{1}{r}\frac{\partial}{\partial r}\left(\frac{r\kappa_e\partial T_e/\partial r}{1+\Omega_e^2\tau_{ee}^2}\right) + R$

(2) Ion energy: $\frac{3n^2e^2K(T_e-T_i)}{m_i\sigma} = -\frac{1}{r}\frac{\partial}{\partial r}\left(\frac{r\kappa_i\partial T_i/\partial r}{1+\Omega_i^2\tau_{ii}^2}\right)$

(3) Pressure balance: $\frac{\partial}{\partial r}\ nK(T_e+T_i) = -\frac{j_z B_\theta}{c}$

(4) Ampere's Law: $\frac{1}{r}\frac{\partial}{\partial r}(rB_\theta) = \frac{4\pi}{c}j_z$

(5) Ohm's Law: $\sigma E_z = j_z$

(6) Faraday's Law: $\frac{\partial E_z}{\partial r} = 0$

where zero diffusion occurs due to the absolute steady state in which j_θ is zero. The classical temperature dependence of $\sigma, \kappa_e, \kappa_i$ are assumed.

By prescribing E_z, B_z, and values at r = 0 of T_e, T_i and n the equations can be integrated numerically by a Runga Kutta technique with the (initial) boundary condition at r = 0 of zero gradients of T_e, T_i and n. Depending on the relative values of these parameters four types of radial variation of T_e, T_i and n are obtained and are illustrated in figures 1 to 4. We employ dimensionless variables $N = n/n_o$, $t_e = T_e/T_{eo}$, $t_i = T_i/T_{eo}$ and $x = r/r_o$, the subscript $_o$ referring to values at r = 0, except for r_o which is an arbitary scale length. The integration proceeds until one of the parameters t_e or t_i go to zero. Iteration methods failed to find solutions for which t_e, t_i and n became zero at some radius which would define the plasma-wall boundary. Indeed it is found both computationally, and analytically by expansion in this region, that the equations only permit two types of solution, viz.,

(i) $t_e \to 0$ with $t_i \neq 0$, $n \neq 0$ as in figs 3 and 4.

(ii) $t_i \to 0$ with $t_e \neq 0$, $n \neq 0$ as in figs 1 and 2.

It could be that inclusion of some further physical processes might relax these conditions, but, as can be seen in the figures, the parameters that remain finite are not small at the wall and imply the tendancy for the plasma to have a finite pressure at the wall, i.e. the plasma is not confined.

If the equipartition and radiation terms are together larger than the Ohmic dissipation at r = 0 then $\partial^2T_e/\partial r^2$ is positive, resulting in curves characterized by figs 1 and 4. If these terms are smaller than Ohmic dissipation at r = 0, then $\partial^2T_e/\partial r^2$ is negative and curves of figs 2 and 3 pertain.

Whilst one might question the conclusions of the wall-boundary solutions because of the assumption of steady state and the neglect of other physical processes that might arise say, due to the presence of neutral particles, the interesting spatial variations of T_e and n are of more general validity. These spatial oscillations are probably the non-linear steady amplitude of an electrothermal instability, and their wavelength is approximately $2\pi a_e(m_i/m_e)^{\frac{1}{2}}$ where a_e is the electron Larmor radius. The Ohmic heating is dominant in the temperature peaks whilst the equipartition is large in the troughs and gives a much enhanced electron energy loss to the ions, perhaps being an explanation for the enhanced electron energy loss in Tokamaks.

Electrothermal instability with $\underline{k}$ perpendicular to $\underline{B}$ and $\underline{j}$. By considering the stability to electrothermal modes to radial wavenumbers $\underline{k}$ we modify the earlier theory of Haines which was for $\underline{k}$ parallel to $\underline{B}$. The obvious modification is that the electron thermal conductivity is reduced by $(1 + \Omega_e^2\tau_{ee}^2)$ so that if ion motion as well as ion temperature variations (unlikely on this scale length) are neglected, the optimum wavelength for growth is now approximately $2\pi a_e(m_i/m_e)^{\frac{1}{2}}$ with an additional factor of $(7.28)^{-1/4}$ for $\beta \ll 1$.

Solutions of the quintic dispersion equation which arises when ion motion is included show a similar optimum wavelength for growth. The equilibrium for the model is assumed flat with $\underline{j}_o \times \underline{B}_o = 0$ because the expected wavelengths are much shorter than characteristic equilibrium scale lengths. The instability occurs when $T_e > 1.32T_i$ and has a growth rate of order $\nu_{ei}\, m_e/m_i$ where ν_{ei} is the electron-ion collision frequency.

Related work. Furth et al have considered equilibrium profiles neglecting electron thermal conduction and pressure balance. In fact n(r) was specified to be proportional to $T_e(r)$. For flat profiles they included electron thermal conduction but in a similar way the boundary condition on the perturbed electron temperature failed at the wall. They noted however that in this case the highest order modes had the fastest growth rate. MacMahon and Ware employed neo-classical transport coefficients to obtain equilibria, but did not identify the problem of the wall boundary condition.

One of us (A.T.) is on leave from the Instituto Militar de Engenharia and partially financed by CAPES, Rio.

References

(1) Furth, H.P., Rosenbluth, M.N., Rutherford, P.M. and Stodiek, N. 1970 Phys. Fluids, 13, 3020.
(2) Haines, M.G., 1974 J. Plasma Physics, 14, 1.
(3) MacMahon, A.B. and Ware, A.A., 1973 Nuclear Fusion 13, 413.

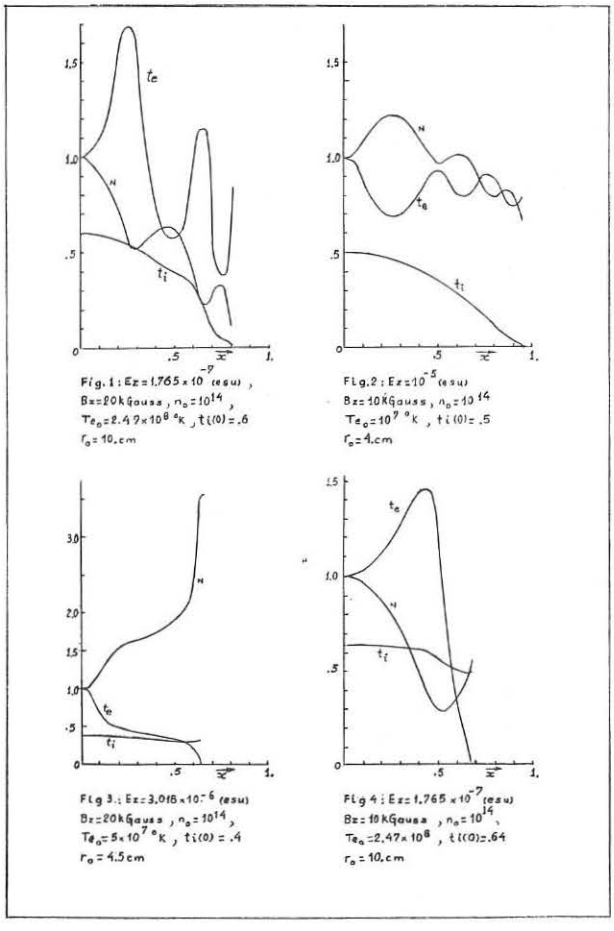

MAGNETO-VISCOUS RESISTIVE TEARING MODES IN CYLINDRICAL GEOMETRY

by

R. J. Hosking

University of Waikato, Hamilton, New Zealand†

Abstract: The direct use of moment equations to formulate plasma transport theory has led to a general form for the stress tensor. "Parallel" viscosity (ion-ion collisions) is likely to be most important at the high temperatures in thermonuclear devices, and it has been found that the resistive tearing mode in compressible plasma is considerably modified.

Introduction: Grad[1] first considered the direct use of moment equations in transport theory for gases, and Herdan and Liley[2] extended this approach to plasmas. There has been a tendency to overlook the generality of results obtained by this moment method, which is independent of assumptions such as no collisions or no magnetic field curvature common elsewhere in the literature.

Stress tensor: Hosking and Marinoff[3] have shown that a result due to Liley for the non-hydrostatic part of the stress tensor in a magneto-plasma may be expanded in terms of small parameter $(\omega_c\tau)^{-1}$, where ω_c is the cyclotron frequency and τ is the collision time, to yield contributions due to "parallel" viscosity, FLR and "perpendicular" viscosity as respective leading terms: i.e., when $\omega_c\tau \gg 1$ the stress tensor is

$$\underset{\sim}{p} = p\underset{\sim}{I} + \underset{\sim}{t} \quad , \qquad \underset{\sim}{t} = \underset{\sim}{t}_{\parallel} + \underset{\sim}{t}_{L} + \underset{\sim}{t}_{\perp} + \ldots \quad .$$

Hence the most important contribution is usually the "parallel" component

$$\underset{\sim}{t}_{\parallel} = -3\mu\, s(\underset{\sim}{b}\underset{\sim}{b} - \tfrac{1}{3}\underset{\sim}{I}) \quad ,$$

where

$$s = \underset{\sim}{s} : \underset{\sim}{b}\underset{\sim}{b}$$

† Presently attached to Culham Laboratory, Abingdon, Oxon. OX14, 3DB, UK.

and μ denotes the viscosity coefficient, $\underset{\sim}{b} = \underset{\sim}{B}/|\underset{\sim}{B}|$ the magnetic field direction, and $\underset{\sim}{s}$ the deformation tensor. The other contributions $\underset{\sim}{t}_{L}$ and $\underset{\sim}{t}_{\perp}$ are given in Ref. 3.

Assuming the simple deformation tensor (ion-ion collisions)

$$\underset{\sim}{s} = \tfrac{1}{2}(\nabla\underset{\sim}{v} + \underset{\sim}{v}\overleftarrow{\nabla}) - \tfrac{1}{3}\nabla\cdot\underset{\sim}{v}\,\underset{\sim}{I} \quad ,$$

one has

$$s = (\underset{\sim}{b}\cdot\nabla)(\underset{\sim}{v}\cdot\underset{\sim}{b}) - \underset{\sim}{v}\cdot(\underset{\sim}{b}\cdot\nabla)\underset{\sim}{b} - \tfrac{1}{3}\nabla\cdot\underset{\sim}{v} \quad .$$

Johnson et al.[4], [5] have shown that all the various terms in the resultant viscosity may be significant in toroidal confinement, and it has been emphasized that generally "parallel" viscosity should be most important in plasma stability theory[3], [6]. In particular, note that the viscosity depends on magnetic field curvature.

Resistive tearing modes: The resistive tearing mode in cylindrical geometry has been considered. For characteristic pinch parameters, numerical results were obtained for the increment in the logarithmic derivative $\Delta(Q)$ of the perturbed radial magnetic field over the (resistive) shock region as a function of the dimensionless growth rate Q. [7] A representative graph of $\Delta(Q)$ for compressible plasma is shown in the accompanying Figure, and it is notable that the viscosity introduces branch point behaviour. If Q_{crit} denotes the singular point, instabilities with relatively small growth $(Q < Q_{crit})$ may occur even when $\Delta < 0$, but larger potential growth rates $(Q > Q_{crit})$ are reduced. The value of Q_{crit} appears to decrease with temperature.

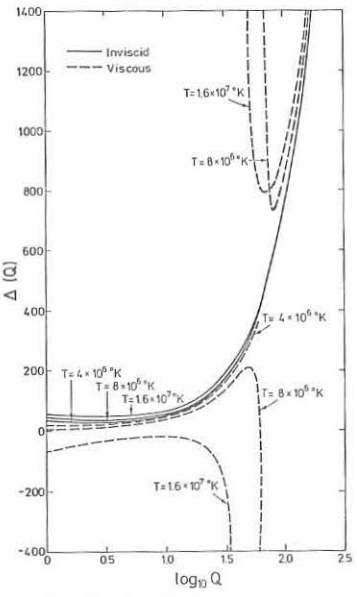

Figure Comparison of viscous and inviscid curves for $n=10^{21}\,m^{-3}(\gamma=5/3)$

A closed solution for $\Delta(Q)$ has since been obtained from Equations (33) - (35) of Ref. 7 : the solution is

$$\Delta(Q) = \frac{2\pi\,\Gamma(\frac{1-\nu}{2})}{\Gamma(-\frac{\nu}{2})}\,Q^{5/4} - \frac{\sqrt{\pi}\,\Gamma(\frac{1-\nu}{2})D\,I(\varepsilon,\tau)}{2^{(\nu+3)/2}\,\ell^6}\,Q^{-1/4}$$

where

$$\nu = -(a+\tfrac{1}{2}) \quad , \qquad a = (\frac{D}{3\gamma\beta} - \frac{S}{8})/(\varepsilon^2 - 2\tau) \quad ,$$

$$\varepsilon^2 = \frac{Q^{1/2}}{3V} \quad , \qquad \tau = \frac{2Q^{3/2}\ell^6}{9\gamma\beta} \quad ,$$

the factor $I(\varepsilon,\tau) \gtrless 0$ according as $Q \lesseqgtr Q_{crit} = \frac{3\gamma\beta}{4\ell^6 V}$ (except in the immediate neighbourhood of Q_{crit} where $\varepsilon^2 - 2\tau = 0$), and the other notation is the same. It is implicit that the pressure gradient and inverse shear parameters (viz., D and S respectively) are small, and that the temperature is fairly high $(\tau \lesssim \varepsilon^2 \ll 1)$.

The term proportional to $Q^{5/4}$ is that given by inviscid, incompressible theory when $\nu = -\frac{1}{2}$, but there is an additional viscous contribution (even in the incompressible limit $\tau \to 0$) proportional to $Q^{-1/4}$. The closed solution reproduces the main features of the results reported in Ref. 7, and in particular the identification of the singular point ($Q_{crit} = \frac{3\gamma\beta}{4\ell^6 V} \sim \mu^{-1}\,\eta^{-3/5}$, where η is the resistivity) confirms that it should decrease with temperature.

Conclusion: Plasma "parallel" viscosity depends on magnetic field curvature and therefore can be most important in plasma stability theory.

References:

(1) H. Grad, Communs. Pure Appl. Math. 2, 331 (1949).

(2) R. Herdan and B.S. Liley, Rev. Mod. Phys. 32, 731 (1960).

(3) R.J. Hosking and G.M. Marinoff, Plasma Phys. 15, 327 (1973).

(4) R.C. Grimm and J.L. Johnson, Plasma Phys. 14, 617 (1972).

(5) M.A. Hellberg, N.K. Winsor and J.L. Johnson, Phys. Fluids 17, 1258 (1974).

(6) R.J. Hosking and G.G. Lister, Plasma Phys. 15, 931 (1973).

(7) G.M. Marinoff, J. Plasma Phys. 11, 253 (1974).

COMPUTATIONS OF THE MAGNETOHYDRODYNAMIC SPECTRUM IN GENERAL AXISYMMETRIC TOROIDAL CONFINEMENT SYSTEMS*

J. L. Johnson,† M. S. Chance, J. M. Greene, R. C. Grimm, and W. Kerner
Princeton University Plasma Physics Laboratory, Princeton, N.J. 08540 USA

Abstract: A numerical program for studying the equilibrium and stability of general axisymmetric toroidal configurations is described and spectra are presented.

Equilibria are determined by solving the usual partial differential equation

$$X \frac{\partial}{\partial X} \frac{1}{X} \frac{\partial \Psi}{\partial X} + \frac{\partial^2 \Psi}{\partial Z^2} = - 2\pi X J_\phi = - 4\pi^2 \left(X^2 \frac{dp(\Psi)}{d\Psi} + \frac{R^2 B_o^2}{2} \frac{dg^2(\Psi)}{d\Psi} \right) \quad (1)$$

with the appropriate boundary condition that the poloidal flux Ψ vanishes along the major axis and far from the plasma. Here

$$\underset{\sim}{B} = \frac{1}{2\pi} \underset{\sim}{\nabla}\phi \times \underset{\sim}{\nabla}\Psi + RB_o g \underset{\sim}{\nabla}\phi \ , \quad (2)$$

$p(\Psi)$, $g(\Psi)$, and J_ϕ describe respectively the plasma pressure and the poloidal and toroidal current distributions, and X, ϕ, Z are the usual cylindrical coordinates. A typical configuration of interest consists of a toroidal plasma column surrounded by a vacuum region and supported by specified currents flowing in external conductors.

Knowing the poloidal flux surfaces $\Psi(X,Z)$, we construct a natural coordinate system ψ, θ, ϕ in which the ignorable variable is used as one coordinate, the second lies on magnetic surfaces, and the third is chosen so that the field lines are straight. This is accomplished numerically by fitting the $\Psi(X,Z)$ with two-dimensional cubic splines and reducing the problem to the integration of ordinary differential equations around the constant Ψ surfaces. Such equations can be derived from the identities

$$\frac{\partial X}{\partial \theta} = \frac{J}{X} \frac{\partial \psi}{\partial Z} \ , \quad \frac{\partial Z}{\partial \theta} = - \frac{J}{X} \frac{\partial \psi}{\partial X} \ . \quad (3)$$

For numerical convenience, we introduce a third r, θ, ϕ coordinate system centered on the magnetic axis and find

$$\partial\theta/\partial v\Big|_\Psi = - \frac{2\pi B_o f r}{\upsilon X(\partial\Psi/\partial X \cos\theta - \partial\Psi/\partial Z \sin\theta)} \quad (4)$$

from which θ can be determined. Here $f \equiv (d\Psi/d\psi)/2\pi B_o$ with B_o the externally imposed toroidal field at the magnetic axis R and $\upsilon \equiv (R/2\pi) \int_p d\tau/X^2 = 2\pi RJ/X^2$ with J the Jacobian. The condition that $\theta(2\pi) = 2\pi$ is used to determine f/υ. Similar equations for $X(\psi,\theta)$, $Z(\psi,\theta)$, and a function $T(\theta)$ that satisfies $\psi(\Psi) = T(2\pi)$ complete the problem of transforming to the operational system.

We introduce the Lagrangian to represent linearized motion about the equilibrium and use the Galerkin method to construct a matrix eigenvalue problem

$$\sum_m \left(\omega^2 < \underset{\sim}{\xi}_n^*, |K| \underset{\sim}{\xi}_m > - < \underset{\sim}{\xi}_n^*, |\delta W| \underset{\sim}{\xi}_m > \right) a_m = 0 \ , \quad (5)$$

where δW is the change in potential energy and $\omega^2 K$ is the kinetic energy associated with a displacement $\underset{\sim}{\xi} = \sum_m a_m \underset{\sim}{\xi}_m$. In order to separate the modes as much as possible, thus keeping the matrix diagonally dominant, we project the displacement vector into components along and perpendicular to the field to isolate the sound modes and then further decompose the perpendicular parts to separate the fast magnetosonic waves from the shear-Alfvén modes. Thus

$$\underset{\sim}{\xi} = (J\xi_\psi/gR^2B_o)\underset{\sim}{\nabla}\theta \times \underset{\sim}{B} + i(J\xi_s/gR^2B_o)\underset{\sim}{B} \times \underset{\sim}{\nabla}\psi + i(\tau/B_o)\underset{\sim}{B} \ ,$$

$$\xi_\psi = \delta - 2\pi i \partial\zeta/\partial\theta \ ,$$

$$\xi_s = 2\pi \partial\zeta/\partial\psi \ , \quad (6)$$

defines the components δ, ζ, and τ. With this decomposition we have been able to determine spectra accurately with eigenvalues varying over eight orders of magnitude. As expansion functions, we utilize a truncated Fourier series in θ and ϕ, noting that only one term in ϕ need be kept since the modes decouple. Finite elements are used to represent the ψ behavior. We treat the vacuum region by using Green's theorem to evaluate a scalar magnetic potential by integrating over the plasma-vacuum interface and the surface of a conducting wall (if it is present). A generalization of the global test-function approach for a particular class of equilibria [1] is being pursued in a complementary program.

As an application, we show in the figure the spectrum associated with a zero-pressure circular cylinder with constant current showing the wall stabilization of the kink mode. It is clear from the left-hand figure that the wall is ineffective unless it is very close to the plasma. We see this mode pass through the shear-Alfvén continuum and then join the fast magnetosonic branch. A small density spread is introduced for the central figure where we show the interaction with the continuous spectrum. Note that this spectrum has been discretized by the finite mesh. To show how the discrete modes can be identified, we plot the radial eigenfunction ξ_ψ as a function of ψ for several modes. Note that the continuous spectrum is characterized by the logarithmic behavior of this function near the singular surface. We have shown that when the coefficient of the logarithmic term vanishes, the associated eigenfunction has finite kinetic energy. Thus, it has the character of a discrete mode.

One of the greatest advantages of our method is that it can generate the whole spectrum of eigenvalues and eigenfunctions; this gives us a rather panoramic view of the properties of magnetohydrodynamics under different equilibrium conditions. This is of great use in integrating the existing analytical theories which are usually restricted to separate regions of the parameter space of the equilibrium. For example, it provides an understanding of how discrete modes can interact with the continua, how the unstable kink can become an integral part of the magnetosonic wave branch and how the interchange modes are intimately related to the continua.

* This work was supported by United States Energy Research and Development Administration Contract E(11-1)-3073. Use was made of computer facilities supported in part by National Science Foundation Grant NSF-GP 579.

† On loan from Westinghouse Research Laboratories, Pittsburgh, Pennsylvania, U.S.A.

[1] W. Kerner and H. Tasso in 5th Conference on Plasma Physics and Controlled Thermonuclear Research, Tokyo, Japan (1974), IAEA-CN-33/A13-1.

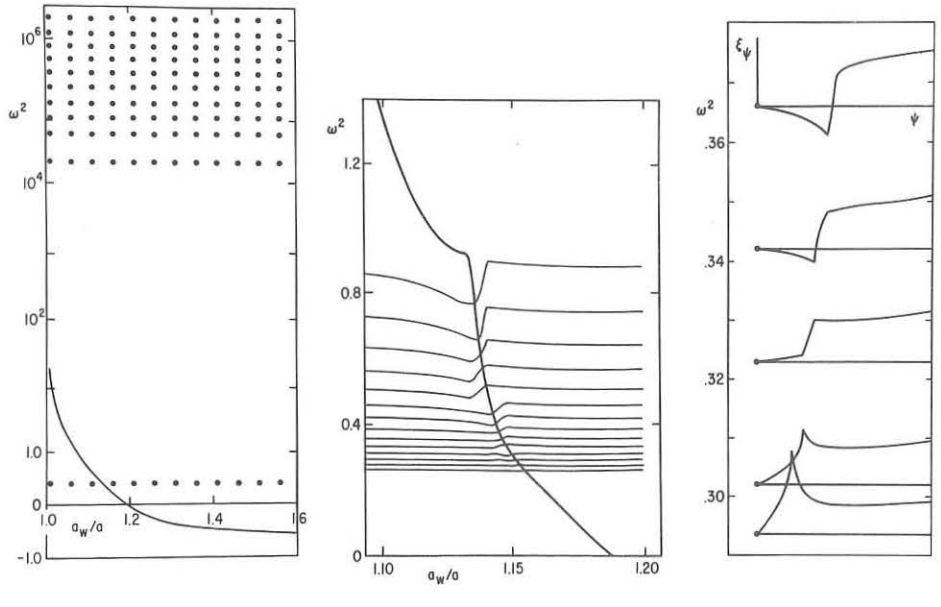

A GENERAL PURPOSE 2D CODE FOR THE COMPUTATION OF THE MHD SPECTRUM OF AN AXISYMMETRIC UNIAXED TOROIDAL CONFIGURATION

R. Gruber, K. Appert, D. Berger, F. Debonneville, F. Troyon

Ecole Polytechnique Fédérale de Lausanne - Switzerland
Centre de Recherches en Physique des Plasmas

Abstract: A full 2D code, which computes the ideal MHD spectrum of an axisymmetric toroidal plasma is described. It utilizes a finite element approach, generalizing a successfull 1D version. The numerical results are compared with exact analytical calculations in a straight elliptical configuration.

1. Introduction:

The computation of the ideal MHD spectrum of a straight cylindrical geometry of circular cross-section can be done either by direct integration of the ordinary second-order differential equation of Hain and Lüst or by variation of the Lagrangian $\mathcal{L} = \delta W - \omega^2 K$, where δW is the usual potential energy and $\omega^2 K$ the kinetiy energy. A finite element approach to the variational problem which is non-polluting and allows a good representation of the continuum as well as of the discrete part of the spectrum has been already described [1]. We have extended this method to toroidal axisymmetric equilibria having only one magnetic axis. Using the expression of δW given by Mercier [2] the Lagrangian may be written as:

$$\mathcal{L} = \iint d\psi d\chi \frac{1}{J}\left\{\frac{1}{B^2 r^2}\left[F(X)\right]^2 + \frac{T^2}{r^2}\left[D - \frac{r^2}{T}F(Y) + r^2 0\left(\frac{1}{r^2}\right)\right]^2 + B^2\left[D - J\,F(Z) + J0\left(\frac{1}{J}\right) + \frac{jX}{JB^2 r}\right]^2 + \right.$$

$$\left. + \gamma p\, D^2 - 2K\, X^2\right\} + \delta W_{VAC}\,(X_s) - \omega^2 \iint d\psi d\chi p\left\{\frac{X^2}{JB^2 r^2} + \frac{r^2}{J}\, Y^2 + JB^2 Z^2\right\}$$

where:

$$F = \frac{\partial}{\partial\chi}\,\frac{1}{J} + in\,\frac{T}{r^2} \qquad D = \frac{\partial X}{\partial\psi} + inY + \frac{\partial Z}{\partial\chi}$$

$$0 = X\,\frac{\partial}{\partial\psi} + Z\frac{\partial}{\partial\chi} \qquad K = \frac{T}{r^2}\,\frac{dT}{d\psi}\,\frac{\partial \log r}{\partial\psi} - \frac{j}{r}\,\frac{\partial \log JB}{\partial\psi}$$

X, Y and Z are related to the displacement ξ through $X = JBr\xi_\psi$, $Y = \frac{J}{r}\xi_\phi$, $Z = \xi_\chi/B$, χ is the azimuthal coordinate orthogonal to ψ and the ϕ variation has been taken as $\exp(in\phi)$, J is the Jacobian, B and T/r the poloidal and toroidal fields, j the current density and p the pressure. The vacuum contribution to the potential energy δW_{VAC} can be expressed in terms of X on the surface by solving Maxwell's equations in the vacuum region.

2. Discretization:

We discretize the variational problem using the finite element approach. As in the 1D case great care has to be exercized in the choice of finite elements if the low frequency part of the spectrum is to be well represented. In the Tokomak regime where $rp^{\frac{1}{2}}/T \sim rB/T \sim a/R$ (a=radius of the plasma column) the low frequency modes are almost incompressible which means $D \approx 0$ and they are localized in the region where $F \approx 0$. For a general choice of elements it will not be possible to have D=0 identically over a cell. δW will then receive from each cell a positive contribution from the second term which is multiplied with the large coefficient T^2/r^2. This leads to a strong coupling of the low frequency modes with the fast modes resulting in a large positive frequency shift (stabilization) and spectral pollution. To improve the accuracy would require an impractical small mesh size, scaling as a (Br/T).

We have chosen the following solution for the the elements:
For X a product of linear functions of ψ and χ, for Y piecewise constant functions in ψ and linear dependency in χ, and for Z a product of a piecewise constant function of ψ and a quadratic function of χ. With this choice of elements on each cell D is piecewise constant in ψ and linear in χ. In any mesh cell D=0 implies then two linear relations between the X, Y and Z coefficients.

F is an algebraic operator in the 1D case. In the 2D case, with our choice of elements, F cannot vanish identically on a mesh cell. This may lead to some spectral pollution but contrary to the ψ pollution of the 1D case it has not led to any problems.

To test the usefulness and the efficiency of the code we have solved some problems for which there are exact analytical results to compare with.

3. Results:

We consider a straight ($r \to \infty, \frac{n}{r} = k$) cylindrical plasma column of elliptical cross-section imbedded in a uniform axial field $B_z = T/r$ with a uniform current density j, and a constant density ρ. The plasma column is surrouded by a confocal elliptical conducting shell characterized by its short axis Ra. The plasma surface is characterized by the small axis a and by the large axis εa. The orthogonal system (ψ,χ) in the plasma is chosen as ($\varepsilon \geq 1$):

$$\psi = \frac{\psi_s}{a^2}\left(x^2 + \frac{y^2}{\varepsilon^2}\right), \qquad \frac{y^2}{x^2} = \frac{(\varepsilon \sin\chi)^2}{\cos\chi}, \qquad \psi_s = \frac{j\varepsilon^2}{2(1+\varepsilon^2)}.$$

In the vacuum we use an orthogonal system μ,χ defined by
$x = a(\varepsilon^2-1)^{1/2}\sinh\mu\cos\chi$, $y = a(\varepsilon^2-1)^{1/2}\cosh\mu\sin\chi$.
The vacuum contribution is evaluated by a Green function technique. The Green function is computed by a finite element representation. To test the validity of the basic concept we compare the numerical results with analytic results in various limits.

R=∞, j=0:

Analytic and numerical calculations have been performed by Dewar et al. [3] using the standard low-beta expansion, keeping only the lowest order (kink ordering). In our notation this corresponds to $R \to \infty, kR \to 0, j \to 0$.
Fig. 1 shows a comparison of the growthrates of the "m=1" external kink between the calculated values with j=.05, R=20 and the analytic results, for a circle and for an ellipse with ε=1.5. N_ψ=14 intervals in the ψ direction,

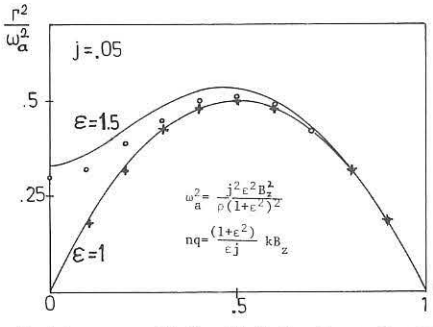

N_χ=16 azimuthal intervals in half the circumference and N_μ=10 intervals in the vacuum region has been used in these runs. The small discrepancy in the circular case for low k is due to the residual wall stabilization effect. Since, for a given R, this stabilizing effect increases with the ellipticity, it may also account for the increased discrepancy. The fact that the agreement improves as nq approaches 1 strongly suggests that the difference is due to the vacuum contribution.

ε=1, R=1:

For this circular case with a rigid boundary the results can be compared with the 1D calculations [1]. The unstable modes which exist around q=m provide a stringent test of the ability of the code to represent the internal kinks which arise with diffuse profiles. The growthrates of these modes are one order higher in the Tokamak expansion and are difficult to reproduce. To test the feasibility of representing such modes with a reasonable number of points we have looked at the modes m=1 at q=1. This is the worst case since F=0 over the whole plasma. Fig. 2 shows a quadratic convergence of the eigenvalue of the most unstable mode as a function of N_χ keeping N_ψ fixed. With this number N_ψ the 1D result is already converged. Comparing with the external kink we see that more points are indeed needed for these modes but that the convergence is still good. Looking at the full spectrum we have observed a pollution of the lowest fast modes by higher m Alfven modes but the "polluters" are easily identified by their azimuthal structure and they do not seem to interfere with the fast modes.

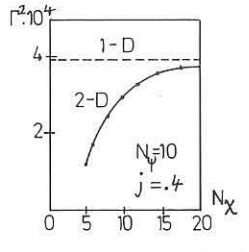

j=0, R=1:

This case can be solved exactly. In elliptic coordinates the eigenfunctions are products of Mathieu functions. Special features are an infinitely degenerate Alfven spectrum and a narrow slow wave spectrum with an accumulation point; both features are reproduced by the code, a crucial test of the choice of the finite elements.

This work was supported by the Swiss National Science Foundation.

References

[1] K. Appert et al., to be published in J.Comp.Physics

[2] C. Mercier, Nucl.Fusion 1, 47 (1960)

[3] R.L. Dewar et al., Phys.Fluids 17, 930 (1974)

MHD Instabilities of Diffuse Helical l = 1 Equilibria as an Initial-Boundary-Value Problem

F. Herrnegger and W. Schneider
Max-Planck-Institut für Plasmaphysik, Garching, Germany, Euratom Association.

Abstract: The gross MHD instabilities of straight helical l = 1 diffuse high-ß plasma equilibria are investigated by solving the linearized MHD equations as an initial boundary-value problem. The method is applied to find the fixed-boundary instabilities of equilibria with at present square cross-section rotating around the symmetry axis of the helical equilibrium.

1. Introduction

The theoretical investigation of the stability properties of helically symmetric high-ß equilibria with arbitrary pressure profiles and vanishing longitudinal current on every flux surface is of great interest for the High-Beta Stellarator experiment HBS II /1/. Marder /2/ has tackled this problem by means of a δW analysis, where the expression for the energy integral is expanded in the small parameter $\varepsilon = a\,h$ (a is the plasma radius, $h = 2\pi/L$ where L is the wavelength of the equilibrium). In this paper another method is described, which should yield the eigenfunctions and the eigenvalues for arbitrary ε without expansions. The method used for the instability calculation is essentially the same as described in /3/: The ideal MHD equations are linearized about a given equilibrium and are Fourier-analyzed in the ignorable coordinate of the equilibrium. The boundary of the domain in which the calcualation is performed coincides with the outermost flux surface of the equilibrium. The boundary conditions are such that the instabilities can be classified as fixed-boundary modes.

To adapt this method to the helical problem, a couple of difficulties have to be overcome: First, the general mechanisms for the instability dynamics are different for equilibria with vanishing longitudinal current; secondly, screw-pinch type equilibria have much higher growth rates, which are therefore easier to calculate; and, finally, the coordinate system which is non-orthogonal, imposes additional complications.

2. Model and Method of Solution

The ideal MHD equations are used as the basic model for describing the gross motion of a plasma; i.e. equations for the velocity $\vec{v}$, the plasma pressure p, and the magnetic field $\vec{B}$; the current density $\vec{J}$ and the electric field $\vec{E}$ are determined from Ampere's law and Ohm's law. These equations are linearized about a given static equilibrium characterized by ($\vec{v}^0 = 0$), p^0 and $\vec{B}^0$. The equilibrium is formally defined by:

$$\nabla p^0 = \vec{J}^0 \times \vec{B}^0 \quad (1), \qquad \vec{J}^0 = \nabla \times \vec{B}^0 \quad (2), \qquad \nabla \cdot \vec{B}^0 = 0 \quad (3).$$

The perturbed state is represented by the variables $\vec{v}^1$, p^1, $\vec{B}^1$ which satisfy the equations:

$$\rho^0 \frac{\partial \vec{v}^1}{\partial t} + \nabla p^1 - \vec{J}^1 \times \vec{B}^0 - \vec{J}^0 \times \vec{B}^1 = 0 \quad (4), \qquad \frac{\partial}{\partial t} p^1 + \nabla (p^0 \vec{v}^1) + (\chi - 1)\, p^0 (\nabla \cdot \vec{v}^1) = 0 \quad (5)$$

$$\frac{\partial}{\partial t} \vec{B}^1 + \nabla \times \vec{E}^1 = 0 \quad (6), \qquad \vec{J}^1 = \nabla \times \vec{B}^1 \quad (7), \qquad \vec{E}^1 + \vec{v}^1 \times \vec{B}^0 = 0 \quad (8).$$

We consider one Fourier harmonic of the perturbation with wavelength λ along the ignorable coordinate, z, of the equilibrium; $U^1(x, y, z) = \mathrm{Re}\,(U^1(x,y)\, e^{ikz})$ where $k = 2\pi/\lambda$. The perturbation vector $U^1(x,y)$ must be complex since its individual components may have different phases along z. Linearization and Fourier analysis reduce the initially posed 3D problem to two dimensions.

The boundary values were chosen to conserve energy and to isolate the system:

$$(\vec{n} \cdot \vec{v}^1) = 0 \qquad (\vec{n} \cdot \vec{B}^1) = 0$$

($\vec{n}$ unit normal vector to the boundary).

The initial conditions are arbitrary distributions of the perturbed velocity field, which ressemble roughly the motion of a particular azimuthal m-mode or a mixture of m-modes. This initial boundary-value-problem is solved by an explicit difference method in an (x,y)-coordinate system rotating around the z-axis with a periodicity number h.

3. Numerical Test of the Model

The 2D equilibria used in this model are numerical solutions of an equilibrium code by Marder /2/. The five parameters for these equilibria are the compression ratio b/a, δ_1 (the helical displacement of the plasma), the longitudinal current J_{zc}, and ß.

The first application of the model described above, was the straight screw pinch equilibrium. The square cross section of the equilibrium rotates around the z-axis. In contrast to the helical equilibrium with vanishing current, this screw pinch configuration is characterized by a longitudinal current density which has a Gauss-like radial profile. For this equilibrium the m = 1 mode is unstable within a certain range of k. The eigenfunctions described in terms of $\vec{v}$, $\vec{B}$, $\vec{J}$ are shown in Fig. 1. The growth rate of this mode is determined by calculating $\iint dx\,dy\, p \cos\varphi = f(t)$. The time behaviour of this quantity is shown in Fig. 2. For the stable region of k this function f clearly shows oscillatory behaviour (Fig. 2).

The first important test of the accuracy of the results was the variation of the grid size. Increasing the number of mesh points from (8 x 8) to (32 x 32) should clearly show a convergence to a specific γ-value. The dependence of γ on the grid-size is plotted in Fig. 3. The numerical results converge with decreasing grid size. That the convergence of the m = 2 mode is worse is qualitatively understandable by the finer spatial structure.

The essential point of this investigation is the shift of the eigenvalues towards stability. This property of the numerical model has an even stronger effect for the Θ - pinch equilibrium, which should show marginal behaviour for k = 0. But as is shown in Fig. 4, the numerical result gives clearly stable oscillations. Since the helical equilibria with moderate values for δ_1 and h can be thought of as small deviations of the Θ-pinch, these helical equilibria will be shifted towards stability in the same way as the Θ-pinch. Because the growth rates are very small, this shift - which is not yet understood - may conceal the unstable character of these modes.

4. Conclusions

: It is demonstrated that for helical equilibria with strong longitudinal current the method yields the eigenfunctions and the eigenvalues of different modes with sufficient accuracy. The application to helical equilibria without longitudinal current and the marginal theta-pinch suffers - mainly because of the numerical shift into the stable regime - from numerically inadequate difference approximations. These problems are further investigated.

References: /1/ E. Fünfer, J. Gruber, M. Kaufmann, W. Köppendörfer, J. Neuhauser: "Wall-Stabilized High-Beta Stellarator", IPP 1/139 (1974). /2/ B. Marder: "Straight l = 1 Equilibrium and Stability", to be published. /3/ G. Bateman, W. Schneider, W. Grossmann, Nucl. Fus. 14, 669 (1974)

Acknowledgements: The authors gratefully acknowledge stimulating discussions with M. Kaufmann, J. Neuhauser, and the HBS II-Group.

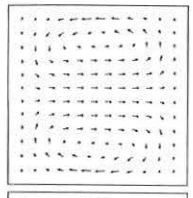

Fig. 1. Eigenfunctions of an m = 1 mode

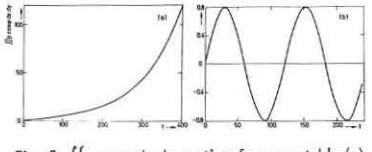

Fig. 2. $\iint p \cos\varphi\, dx\, dy$ vs time for an unstable (a) and a stable (b) mode

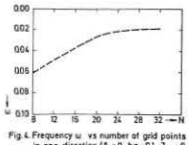

Fig. 4. Frequency ω vs number of grid points in one direction ($\delta_1 = 0$, $ha = 0.1$, $J_{zc} = 0$, $\beta = 0.5$)

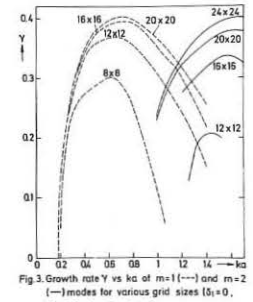

Fig. 3. Growth rate γ vs ka at m=1 (---) and m=2 (—) modes for various grid sizes ($\delta_1 = 0$, $ha = 0.1$, $J_{zc} = 2$, $\beta = 0.5$)

NONLINEAR EVOLUTION OF MHD INSTABILITIES*

Glenn Bateman, H. R. Hicks, J. W. Wooten, R. A. Dory

Oak Ridge National Laboratory, Oak Ridge, Tennessee USA

Abstract: We have used a 3-D nonlinear MHD computer code to study the time evolution of internal instabilities. Velocity vortex cells are observed to persist into the nonlinear evolution. Pressure and density profiles convect around these cells for a weak localized instability, or convect into the wall for a strong instability.

We have developed a series of computer codes [1,2,3] which treat MHD instabilities as an initial value problem. Like Sykes and Wesson [4] we use a Cartesian grid and an explicit difference scheme - but since we use the primitive MHD equations (variables $\underset{\sim}{v}$, $\underset{\sim}{B}$, p, ρ) we have been able to write our nonlinear code as a direct extension of our linear code. Brackbill's code [5] is more sophisticated and flexible than ours but it takes much longer to run (our nonlinear results shown in Fig. 1 required less than 8 minutes on an IBM 360/91). The method of Rosenbluth, et al [6] uses an expansion in low β or large aspect ratio - since we use no expansion we can reliably work in the regime $\beta \gtrsim 10\%$ where reactor tokamaks should operate, especially if they have elongated cross section.

A typical weak m = 1 instability is presented in illustrations below. Here the equilibrium plasma completely fills a straight cylinder with square cross section. The central q-value is 0.9 and periodic end conditions are used so that k·a = 1. The pressure profile, $p'(\psi) \sim \psi$, is described in [3].

A mild density profile such as the one used here ($\rho_{edge} = 0.5\ \rho_{center}$) seems to have little effect on the nonlinear evolution of all variables other than the density; its effect on the evolution of density is to enhance convection over compression. As reported before [2,3] this fixed-boundary instability is characterized by a pair of vortex cells which are helically twisted down the tube. The vortex cells persist, essentially unchanged, throughout the nonlinear evolution. However, sizable velocities are excited along the axis of the cylinder as the peak pressure profile, shown in time-sequence below, convects around the vortex pattern so that the central region of high pressure is pulled up and around to form an annulus surrounding a region of lower pressure. The effects of compression and expansion are also observed below and above (resp.) the center of the cylinder. The vortex velocity saturates at a few tenths of the Alfvén velocity (after the pressure has moved off center and bent around) but the kinetic energy integrated over the cross section continues to grow at a slightly diminished rate. The continued growth of the kinetic energy is attributed to the onset of velocity along the axis of the cylinder. Finally, it is observed that the B-field at the end of the nonlinear evolution has the same form as the equilibrium B-field. The longitudinal field is somewhat compressed in the center and reduced near the mode-rational surface. The profile of the poloidal field is flattened at the mode-rational surface. There is very little shear near the center of the plasma for this equilibrium.

We observe that a stronger m = 1 mode (lower q-value, larger growth rate, broader spatial extent) drives the pressure profile atainst the wall where it appears to splash. For an m = 2 mode there are four vortex cells; the pressure profile is pulled out and around these. The same basic phenomena persist when the cross section of the plasma is elongated.

References

*Research sponsored by U. S. Energy Research and Development Administration under contract with Union Carbide Corporation.

[1] J. W. Wooten and H. R. Hicks, Report UCC-CSD-INF-21, "Preliminary Description of the Linear and Nonlinear Ideal MHD Codes", May 1975; see also Seventh Conference on Numerical Simulation of Plasmas, June 1975.

[2] J. W. Wooten, H. R. Hicks, G. Bateman, R. A. Dory, Report ORNL-TM-4784, "Preliminary Results of the 3-D Nonlinear Ideal MHD Code", Nov. 1974.

[3] G. Bateman, W. Schneider, W. Grossmann, Nuclear Fusion 14, 669-683, (1974); Fifth Conf. on Plasma Phys. and Cont. Nuc. Fus. Res. (Tokyo Conference) IAEA-CN-33/A12-1, Nov., 1974.

[4] A. Sykes and J. A. Wesson, Nuclear Fusion 14, 645 (1974); Tokyo Conference, IAEA-CN-33/A12-3 (1974).

[5] J. U. Brackbill, Bulletin A.P.S. 19, 904 (1974).

[6] R. White, et al, Tokyo Conf., IAEA-CN-33/A13-3 (1974).

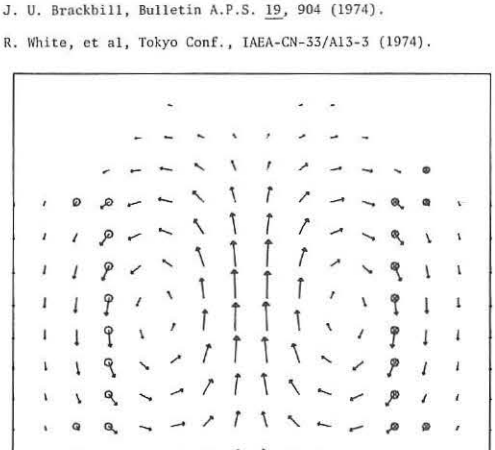

Cross section of velocity for linear m = 1 instability

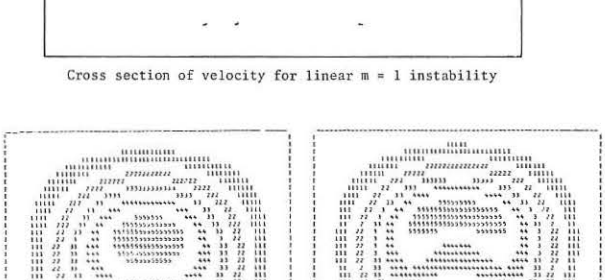

t = 4.44 t = 6.21

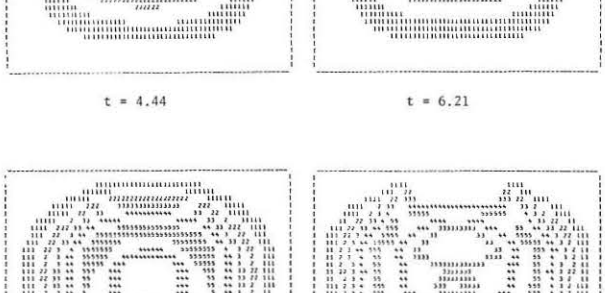

t = 7.85 t = 10.2

Time sequence of pressure profiles at a given cross section. (t in units of Alfvén transmit time [2,3])

NON-LINEAR DEVELOPMENT OF THE KINK INSTABILITY

A. Sykes and J.A. Wesson
Culham Laboratory, Abingdon, Oxon, UK
(Euratom/UKAEA Fusion Association)

Abstract: The hydromagnetic equations have been solved numerically to obtain the three dimensional, non-linear, time development of a kink instability.

Introduction There has been an extensive study of the linear hydromagnetic stability theory of tokamaks and pinches but it seems that a theory of the non-linear behaviour is necessary for a satisfactory integration of theory with experiment. The present work represents a preliminary non-linear study of one particular instability - the kink mode. Our approach follows that of Wooten et al.[1] but a different numerical method is used.

We take a straight system having a square cross-section, the plasma carrying an axial current and having an axial magnetic field. The time dependent, non-linear, hydromagnetic equations are then solved numerically to follow the growth of the internal kink instability. The code uses a finite difference Lax-Wendroff technique based on a 16 × 16 × 10 point grid.

Model We shall describe here a typical calculation in which the resistivity has been put to zero but in which a small viscosity is included. The initial axial magnetic field, B_z, is constant in space. The initial current is chosen to give a central value of q just less than unity, $q_o = 0.94$. The current distribution is $j_z = j_{zo} \cos(\pi x/2a) \cos(\pi y/2a)$ where a is the half-length of the sides of the square. The periodicity length in z is $2\pi a$ and the calculated values of q use this length. The shear is small in the interior of the plasma but increases rapidly at the edge. We shall now describe the time development which follows the introduction of a small velocity perturbation at t = 0. The unit of time is $\tau = a/(B_{zo}/\rho_o^{\frac{1}{2}})$. The viscosity used is $\nu = 0.01\, \rho_o a^2/\tau$ where ρ_o is the initial density.

Non-linear Development Two of the key variables are plotted as a function of time in figure 1. These are the value of q on the magnetic axis, q_o, and the total kinetic energy of the plasma, the latter being an indicator of the growth of instability. At early times the gross properties of the plasma are unchanged but after t = 8 the instability grows rapidly. The azimuthal flow pattern of the plasma is shown in figure 2 and it is clear from this that the instability is an m = 1 kink mode[2]. This instability causes the high pressure plasma to be displaced away from the magnetic axis into a helical form which persists throughout the rest of the run. The resulting

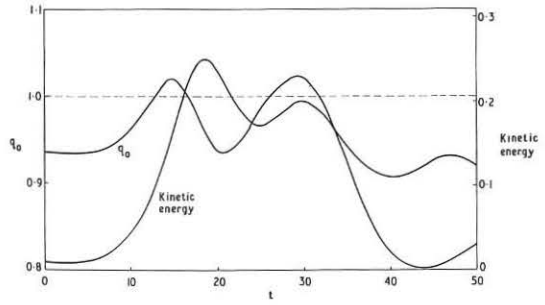

Figure 1 Graphs of the safety factor on the magnetic axis, q_o, and the kinetic energy (as a percentage of the total energy) plotted against time (measured in units of $a/(B_{zo}/\rho_o^{\frac{1}{2}})$).

fall in kinetic pressure is compensated by an increase in B_z, which in turn produces the observed increase in q_o.

After q_o has increased to unity the growth of the instability slows and the growth stops at t = 19. The value of q_o now falls back to its original value below unity and this is followed by a small growth in kinetic energy between t = 25 and t = 30. However, the configuration is no longer simple and $q_o = 1$ no longer has its original significance.

Contours of kinetic pressure and the axial magnetic field are shown in figures 3 and 4 for a given z plane at time t = 27. The kinetic pressure has fallen into a horse-shoe configuration and is only prevented from reaching the wall by the shear near the surface. The contours of B_z show an increased magnetic field in the inner region. This behaviour is very similar to that suggested by Kadomtsev[3] except that the "magnetic bubble" arises here, not through a penetration of magnetic flux from the outer vacuum region[4] but rather by a rearrangement of the magnetic field in the comparatively shear free central region. There has also been a considerable redistribution of the axial current, its direction actually being reversed in the high pressure region of the helix whereas it has increased by 50% in the region of enhanced B_z. Another interesting feature is the reduction of

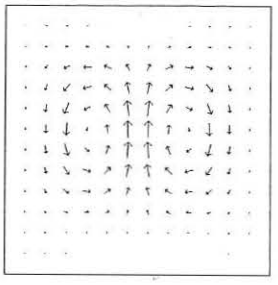

Figure 2 The azimuthal velocity field at t = 16, showing the m = 1 instability

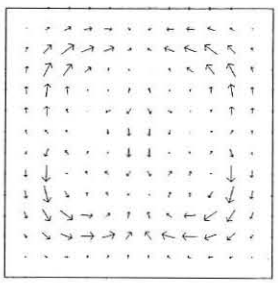

Figure 5 The azimuthal velocity field at t = 46, showing the m = 2 instability

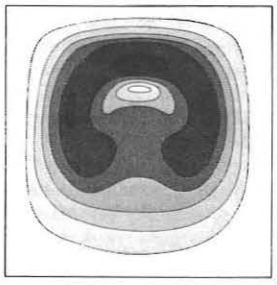

Figure 3 Contours of constant pressure across the minor cross-section at t = 27. (Equal spacing between contours, the lowest value of p being zero)

Figure 4 Contours of constant B_z across the minor cross-section at t = 27. (The contours are equally spaced between 0.70 and 1.20 of the initial constant value)

the axial magnetic field in the outer regions. The resulting value of B_z is only one half of that at the centre. This is very similar to the behaviour observed in high-β pinches[5].

Following the rearrangement of the plasma as described above the value of q_o falls to 0.8 at t = 40. However the plasma pressure is no longer concentrated around the magnetic axis and no m = 1 instability results. Up to this time the kinetic energy has been falling, but now an m = 2 instability becomes apparent in the region of higher q. This results in a small growth in the kinetic energy but saturation is soon reached. The azimuthal flow corresponding to this instability is shown in figure 5.

Conclusions In the calculation described above the kink instability grows until the value of q on the axis is greater than unity. The plasma forms a helical configuration which persists throughout the calculation. These two phenomena are related in that when there is a fall in the kinetic pressure on the magnetic axis there is a compensating increase in the axial magnetic field and this in turn leads to the increase in q. In the final configuration the high pressure plasma is much closer to the wall than in the initial state and in a collisional plasma this would result in a greatly enhanced diffusion.

The calculation is one of a number which have been carried out and which, it is hoped, will give some insight into the actual behaviour of tokamaks and pinches.

Acknowledgment We would like to acknowledge the kindness of Dr Dory and his colleagues in sending us an early account of their work at the Oak Ridge National Laboratory.

References

1. Wooten, J., Hicks, H.R., Bateman, G. and Dory, R.A. ORNL TM 4784, 1974.
2. Rosenbluth, M.N., Dagazian, R.Y. and Rutherford, P.H. Phys. Fluids 16, 1894 (1973).
3. Kadomtsev, B.B. and Pogutse, O.P. Proc. 6th. Conf. on Controlled Fusion and Plasma Physics, Moscow 1973, Vol. 1, p. 59.
4. White, R., Monticello, D., Rosenbluth, M.N., Strauss, H. and Kadomtsev, B.B. Proc. 5th. Conf. on Plasma Physics and Controlled Nuclear Fusion Research, Tokyo 1974, paper CN-33/A13 - 3.
5. Allen, N.L. and Liley, B.J. Proc. 4th. Int. Conf. on Ionization Phenomena in Gases, Uppsala, 1959, Vol. 2, p. 937.

THE DEVELOPMENT AND EQUILIBRIUM STRUCTURE OF MAGNETIC ISLANDS.

David Potter* and T. Kamimura+

* Imperial College, London SW7, England
+ University of California at Los Angeles, U.S.A.

Abstract: A simple heuristic model for the non-linear development of magnetic islands is developed. The model describes a change of equilibrium in the Tohamak, subject to a sequence of integral constraints, to a new three-dimensional helical structure.

We describe the development of magnetic islands through a sequency of equilibrium states satisfying:

$$\nabla^2\psi = -J(\psi), \tag{1}$$

where ψ is the magnetic flux in the helical plane containing the instability and J is the normal current density defined by a set of integral adiabatic constraints on each magnetic surface:

$$\delta \int_\psi \frac{d\ell}{|\nabla\psi|} = 0. \tag{2}$$

By employing a variational procedure (Sec. B), the non-linear path of the instability is followed through a succession of equilibrium states to the final (minimum energy) island state. Such a model may be applied to the Tohamak and suggests the early change of the equilibrium from an initial axisymmetric configuration to a three-dimensional helical equilibrium.

A. Application of the Model to the Tokamak. The geometry of the Tohamak is simplified by employing a doubly periodic slab model, topologically equivalent to the torus (Fig. 1). Assuming a low-beta plasma, the à priori condition for the linear growth of the instability is:

$$\underline{k}\cdot\underline{B}^0 = 0, \tag{3}$$

where $\underline{k}$ is the initial wavenumber of the instability and $\underline{B}^0$ is the initial equilibrium field. By considering the plane which contains both the initial $\underline{k}$ and x (the co-ordinate describing the initial equilibrium), the non-linear development of the instability remains two-dimensional.

The occurrence of a neutral line in the field (Eq. 3) suggests the possible growth of an island by the mechanism of the tearing mode. Consistent with linear theory (1) in the Tokamak, it is assumed that the growth time of the instability is short compared to the resistive diffusion time τ_R, but long compared to the time of flight of Alfvèn waves and sound waves τ_H,

$$\tau_R >> \tau >> \tau_H . \tag{4}$$

The second inequality suggests that the plasma always remains in equilibrium with the field during the development of the island. Thus the equilibrium equation for the flux ψ in the plane of the instability may be applied throughout the evolution of the system:

$$\nabla^2_\psi = -h^\xi \frac{dp}{d\psi} - \frac{f(\psi)}{h^\xi}\frac{df}{d\psi} , \tag{5}$$

with the pressure $p = p(\psi)$ and axial flux $f = f(\psi)$. Since h^ξ, the length scale normal to the plane (Fig. 1), is constant in the slab:

$$\nabla^2\psi = -J(\psi) \tag{6}$$

where J is the current normal to the plane.

On the other hand, according to the first inequality (Eq. 4), the island develops adiabatically, so that significant diffusion of the surfaces does not occur. In terms of the flux co-ordinates (ψ,χ) with metric:

$$ds^2 = (h^\chi d\chi)^2 + (h^\psi d\psi)^2 + (h^\xi d\xi)^2 , \tag{7}$$

the absence of diffusion suggests that the area of each magnetic surface in low-beta is preserved(2):

$$\delta \int_\psi h^\psi h^\psi d\chi = 0 \tag{8}$$

namely Eq. (2). Unlike the ideal local MHD equations, this model, while adiabatic, still permits a change of topology and the development of an island by a changing separatrix.

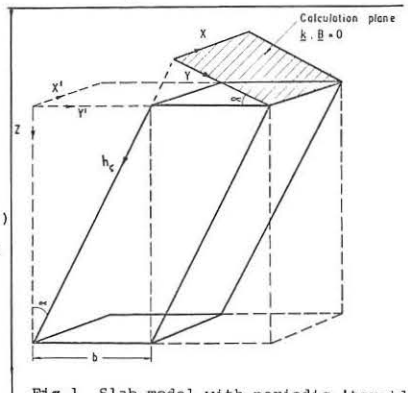

Fig.1 Slab model with periodic 'toroidal' (z) and 'poloidal' (y') directions. With a rational surface, the field vanishes in one of the planes containing a wave-number.

B. Variational Procedure. The potential energy of the system is:

$$E = \tfrac{1}{2}\int\int(\nabla\psi)^2 ds . \tag{9}$$

The equilibrium is varied, $\delta\psi$, over a succession of steps, or iterations, while keeping the flux at the non-periodic boundaries constant. Introducing Lagrange multipliers $g(\psi)$ for each surface ψ to satisfy the constraint equations (8), the resultant change of energy is:

$$\delta E = \int\int -\delta\psi(\nabla^2\psi - g(\psi)) \, ds . \tag{10}$$

A variety of variational procedures may now be defined which ensure a dimunition of the energy at each step. One such procedure is:

$$\delta\psi(x,y) = \varepsilon(\nabla^2\psi - g(\psi)), \tag{11}$$

with,

$$g(\psi) = \frac{1}{A'(\psi)}\int_\psi \nabla^2\psi \, h^\psi h^\chi d\chi , \tag{12}$$

where $A'(\psi)$ is the differential area of each surface and ε is a small positive constant.

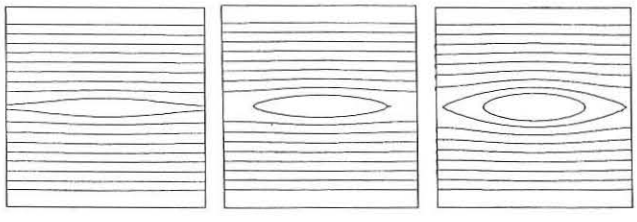

Fig.2. The non-linear evolution of an island state (left to right) for a symmetric Gaussian distribution. The final equilibrium state ($\delta E=0$) is illustrated on the right.

C. Example of Solutions. The non-linear development of the instability, with the final island state ($\delta E = 0$) is illustrated in Fig. 2.

Solutions with this model demonstrate the fall of the current density at the centre of the island. The separatrix acts like a shock, with a discontinuity of the current density across the separatrix and dissipation necessarily occurring in an infinitesimal layer on the separatrix. Dependence of the solutions on mode numbers and current radius will be presented.

References

(1) FURTH, H.P., KILLEEN, J., and ROSENBLUTH, M.N. (1963). Phys. Fluids 6, 459.

(2) POTTER, D.E. (1975). "Waterbag Methods in Magneto-hydrodynamics" to be published in Methods in Computational Physics (Killeen, J., ed.), Vol. 16.

RESISTIVE INSTABILITIES IN A TOKAMAK*

A. H. Glasser

Princeton University Plasma Physics Laboratory, Princeton, N.J. 08540 USA

Abstract: Application of resistive instability theory shows that toroidal effects can stabilize the tearing mode in devices like the Princeton Large Torus. Contraction of the current channel is destabilizing. Finite fluid compressibility is crucial to this phenomenon.

The Mirnov oscillations with poloidal mode number $m \geq 2$ which precede disruptions in tokamak discharges [1] are usually interpreted as tearing modes, with the analysis done for a cylindrical model tokamak [2]. We have studied resistive instabilities in an arbitrarily shaped torus [3], and found that favorable average curvature can stabilize the tearing mode as well as the resistive interchange. Application of this theory to a tokamak shows that the effect is large enough to stabilize these modes in devices such as PLT.

The central result of Ref. 3 is the dispersion relation,

$$\Delta = 2.1 \frac{V_s}{X_o} Q^{5/4}\left(1 - \frac{\pi}{4}\frac{D_R}{Q^{3/2}}\right) . \qquad (1)$$

Here Δ is the jump in the logarithmic derivative of the normal component of the perturbed magnetic field across the narrow singular layer where resistive effects are important. It is obtained by solving the ideal MHD equations in the regions outside the singular layer. It carries the destabilizing influence of the Ohmic heating current. The ratio V_s/X_o of a macroscopic length to the resistive layer thickness is large since it varies with resistivity as $\eta^{-1/3}$. The dimensionless quantity Q is the complex growth rate divided by a scale factor which varies as $\eta^{1/3}$. The essential effects of toroidal curvature are carried by D_R. For $D_R = 0$, Eq. (1) reduces to the usual equation for the tearing mode, which is unstable for $\Delta > 0$. For $D_R > 0$, the approximate vanishing of the quantity in parentheses gives the resistive interchange. For $D_R < 0$, all values of $\Delta < \Delta_C = 1.54\,(V_s/X_o)|D_R|^{5/6}$ are stable. The region $0 < \Delta < \Delta_C$ represents curvature stabilization of the tearing mode.

The quantity D_R is given in [3] as a sum of field line averages on the singular surface. It is closely related to D_I, the quantity involved in the Mercier criterion for ideal interchange stability, and to the well-known stability concept of minimum average B or negative V". A large aspect ratio expansion for a circular tokamak yields

$$D_R = \frac{2q^2}{B_o^2}\frac{1}{r}\frac{dp}{dr}\left(\frac{q}{dq/dr}\right)^2\left[1 - \frac{1}{q^2} + \frac{q}{r^3}\frac{dq}{dr}\int_o^r dr'\left(\frac{r'^3}{q^2} - 2\frac{R^2}{B_o^2}\frac{1}{r}\frac{dp}{dr}\right)\right] , \qquad (2)$$

where the safety factor q and the pressure p are arbitrary functions of the minor radius r. For parabolic profiles, $p = p_o(1 - r^2/a^2)$, $q = q_o(1 + sr^2/a^2)$, this reduces to

$$D_R = -\frac{\beta_p a^4}{s^2R^2r^2}\frac{(1 + sr^2/a^2)^4}{(1+s)^2}\left[\left(\frac{1 + sr^2/a^2}{sr^2/a^2}\right)\ln(1 + sr^2/a^2) - \frac{1}{q_o^2(1 + sr^2/a^2)^2} + \frac{2\beta_p}{(1+s)^2}(1 + sr^2/a^2)\frac{sr^2}{a^2}\right] , \qquad (3)$$

with $\beta_p \equiv \left[2q(a)R/B_o a^2\right]^2 \int_o^a p(r)rdr$. Note that $D_R < 0$ if $q_o > 1$.

The solid curves in Fig. 1 show the values of Δ_C vs. minor radius for

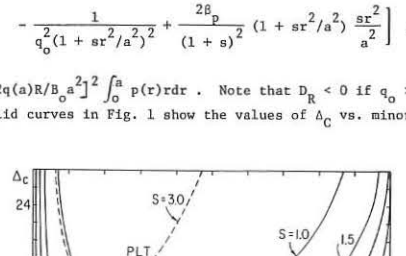

Fig. 1. Δ_C vs. r/a in the ST and PLT tokamaks, with $q_o = 1.1$ and $\beta_p = 0.8$.

this model of the ST tokamak, with $q_o = 1.1$ and $\beta_p = 0.8$. The m = 2 mode is stable until the q = 2 surface drops below the line Δ_2, calculated in [2]. Increasing the value of s, representing contraction of the current channel, is destabilizing. The dashed curve, for PLT with s = 3, shows that this device is much more stable. This is because of its smaller aspect ratio R/a, and its higher temperature and correspondingly lower resistivity. Figure 2 shows Δ_C vs. s at the q = 2 surface in ST and PLT.

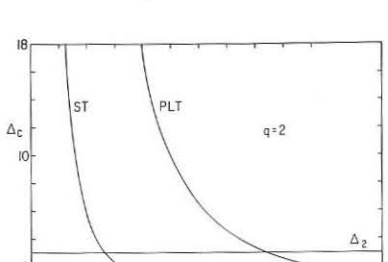

Fig. 2. Δ_C vs. s at the q = 2 surface in the ST and PLT tokamaks.

Furth et al., [2] state that curvature cannot stabilize the tearing mode. They base this conclusion on a dispersion relation which represents a particular low-β limit of a more general dispersion relation, given in the Appendix of [3]. There are two reasons why this limit is inappropriate to a tokamak. First, β affects Δ_C through the ratio $|\beta/D_R|$. Since D_R is proportional to β, the ratio is not necessarily small, and does not vanish as β goes to zero. Second, its effect on Δ_C is very weak. As shown in Fig. 3, Δ_C falls off as the 1/6 power of $|\beta/D_R|$ as $|D_R/\beta|$ gets large. Earlier indications that toroidal curvature does not affect the tearing mode were based on the limit where Δ_C vanishes. Our study indicating strong stabilization utilizes the opposite limit, denoted here by Δ_o. In ST and PLT, $\Delta_C/\Delta_o \simeq 0.8$. The frequently made assumption that the fluid is incompressible, or the use of a fictional gravitational force to simulate curvature, leads to the same inappropriate limit of vanishing Δ_C, and thus misses the crucial effect.

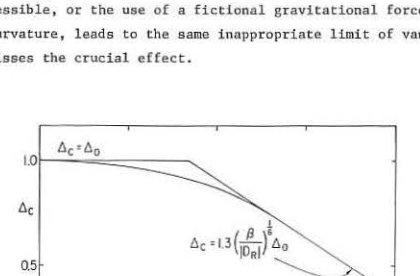

Fig. 3. Log-log plot of Δ_C vs. $|D_R|/\beta$.

* This work was supported by United States Energy Research and Development Administration Contract E(11-1)-3073. Use was made of computer facilities supported in part by National Science Foundation Grant NSF-GP 579.

[1] S. V. Mirnov and I. V. Semenov, in Plasma Physics and Controlled Nuclear Fusion Research (IAEA, Vienna, 1971), Vol. II, p. 401.

[2] H. P. Furth, P. H. Rutherford, and H. Selberg, Phys. Fluids 16, 1054 (1973).

[3] A. H. Glasser, J. M. Greene, and J. L. Johnson, Phys. Fluids (in press).

EFFECTS OF EQUILIBRIUM FLOW, RADIATION AND RESISTIVE WALLS ON MHD AND TEARING MODES IN A PINCH

A.S. Furzer*, D.C. Robinson

* Royal Holloway College, London, U.K.
Euratom-UKAEA Association for Fusion Research, Culham Laboratory, Abingdon, Oxon. U.K.

Abstract The effects of radial equilibrium flow on gross MHD and resistive modes are investigated. The influence of three types of radiation loss, Bremsstrahlung, recombination and line radiation on the growth of kink and tearing modes has been studied. The consequences of a resistive wall are considered.

Introduction The stability of a variety of cylindrical pinch equilibria to gross resistive modes has been considered in some detail[1,2,3]. The stabilising effects of ion viscosity, particularly on localised short wavelength Suydam modes for the reversed field pinch, at relatively low magnetic Reynolds numbers (S ≲ 1000) has been demonstrated[4]. Measurements on the HBTX experiment are in good agreement with theory for gross MHD modes and gross resistive modes if the more complete theory is used[4].

Radial Flow In studying the stability of a configuration at modest values of S the question arises as to the significance of instabilities whose growth time is not very different from the resistive diffusion time. As the tearing mode growth rate varies as $S^{2/5}$ it is deduced from examples studied that diffusion effects can be considered insignificant when S exceeds 10^6. From more basic considerations Taylor[5] has indicated that diffusive effects in the resistive layer can have a significant effect on the stability of the tearing mode.

Previously $\underline{B}(\underline{r})$ has been taken to be constant in time. For V = 0 this yields $J_\theta = 0$ and $\eta(r)\, J_z(r) = \text{const}$ (where η is the resistivity). This case has been used to study tearing mode effects in a Tokamak. If $V \neq 0$, and we take $\eta(r)$ = constant to avoid rippling modes and $\nabla p = 0$ we obtain the force-free paramagnetic model with $v_r = -E_z B_\theta / B^2$.

Outside a singular surface $(\underline{k}.\underline{B}) = 0$ the system is potentially MHD unstable ($g < 0$)[6] but is more unstable to a tearing mode because of the connection through the surface. The radial field perturbation which is peaked outside is now carried inwards by the flow thus making the situation more unstable.

Fig.1 shows the resultant growth (or decay) with zero diffusion velocity for the force-free paramagnetic model for m = 1 as a function of the mode number K for a variety of normalised wall radii (iow viscosity and thermal conductivity are included here). The arrows indicate the MHD marginal stability K numbers for $P_w = 4.0$. The curve AVISC = 0.1 indicates the enhanced growth associated with artificially reducing the viscosity to a small value. For $P_w = 4.0$ the pure tearing mode lies to the left of K = -0.6. Fig.2 shows the effect of the flow on the tearing mode for two values of S. AVO = 1.0 corresponds to inward flow, AVO = 0 to no flow and AVO = -1.0 to an outward flow. The destabilising nature of the inward flow in this case is apparent.

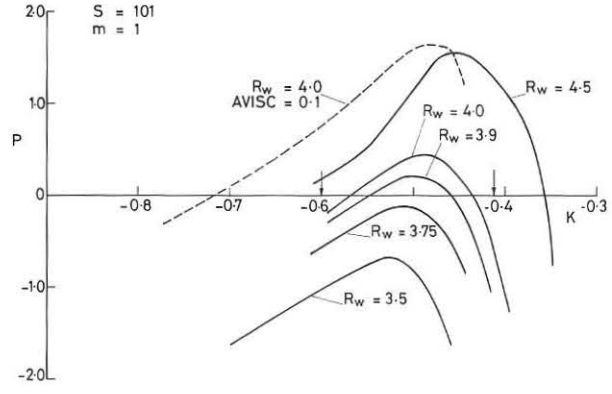

Fig.1 Growth rate as a function of wall radius and wave number for the F.F.P.M. with zero diffusion velocity.

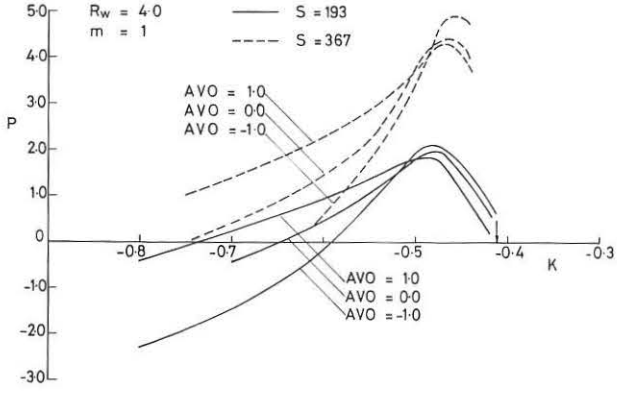

Fig.2 Growth rate as a function of wavenumber for differently directed diffusion velocities.

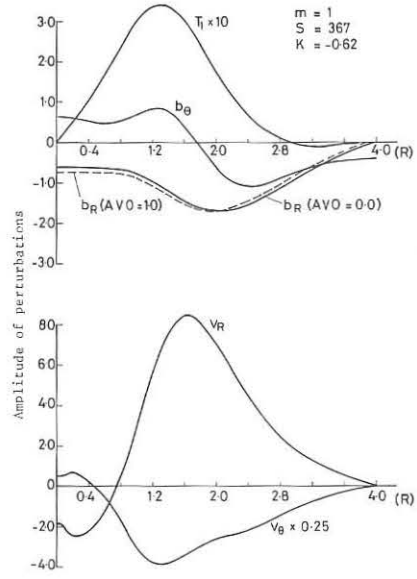

Fig.3 Normalised field, velocity and temperature perturbations.

Fig.3 shows the resultant perturbations for a typical case. The singular surface is at R = 1.25 and the inward shift of the radial field for the inward flow case is apparent.

Radiation effects To the perturbed energy equation we have added a radiation loss term

$$n_o^2 T_o^{\frac{1}{2}} \{\alpha_1 (\frac{2n_1}{n_o} + \tfrac{1}{2}\frac{T_1}{T_o}) + \alpha_2 \frac{Z^4}{zT_o} (\frac{2n_1}{n_o} - \tfrac{1}{2}\frac{T_1}{T_o}) + \alpha_3 \frac{Z^6}{zT_o^2} (\frac{2n_1}{n_o} - \frac{3}{2}\frac{T_1}{T_o})\}$$

where $n_o T_o$ are the equilibrium values of density and temperature, n_1, T_1 the perturbed values, Z the charge of the impurity, and z the effective charge. The Bremsstrahlung coefficient is α_1, α_2 is the recombination and α_3 a line radiation term. (The nuclear heating term has been treated similarly.) If $n_1 > +\frac{3}{4} T_1$ then the terms can only damp the instability however a negative correlation between n_1 and T_1 appears to be destabilising. We have investigated the effects of these terms on unstable MHD and resistive modes for power losses of up to 50%. Both the MHD mode and the resistive mode studied possess positively correlated density and temperature perturbations, in the MHD case the individual perturbations change sign. The effect of all or any of the radiation loss terms is to reduce the growth rate by ~ 2% and 13% for radiation powers of 18% and 50% respectively of the ohmic input power. If the power loss is larger than 50% the correlation of n_1 and T_1 becomes negative and the growth rate increases considerably.

Pesistive Walls A reversed field pinch requires a conducting wall to give it stability to long wavelength kink and tearing modes. The finite conductivity of such a wall, σ_w, will lead to slowly growing kink modes. MHD calculations for a thin walled vessel give instability growth times close to the field penetration time through the wall, τ_w; however, close to marginal stability points for a perfect wall the growth rate can vary as $\tau_w^{-1/3} \cdot \tau_A^{-2/3}$ where τ_A is the Alfven transit time. A good conducting wall yields values for τ_w comparable with the field diffusion time of the plasma so that considerations of the first section are necessary in determining a full solution to the problem.

Conclusions A radial velocity directed inwards destabilises the tearing mode whereas an outward velocity gives greater stability. Radiation losses at the level of a few percent of the ohmic input power reduce the growth rate of both MHD and resistive instabilities. A resistive wall leads to instability growth in a field penetration time and this can be modified by radial flow effects.

References

(1) H P Furth et al. Phys Fluids 16, 1054, 1973.

(2) J E Crow et al. 6th European Conference on Controlled Fusion and Plasma Physics, Moscow, p.269, 1973.

(3) J A Dibiase., University of California, Lawrence Livermore Laboratory UCRL-51591, 1974.

(4) E P Butt et al. 5th Conference on Plasma Physics and Controlled Nuclear Fusion, Tokyo, CN-33, E9-2 1974.

(5) J B Taylor., Phys. Rev. Letters 33, 1139, 1974 and private communication.

(6) D C Robinson., Plasma Physics, 13, 439, 1971.

IMPURITY DRIVEN DISSIPATIVE FLUID MODES

T.J. Schep
Association Euratom-FOM, FOM-Instituut voor Plasmafysica
Rijnhuizen, Jutphaas, The Netherlands

B. Coppi and G. Rewoldt
Massachusetts Institute of Technology, Cambridge, U.S.A.

Abstract: Dissipative fluid modes driven by a small concentration of impurity ions are discussed. When collisions between the two ion species are dominant, these modes will tend to redistribute the ion populations so as to make their radial density distributions nearly equal.

We refer to a low-β, one-dimensional equilibrium configuration, in which all quantities are x-dependent. The confining magnetic field is in the z-direction. The plasma is assumed to consist of the species: e, electrons, i, main ion population with charge number $Z_i = 1$, and I, impurity ions with $Z > 1$. Thus, assuming charge neutrality, we have $n_e = n_i + Zn_I$. We consider the high temperature limit where the average collision frequencies for each species are smaller than their gyration frequencies. We neglect all finite gyro-radius effects. Therefore, we can adopt a guiding centre description for all species. We consider electrostatic modes $\tilde{E} = -\nabla\tilde{\phi}$, $\tilde{\phi} = \hat{\phi}(x)\exp[-i\omega t + ik_y y + ik_\parallel z]$. When the ion mean free paths are shorter than the longitudinal wavelengths, the relevant modes are of fluid type[1,2,3] and can be described by moment Eqs.[4]. They are associated with the finite thermal conductivity, along the magnetic field, of the main ion population, the thermal electric effect and the friction arising from i-I collisions. They are found in the frequency range

$$v_{tI} < \omega/k_\parallel < v_{ti} < v_{te} \quad . \tag{1}$$

The relevant range of mean free paths is such that

$$k_\parallel^2 v_{tI}^2/\nu_I < \omega \lesssim k_\parallel^2 v_{ti}^2/\nu_i < k_\parallel^2 v_{te}^2/\nu_e \quad , \tag{2}$$

v_{tj} and v_j representing the thermal velocity and the average collision frequency for each species, respectively. In particular, we have $\nu_i = \nu_{ii} + \nu_{iI}$, and we will consider the situation where $Z_e \equiv \nu_{iI}/\nu_{ii} = n_I Z^2/n_i$ is 0(1).

The electrons are in equilibrium along the magnetic field, so that $\tilde{n}_e = n_e e\tilde{\phi}/T_e$ and the quasi-neutrality condition gives

$$Z\tilde{n}_I = \tilde{n}_i + n_e e\tilde{\phi}/T_e \quad . \tag{3}$$

The linearized main ion and impurity ion mass conservation equations are

$$\omega\tilde{n}_j = -n_j\,\omega_{*j}\,e\tilde{\phi}/T_i + k_\parallel\tilde{u}_{j\parallel} \quad , \tag{4}$$

where $j = i, I$ and $\omega_{*j} \equiv k_y(cT_i/eB)(d\ln n_j/dx)$. The two ion momentum balance equations along the magnetic field are

$$0 = \left[n_i e\nabla_\parallel\tilde{\phi} + T_i\nabla_\parallel\tilde{n}_i + (1+\alpha_{iI})n_i\nabla_\parallel\tilde{T}_i\right] - \beta_{iI}m_i n_i\nu_{iI}(\tilde{u}_{i\parallel} - \tilde{u}_{I\parallel}), \tag{5}$$

$$m_I n_I \frac{\partial\tilde{u}_{I\parallel}}{\partial t} = -\left[Zn_I\nabla_\parallel\tilde{\phi} + T_i\nabla_\parallel\tilde{n}_I - \alpha_{iI}n_i\nabla_\parallel\tilde{T}_i\right] + \beta_{iI}m_i n_i\nu_{iI}(\tilde{u}_{i\parallel} - \tilde{u}_{I\parallel}), \tag{6}$$

respectively, where the α_{iI} terms correspond to the thermal force resulting from collisions between the two ion species, and the β_{iI} terms correspond to the analogous friction force. The main ion thermal energy balance equation is

$$\left[\frac{3}{2}n_i\frac{\partial}{\partial t} - \nabla_\parallel\left(\chi_i\frac{n_i T_i}{\nu_i m_i}\nabla_\parallel\right)\right]\tilde{T}_i = \frac{3}{2}c\frac{\nabla\tilde{\phi}\times\mathbf{B}}{B^2}\cdot\nabla T_i - n_i T_i\nabla_\parallel\tilde{u}_{i\parallel} - \alpha_{iI}n_i T_i\nabla_\parallel(\tilde{u}_{i\parallel} - \tilde{u}_{I\parallel}) \quad . \tag{7}$$

Here the χ_i term arises from the main ion thermal conductivity along the field lines. Since we take $n_I/n_i < 1$, we may neglect the collisional energy transfer to the main ions. The coefficients α_{iI}, β_{iI} and χ_i are tabulated in Ref.5 for a number of values of Z_e. They are all of order unity, except for α_{iI}, which is proportional to Z_e for small values of Z_e.

We consider the realistic limit in which main ion-impurity ion collisions are dominant, so that

$$\frac{m_i n_i}{m_I n_I}\frac{\nu_{iI}}{\omega} > 1 \quad . \tag{8}$$

In this limit the two ion momentum balance equations (5) and (6) reduce to

$$n_e e\tilde{\phi} + T_i\tilde{n}_i + n_i\tilde{T}_i + T_I\tilde{n}_I = 0 \quad , \tag{9}$$

$$\frac{k_\parallel}{\omega}(\tilde{u}_{i\parallel} - \tilde{u}_{I\parallel}) = \frac{-i}{\beta_{iI}}\frac{k_\parallel^2 T_i}{\omega\nu_{iI}m_i}\left[\frac{\tilde{n}_i}{n_i} + \frac{e\tilde{\phi}}{T_i} + (1+\alpha_{iI})\frac{\tilde{T}_i}{T_i}\right] \quad . \tag{10}$$

Eliminating $\tilde{n}_I$ with the aid of Eq. (3) and neglecting quantities of order, we obtain from Eqs. (9) and (10)

$$n_e e\tilde{\phi}/n_i T_i + \tilde{n}_i/n_i + \tilde{T}_i/T_i = 0 \quad , \tag{11}$$

$$\frac{k_\parallel}{\omega}(\tilde{u}_{i\parallel} - \tilde{u}_{I\parallel}) = \frac{i}{\beta_{iI}}\frac{k_\parallel^2 T_i}{\omega\nu_{iI}m_i}\left[\frac{A}{2}\frac{e\tilde{\phi}}{T_i} - \alpha_{iI}\frac{\tilde{T}_i}{T_i}\right] \quad , \tag{12}$$

where $A = n_I Z^2/n_i + n_e T_I/n_i T_e + T_I/T_i$.

Subtracting the two ion particle conservations Eqs. (4) and eliminating $\tilde{n}_I$ gives

$$\frac{\tilde{n}_i}{n_i} = \frac{e\tilde{\phi}}{T_e} + \frac{n_I Z}{n_e}\frac{\omega_{*I} - \omega_{*i}}{\omega}\frac{e\tilde{\phi}}{T_i} + \frac{n_I Z}{n_e}\frac{k_\parallel}{\omega}(\tilde{u}_{i\parallel} - \tilde{u}_{I\parallel}) \quad . \tag{13}$$

Equation (7) can be written as

$$\left[\frac{3}{2} + i\chi_i\frac{k_\parallel^2 T_i}{\omega\nu_i m_i}\right]\frac{\tilde{T}_i}{T_i} = -\frac{e\tilde{\phi}}{T_i}\frac{\frac{3}{2}\omega_{Ti} - \omega_{*i}}{\omega} + \frac{\tilde{n}_i}{n_i} + \alpha_{iI}\frac{k_\parallel}{\omega}(\tilde{u}_{i\parallel} - \tilde{u}_{I\parallel}) \quad , \tag{14}$$

where $\omega_{Ti} \equiv k_y\,(c/eB)(dT_i/dx)$.

From the set of Eqs. (10)-(13) we obtain the following dimensionless dispersion relation

$$\hat{\omega} + (n_I Z/n_e)\left[A_1(\sigma_I - 1) + A_2\,(\hat{\alpha}_{iI}/\hat{\chi}_i)\left(\frac{3}{2}\eta_i - 1\right)\right]$$
$$= i\hat{\omega}\hat{C}\left[\hat{\omega} + A_2(n_I Z/n_e)(\sigma_I - 1) - \frac{2}{5}A_2\left(\frac{3}{2}\eta_i - 1\right) - A_3 A/Z^2\hat{\omega}\hat{C}^2\right] \quad , \tag{15}$$

where

$\hat{\omega} = \omega/\omega_{*i}$, $\sigma_I = \omega_{*I}/\omega_{*i}$, $\eta_i = \omega_{Ti}/\omega_{*i}$, $\hat{C}^{-1} = \frac{2}{5}\hat{\chi}_i k_\parallel^2 T_i/\omega_{*i}\nu_i m_i$,

$A_1 = (T_i/T_e + n_e/n_i)^{-1}$, $A_2 = (T_i/T_e + 3n_e/5n_i)^{-1}$,

$\hat{\alpha}_{iI} = \alpha_{iI}\nu_i/\beta_{iI}\nu_{iI}$, $\hat{\chi}_i = (\chi_i + \alpha_{iI}\hat{\alpha}_{iI})A_2 A_1^{-1}$,

$A_3 = \frac{5}{2}A_2\chi_i\nu_i/\hat{\chi}_i^2\beta_{iI}\nu_{ii}$.

Equation (15) may be solved for $\hat{\omega} \equiv \hat{\omega}_R + i\hat{\gamma}$ to yield

$$\hat{\omega} = -\left[(n_I Z/n_e)\left\{A_1(\sigma_I - 1) + A_2(\hat{\alpha}_{iI}/\hat{\chi}_i)\left(\frac{3}{2}\eta_i - 1\right)\right\} - iA_3 A/Z^2\hat{C}^2\right]$$
$$\times \frac{1 + \hat{C}\hat{\gamma} + \hat{C}\left\{\hat{\omega}_R + A_2(Zn_I/n_e)(\sigma_I - 1) - \frac{2}{5}A_2\left(\frac{3}{2}\eta_i - 1\right)\right\}}{(1+\hat{C}\hat{\gamma})^2 + \hat{C}^2\left[\hat{\omega}_R + A_2(Zn_I/n_e)(\sigma_I - 1) - \frac{2}{5}A_2\left(\frac{3}{2}\eta_i - 1\right)\right]^2} \quad , \tag{16}$$

so that the condition for instability is

$$-\left[A_1(\sigma_I - 1) + A_2\frac{\hat{\alpha}_{iI}}{\hat{\chi}_i}\left(\frac{3}{2}\eta_i - 1\right)\right]\left[\hat{\omega}_R + A_2\frac{n_I Z}{n_e}(\sigma_I - 1) - \frac{2}{5}A_2\left(\frac{3}{2}\eta_i - 1\right)\right]$$
$$- A_3\,n_e A/n_I Z^3\hat{C}^2 > 0 \quad . \tag{17}$$

We see that if the last term of Eq. (17) is dominant no instability can occur.

We consider the realistic case where $n_I Z^2/n_e < 1$ and $\eta_i = 0(1)$. From equilibrium considerations one would expect that the impurities are concentrated in the centre of the plasma column and that $\sigma_I = 0(Z)$. In that case we obtain from Eq. (16) for

$$Z^{-2} < \hat{C}^2 < 1 \quad , \tag{18}$$

the following expression for the real part of the frequency

$$\hat{\omega}_R = -(n_I Z/n_e)A_1(\sigma_I - 1) \quad , \tag{19}$$

so that the instability condition is

$$(\sigma_I - 1)\left[\frac{3}{2}\eta_i - 1 - \frac{n_I Z}{n_e}\left(1 + \frac{n_i T_i}{n_e T_e}\right)^{-1}(\sigma_I - 1)\right] > 0 \quad . \tag{20}$$

In Eqs. (19) and (20) we have neglected terms of order Z^{-1}.

In particular, we see from Eq. (20) that if $\sigma_I > 1$ corresponding to impurity ions being concentrated in the centre of the plasma column , the relevant instability can be excited if $\eta_i > \frac{2}{3}$, and we may argue that this will tend to redistribute the ion populations so as to make $\sigma_I \simeq 1$.

The instability will tend to produce enhanced ion thermal energy conductivity, but will not be accompanied by a net electron transport across the field lines.

On the other hand, when $\sigma_I = 0(1)$ the instability condition is

$$\left(\frac{3}{2}\eta_i - 1\right)\left[A_1(\sigma_I - 1) + A_2(\hat{\alpha}_{iI}/\hat{\chi}_i)\left(\frac{3}{2}\eta_i - 1\right)\right] > 0 \quad . \tag{21}$$

In this latter case the growth rate is a factor Z^{-1} smaller than in the previous one.

References:

1. B. Coppi and T.J. Schep, Phys. Lett. 46A, 361 (1974).
2. B. Coppi, R. Pozzoli, G. Rewoldt, and T. Schep, in Proceedings of the Fifth International Conference on Plasma Physics and Controlled Nuclear Fusion Research, (International Atomic Energy Agency, Vienna, 1975), paper CN-33/A14-4, (to be published).
3. S.K. Wong, Phys. Fluids 18, 391 (1975).
4. S.I. Braginskii, in Reviews of Plasma Physics, edited by M.A. Leontovich (Consultants Bureau, New York, 1965), Vol.1, p.205.
5. P.H. Rutherford, Phys. Fluids 17, 1782 (1974).

STUDY OF PLASMA PROPERTIES IN THE TRAPPED ELECTRON REGIME IN THE FM-1 SPHERATOR

K. ANDO, V. ARUNASALAM, S.L. DAVIS, R.J. HAWRYLUK, M. OKABAYASHI, N. SAUTHOFF, J.A. SCHMIDT, S. SUCKEWER and M. YAMADA

Plasma Physics Laboratory, Princeton University

Princeton, New Jersey, United States of America

Abstract:

Recent experiments on drift wave mode structure, current driven instabilities, neutral beam injection and auxiliary heating near the lower hybrid frequency are described.

The next generation of large tokamak devices such as PLT and T-10 will operate in the trapped electron and possibly in the trapped ion regime. According to available theory in these regimes, the plasma transport properties will be significantly affected. In fact, experiments in the FM-1 spherator on particle confinement [1] and electron thermal conductivity [2] have indicated the presence of a new scaling law in the trapped electron regime different from that in the pseudoclassical collisional regime. Recent FM-1 spherator experiments are devoted to the study of plasma properties in the trapped particle regime. Our most recent experiments include (1) the detailed study of fluctuations in the trapped electron regime, (2) current driven effects in the trapped electron regime, (3) injection of a high power neutral beam (~ 100 kW) to obtain a plasma of the trapped ion regime and also to study the effect of a non-Maxwellian ion distribution function on plasma confinement, and (4) the study of auxiliary heating near the lower hybrid frequency. (At present (3) is under preparation). The typical plasma parameters (n_e, T_e) in these experiments are shown in Fig. 1, where the transition between the collisional regime and trapped electron regime is estimated from the observed transition between the pseudoclassical confinement scaling law and the Bohm type scaling law (τ = 200~300τ_B)[1].

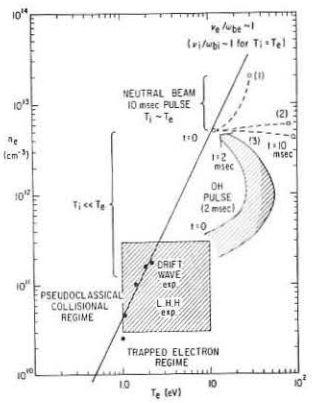

Fig. 1. Parameter regime in the FM-1 experiments. Black points are obtained from Ref. [1].

In order to study this range of plasma parameter we have built several new diagnostics for FM-1 including: (1) laser scattering for T_e and n_e, (2) 8mm microwave scattering for fluctuation studies, (3) spatially resolved light intensity measurement, (4) Doppler broadening measurement for T_i and (5) magnetic pick up probes.

1. Drift wave mode structure in the trapped electron regime

Drift wave mode structure was studied to clarify the effect of shear stabilization on the anomalous transport in the trapped electron regime. It is experimentally observed that fluctuations exist even when the shear is an order of magnitude greater than the value predicted for stability. It has been proposed that the peaking of the diamagnetic frequency profile could explain the failure of shear stabilization [3]. The mode structure was studied by using two probes movable in the radial and the azimuthal directions. The toroidal wavelength is quantized by the poloidal rather than the toroidal periodicity. The mode structure along the field line was investigated by aligning two probes using an electron gun. A theory was developed to calculate the amplitude and phase shift of the fluctuations at the magnetic field maximum and minimum based on periodically dependent driving terms. Experimental results show relatively strong coupling between adjacent mirrors.

2. Current driven effects in the trapped electron regime

There has been considerable interest in whether the well known simple current driven drift waves or ion accoustic waves can be excited in the trapped electron regime. In this regime, the majority of the current is carried by the circulating particles. Consequently a shifted electron Maxwellian distribution may not be produced. To investigate microinstabilities in this regime, we applied inductively an ohmic heating current in the poloidal direction. The ohmic heating current was 100~150 kA with one cycle at 500 Hz. Since the preionized plasma n_e~5×10^{11} cm^{-3} and T_e~5eV was not fully ionized, the plasma density and electron temperature change due to ionization is illustrated in Fig. 1.

The particle confinement time estimated from the observed plasma loss rate across the magnetic surfaces was τ_p = 5-15 msec, which was slightly lower than the τ = 200~300 τ_B scaling. Doppler broadening measurement show that the ion temperature was increased from T_i = 3eV to 10eV at the end of the ohmic heating pulse. Micro instabilities associated with the high ohmic heating current (estimated particle drift velocity~electron thermal velocity) were studied by 8mm microwave scattering (incident power of 1W, sensitivity for scattered power is 10^{-12}W). The frequency spectrum measurements showed strong fluctuations at low frequencies (f<5MHz). Preliminary results indidate that relatively weak current driven ion accoustic waves may exist under certain conditions.

3. Neutral Beam Injection

A high power neutral beam will be injected into a target plasma produced by ohmic heating. The evolution of the plasma density and temperature will be significantly affected by the neutral density in the plasma which will be determined by the operation of the FM-1 poloidal divertor. This is illustrated in Fig. 1 for a 15keV, 5A and 10 msec neutral beam pulse by assuming the capture efficiency of the plasma loss by the divertor chamber to be (1) 0%, (2) 80% and (3) 90%. We expect to obtain high plasma densities with T_i~ T_e, so that the trapped ion regime will be achieved.

4. Auxiliary heating near lower hybrid resonance

Auxiliary plasma heating experiments at frequencies near the lower hybrid frequency have been carried out at modest powers (.05-2kW). The antenna structure operating at 68MHz was comprised of two plates driven out of phase on the exterior of the plasma. High electron heating efficiency (>40%) in both Helium and Argon plasmas was observed with only a weak density dependence. At low densities ($n_e \lesssim 1\times10^{11}$cm^{-3}), the heating was uniform across the plasma while at higher densities the heating was preferentially on the exterior portion of the plasma. The heating of exterior of the plasma was found not to correspond to absorption at the lower hybrid resonance layer. The electron heating efficiency was found to be a weak function of rf power when the incident rf power was varied from 10 to 200 times the experimental observed threshold power for parametric instabilities. The ion temperature was determined by measuring the Doppler boradening of an Argon ion line using a Fabry-Perot interferometer. Low efficiency ion heating (1-3%) was observed.

References

[1] J. Sinnis et al., Phys. Rev. Lett. 29 1214 (1972).

[2] S. Ejima and M. Okabayashi, to be published in Phys. Fluids.

[3] N. Sauthoff et al., to be published in Phys. Fluids.

HEATING AND THERMAL ISOLATION OF CURRENT DISCHARGE PLASMA IN A CLOSED MAGNETIC TRAP

Volkov E.D., Latsko E.M., Rubtsov K.S., Rudakov V.A.
Physical-Technical Institute of Academy of Sciences of Ukr.SSR, Kharkov, U.S.S.R.

Investigations of thermal isolation of current-caryying plasma in tokamaks and stellarators at moderate current values confirm the empirical formula by L.A.Artsimovich [1]

$$\chi_e = C^2 \rho_\theta^2 \nu_{eff} \qquad (1),$$

which connects a thermal conductivity mechanism with anomalous resistance of a plasma.

In this paper we present the experimental results obtained in the "Sirius" stellarator which allow to make some conclusions about possible mechanism of pseudoclassical thermal conductivity.

It was shown earlier [2], that with electric field in a plasma $E \gg E_c$ (E_D is Draicer's field) the following dependence is observed:

$$\frac{\sigma_c}{\sigma} = C_1 E/E_D \qquad (2)$$

Here σ_c is the Coulomb conductivity, σ is measured experimentally. In this case the stabilization of current velocity was obtained $U = \alpha_s V_s = a_s \sqrt{\frac{T_e}{M_i}}$ which in combination with measurement results of oscillation spectrum and of noise level [3,4] allowed to interpret the dependence (2) as a result of the ion-acoustic instability development. However, in the region $E/E_D < 10$ the anomaly resistivity behaviour is different [5] from that (2) and $\frac{U}{V_s}$ value changes with the changing of E/E_D. In these conditions the assumption about an ion-acoustic nature of the anomaly has probably to be excepted. The latter conclusion is confirmed by theoretical consideration [6] as well .

It is of interest to compare the laws of energy losses in these two regions with pseudoclassical one. If to suppose pseudoclassical losses in stellarators, then the relation $nT = A i_\Sigma J$ must be fulfilled. Here nT is the unit-volume energy content in a plasma, and i_Σ is the total rotational transormation angle from the plasma current and helical windings.

Fig.1a and 1b show the dependences $nT(i_\Sigma J)$ for cases $E/E_D < 10$ and $E/E_D > 10$, respectively. It is easily seen that in the case "a" the energy losses correspond well to pseudoclassical ones. The case "b" corresponds to the ion-acoustic instability excitation and is not described by the equation (1).

Notice that pseudoclassical energy losses are observed in the most of current heating toroidal experiments at a small value of anomaly: $\frac{\sigma_c}{\sigma} \lesssim 10$, $E/E_D \gtrsim 1$. At the same time in many of these experiments the condition $U \geq \frac{\omega^*}{k_\parallel}$ is valid where $\omega^* = e k_\perp \nabla_r T_e / eH a$ and $a = \left(\frac{d \ln n}{dr}\right)^{-1}$, that is, the current velocity is larger or of the order of a phase velocity of drift oscillations.

The existance of such oscillations can essentially effect the rate of losses. In particular using the "Syrius" stellarator it was shown experimentally that the plasma diffusion is completely defined by drift fluctuations during the current flow stage [7].

If to assume that there is a limitation of a current velocity near the level of $U = \alpha \frac{\omega^*}{k_\parallel}$ at small values E/E_D then by the use of $k_\parallel = i/L = H\theta/rH$ it is easy to derive from the balance equation the expression which is similar to (1):

$$\chi_e = \frac{1}{9} \frac{\alpha^2 k_\perp^2 r^4}{a^2} \rho_\theta^2 \nu_{eff} \qquad (3),$$

where $\nu_{eff} = \frac{eE\omega_p}{m_e e V_{Te} \sqrt{\alpha k_\perp}}$, ω_p is the electron plasma frequency, the comparison of U, V_s and $\omega^*/k_\parallel$ shows that in given experiment $U = \alpha_s V_s < \omega^*/k_\parallel$ at $E/E_D > 10$ (Fig.2) and $U > \frac{\omega^*}{k_\parallel}$ at $E/E_D < 10$ (Fig.3). It was found that expression (3) is satisfied only in the case $U \gtrsim \frac{\omega^*}{k_\parallel}$.

These data allow us to make following conclusions:

1) the pseudoclassical thermal conductivity can be explained as a consequence of resistance canomaly appearance due to the current limitation on drift oscillations, i.e. as a result of interaction of current with these oscillations;
2) an ion-acoustic anomaly of resistance is developed at high electric field and this leads to the rates of losses which differ from pseudoclassical one .

REFERENCES

1. Artsimovich L.A. JETP Letters 13 (1971) 101
2. Burchenko P.I., Volkov E.D., Rudakov V.A., Sizonenko V.A., Stepanov K.N. IAEA, Madison (1971), v.III, 119.
3. Barkov A.P.Burchenko P.I., Volkov E.D., Rudakov V.A., Tereschenko F.F. JETP 43 (1973) 1170.
4. Barkov A.P.,Burchenko P.I., Volkov E.D. Rutsyn A.A., Maznichenko M.E., Pavlichenko O.S., Rubtsov K.S. "Voprosy atomnoy nauki i techniki", seris "physica plazmy i problemy UTS" Wyp I(2), Kharkov (1974) 60.
5. Burchenko P.I., Vasilenko B.T., Volkov E.D., Potapenko V.A., Rudakov V.A. "Physica plasmy i problemy UTS" AN Ukr.SSR, Kiev I (1971) 194.
6. Kadomtsev B.B., Pogutse O.P. JETP 53 (1967) 2025.
7. Burchenko P.I., Volkov E.D., Latsko E.M., Rudakov V.A. "Voprosy atomnoy nauki i techniki" seria "Physica plasmy i problemy UTS" wyp I(2), Kharkov (1974) 57.

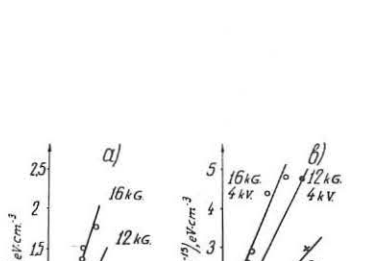

Fig.1. $nT(i_\Sigma J)$, dotted line corresponds to Artsimovich's formula with $C^2 = 5$.

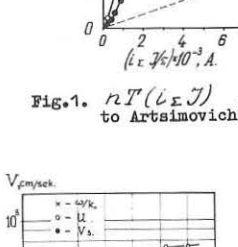

Fig.2. $n = 3 \div 5 \cdot 10^{13}$, $B = 16$ KG

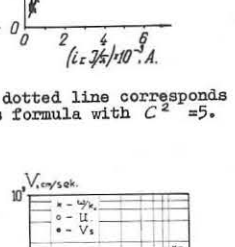

Fig.3. $n = 4 \cdot 10^{12} - 2 \cdot 10^{13}\,cm^{-3}$, $B = 16$ KG

ENHANCED TRANSPORT IN NON-AXISYMMETRIC TOROIDAL DEVICES DUE TO CONVERSION OF TRAPPED TO CIRCULATING PARTICLES BY FLUCTUATIONS

J. L. Shohet

The University of Wisconsin, Madison, Wisconsin 53706 (USA)

Abstract: In non-axisymmetric devices that exhibit a separatrix such as stellarators, enhanced transport can occur whenever trapped particles are converted to circulating particles outside of the separatrix. Transit-time magnetic pumping produces such conversions and the change in confinement obtained from experiments is in quantitative agreement with this mechanism.

Non-axisymmetric toroidal devices such as stellarators contain three classes of particles: 1) circulating, 2) particles trapped in mirrors of the helical field, and 3) particles trapped in mirrors of the toroidal field. Circulating particles tend to be contained inside magnetic surfaces, but trapped particles drift across the magnetic surfaces and, instead, are confined on drift surfaces which are bounded by mod-B surfaces. [1] In a stellarator, the mod-B surfaces deviate considerably from the flux surfaces, [2] and in fact, pass across the boundary between closed and open flux surfaces, i.e., the separatrix.

Hence, if some process converts a trapped particle to a circulating particle while it is outside of the separatrix, that particle will be lost. Normally, as long as the action is an adiabatic invariant, this will not happen, even if there are temporal and spatial variations in the fields.

Furth and Rosenbluth [3] developed a theory of enhanced transport for non-axisymmetric devices in which low-frequency electrostatic potentials caused either trapping of circulating particles, or additional trapping of trapped particles to produce the additional transport. It is proposed here that the inverse process, that is, "untrapping" of trapped particles due to electrostatic or magnetic fluctuations may also produce enhanced transport in non-axisymmetric devices. The fluctuations must add energy to the trapped particles in the direction parallel to the d.c. magnetic field, so that they will be untrapped. One possible method to do this occurs when the fluctuation frequency is of the order of the trapped particle bounce frequency. If parallel energy is added to these particles, the action is no longer an adiabatic invariant.

As an example of this transport, a model in which a temporal and spatial modulation of the toroidal field is produced, either deliberately, as in transit time magnetic pumping, [4] or spontaneously, because of fluctuations produced in the plasma, is considered. The fluctuation exerts a force on the trapped particle of magnitude $\mu_m \nabla B$ in the direction parallel to the toroidal magnetic field. μ_m is the particle's magnetic moment and ∇B is the field gradient produced by the fluctuation. The change in parallel velocity over a bounce period is obtained from eqn. (1).

$$\frac{1}{2} m V_{\parallel 2}^2 \simeq \frac{1}{2} m V_{\parallel 1}^2 + (\mu_m \nabla B) 2L \qquad (1)$$

where L is the length of the trapped particle's orbit, $V_{\parallel 2}$ is the velocity at the end of the orbit, and $V_{\parallel 1}$ is the velocity at the beginning of the orbit. In TTMP it is usually true that the wavelength of the fluctuation is approximately equal to the length of the trapped particle's orbit, since $V_{ph} \simeq V_{th}$ or

$$f_{TTMP}\, \lambda_{TTMP} \simeq f_{bounce}\, L$$

The fluctuation induced gradient, ∇B, can be approximated by assuming a field modulation amplitude b, so that

$$\nabla B \simeq \frac{2b}{L}$$

Equation (1) thus becomes

$$V_{\parallel 2}^2 - V_{\parallel 1}^2 = \frac{4\mu_m b}{m} = 2V_\perp^2 \frac{b}{B} \qquad (2)$$

From eqn. (2) we may compute the change in velocity $\Delta V_\parallel$ by factoring the left hand side to give, for $V_{\parallel 2} - V_{\parallel 1} = \Delta V_\parallel \ll 1$

$$(V_{\parallel 2} + V_{\parallel 1})(V_{\parallel 2} - V_{\parallel 1}) \simeq 2V_{\parallel 1} \Delta V_\parallel = 2V_\perp^2 \frac{b}{B} \qquad (3)$$

The determination of whether a particle is trapped or circulating depends upon its pitch angle θ with respect to the magnetic field. The change in pitch angle per bounce period is computed as follows:

$$\tan\theta_2 - \tan\theta_1 = \frac{V_\perp}{V_{\parallel 1}} - \frac{V_\perp}{V_{\parallel 1} + \Delta V_\parallel} \simeq -\frac{V_\perp}{V_{\parallel 1}^2} \Delta V_\parallel \qquad (4)$$

$$\simeq \frac{2\Delta\theta}{\cos\theta_1} \qquad \text{where } \Delta\theta = \theta_2 - \theta_1 \ll 1$$

Thus, the change in pitch angle per bounce period, $\Delta\theta$, is

$$\Delta\theta \simeq \frac{-V_\perp \Delta V_\parallel \cos\theta}{2V_\parallel^2} = -\frac{V_\perp^3 b}{B\sqrt{V_\parallel^2 + V_\perp^2}\, 2V_\parallel^2} \qquad (5)$$

As an example, let $V_\parallel \simeq V_\perp$, $\frac{b}{B} = .01$. Then $\Delta\theta = -.005$ radians/bounce period. For θ to change by θ_L radians, the number of bounce periods is

$$N_{\theta_L} = \frac{2B}{b}\theta_L \cong 100 \text{ bounce periods for } \frac{\pi}{2} \text{ radians.} \qquad (6)$$

This result is now applied to the enhanced transport observed in the Proto-Cleo stellarator under TTMP conditions. In order to obtain the enhanced transport, it can be shown that it is sufficient to convert trapped particles into circulating particles outside the separatrix. These circulating particles are then free to drift out of the confinement region.

In the Proto-Cleo experiment, with $\ell = 2$ windings, for which this analysis is developed, $R_o = 0.4$ m and $r_s \cong 0.05$ m. R_o is the major radius and r_s is the average separatrix radius. Figure 1 shows both the separatrix and the mod-B surfaces and thus the trapped particles can easily pass outside of the separatrix.

In Proto-Cleo many of the trapped particles are trapped in mirrors of the toroidal field, rather than localized in the helical mirrors. These particles are more nearly circulating than the localized particles. Also it was observed that the difference in containment times with and without TTMP decreased as the current in the helical windings was decreased, which lowered the number of trapped particles. Thus, trapped particles do seem to play a significant role in the enhanced transport. The bounce period was approximately $\tau_B = 10^{-5}$ sec. 100 bounce periods is about 1 msec.

Figure 2, taken from reference [4], shows that with 1% modulation, ($\frac{b}{B} = .01$) the particle containment time is reduced to approximately 1 msec. Equation (6) implies that the decrease in containment time varies linearly with modulation and shows no threshold effect, which is the result shown in Figure 2. Thus, conversion of trapped to circulating particles outside of the separatrix, [5] is consistent with the results; both qualitatively and quantitatively.

The helpful conversations with J. L. Johnson, H. Grad, D. J. Lees and W. Millar are gratefully acknowledged. This work was supported by the National Science Foundation under grant ENG-7203778 A01.

References:

[1] H. Grad, Phys. Fluids 10, 137 (1967).

[2] S. Fisher, H. Grad, Y. Sone and J. Staples, in Plasma Physics and Controlled Nuclear Fusion Research (International Atomic Energy Agency, Vienna, 1969) Vol. 1, p. 899.

[3] H.P. Furth and M.N. Rosenbluth, in Plasma Physics and Controlled Nuclear Fusion Research (International Atomic Energy Agency, Vienna, 1969) Vol. 1, p. 821.

[4] D.J. Lees, W. Millar, R.A.E. Bolton, G. Cattanei and P.L. Plinate, in Proceedings of the Fifth European Conference on Controlled Fusion and Plasma Physics, Grenoble, France, 1972 (Service d'Ionique Generale, Association EURATOM-Comissariat à l'Energie Atomique, Centre d'Etudes Nucléaires de Grenoble, Grenoble, France, 1972) Vol. II, p. 135.

[5] J.L. Shohet, Phys. Rev. Lett 34, 310 (1975).

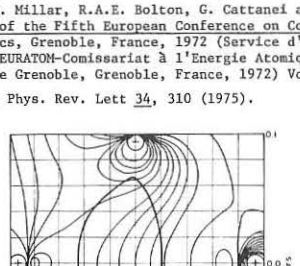

Fig. 1. Mod-B surfaces and the separatrix for the Proto-Cleo $\ell = 2$ stellarator. The conductors are shaded and the + or - sign shows the direction of the current in the helical windings. The major axis is to the left-hand side.

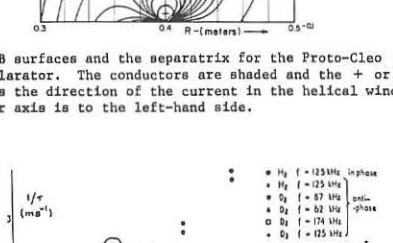

Fig. 2. Inverse of density confinement time, as a function of RF voltage. The modulation factors (ringed) are for a frequency of 122 kHz, and vary as 1/frequency.

Neoclassical Equilibrium and Transport Calculations
for the Full Range of Collisionality*

C.O. Beasley, J.E. McCune+, H.K. Meier, W.I. van Rij and J.D. Callen
Oak Ridge National Laboratory, P.O. Box Y, Oak Ridge, Tenn. 37830 U.S.A.

Abstract: The new Collisional Plasma Model, used to obtain neoclassical equilibria and transport in tori, is described. Results over the full collisionality range (banana through Pfirsch-Schlüter) show the distribution function, radial flux, bootstrap current and other important macroscopic quantities, and are compared with earlier, more approximate results.

Introduction: The general approach to calculating neoclassical transport is to approximate the Fokker-Planck collision operator by a model valid in some region of collisionality [1]. By use of a drift-kinetic equation, one may obtain an equilibrium distribution function, usually divided into a part describing trapped particles, and a part describing untrapped particles. However, since the effective collisionality of the plasma near the trapped-untrapped particle boundary pitch angle is greater than in other regions of velocity space, this region must be separately analyzed in an approximate way in order to include the effects of the distribution function in that region. Having the resulting composite distribution function, one can then calculate the various transport coefficients, or, more correctly, the desired moments of the distribution function, yielding currents, pressures, velocities, fluxes, etc.

In this paper, we present the results of neoclassical calculations obtained from an application of the Collisional Plasma Model (CPM). In the CPM, an exact treatment of the Fokker-Planck collision operator and the drift-kinetic equation through a particular choice of an expansion of the distribution function in velocity space, using a set of functions described below, permits us to calculate the distribution function to arbitrary accuracy in the Fokker-Planck - drift-kinetic sense. It is important to note that this model permits all particles, trapped or untrapped, to be treated on the same footing, thus removing the difficulties associated with the boundary layer. Moreover it does not entail any basic restriction on the range of collisionality to be considered. As in other neoclassical calculations, we have so far chosen to calculate locally on a given (circular) flux surface. If we relax this restriction, and use the full set of Maxwell's equations to include finite-β effects, in the Pfirsch-Schlüter regime, such calculations would be equivalent to a three-dimensional non-ideal MHD calculation except that all transport coefficients, inertial effects, etc., are calculated self-consistently, and are, in fact, an inherent part of results of CPM calculations.

In this paper, we briefly describe the model, and how we obtain our results. We then show the structure of the distribution function, radial flux, bootstrap current, toroidal and poloidal drifts, pressure tensors and heat fluxes in the banana, plateau, and Pfirsch-Schlüter regimes.

The Collisional Plasma Model: By choosing a suitable representation to expand $f(\vec{v})$, it is possible to write down analytically the elements of the Fokker-Planck collision operator. The expansion is useful if relatively few terms are needed to obtain convergence. One expansion we have found to have these properties is a modified Laguerre-Spherical Harmonic expansion:

$$f^s(\vec{r},\vec{v}) = \sum_{\ell,n,m} f^s_{\ell nm}(\vec{r})(\rho v^2)^{\ell/2} e^{-\rho v^2/2} L_n^{\ell+1/2}(\rho v^2) Y_{\ell m}(\alpha,\beta)$$

where s refers to species, v the velocity, $\rho = m_s/kT_s$, α is the angle (in velocity space) between the magnetic field direction and $\vec{v}$, and β the gyro-angle. (In a drift-kinetic equation, only the m = 0 term will appear; we henceforth drop this subscript.) Our drift-kinetic equation, in the absence of self-consistent electric fields, is

$$\frac{\partial f^s}{\partial t} + \frac{1}{\tau}\left[\sqrt{\rho}\, v\cos\alpha \frac{\partial f^s}{\partial\theta} + \frac{\epsilon\sin\theta}{2(1+\epsilon\cos\theta)}\sqrt{\rho}\, v\sin\alpha\frac{\partial f^s}{\partial\alpha}\right] - \frac{1}{\tau'}\left[2\rho v^2(1+\cos^2\alpha) \times (\sin\theta\, r\frac{\partial f^s}{\partial r} + \cos\theta\frac{\partial f^s}{\partial\theta})\right] = \sum_p C^{sp}_o f^s f^p \quad .$$

We further assume an axisymmetric equilibrium. Then using the poloidal periodicity, we write

$$f^s_{\ell n}(\vec{r}) = \sum_\mu f^s_{\ell n\mu}(r)\, e^{i\mu\theta} \quad .$$

Since our distribution function is approximately a Maxwellian, we may use the linearized form of the collision operator. In our representation, f is approximately (to one part in 10^3)

$$f(\vec{r},\vec{v}) \simeq f_{oo}(\vec{r})\, e^{-\rho v^2/2} L_o^{1/2}(\rho v^2) Y_{oo}(\alpha,\beta) = \frac{1}{2\sqrt{\pi}} f_{oo}(\vec{r})\, e^{-\rho v/2}$$

Then, symbolically, our drift-kinetic equation may be written in the form

$$\frac{\partial f^s_{\ell n\mu}(r)}{\partial t} + \sum_{\substack{n'=n-2\\ \ell'=\ell-2\\ m'=m-2}}^{\substack{m'=m+2\\ \ell'=\ell+2\\ n'=n+2}} K_{\ell\ell' nn'\mu\mu'}(r)\, f^s_{\ell' n'\mu'}(r) = \sum_{\substack{n'=0\\ \mu'=-\infty}}^{\infty}\Big[C^{ss}_{\ell nn'}(r)\, f^s_{oo\mu}(r)\, f^s_{\ell n'\mu-\mu'}(r) + \sum_p\left(C^{sp}_{\ell nn'}(r)\, f^s_{oo\mu}(r)\, f^p_{\ell n'\mu-\mu'}(r) + C^{ps}_{\ell nn'}(r)\, f^s_{\ell n\mu'}(r)\, f^p_{oo\mu-\mu'}(r)\right)\Big]$$

Method: We calculate the equilibrium by treating an initial value problem, where the plasma begins as a homogeneous Maxwellian with imposed radial density and temperature gradients, with and without applied toroidal voltage. We then follow the time evolution of $f(\vec{r},\vec{v})$, until it reaches a quasi-equilibrium. In this time-dependent problem, the various time scales inherent to the problem become apparent. These include the collisional time, the bounce time, the various diffusivity times, the velocity development times, and times associated with the flux. (The ordering of some of these time scales will depend on the collisionality regime.) The quasi-equilibrium of interest is one in which f is no longer evolving on any time scale except the latter.

Results: Space does not permit a detailed presentation of results. We do show two typical trapped-particle distribution functions in the banana, plateau and Pfirsch-Schlüter regimes (Figs. 1 and 2). These are actually perturbations of $f(\alpha)\,|_{v=2\sqrt{kT/m}}$, and $f(v)|_{\alpha=60^\circ}$ and are proportional to the number of particles at a given α (or v), on the inside of the torus ($\theta = 180^\circ$). The magnitudes of these perturbations (in comparison with the Maxwellian, magnitude = 1) are given by SF, the scale factor.

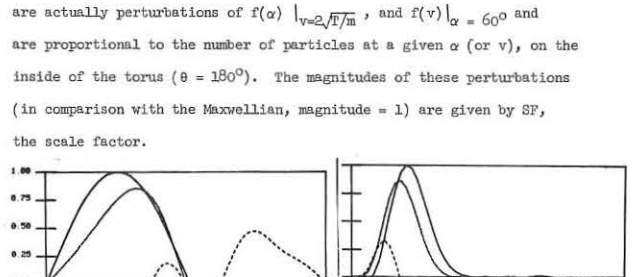

Fig. 1: $f(\alpha)$ at $v = 2\sqrt{kT/m}$

Fig. 2: $f(v)$ at $\alpha = 60^\circ$

It should be mentioned that we get good agreement for the radial particle flux, $\Gamma(\nu_*)$, in comparison with other work.

References:

[1] R.D. Hazeltine and F.L. Hinton, Phys. Fluids 16, 1883 (1973) and references cited therein.

+ Permanent address: Massachusetts Institute of Technology.

* Work supported by the U.S. ERDA under contract with Union Carbide Corp.

Neoclassical Diffusion and Dissipative Trapped-Electron Instabilities in the Transition from the Banana to Plateau Collisionality Regime*

J. D. Callen and K. T. Tsang
Oak Ridge National Laboratory, P.O. Box Y, Oak Ridge, Tenn. 37830 U.S.A.

Abstract: A phenomenological procedure of separating velocity space into various regions of collisionality (banana, plateau, boundary layer), calculating the perturbed distribution functions accordingly, and appropriately averaging over velocity space, is used to analytically reproduce neoclassical diffusion and facilitate investigation of dissipative trapped-electron modes in this important transition regime.

Introduction: Of the various types of low frequency drift and trapped-particle instabilities [1], the most relevant mode in present tokamaks is the drift-dissipative trapped-electron instability. This mode has previously been derived only in the banana regime where the trapped-electrons are very collisionless. However, present experiments tend to operate in the transition ($\nu_* \sim 1$) between the banana ($\nu_* \ll 1$) and plateau ($1 \ll \nu_* \ll \epsilon^{-3/2}$) regimes. We investigate this transition region with a phenomenological model based upon separating velocity space into the various regimes of collisionality.

Partitioning of Velocity Space: Since the collision frequency and bounce time for a given particle are dependent on its kinetic energy, we can separate velocity space into Pfirsch-Schlüter, plateau and banana regimes, as shown in Figure 1. In the banana regime the effective collision frequency for trapped-particles [$\nu_{eff}(E) = \nu_{ei}(E)/\epsilon = 3\sqrt{2\pi}\,(T_e/2m_e)^{3/2}/2\epsilon\tau_{ei}$, in a Lorentz gas] is less than the trapped-particle bounce frequency [$\omega_b^T = \sqrt{2\epsilon E}/R_o q$], and hence this region is defined by $E > E_c \equiv 0.97\sqrt{\nu_*}\,T_e/m_e$, or $v > 0.985\,\nu_*^{1/4} v_T$, where $v_T = \sqrt{2T_e/m_e}$ is an electron thermal velocity, and ν_* is the ratio of effective collision frequency to bounce frequency for a thermal, trapped-electron. In the banana regime particles can be distinguished as trapped or untrapped according to their pitch-angles in velocity space. Between the trapped and untrapped regions, there is a collisional boundary layer in which the bounce time is longer than the time required for collisions to scatter particles out of this region. As we progress from the banana regime to lower energies in Fig. 1, we first encounter the plateau regime, and finally for sufficiently low energies ($v < 0.985\,\epsilon^{3/8}\nu_*^{1/4} v_T$) reach the very collisional Pfirsch-Schlüter regime.

Neoclassical Diffusion: As an example of the usefulness of this partitioning of velocity space, we calculate the neoclassical particle flux in equilibrium by solving for the distribution function in the various collisionality regimes and then appropriately adding up the various velocity space contributions to the particle flux integral $\Gamma = (m_e/2\pi|e|B_\theta)\int d\theta\,(1+\epsilon\cos\theta)\int d^3v\, v_\parallel C_{ei}(f_e)$. For a Lorentz collision model and density gradient only, we obtain [2]

$$\Gamma = -K_{11}\,\epsilon^{1/2}\,\rho_{e\theta}^2\,n_e'/\tau_{ei}$$

where

$$K_{11} = 0.73\,e^{-x_c}\,[1 - 0.89\sqrt{\nu_*}\,e^{x_c}\,E_1(x_c)] + (\sqrt{2\pi}/8\nu_*)\,[e^{-y_c}(2+2y_c+y_c^2) - e^{-x_c}(2+2x_c+x_c^2)] + \frac{\pi\epsilon^{3/2}}{32}\left[\frac{75}{16}\,\mathrm{erf}\sqrt{y_c} - e^{-y_c}\sqrt{\frac{y_c}{\pi}}\left(\frac{75}{8}+\frac{25}{4}y_c-\frac{3}{2}y_c^2\right)\right]$$

in which $x_c = 0.97\sqrt{\nu_*}$, $y_c = \epsilon^{3/4}x_c$. We can recognize the first, second and third terms in square brackets in K_{11} as the contributions from the banana (including boundary layer), plateau and Pfirsch-Schlüter regimes, respectively. These analytic results compare quite favorably with the numerical formulae of Hazeltine and Hinton [3] (cf. Ref. 2). The reason why this separation of velocity space primarily by energy works so well is that energy scattering is weak in a neoclassical plasma; pitch-angle scattering is the dominant collisional process.

Dissipative Trapped-Electron Instabilities: For the temperature-gradient-driven version of these modes the dominant destabilizing contribution comes from the trapped-electrons in the banana regime -- region I in Fig. 1. Taking account of our separation of velocity space, we find that as ν_* increases this destabilizing integral does not change sign; however, it does decrease as $\exp(-\sqrt{\nu_*})$ for large ν_*. In the plateau region (II in Fig. 1) there is a collisional broadened Landau-type resonance, which, for $\omega \simeq \omega_*$ in the presence of a termperature gradient, has a stabilizing effect similar to that in collisionless drift modes [4]. The effective $k_\parallel$ here is $s/R_o q$, where s is an integer, and not $|sq-m|/R_o q \ll s/R_o q$ because for $\nu_* \sim 1$ the plasma is sufficiently collisional that the parallel variation of the potential seen by a particle is that seen within one bounce period and not the average seen over many bounce periods. Finally, there are contributions from the boundary layer between trapped and untrapped particles depending upon whether the wave frequency is larger (region III) or smaller (region IV) than the effective trapped particle collision frequency. The contribution from region IV is small because collisions simply further smear out the already small perturbed distribution function there. The contribution from region III, in which little diffusion takes place in the short period of the wave so that the diffusion is localized to the boundary layer, is similar to that calculated by Rosenbluth et.al. [5] for ions in the dissipative trapped-ion instability. Magnetic shear has a stabilizing effect on these modes that is found to be independent of the degree of collisionality. Stabilization of the temperature-gradient-driven version of the dissipative trapped electron instabilities occurs when ν_* becomes large enough so that the destabilizing contribution from region I becomes smaller than the stabilizing ones due to shear and the wave-particle resonance term. Specific numerical calculations of these effects are being performed.

References:

[1] B.B. Kadomtsev and O.P. Pogutse, Nuclear Fusion 11, 67 (1971).
[2] K.T. Tsang and J.D. Callen, "On the Smooth Transition of Neoclassical Diffusion from the Banana to Pfirsch-Schlüter Regime," ORNL-TM-4848, Feb., 1975 (to be published).
[3] R.D. Hazeltine and F.L. Hinton, Phys. Fluids 16, 1883 (1973).
[4] See for example: J.N. Davidson and T. Kammash, Nuc. Fus. 8, 203 (1968).
[5] M.N. Rosenbluth, D.W. Ross and D.P. Kostomarov, Nuc. Fus. 12, 3 (1972).

* Work supported by the U.S. ERDA under contract with Union Carbide Corp.

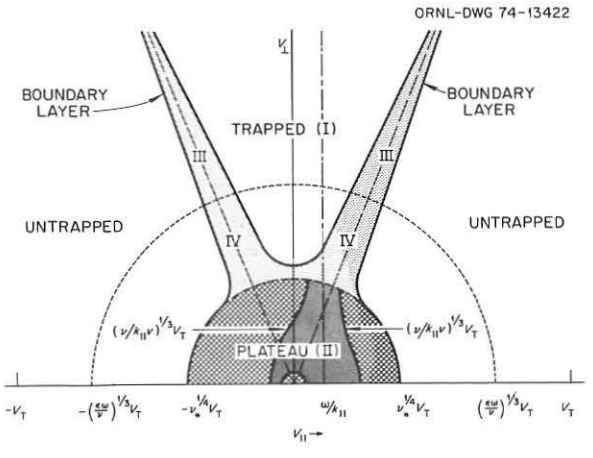

Figure 1 Regimes of collisionality in velocity space as seen on the outside of the torus.

MULTISPECIES DIFFUSION COEFFICIENTS IN THE PFIRSCH-SCHLUTER AND BANANA REGIMES FOR ALL TEMPERATURE AND MASS RATIOS

P. ROLLAND - F. WERKOFF

ASSOCIATION EURATOM-CEA
Département de Physique du Plasma et de la Fusion Contrôlée
Service IGn - Centre d'Etudes Nucléaires
B.P.85 - Centre de Tri - 38041
GRENOBLE CEDEX (France)

ABSTRACT : A general expression for the parallel friction is straightforwardly derived by using only the fact that the Fokker-Planck operator conserves momentum. Assuming the galilean invariance of the F.P operator, we obtain a simplified operator for unlike particle collisions, which gives the correct expression for the friction force. The inspection of the influence of the shape of the distribution function on the friction allows us to show that the fluid description of the Pfirsch-Schluter regime fails out when temperature gradients are taken into account. In the case of banana regime our results differ from those previously derived for multi species in /7/.

1 - FRICTION FORCE AND COLLISION OPERATOR. Starting with $f_j = f_{oj} + f_{1j}$ where f_{oj} is maxwellian and $f_{1j} \ll f_{oj}$, the friction force /1/ is given by :

$$R_{jk} = m_j \int \underline{dv}\, \vec{v}\, C_{jk} = m_j \int \underline{dv}\, \vec{v}\, C(f_{1j}, f_{ok}) + m_j \int \underline{dv}\, \vec{v}\, C(f_{oj}, f_{1k}) \qquad (1)$$

where $C(f_a, f_b)$ is the full Fokker-Planck (F.P) operator /2/. The conservation of momentum gives us :

$$R_{jk} = m_j \int \underline{dv}\, \vec{v}\, C(f_{1j}, f_{ok}) - m_k \int \underline{dv}\, \vec{v}\, C(f_{1k}, f_{oj}) \qquad (2)$$

For azimutal symetry and f_1 regular we have :

$$\int \underline{dv}\, v_\parallel C(f_{1j}, f_{ok}) = \int \underline{dv}\, pv \frac{\nu_{jk}}{2} L_p(f_{1j}) = -\int \underline{dv}\, v_\parallel \nu_{jk} f_{1j} \qquad (3)$$

where L_p is the Legendre operator $L_p = \partial_p\left[(1-p^2)\partial_p\right]$, $p = \frac{v_\parallel}{v}$ and ν is given in /3/.

(In (3), the terms whose contribution to R_{jk} vanishes are not written). Then :

$$R''_{jk} = -m_j \int \underline{dv}\, v_\parallel \nu_{jk} f_{1j} + m_k \int \underline{dv}\, v_\parallel \nu_{kj} f_{1k} \qquad (4)$$

Assuming that the F.P equation is galilean invariant - as previously done in /3/ for like particle collisions - we can derive /4/ a simplified F.P operator giving the correct expression (4) for R''_{jk} :

$$C_{jk} = \frac{\nu_{jk}}{2} L_p(f_{1j}) + \nu_{jk} v_\parallel f_{oj} \frac{m_k}{A_{jk}} \int \underline{dv}\, v_\parallel \nu_{kj} f_{1k} \qquad (5)$$

The following coefficients are defined :

$$A_{jk} = m_j \int \underline{dv}\, v_\parallel^2 \nu_{jk} f_{oj} = \frac{4}{3}(2\pi)^{\frac{1}{2}} e^4 \mathrm{Ln}\, D\, n_j n_k Z_j^2 Z_k^2 \left\{ \frac{(T_k m_j + T_j m_k)^{\frac{1}{2}}}{T_j (m_j m_k)^{1/2}} - \frac{m_j^{1/2}}{T_j^{3/2}} \frac{T_k}{m_k} \mathrm{In} \frac{(T_j/m_k)^{1/2} + (T_j m_k + T_k m_j)^{1/2}/(T_k m_j)^{1/2}}{} \right\}$$

$$B_{jk} = m_j \int \underline{dv}\, v_\parallel^2 v^2 \nu_{jk} f_{oj} = \frac{8}{3}(2\pi)^{1/2} e^4 \mathrm{Ln}\, D\, n_j n_k Z_j^2 Z_k^2 \frac{T_j}{m_j^{3/2}} \left(\frac{m_k}{m_k T_j + m_j T_k}\right)^{1/2}$$

$$D_{jk} = m_j \int \underline{dv} v_\parallel^2 v^4 \nu_{jk} f_{oj} = \frac{8}{3}(2\pi)^{\frac{1}{2}} e^4 \mathrm{Ln}\, D\, n_j n_k Z_j^2 Z_k^2 \frac{m_k^{1/2}}{m_j^{5/2}} T_j^2 \frac{(5T_k m_j + 4T_j m_k)}{(m_k T_j + m_j T_k)^{3/2}} \qquad (6)$$

In order to compare our result (4) with that of Braginskii (/1/ eq. 7-3, 7-6) we suppose $m_k \gg m_j$ and we consider a special form for the distribution function :

$$f_{1j} = f_{oj}\, \beta_{oj}\, v_\parallel \qquad (7)$$

Our equation (4) gives :

$$R_{jk} = -m_j \frac{A_{jk}}{T_j}(V_j - \frac{T_j}{T_k} V_k) \text{ where } V_j = \beta_{oj} \frac{T_j}{m_j} \qquad (8)$$

The expression given by Braginskii can be written :

$$R_{jk} = -\frac{m_j}{T_j} A_{jk} (V_j - V_k) \qquad (9)$$

The reason for this difference is that eq. (9) has been obtained by assuming that R_{jk} was a Galilean invariant, whereas eq. (4) and (7) show that this property is fulfilled only when $\frac{m_j}{T_j} A_{jk} = \frac{m_k}{T_k} A_{kj}$. When $m_k \gg m_j$, this last relation implies $T_j = T_k$.

2 - MULTISPECIES COEFFICIENTS OF THE PFIRSCH-SCHLUTER REGIME. Recent calculations /5/, /6/ of the diffusion coefficients in the Pfirsch-Schluter regime have led to discrepancies on the effect of the temperature gradients.
The inspection of the influence of the form of the distribution function on the friction force gives some light on this point :

In his calculation Samain /5/ uses a kinetic treatment and assumes that the distribution function is of the form :

$$f_{1j} = f_{oj}(\beta_{oj} v_\parallel + \beta_{1j} v^2 v_\parallel) + \text{even function of } v_\parallel \qquad (10)$$

On the other hand, Rutherford /6/ uses a fluid treatment with a term of parallel friction of the form (9), given in /1/. As a matter of fact, we shall see that R_{jk} is generally not of the form (9) even when $T_j = T_k$, $m_j \ll m_k$. For instance, if the distribution function is of the form (10), we obtain :

$$R_{jk} = -(A_{jk}\beta_{oj} + B_{jk}\beta_{1j}) + (A_{kj}\beta_{ok} + B_{kj}\beta_{1k}) \qquad (11)$$

$$R_{jk} = 4\frac{\sqrt{2\pi}}{3} \mathrm{Ln}\, D\, n_j n_k Z_j^2 Z_k^2 \left\{ \frac{m_j^{1/2}}{T_j^{3/2}}(V_{\parallel k} - V_{\parallel j}) + 3(T_j m_j)^{1/2}\left(\frac{\beta_{1j}}{m_j^2} - \frac{\beta_{1k}}{m_k^2}\right) \right\} \qquad (12)$$

where $V_{\parallel j} = \frac{T}{m_j}(\beta_{oj} + \frac{5T}{m_j}\beta_{1j})$. As we shall see later, f_1 is effectively of the form (10) in the P.S. regime, and (9) is no longer valid.
The linearized drift kinetic equation reads /3/ :

$$-\frac{\sin\theta}{2\omega_{cj}R} v^2(1+p^2)\partial_r f_{oj} - \frac{\textcircled{N}v}{r} p\, \partial_\theta f_{1j} + \frac{\textcircled{N} v \sin\theta}{2Rh}(1-p^2)\partial_p f_1 = \sum_k C_{jk} \qquad (13)$$

where $\textcircled{N} = -B_\theta/B$, $p = \frac{v_\parallel}{v}$, $h = 1 + r\cos\theta/R$. The matter and heat fluxes are given by /3/ :

$$\Gamma_j = \int \frac{d\theta h^2}{2\pi\omega_{cj}\textcircled{N}} \int \underline{dv}\, v_\parallel \sum_k C_{jk} = -\frac{1}{Z_j e B_\theta} \int \frac{d\theta h^2}{2\pi} \sum_k R''_{jk}$$

$$Q_j = \int \frac{d\theta h^2}{2\pi\omega_{cj}\textcircled{N}} \int dv\, v_\parallel v^2 \sum_k C_{jk} \qquad (14)$$

We expand f_1 in Legendre polynomials $f_1 = \sum_n P_n(p)\,\phi_n(\theta, v)$. Only ϕ_1 gives a contribution to the fluxes. Integrating eq. (12) from p = - 1 to p = 1 gives:

$$\phi_{1j} = \frac{2r\cos\theta\, v}{R\omega_{cj}\textcircled{N}} f_{oj}\left(\mathcal{A}_{1j} + \frac{m_j v^2}{2}\mathcal{A}_{2j}\right) \text{ where } \mathcal{A}_{1j} = \left(\frac{N'}{N} - \frac{3}{2}\frac{T'}{T}\right)_j ; \mathcal{A}_{2j} = \frac{T'_j}{T_j^2} \qquad (15)$$

As we see, f_1 is effectively of the form (10) with $\beta_1 \neq 0$, as it has been supposed by Samain. β_1 is proportionnal to T'. Eq. (14) gives:

$$\Gamma_j = \frac{2r^2}{R^2 B_\theta^2 Z_j e^2} \sum_k \left\{ \frac{m_k}{Z_k} A_{kj}\mathcal{A}_{1k} + \frac{m_k^2}{2Z_k} B_{kj}\mathcal{A}_{2k} - \frac{m_j}{Z_j} A_{jk}\mathcal{A}_{1j} - \frac{m_j^2}{2Z_j} B_{jk}\mathcal{A}_{2j} \right\} \qquad (16)$$

$$Q_j = \frac{2r^2}{R^2 B_\theta^2 Z_j e^2} \sum_k \left\{ \frac{m_k}{Z_k}\frac{B_{jk}}{A_{jk}} A_{kj}\mathcal{A}_{1k} + \frac{m_k^2}{2Z_k}\frac{B_{jk}}{A_{jk}} B_{kj}\mathcal{A}_{2k} - \frac{m_j}{Z_j} B_{jk}\mathcal{A}_{1j} - \frac{m_j^2}{2Z_j} D_{jk}\mathcal{A}_{2j} \right\} \qquad (17)$$

When the masses are very different, we have $B_{jk} = \frac{2T_j}{m_j} A_{jk}$ and in eq. (16) we recover the term $\frac{N'}{N} - \frac{1}{2}\frac{T'}{T}$ of Samain /5/. If the distribution had been chosen a priori of the form (7) the integration of eq. (13) over all the velocity space would have given the wrong dependence $\frac{N'}{N} + \frac{T'}{T}$.

3 - MULTISPECIES COEFFICIENTS OF THE BANANA REGIME. We shall use our F.P. operator (5) within the standard technic /3-7/. :

$$f_{1j} = -\frac{m_j}{Z_j e B_\theta} qh\, \partial_r f_{oj} + g(\mu, \varepsilon, \sigma)$$

For the passing particles (with $v_\parallel = \sigma v\left(1 - \frac{\lambda}{h}\right)^{1/2}$) we obtain :

$$\partial_\lambda g_j = \frac{v\sigma}{2<(1-\frac{\lambda}{h})^{1/2}>} \frac{f_{oj}}{} \left\{ -\frac{m_j}{eB_\theta Z_j}\left(\mathcal{A}_{1j} + \frac{m_j v^2}{2}\mathcal{A}_{2j}\right) + \frac{1}{\sum_{a,b} m_a A_{ab}} \sum_{ab} \left(\frac{m_a}{Z_a} A_{ab}\mathcal{A}_{1a} + \frac{m_a^2}{2Z_a} B_{ab}\mathcal{A}_{2a}\right) \frac{m_j}{eB_\theta} \right\}$$

With the expression A-40 of /3/ for Γ_j, we obtain :

$$\Gamma_j = \frac{m_j}{Z_j e^2 B_\theta^2} 1.46\sqrt{\epsilon} \sum_k A_{jk} \left\{ -\frac{1}{Z_j}\left(\mathcal{A}_{1j} + \frac{m_j}{2}\frac{B_{jk}}{A_{jk}}\mathcal{A}_{2j}\right) + \frac{\sum_{ab}(m_a A_{ab}\mathcal{A}_{1a}/Z_a + m_a^2 B_{ab}\mathcal{A}_{2a}/2Z_a)}{\sum_{ab} m_a A_{ab}} \right\}$$

$$Q_j = \frac{m_j}{Z_j e^2 B_\theta^2} 1.46\sqrt{\epsilon} \sum_k B_{jk} \left\{ -\frac{1}{Z_j}\left(\mathcal{A}_{1j} + \frac{m_j}{2}\frac{D_{jk}}{B_{jk}}\mathcal{A}_{2j}\right) + \frac{\sum_{ab}(m_a A_{ab}\mathcal{A}_{1a}/Z_a + m_a^2 B_{ab}\mathcal{A}_{2a}/2Z_a)}{\sum_{ab} m_a A_{ab}} \right\}$$

These expressions are somewhat different from those of Connor /7/, because the collisions jj give a non vanishing contribution, although $\sum_j Z_j \Gamma_j = 0$ /3/.
In the case of different temperatures our results differ from those of Rosenbluth et al. /3/, because their e.i collision operator gives in this case an expression different from our eq. (4). To obtain C_{ei} in /3/, $\hat{f}_e$ is linearized in $\bar{v}_i (m_e/T_e)^{1/2}$ (/3/ eq.D 18). As a matter of fact, the correct linearization could be the following : $\hat{f}_j$ is proportional to the ratio of the shift velocity to the thermal velocity : $\hat{f}_e \sim \bar{v}_e (m_e/T_e)^{1/2}$. In diffusion theories the perturbed distribution functions are of the form : $\hat{f}_j \sim \frac{v_\parallel m_j}{Z_j e B}\mathcal{A}_j$. Then $|\bar{v}_j| \sim \frac{m_j}{eB_\theta}\frac{T_j}{m_j}\mathcal{A}_j$, i.e $\bar{v}_j$ scales as T_j and $\hat{f}_e$ must be linearized in $\bar{v}_i \frac{e}{T_i}\left(\frac{m_e}{T_e}\right)^{1/2}$. Following the same procedure as in /3/(Eq. D-18 to D-20) we obtain for C_{ei} an expression which differs from eq. D-20 by a factor T_e/T_i in front of $\bar{v}_i$, and then this modified operator leads to an expression of R_{ie} equivalent to our eq. (2). In the case of e.i collisions and equal temperatures and with
$I_{oa} = \sum_b \frac{3}{2\sqrt{2}} \frac{m_a A_{ab}}{4\pi e^4 \mathrm{Ln}\, D\, Z_a^2 Z_b^2}$, $I_{1a} = \sum_b \frac{3}{4\sqrt{2}} \frac{m_a B_{ab}}{4\pi e^4 \mathrm{Ln}\, D\, Z_a^2 Z_b^2}$, where the I are defined in /3/, $m_i A_{ie} = m_e A_{ei} = m_e^2 \frac{B_{ei}}{2T} = m_i^2 \frac{B_{ie}}{2T} = \frac{4}{3}\sqrt{2\pi} e^4 Z_i^2 N_i N_e \mathrm{Ln}\, D \sqrt{\frac{m_e}{T_e}}$,
it is easy to see that our results agree with eq. (88-92) of Rosenbluth et al. /3/.

REFERENCES :

/1/ - S.I. BRAGINSKII, Review of Plasma Physics 1, 214 (1965).
/2/ - M.N. ROSENBLUTH, W.M Mac DONALD, D.L. JUDD, Phys. Rev. 107, 1 (1957).
/3/ - M.N. ROSENBLUTH, R.D. HAZELTINE, F.L. HINTON, Phys. of Fl. 15, 116 (1972).
/4/ - P. ROLLAND, F. WERKOFF, Physics Letters (to be published) (1975).
/5/ - A. SAMAIN, Report EUR-CEA-FC 745 (1974).
/6/ - P.H. RUTHERFORD, Phys. of Fluids 17, 1732 (1974).
/7/ - J.W. CONNOR, Plasma Phys. 13, 765 (1973).

NEW FLUID THEORY OF THE DISSIPATIVE TRAPPED-ION INSTABILITY

H.K. Wimmel

Max-Planck-Institut für Plasmaphysik, 8046 Garching bei München, Federal Republic of Germany

Abstract: An improved set of dissipative, trapped-fluid, drift equations for anomalous plasma transport in tokamaks is established. The anomalous diffusion coefficient due to the dissipative trapped-ion instability is derived from these equations, and the result is compared with the diffusion formula of KADOMTSEV and POGUTSE [1].

The macroscopic theory by KADOMTSEV and POGUTSE [1] of anomalous diffusion in a tokamak due to the dissipative trapped-ion instability neglects the effects of $E_\parallel$ and of $\nabla\delta_0$, where $\delta_0 = n_0/N_p$ is the equilibrium fraction of trapped particles. Improved macroscopic equations are presented that include these effects to linear order in the perturbation. Specifically, $E_\parallel$ perturbs the distribution functions $f_{i,e}$, the instantaneous loss cone factors $\delta_{i,e} \equiv |v_\parallel/v|_{crit}$, and the instantaneous "equilibrium densities" $n_{i0}(t)$, $n_{e0}(t)$ of the trapped particles. The latter quantities enter in the collision terms of the dissipative continuity equations for trapped particles. The collision terms are also affected by the $\underline{E} \times \underline{B}$ drift of the particles, because the drift contributes to varying the instantaneous trapped equilibrium densities. On the other hand $\nabla\delta_0 \neq 0$ provides for additional particle sources, or sinks, in the dissipative continuity equations. The new equations read:

$$\frac{\partial n_i}{\partial t} + \underline{v}\cdot\nabla n_i = -\nu_{eff}(n_i - n_{i0}) + \left(\frac{\partial n_i}{\partial t}\right)_{E_\parallel} + N_p\,\underline{v}\cdot\nabla\delta_0 \qquad (1)$$

$$\frac{\partial n_e}{\partial t} + \underline{v}\cdot\nabla n_e = -\nu_{eff}(n_e - n_{e0}) + \left(\frac{\partial n_e}{\partial t}\right)_{E_\parallel} + N_p\,\underline{v}\cdot\nabla\delta_0 \qquad (2)$$

$$N_i + n_i = N_e + n_e \qquad (3)$$

$$\underline{v} = \frac{c}{B^2}\,\underline{B}\times\nabla\Phi \qquad (4)$$

with

$$N_i = N_0 + \frac{1-\delta_0}{\delta_0}\cdot\frac{e N_p \Phi}{T_i} \qquad (5)$$

$$N_e = N_0 - \frac{1-\delta_0}{\delta_0}\cdot\frac{e N_p \Phi}{T_e} \qquad (6)$$

$$\left(\frac{\partial n_i}{\partial t}\right)_{E_\parallel} = -\frac{e N_p}{T_i\,\delta_0}\,\frac{\partial\Phi}{\partial t} \qquad (7)$$

$$\left(\frac{\partial n_e}{\partial t}\right)_{E_\parallel} = +\frac{e N_p}{T_e\,\delta_0}\,\frac{\partial\Phi}{\partial t} \qquad (8)$$

$$n_{i0} = n_0 + \delta_0(n_i - n_0) + \frac{T}{2T_i}(n_i - n_e) \qquad (9)$$

$$n_{e0} = n_0 + \delta_0(n_e - n_0) - \frac{T}{2T_e}(n_i - n_e). \qquad (10)$$

Here N_i, N_e, and n_i, n_e are the actual untrapped and trapped densities; N_p, N_0, and n_0 are the total, untrapped, and trapped equilibrium densities, and the remaining notation is standard. The approximations $\nabla(T/N_p) = \nabla B = 0$, $\nabla\cdot\underline{v} = 0$ are used. The potential Φ can be eliminated by

$$\Phi = -\frac{T\,\delta_0}{2eN_p(1-\delta_0)}(n_i - n_e), \qquad (11)$$

with $T = 2T_eT_i/(T_e + T_i)$; $\Phi = 0$ at $B = B_{max}$. This differs in sign as well as in magnitude from analogous equation of KADOMTSEV and POGUTSE [1]. Alternative sets of equations proposed by HORTON et al. [2] and LAQUEY et al. [3] do not agree with the above system because these authors neglect the temporal variations of the loss cone factors $\delta_{i,e}$ although they are predominant effects, and omit the effect of $\nabla\delta_0$. In particular their expressions for $N_{i,e}$, $(\partial n_{i,e}/\partial t)_{E_\parallel}$, and n_{i0}, n_{e0} are not correct.

By a critical-mode, mixing-length method the anomalous diffusion flux due to the dissipative trapped-ion instability can be derived from eqs.(1) to (11) for the case of strong, isotopic, small-scale turbulence (WIMMEL [4]). This method is superior to the one used by KADOMTSEV and POGUTSE [1] in that it determines to what density gradient (∇N_p, ∇n_0, or whatever) the diffusion flux is proportional. So it is possible to decide whether the trapped-particle diffusion is inward or outward near the magnetic axis. The diffusion flux density for a slab model is:

$$\gamma_x = -\frac{cT\,\delta_0^2}{2eBN_p\,\nu_{eff}(1-\delta_0)^3}\,\langle\partial_t\varrho\cdot\partial_y\varrho\rangle, \qquad (12)$$

with $\varrho = n_i - n_e$, or, explicitly:

$$\gamma_x = -\frac{1}{2\sqrt{5}}\left(\frac{cT\,\nabla n_0}{2eBN_p}\right)^2\frac{\delta_0}{\nu_{eff}}\,\frac{\partial N_p}{\partial x}\,K_1\left(\delta_0, \frac{T}{T_e}\right), \qquad (13)$$

$$K_1 = \frac{2\delta_0^2}{1-\delta_0}\left\{\left(1-\delta_0-\frac{T}{2T_e}\right)^2 + \delta_0^2\right\}^{-1}. \qquad (14)$$

This result exhibits a more complicated dependence on δ_0 than the original formula by KADOMTSEV and POGUTSE [1]. It shows explicitly that the diffusion flux is proportional to ∇N_p rather than ∇n_0. If the effects of $\nabla\delta_0$ and $E_\parallel$ were omitted as was done by KADOMTSEV and POGUTSE [1], the mixing-length method would yield, instead of eqs. (13), (14), the following:

$$\tilde{\gamma}_x = -\frac{1}{2\sqrt{5}}\left(\frac{cT\,\nabla n_0}{2eBN_p}\right)^2\frac{1}{\nu_{eff}}\,\frac{\partial n_0}{\partial x}, \qquad (15)$$

a paradoxical result because it would predict inward rather than outward diffusion near the magnetic axis.

[1] KADOMTSEV B.B. and POGUTSE O.P., Reviews of Plasma Physics (LEONTOVICH M.A. Editor) Vol. 5, p. 249 (1970). Nuclear Fusion 11, 67 (1971).

[2] HORTON, JR., W. et al., Plasma Physics and Controlled Fusion Research (Proc. 5th Conf. Tokyo), Paper IAEA-CN-33/A14-3 (1974).

[3] LAQUEY R.E. et al., Phys. Rev. Lett. 34, 391 (1975).

[4] WIMMEL H.K., Plasma Physics, to be published.

"This work was performed under the terms of the agreement on association between the Max-Planck-Institut für Plasmaphysik and EURATOM".

ANOMALOUS ION TRANSPORT IN A MAGNETIZED DISCHARGE PLASMA

G. Popov

Institute of Electronics, Bulg. Acad. Sci., Sofia, Bulgaria

Abstract: The transverse ion transport in an Argon magnetoplasma column was studied experimentally. The B-field dependence of the wall ion flux for $B > B_c$ can be understood only if the anomalous part of the diffusion coefficient is taken into account. Onset of cathode region instabilities causes rise of the wall ion flux in the column.

The paper is aimed at elucidating the nature of enhanced ion transport in a magnetoplasma column. Changing the boundary conditions at the beginning of the plasma column, we looked into effects due to long-distance interactions in a turbulent plasma column.

In our experiments we made use of the idea of ECKER /1/ who described the enhanced transport processes by introducing an effective electron-ion relaxation time. Recently this idea was refined by several workers, e. g. /2/ who related the effective collision frequency corresponding to the diffusion process to the anomalous part of the diffusion coefficient.

1. A plasma was produced in hot-cathode discharge tubes with diameters 40 to 70 mm and lengths 50 to 60 cm. The experiments were made in Argon (0.2 to 1.0 torr) in order to separate the beam and secondary electrons. The axial magnetic field was produced by water-cooled magnetic coils. The unformity region (<5%) was greater than the tube length. The tube and the coils were exactly coaxial. The magnetic induction was changed from 0 to 0.2 Tesla. Density and potential profiles were obtained using Langmuir probes, the axial and azimuthal correlations of light-output and potential fluctuations being also recorded.

The change of the boundary conditions was provided by variation of the cathode thermionic-emission/discharge current ratio, I_{em}/I_d. The transition from glow-like discharge (GLD), $I_{em}/I_d < 1$, to thermionic-emission controlled discharge (TECD), $I_{em}/I_d > 1$, is connected with the change of the beam electrons energy dissipation mechanism /3/ which leads to onset of various kinds of instabilities:

a) Because of similarity between GLD- and TECD-cathode fall region the discharge balance equation for $I_{em}/I_d = 1$ is transformed into $\gamma M = 1$, M = 1 /3/ and the γ-δ instability takes place /4/ (γ = cathode efficiency, δ = plasma efficiency, M = ectron multiplication rate in the cathode sheath).

b) Ion-acoustic waves instability may be excited by the electron beam from the cathode if the electron drift velocity exceeds some critical value (/2/, chap. 7, 11).

c) Nonlinear interaction between the slow electrons at the Ramsauer's minimum and the plasma causes rotation of the positive column head /5/ in the case of GLD.

Therefore the onset of various kinds of instabilities at the beginning of plasma column can be controlled by variation of I_{em}/I_d - ratio. We can also study their interaction with the intrinsic plasma column instabilities.

The choice of a reliable and sensitive method for measurments of the particle losses proves to be the most complicated problem. ECKER /1/ suggested that the use of simple density and profile functions

$$U_r = -a.\ln(n_o/n_r) + b(n_o).\ln(n_o/n_r) \qquad (1)$$

offers a sensitive method for studying the particle losses. From the dependence of U_r on $\ln(n_o/n_r)$ we can draw a conclusion about processes taking place in the plasma volume. A deviation from linearity occurs if the second term in (1) due to Coulomb-interaction is nonzero. Such a presentation has the advantage that it doesnot depend on the radial density profile. Fig.1 shows the effect of the magnetic induction on U_r as a function of $\ln(n_o/n_r)$, obtained in a discharge tube with 50 mm diameter, I_d = 20 ma, I_{em}/I_d = 0.1, p = 0.5 torr. For B = 0 a deviation from linearity occurs only near the wall where the nonlinear plasma-sheath interaction takes place. For B > 0.07 T nonlinear dependence is obtained, e. g. the collective phenomena take place in the whole plasma volume. In our case the curvature of the plot is opposite to that evaluated from ECKER. A critical value, $B_c \simeq 0.072$ T, was obtained by light-emission and correlation measurements. We didnot observe the development of zero-mode helical instability accompanied by concentration of the current within screw-chaped channel. In Argon, the helical instability breaks, possibly, into turbulence. The radial density profile for B>0.09 T is Gaußian [x].

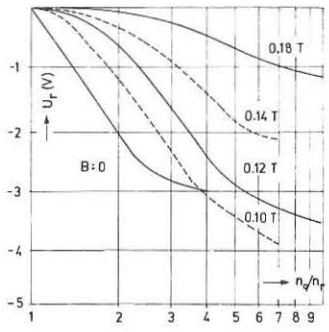

Fig. 1

2. In order to study the effect of the boundary conditions on the anomalous transport we measured the ion flux to the wall. The ion satturation current in the wall vicinity, I_{is}, was picked up by spherical Langmuir probes. In the B-field region under investigation the ion Larmor radius was always greater than the probe radius. The I_{is} - values were corrected according to the B-field variation of the floating potential.

The ion satturation current density obtained in this way depends only on the diffusion rate and the plasma density profile if ambipolarity takes place in the volume:

$$j_{is} = - D(B)n_o(B)f(r,B) \qquad (2)$$

where $n_o(B)$ = plasma density on tube axis, $n_o(B) = n_o(0)(1+\chi(I_{em}/I_d).B)$ for $B \leq 0.15$ T, and $n_o(B) = n_o(0)(1+ 0.15\chi)$ for $B > 0.15$ T.

In the first approximation the density profile function, f(r,B), can be given in the form:

$$f(r,B) = \begin{cases} -J_1(2.4r/R)2.4/R & \text{for } B < B_c \\ -\exp(-r^2/r_o^2)2r/r_o^2 & \text{for } B > 1.5\ B_c \end{cases} \qquad (3)$$

(J_1 is the first-order Bessel function, $r_o = (0.7...0.8)R_{tube}$) For $r/R_{tube} = 0.75$, $R_{tube} = 2$ cm we obtain (see Table1 in/6/):

$$j_{is} = 0.7e(1 + \chi B)D_a(1 + 28.4B^2[T])^{-1}, \quad B < 0.07 \text{ T} \qquad (4)$$

$$j_{is} = 0.5e(1 + \chi B)(D_a(1+28.4B^2[T])^{-1} + D_{Bohm}), \quad B > 0.1 \text{ T} \qquad (5)$$

At $B < 0.07$ T, j_{is} doesnot depend on B if $I_{em}/I_d > 1$, $\chi = 2$ Tesla^{-1} and grows slightly if $I_{em}/I_d < 1$, $\chi = 4$ T^{-1}. For $B > 0.1$ T correct j_{is}-values can be obtained only taking into account the anomalous part of the diffusion coefficient (in our case for slightly turbulent plasma with $T_i \ll T_e$, /2/ Chap. 11).

$$D_{Bohm}\left[cm^2/sec\right] = \frac{10^3(T_i[eV] \times T_e[eV])^{1/2}}{(n[cm^{-3}]\lambda_D^3[cm])^{1/2} B[T]}$$

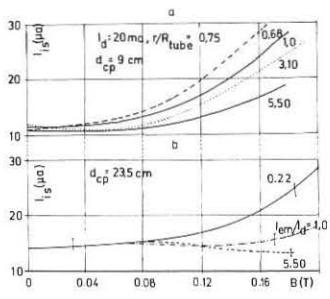

Fig. 2

Fig. 2 shows the I_{is} vs B plot for two tube cross-sections: at the beginning, d_{ep} = 9 cm (a) and in the middle of the column (b), $r/R_{tube} = 0.75$, R_{tube} = 2 cm; parameter being the I_{em}/I_d-ratio. At $I_{em}/I_d > 1$ the negative space charge near the cathode suppresses the cathode region instabilities. I_{is} for B > 0.1 T (Fig. 2b) depends on the intrinsic, turbulent-column diffusion and can be described by eq. (5). The onset of cathode region instabilities causes at least twofold increase of I_{es} for B = 0.2 T which isnot taken into account in eq. (5). The long-distance interactions lead possibly to the broadening of the turbulence spectrum.

[x] A Gaußian density profile may also be caused by end effects: B-field inhomogenity, small $r_{cathode}/R_{tube}$- ratio etc.

REFERENCES

/1/ G. ECKER, Phys. Fluids 4(1961)127

/2/ S. ICHIMARU, "Basic Princ. Plasma Phys.", Moscow 1975

/3/ G. POPOV, Proc. 3d Int. Conf. Gas Disch., London 1974, p. 163

/4/ G. ECKER, W. KRÖLL, O. ZÖLLER, Ann. Phys. 15(1965)60
K. G. EMELEUS, Int. J. Electronics 32(1972)593

/5/ G. POPOV, L. ROTHHARDT, 9th ICPIG, Bucharest 1969, p. 154

/6/ G. POPOV, 11th ICPIG, Prague 1974, p. 112

Theory of Anomalous Electron Transport.

C. T. Dum

Max-Planck-Institut für Plasmaphysik, 8046 Garching bei München, Federal Republic of Germany

Abstract: A complete set of anomalous electron transport coefficients is derived for ion sound and related instabilities. As compared to classical theory, not only can effective collision frequencies be very much larger but there are interesting differences in the structure of the transport equations as well.

The effect of turbulence on transport phenomena such as resistivity and heat-conduction is of great interest to many problems, e.g. turbulent heating, shock waves, laser -pellet interaction and the solar wind. By now there is good evidence that ion sound and related instabilities are responsible for anomalous transport in all of these cases. Just as for a collision dominated plasma [1], one would like to obtain a closed set of transport equations relating the macroscopic variables. In classical theory the possibility of such a description arises from the existence of a universal relaxation process, causing any distribution function to relax to a Maxwellian. Thus for phenomena which occur on time scales long compared to the relaxation time τ and on length scales long compared to the meanfree path $\lambda=v_e\tau$, the deviation f_1 of the distribution function from a local Maxwellian can be treated as a small perturbation. Transport coefficients are determined from f_1 which is proportional to the perturbing gradients, electric field, etc. Small scale turbulence also leads to very effective scattering of particles, but there is no universal relaxation law for the distribution function. The fluctuation spectrum is no longer a given functional of the distribution but is determined in general by nonlinear dynamic processes, such as mode coupling and quasi-linear flattening of the distribution. One can thus hardly expect to obtain a universal, closed macroscopic theory of anomalous transport and so far ,at best, only order of magnitude estimates of effective collision frequencies have been given.

We show in this paper that for a very important class of instabilities it is nevertheless possible to give a complete description of transport processes, analogous to classical theory. We consider the effect of a given spectrum of low phase velocity waves, $v_{ph} \ll v_e$, on electron transport. The predominant effect of such fluctuations, e.g. ion sound, is pitch angle scattering, much like that of electron-ion collisions. The distribution function, however, does <u>not</u> relax to a Maxwellian equilibrium but assumes the <u>selfsimilar form</u>

$$f_o(\underline{w}) = C_5 \exp\left[-(w/w_o)^5\right] \qquad (1)$$

where the time dependence is through $w_o(t)$, describing electron heating. In our theory this relaxation to a selfsimilar isotropic distribution plays the same role as the relaxation to a Maxwellian in classical transport theory, and the assumption $(v_{ph}/v_e)^2 \ll 1$ replaces $m/M \ll 1$. We consider transport in a weak magnetic field $k\rho_L \gg 1$ (k typical wave number, ρ_L electron Larmor radius) and inhomogeneity scales large compared to the wavelengths, $kL \gg 1$. The kinetic equation for the electrons is then

$$\frac{\partial f}{\partial t} + \underline{v}\cdot\frac{\partial f}{\partial \underline{x}} + (\underline{\Omega}\times\underline{v})\cdot\frac{\partial f}{\partial \underline{v}} + \frac{e}{m}\underline{E}_o\cdot\frac{\partial f}{\partial \underline{v}} = \frac{\partial}{\partial \underline{v}}\cdot\underline{\underline{D}}(v)\cdot\frac{\partial f}{\partial \underline{v}} \qquad (2)$$

where $\underline{\underline{D}}$ may be taken to be the unmagnetized quasilinear diffusion tensor [2]. The main physical ideas become more apparent, if we consider, for now, an isotropic (in the ion frame) turbulent spectrum. In spherical coordinates (w,θ,ϕ) the only nonvanishing components of the diffusion tensor are then

$$D^{vv} = \pi\omega_e \frac{W}{nT_e} v_e^2 \langle (\omega_e/kv_e)(\omega_k/kv_e)^2 \rangle (v_e/v)^3 \qquad (3)$$

and

$$D^{\theta\theta} = D^{\phi\phi} = \frac{1}{2}\left[\pi\omega_e \frac{W}{nT_e} v^2 \langle\omega_e/kv_e\rangle (v_e/v)^3 - D^{vv}\right], \qquad (4)$$

where the average is over the spectrum $W(k)$ resonating with electrons of speed $v,\omega/(kv)<1$. Temperature and thermal velocity are defined by (3/2) $T_e = m\langle w^2/2\rangle = (3/2)\, mv_e^2 = (3/2)\,\mu_3\, m w_o^2$, where for (1) $\mu_3=0.2238$. $\underline{w}=\underline{v}-\underline{u}$ is the velocity in the electron rest frame. In the absence of spatial gradients and electric field $\underline{E}_o$ it can be verified that (1) is the self-similar solution of (2) with the heating rate

$$Q_o = (3/2)(nT_e/\tau_e)\, 2\langle(\omega_e/kv_e)(\omega_k/kv_e)^2\rangle / \langle\omega_e/kv_e\rangle \qquad (5)$$

where the effective collision time has been defined such that

$$\underline{R}_o = -\, n\, m\, \underline{u}/\tau_e \qquad (6)$$

is the friction force on distribution (1) shifted by the drift velocity $\underline{u}$

$$1/\tau_e = (1/3)\,(2\pi)^{1/2}\mu_2\,\omega_e\,(W/nT_e)\,\langle\omega_e/kv_e\rangle, \qquad (7)$$

$\mu_2 = 0.445$.

The validity of such a description is verified by Computer simulation of the current driven ion sound instability, [2]. Assuming, now, small gradients, electric field and drift velocity $u/v_e \ll 1$, we find the distribution function in the form $f=f_o + f_1$, where f_o is the shifted selfsimilar distribution (1) with local parameters $n(\underline{x},t)$, $\underline{u}(\underline{x},t)$ and $T(\underline{x},t)$. It is convenient to transform (2) to the electron rest frame. The dominant terms are then assumed to be pitch angle scattering and the magnetic term, both tending to isotropize $f(\underline{x},\underline{w},t)$. The lowest order moment equations for f_o are solubility conditions for f_1 and are used to express the time derivatives in terms of the local parameters. The resulting equation for f_1 is

$$C_L^o(f_1) + (\underline{w}\times\underline{\Omega})\cdot(\partial f_1/\partial\underline{w}) = \Big\{\left[1-\mu\mu_3(w/w_o)^{\mu-2}\right]\underline{w}\cdot\nabla\ln n + \left[\mu\mu_3(w/w_o)^{\mu-2}(-1+mw^2/2T) - 3/2\right]\underline{w}\cdot\nabla\ln T_e + \mu\mu_3(w/w_o)^{\mu-2}\left[\underline{\underline{W}}:\underline{\underline{U}}\,(m/2T_e) + \underline{R}\cdot\underline{w}/(n\,T_e)\right]\Big\} f_o \qquad (8)$$

where $\underline{\underline{W}} = \underline{w}\,\underline{w} - (1/3)w^2\,\underline{\underline{I}}$ and C_L^o describes pitch angle scattering with frequency

$\nu(w) = (\mu_4/\tau_e)(w_o/w)^3$. For (1) $\mu=5$, $\mu_4 = 0.893$.

For the classical Lorentz gas, $Z_{eff}\to\infty$ $\mu=2$, $\mu_3=1/2$, (f_o Maxwellian), the terms proportional to ∇n vanish. Equ. (8) is linear in the perturbing factors u, ∇n ∇T, and $U^{ik} = \partial u^i/\partial x_k + \partial u^k/\partial x_i - (2/3)\delta^{ik}\nabla\cdot\underline{u}$ and they may be treated separately, according to their tensorial character. (Note however that there is an implicit nonlinear dependence through the wave spectrum). The rate of momentum transfer $\underline{R} = \underline{R}_o + \underline{R}^1$ consists of the friction force $\underline{R}_u = \underline{R}_o + \underline{R}_u^1$ proportional to u, the thermal force $R_T \propto \nabla T_e$ and, in our case, $\underline{R}_n$, which is proportional to ∇n. Similarly, the heat flux $\underline{q}$ consists of terms proportional to the same perturbing factors, and there are five viscosity coefficients. All these coefficients and their magnetic field dependence have been found, e.g.

$$\underline{q}_T = -\frac{nT_e\tau_e}{m}\left[\kappa_o\nabla_\mu T_e + \kappa_\perp\nabla_\perp T_e + \kappa_\wedge(\underline{\tau}_o\times\nabla T_e)\right] \qquad (9)$$

where $\kappa_o=1.50$ $\kappa_\perp=4.05/(\Omega_e\tau_e)^2$, $\kappa_\wedge=1.46/(\Omega_e\tau_e)$; $\Omega_e\tau_e\gg1$, $\tau_o = \underline{B}/B$.

It is also planned to discuss the effect of anisotropy in the spectrum on the transport equations.

[1] S.I. Braginskii, Reviews of PlasmaPhysics, Vol I, 205, 1965

[2] C.T. Dum, R. Chodura, D. Biskamp, Phys.Rev.Letters 32, 1231, 1974; 34, 131, 1975

"This work was performed under the terms of the agreement on association between the Max-Planck-Institut für Plasmaphysik and EURATOM".

Renormalized Turbulent Transport Theory in Strongly Magnetized Plasma

Guy PELLETIER and Claude POMOT

Laboratoire de Physique des Plasmas - Université de Grenoble
Equipe de Recherche Associée au CNRS - FRANCE

Abstract : The turbulent transport coefficients are derived with the average orbit theory formalism. A generalisation of the dressed test - particles method leads to a fluctuation - dissipation theorem giving the electric fiels spectrum.

The usual dressed-test particles method in kinetic theory [1] breaks down when the plasma becomes linearly unstable. Dupree-Weinstock formalism [2] , [3] allows to describe a weak-turbulent state which can be stabilised by non-linear effects ; a non-linear permittivity and a non-linear growth rate can be defined, including resonance broadening and frequency-shift due to turbulent orbits diffusion. In this situation of a weak turbulence non-linearly stabilised, we investigated the extension of the dressed-test particles method [4]. We considered the test particles had no more free motions but brownian motions, experiencing a drag-force and a diffusion generated by the turbulence. The wave absorbtion is balanced by the Cerenkov emission of the test-particles dressed with their polarisation clouds ; so a stationary spectrum is obtained and the turbulent transport coefficients can be calculated.

In this communication we expose the results of this theory in a strongly magnetized plasma. Our results differ from those of I. Cook and J.B. Taylor [5] in that they included non-linear effects in the permittivity only.

In a guiding-center plasma, the Vlasov equation is :

$$\left(\frac{\partial}{\partial t} + \vec{v}_{//} \cdot \frac{\partial}{\partial \vec{x}_{//}} + \frac{\vec{E}^{\perp} \times \vec{B}}{B^2} \cdot \frac{\partial}{\partial \vec{x}_{\perp}} + \frac{q}{m} \vec{E}^{//} \cdot \frac{\partial}{\partial \vec{v}_{//}}\right) f_t = 0 \qquad (1)$$

The averaged distribution function satisfies a Fokker-Planck equation :

$$\left(\frac{\partial}{\partial t} + \vec{v}_{//} \cdot \frac{\partial}{\partial \vec{x}_{//}}\right) \langle f_t \rangle = \left(- \frac{\partial}{\partial \vec{v}_{//}} \vec{F}_{//} + \frac{\partial}{\partial \vec{v}_{//}} \cdot D_{//} \frac{\partial}{\partial \vec{v}_{//}} + \frac{\partial}{\partial \vec{x}_{\perp}} \cdot D_{\perp} \frac{\partial}{\partial \vec{x}_{\perp}}\right) \langle f_t \rangle \qquad (2)$$

The derivation of the equation (2) from the equation (1) requiresthat the correlation time τ_c is shorter than the diffusion-times $(k_{//}^2 D_{//}^2)^{-1/3}$ and $(k_{\perp}^2 D_{\perp})^{-1}$; it requires also, in this simple form, that $E^{//}$ and $E^{\perp}$ be stochastically independant.

For a locally homogeneous and quasi-stationary turbulence, the diffusion coefficients are :

$$D_{//} = \frac{q^2}{m^2} \langle E_t^2 \rangle \tau_c^{//} (\vec{v}_{//}) \qquad ; \qquad D_{\perp} = \frac{1}{B^2} \langle E_t^2 \rangle \tau_c^{\perp} (\vec{v}_{//})$$

with

$$\tau_c^{\alpha} (\vec{v}_{//}) = \langle E_t^2 \rangle^{-1} \int_0^{\infty} d\tau \, \langle \vec{E}_t^{\alpha} . \vec{U}(\tau) \, E_{t-\tau}^{\alpha} \rangle \qquad \alpha \text{ is } // \text{ or } \perp$$

$\vec{U}$ is the average Vlasov propagator [3] .

These correlation times can be calculted by means of the normalized spectrum density, $S_{\vec{k},\omega}$ defined by :

$$\langle \vec{E}_{\vec{k},\omega} \cdot \vec{E}^{*}_{\vec{k}',\omega'} \rangle = \langle \vec{E}_t^2 \rangle \; S_{\vec{k},\omega} \; \delta(\omega-\omega') \; \delta(\vec{k}-\vec{k}')$$

and the broadened resonance function $g_{\vec{k},\omega}$ defined by :

$$g_{\vec{k},\omega} (\vec{v}_{//}) = \int_0^{\infty} d\tau \, e^{i(\omega\tau - \vec{k}.\vec{x})} \, \vec{U}(\tau) \, e^{i\vec{k}.\vec{x}}$$

So

$$\tau_c^{\alpha} (\vec{v}_{//}) = \int_{\mathbb{R}^3} \frac{d\vec{k}}{(2\pi)^3} \int_{\mathbb{R}} \frac{d\omega}{2\pi} \, \frac{k_{\alpha}^2}{k^2} \, S_{\vec{k},\omega} \, \mathrm{Re} \, g_{\vec{k},\omega} (\vec{v}_{//})$$

This resonance function has been derived in the litterature [4] :

$$g_{\vec{k},\omega} (\vec{v}_{//}) = \int_0^{\infty} d\tau \, \exp\left[i(\omega - k_{//} v_{//})\tau - i\frac{\tau^2}{2} k_{//} \left(F_{//} + \frac{\partial D_{//}}{\partial v_{//}}\right) - \frac{\tau^3}{3} k_{//}^2 D_{//} - \tau k_{\perp}^2 D_{\perp} \right]$$

Consider now the drag-force $F_{//}$; this is generated by the correlation of the ballistic streams of test-particles with the collectif field.

The initial perturbed distribution function δf_{t_o} is the sum of two parts : the one is the difference between the averaged distribution function and this of an assembly of non-interacting particles, the other one is any "smooth" perturbation the contribution of which disappears by phase-mixing in the asymptotic limit. This perturbation is propagated by a Green operator U_A introduced by Weinstock [3], so the ballistic perturbed distribution function is defined by :

$$\delta f_t^b = U_A (t, t_o) \, \delta f_{t_o}$$

The drag-force is related to this ballistic perturbation by :

$$\langle \vec{E}_t^{//} \, \delta f_t^b \rangle = \vec{F}_{//} \langle f_t \rangle$$

A ballistic charge $\delta \rho_t^b$ is associated to δf_t^b which acts as a source in the Poisson equation. So we obtain a relation between the electrostatic field and the streaming test-charge :

$$\vec{E}_{\vec{k},\omega} = - \frac{i\vec{k}}{k^2} \, \frac{\delta \rho^b_{\vec{k},\omega}}{\varepsilon_o \varepsilon_{NL}}$$

ε_{NL} is the non-linear permittivity, the non-linear effects appearing in the broadened resonance function $g_{\vec{k},\omega}$:

$$\varepsilon_{NL} = 1 - i \frac{\omega_p^2}{k^2} \int_{\mathbb{R}^3} d\vec{v} \, g_{\vec{k},\omega} (\vec{v}_{//}) \, \vec{k}_{//} . \frac{\partial}{\partial \vec{v}_{//}} \langle f_t \rangle$$

Assuming $\gamma_{NL} < 0$, the stationary spectrum is therefore :

$$\langle \vec{E}_{\vec{k},\omega} \cdot \vec{E}^{*}_{\vec{k}',\omega'} \rangle = \frac{1}{k^2 \varepsilon_o^2 |\varepsilon_{NL}|^2} \langle \delta \rho^b_{\vec{k},\omega} \delta \rho^{b^*}_{\vec{k}',\omega'} \rangle$$

Its determination requires the knowledge of the correlation function :

$$\langle \delta f_t^b(1) \, \delta f_t^b(2) \rangle$$

In the framework of the Dupree-Weinstock formalism, it can be shown [4] that

- 1) For $t' \geq t$ $\quad \langle \delta f_{t'}^b(1) \, \delta f_t^b(2) \rangle = \bar{U}_1 (t'-t) \, g_t^b(1,2)$

  where $\quad g_t^b(1,2) = \langle \delta f_t^b(1) \, \delta f_t^b(2) \rangle$

- 2) $\quad g_t^b(1,2) = \bar{U}_{12}(t-t_o) \, g_{t_o}(1,2)$

  where $\bar{U}_{12}$ is the two-particles average Vlasov propagator..

- 3) The test-particles providing initialy the self-correlation

$$g_{t_o}(1,2) = \frac{1}{n_o} \, \delta(x_1 - x_2) \, \delta(v_1 - v_2) \langle f_{t_o}(1) \rangle,$$

one finds that this correlation is maintained at time t through the ballistic streams , that is :

$$g_t^b(1,2) = \bar{U}_{12}(t - t_o) \, g_{t_o}(1,2) = \frac{1}{n_o} \, \delta(1 - 2) \langle f_t (1) \rangle$$

These properties allow to calculate the drag-force and the spectrum, one finds

$$\vec{F}_{//} (\vec{v}_{//}) = \frac{2\omega_p^4}{n_o} \int_{\mathbb{R}^3} \frac{d\vec{k}}{(2\pi)^3} \int_{\mathbb{R}} \frac{d\omega}{2\pi} \, \frac{k_{//}^2}{k^2 |\varepsilon_{NL}|^2} \int_{\mathbb{R}^3} d\vec{v}' \, \mathrm{Re} \, g_{\vec{k},\omega}(\vec{v}'_{//}) \times$$
$$\times \, \mathrm{Re} \, g_{\vec{k},\omega}(\vec{v}_{//}) \, \frac{\partial}{\partial \vec{v}'_{//}} \langle f_t(v') \rangle$$

$$S_{\vec{k},\omega} = \frac{2 \langle F_E^2 \rangle^{-1}}{\varepsilon_o^2 k^2} \, \frac{n_o q^2}{|\varepsilon_{NL}|^2} \int_{\mathbb{R}^3} d\vec{v} \, \mathrm{Re} \, g_{\vec{k},\omega}(\vec{v}_{//}) \langle f(\vec{v}) \rangle$$

This two last results and also the two diffusion coefficients, in which the spectrum is inserted, provide the basic equations describing the turbulent transport. One finds that the resonant particles diffuse much more than the non resonant particles across the magnetic field ; this spatial diffusion of the resonant particles would be a Bohm-like diffusion ($D_{\perp} \sim 1/B$) if the spectrum would be independant of the magnetic field as the usual thermal noise ; in fact the non-linear effects introduce a significant modification of the spectrum and therefore of the diffusion coefficient $D_{\perp}$.

The excitation of ion sound turbulence by a current gives rise to an anomalous resistivity which can be calculated starting from the expression of the drag-force we found, provided the assumptions of weak turbulence and of non-linear stability are valid.

[1] N. Rostoker (1961) Nuclear Fus. 1, 101
[2] Th. Dupree (1966) Phys. Fluids 9, 1773
[3] J. Weinstock (1969) Phys. Fluids 12, 1045
[4] G. Pelletier and Cl. Pomot (1975) J. of Plasma Phys. (to be published)
[5] I. Cook and J.B. Taylor (1973) J. of Plasma Phys. 9, part 1, 131

The Effect of Turbulent Energy Transport on the Ablation Rate of a Refuelling Pellet.

C.T. Chang
Association Euratom - AEK
Danish AEC Research Establishment Risø, Roskilde, Denmark

Abstract Under the same reactor condition, the ablation rate of a given pellet in the presence of turbulent energy transport is found to be more than an order of magnitude higher than that of a laminar flow.

Introduction In the magnetic shielding model considered previously[1], the ablated plasma emerges from the pellet as a cold jet against the background of a hot fusion plasma. The situation could easily cause the onset of Helmholtz instability and eventually leads to turbulent energy transport across the field lines. In this note, we like to estimate to what extent the occurence of turbulence will affect the ablation rate of the pellet.

Theoretical considerations In view of the lack of knowledge of the spectrum of the turbulent flow, the exact values of the thermal transport coefficients are difficult to assess. However, one may use the intuitive argument that the turbulent energy transport coefficient is about the same order of magnitude as that of a laminar flow corresponding to the maximum fluctuation. According to Braginskii[2], the perpendicular thermal transport coefficient of a laminar flow is

$$\kappa_\perp^i = n_i T_i \tau_i f(x)/m_i \qquad (1)$$

where

$$f(x) = (2x^2+2.645)/(x^4+2.70x^2+0.677) \quad , \quad x = \omega_i \tau_i \ ,$$

and has a maximum at $x = 1.02$. If we take $(\kappa_\perp^i)_{tur.} \approx cn_i T_i/eB$, and approximate $\nabla T_i \approx T_i/r_{ci}$, where r_{ci} is the ion Larmor radius, we have the corresponding energy flux across the field lines as

$$F_\perp^i = k\nabla T \approx n_i T_i \langle v_i \rangle /3 \qquad (2)$$

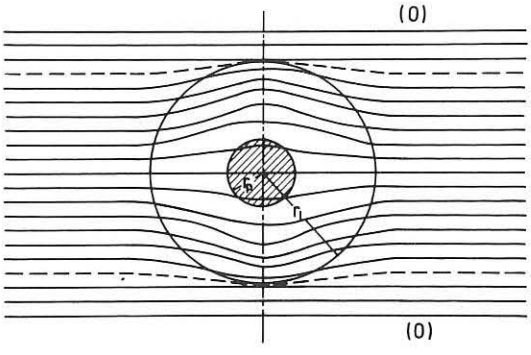

Fig. 1. Schematic drawing showing the equivalent boundary through which turbulent energy transport across the field lines takes place.

By averaging the plasma parameters across the field lines and assuming the existence of a nozzle flow in the direction of the field lines[1] see fig. 1, we obtain the following system of conservation equations

$$2\pi r_p^2 n_l \langle v_l \rangle e T_l = Gh \quad (r_g \approx r_p) \qquad (3)$$

$$2\pi r_l r_c n_o \langle v_o \rangle_i T_o = G(h+3T_l) \qquad (4)$$

$$2n_l T_l (1+\varepsilon) = 2n_o T_o (1+1/\beta_o) = B_c^2/2\mu \qquad (5)$$

$$G = 2\pi r_l^2 n_l v_{la} \alpha(\varepsilon) \qquad (6)$$

where subscripts 0 and 1 refer to the state of the fusion plasma and the state of the ablated plasma near the pellet, respectively. $\varepsilon = \frac{B_l^2}{2\mu}/p_l$, $\beta_o = 2n_o T_o/\frac{B_o^2}{2\mu}$ and is related to β with respect to the confinement field B_c by

$$\beta_o = \beta/(1-\beta) \qquad (7)$$

G is the ablation rate, h is the energy required for phase transition $\langle v \rangle_{l,0}$ are the average thermal speed in region 1 and region 0, respectively. ($T_{io} = T_{eo} = T_o$, $T_{il} = T_{el} = T_l$ are assumed). v_{la} is the ion acoustic speed near the pellet, $\alpha(\varepsilon)$ is the nozzle factor. (Fig. 4, ref. 1).

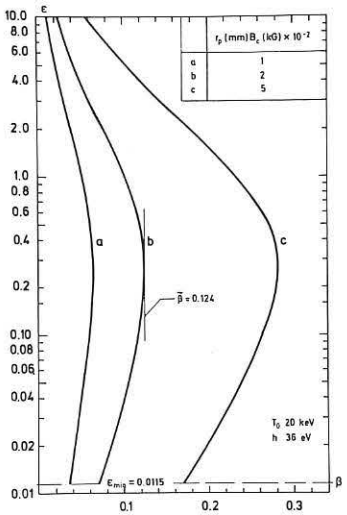

Fig. 2. Critical value of $\tilde{\beta}$ and permissible range of ε for the existence of a nozzle flow.

From the above system of equations, one can deduce that as a necessary condition of $T_l > 0$ there exists a critical value of $\tilde{\beta}$ for given combinations of T_o/h and $r_p B_c$. For $\beta < \tilde{\beta}$, a nozzle exists only for those values of the field trapping parameter ε in the range shown in fig. 2. For $\beta > \tilde{\beta}$, any value of ε above the minimum field trapping parameter[1], $\varepsilon_{min.} = 0.012$, is possible.

Computational result Taking the given condition of $T_o = 20$ keV, $B_c = 100$ kG, $\beta = 0.15$, $h = 36$ ev. and $r_p = 2$mm, for comparison purpose, we have calculated the ablation rate and the state of the ablated plasma corresponding to the two states of flow. The result is shown in the following table.

	Laminar		Turbulent	
ε	5	2.5	2.5	0.02
$g, 10^{-26}(cm^{-2}sec^{-1})$	0.176	0.289	1.33	3.58
$t_d, 10^4$(sec)	0.380	0.231	0.050	0.019
r_l/r_p	1.007	1.024	6.64	13.86
T_l(ev.)	0.842	0.778	16.30	9.99
$n_l, 10^{-19}(cm^{-3})$	1.23	2.28	0.218	1.22

In the table, $g = G/4\pi r_p^2$. t_d is the disintegration time of the pellet assuming a uniform ablation process.

One observes that as a result of the turbulent energy transport across the field lines a bulge is formed around the pellet. Both the temperature of the ablated plasma and the ablation rate of the pellet are increased by more than an order of magnitude.

References:

1) C.T. Chang, Nuclear Fusion, to be published.
2) S.I. Braginskii, article in "Review of Plasma Physics", vol. I, p. 250 (1950, Consultants Bureau).

ON THE QUASI-STEADY STATE OF PERMEABLE PLASMAS

B. Lehnert
Royal Institute of Technology, S-10044 Stockholm 70, Sweden

Abstract: Quasi-steady plasmas are divided into three types with respect to the density range. In plasmas being permeable to neutral gas the immersed neutral density becomes related to the diffusion rate. The equilibrium state and relaxation times are affected substantially by neutral gas interaction.

1. Classification of Density Ranges: Neutral gas which penetrates into a hot plasma of the characteristic dimension L_b, average ion density $\bar{n}$, and temperature T, consists mainly of a slow and a fast component of densities n_{ns}, n_{nf} and temperatures $T_{ns}\ll T$, $T_{nf}\approx T$, having the e-folding penetration lengths [1,2]

$$L_{ns}=1/\sigma_{cs}\bar{n}=n_{cs}L_b/\bar{n}\approx(2k\bar{T}_{ns}/m_i)^{1/2}/(\xi+\xi_{ins})\bar{n} \quad (1)$$

$$L_{nf}=1/\sigma_{cf}\bar{n}=n_{cf}L_b/\bar{n}\approx\left[2kT/m_i\xi(\xi+\xi_{inf})\right]^{1/2}/\bar{n} \quad (2)$$

where $\bar{T}_{ns}\approx 2m_e\xi_{en}T/3m_n(\xi+\xi_{ins})$, $\xi\approx\langle\sigma'_{en}w_{en}\rangle$, $\xi_{en}=\langle\sigma_{en}w_{en}\rangle$, $\xi_{inv}=\langle\sigma_{in}w_{in}\rangle_v$, $v=(s,f)$, σ'_{en} and σ_{en} are cross sections of ionizing and non-ionizing electron-neutral collisions, σ_{in} is the total cross section of ion-neutral collisions including charge transfer, and w_{en} and w_{in} are mutual particle velocities. The lengths L_{nv} give direct information on the depth to which the neutral gas penetrates into a plasma in a quasi-steady state; such information is not merely given by adding the inverted mean paths of free flight obtained from the cross sections σ'_{en}, σ_{en}, and σ_{in}. For hydrogen $2\times10^{18}<1/\sigma_{cs}\approx100/\sigma_{cs}<8\times10^{18}\,m^{-2}$ in the range $10^5<T<10^7$ K. Thus, three plasma classes are defined in respect to the ion density range (Table 1), having different equilibrium and stability properties and being affected in different ways by the neutral gas-wall balance and its associated vacuum conditions [2].

2. Permeable Plasmas: Wall interaction becomes especially important to permeable plasmas. A distinction should be made between two situations in respect to the circulation of matter. When the neutral gas-wall balance with its pumping and sputtering processes has much longer relaxation times than the plasma-neutral gas balance, the system is subject to "closed circulation" with approximately constant total mass. If instead the relaxation times of the neutral gas-wall balance become comparable to or shorter than those of the plasma-neutral gas balance, there is "open circulation" and the total mass of the system is no longer conserved.

Table 1. Plasma classification with respect to density range.

Properties \ Type	PERMEABLE: Dilute	PERMEABLE: Non-Dilute	IMPERMEABLE
Ion density	$\bar{n}\lesssim n_{cs}\ll n_{cf}$	$n_{cs}\ll\bar{n}\lesssim n_{cf}$	$n_{cs}\ll n_{cf}\ll\bar{n}$
Fast neutrals $L_b/L_{nf}=\bar{n}/n_{cf}$ penetrate by	$\ll1$ free streaming	$\lesssim1$ free streaming	$\gg1$ diffusion
Slow neutrals $L_b/L_{ns}=\bar{n}/n_{cs}$ penetrate by	$\lesssim1$ free streaming	$\gg1$ diffusion	$\gg1$ diffusion
Examples on experiments	Most internal conductor devices, most Stellarators.	Tokamaks, some Stellarators, and similar devices.	Reactors, and some toroidal, theta pinch, and internal conductor devices.

In the quasi-steady state of closed circulation, the densities of the plasma and neutral gas components become related to the plasma confinement which, in its turn, depends on the gradient of the pressure p and on the diffusion processes being involved. Thus, in an axisymmetric magnetic bottle [2]

$$\nabla_{11}p\approx-(B^2/n\eta_c\delta_\perp S)\int n(n_{ns}+n_{nf})\xi dV-\underline{j}_{22}\times\underline{B}_{12}-(3nk/2\delta_\perp)\nabla_{11}T \quad (3)$$

where $(_{22})$ denotes the direction parallel with the main vacuum field $\underline{B}$, $(_{11})$ the direction perpendicular to this field and to the magnetic surfaces, $(_{12})$ the direction perpendicular to both $(_{22})$ and $(_{11})$, $\delta_\perp\eta_c$ and η_c the resistivities due to anomalous and classical diffusion, V the plasma volume inside a magnetic surface of area S, and the last two terms represent the pinch effect due to a current $\underline{j}_{22}$ and the Nernst effect, respectively. Here a substantial fraction of the plasma pressure drop is assumed to be balanced by the force $\underline{j}_{12}\times\underline{B}_{22}$.

2.1. Density Relationships: Eq.(3) is now used in an order-of-magnitude estimate of the density relationships. With $\rho_c=(B_oL_b)^2\xi_m/2kT_o\eta_{co}$ and subscript $(_o)$ indicating characteristic (maximum) values within the plasma body, we obtain:
(i) In dilute plasmas where T is large enough for the ionization rate ξ to become equal to its "saturation" value $\xi_m=10^{-14}\,m^3/s$ within almost the entire plasma body, we have $n_{nf}\ll n_{ns}$ and $n_{ns}\approx n_o(1+\delta_\perp)/\rho_c\approx$ const. in space.
(ii) In non-dilute plasmas $n_{nf}\approx n_o(1+\delta_\perp)/\rho_c\approx$ const. and $n_{ns}\approx0$ within the inner hot region when $L_{ns}\ll L_b$.

2.2. The Pressure Gradient: With the condition $p(S_b)\ll p_o$ at the surface $S=S_b$ touching a wall, it is seen from Eq.(3) that the pressure gradient is due to a balance between the ionization rate which "pumps up" the plasma density, and the rate of plasma diffusion which drains the plasma. This sometimes results in a steepening of the pressure distribution [2]:
(i) In dilute plasmas where kT_o becomes comparable to the ionization energy $e\phi_i$, $L_p\equiv p/|\nabla_{11}p|$ should decrease in the outer plasma layers at increasing T_o, i.e. when ξ approaches ξ_m within an increasing part of these layers.
(ii) In non-dilute hot plasmas where $\bar{n}$ approaches the transition region $\bar{n}=n_{cf}$ from below, L_p should decrease gradually in the outer layers to a minimum value $L_p=L_{ns}$ at $\bar{n}=n_{cf}$.

2.3. The Relaxation Times: The presence of immersed neutral gas affects the plasma energy and particle containment times, τ_E and τ_p. The former is determined by $1/\tau_E=(1/\tau_{ch})+(1/\tau_n)$ where τ_{ch} represents the losses due to diffusion and heat conducting by Coulomb collisions, $1/\tau_n=\overline{n_{ns}F_s+n_{nf}F_f}$ with a bar indicating mean value formation over the plasma body, $F_v\approx(e\phi_i\xi/3kT)+(T-T_{nv})\xi_{inv}/2+f_{en}\xi_{en}$, and f_{en} is the average fraction of the energy lost by an electron in a non-ionizing collision with a neutral particle. The latter is usually defined as $\tau_p=\bar{n}/|\overline{nv_{11}}|_b$ where v_{11} is the velocity of particle diffusion across the magnetic surfaces, and the particle flux $\overline{nv_{11}}$ is measured at $S=S_b$. With this definition $\tau_p=\bar{n}/n(n_{ns}+n_{nf})\xi$.

In the case of classical diffusion and heat conduction, not only τ_E but also τ_p can deviate considerably from the square root dependence of T_o due to Coulomb collisions. This is caused by at least three effects. The first is an increase in n by the rapid growth of ξ with T, leading to an increase in $|v_{11}|\propto Zn/L_pT^{1/2}$. The second is an amplification of v_{11} by wall-released high-Z impurities. The third is caused by the decrease in L_p discussed in Section 2.2.

3. Applications: The following problems are considered:
(i) In earlier experiments with Tokamaks at $n_o=3\times10^{19}\,m^{-3}$, a neutral gas density $n_{nf}=2\times10^{14}\,m^{-3}$ has been measured [3]. With relevant parameter data Section 2.1(ii) then yields $\delta_\perp\approx10^3$, being consistent with the large observed anomalous losses.
(ii) The maximum pressure gradient of non-dilute plasmas in Section 2.2(ii) can become a driving force of instabilities. Thus, the maximum parameter data obtained so far in Tokamak experiments have been reached in the transition region $\bar{n}=n_{cf}$. The stability limit of collisionless ballooning modes agrees with the onset of the observed disruptive instabilities, but there may also exist other explanations of the latter [2].
(iii) In experiments with the Princeton Spherator, a Bohm-like behaviour of τ_E and τ_p has been observed for $3\times10^4<T<10^6$ K [4]. Since the confinement is efficient, the plasma density low, and the temperature moderately high here, τ_E and τ_p become sensitive functions of the neutral gas interaction and the vacuum conditions, as described in Sections 2.3 and 2.2(i). Thus insertion of the Spherator data into the classical expressions for τ_E and τ_p yields results being roughly in agreement with the observations. Therefore the latter need not be explained in terms of anomalous losses at temperatures above 3×10^4 K.

At the comparatively large loss rate and high temperature in Tokamak plasmas, the neutral gas should on the other hand have only moderately large effects on the energy containment time.

[1] B.Lehnert, Arkiv f. Fysik 18(1960)251; Nuclear Fusion 8(1968)173, 11(1971)485, 13(1973)781.
[2] B.Lehnert, Roy. Inst. of Technology, TRITA-EPP-75-06(1975).
[3] L.A.Artsimovich et al., Fourth European Conf. on Controlled Fusion, Rome(1970), CNEN, page 18.
[4] R.Freeman et al., Plasma Physics and Controlled Nuclear Fusion Research, I.A.E.A., Vienna I(1971)58.

WALL-CONFINED, $\beta > 1$, PLASMA PHYSICS

Robert A. Gross
Plasma Physics Lab, Columbia University, N.Y.,N.Y., U.S.A.

Abstract: Physics associated with wall-confined, high-beta, plasma have been studied by experiments and computer simulations. Energy transfer rate from a $\beta > 1$ plasma to a wall has been measured and compared with theory. Studies of plasma confinement by a cylindrical wall and an axial magnetic dam are described.

INTRODUCTION: This paper summarizes some recent studies of high-beta, plasma-wall energy transfer and confinement, and plasma trapping by a magnetic dam. A power cycle employing wall confinement of a shock heated fusion system has been previously described (1). There are several groups currently pursuing various types of wall-confined fusion concepts. These include the Novosibirsk investigations under Budker (2), the Netherlands studies under Braams (3), and Swedish research under Lehnert (4). Wall confinement of plasma requires a transverse magnetic field with $\beta > 1$ to decrease energy loss by heat conduction. $\beta > 1$ implies that magnetic pressure alone is insufficient for static plasma confinement. A combination of magnetic field plus physical walls can however provide confinement. In a cylindrical geometry, longitudinal plasma trapping may be achieved by one or more magnetic mirrors.

PLASMA-WALL ENERGY TRANSFER: The physics of $\beta > 1$ plasma-wall confinement has a number of interesting effects. When a hot plasma is brought into sudden contact with a wall, a thermal boundary layer forms adjacent to the wall, and magnetosonic waves rapidly propagate into the hot plasma interior, creating essentially a spacially uniform pressure (both plasma and magnetic) which varies with time. This constant pressure is common in boundary-layer phenomena and is particularly applicable to this problem because the magnetosonic speed is large and the characteristic distance, the thermal boundary layer thickness, is small. In response to the magnetosonic signals from the cooling boundary layer, plasma is convected toward the wall. Induced currents are created and their magnetic field stiffens the plasma and impedes motion toward the wall. Thus, a transverse magnetic field in a $\beta > 1$ plasma not only can drastically reduce heat transfer to the wall, but helps retard plasma motion toward the wall. Some of these interesting plasma-wall effects caused by the cooling boundary layer have been studied analytically by M.S. Chu (5).

An experimental study of the energy transfer rate from a hot, dense plasma brought into sudden contact with a cold wall has been performed by B. Feinberg (6). He employed a fast response ($\tau \sim 200$ nsec) infrared bolometer to determine the rate of energy transfer from a shock created plasma whose properties were typically, $T_i \sim 500$ eV, $T_e \sim 30$ eV, $n \sim 1 \times 10^{16}$ cm^{-3}. This plasma contained a transverse magnetic field, $B \sim 10^4$ G, ($\beta \sim 2$) and was brought into sudden contact with the wall. The measured energy transfer rate to the wall is compared to a simple classical plasma thermal conduction prediction. At early time, the energy transfer rate agrees with the classical prediction, but after ~ 1 μsec, the rate exceeds the classical prediction by about a factor of 2. Considering effects of convection and radiation which are not included in the theoretical prediction, the agreement is rather good. It is important to observe that if, during the early time, the thermal boundary layer had been unstable or turbulent, a much greater energy transfer rate would occur. The fact that this was not observed is encouraging.

PLASMA CONFINEMENT: Radial confinement of a dense, high-beta plasma within a cylindrical tube takes place in a subtle way. As the cool, dense, plasma thermal boundary layer forms near the wall, the radial density, temperature, and transverse magnetic field distributions look like those illustrated in fig. 1. Charged particles which spiral around the cylinder axis experience increasing gradients in both density and azimuthal magnetic field. Both of these boundary layer gradient effects tend to reflect particles back into the interior of the plasma. The increasing radial magnetic field acts like a magnetic mirror, and the density gradient causes hot particles to collide with the cooler particles in the thermal boundary layer and consequently be scattered toward the plasma interior. The energy exchange in these scatterings is the kinetic mechanism for the radial thermal conduction discussed previously.

Confinement in the axial direction requires some type of magnetic trap. We have studied a single strong magnetic dam as a means to trap the plasma. Erection of a magnetic dam in a coaxial system involves a number of interesting phenomena. When the magnetic dam is turned on it must punch through a layer of plasma and penetrate to the inner wall. Todd (7) has studied numerically the problem of erecting the dam and the physical parameters required to achieve penetration to the opposite wall. Some of his numerical results are illustrated in fig. 2. Exploratory magnetic dam experiments have been carried out and the first results are encouraging. Further details are available in ref. 8.

ACKNOWLEDGEMENT: This summary contains contributions by Columbia colleagues and our students, and has been supported by the U.S. ERDA under contract AT(11-1)2456.

REFERENCES:

1. R.A. Gross; Nuclear Fusion 13, 293 (1973).
2. G.I. Budker; 6th European Conf. on Controlled Fusion & Plasma Physics, vol. 2, 136 (1973).
3. F.C. Schuller et al., IAEA 5th Conf. on Plasma Physics & Controlled Fusion Research, Tokyo, Nov. (1974) paper H7-2.
4. B. Lehnert; Nucl. Fusion 13, 781 (1973).
5. M.S. Chu; Phys. Fluids 16, 1441 (1973).
6. B. Feinberg; Ph.D. Thesis, Columbia University (1974).
7. A.M.M. Todd; Ph.D. Thesis, Columbia University (1974).
8. R.A. Gross; Physics of a Wall-Confined Fusion System, Columbia Plasma Lab preprint, Feb. 1975.

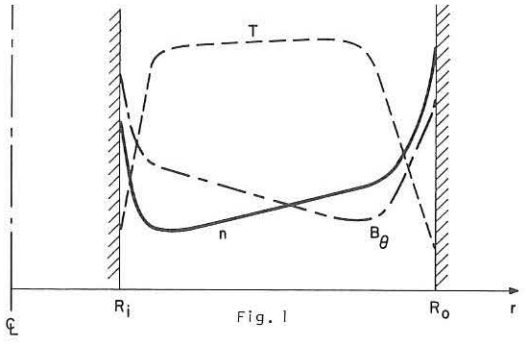

Fig. 1

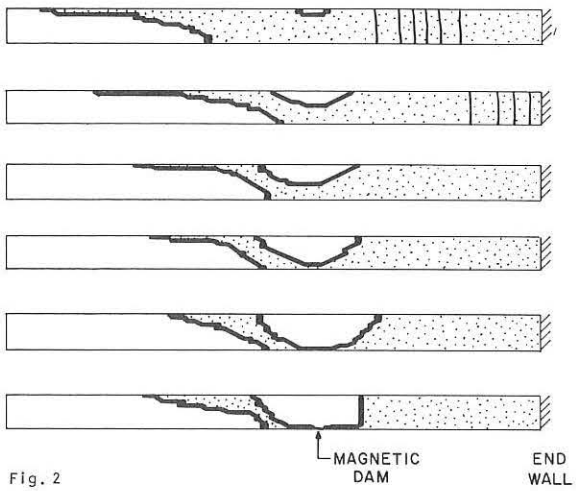

Fig. 2

RINGBOOG: A TOROIDAL DISCHARGE IN A GAS BLANKET

F.C. Schüller, R.S. de Haas, L.Th.M. Ornstein, L.C.J.M. de Kock, W.J. Schrader and J. van Os

Association Euratom-FOM, FOM-Instituut voor Plasmafysica, Rijnhuizen, Jutphaas, The Netherlands.

Abstract: A magnetized toroidal discharge with currents up to 25 kA is studied in a hydrogen atmosphere with pressures up to 0.1 Torr. Anomalous plasma heating is found; there are clear indications of weak plasma turbulence at low ratios of electron drift velocity to ion sound speed.

Introduction: A toroidal discharge is studied to gather experimental information about the properties of the transition layer between a neutral gas blanket and a fully ionized plasma core. The conditions are made similar to those expected to prevail in the outer layers of a thermonuclear reactor with a protective envelope of low-temperature plasma and cold gas[1]. If the outside density is sufficiently high energetic plasma neutrals are stopped in the impermeable layer[2] and thus plasma contamination through wall sputtering is avoided.

Experiment: The experimental facility RINGBOOG[3] is a Tokamak-like device with dimensions R_o = 0.52 m, r_o = 0.087 m, and B_T = 3.2 T (maximum). The discharge is struck in a quartz torus. The induction circuit consists of an 1.2 Vs iron core; the primary is fed by capacitor batteries. There is no copper shell; plasma equilibrium can be obtained by careful tuning of various vertical and horizontal magnetic fields.

The first results of the experiment as reported earlier[4] (quoted here again as regime I) were obtained at discharge currents I = 7.5 kA and $B_T(R_o)$ = 1.65 T. Recently discharge currents in the range of 25 kA with a duration of 3 ms were obtained at $B_T(R_o)$ = 1.65 T and at various filling pressures (regimes II and III). No limiter was used. The results, as presented in the table, as well as a number of newly installed diagnostics are commented upon below.

With an HCN-laser interferometer the value for the electron density derived from H_β Stark broadening is confirmed. In the already rather high density of reg. II dispersion of the probing waves prevents observation of more than 11 fringes in the afterglow. Still, this allows a realistic extrapolation for $\int n_e\, dL = 8 \times 10^{19}$ m^{-2}, which with an estimated optical path of 0.14 m yields $\langle n_e \rangle = (6 \pm 1) \times 10^{20}$ m^{-3}. Stronger dispersion allows one only to establish a lower limit for the density in regime III.

A double vortex was found with a low flow velocity: this proves that plasma equilibrium was maintained throughout the duration of the discharge[4].

The current density profiles shown in Figs. 1 and 2 are obtained by differentiation of magnetic probe measurements. When $T_\sigma(R_o)$ is calculated from the local conductivity on the axis the low value of 4.6 eV is found in reg. II in contradiction with a number of other measurements:

- The average ion temperature in the plasma core is found to be 12 ± 3 eV from Doppler broadening of the 4686 Å He II line, under admixture of 15% helium[5]. The emission was not detectable in reg. III, which indicates a considerably lower temperature.
- The local diamagnetism $\Delta B_T(R)$ as measured with a magnetic probe, when integrated over the plasma cross section agrees with the total diamagnetic flux, $\Delta\Phi_D$, measured with an external loop. Also, the measured increase ΔB_T just outside the plasma is in good agreement with $\Delta\Phi_D/\pi r_B^2$ (r_B = bore radius of the coils). From the calculated pressure profile p(R) and the measured $\langle n_e \rangle$ we conclude that $\frac{1}{2}\langle T_e + T_i \rangle$ = 14.5 eV in reg. II. If we assume a flat density profile the temperature on the axis would even be higher. In reg. III the central conductivity temperature is close to the average temperature.

The anomalous plasma heating in reg. II and possibly to a lesser extent also in reg. III, is believed to be due to the occurrence of weak plasma turbulence. This is supported by further observations:

- In both regimes II and III there is some indication that the H_α and the Stark-broadened H_β line profiles have weak satellites near ω_{pe} and harmonics thereof[6].
- By means of a wide-band antenna and band-pass filters emission of r.f. radiation around 2 GHz - corresponding to values somewhat below ω_{pi} - was detected in reg. II. In reg. III the radiation level was much lower (- 25 dB). In cases of bad plasma equilibrium, due to improper choice of $B_\perp$, the radiation was strongly enhanced (+ 10 dB) in both regimes.
- Plasma turbulence made it impossible to draw conclusions about $T_e(r)$ from preliminary Thomson-scattering measurements since the scattered intensities at shifted wavelengths ($\Delta\lambda$ = 10 to 50 Å) showed shot-to-shot variations up to a factor of 2.5. Furthermore, the total amount of scattered light appears to be too high by factors of 10 (reg. II) and 3 (reg. III) to be compatible with densities measured otherwise. A more precise scanning of the scattered spectrum will yield information about disturbances e.g. by satellites at ω_{pe} and harmonics as reported by others for comparable discharges[7,8,9].

TABLE OF EXPERIMENTAL RESULTS (WITH SHOT-TO-SHOT VARIATIONS) t = 1.8 ms

Regime	I	II	III	
Hydrogen pressure p_o	2.5×10^{-2}	2.5×10^{-2}	10^{-1}	Torr
Tor. magnetic field $B_T(R_o)$	1.65	1.65	1.65	T
Discharge current I	7.5 ± 0.5	24 ± 1	20 ± 1	kA
Loop voltage V	190 ± 10	300 ± 25	400 ± 25	V
Current density $j_p(R_o)$	0.8 ± 0.1	2.1 ± 0.1	1.2 ± 0.1	MA/m^2
Electron density $\langle n_e \rangle$				
HCN interferometer	-	6 ± 1	inconclusive	10^{20}/m^3
H_β Stark broadening	6 ± 1	5 ± 1	20 ± 2	10^{20}/m^3
Conduct. temp. $T_\sigma(R_o)$	3.2	4.6	2.4	eV
Ion temperature $\langle T_i \rangle$	-	12 ± 3	undetectable	eV
Diamagnetism				
total flux $\Delta\Phi_D$	- 2 ± 0.5	- 19 ± 2	- 8 ± 2	10^{-6} Vs
local field $\Delta B_T(R_o)$	-	- 26 ± 2	- 13 ± 2	10^{-4} T
Vortex flow speed v_{hor}	4.7 ± 0.5	4.2 ± 0.5	4.4 ± 0.5	10^2 m/s
β_p	2.0 ± 0.2	1.9 ± 0.2	1.5 ± 0.2	
$\langle T_e + T_i \rangle$	3.5	29	5	eV
$\langle v_{de} \rangle / \langle c_s \rangle$	0.30	0.38	0.22	
τ_E	19	37	18	μs

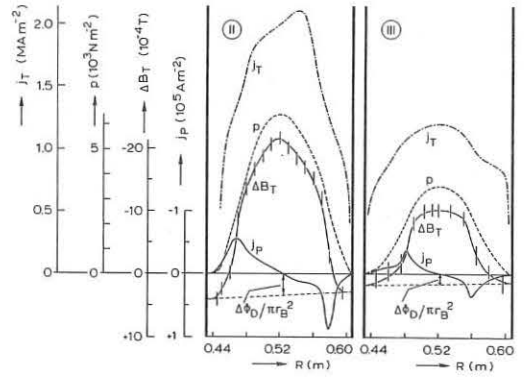

Figs. 1,2: Radial profiles of toroidal current density $j_T(R)$, local diamagnetism $B_T(R)$, diamagnetic current density $j_p(R)$, local pressure p(R).

Conclusion

- The plasma confinement in the toroidal discharge is partly diamagnetic $\beta_p = 1 - \frac{8\pi\,\Delta\Phi_D\,B_T}{\mu_o I^2}$ always exceeds 1.
- There is evidence for anomalous plasma heating in reg. II: $\frac{1}{2}\langle T_e + T_i \rangle = \frac{\beta_p B_p^2(a)}{4\mu_o e \langle n_e \rangle}$ exceeds the central conductivity temperature by a factor of about 3.
- The occurrence of weak plasma turbulence is evident even though the average $\langle v_{de} \rangle / \langle c_s \rangle = 2.87 \times 10^{14}\, I/\langle n_e \rangle a^2 \langle T_e + T_i \rangle^{\frac{1}{2}}$ is only 0.38.
- Whereas the loss mechanism in reg. II is not yet understood, the energy confinement time $\tau_E = \frac{3}{8}\mu_o \beta_p R_o I / V$ in reg. I and III agrees with collision-dominated classical heat losses (c.f. Ref. 4).

Acknowledgement: The authors are indebted to the diagnosticists Messrs C.A.J. Hugenholtz and B.J.H. Meddens (HCN-laser interferometer), Dr. E.P. Barbian and Mr. C.J. Barth (Thomson scattering), Mr. A. Ravestein (spectroscopy), Mr. H.G. Polderman (electrostatic probing) and to the devoted technical team Messrs J.J. Busser, O.G. Kruyt, W. van den Boom, and M.J. Goedkoop.

This work is part of the research programme of the Euratom-FOM Association Agreement with financial support from ZWO and Euratom.

References

[1] G.K. Verboom and J. Rem, Nucl. Fusion 13 (1973) 69.
[2] B. Lehnert, Nucl. Fusion 13 (1973) 781.
[3] R.S. de Haas, Proc. 8th Symp. on Fusion Technology, Noordwijkerhout (1974) 39.
[4] F.C. Schüller et al., Proc. 5th Int. Conf. on Plasma Phys. and Contr. Nucl. Fusion Res., Tokyo (1974) paper CN 33/H 7-2.
[5] T. Sato et al., Plasma Physics 15 (1973) 921.
[6] W.R. Rutgers and H.W. Kalfsbeek, accepted for publication in Z. Naturforsch. (1975).
[7] H. Ringler and R.A. Nodwell, Proc. 3rd Eur. Conf. Contr. Fusion and Plasma Physics, Utrecht (1969) 111.
[8] C.R. Neufeld, Phys. Letters 31A (1970) 19.
[9] P.K. John et al., Phys. Letters 36A (1971) 277.

POSSIBILITY OF USING TURBULENT PLASMA BLANKET

A.V.Nedospasov

Institute for High Temperatures of the
USSR Academy of Sciences, Moscow, USSR

The problem of contamination of plasma in a stationary thermonuclear reactor by the products of sputtering of the walls apparently can not be solved by selection of the wall material alone. The solution of this problem can be obtained by means of special constructive measures which either prevent penetration of impurities into the central zone of the reactor or reduce the energy of the ions and neutrals striking the wall below the sputtering threshold (30-50 eV).

The typical value of the radial temperature gradient in the reactor is determined by the ratio of the axial temperature to the small torus radius (a) and is equal to 10 keV/m. In this case the energy of the neutral particles emitted after the recharging is equal to hundreds of electron volts.

The sputtering can be reduced considerably by a sufficiently thick ($\sim$10cm) layer of cold plasma near the wall. The difficulty consisting in creating such a plasma is that it should pass a heat flux of $q \simeq 10^1 - 10^2$ W/cm^2 coming from the core. This difficulty can be overcome by reducing the temperature gradient near the walls by one order of magnitude by turbulizing the plasma with any instability. Such instability can be current convective instability excited by special longitudinal current.

Owing to the fact that in the case of current-convective instability the transfer coefficients grow with a decrease in temperature /1,2/, the temperature profile should have mildly sloping "wings" near the walls. An identical picture is observed in a turbulent positive column of a gas discharge, in which the current-convective instability develops at the gradient of the plasma concentration /3,4/.

The estimation can be made using the formula for the coefficient of the turbulent temperature conductivity /1,2/

$$\chi \sim 10 \frac{R^4}{\chi_{11}} \left(\frac{c E_0}{H_z T} \cdot \frac{dT}{dz} \right)^2 \qquad (1)$$

Here R is the great radius of the torus, χ_{11} is the longitudinal temperature conductivity, E_0, H_z are the intensities of the longitudinal electric and magnetic fields.

Let us take $\frac{1}{c}\frac{\partial \varphi}{\partial z} = 10^2$ eV/cm and $\chi_0 = 10^4$ cm^2/sec for smooth "stitching" of the temperature profile near the boundary with the hot plasma. The plasma concentration is taken constant ($n=10^{13}$cm^{-3}). The integration of the temperature profile

$$\frac{d}{dx}\left(n \chi \frac{dT}{dx} \right) = 0 \qquad (2)$$

with due account of (1) gives temperature profiles shown in Fig. 1. The corresponding values of E_0 are given in the following table

T_0 (eV)	100	70	50
E_0 (V/m)	6.1	2.6	1.2

For T_0=50 and 70 eV in a reactor with a = 1.5 m we need a current of 20 and 90 kA, respectively, while the additional Joule heat is equal to $\sim$0.4 and 2.6 W per cm^2 of the wall. Since the concentration near the walls must be equal to several units per 10^{14}cm^{-3}, i.e. exceed the design value by one order of magnitude, the required currents and Joule losses will be much lower than those given above. This justifies the neglect of the Joule heat in (2) in the turbulent region compared with the heat flow from the central zone of the reactor.

The using of the solution with decreasing temperature of the electrons implies good contact of the electron gas with the wall. It can be provided by photoelectric and thermoelectric emission of electrons from the surface. Thus, we may indicate to some materials (TaB_2 ; LaB_6 ; TiN ; W) having thermoemissive current density of $\sim$ 1 A/cm^2 at temperatures considerably lower than their melting point. In this case the ratio of the number of evaporating atoms to the number of electrons is in the order of 10^{-6}-10^{-10}, i.e. contamination of the plasma due to the evaporation is much less than the contamination during the sputtering.

It should be noted that a very low plasma temperature in the planket hinders the heat removal to the wall. In order to increase the temperature in the turbulent blanket without increasing the losses, we can try to increase the turbulent pulsations by breaking the magnetic surfaces.

The turbulent transfer is hindered near the equipotential metal wall. However, in view of inavoidable corrugation of the magnetic field, the plasma can pass along the magnetic lines of force in the immediate vicinity to the wall.

Since these estimations do not exclude principal possibilities of formation of a turbulent blanket with L 10 cm and a plasma temperature of a few electron volts, the question of such a blanket deserves more detailed discussion.

The author would like to express his gratitude to B.B. Kadomtsev for valuable discussion having stimulated this work and thanks V.E.Lukash and N.N.Vasiliev for their assistance.

REFERENCES

1. B.B.Kadomtsev in "ZTF" Journal, 31, 1209 (1961)
2. B.B.Kadomtsev , O.P.Poguze "Turbulent Processes in Toroidal Systems" in "Vorposy Teorii Plazmy", v.5, "Atomizdat" Publishers, 1967
3. B.B.Kadomtsev in "ZTF" Journal, 31, 1273 (1961)
4. L.L.Arzimovich, A.V.Nedospasov in "DAN" USSR 145, 1022 (1962)

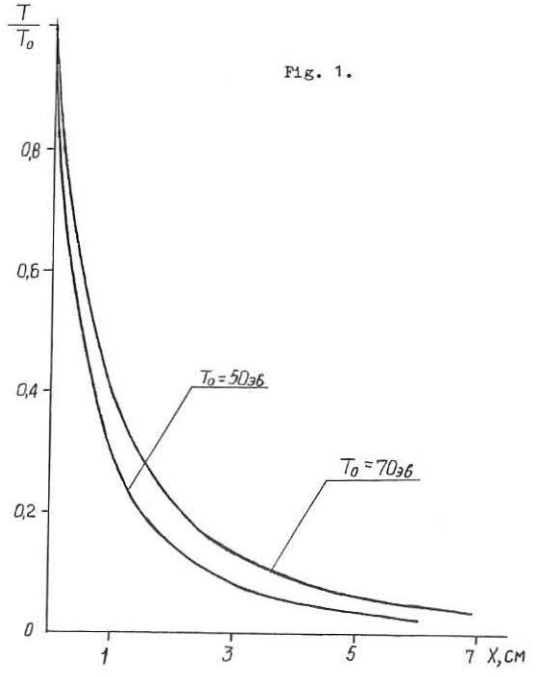

Fig. 1.

A STATIONARY FLOW IN GAS-KINETIC CONFINEMENT OF A MAGNETIZED PLASMA

S.G.Alikhanov, I.S.Glushkov

The Kurchatov Institute of Atomic Energy. Moscow
USSR

Abstract. A stationary cooling wave, travelling across a magnetized plasma is considered. Plasma flow rate, as a function of pressure to magnetic field intensity ratio is determined.

Use of a magnetic field for plasma thermoisolation only has been proposed by different authors before /1,2/. However, as shown in /3/, without plasma motion across the magnetic field a stationary state does not exist. This is due to radiation power loss of a dense plasma, being in direct contact with the walls, which is not compensated by the heat conduction flow. Stationary solution for particular cases /4,5/ does not allow to reveal general process regularity in a not plasma interaction with cold walls. Knowledge of the plasma flow dependence on pressure, magnetic field intensity and temperature provides the possibility for loss evaluations for choice thermonuclear reactor parameters, based on the gas-kinetic confinement principle.

Because a stationary state is considered, all equations,then have to be written in the system, where temperature and magnetic field profiles are stationary, and the plasma flow with magnetic field penetrates the cooling wave. In one-dimensional case for hydrodynamic, one-fluid approximation of equations of motion, Ohm's low and heat conduction /6/ it is convenient to write as follow:

$$\frac{dV}{dx}=\left(\frac{2}{m_i V}\frac{dT}{dx}+\frac{H}{4\pi m_i q}\frac{dH}{dx}\right)\Big/\left(\frac{2T}{m_i V^2}-1\right) \qquad (1)$$

$$\frac{dH}{dx}=-\frac{4\pi\sigma_\perp}{c^2}\left(VH-\frac{c}{e}\frac{\beta_\wedge^{uT}}{q}V\frac{dT}{dx}+const\right) \qquad (2)$$

$$\frac{d^2T}{dx^2}=\left\{3q\frac{dT}{dx}+2q\frac{T}{V}\frac{dV}{dx}-\frac{c^2}{4\pi\sigma_\perp}\left(\frac{dH}{dx}\right)^2-\frac{c\beta_\wedge^{uT}}{4\pi eq}V\frac{dH}{dx}\frac{dT}{dx}-\right.$$
$$-\frac{dT}{dx}\frac{d}{dx}\left[\varkappa_\perp^e+\varkappa_\perp^i-\left(\frac{\beta_\wedge^{uT}V}{qe}\right)^2\sigma_\tau T\right]-\frac{d}{dx}\left[\frac{\beta_\wedge^{uT}T}{qec}\sigma_\perp V(VH+ \qquad (3)$$
$$\left.+const)\right]+\left(\alpha_{Br}T^{1/2}+\alpha_{Rec}T^{-1/2}\right)\frac{q^2}{V^2}-Q_{N.E}\Big\}\Big/\left[\varkappa_\perp^e+\varkappa_\perp^i-\left(\frac{\beta_\wedge^{uT}V}{eq}\right)^2\sigma_\perp T\right]$$

where q=nV = Const, other designations are the same with ones in /6/.

The calculation were performed with a M-222 computer for a wide range of parameters of interest for the CTR problem: pressure was 32 to $3{,}2\cdot10^9$ atm, β =10÷1000. Fig I shows typical T,H,V, $\omega_e\tau_e$ profiles for one case. On condition that HV=const for completely magnetized plasma H must increase to a cold boundary but diffusion changes sign of the gradient near the wall, and thermoelectromotive force in the region $\omega_e\tau_e\simeq1$. Hence the magnetic field intensity is of two-hump shape, so that increasing of H at given P approximates the second maximum to the cold wall, decreasing the distance between the hot and cold regions. Basic results of the work are plotted in Fig 2, where dependence of flow rate of the hot magnetized plasma V_f on ratio P/H_f is shown. Circles represent the results of the calculations which have been checked on from the standpoint of hydrodynamic model and one-fluid consideration applicability. The solid line shows an averaged dependence

$$V_f=3{,}31\cdot10^3\left(\frac{P}{H_f}\right)^{0.32} \qquad (4)$$

here all is in CGSM system.

Hence, the power flow to the wall is given by

$$W=8{,}28\cdot10^3\ P^{1.32}/H_f^{0.32} \qquad (5)$$

Fig 3. (upper line) shows dependence of the layer thickess on the magnetic field in high temperature plasma regions. As shown, calculated points perfectly fall in line with the dependence

$$\ell=1{,}1\cdot10^4\ /H_f^{0.912} \qquad (6)$$

Results obtained can be compared to the estimate with rough assumptions in formula(3) omiting all the terms, except those for power radiation loss and electron non-magnetized thermal conduction.

Power flow at point $\omega_e\tau_e$=1 appears proportional to $P^{1,4}/H_f^{0,4}$, and the coordinate, where $\omega_e\tau_e$=1, $\ell_e\sim H_f^{-1}$, which roughly corresponds to those obtained from exact solution (bottom line in Fig 3). This can be explained by substantial radiation loss fraction being in the region of $\omega_e\tau_e\leq1$.

In this sense formulae (4)-(6) will not greatly change with the coefficients becoming of Bohm's form.

By use of formula (4) we estimate parameters of the thermonuclear system, based on the principle of gas-kinetic magnetized plasma confinement. Total plasma energy for $n\tau=10^{15}$ is

$$Q(MJ)=4{,}5\cdot10^3\left(\frac{I}{H}\right)\beta^{0.5}/P^{1.5} \qquad (7)$$

pressure in this case is 10^6 atm.

Now it is easy to see, that the pressure range is $>10^8$atm, which is of practical interest at reasonable choice of the length to radius ratio of the system.

The authors are grateful to E.P.Veliknov for support and interest in the work, as well as V.D.Konyukova for help in the program preparation.

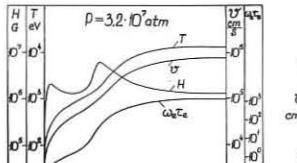

Fig. 1

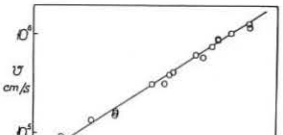

Fig. 2

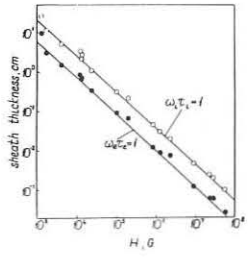

Fig. 3

Literature

1. A.D.Sakharov. Plasma Physics and CTR problems,I,p.20,M,1958.
2. H.Alfen,E.Smars Nature vol.188,p.861, 1961
3. S.G.Alikhanov et al.Nuc.Fusion vol.10, 1973
4. P.Z.Chebotayev et al. VI European Conference on Plasma Physics,vI,p.411,M, 1973
5. M.S.Chu Phys.Fluids vol.16,p.1441, 1973
6. S.I.Braginsky, Questions of plasma theory,v.1,p.183,M.1963.

IMPURITY PROFILES IN A STEADY-STATE D-T REACTOR

J.A. Markvoort and J. Rem

Association Euratom-FOM, FOM-Instituut voor Plasmafysica
Rijnhuizen, Jutphaas, The Netherlands

Abstract: The density profile of an impurity in a cylindrical model of a gas-blanket reactor is investigated on the basis of the multi-fluid MHD-equations. The effect of ion-ion collisions in the thermal force is found to dominate the contribution from the electron-ion collisions, and leads to an impurity profile that has a minimum in the centre of the plasma column.

Introduction

The level of impurities in a D-T reactor should be kept low in order not to give rise to a large "Bremsstrahlung" loss that might make a self-sustained fusion reaction impossible. In this paper we investigate the behaviour of an impurity in a model of a gas-blanket reactor[1,2].

Our reactor model is that of a cylindrical plasma column embedded in a strong longitudinal magnetic field in which the fuel supply, a 50/50% deuterium-tritium mixture, and the ash (helium) removal are effectuated by diffusion, and where the fusion reaction energy is balanced by heat conduction in addition to Bremsstrahlung and neutron radiation; the neutrons are supposed to leave the plasma without interaction. From the variety of possible nuclear reactions in a D-T mixture we consider the deuterium-tritium reaction only. Furthermore, we restrict ourselves to the region where the plasma is fully ionized and assume that the transport processes are describable by the multi-fluid MHD-equations. These equations differ in one aspect from the ones usually considered to yield a sufficient description: the thermal force in the momentum equations must be taken along. It is this "Nernst" effect that drives the poloidal current which together with the longitudinal magnetic field assures the confinement of the plasma. To reduce the number of components we neglect the difference between a deuteron and a triton by introducing a new particle "deuterium" with mass number 2.5; subscripts e, d, 4, and c refer to electrons, the "deuterium" particle, helium, and the impurity, respectively.

The analysis consists of two parts. In the first part we take carbon as a representative impurity and assume only electron-ion collisions to contribute to the thermal force. We show that the results of this calculation - the equations are solved numerically by a Runge Kutta method - can be understood on the basis of a simple analytical analysis. From this analysis it is clear why the relationship $\nabla p_d/n_d \approx \nabla p_4/2n_4 \approx \nabla p_c/z_c n_c$ as found by Braginskii[3] for a plasma where the "Nernst" term was not considered, holds also in this case except for small radii where the radial velocities play a role. Having established the range of validity of the analytical approach we complete the model by adding the effect of ion-ion collision to the thermal force.

The transport equation

The following assumptions are made in the model. The kinetic energy of the helium atoms created in the reaction is instantaneously given off to the surrounding plasma, all species have the same temperature, quasi neutrality, no viscous or inertia effects, no momentum transfer by inelastic collisions, $\omega_i\tau_i >> 1$ the product of the cyclotron frequency and the collision time for each component, no reabsorption of Bremsstrahlung, no cyclotron radiation, the magnetic field has only an axial component and all velocities in the axial direction are zero. The plasma cylinder is placed along the z-axis of the cylindrical coordinate system (r,ϕ,z).

The momentum equation for the i^{th} component is

$$0 = -\nabla p_i + n_i z_i e(\bar{E} + \bar{v}_i \times \bar{B}) + \sum_j \overline{R_{ij}} \quad (j = e,d,4,c;\ i \neq j), \qquad (1)$$

where $\overline{R_{ij}}$ represents the force per unit volume due to collisions of particles i and j (Ref. 3):

$$\overline{R_{ij}} = -n_i n_j \varepsilon_{ij}(\bar{v}_i - \bar{v}_j) + \tfrac{3}{2}\alpha_{ij}\frac{n_i k}{\omega_i \tau_{ij}}\frac{\bar{B}\times\nabla T}{|B|};\quad \tau_{ij} = \sqrt{\frac{m_i m_j}{m_i+m_j}}\frac{(kT)^{3/2}}{\sqrt{2\pi}}\frac{12\pi^2\varepsilon_0^2}{n_j e^4 z_i^2 z_j^2 \ln\Lambda}$$

$$\omega_i = \frac{z_i eB}{m_i},\quad \varepsilon_{ij} = \left(\frac{m_i m_j}{m_i+m_j}\right)\frac{1}{\tau_{ij} n_j}. \qquad (2)$$

The sign and magnitude of the charge of an ion of specie i is designated by $z_i e$; all other symbols have the usual meaning. The coefficient α appearing in the "Nernst" term is equal to unity when $m_j >> m_i$ but differs from this otherwise. For an extensive discussion of the model and the equations used to describe it, the reader is referred to Ref. 1.

Results

In Fig. 1 it is shown to what impurity profile our reactor model gives rise if the effect of ion-ion collisions is neglected in the thermal force, i.e. the profile that an impurity would have in the model of Ref. 1. As representative impurity we have taken carbon $z_c = 6$ and the equations are solved numerically. These figures show that the "deuterium" density increases with r while those of helium and carbon decrease. The carbon density (z=6) is seen to change ten orders of magnitude from r = 0 to the radius where $T = 10^5$ K is reached (the "wall"). The forces in this model thus lead to a strong concentration of high z-impurities on the z-axis.

A simple analytical analysis is able to explain the numerical result. If in the momentum equations all radial velocities are taken zero, then upon elimination of the ϕ-components of the velocities from the r and the ϕ-components we arrive at

$$\frac{dp_i}{dr} + \frac{n_i z_i}{n_e}\frac{dp_e}{dr} = \frac{3}{2} n_i z_i k \frac{dT}{dr},\ \text{or}\ n_i n_e^{(z_i)}\, T^{(1-z_i/2)} = \text{constant}, \qquad (3)$$

where i stands for the ions: d, 4, and c; $n_e = n_d + 2n_4 + z_c n_c$. As the temperature is a decreasing function of r this shows that n_d will be an increasing one while n_4 and n_c are decreasing functions of r. By elimination of dp_e/dr two of these equations can be replaced by:

$$\frac{1}{n_d}\frac{dp_d}{dr} = \frac{1}{2n_4}\frac{dp_4}{dr} = \frac{1}{z_c n_c}\frac{dp_c}{dr}. \qquad (4)$$

This relationship is identical to the one derived in Ref. 3 for an impurity in a fully ionized plasma where no "Nernst" collision terms were considered. Why this is so, is evident from the above differential equation, when dp_e/dr is eliminated; so is dT/dr. The neglect of the radial velocities can also be expressed in the form: $v_{d\phi} - v_{4\phi} = v_{c\phi} - v_{d\phi} = v_{4\phi} - v_{c\phi} = 0$.

In Fig. 2 we have plotted the deviation from relationship (4) due to the radial diffusion of "deuterium" and helium. Only in the centre of the column this is seen to have an effect.

The fact that the "Nernst" term for ion-ion collision depends on the charge number of both ions, indicates that this term does not cancel in deriving Eq. (4) if it would be included in the momentum equations for the ions. Since the masses of "deuterium" and helium are close together we cannot use the formula derived in Ref. 3. To derive an expression valid for collisions between ions of arbitrary masses we have to evaluate the average momentum loss of ion 1 (mass m_1) due to collisions with ions of type 2 (mass m_2). This averaging means integrating over the distribution functions of both ions in which the non-Maxwellian character due to the temperature gradient is taken into account:

$$\left\langle\frac{d\bar{p}}{dt}\right\rangle_{12} = -\frac{e^4 z_1^2 z_2^2 \ln\Lambda}{4\pi\mu\varepsilon_o^2}\int d\bar{v}_1 d\bar{v}_2 \frac{\bar{v}_1 - \bar{v}_2}{|v_1 - v_2|^3} f_1 f_2,\quad \mu = \frac{m_1 m_2}{m_1+m_2}$$

$$f_i = n_i\left(\frac{m_i}{2\pi kT}\right)^{3/2}\left[1 - \frac{v_{ir}}{\omega_i T}\frac{dT}{dr}\left(\frac{5}{2} - \frac{m_i v_i^2}{2kT}\right)\right]\exp\left(-\frac{m_i v_i^2}{2kT}\right);\ i = 1,2.$$

The integrations can be carried out without approximations and result in a force in the ϕ-direction:

$$\left\langle\frac{dp}{dt}\right\rangle_{12\phi} = \frac{3}{2}\alpha_{12}\frac{n_1 k}{\omega_1\tau_{12}}\frac{dT}{dr},\ \text{where}\ \alpha_{12} = \frac{m_2^2}{(m_1+m_2)^2}\left(1 - \frac{m_1^2\omega_1}{m_2^2\omega_2}\right).$$

If in the momentum equations these extra ion-ion Nernst terms are taken into account (in $\overline{R_{d4}}$, $\overline{R_{4c}}$, and $\overline{R_{dc}}$) we obtain with $z_c^2 n_c << n_d, n_4$, and $m_c >> m_4, m_d$ instead of (4)

$$\frac{1}{n_d}\frac{dp_d}{dr} - \frac{1}{z_c n_c}\frac{dp_c}{dr} = \frac{3}{2}k\frac{dT}{dr}\left[6n_4\sqrt{\frac{m_4}{m_d}}\,m_4(m_4+m_d)^{-1} + n_d\right]\left[4n_4\sqrt{\frac{m_4}{m_d}} + n_d\right]^{-1}.$$

Contrary to (4) the velocity differences of these ions in the ϕ-directions are no longer zero. From the complete set of equations which can be derived in this manner, it is seen that the impurity profile has now a minimum at r=0. In the particular limits $n_4 >> n_d$ and $n_4 << n_d$ we arrive at the following relationship between n_c and T,

$$n_c T^{(1+z_c/4)} = \text{constant and } n_c T^{(1+3/4z_c)} = \text{constant}.$$

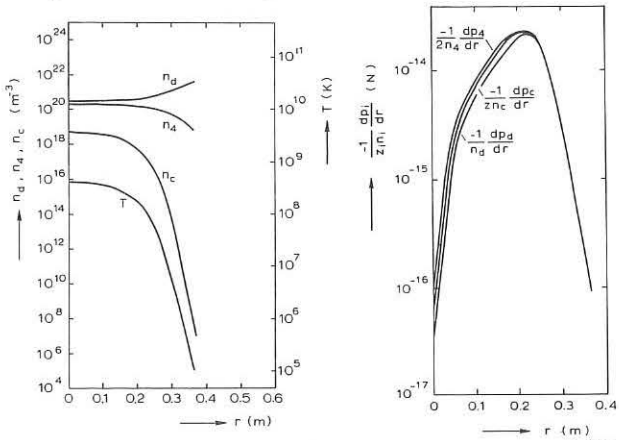

Fig.1. Radial profiles of n_c, n_4, n_d, and T. Fig.2. Radial profiles of $-\frac{1}{z_i n_i}\frac{dp_i}{dr}$ z=6; $T_{axis} = 0.4\times10^9$; $B_{axis} = 2.7$ T; $n_{4axis}/n_{daxis} = 0.8$, $p_{axis} = 75$ atm; $n_{caxis} = 5\times10^{18}$ m^{-3}.

Acknowledgement: The authors are deeply indebted to Prof. C.M. Braams for many fruitful discussions.

References

[1] G.K. Verboom and J. Rem, Nucl. Fusion 13 (1973) 69.
[2] B. Brandt and C.M. Braams, Nucl. Fusion Spec.Suppl. (1974) 385.
[3] S.I. Braginskii, Reviews of Plasma Physics 1, New York Consultants Bureau Enterprises (1965).

ON THE PLASMA WALL INTERACTIONS IN T.F.R.

T.F.R. Group presented by P. BROSSIER

ASSOCIATION EURATOM-CEA SUR LA FUSION
Département de Physique du Plasma et de la Fusion Contrôlée
Centre d'Etudes Nucléaires
Boite Postale n° 6. 92260 FONTENAY-AUX-ROSES (FRANCE)

Experiments have been carried out to analyze the mechanism responsible for the damages observed in the first vacuum chamber of TFR[1]. We recall that impacts, regularly spaced around the torus, had been observed. In one of these spots the amount of energy locally deposited on the chamber wall was sufficient to melt the 0.5 mm tick stainless steel wall, thus creating a leak ; the whole assembly had to be dismantled for repairs and the experiment was shut down for 9 months.

In the new TFR vacuum chamber, the walls are protected from the plasma by a 2 mm thick stainless steel shield. Since the observed impacts were located below the troughs of the toroidal field, a target has been installed in a lower port, in order to study the mechanism involved in the energy deposit on the walls. The target was observed with a near infrared television camera and an X-ray detector sensitive in the energy range from 4 to 100 keV. The current collected by the target was also measured. The other machine diagnostics have been listed in[2].

The energy deposit is a highly localized phenomenon. Every impact is roughly 1 cm^2 in area. The toroidal extension is $\simeq$ 0.5 cm and the poloidal extension is $\simeq$ 2.0 cm. Melting the initial vacuum chamber on such a small area requires an energy of about 200 J. Since the observed spots have the toroidal field coils periodicity (24) the total amount of energy released to the wall is of the order of 5kJ, which is only a small fraction of the total energy in the discharge (200 to 300 kJ).

The last few discharges run in the first TFR vacuum chamber were characterized by low value of the electron density $\bar{n}_e$ and a large number of runaways. Accordingly the experiments described below have been carried out in this regime. A few observations have been given in[3]. The main findings are the following :

- in most of the cases the interaction occurs only when the average electron density $\bar{n}_e$ is smaller than a critical density $\bar{n}_c$. For a plasma current I_p = 130 kA and a toroidal magnetic field B_t = 25 kGs, $\bar{n}_c \simeq 10^{13}$ cm^{-3}. If $\bar{n}_e$ keeps below $\bar{n}_c$ during the whole discharge, the interaction, that is the energy deposit on the walls, starts early (~50 ms) and lasts until the end of the discharge. If $\bar{n}_e \geq \bar{n}_c$ early in the discharge, the interaction starts during the density decay (fig. 1). The lower the density, the larger the amount of energy released to the wall. The critical density $\bar{n}_c$ depends upon the discharge parameters such as I_p, B_t ,... but no systematic study of this dependence has been made. In a few exceptionnal cases, when the breakdown delay is longer than usual, an interaction has been observed even though $\bar{n}_e$ was somewhat larger than $\bar{n}_c$.

- in these particular discharges, the amount of runaways is larger than usual. The loop voltage drop observed (fig. 1b) at the time where the interaction starts shows that, during the interaction, the runaways can carry up to 40% of the total plasma current I_p. The parallel energy of these runaways has been measured and is close to 6 MeV as compared to 10 MeV, or more, in normal Tokamak discharges. In this regime the continuous acceleration of runaways is inhibited, although their density and creation rate are larger than in normal discharges. That the runaways behaviour is modified by the interaction is also shown by the hard X-rays flux emitted by the limiter (fig. 1c). This flux, which corresponds to the runaway electrons lost onto the limiter, stops growing when the interaction starts.

- the energy deposited locally on the walls is carried away from the plasma by electrons which are trapped in the local magnetic mirrors of the toroidal field. They drift vertically upwards when the toroidal field is clockwise, seen from the top of TFR, and downwards when the toroidal field is reversed. Those trapped electrons have an energy close to 50 keV. The current collected by the target, and the duration of the interaction vary from shot to shot . Observed values such as $3.5\ 10^{-4}$ A and 200 ms correspond to an energy of 4 J per impact. This figure is in agreement with the heating of the target as measured by the infrared camera. It must be noted however that the amount of energy released to the walls varies with the experimental conditions such as I_p, B_t , n_e, as well as with the limiter radius. Energy deposits as high as 180 J per impact have been measured with the TV camera. Such an energy would be sufficient to explain the melting of the wall.

- the 50 keV electrons impiging upon the wall are created near the plasma magnetic axis ; by varying the distance between the target and the plasma it was shown that they drift on the B = cte surfaces coming from a region of the plasma inside a radius r $\simeq$ 5 cm (see Ref. 3).

- in these discharges the electromagnetic energy emitted in the neighbourhood of the electron cyclotron frequency and its harmonics has clearly a non-thermal origin[3] : the emitted power is approximately an order of magnitude above that in "normal Tokamak discharges"[4] and peaks up at frequencies close to 0.5 ω_{ce}, 1.5ω_{ce},... We interpret this spectrum as a continuous spectrum partially reabsorbed by the bulk of the plasma near ω_{ce} and its harmonics.

- the plasma-wall interaction is a relaxation phenomenon ; the electrons leave the plasma in bursts which occur every 200 to 300 µs. This is shown by the modulation observed on a) the target current, b) the X-ray flux emitted by the target hit by the 50 keV electrons (fig. 2) and c) the total emitted electromagnetic power integrated over the 0.4 ω_{ce} - 4 ω_{ce} frequency range.

To conclude, we observe that the relaxation period (300 µs) is of the order of the time necessary to decouple electrons from the thermal bulk. The distribution function is theoretically isotropic[5] up to an energy of the order of 50 keV in our case. 50 keV electrons which are trapped in the toroidal field modulation $\delta B/B$ may drift up to the wall without undergoing too many collisions. We may then consider that the total number N of trapped electrons collected on the target during one pulse is related to the total number N_T of runaways produced during this pulse by $N \simeq N_T(\delta B/B)^{1/2}$. Each pulse would correspond to an increase of the runaway current of 1000 A. This is consistent with 30 % of the discharge current being carried by runaways after ~ 10 ms. In a time of 300 µs a beam of runaways with a relatively large density current is produced on the magnetic axis. It is possible that this beam is unstable. This would explain the observed relaxations.

REFERENCES.

(1) - P.M. Rebut, R. Dei-Cas, P. Ginot, J.P. Girard, M. Huguet, P. Lecoustey P. Moriette, Z. Sledziewski, J. Tachon and A. Torossian. "Plasma-wall interactions in the TFR machine" Journal of Nuclear Materials, 53, 1974, p. 16.

(2) - Equipe TFR "Neutres atomiques et impuretés dans TFR" 5th IAEA conference, Tokyo, november 1974.

(3) - Equipe TFR "Décharges à fort courant dans TFR". 5th IAEA conference, Tokyo, november 1974.

(4) - TFR Group "Measurements of the electron cyclotron emission from the TFR Tokamak plasma and comparisons with theory" this conference.

(5) - A.V. Gurevich, " On the theory of runaway electrons" Sov. Phys., JETP, 12, 5, 1961, 904,

FIGURE CAPTIONS

Fig. 1 - The interaction starts 160 ms after the beginning of the discharge (arrow).
Fig. 2 - Relaxation on the target current and X-ray flux. Top times : 50 ms/div. Bottom traces : 200 µs/cm.

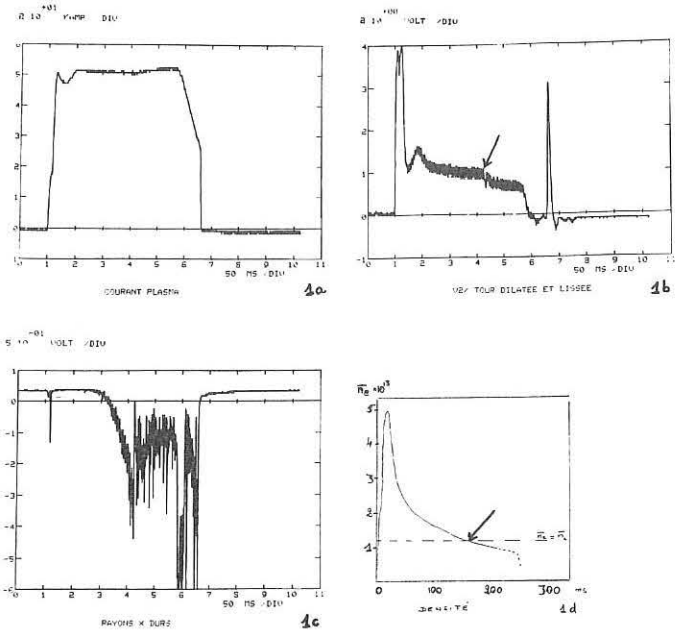

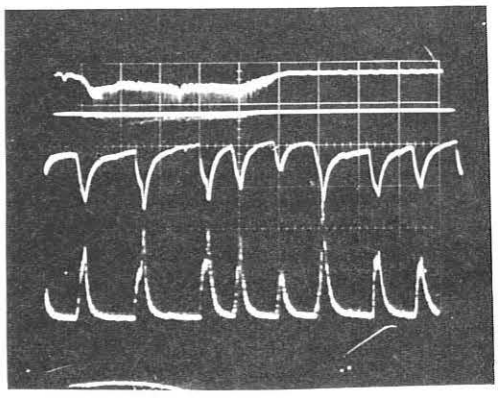

QWAAS a New Tool for Investigation of Plasma-Wall Interaction in Fusion Research

P. STAIB, R. BEHRISCH, W. HEILAND and G. STAUDENMAIER
MPI für Plasmaphysik, EURATOM Association, D-8046 Garching, Germany

Abstract : A sample is introduced to the wall of the PULSATOR I tokamak. After exposure to several discharges its surface composition is determined in a UHV analysing chamber using different methods. Absolute calibrations give a mean deposition rate of 1×10^{13} atoms/cm^2 per discharge for Mo (limiter material).

The discharge times reached in today's tokamak machines is much longer than the confinement time of the particles in the plasma, and so the plasma-wall interaction is a dominating process in these devices (1-3). This interaction leads to an impurity flow from the wall to the plasma, the consequence being an enhancement of Z_{eff}, as measured by other diagnostics.

The experiment QWAASS (Quantitative Wall Analysis by means of Auger and Secondary Ion Mass Spectroscopy) opens the possibility of measuring directly such interactions by making a chemical analysis of a probe before and after its introduction to the wall of the plasma vessel. The analysis of the surface are performed by combination of

1. SIMS, Secondary Ion Mass Spectroscopy, the most sensitive method available for surface analysis providing qualitative detection of all elements (and isotopes)(4).
2. AES, Auger Electron Spectroscopy, applicable for $Z \geq 4$, which yields quantitative information (5).
3. EID, Electron Induced Desorption, which yields information on the binding of sorbed layers (6).

By these methods both deposition and removal of material from the sample can be observed. Thus QWAASS is suitable for investigating (a) the material transport (absolute calibration) occurring in tokamak discharges, (b) the effects of pulse cleaning on the first wall, (c) the amount of hydrogen on and in the sample (recycling), (d) the dependence of measured data on the sample-to-plasma distance, (e) the microscopic distribution of materials deposited on the sample.

The experimental arrangement (Fig. 1) consists of an ultra-high vacuum chamber containing the analysis systems and a long manipulator. For surface analyses, the sample is located at the center of the analyzing chamber, and the metallic valve between the chamber and the plasma vessel is closed. After determination of the chemical composition of the sample (taking about 2 minutes), the sample can be introduced into the machine. The manipulator, driven by a remote-controlled step motor, is first introduced through a metallic fitting allowing a backlash of only 0.02 mm with the manipulator, thus achieving excellent vacuum isolation between the two vessels. Then the valve is opened and the sample is moved to the wall of the plasma vessel. Since the vacuum vessels are always separated a background pressure of about 2×10^{-9} torr can be maintained in the analyzing chamber even for a filling pressure of several 10^{-4} torr.

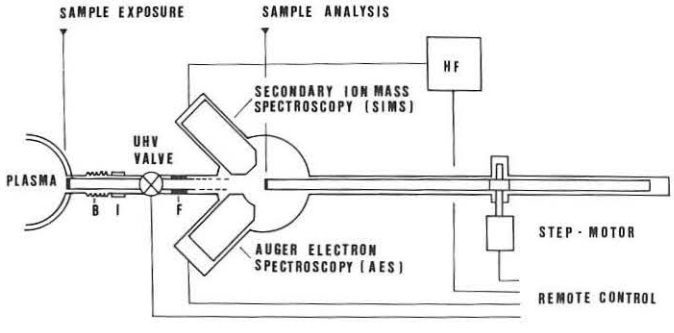

Fig. 1 : Schematic view of QWAASS

At present QWAASS is mounted on the PULSATOR I tokamak at Garching. It should be mentioned that the sample of QWAASS is mounted at a position on the torus 90° apart from the position of the limiter, and there is no line of sight between the two. The aim of our first experiment is to analyze deposited material for a certain number of discharges with SIMS and perform an absolute calibration of the deposited material.

In Fig. 2 SIMS spectra of the Al sample before exposure and after 120 discharges are shown. The appearance of Cr^+ and Fe^+ (stainless-steel liner) and Mo^+ (limiter) is obvious. It is noteworthy that molybdenum oxide was definitely detected, whereas no oxide of iron or chromium was found. The total amount of material deposited at the sample as determined by Rutherford backscattering (5) was 1×10^{15} Mo atoms/cm^2 and 3×10^{15} Fe and Cr atoms (not resolvable) for 120 discharges. Hence mean values of 0.8×10^{13} atoms/cm^2 per discharge for Mo and $2,5 \times 10^{13}$ for Fe and Cr are obtained. SIMS is sensitive enough to allow qualitative detection of impurities deposited after one discharge, however, a larger number of discharges was necessary for quantitative analysis by Rutherford backscattering.

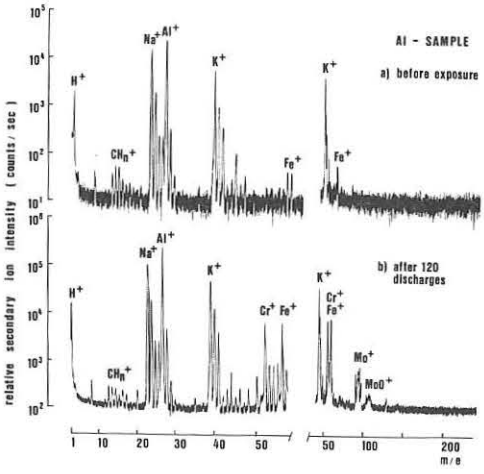

Fig. 2 : SIMS spectra of Al sample
a) before exposure to plasma, primary ions : 2 keV Ar^+, $2,1 \times 10^{-8}$ A.
b) After exposure to 120 discharges, primary ions : 2 keV Ar^+, $2,1 \times 10^{-7}$ A.

After analysis the targets can be cleaned by sputtering with Ar^+ ions. The complete disappearance of Mo indicated that the deposition of impurities on the sample is homogeneous. In addition surface investigations performed with a scanning electron microscope (resolution 200 Å) combined with x-ray analysis show no droplets of Mo supporting also a homogeneous distribution. Assuming that the distribution of deposited impurities is homogeneous over the liner, and further assuming that the confinement time for the impurities is equal to the particle confinement time of about 10 ms, and a discharge time of 150 ms, the corresponding mean impurity densities are 9×10^{10} cm^{-3} for Mo and 3×10^{11} cm^{-3} for Fe and Cr. These values amounting to about 1 % of the plasma density are in rough agreement with soft x-ray spectroscopy measurements (8). A comparison between these quantitative results of QWAASS and absolutely calibrated impurity concentrations, if available, would allow determination of the impurity confinement time.

References :

(1) E. Hinnov, J. Nucl. Mater. 53 (1974) 9
(2) R. Behrisch and B.B. Kadomtsev, Proc. 5th Conf. Plasma-Phys. and Contr. Nucl. Fus., Tokyo 1974 Paper CN-33/S-2
(3) D. Düchs, G. Haas, D. Pfirsch and H. Vernickel, J. Nucl. Mater. 53 (1974) 102
(4) A. Benninghoven, Surf. Sci, 28 (1971) 541
(5) P. Staib and J. Kirschner, Appl. Phys. 3 (1974) 421
(6) T.E. Madey and J.T. Yates, jr., J. Vac. Sci. Technol. 8 (1971) 525
(7) R. Behrisch, B.M.U. Scherzer and P. Staib, Thin Solid Films 19 (1973) 57
(8) S. Sesnic, private communication

INTERACTION OF NEUTRAL HYDROGEN AND PLASMA INCLUDING WALL REFLECTION

J.F. Clarke[+] and D.J. Sigmar[*]
[+]Oak Ridge National Laboratory and [*]Massachusetts Institute of Technology
U.S.A.

Abstract: We solve the kinetic equation for the neutral hydrogen in a hot plasma taking into account gas feed, Frank-Condon neutrals, wall absorption and re-emission of neutrals, electron impact ionization and charge exchange reactions. Steady state neutral profiles are obtained showing the effect of neutral hydrogen on the ion momentum and energy balance.

The presence of neutral hydrogen in Tokamak reactors is unavoidable (refuelling, outgassing) as well as desirable (wall protection, plasma profile control). Combined with the choice of wall reflection properties, one can achieve control of boundary conditions for the plasma, extending some depth into the plasma. The full problem entails the simultaneous solution of the coupled kinetic equations for the proton and the neutral hydrogen distribution functions. In this paper we assume the proton distribution function given and using a simple model, address the steady state kinetics of the various neutral components, shown schematically in Fig. 1. f_{H2} is the source distribution of molecular hydrogen producing the distribution f_{FC} of Frank-Condon neutrals, F_w describes the net amount of atomic hydrogen reflected off the wall and f_o describes warm charge exchange neutrals born inside the plasma. In the figure, the superscripts + and - refer to the direction with respect to z, the slab model equivalent of the radial coordinate. We assume the mean free path of a neutral against charge exchange (CX) to be much smaller than a, and

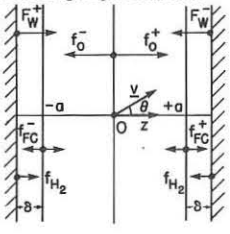

Fig. 1 Slab model

that of a proton against charge exchange smaller or equal to a. The distance $\delta \ll a$ in Fig. 1 characterizes the source of the Frank-Condon neutrals, whose location depends on the shape of the plasma temperature profile near the edge. The kinetic equation for f_o is [1]

$$v_z \frac{\partial f_o}{\partial z} = n_w \langle \sigma_{cx} v \rangle_i f_i - n_e \langle \sigma_{ion.} v \rangle_e f_o + n_o \langle \sigma_{cx} v \rangle_o f_i - n_i \langle \sigma_{cx} v \rangle_i f_o \quad (1)$$

n is the density. The indices on the density w, e, o, and i stand for neutrals born outside the plasma region, electrons, neutrals born inside the plasma region and ions (protons). The first term is gain from CX of a wall neutral with a proton, the second loss due to electron impact ionization, the third gain from CX of an "interior" neutral with a proton, the fourth loss of interior neutrals due to CX with protons. A more rigorous CX collision operator has been given elsewhere [2]. This simplified operator allows the analytic solution

$$f_o = \left(\overline{\sigma v}/\mu v\right) \int_{-a}^{z} dz' f_i \left(n_o + n_w\right) \exp - A(z', z) \cdots \mu > 0 \quad (2a)$$

$$f_o = -\left(\overline{\sigma v}/\mu v\right) \int_{z}^{a} dz' f_i \left(n_o + n_w\right) \exp + A(z, z') \cdots \mu < 0 \quad (2b)$$

Here,

$$A(z_1, z_2) = \int_{z_1}^{z_2} dz'' n_i \overline{\overline{\sigma v}}/v\mu \quad (3a)$$

$$\mu = \cos\theta, \quad \overline{\sigma v} = \langle \sigma_{cx} v \rangle_o, \quad \overline{\overline{\sigma v}} = \langle \sigma_{cx} v \rangle_i + \langle \sigma_{ion.} v \rangle_e \quad (3b)$$

To keep the theory analytically tractable, we choose the model for the proton distribution function

$$f_i = n_i \, \delta(v - \alpha_i)\left(1 + 3 v_x u_i / \alpha_i^2\right) / 4\pi v^2 \quad (4)$$

a finite temperature "Maxwellian" containing a toroidal flow velocity u. (We have in mind the neoclassical pressure gradient driven ion flow [3,4].)

One obtains

$$n_o = \tfrac{1}{2} \int_{-a}^{a} dz' \left(n_o + n_w\right) n_i \, \sigma_{cx} \, E_1\left[\left|\bar{A}(z', z)\right|\right] \quad (5)$$

where

$$\bar{A}(z', z) = \int_{z'}^{z} dz'' \, n_i \, \overline{\overline{\sigma v}}/\alpha_i(z') \quad (6)$$

and E_1 is the first exponential integral.

If the density of wall originating neutrals n_w is assumed given, Eq. 5 can be solved straightforwardly numerically for $n_o(z)$, which inserted in Eq. 2 completes the problem [1]. However, as can be concluded from Fig. 1, $n_w = n_{FC} + n_R$ where n_{FC} is the density of Frank-Condon neutrals and n_R the density of neutrals reflected from the wall. n_R is therefore dependent on n_o, the density of energetic neutrals originating inside the plasma, and a further integral equation for n_w must be found. Motivated by a detailed study of the wall absorption and re-emission problem of warm CX neutrals, we assume that on re-emission the neutrals have a flat distribution in energy ($0 \leq E' \leq E$) and in angle ($0 \leq \theta' \leq \frac{\pi}{2}$). Introducing a reflection transfer function R (E, μ) [where (E, μ) describes the neutral before absorption and (E', μ') after], one finds for the distribution of reflected neutrals

$$f_R(v', \mu') = \left(\sqrt{m/2}/v'\right) \int_{E'}^{\infty} dE \, E^{-\frac{1}{2}} \int_{o}^{1} d\mu \, R(\mu, E) \, f_o(\mu, E, z = \pm a) \quad (7)$$

This distribution is attenuated as the reflected neutrals penetrate into the plasma, so that the neutral distribution due to wall reflection becomes, at point z

$$F_w^{\pm} = f_R(v, \mu) \begin{cases} \exp - A(-a, z) \cdots \mu > 0 \\ \exp \; A(z, a) \cdots \mu < 0 \end{cases} \quad (8)$$

with A as defined in Eq. 6. A similar equation describes the Frank-Condon distribution $f_{FC}^{\pm}$ within the plasma. Thus, the total density of wall originated neutrals is given by

$$n_w = \sum_{\pm} \int d^3v \left(F_w + f_{FC}\right) \quad (9)$$

and the total density of all neutrals becomes $n_T = n_o + n_w$, where n_o has been given in Eq. 5. This completes the formulation of the problem. Combining the integral equations 5 and 9

$$n_w = \int_{-a}^{a} dz' \, K_1(z', z) \, n_T + S_{FC}; \quad n_T = \int_{-a}^{a} dz' \, K_1 + S_{FC}^{*} \quad (10)$$

where the kernels $K_{1,2}$ are similar to that shown in Eq. 5 and S_{FC}, S_{FC}^{*} are Frank-Condon source terms. Numerical solutions are in progress. A simple case results by omitting the contribution of wall reflected neutrals (i.e., setting R (E, μ) = o, $n_w = n_{FC}$). After solving for n_o, f_o we calculate the moments $n_o u_o = \int d^3v \, v_x f_o$ and $n_o E_o = \int d^3v \, \frac{mv^2}{2} f_o$, the toroidal flow velocity and heat content of "interior" neutrals. Typical results are shown in Figs. 2,3,4. Particularly noteworthy is the fact that one deduces from Fig. 3 a finite friction $R_{cx} = -m n_i \nu_{cx} (u_i - u_o)$ between the toroidal ion flow

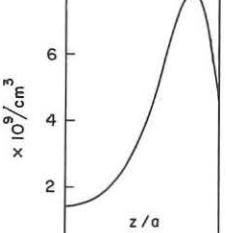

Fig. 2 Neutral density n_o

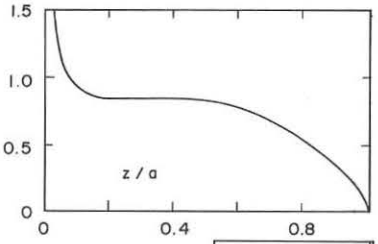

Fig. 3 Ratio $n_o u_o / n_i u_i$

velocity u_i and the neutral flow velocity u_o which reverses over the plasma radius owing to momentum transport from neutrals originating in the outer region. This friction leads to non-ambi-polar ion diffusion [2,4]. From Fig. 4, the ion energy loss $Q_{cx} = -m_i n_i \nu_{cx} (T_i - E_o)$ by CX is seen to be reduced by the finite neutral energy in the plasma core and reversed near the edge where the fast neutral energy exceeds the ion temperature. These effects will be explored parametrically, allowing the ratio of neutral and proton CX mean free path over device size to vary.

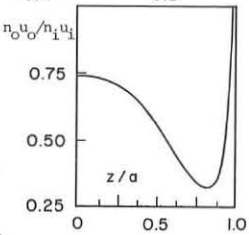

Fig. 4 $n_o E_o / n_i T_i$

Acknowledgements: We thank J.T. Hogan and S.P. Hirshman for valuable discussions. The numerical work was performed by R. Fowler, K. Rothe & B. Clark. Work sponsored by ERDA under contract W7405-eng-26 with Union Carbide Corp. at ORNL, and contract AT(11-1)3070 at M.I.T.

References: [1] J.T. Hogan and J.F. Clarke, Proceedings, Journal of Nucl. Materials 53, 1 (1974).
[2] D.J. Sigmar and J.F. Clarke, ORNL-TM-4606, to be published in Physics of Fluids.
[3] M. Rosenbluth, R. Hazeltine, and F. Hinton, Phys.Fl. 15 (1972) 116.
[4] D. Sigmar, J. Clarke, R. Neidigh, K. Vander Sluis, Phys. Rev. Lett. 33 (1974), 1376.
[5] M.T. Robinson, paper presented at 3rd Intl. Conf. Atomic Collisions with Solids, Kiev, U.S.S.R., Oct. 1974.

WALL LOSS LIMITS IN HALL ACCELERATORS

P.J. Lomas and J.D. Kilkenny
Imperial College, London, United Kingdom

Abstract: This paper demonstrates that wall impact can be a serious problem for high current density Hall Accelerators. This effectively prevents the scaling up of the stage length of existing devices in order to obtain useful ion energies.

It is important when considering the merits of Hall Accelerators in producing plasma beams, to know how they might scale up for application in neutral beam injection into containment experiments. To date, operation has covered the range 1Amp at 20KV to 3KA at 1KV (1, 2). We would like to increase the number of stages at the higher currents to give the 20keV optimum ion energy required for injection (3).

Electric and magnetic probe and spectroscopic diagnostics have been applied to the accelerating hydrogen plasma in the 2-stage device of Cole (2). Density and temperature estimates from the interpretation of hydrogen Balmer line intensities show that $\omega\tau$ is large ($\sim$ 1000). However, the effective plasma conductivity for electron current is much less than the collisional value of $\sigma/1+(\omega\tau)^2$. We find that a fast instability (frequency $\sim$1Mc/s) dominates the conductivity, in a similar manner to Russian (4) observations in Argon. We determine the build up and geometry of the ion flux by an ion probe, and the ionisation rate from the absolute H_α intensity. As can be seen in figs. 1 and 2, the build up of ion current is most pronounced in stage 2, whereas ionisation occurs in both. This contrasts with other work (5) in much lower current density devices. We observe $\sim$300KW of $\sim$1keV ions at the cathode. However the ion probe shows that the beam diverges with an half angle of $\sim 45^\circ$, so that the beam power is wasted.

Ion trajectory calculations in the experimentally determined electric and magnetic fields can account for the form and divergence of the ion current. Ions created in the first stage tend to undergo wall impact, whereas those created in stage-2 are strongly divergent. This occurs because there is no mechanism to counteract the centrifugal effects of azimuthal motion since E_r and B_z are too weak. The ions created in stage two do not have their azimuthal velocity reduced by any reversal in B_r and so diverge in the field free region. The addition of a judicious amount of B_z would reduce both these effects if the consequent $V_\theta B_z$ force were inward. An example of the un-focussed trajectories of an H^+ ion is shown in fig. 4 for the 0.05T field of fig. 3 with a discharge voltage of 1.5KV.

We see that a many stage extension of this accelerator would produce no benefits since only the final stage would be effective; ions created in earlier stages would be lost. In fact, calculations performed for the fields of the six-stage device of Cole show that not only is this the case, but his poor efficiencies $\sim$ 10% or less (1) can be explained on this basis.

A field which has such an inbuilt focussing mechanism is the multi-cusp (6). This field would reduce wall loss, improving the efficiency of acceleration, and also as a bonus, improve beam divergence. Here we might find scale up of stage length much more worthwhile. However for maximum effect it would be essential to control the ionisation region by means of some pre-ionisation technique. The feasibility of such techniques has yet to be demonstrated.

I gratefully acknowledge the use of U.K.A.E.A. Culham Hall Accelerator facilities and I warmly thank Dr. H.C. Cole for many discussions.

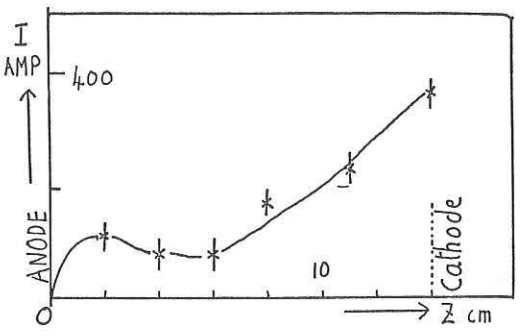

Fig 1. Axial Distribution of Ion Current

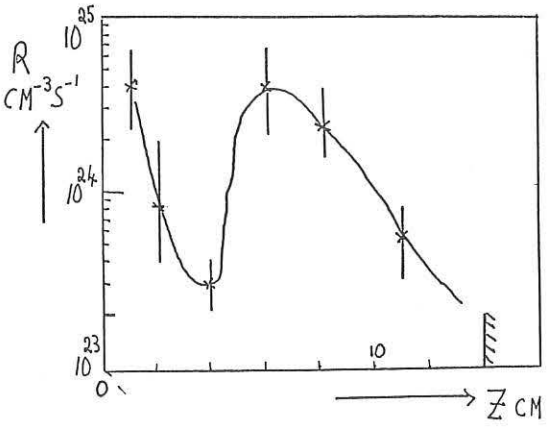

FIG 2. Axial Dependence of Ionisation Rate

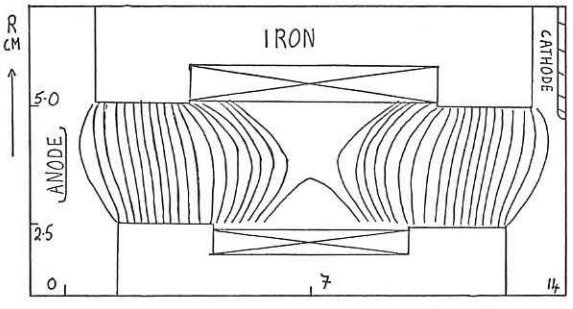

FIG.3. Magnetic Field

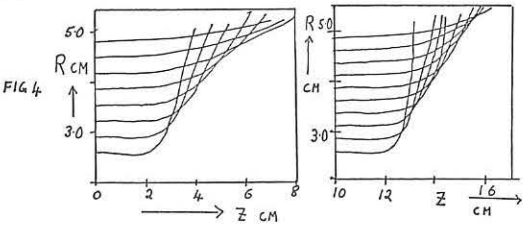

References

(1) H.C. Cole et al. (1974)

(2) H.C. Cole (1970), Nucl. Fusion 10, p. 271.

(3) T.H. Stix (1972), Plasma Physics 14, p. 367.

(4) A.I. Morozov (1973), Sov. Phys. Tech.Phys. 18, No. 5.

(5) I.P. Zubkov et al. (1971), Sov. Phys. Tech. Phys. 16, No. 3.

(6) J.D. Kilkenny et al. (1973), Plasma Physics 15, p. 1197.

LOWERING THE IMPURITY LEVEL IN PULSATOR BY PULSED GAS INFLOW

B. Cannici, W. Engelhardt, J. Gernhardt, E. Glock, F. Karger, O. Klüber, G. Lisitano, D. Meisel, P. Morandi, S. Sesnic
Max-Planck-Institut für Plasmaphysik, 8046 Garching, Germany

Abstract: An increase of the electron and proton density is achieved by fast inflow of hydrogen during the discharge. The result is an appreciable decrease of Z_{eff}. The particle confinement properties are shown to depend on the stability behaviour.

Most Tokamak discharges last longer than the particle confinement time which means that, in the absence of other sources, lost particles must be recycled from the wall. Assuming a recycling coefficient of 1, the density is expected to be proportional to the filling pressure. Experiments on Pulsator show, however, that only the density reached in the first 0.5 ms follows this expectation. Generally after $\approx$ 20 ms a steady-state value is reached which can be higher or lower than the filling density, depending on the discharge current and on the vacuum conditions. Frequent opening of the torus, for example, may lead to a plateau density which is more than five times the filling density. On the other hand, during a series of 2000 shots where no opening took place, the plateau density decreased continuously, the value $1.5 \cdot 10^{13}$ cm^{-3} not being exceeded regardless of the filling pressure. These observations led us to the following conclusions: 1)the recycling coefficient of hydrogen is less than 1, 2)wall recycling may cause a considerable contamination by impurities, whose influx decreases with progressive cleaning during many shots. In order to control the density in an independent way and moreover to lower the relative impurity content, experiments have been started to replace lost hydrogen by pulsed gas inflow. /1/

The experimental setup is shown in Fig. 1. Access to the torus is provided by four ducts, which are connected to the vacuum pumps via large conduits. In the type A operation mode (no pulsed inflow) hydrogen is slowly pumped through the torus. In type B discharges, after a start as in type A, a volume of $\approx$ 100 cm^3 filled with hydrogen in the torr range is expanded into one of the conduits $\approx$ 20 ms later.

Both types of discharges are compared in Fig. 2. In case A the loop voltage, electron density and Z_{eff} are nearly constant, while in case B the loop voltage drops when the density is increased by the additional gas input. Since the electron temperature does not vary appreciably in time, the loop voltage decrease is mainly due to that of Z_{eff}. This is consistent with the observation that the O VI line emission remains constant during the current flat-top. Moreover, the absolute amount of heavy impurities seems to be reduced by the gas input: The L-line emission of Mo and of the wall components (Fe,Cr,Ni) as well as the X-ray continuum emission decreases during the discharge. This has never been observed in type A. The X-ray spectra show additional striking differences (Fig.3): in case B the continuum exhibits a more extended thermal slope. The K-lines, excited by soft runaways, are much weaker than in case A. Furthermore, the reduction of Z_{eff} is reflected by the reduction of the emitted intensity. It should be added that τ_E in case B is increased by a factor of 3, i.e. roughly by the same factor by which Z_{eff} is decreased.

From our experiments we can also draw some conclusions concerning the particle confinement properties of the plasma. Fig. 4 shows two type B discharges with the same gas input but with different limiter q values. The density increase is slower in the $q \approx 3$ discharge where strong MHD-modes are observed. This suggests that the particle confinement time has been reduced by these instabilities. Damping the MHD-modes by applying helical $\ell = 2$ fields /2/ increases again the density. Clearly, a net effect can only be observed when the recycling coefficient r is less than 1. As only the ratio $\tau_p/(1-r)$ enters the equation for the density evolution, an independent measurement of τ_p is necessary. Unfortunately this is not possible at the moment for the following reason: An absolute $L\alpha$ measurement at one of the 4 ducts is not representative of the whole torus surface, since gas flowing from the conduit into the plasma causes an increased emission. This is supported by $H\alpha$ measurements performed by means of a 7 channel system as indicated in Fig. 1. The emission at the plasma surface facing the conduit is much larger than that at the inner side of the torus (Fig.5). Suitable modifications of the machine should enable measurements of τ_p. Further, experiments with gas inflow should allow estimates of the recycling coefficient. Summarizing we can make the following statements concerning our experiments:

1) The recycling coefficient of hydrogen is appreciably < 1.
2) Replacing lost hydrogen by gas inflow lowers Z_{eff} by reducing the relative impurity level and probably the absolute value as well. As a consequence energy confinement is improved.
3) Particle confinement is strongly influenced by MHD-stability.

References: /1/ E.P.Gorbunov et al.,Nucl.Fusion 11, 433 (1971)
/2/ F.Karger et al.,Tokyo Conference, PD-2,(1974)

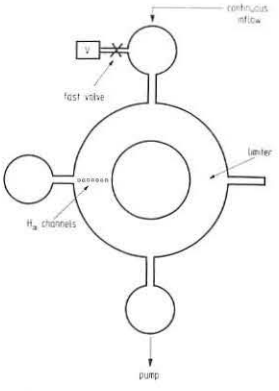

Fig. 1 Schematic view of the vacuum setup

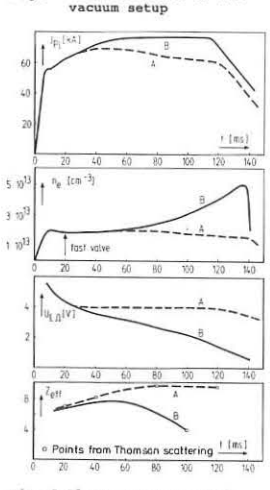

Fig. 2 Plasma parameters of type A and B discharges

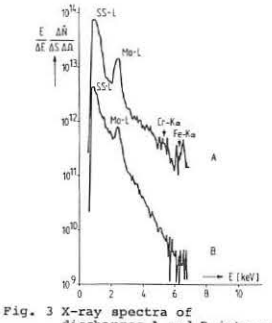

Fig. 3 X-ray spectra of discharges A and B integrated between 60 and 120 ms

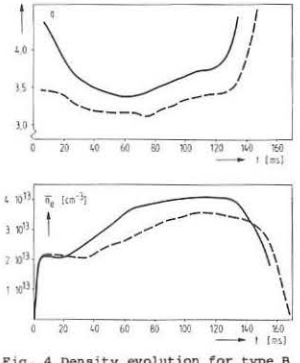

Fig. 4 Density evolution for type B discharges different in q

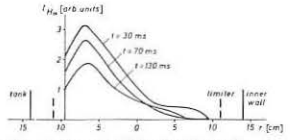

Fig. 5 Case A distribution of H_α emission (chord average)

TRANSPORT OF INJECTED IMPURITIES IN ATC

S. A. Cohen, E. S. Marmar, J. L. Cecchi

Princeton Plasma Physics Laboratory, Princeton University

Princeton, N. J. 08540, U.S.A.

Abstract. Using a new technique for producing short intense bursts of high-Z atoms, we have injected aluminum into ATC and measured the time evolution of the radial distributions of AlVII → AlXI. When intrinsic impurities are taken into account the inferred diffusion coefficient is in good agreement with that predicted by neoclassical theory [1][2].

The effects of impurities in CTR plasmas have been considered by numerous authors [3]. One important unknown is how rapidly impurities are transported through the edge region of a plasma. We have developed a new impurity injection technique that makes possible a dynamic measurement of impurity transport in this region.

The injection system consists of an aluminized glass slide in a vacuum system and a 2 joule Q-switched ruby laser. A 2 mm diameter spot on the aluminum-glass interface is irradiated by the focussed laser beam. This produces a 300 μsec burst of 5×10^{16} neutral aluminum atoms with 3 eV mean energy. (The total number of electrons in the plasma is 10^{19}.) Aluminum neutrals with this energy should penetrate 1 to 2 cm into the ATC plasma before being ionized. They then rapidly circulate along the field lines and, less rapidly, are transported across them. The radial location of each ionization state is measured using an absolutely calibrated, scanning, grazing incidence, vacuum ultraviolet monochromator. Observations are made of the strongest lines, Δn=0 transitions to the ground state.

During these experiments magnetic probes showed that no large MHD kink-like modes were present and that the up-down and in-out stability was $\pm$ 0.5 cm. Using a 4 mm microwave interferometer, the average electron density, $< n_e >$, was measured. Within 4 ms after aluminum injection $< n_e >$ increased 5% above the no-injection case. This change in $< n_e >$ decayed with a 7 ms time constant. The 5% increase is consistent with the amount of aluminum injected. Thomson scattering measurements of the radial electron density and temperature profiles showed no change upon injection. The peak electron density and temperature were 2.5×10^{13}cm^{-3} and 1400 eV, respectively. The proton temperature profile was assumed to be parabolic, with a peak temperature of 180 eV as previously measured on ATC for this type discharge. The proton density, n_p, is assumed to equal 60% of the electron density. This is because Z_{eff} was 4.6. Most of this is accounted for by the measured oxygen concentration. Z_{eff} is assumed constant across the plasma. The safety factor, q, was calculated to be 0.6 on axis and 2.5 at the edge.

After injection of aluminum, observations of different Al ionization states were made along chords of the minor cross section. These were Abel inverted and the density unfolded from the photon signals. The results show the surprising feature that each ionization state appears in a particular shell of the plasma, becomes bright, then dim, but does not move discernably from that shell. The normalized radial distributions of three adjacent ionization states, AlIX → AlXI, are shown in Figure 1. The time evolution for the normalized line integral (across the minor diameter) photon signals of 5 consecutive ionization states is shown in Figure 2. The peak absolute brightness of each line is shown in Figure 3a. These three measurements-the radial distributions, the time evolutions, and the absolute brightness-form a complete description of aluminum transport in the region 8 to 14 cm.

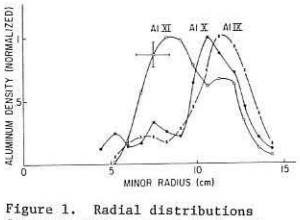

Figure 1. Radial distributions for AlIX → XI measured at the time of their peak intensity.

To compare these results with theory we have developed a one-dimensional computer code that describes impurity transport in the Pfirsch-Schlüter regime. This code advances each ionization state in space and time according to the diffusion equation,

$$1)\quad \frac{\partial I_j}{\partial t} = \frac{1}{r}\frac{\partial}{\partial r}\left\{ r\,\frac{m_p}{m_{Al}}\,\rho_j^2\,\nu_{pj}(1+q^2)\left[A\,\frac{jI_j}{n_p}\,\frac{\partial n_p}{\partial r} - B\,\frac{\partial I_j}{\partial r}\right]\right\} + S$$

where I_j = density of the j^{th} state of ionization; e.g., j=5 for AlVI; A = inward transport factor; B = spreading transport factor. A and B are functions of the impurity content in the plasma; $\rho_j = mv_j/jeB$; $\nu_{pj}=4\sqrt{2\pi}\,(j)^2\,e^4\,n_p \ln\Lambda/3(4\pi\varepsilon)\,\sqrt{m_p}(kT_p)^{3/2}$; and S = source terms. These include radiative and dielectronic recombination and electron impact ionization.

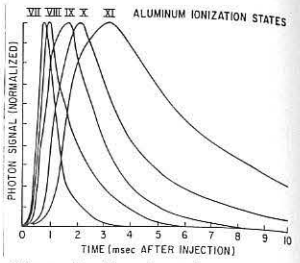

Figure 2. Experimental measurement of time evolution of line integral Al photon signals.

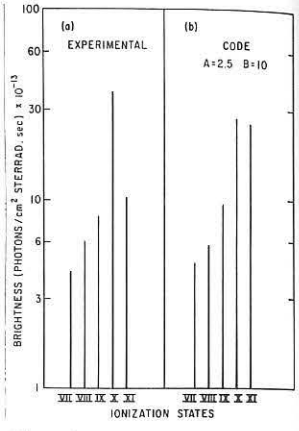

Figure 3. Absolute peak brightness of Al lines. (a) is measured, (b) is computed using 1) with A=2.5, B=10.

Diffusion caused by the temperature gradients or collisions with different Al ionization states are estimated to have a negligible effect. The electron, proton and oxygen profiles used in the code are those previously described. They are assumed to be stationary in time. The initial AlII radial distribution is calculated assuming electron impact ionization of the aluminum neutrals. There is no recycling of impurities lost at the edge.

The results of the code for Pfirsch-Schlüter Al diffusion in a background hydrogen plasma; i.e., A=B=1, do not agree with the experiment. However, a parametric study of the code, varying A and B independently from 0 to 15, did reveal an excellent fit to the data for $A=2.5^{+2}_{-1}$ and $B=10^{+1}_{-2}$. Some results are shown in Table II and Figures 3b and 4.

Table II: Radial Distribution (RL/FWHH) of Aluminum IX, X and XI(in cm.)

	Experimental		Code A=2.5,B=10	
IX	11.4	3.7	11.3	4.4
X	10.5	2.7	10.6	4.7
XI	8.4	4.6	9.2	5.2

The code does predict the "stationary shell" effect. For A=2.5, B=10, the calculated radial locations (RL) and shell widths (FWHH) for AlIX → AlXI agree with the experiment (see Table II). Also, the time evolution of the normalized brightness of each ionization state (Figure 4), and the absolute peak intensity for each line, Figure 3b, agree reasonably well.

We take the 5% oxygen concentration into account by using the scaling laws found in [1]. From these we calculate that A=3.6 and B=13.8, which are near the inferred values. We conclude that impurity transport in ATC can be explained by neoclassical theory.

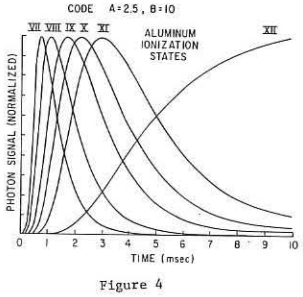

Figure 4

We thank C. Daughney for the Thomson scattering measurements. This work was partially supported by USERDA Contract E(11-1)-3073.

References

[1] J. W. Connor, Plasma Physics 15, 765 (1973)

[2] P. H. Rutherford, Phys. Fluids 17, 1782 (1974)

[3] See, for example, J. P. Girard, D. Marty and P. Moriette, 5th Int. Conf. on Plasma Physics and Controlled Nuclear Fusion Research, Tokyo, 1974, Paper A17-2.

ON THE IMPURITIES IN THE OHMICALLY HEATED PLASMA OF THE WENDELSTEIN II b STELLARATOR.

H. Hacker, E. Hinnov+, H. Renner, H. Ringler, E. Würsching
Max-Planck-Institut für Plasmaphysik, Garching, W. Germany, EURATOM-Ass.
+) Princeton Univ., USA

Abstract: The impurity content of the plasmas was measured by spectroscopic methods. The densities of the main components O, N, C are less than 10^{11} cm^{-3} compared to plasma density 10^{13} cm^{-3}. This low value does not explain the discrepancy of energy and particle confinement times.

I. Energy and particle confinement

In the Wendelstein W II b stellarator [major radius 0.5m, minor radius 0.05 m; main field Bo $\lesssim$ 1.2 T; helical windings: l = 2, m = 5] with ohmic heating in H_2 and He gas at densities $n_e = 10^{13}$ cm^{-3}, electron temperatures $kT_e \lesssim$ 300 eV and ion temperatures $kT_i \lesssim$ 100 eV have been reached.

As reported at the Tokyo conference 1974 [1] an anomalous electron energy loss for both types of discharges was observed. The energy confinement time τ_E = plasma energy / power input was in agreement with the assumption of the pseudoclassical electron heat loss, if the additional rotational transform ι_o produced by the helical current transform ι_p was considered $\tau'_E \sim (1 \pm \iota_o/\iota_p)\cdot\sigma$, with σ electrical conductivity. The behaviour of σ, deduced from total resistance and the radial temperature profiles measured by laser scattering, is observed to be classical, with an effective ion charge $Z_{eff} \approx 2$.

The particle confinement time τ_p was determined from the equation of particle balance between ionization of neutrals and particle loss rate. Using the relative rate coefficients for excitation and ionization [2] we obtain the ionization rate from measurements of the intensity of H and He lines. The resulting τ_p were by a factor 10 larger than τ'_E and show a different behaviour with respect to changing plasma temperature, kT_e.

Impurities can affect the calculated confinement times if the additional radiation loss is a significant fraction of the power input, or the additional ionization rate is non-negligible compared to the ionization rate of the working gas.

II. Impurities

1. Characteristics of the device

Because of the characteristics of the stellarator W II b [air core transformer, 8 Vp loop voltage] the following procedures are necessary for running a discharge:

a) Preceeding cleaning discharge: Ne at 50 Hz, 2 - 4 hours.
b) Additional neutral flux by a fast acting valve during the discharge in H_2, to compensate for the gas loss. (Not necessary for He)
c) Starting the discharge with $\iota_o > 0$ and sufficient far from rational values, to provide the confinement and the cleanliness.

The discharge reacts very sensitivly to impurities. A small amount of neon - e.g. 0.5 % added - reduces severely the achievable plasma current.

2. Diagnostics

The normal incidence and grazing incidence monochromators are calibrated for the measurements of the absolute intensity in the vacuum ultraviolett range by the branching ratio method to visible lines [3]. The visible line intensity is deduced from a tungsten standard lamp. The observed resonance line intensity of the impurities is averaged along a diameter in the horizontal plane. Recently we have improved the scanning system by mirrors. This system allows now after an Abel inversion the description of the radial distribution.

Results

For proper discharges in H_2 and He the measured impurity concentration (error about 50%) as deduced from the individual line intensities (ni indicates by normal incidence spectrometer and gi by grazing incidence spectrometer) is given in Fig.1 and Fig.2. In both cases the electron temperature varies from 100 - 250 eV in time. The H_2 discharge is fed by an additional gas flux, which starts a few ms after the current.

The line-averaged density is determined by µ-wave interferometry. O, C and N have been observed as the main impurities. Their densities remain to below 10^{11} cm^{-3}. This low level is consistent with the measured $Z_{eff} = 2$ from resistivity. The power by radiation can be estimated to a few kW and is small compared to the 25 kW input power. The effect of the ionization rate of impurities on the particle confinement time is negligible.

References

[1] H. Hacker et al. IAEA-CN33-B1, Tokyo 1974.
[2] L.C. Johnson, E. Hinnov, J.Quant.Spectr.Rad.Trans. 13 (1973), p.333
[3] E. Hinnov, F.W. Hofmann, J.Opt.Soc.Am. 53, 1259 (1963)

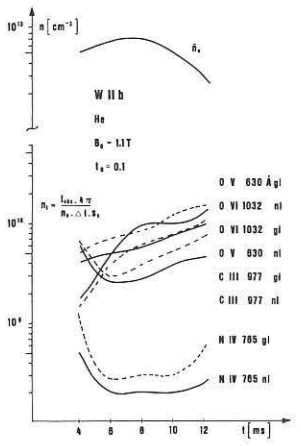

Fig.1

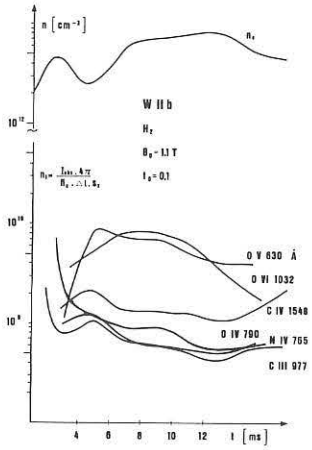

Fig.2

EXTRACTION OF IMPURITIES FROM A TOKAMAK

T. CONSOLI - R. LEGARDEUR - G.F. TONON

ASSOCIATION EURATOM-CEA
Département de Physique du Plasma et de la Fusion Contrôlée
Service IGn - Centre d'Etudes Nucléaires
B.P.85 - Centre de Tri - 38041
GRENOBLE CEDEX (France)

ABSTRACT : In the electrodynamical divertor here described, the neutral atoms emitted by the wall after being ionized in the low density plasma corona surrounding the dense and hot plasma core, are expelled by an $\vec{E} \times \vec{B}$ force. This divertor may be made more efficient if a low density plasma flow is maintained and controlled between the liner and the limiter by means of external plasma injectors.

It has been proposed in a previous publication /1/ to expel the neutral atoms (light and heavy) emitted by the wall of the liner of a TOKAMAK by means of an electrodynamical divertor based on the $\vec{E}_r \times \vec{B}_\phi$ force. This force acts upon the low density plasma corona which is located between the liner and the limiter. This force permits the elimination of impurities and more generally of any atoms ionized in the low density plasma corona.
Ionization would take place it the mean free path of ionization λ_i is less than the thickness of the corona.
This mean free path $\lambda_i = \frac{1}{n_{pe} < \sigma_i v_{pe}}$ is a function of the density n_{pe} and of the electron thermal velocity v_{pe} of the low density plasma which is submitted itself to the same force and tends to depopulate. The elimination process under these conditions would stop of itself and neutrals would penetrate freely into the dense plasma core.

In this paper the improvements brought to the divertor (cf. Réf./1/) are described, and in particular those concerning the maintenance and control of the corona parameters.

DESCRIPTION AND PRINCIPLE. A radial $\vec{E}_r$ steady state electric field is applied between the liner (ground potential) Fig.1.1 and a second stainless steel grid Fig. 1.3 , coaxial to the first and located just inside in the limiter shadow. This grid can be either a complete torus or be limited to a certain number of p sectors (p < number of toroidal coils) each sector forming an electro dynamical divector. Even when the grid is a complete torus, its surface could be only 5% of the total liner surface. In each sector the coaxial structure is continued towards the outside in a vertical direction between two successive B_ϕ coils (injection and extraction regions Fig.1.5 and 1.6 of the divector). In these regions the electric and magnetic fields are in an horizontal plane. They are linked to the $\vec{E}_r$ and $\vec{B}_\phi$fields in the torus.
The Hall injector Fig. 2 differs from the previously known /2/ and /3/ and works under the following conditions : the magnetic field $\vec{B}_H$ which continues B_ϕ is constant and weaker, for example, $\vec{B}_H$ = 3000 Gauss. A neutral gas (pure Deuterium) is injected from the outside Fig.1.5, becomes ionized (region I in Fig. 2) and heated by the $\omega_{ce} = \omega_{HF}$ resonance (10 GHz in this case). Densities of $10^{12} cm^{-3}$ with $10 < T_e < 10^3$ eV can be obtained /4/. The $\vec{E}_H \times \vec{B}_H$ force acts on this ionized medium, which is propulsed toward the plasme torus. With intense pumping (Fig. 2 region II) one can obtain /2/ a ratio $\frac{ne\ (plasma)}{na\ (neutral\ atoms)}$ of the order of 3×10^2, that is 3.10^9 neutrals by cm^{-3}.
The plasma jet sweeps out the two halfs of the torus with the drift v_d speed greater than the thermal speed. A plasma corona density of 10^{11} to $10^{12} cm^{-3}$ can be achieved.
On the other hand in the divertor ejection regions Fig. 1.6 where B_H approaches zero, a charge separation permits recovery of the electrons and ions, like in energy conversion systems /5/.

EVALUATION OF THE NECESSARY PARAMETERS. The fluid mouvement considering the low densities, is similar to that of individual particles (cf. Ref. 1). The total number N of particles which could be extracted is :

$$N_{min} = n_{pe} \cdot \frac{\pi^2 (r_1^2 - r_2^2) R t}{\tau},$$

t being the duration of one shot, τ the energy life time, n_{pe} the corona density. N_{min} is the minimum number of particles to be injected in order to maintain constant the density n_{pe}. If $N > N_{min}$, a larger density n_{pe} could be obtained.
Presuming that the injection time is equal to τ, the injected density is :

$$n'_{inj} = \frac{\pi^2 n_{pe} (r_1^2 - r_2^2) R t\ p}{v_d\ S\ \tau^2},$$

v_d being the directed beam velocity, S the beam cross section and p the total number of divertors. The necessary powers for ionization and maintenance of this flux are :

$$P_{HF} = \frac{V_i N \times 1{,}6 \times 10^{-19}}{\eta \tau p} \text{ in watts,}$$

V_i being the first ionization potential in electron wolts, η = the H.F. overall efficiency

$$P_{DC} = \frac{N(V_f - V_i)}{p \tau \eta}$$

is the power required to raise the ion directed energy from V_i (eV) to V_f(eV)
In a typical TOKAMAK having the following characteristics :
r_1 = 1,5 m, r_2 = 1,3 m, R = 3 m, $n_{ep} = 10^{11} cm^{-3}$, $S = 10^3 cm^2$, p = 10, V_i = 20 eV, $V_f = 10^2$eV, τ = 0,1 s, t = 1 s, $T_e = 10^2$eV, η = 0,5, gas = deuterium, gives N equal to 3×10^{20} p/cm^3, $n_{inj} = 10^{10} cm^{-3}$ and requires less than 50 kW for both ionization and acceleration.

CRITICAL PARAMETERS FOR THE IONIZATION CORONA. The divertor cannot eliminate those neutrals coming out of the liner wall unless they can be ionized in the shell of thickness $(r_1 - r_2)$, of density n_{pe} and of temperature T_e.
Considering three typical elements : a light one, (D) two impurities (one light (O) and one heavy (W) the necessary shell thickness is given in Fig.3, under the condition that neutrals are emitted from the liner wall with an energy of 0,1 eV. One can see that the corona plasma density and thickness are such that all neutrals coming from the wall are ionized in typical TOKAMAKS.

IN CONCLUSION. The application of a steady state electric field of the order of few kilovolts /1/, being localized in the low density plasma regions, does not disturb the confined plasma.
It has been proved experimentally /6/ that the main contribution to the pollution of TOKAMAK'S plasma comes from the liner (more than 90% of the plasma energy is deposed on the wall).
The grid electrode surface being very transparent, lower than (5% of the liner surface), the pollution due to its presence is small.
With the electron dynamical divertor the heavy mass impurities having been expelled, their replacement by ions of low mass, reduces the radiation loss in the plasma core.

REFERENCES. /1/ - T. CONSOLI, R. LEGARDEUR, G.F. TONON, Vth Conf., TOKYO, 11-15 Novembre 1975, IAEA A/N2.
/2/ - H.C. COLE, III^{d} European Conf. on Controlled Fusion and Plasma Physics, UTRECHT, June 1969.
/3/ - A.I. MOROZOV and al., J.E.T.P. Letters 7, 199, (1968).
/4/ - R. BARDET, P. BRIAND, G. GORMEZANO, G. MELIN, F. WERKOFF, Vth Conf., TOKYO, 11-15 Novembre 1975, IAEA D/5-1.
/5/ - R.N. MOIR, W.L. BARR, G.A. CARLSON, Vth Conf., TOKYO, 11-15 Novembre 1975, IAEA G/3-1.
/6/ - T.F.R. Group. Energy Confin. in T.F.R. Analysis of Losses sources internal note, N.T. 111.

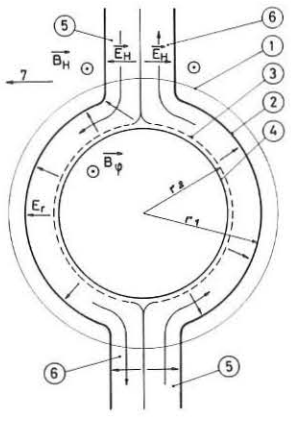

Fig. 1 The electrodynamical divertor.
1.1 Boundary of the toroidal B_ϕ field, 1.2 The liner, 1.3 The internal grid, 1.4 The plasma section, 1.5 The plasma injecting channel, 1.6 the plasma ejecting channel, 1.7 Toward the vertical axis of the torus.

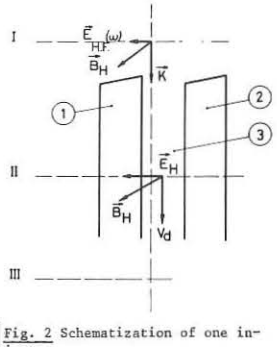

Fig. 2 Schematization of one injector.
1 and 2 parallele plates at the ground and at high voltage
3 region of plasma flow
I - Ionization region, II - pumping region, III - connection of the injector to the toroidal plasma chamber.

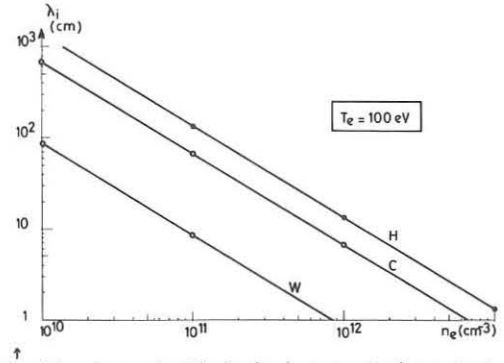

Fig. 3 Mean free path of ionization λ_i versus density n_e for H, C and W.

NUMERICAL CALCULATIONS OF IMPURITY TRANSPORT IN TOKAMAK PLASMAS

M H Hughes

Culham Laboratory, Abingdon, Oxfordshire, England
(Euratom/UKAEA Fusion Association)

Abstract: The effect of plasma contamination by high-Z materials released from the walls and limiter by escaping ions and neutrals is considered. Ionization parameters and impurity radiation losses are determined from the steady-state corona model while neoclassical transport theory is used to describe the impurity transport within the plasma.

Introduction. In the next generation of Tokamak experiments, with their large energy fluxes and long pulse lengths, it is anticipated that contamination of the plasma by high-Z materials arising from bombardment of the walls and limiter will play a significant role in the plasma energy balance. Transport theory indicates that impurities which enter the plasma at the edge can diffuse to the centre of the discharge where they accumulate. Estimates of the effects of impurities suggest that the subsequent power loss through line radiation and bremsstrahlung can prevent ignition unless the impurity content can be kept sufficiently small. To investigate the distribution of impurities and their effect on a Tokamak plasma we have devised a simple numerical model for impurity diffusion and plasma-wall interactions. This paper outlines the model and illustrates results obtained using a modified version of Düchs' 1-D radial transport code [1].

Physical Model: The essential features of the model can be summarised as follows. If the spatial distribution of the plasma temperature is known we can find from the corona model the average ionization state of the impurity atom at any point and correct those diffusion coefficients dependent on Z. Subsequently, if we also know the electron and impurity concentrations we can calculate the total impurity radiation losses at each point. We then have sufficient information to follow the evolution of the plasma parameters and the impurity concentration.

The coronal equilibrium model is based on a code written by Mosher [2]. We suppose that the plasma is everywhere in a state of ionization equilibrium; this assumption is valid if the time τ over which the macroscopic plasma parameters change satisfies the condition

$$\tau \geq \frac{10^{12}}{n_e(\mathrm{cm}^{-3})} \quad \text{sec} \quad .$$

Thus, for the simulation of large future machines where diffusion timescales $\sim$1 sec are expected the steady-state model is appropriate.

For the plasma transport we use Düchs' 1-D radial transport code in which the ion thermal conduction is neoclassical while the particle diffusion and electron thermal conduction is pseudo-classical, i.e.

$$D = \kappa_e = \gamma(Z_{eff})\, Z_{eff}\, \nu_{ei}\, \rho_{e\theta}^2$$

where $\gamma = \dfrac{0.457}{1.07 + Z_{eff}} + 0.29$.

Alternatively we can use the empirical law suggested by Soubbarameyer and Mercier [3] which is

$$D = \kappa_e = 400\, Z_{eff}\, (1 + 1.6q^2)\, \nu_{ei}\, \rho_{eZ}^2 \quad .$$

This law seems to predict quite accurately the behaviour of existing Tokamaks.

For the impurity transport we solve a single diffusion equation for the sum $n_I = \sum_Z n_Z$ over all charge species. The impurity diffusion flux is that given by neoclassical theory [4] with the coefficients smoothed into the plateau regime.

Boundary conditions. The Düchs code includes an influx of cold neutral gas at the boundary together with some number of generations of hot neutrals produced by successive charge exchange collisions; the version of the code used here can follow up to 20 generations of hot neutrals. From the hot neutral calculation we can distinguish the escaping flux Γ_j^o of each generation. Moreover, the temperature T_j^o of a particular generation is calculated by averaging over the temperatures at the points of creation. We can then define a sputtering coefficient $\alpha(T_j^o)$ for each generation to determine the influx of heavy atoms released from the walls by neutral bombardment. Similarly, escaping ions can release impurities to give a net influx

$$\Gamma_Z = \alpha(T^+)\Gamma^+ + \sum_j \alpha(T_j^o)\Gamma_j^o$$

of impurities.

The sputtering coefficient for protons incident on niobium, measured experimentally by Berrisch, can be fitted quite accurately by the formula [5]

$$\alpha = \frac{9 \times 10^{-3}}{[E/2 + 2/E^2]^{\frac{1}{2}}} \exp(-0.017\,E)$$

where E(keV) is the energy of the incident particle. We have used this formula multiplied by a factor 3 for stainless steel. The threshold energy for sputtering is calculated from

$$E_{thr} = \frac{(m_1 + m_2)^2}{4 m_1 m_2}\, Q$$

where m_1 and m_2 are the atomic weights of the incident particle and target material and Q is the sublimation energy (e.g. 4.3 eV for iron).

The model described above has been used in a study of the proposed JET machine. The main parameters for these calculations are as follows: major radius 2.93 m; minor radius 1.28 m; toroidal field 30 kG; Tokamak current 3 MA. The rapid penetration of the skin current during the current rise phase in a Tokamak is not described by 1-D codes without making some ad hoc assumption about the diffusion in this regime. To circumvent this difficulty we assume that the full current is initially distributed throughout the plasma volume and maintained constant in time. The electron and ion temperature profiles are initially parabolic with peak values of 100 eV; the electron density profile is also parabolic giving a mean density of 5×10^{13} cm^{-3}.

Results: Using the pseudo-classical scaling law, the temperatures of the escaping protons and hot neutrals rapidly become large enough to initiate sputtering of material (assumed to be iron) from the walls. Impurity atoms entering the plasma diffuse to the centre where they accumulate, forming a peaked distribution as shown in Fig.1. After 3 sec the accumulation of impurities in the central core begins to modify the plasma profiles by excluding current from this region. At later times the build-up of the impurity concentration results in cooling of the core. For example, Fig.2 shows the temperature profile after 6 sec. Impurity radiation cooling has by this time caused a significant depression of the central temperature resulting in an unstable configuration.

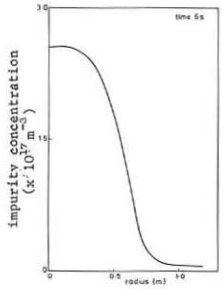

Fig.1 Radial distribution of impurity concentration.

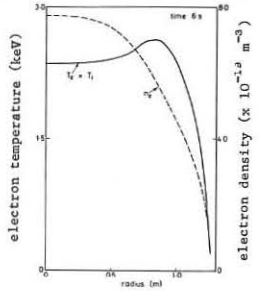

Fig.2 Radial distributions of electron temperature and density (pseudo-classical scaling).

When the particle diffusion and electron thermal conduction coefficients are replaced by the Mercier-Soubbaramayer form the most important difference is a large increase in the outflux of escaping particles and a corresponding increase in the influx of cold neutrals required to maintain the total number of particles. The incoming neutrals are ionized in a narrow region near the edge ($\sim$ 10% of the plasma radius) which is consequently maintained at a relatively low temperature (Fig.3). Thus, the only escaping particles with sufficient energy to release material from the wall are the higher generations of neutrals emanating from the hot central region. The net result is a much smaller influx of impurities compared with the previous case (by a factor $\sim$ 10). The build-up of impurities in this case was therefore negligible. It appears therefore that it may be possible to shield a Tokamak plasma from impurities by a thin shell of cold plasma.

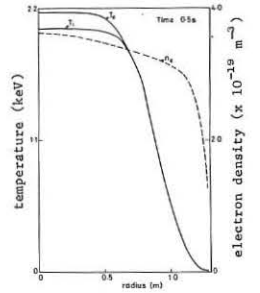

Fig.3 Radial distributions of temperature and density (Mercier-Soubbaramayer scaling).

References

1. Düchs, D F, Furth, H P and Rutherford, P H. Proc.4th Int.Conf. on Plasma Physics and Controlled Nuclear Fusion Research, Madison, 1, 369, 1971.
2. Mosher, D. NRL Memorandum Report 2563, March 1973.
3. Soubbaramayer and Mercier, C. Proc.4th European Conf. on Controlled Fusion and Plasma Physics, Rome, 1, 16, 1970.
4. Connor, J W. Plasma Physics 15, 765, 1973.
5. McCracken, G M. Private communication.

NUMERICAL SIMULATION OF THE ENERGY BALANCE AND IMPURITY DIFFUSION IN TOKAMAKS

Y.N.Dnestrovskii, S.E.Lysenko
I.V.Kurchatov Institute of Atomic Energy, Moscow, USSR
I.N.Inovenkov, D.P.Kostomarov
Moscow State Iniversity, Moscow, USSR

1. Influence of magnetic field ripples on the energy balance.

At low collision frequencies, the ripples of the magnetic field are the main factors responsible for the transport processes in plasmas.

In this case [1]

$$\chi_i = \frac{40.6}{\nu_i}\Delta^{3/2}\left(\frac{T_i}{eHR}\right)^2 n \qquad (1)$$

Here χ_i is the ion heat conductivity, 2Δ is the depth of a ripple along the line of force. In the paper [1] it was assumed that Δ is constant on the magnetic surfaces $\Delta = \Delta(r)$. We have used a more exact formula for χ_i, by replacing $\Delta^{3/2}$ in (1) with the value $\langle \Delta^{3/2} \rangle$ averaged over θ, where θ is the angular coordinate in the small cross-section of a torus.

The magnetic field ripples can be described by the formula

$$H \approx H_\varphi = H_0\left\{1 - \frac{r}{R}\cos\theta - \hat{\delta}(r,\theta)\cos N\varphi\right\} \qquad (2)$$

where φ is the angular coordinate along the magnetic axis, N is the number of magnetic coils. The numerical calculations of the magnetic field have shown that the function $\hat{\delta}(r,\theta)$ is well approximated by the expression

$$\hat{\delta}(r,\theta) = \delta_{max} I_0\left(\frac{\beta N J(r,\theta)}{R}\right) \Big/ I_0\left(\frac{\beta N J(a,\theta)}{R}\right) \qquad (3)$$

Here I_0 is the modified Bessel function, $\beta \approx 0.6 \div 0.7$ is the parameter depending on the coil configuration

$$J(r,\theta) = \left[r^2 + 2r\Delta r\cos\theta + (\Delta r)^2\right]^{1/2},$$

Δr is the departure of the $\hat{\delta}$ minimum from the magnetic axis. In the region of maximum corrugation ($\theta \approx 0$, $r \approx a$, $\Delta r \ll r$), one can use an asymptotic formula for the Bessel functions, expand J into power series of Δr and expand $\cos\theta$ into power series of θ. As a result, we obtain $\langle \Delta^{3/2} \rangle = \delta^{3/2} J(\alpha,\mu)$

$$J(\alpha,\mu) = \frac{1}{\pi}\int_{-\pi}^{\pi} \exp\left(-\frac{3}{2}\mu\theta^2\right) f^{3/2}\sin^2\theta\, d\theta, \qquad (4)$$

$$\delta = \delta(r) = \delta_{max}\exp\left[\frac{\beta N(r-a)}{R}\right], \quad \mu = \frac{\beta N \Delta r}{R}, \quad \alpha = \frac{r}{RN\delta},$$

$$\hat{\alpha} = \alpha\exp(\mu\theta^2), \quad f = (1 - \hat{\alpha}^2\sin^2\theta)^{1/2} - \hat{\alpha}|\sin\theta|\arccos(\hat{\alpha}\sin\theta).$$

When $\mu = 0$ Eq.(4) exactly matches the results obtained by Stringer [2], where the dependence of $\hat{\delta}$ on θ was neglected. Fig.1 presents $J(\alpha,\mu)$ as a function of α for $\mu = 0,\ 0.5,\ 0.7,\ 1$. Near the plasma boundary, $\alpha \sim 0.05 \div 0.4$. It is seen that $J(\alpha,\mu) \sim 0.05 \div 0.1$ if $\mu \sim 1$ in this region. The present model has been used for calculating the energy balance in the tokamak T-11 installation ($R = 70$ cm, $a = 20$ cm, $N = 24$, $n = 10^{13}(1.2 - r^2/a^2)$ cm^{-3}) with the injection of hot neutrals of the energy $E_0 = 20$ keV and current $i \sim 10$ A. Fig.2 shows the dependence of the ion temperature $T_{i\,max}$ on the current i for three different positions of the plasma column inside the chamber:
(I) the plasma column is displaced 5 cm inside the chamber, $\mu = 0.3$, $\delta_{max} = 0.066$, (II) the plasma column is in the centre of the chamber $\mu = 0.4$, $\delta_{max} = 0.02$, (III) the plasma column is displaced outside the chamber $\mu = 0.7$, $\delta_{max} = 0.05$. For comparison, we have drawn a dotted line for $\delta_{max} = 0.06$ which matches that obtained by Stringer model [2].

2. Diffusion of the impurities.

It is well known that the impurities play the essential role in the tokamak plasma dynamics. We have described the results obtained from the calculations of the density profiles for light impurity ions (carbon and oxygen). We have taken into account the diffusion of particles and such atomic processes as ionization by electron impact and radiative recombination. The initial system of the equations is of the form

$$\begin{aligned}
\frac{\partial n_e}{\partial t} &= -\frac{1}{r}\frac{\partial}{\partial r} r\,\Gamma_e + n_e\sum_{j=0}^{z-1}\left(I_j n_j - R_{j+1} n_{j+1}\right)\\
\frac{\partial n_p}{\partial t} &= -\frac{1}{r}\frac{\partial}{\partial r} r\,\Gamma_p \qquad (5)\\
\frac{\partial n_j}{\partial t} &= -\frac{1}{r}\frac{\partial}{\partial r} r\,\Gamma_j + n_e\left\{I_{j-1} n_{j-1} - n_j(I_j + R_j) + R_{j+1} n_{j+1}\right\},\ j = 1,2\ldots z
\end{aligned}$$

where n_e, T_e, n_p, T_p, n_0, T_0, n_j, T_j are the densities and temperatures of the electrons, protons, impurity atoms and ions, Γ_e, Γ_p, Γ_j are the neoclassical diffusion fluxes [3], Γ_0 is the flux of the impurity atoms, I_j and R_j are the ionization and recombination rates [4,5]. The radial profile of the impurity atoms n_0 was determined from the stationary kinetic equation. It is assumed that $T_j = T_p$. We have used the following initial and boundary conditions :

$$\left.\begin{aligned}
&\Gamma_{jp}\big|_{r=a} = 0,\\
&n_e\big|_{r=a} = n_{e0},\ \left(n_p + \textstyle\sum n_j z_j - n_e\right)\big|_{r=a} = 0,\\
&n_e(r,0) = n_p(r,0) = \left[n_{e0} + n_{e1}\left(1 - r^2/a^2\right)\right], 10^{13}\,\mathrm{cm}^{-3},\\
&n_j(r,0) = 0,\ (j = 1,2,\ldots,z)
\end{aligned}\right\} \qquad (6)$$

Here Γ_{jp} is the partial proton-impurity flux. Conditions (6) assume that the particle losses from the plasma are determined solely by collisions with the electrons. We have assumed in the above calculations that $T_p(r) = \mathrm{const}\,t$, thus neglecting the thermal diffusion.

Fig.3 presents the results of the calculations for tokamak TM-3 ($R = 40$cm, $a = 8$cm). The radial profiles of C^{5+}, C^{6+}, Z_{eff} are shown for $t = 10, 20, 30$ msec. The dotted lines correspond to the electron and proton profiles. Fig.4 presents the similar curves for oxygen in tokamak ST ($R = 109$cm, $a = 12$cm).

Certain features characteristic of these processes should be pointed out.

1) In a time $t \sim 5$ msec the density profiles of the C^{6+} and O^{8+} nuclei arrange themselves to the density profile of the protons with an accuracy of 2÷3 per cent according to the Braginsky condition ($\partial/\partial r(\ln n_p z) = \partial/\partial r \ln n_z$). At this stage, the impurities should move towards the plasma column centre, the diffusion rate of the protons being sufficiently low.

2) When the impurity concentration reaches $n_z > 0.03\, n_p$ the proton density profiles rapidly flatten, causing the flattening of the impurity profiles.

3) With the concentrations up to $n_z \sim 0.1\, n_p$ the amount of impurities lost from the plasma column is appreciably less than that of the protons.

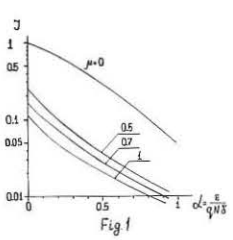

Fig 1

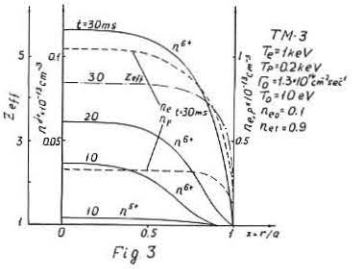

Fig 3

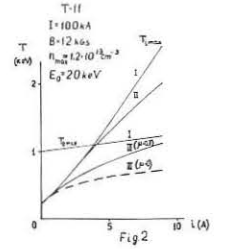

Fig 2

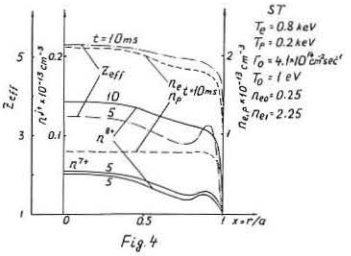

Fig 4

REFERENCES

1. J.W.Connor, R.J.Hastie, J.B.Taylor. V European Conf. Contr. Fusion and Plasma Phys., Grenoble, 1 (1972) 15.
2. T.E.Stringer. Nucl.Fusion, 12 (1972) 689.
3. J.W.Connor. Plasma Phys., 15 (1973) 765.
4. E.Hinnov. MATT-777, Princeton University (1970).

PLASMA-WALL INTERACTION THROUGH RIPPLE CONVECTION IN TOROIDAL DEVICES

F. Engelmann*) and A. Sestero

Centro Gas Ionizzati, Associazione
EURATOM-CNEN, Frascati, Italy

*) Also at the FOM-Instituut voor Plasmafysica, Rijnhuizen, Associatie EURATOM-FOM, Jutphaas, The Netherlands.

Abstract: It is shown that under certain circumstances ripple convection may lead to a strong localized plasma-wall interaction in Tokamaks. The relevance of the result to recent findings on TFR is discussed.

As any deviation from axisymmetry in toroidal devices leads to the formation of loss-cones, in such a case a certain number of charged particles can reach the chamber wall in spite of the presence of a limiter. In particular, if a sufficient number of highly energetic particles (e.g. electrons) can enter these loss-cones, a strong plasma-wall interaction, usually localized in certain areas, is to be expected. We specifically consider here the effect of the presence of a toroidal field ripple in Tokamaks, but the situation is quite analogous in Stellarator geometry.

The loss-cones created by the ripple are related to the free ∇B-drifting of the particles trapped in the ripple mirrors, occurring at a velocity

$$v_D = \frac{\varepsilon_\perp}{eBR} \quad , \tag{1}$$

where $\varepsilon_\perp$ is the kinetic particle energy perpendicular to the magnetic field B, R the torus' major radius, and e the elementary charge. For a group of particles of density n this implies a vertical energy flux

$$F = \frac{n\,\varepsilon_\perp^2}{eBR} \quad , \tag{2}$$

which may be considerable for large $\varepsilon_\perp$.

Through this mechanism electrons may convect to the wall from the plasma edge or even from its interior. In the first case, this happens if the effective mean free path λ for scattering the electrons out of the loss-cone is larger than the extension of the limiter shadow h, i.e.,

$$\lambda \equiv \frac{v_D}{\nu_{eff}} > h \quad , \tag{3}$$

where, for $\varepsilon_\perp$ more than three times larger than the bulk plasma temperature[1].

$$\nu_{eff} = 2\sqrt{2}\,\pi\,\frac{e^4 \ln\Lambda}{m\,\varepsilon_\perp^{3/2}}\,\frac{(1+Z_{eff})\,n}{\delta B_e/B} \quad , \tag{4}$$

with Z_{eff} the effective ion charge, δB_e the amplitude of the field ripple, m the electron mass, and $\ln\Lambda$ the Coulomb logarithm. Combining Eqs. (1) and (3) yields for R = 100 cm, h = 3 cm, B = 40 kG, $\delta B_e/B$ = 5%, and Z_{eff} = 3

$$\frac{\varepsilon_\perp^{5/2}}{n} > 4\cdot 10^{-11} \tag{5}$$

when $\varepsilon_\perp$ is in keV and n in cm^{-3}.

On the other hand, for a system of N = 24 coils and a strongly corrugated liner (radius of curvature of about 2 cm), the area hit by the convecting electrons extends less than 1 mm in toroidal direction, corresponding to an effective concentration of the energy flux by more than 2 orders of magnitude[1]. Melting of the surface material after 0.4 s is then possible if $F \gtrsim 8$ Watt/cm^2, equivalent to a loss of 200 Watt per ripple over 1 cm in the direction of the torus' major radius. Condition (5) then requires the presence of electrons with at least $\varepsilon_\perp$ = 2.5 keV, having a density $n = 3\cdot 10^{11}$ cm^{-3}. It may be noted that charge neutrality in the shadow of the limiter can presumably be ensured through ionization of cold neutrals by the convecting electrons[1].

In the second case, the effective mean free path λ must be larger than the distance from the wall to the hot inner plasma, that is condition (3) must be satisfied with h being now this latter distance, and in Eq. (4) n being replaced by the plasma density n_p, as well as δB_e by the ripple amplitude δB_i in the plasma interior. Taking $n_p h = 5\cdot 10^{13}$ cm and $\delta B_i/B$ about 1 to 2 $^{o}/_{oo}$ (R, B and Z_{eff} being as above) yields $\varepsilon_\perp \gtrsim 50$ keV. As at the lower limit of this energy range only deeply trapped electrons (typically those whose oscillation amplitude is less than half the maximum amplitude possible) have a high probability of reaching the wall, surface damage is to be expected if there are electrons of this kind with a density of about $n = 1.6\cdot 10^9$ cm^{-3} or larger. For isotropic distributions, such a density corresponds to somewhat less than 1% of the plasma electrons trapped in the relevant part of the ripple mirror. An important property of ripple convection from the plasma interior is also that the extension of the convecting beam in toroidal direction decreases considerably from inside to outside, due to the increase of the field ripple. Using the constancy of the longitudinal adiabatic invariant and taking $\delta B_i/\delta B_e$ about 0.02 to 0.04 yields, for the example considered, a decrease of the beam extension L by about a factor of 3 to $L_e \approx 4$ cm at the wall.

In conclusion, the conditions to be satisfied for ripple convection to create dangerous plasma-wall interactions are stringent, but by no means forbidding. In particular, the effects observed on TFR[2] seem to be marginally consistent with the properties of ripple convection of a group of highly energetic electrons originating from the plasma interior.

Acknowledgements: The authors gratefully acknowledge the fruitful interaction with the TFR group, and in particular with Drs. P. Ginot and J. Tachon. Thanks are also due to Drs. L. Enriques and F. Santini for suggestions and criticism.

References:

1) F. Engelmann and A. Sestero: Report C.G.I.-R-TEO-75.5-E Centro Gas Ionizzati (Associazione EURATOM-CNEN sulla Fusione) Frascati, Italy.

2) Equipe TFR: Proc. 5th Int. Conf. on Plasma Phys. and Contr. Nuclear Fusion Res., Tokyo, November 11-15 (1974), Paper IAEA-CN-33/A6-2.

THE EFFECT OF HEAVY IMPURITIES ON PLASMA MOTION IN A MULTIPLE MIRROR MAGNETIC FIELD

V.V.Mirnov, D.D.Ryutov
Institute of Nuclear Physics, Siberian Division
of the USSR Academy of Sciences, Novosibirsk, USSR

Abstract: It is shown that by inserting a certain amount of heavy impurities into a DT-plasma one can considerably decrease a longitudinal plasma expansion velocity.

At a temperature T = 10 KeV the fusion power output in a pure DT-plasma is known to be aproximately 30 times greater than the bremsstrahlung losses. By inserting the impurities with a charge $Z \gg 1$, the bremsstrahlung losses rise by a factor of $n_z Z^2/n_H$, where n_z and n_H are, respectively, the densities of impurities and of hydrogen isotopes (the density of impurities is assumed to satisfy the condition $n_z Z \lesssim n_H$, under which the electrons have mainly a "hydrogen" origin). Therefore an ultimate permissible density of impurities is determined by the condition:

$$n_z Z^2/n_H \lesssim 30 \qquad (1)$$

On the other hand, at the densities $n_z Z^2/n_H \gtrsim 1$ the impurities can considerably affect the scattering frequency of electrons and hydrogen ions. Dawson et al.[1] have suggested to use this circumstance to decrease absorbtion length of a CO_2-laser radiation in a plasma (the absorbtion length is inversely proportional to the scattering frequency of electrons on ions). It is evident that by inserting impurities one can reduce an absorbtion length by the order of magnitude without violation of the condition (1).

In the present paper, it is noticed that in the same way one can apreciably reduce the length of a multiple mirror trap [2,3]. Indeed, if $n_z Z^2/n_H \gtrsim 1$, the hydrogen ions scattering path decreases by a factor of $n_z Z^2/n_H$ in comparison to the case of a pure plasma. The scattering path reduction results in slowing down of a plasma diffusion along the multiple mirror magnetic field. This allows to reduce installation length needed to provide the chosen confinement time.

In the case of $n_z Z^2/n_H \gtrsim 1$ the hydrogen ions mean-free path λ_{HH} with respect to the collisions between them themselves is connected with their mean-free path λ_{Hz} with respect to the collisions with impurities and with impurity mean-free path λ_{zz} by the relationships: $\lambda_{zz} \sim \lambda_{Hz}/Z^2 \sim \lambda_{HH}\, n_H/n_z Z^4$

For the quantitative illustration of the impurity effect on the expansion velocity, the case will be examined when the spacing l between two mirrors is smaller than the minimum scattering path, namely, λ_{zz}. Thereby, either among electrons and light ions, or among heavy ions there are groups of trapped and untrapped particles. Respectively, for the longitudinal diffusion coefficients of the various components according to [2] one can write down the following estimates:

$$\mathcal{D}_e \sim v_{Te}\lambda_{Hz}/K^2,\quad \mathcal{D}_H \sim v_{TH}\lambda_{Hz}/K^2,\quad \mathcal{D}_z \sim v_{Tz}\lambda_{zz}/K^2 \qquad (2)$$

(the mirror ratio K is supposed to be large, $K \gg 1$, and the width of the mirrors is assumed to be smaller than the distance l between them). Here, in the order of magnitude estimates, we neglect the difference between deuterium and tritium masses.

The estimate (2) shows, that the electron diffusion is faster then that of the other species. However, in the case when plasma expands to vacuum the electrons move together with light ions due to the effect of a polarization electric field. As to the heavy ions, they can be regarded as immovable (due to their very small diffusion coefficient) within the scale of a light component expansion time.

Basing on estimates (2), let us compare numerically the cases of confinement of a pure DT-plasma and of a plasma with a small heavy ions admixture. For the parameters $T \sim 10$ KeV, $n \sim 3\cdot 10^{17}$ cm^{-3}, the length L of the multiple mirror machine providing a pure plasma confinement for the Lawson time, $t_L \sim 3\cdot 10^{-4}$ sec, under the mirror ratio K = 3, must be of the order of 30 m. If 10% of impurities with Z = 10 are inserted, the length of the machine can be reduced to 10 m (to obtain this, one should note that for a given confinement time, the installation length is proportional to the square root of a diffusion coefficient). However, in this case the mean-free path λ_{zz} equals to 0.6 cm, so it is rather hard to satisfy the condition $l < \lambda_{zz}$ with a reasonable installation diameter. Therefore we shall analyse the case of $\lambda_{zz} \ll l \ll \lambda_{Hz}$.

Over this range of parameters the impurity flow is purely hydrodynamic ($\lambda_{zz} \ll l$!), whereas the light ions motion is diffusive as before. The expansion velocity of a heavy component is defined by the balance of two forces: the accelerating force, which is due to the polarization electric field, and the friction force against the magnetic field, which is connected with a longitudinal ion viscosity: $\eta_{\parallel z} u_z/l^2 \sim e Z n_z E$ (this estimate holds for not too large mirror ratios, K-1~K). Hence, taking into account that $\eta_{\parallel z} \sim \lambda_{zz} v_{Tz} Z M_z n_z$ and $E \sim T/eL$, one gets $u_z \sim v_{TH}\sqrt{Z}\, l^2/\lambda_{zz} L$. Comparing it with (2), we find the condition $l < Z^{3/4}\lambda_{zz}$ for the heavy component expansion to be slower than the light one. For the numerical example considered above this inequality gives $l \lesssim 5$ cm, this estimate being quite acceptable if an installation radius is smaller than $2 \div 3$ cm.

Since in the case of $l < Z^{3/4}\lambda_{zz}$, the heavy ions can be considered as immovable within the scale of a light component expansion time, the exact equations describing a light component flow can be obtained in the way analogous to that used in [3]. Thereby it is quite sufficient to take into account only the collisions of electrons and light ions with heavy ions (Lorentz plasma model). As it was shown in [3], the temperatures of all species can be considered to be equal ($T_e = T_H = T_z = T$) and constant ($\partial T/\partial x = 0$) along the plasma column in many cases of practical interest. Under these assumptions the equations for deuterium and tritium densities have a form:

$$\frac{\partial n_{D,T}}{\partial t} = \frac{3T^{5/2}}{\sqrt{2\pi^3}\, m_{D,T}^{1/2}\Lambda e^4 Z^2 K^2}\,\frac{\partial}{\partial x}\left\{\frac{1}{n_z(n_D+n_T)}\left[\left(2n_{D,T}+n_{T,D}\right)\frac{\partial n_{D,T}}{\partial x}+n_{D,T}\frac{\partial n_{T,D}}{\partial x}\right]\right\}$$

where Λ is the Coulomb logarithm and $n_z \equiv n_z(x)$ is an initial distribution of impurities (the polarization electric field is excluded by means of a quasineutrality condition). These equations allow to predict exactly a time-space evolution of a DT-plasma with heavy impurities in a multiple mirror magnetic field.

References

1. J.M.Dawson, R.E.Kidder, A.Hertzberg. Plasma Physics Lab., Princeton University, preprint MATT-782, September 1971
2. G.I.Budker, V.V.Mirnov, D.D.Ryutov. JETP Letts., 14, 320, 1971
3. V.V.Mirnov, D.D.Ryutov. Nuclear Fusion, 12, 627, 1972

ELECTRON CYCLOTRON RESONANCE HEATING ON TM-3 TOKAMAK AT MAGNETIC FIELDS UP TO 25 kOe

Alikaev V.V., Bobrovskii G.A., Poznjak V.I., Razumova K.A., Sannikov V.V., Sokolov Yu.A., Shmarin A.A.

I.V.Kurchatov Institute of Atomic Energy, Moscow USSR

Experiments on additional HF-heating of plasma at electron cyclotron resonance (ECR) frequency and its second harmonic are continued. Thomson scattering measurement of electron temperature has been used.

The perspective of ECRH for reactor is strongly depended on results of investigations of this method at large magnetic fields. In the experiments the HF-generator which provided the heating at the magnetic field $H_z = 20\text{–}25$ kOe was used. The power of the generator was $\lesssim 60$ kW, the pulse duration was up to 1 msec. The heating was investigated at H_z which corresponded to the first and second harmonics of ECR, and the averaged density $\bar{n}_e = (3\div10)10^{12}$ cm^{-3}.

The results of the experiments are similar to those obtained at the resonant magnetic field $H_z \simeq 10$ kOe/1/ :

1. The maximum additional Δ (nT) measured by a diamagnetic loop at the ECR-frequency are the same in the both cases: Δ (nT) = (6–8)10^{14} eV.cm^{-3};

2. The typical features of the runaway electrons heating are observed when $\bar{n}_e$ is decreased (Δ(nT) value, the additional EC-emission and the plasma column shift drop slow after the heating pulse /1/).

3. The Δ (nT) value is decreased somewhat by the higher density or discharge current.

The increase of the electron temperature $\Delta\bar{T}_e$, averaged over the column cross section, has been measured by the diamagnetic loop, the increase of T_e in the center of the column $\Delta T_e(0)$ has been measured by 90° Thomson scattering. In the latter case the ruby laser with Q-switched mode was employed.

As the value $\Delta T_e(0)$ corresponds to the heating of the bulk electrons and the value $\Delta\bar{T}_e$ characterises the heating both of the bulk electrons and of the runaway electrons, the ratio between $\Delta\bar{T}_e$ and $\Delta T_e(0)$ may be arbitrary. For instance, the ratio $\Delta\bar{T}_e/\Delta T_e(0) = \frac{20\text{eV}}{170\text{eV}}$ was registered at the first and the second harmonics of ECRH of the plasma with $\bar{n}_e \sim 8.10^{12}$ cm^{-3}. This fact seems to correspond to the heating of the bulk electrons in the narrow central region of plasma column. On the other hand the ratio $\frac{\Delta\bar{T}_e}{\Delta T_e(0)} = \frac{125\text{eV}}{160\text{eV}}$ observed at the second harmonic in the plasma with $\bar{n}_e \sim 4.10^{12}$ cm^{-3} is the result of the heating either of the bulk electrons all over the cross section or both of the bulk electrons and of the runaway electrons. However, in any case, the $T_e(0)$ increase, obtained by scattering measurements, proves the heating of the bulk electrons during the HF-pulse.

It should be noticed that the $T_e(0)$ may increase in part because the ohmic heating becomes more significant. This can be attributed to the improvement of the plasma confinement in the inner regions of the column at additional heating of the plasma periphery.

The additional HF-heating makes it possible to investigate the fundamental properties of plasma in tokamak. The confinement of plasma with high β_I produced by ECRH has been investigated. The experiment was fulfilled at the second harmonic with $\lambda = 1$ cm HF-generator(H_z = 5 kOe). The Fig.1 shows some characteristics of this regime. One can see that no ill effects are observed at $\beta_I \simeq 2.2$. It should be noticed, however, that the marked part of the additional energy seems to be accumulated by the runaway electrons (as the scope traces show).

An other interesting possibility is the estimation of the runaway electrons confinement time by the measurement of the delay time of their additional energy, provided by ECRH. For this purpose we investigated the EC-emission of plasma at $\lambda \simeq 1.2$ cm and $\lambda \simeq 2.0$ cm. This emission (at $H_z \simeq 13$ kOe) is the one of the runaway electrons with longitudinal energy $E_\parallel \geqslant 10$keV and $E_\parallel \geqslant 60$ keV accordingly (Fig.2). As the electron distribution function is approximately exponential (as X-ray measurements show / 1 /), the registered EC-emission is attributed to the electrons with threshold energy. The time of delay of the additional emission points out that the runaway electrons are contained not less than 2 msec at $E_\parallel \simeq 10$keV and not less than 9 msec at $E_\parallel \simeq 60$ keV.

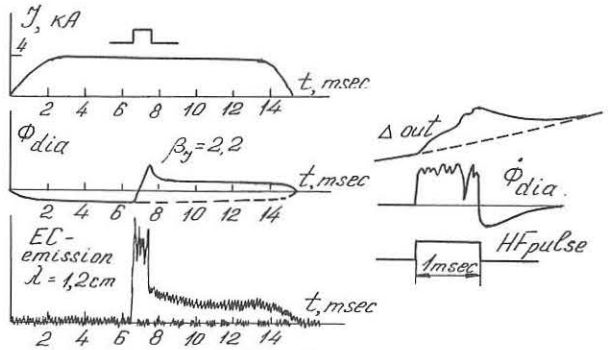

Fig. 1

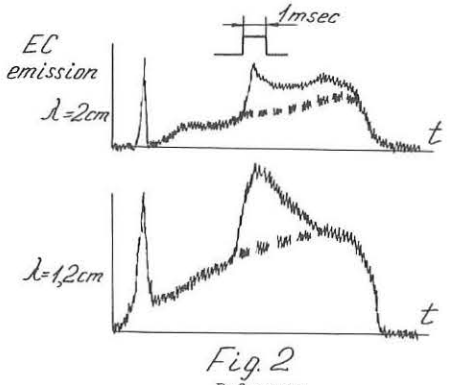

Fig. 2

Reference

/1/. Alikaev V.V. et al. 5th Conf. on Plasma Phys. and Contr. Nuclear Fusion Res., Tokyo (Japan), 1974, Paper CN 33/A9-4.

Fast Magnetosonic Wave Heating at the Second Ion-Cyclotron Harmonic in Tokamak Plasmas

John E. Scharer, Tak-Kuen Mau,
Donald T. Blackfield and Brian D. McVey
University of Wisconsin, Madison, Wisconsin 53706, U.S.A.

Abstract: Hot ion and electron absorption effects are included in the dispersion relation for second ion cyclotron harmonic heating. It is shown that mode conversion problems can be eliminated for UWMAK-II parameters by imposing sufficiently short parallel wavelenghts ($k_\parallel = 10m^{-1}$). The density of toroidal eigenmodes for reactor size plasmas is considered.

It is well recognized that in order to ignite a tokamak reactor, a supplementary heating mechanism in addition to ohmic heating will have to be employed. Magnetosonic wave heating at the ion-cyclotron frequency and its second harmonic has been studied by Adam and Samain [1], Perkins [2], and Weynants [3]. The significant ion heating and wave penetration to a tokamak plasma core that are predicted make the compressional hydromagnetic or fast wave a most interesting candidate for supplementary heating in a tokamak.

Assuming an $e^{-i\omega t + i\bar{k}\cdot\bar{r}}$ Fourier component of wave quantities, the wave equation is obtained as $\bar{k} \times (\bar{k} \times \bar{E}) + (\omega/c)^2 \bar{\bar{K}} \cdot \bar{E} = 0$ where $\bar{\bar{K}}$ is the dielectric tensor as defined in Stix [4]. By noting that in the magnetosonic regime that the Bessel function argument $\lambda_j = k_\perp^2 \rho_j^2/2$ is small for both ion and electron terms, one can obtain a tractable dispersion relation in which first-order finite gyroradius effects are included by expanding to first order in λ_j. Further, the K_{zz} component of the dielectric tensor is so large compared to other elements involving the z component that the dispersion relation can be obtained to a very good approximation by expanding the 2 x 2 minor of the K_{zz} component. The dispersion relation then becomes ($k_\perp = k_x$) to fourth order in $k_\perp$

$$\begin{vmatrix} (\omega/c)^2 K_{xx} - k_\parallel^2 & (\omega/c)^2 K_{xy} \\ (\omega/c)^2 K_{yx} & (\omega/c)^2 K_{yy} - k_\parallel^2 - k_\perp^2 \end{vmatrix} = 0 \qquad (1)$$

where

$$K_{xx} = 1 + \sum_{\alpha=i,e} (\omega_{p\alpha}^2/2\omega k_\parallel v_\alpha)(Z_1^\alpha + Z_{-1}^\alpha) - k_\perp^2 \sum_{\alpha=i,e} (\omega_{p\alpha}^2 v_\alpha/4\omega k_\parallel \Omega_\alpha^2)(Z_1^\alpha + Z_{-1}^\alpha - Z_2^\alpha - Z_{-2}^\alpha),$$

$$K_{yy} = K_{xx} + k_\perp^2 \sum_{\alpha=i,e} (\omega_{p\alpha}^2 v_\alpha/\omega k_\parallel \Omega_\alpha^2)\,[Z_0^\alpha - 1/2(Z_1^\alpha + Z_{-1}^\alpha)],$$

$$K_{xy} = -K_{yx} = -i \sum_{\alpha=i,e} (\omega_{p\alpha}^2/2\omega k_\parallel v_\alpha)(Z_1^\alpha - Z_{-1}^\alpha) + ik_\perp^2 \sum_{\alpha=i,e} (\omega_{p\alpha}^2 v_\alpha/4\omega k_\parallel \Omega_\alpha^2)(2Z_1^\alpha - 2Z_{-1}^\alpha - Z_2^\alpha + Z_{-2}^\alpha)$$

and Z_ℓ^α denotes the Fried and Conte Plasma dispersion function $Z((\omega + \ell\Omega_\alpha)/k_\parallel v_\alpha)$. The dispersion relation then includes wave absorption due to ion finite gyroradius and cyclotron damping effects and electron transit-time damping.

We now present results for Eq.(1) which yields the same dispersion relations for the cases treated in Weynants' paper. The particular case we wish to study is that of the UWMAK-II conceptual fusion design reactor [5]. The deuterium plasma parameters are $6x10^{13}/cm^3$, $T_D = 15.2$ keV, $T_e = 13.5$ keV, B_o on axis = 35.7 kG, R = 13 m, and a = 5 m. They are obtained from a global energy and particle balance assuming trapped particle scaling. We assume that the $k_\parallel$ spectrum excited within the plasma torus is the same as that excited by a launching structure located near the walls in the vacuum region.

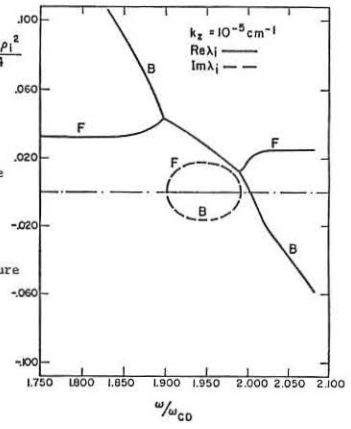

Figure 1

Figure 1 shows a plot of the fast magnetosonic (F) and Ion Bernstein (B) wave modes for the UWMAK parameters for very small $k_\parallel$. A region of mode conversion is noted for $1.90 < \omega/\omega_{CD} < 1.98$. This is quite detrimental for ion heating for waves penetrating from the high magnetic field side. The $k_\parallel = 0$ case can be expected to be the dominant Fourier spectrum of a single excitation structure. Fast wave tunneling and Ion Bernstein electron Landau damping can be expected to assist in power absorption of the wave incident from the high field side.

If the parallel wavelength is decreased so that $k_\parallel = 10m^{-1}$, the mode conversion is eliminated as shown on Figure 2 for the same plasma parameters. Note that even though $\omega/k_\parallel v_e \sim 1$, the dispersion relation is little affected from that for cold electrons. Appropriately spaced and phased poloidal hoops or waveguide feeds mounted in the outside torus wall could be envisioned to provide the desired excitation spectrum.

For large reactor devices such as UWMAK-II, the density of toroidal eigenmodes such as those observed on ST [6] approaches a continuum when the width of the individual modes due to absorption effects and the multiplicity of radial and poloidal mode numbers yielding the transverse wavenumber are taken into account. The toroidal, poloidal, and radial mode numbers are given for a uniform bounded plasma by $n = k_\parallel R$, m, and a boundary value equation involving Bessel functions

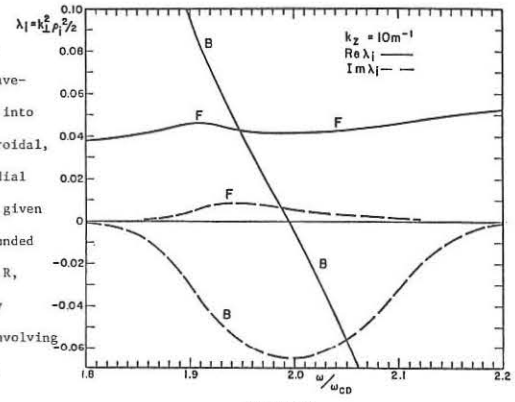

Figure 2

and their derivatives of large argument $k_\perp a$ and the wave and plasma parameters [7]. The width of a given mode can be estimated from equations for second harmonic damping averaged over the minor cross section as $\gamma_i(2\Omega_{CD}) \sim k_\perp^2 \kappa T_i R/m_i \Omega_{CD} a \sim 4 \times 10^6 sec^{-1}$ which can be shown to be large compared to the mode separation $\Delta\omega(n,m,k_\perp)$. It is desirable to excite low m numbers in order to obtain core rather than edge heating. A launching structure which has a significant amplitude of low $k_\parallel$ in its spectrum will excite waves which undergo mode conversion, change the antenna loading, and possibly heat electrons via Landau damping of the Ion Bernstein mode. Thus for large reactors it will be difficult to design a launching structure which provides a particular amount of core vs. edge and ion vs. electron heating.

Skin effect losses for a stainless steel wall at the operating frequency of 54.4 MHz are small compared to the plasma absorption.

$$\gamma_{ss}(500°C) \sim \Omega_{CD}\delta_{ss}/a \sim 3.4 \times 10^3 sec^{-1} \ll \gamma_i(2\Omega_{CD})$$

If a carbon curtain is introduced to reduce the Z_{eff} and impurity line radiation to lower the ignition power requirements, the skin effect losses become

$$\gamma_{cc}(500°C) \sim \Omega_{CD}\delta_{cc}/a \sim 2 \times 10^4 sec^{-1} \ll \gamma_i(2\Omega_{CD}).$$

Thus it appears that a carbon curtain does not obviate the possibility of fast magnetosonic wave heating in a reactor if the wave energy can be introduced between the carbon curtain and plasma column.

References

[1] Adam, J., and Samain, A., Fontenay-aux-Roses, Report EUR-CEA-FC-579, 29 (1971).
[2] Perkins, F. W., Symposium on Plasma Heating and Injection, Varenna, 20 (1972).
[3] Weynants, R. W., Phys. Rev. Letters 33, 78 (1974).
[4] Stix, T. H., The Theory of Plasma Waves, McGraw Hill, New York (1962).
[5] Conn, R. W., et al., Proc. 5th Intl. Conf. on Plasma Physics and Controlled Nuclear Fusion Research, Paper CN-33/G1-2, Tokyo (1974).
[6] Adam, J., et al., Proc. 5th Intl. Conf. on Plasma Physics and Controlled Nuclear Fusion Research, Paper CN-33/A3-2, Tokyo (1974).
[7] Stix, T. H., Princeton MATT Report 1113 (1975).

TRANSFORMATION OF ELECTRON SOUND WAVES IN A HOT-ION PLASMA

N.F.Perepelkin, O.M.Shvets, M.P.Vasil'ev, A.G.Diky.
Physical-Technical Institute, Academy of Sciences of Ukr.SSR, Kharkov, U.S.S.R.

The current-carrying plasma instabilities in the anomalous resistivity regime were studied in the "Uragan" stellarator in works [1,2]. Intensive long-wave $K \ll K_d$ noises with frequency spectra $\omega \sim \omega_{pi}$ and $\sim 2\omega_{pi}$ have been observed, and these noises were explained as a result of the transformation of the short-wave ($K_s \sim K_d \sim \frac{\omega_{pi}}{v_s}$) ion sound waves excited in a nonisothermal plasma ($T_e \gg T_i$). However, at a quasistationary current heating these noises were observed in the form of separate short bursts followed by the bursts of hard X-rays from a traget in a plasma, as well as by microwave (UHF) superthermal noises. These circumstances caused some difficulties for interpretation of results. In this respect the current-less plasma, where the quasi-stationary acceleration of electrons is absent, is more suitable for investigation of the turbulence.

In this work the microinstabilities of a plasma with hot ions were studied during the ion-cyclotron heating (ICRH) in the "Uragan" stellarator. The noise spectrum in the vicinity of ω_{pi} was investigated by two methods. In the first method these noises were picked up by means of the magnetic loop outside the plasma. Relative intensity changes of these noises were studied varying the magnetic field within the resonance curve of the ion-cyclotron wave (ICW) absorption. In the second method the fluctuation-spectral characteristic $m^2(\Omega) = \frac{\bar{S}_{\Delta\Omega}(\Omega)}{\bar{S}_{\Delta\omega}}$ of the thermal UHF emission of the hot-ion plasma was determined (see [1]) and compared with similar characteristic of the UHF standard black-body radiation. Here $\bar{S}_{\Delta\Omega}(\Omega)$, $\bar{S}_{\Delta\omega}$ are the fluctuating and statistical parts of the varience of noise on the exit of square-law UHF detector; Ω is the frequency of fluctuations; $\Delta\omega = 10^3 \Delta\Omega = 1$ Gcps is the bandwidth of analyzed frequencies Ω and the UHF band-pass; $\Delta\Omega$ is the bandwidth of the low-frequency analyzer.

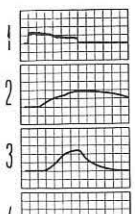

Fig.1

Ion heating in the stellarator was realized at magnetic fields H =3,8 kOe; 7 kOe; 12,6 kOe, that being in agreement with the condition of ICW excitation in plasma for two gases; hydrogen and deuterium at pumping frequencies f =5,2 and 9,4 Mcps. The typical behaviour of plasma parameters is illustrated in fig.1, where; 1 - current in the coupler (f = 9,4 Mcps); 2 - plasma density $1{,}7 \cdot 10^{12}$ cm^{-3}/div; 3 - diamagnetic signal $1.87 \cdot 10^{14}$ ev$\cdot$cm^{-3}/div; 4 - UHF noises $\lambda \approx 2{,}5$ cm; 5 - intensity of radio noises Ω = 290 Mcps (time scale is 0,2 msec/div). The distinguishing feature of plasma behaviour at fast switching-off ($\sim$10 sec) the pumping generator is a slow decay of the diamagnetic signal (3) and the UHF noise (4) and a rapid decay of noises in a radio frequency band (5). The behaviour of ion temperature (T_i), plasma density (n_e) and radio noises (W) at changing of magnetic field strength in the vicinity of ICR in deuterium plasma is shown in fig.2 (at t =0,7 msec). Regime of experiment was chosen from the condition of maximum excitation of turbulent noises. These conditions were $T_i \gg T_e$ which were realized when $\frac{H}{H_{ci}} \sim 1$. The noise intensity W decreased at the transition to the higher magnetic field $\frac{H}{H_{ci}} > 1$ where plasma density increased and $\frac{T_i}{T_e} \to 1$. The similar character of ICW absorption was observed in a hydrogen plasma.

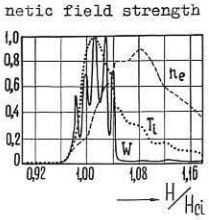

Fig.2

The spectrum of plasma radio noises for the moment of 0,7 msec was obtained by means of a magnetic loop. Fig.3 gives the relation of spectral intensitites $\frac{W'}{W''}$ as a function of frequency Ω (here $\frac{H'}{H_{ci}}$=1,015 and $\frac{H''}{H_{ci}}$=1,045, see fig.2). In this spectrum there are two maxima at frequencies close to the lower hybrid resonance ω_L and $2\omega_L$. In experimental conditions $\omega_{ce} \gg \omega_{pe}$ this spectrum is satisfactorily described by the following relation: $\omega_L^2 = \omega_{ce}\omega_{ci}(1 + \frac{\omega_{ce}^2}{\omega_{pe}^2})^{-1} \sim \omega_{pi}^2$ at changing discharge parameters n_e, H and f and m_i, respectively. Additional probe measurements showed that $\frac{K_\perp}{K_\parallel} \geq 10$ with $\lambda_\perp = 4 \div 5$ cm. All our data allowed us to come to the conclusion that the turbulent noises at $\omega \sim \omega_{pi}$ are fast magneto-acoustic waves close to the lower hybrid resonance which propagate across the magnetic field with the velocity $v_\perp \geq v_{Te}$.

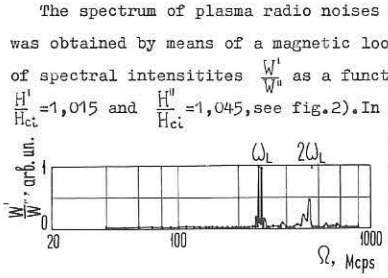

Fig.3

UHF emission (see fig.1(4)) took place at frequencies near $\omega_L = (\omega_{pe}^2 + \omega_{ce}^2)^{\frac{1}{2}}$ and its power P_h was proportional to T_e. The fluctuation spectrum of this UHF emission obtained at the condition: $n_e = 2 \cdot 10^{12}$ cm^{-3}, T_i=300 ev, $T_e \approx 30$ ev, H=3,8 kOe, f=5,2 Mcps is presented in fig.4 (solid line) where for a comparison the spectrum of UHF-standard semiconductor noise source is shown too (broken line). The odd harmonics of the lower hybrid resonance $\omega \sim \omega_L$ and $\sim 3\omega_L$ may be explained as a result of scattering of thermal UHF radiation on plasma fluctuations with $\omega \sim \omega_L$. Relative intensity of the first harmonic ($\frac{\bar{S}(\omega_L)}{\bar{S}_{\Delta\omega}} \sim 5 \cdot 10^{-2}$) allowed to estimate a level of turbulence at $\omega \sim \omega_L$ as $\frac{W_L}{nT} \sim 10^{-2} \div 10^{-3}$.

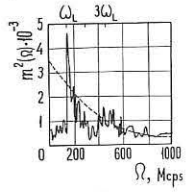

Fig.4

The analysis of all available experimental data showed that the plasma fluctuations at $\omega \sim \omega_L$ during the ICRH might be a result of an electron sound instability [4,5]. According to this theory, a short-scale electron sound instability with $\omega = K_\parallel (T_i m_e^{-1})^{\frac{1}{2}} (1 + K^2 d_i^2 + K^2 \rho_i^2 \frac{m_e}{m_i})^{-\frac{1}{2}}$ can be excited in a nonisothermal ($T_i \gg T_e$) plasma by a transverse current when a current velocity is $v_\perp \geq v_{ti}$. In our case at T_i =300 ev, $T_e \approx 30$ ev, $H_\perp$=10÷20 Oe the transver-current velocity was $v_\perp^e \approx 10^7$ cm$\cdot$sec$^{-1} \geq v_{ti} \approx 1{,}2 \cdot 10^7$ cm$\cdot$sec^{-1}. The long-wave plasma noises at $\omega \sim \omega_{pi}$ and $\sim 2\omega_{pi}$ are, in our opinion, a result of non-linear transformation of electron sound waves in the low-hybrid resonance region of inhomogeneous plasma column.

The conclusion about possible transformation of short scales in an electron sound spectrum is in agreement with the results obtained earlier in the "Uragan" stellarator [1,2] when the ion sound decays in hot electrons plasma have been studied.

The authors are grateful to Prof.K.N.STEPANOV and Dr.V.A.SUPRUNENKO for useful discussion.

References

1. N.F.Perepelkin et al. "III Intern.Symp.on Plasma Toroidal Confinement". E 19. Garching (FRG), 1973.
2. A.G.Diky et al. "V Intern.Conf.on Plasma Phys. and Contr.Nuc - lear Fusion Research". Report CN-33/B3-1. Tokio. 1974.
3. A.G.Diky et al. "III Intern.Symp.on Plasma Toroidal Confinement" E 17. Garching (FRG), 1973.
4. V.L.Sizonenko, K.N.Stepanov. "Nuclear Fusion", 7, 131, 1967.
5. A.A.Galeev, R.Z.Sagdeev. "Voprosi Teorii Plasmi", 7, Atomizdat. Moscow, 1973.

WAVE PROPAGATION AND RF PLASMA HEATING NEAR AND ABOVE THE LOWER HYBRID FREQUENCY IN THE W II A STELLARATOR

P. Javel, G. Müller, A. v.H. van Oordt, and U. Weber
Max-Planck-Institut für Plasmaphysik, Garching b. München

and

R.R. Weynants
Laboratorium voor Plasmafysica, Associatie EURATOM-Belgische Staat, Koninklijke Militaire School, 1040 Brussels

Abstract: Strong absorption of electron plasma waves which leads to a very localized energy deposition via the resonance cones is observed. Ion heating by parametric decay is demonstrated.

Introduction. The target plasma used in the RF heating experiments now being conducted on the W II A stellarator [1] is produced with radio-frequencies and sustained by electron plasma waves. Owing to the self-consistent propagation of these waves, the energy transfer can be studied under conditions quite similar to present lower hybrid wave experiments. An important aspect is the occurrence of resonance cones. In a previous paper [1] we reported on the kinematical aspects of the cone propagation. Here we describe some of the pronounced effects of the cones on the wave-plasma interaction processes, in particular on the electron and ion heating.

Experimental apparatus. The machine characteristics are R = 50 cm, a = 9 cm, and B_o = 5 kG, and the rotational transform is in the range $0 < \iota < 0.2$. The gas used is H_2 at filling pressures of $5 \cdot 10^{-6}$ to $5 \cdot 10^{-5}$ torr. The coupling structure is a metal ring 10 cm in diam.; $P_{inc} \leq 300$ W cw at 35 MHz $\leq f \leq$ 200 MHz. Breakdown requires from 30 to 200 W in the specified pressure and frequency ranges. After ignition, the plasma can be maintained with a power as low as 1 W, and the coupling efficiency ranges from 70 % to 100 % without the use of a matching network. The diagnostics comprise Langmuir probes (only at high pressures) for n_e and T_e, 4 mm interferometry for n_e, and electrostatic analyser for T_i near the plasma boundary, and Doppler-broadening spectroscopy+) of Ba^+ impurities for T_i and coaxial RF probes.

Interdependence between resonance cones, density and temperature profiles. With increasing power, at fixed frequency, the line density $\int n_e\, dr$ varies as shown in Fig.1. A corresponding set of radially resolved ion-saturation current measurements is also shown. These results can be explained in terms of the existence domain of the electron plasma waves. Under the conditions studied here, the maximum attainable densities are such that the corresponding lower hybrid frequency (f_{lh}) equals the applied frequency. These densities are indicated in Fig.1 for a square profile of 6 cm or a parabolic one of 9 cm. For the higher frequencies the lower hybrid density is not reached since profile broadening results from a sudden density redistribution in which the total number of particles is conserved for power levels critically dependent on ι. The profile flattening strongly affects the wave propagation. The angle of propagation of the cones with respect to the magnetic axis is given by

$$tg\,\psi = \left(\frac{f^2 - f_{lh}^2}{f_{pe}} \right)^{1/2},$$

where f_{pe} is the electron plasma frequency and f_{lh} practically equals f_{pi}. If the cone encounters a high density as soon as it enters the plasma, the energy will have to travel a long way before reaching the center. In order for the energy to pervade the whole plasma column, (a) the lower hybrid layer should be present along the density profile and (b) the absorption length must be longer than the said path length. Collisional absorption lengths are expected to be of the order $L_c = (10^{-1} \ldots 4)\omega_{pe}\nu^{-1}$ cm (where ν is the collision frequency of electrons with ions and neutrals), i.e. typical values of 100 to 1000 m. Landau damping is expected to take even longer. In contrast, an energy packet leaving the RF structure would reach the center after passing 2 (5) m through a square plasma profile with a density value equal to 50 % (90 %) of the lower hybrid density.

Figure 2 shows a set of radial electron temperature profiles for different powers at f = 35 MHz. With increasing power, heating preferentially occurs towards the outer plasma layers. At fixed power, parabolic profiles can be found at the higher frequencies, and a strong non-uniformity develops at lower frequencies even under conditions where the maximum density remains well below the lower hybrid density. These results point to absorption lengths at least two orders of magnitude smaller than L_c. These might be brought about by the observed parametric decay of the electron waves into another electron plasma wave and an ion wave with a frequency slightly above the ion cyclotron frequency.

Of course, decreased heat deposition in the center is not enough to explain the observed temperature minimum. From the heat balance equation it is clear that this power has to be more than balanced by a loss which is not due to conduction. On the basis of the measured field distributions and the density decay times, we conclude that ionization, heating of the newly created particles, and radiation constitute a plausible explanation.

Ion Heating. Ion heating might occur as a result of ion-electron equilibration with a power input $P_{ei} = 1.3 \cdot 10^{-26} \alpha n_e^2 T_i^{-1/2}$ W/cm^3 (n_e in cm^{-3} and T_i in eV). α is a function of T_e/T_i which varies only slightly around a mean value of about 0.3 in the range $1.5 < T_e/T_i < 10$. Equating P_{ei} with the ion losses (elastic collisions with neutrals, diffusion, and conductivity), one expects T_i to be about 0.6 to 2 eV for densities of $5 \cdot 10^{10}$ to $3 \cdot 10^{11}$ cm^{-3} and $p \gtrsim 10^{-5}$ torr with a $T_i \approx n^{2/3}$ dependence. Fig.3 shows a typical radial distribution of T_i and the corresponding T_e. The presence of a T_i minimum cannot be accounted for by equilibration heating since P_{ei} is practically uniform over the plasma radius. Equilibration is also insufficient to explain the high ion temperatures measured at low density (low frequency) and the observed power dependence. However, the parametric decay phenomena mentioned appear to supplement the equilibration heating adequately:

(i) The spatial field distribution of the ion waves shown in Fig.4 is "cone-like" (see also (ii)), and similar arguments as for T_e can be deduced.

(ii) Preferential heating at low frequencies is expected on the basis of the Manley-Rowe relations, which are found to apply.

(iii) It is found that the increment of T_i with respect to the value before threshold is correlated with the measured instability amplitude.

It was not possible to determine to what extent the ion heating at low frequencies is favourably influenced by the fact that the lower hybrid density can practically be reached.

Conclusions. The experiments confirm in toroidal geometry the good source performances reported in Ref. [2]. Preliminary efficiency evaluations turn out to be quite favourable at high frequencies although both particle and energy losses are expected to be accentuated at higher power levels since ionization and heating increasingly occur in the outer layers.

References

[1] Javel, P., G. Müller, U. Weber and R.R. Weynants, IPP-Report 2/228 (1975)
[2] Bernabei, S., W.M. Hooke, D.L. Jassby and R.W. Motley, Proc. of 2nd Topical Conference on RF Plasma Heating, Lubbok, Texas (1974), Paper C 5.

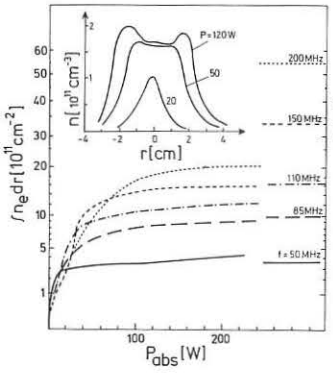

Fig.2 Typical electron temperature radial profiles.

Fig.1 Line density vs. absorbed power at different frequencies. The inset shows radial density profiles at f = 110 MHz for various powers. The pressure $p = 1.0 \cdot 10^{-5}$ torr. Furthermore, in common with all figures: B_t = 5 kG, ι = 0.11.

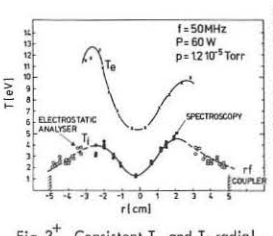

Fig.3+ Consistent T_e and T_i radial profiles. The density is about $5 \cdot 10^{10}$ cm^{-3}

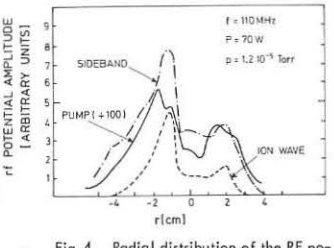

Fig.4 Radial distribution of the RF potential amplitudes of the three waves present.

+) The spectroscopic ion temperature measurements were performed by E. Hinnov and H. Ringler.

PLASMA HEATING IN A TOROIDAL TRAP BY A HELICAL H.F. MULTIPOLE MAGNETIC FIELD

R.A.Demirkhanov, A.G.Kirov, S.E.Il'insky, S.N.Lozovsky, V.B.Maiburov, I.Ya.Kadysh, L.Ya.Malykh

Institute of Physics and Technology, Sukhumi, USSR

Abstract: The results of experimental studies on plasma heating in a stellarator "R-02" by a helical quadrupole h.f. field are given. During the heating, the h.f. field energy is transported predominantly to plasma ions. Possible mechanisms of heating are discussed.

The methods of plasma heating at frequencies $\omega < \omega_{Bi}$ attract some attention last time. The experiments in this field are presented, in particular, by TTMP method /1/. Another possibility is indicated by us in /2/. In the present paper which continues /2/ we give experimental results of the ion heating by a helical quadrupole h.f. field.

The exreriments have been carried out on a circular stellarator "R-02" with a plasma resistively heated in advance.

The parameters of the machine are the following: the quartz discharge chamber - D = 130 cm, d = 8 cm, B_o = 15 kGs, i_o = 1,5π, $I_p \leq$ 2 kA.

The h.f. field is generated by 8 helical windings. They make 3 turns around the minor section of the chamber when one turn along the torus is made, the winding system being similar to a helical stellarator winding. A whole set of windings and condensers forms the closed LC-line fed at a resonance frequency by a four-phase oscillator with independent excitation and maximum power ~ 40 MW. In the neighbouring windings, the h.f. currents are shifted in phase at 90°. As a result a helical quadrupole (m_o = 2) h.f. magnetic field ($\omega = 8.10^6 sec^{-1}$, $\tilde{B}_\varphi \simeq 150$ Gs, pulse duration $\tau \simeq 1,5$ msec) rotating around and running along the plasma column is created. Six periods (n_o = 6) of the h.f. field with the period length $\tilde{\lambda}$ = 68 cm are arranged along the plasma column.

The plasma density averaged over the diameter has been measured by the microwave interferometer with λ = 2,3 mm, the specific plasma energy averaged over the cross-section has been registered by diamagnetic probes. The electron temperature was deduced from the plasma conductivity $\sigma \sim \frac{U_{f\,esop.}}{J_p}$. The temperatures of impurity ions were estimated according to Doppler broadening of spectral lines (SiII, SiIII, OII, OIII etc.).

The ohmically heated discharge was unstable and the plasma escaped rather rapidly. On switching the h.f. field the discharge was getting more stable /3/ and the plasma density reached the value corresponding to the density of neutral gas (He or H_2) before breakdown.

The h.f. field interaction with the plasma shows a well-defined resonant character. At a certain density value in the range of magnetic fields B_o = 8 ÷ 15 kGs there exist such values of B_o at which the h.f. power is effectively absorbed by the plasma which is intensively heated in result. Two regimes of the resonance heating for plasma densities $n \simeq 2.4 \cdot 10^{13} cm^{-3}$ and $n \simeq 5 \cdot 10^{13} cm^{-3}$ are shown in Fig.1 where the specific plasma energy is presented VS B_o. It follows from the experimental data that $B_o \sim n^{1/2}$. At the same time, for a hydrogen plasma, the h.f. energy effective absorption at the same magnetic field occurs at the densities which are four times the density for helium, i.e., $(B_o)_{res} \sim (nm_i)^{1/2}$. As a whole, the stationary magnetic field resonance value satisfies fairly well the relation:

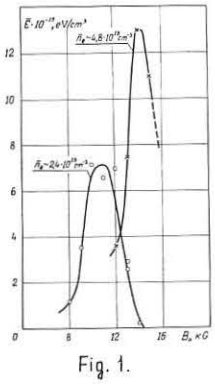

Fig. 1.

$$\frac{(B_o)_{res}}{\sqrt{4\pi n m_i}} = \alpha \frac{\omega}{k_z}; \quad k_z = \frac{2\pi}{\tilde{\lambda}}; \quad \alpha = 1 \div 2 \qquad (1)$$

The relation (1) being fulfilled, the specific plasma energy dependence upon the h.f. field strength is shown in Fig.2. It is seen that the h.f. field strength threshold value exists at which an intense heating beings.

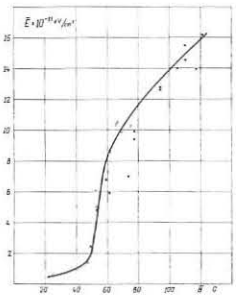

Fig. 2.

The maximum specific plasma energy averaged over the cross-section obtained from diamagnetic measurements is $\simeq 1,6 \cdot 10^{16} ev \cdot cm^{-3}$, the corresponding diamagnetic temperature being $T_d = T_e + T_i \simeq 450 ev$ at the plasma density $n \simeq 2,5 \cdot 10^{13} cm^{-3}$.

The spectroscopic measurements averaged both over the discharge duration and the plasma cross-section give the Si^{++} ion temperature $T_{is} \simeq 250$ ev. The spectroscopic measurements carried out at various strengths of the h.f. field show that the ion spectroscopic temperature is proportional to the diamagnetic temperature: $T_{id} \simeq T_{is}$. The electron temperature estimated from the conductivity is $T_e \simeq 50$ ev.

All these facts indicate that it is ion component of the plasma that is effectively heated. One of the most probable treatments of the observed plasma heating effect is the mechanism of the resonance excitation of proper helical modes of the plasma column by the h.f. field. The theoretical analysis leads to the following expression for the h.f. field B_φ -component excited by a helical h.f. current in an uniform cylindrical plasma column with the radius r_p in which a stationary longitudinal homogeneous current flows:

$$\tilde{B}_\varphi(r) = \frac{4\pi}{c} \tilde{J}_{oz} \left(\frac{r}{r_c}\right)^{m_o - 1} \frac{k_z^2 c_A^2 \left(1 + \frac{n_o}{m_o} q_i\right)}{2k_z^2 c_A^2 F(q_i) - \omega^2};$$

$$F(q_i) = 1 + \frac{m_o}{n_o q_i} + \frac{m_o(m_o - 1)}{2 n_o^2 q_i^2}; \qquad (2)$$

$$\tilde{J}_z = \tilde{J}_{oz} e^{i(\omega t - m_o \varphi - k_z z)}; \qquad \tilde{J}_\varphi = -\frac{k_z r_c}{m_o} \tilde{J}_z,$$

where r_c is the radius of the current sheath, $q_i = \frac{B_o}{B_{o\varphi}(r_p)} \cdot \frac{r_p}{R}$ is the stability safety factor, $B_{o\varphi}$ is the poloidal magnetic field, $c_A^2 = \frac{B_o^2}{4\pi n m_i}$.

The resonance condition $\sqrt{2} \frac{H_o}{\sqrt{4\pi n m_i}} \sqrt{F(q_i)} = \frac{\omega}{k_z}$ (3) coincides, naturally, with the dispersion law for helical modes /4/ (in their stability region). It follows from (3) that $(B_o)_{res} \sim \sqrt{n m_i}$ (the remaining parameters being fixed) which agrees with the experimental data given above.

Dissipation of the h.f. power absorbed by the plasma at the resonance is realised probably by means of nonlinear mechanism of parametric excitation of short-wave oscillations which can effectively dissipate due to collisions or Landau damping.

The temperature of helium ions was not determined because of low luminosity of HeII lines and small light-power of the apparatus. We have also not yet defined the percentage of impurities in plasma.

These two circumstances lead to some uncertainty in the treating the experimental results since the cyclotron frequencies of impurities (SiII, SiIII, OII) are in the region of operating values of B_o, and the effect of cyclotron heating of impurity ions is not excluded.

We express our acknowledgements to V.A.Miloserdov for help in work and F.M.Nekrasov and A.G.Elfimov for useful discussions.

References

1. M.Bernar. Paper presented at the Soviet-French symposium on h.f. methods of plasma heating (Leningrad, June 1974). Leningrad, "Nauka", p.12, 1974.

2. R.A.Demirkhanov, A.G.Kirov et al. Ibid., p.15.

3. R.A.Demirkhanov et al. Proc. of the VI European Conf. on CTF and Plasma Physics. V.I, 169, Moscow, 1973.

4. V.D.Shafranov. Atomnaya Energiya, 5, 38, 1956.

PLASMA ELECTRON HEATING AT FREQUENCIES ABOVE THE LOWER-HYBRID FREQUENCY BY PARAMETRIC EFFECTS IN A BOUNDED PLASMA.

V. BHATNAGAR, G. VAN OOST, A.M. MESSIAEN, P.E. VANDENPLAS, A. PAITHANKAR, W. VAN HOVE

Laboratoire de Physique des Plasmas - Laboratorium voor Plasmafysica

Association "Euratom-Etat belge" - Associatie "Euratom-Belgische Staat"

Ecole Royale Militaire - 1040 Brussels - Koninklijke Militaire School

Abstract. Two parametric instabilities have been simultaneously observed above a certain pump threshold. The pump and the first decay wave are identified as Trivelpiece-Gould modes of the bounded plasma and the second decay wave is identified either as an ion-acoustic mode and/or an ion-cyclotron mode. Spectroscopic measurements show strong increase of electron temperature with increasing pump amplitude.

During the last few years plasma heating via the excitation of parametric instabilities has been of considerable theoretical and experimental interest ; see e.g. 1 - 4. As an example, the pump wave (e.g. Trivelpiece-Gould (T-G) mode, $f_{LH}<f<f_{pe},f_{ce}$) excites, above a certain threshold, an instability which produces simultaneously two decay modes i.e. an electron mode (e.g. T-G mode) and an ion mode (e.g. ion-acoustic (IA) mode, $f \lesssim f_{ci}$ or ion-cyclotron (IC) mode, $f \gtrsim f_{ci}$). The decay modes then interact with the plasma particles resulting in plasma heating. Such parametric instabilities have been observed in the present nonlinear experiment in which both the pump wave and the decay waves obey the linear dispersion relation of the bounded plasma system[5].

A schematic diagram of the experimental apparatus is shown in Fig.1. The pump wave is excited by one section of the split-cylindrical coupler shown. The pump and the decay modes are detected by spatially movable RF double probes and a spectrum analyzer ; $k_{//}$ is measured by the interferometric technique. Electron temperature is measured spectroscopically (helium line-intensity ratio technique). Basic plasma parameters are $N_o \simeq 1\times10^{10} cm^{-3}$; $B_o=0.8-2kG$; $T_e \simeq 8eV$; length of the column $\simeq 1m$; diameter $\simeq 1.2cm$ and helium gas pressure $\simeq 4\times10^{-4}$ Torr.

The dispersion diagram of a warm-electron, cold-ion,magnetized plasma waveguide (plasma radius $=a$, metal tube radius $=d$) is shown in Fig. 2 for the azimuthal mode $n=o$. V_S, V_e and V_A represent plasma sound speed, electron thermal velocity and Alfvén velocity respectively. Warm plasma effects appear above the V_e line. There are four sets of modes viz. T-G modes, surface wave, IC modes and IA modes that exist in the frequency domain shown. By linear excitation, existence of these waves and their dispersion characteristics have been experimentally verified[5]. At higher RF power, excitation of the IA and IC modes by nonlinear coupling has been observed. In general, the frequency spectrum is complicated with side bands and harmonics appearing on both sides of the applied signal in the T-G mode region. However for certain ranges of parameters, the situation schematically shown in Fig.3 is observed. Below threshold, the frequency spectrum consists essentially of a single peak at the pump frequency. Above a first threshold (a few Volts on the coupler) a sharp lower side band and a low-frequency decay signal (*kHz* range) appear in the spectrum. Above a second threshold (which can be lower or higher than the first one depending on plasma parameters), a rather broad lower side band and a broad low-frequency decay mode (*MHz* range) appear as shown in Fig. 3.

The frequency spectrum containing the *kHz* signal and one side band is shown in Fig. 4 for certain parameters. The amplitude of the side band(f_1) is about 20 *db* below the pump (f_o) amplitude but that of the low-frequency mode (f_2) could not be compared due to the frequency-dependent capacitive coupling of the probe. The frequency condition $f_o=f_1+f_2$ is satisfied. Axial wavelength measurements of the pump and decay waves provide $k_{//}(f_o)=0.6cm^{-1}$, $k_{//1}(f_1)=1.6cm^{-1}$, $k_{//2}(f_2)=1.1cm^{-1}$ and roughly satisfy the condition $k_{//o}=k_{//1}-k_{//2}$. The high-frequency (i.e. the side band) and low-frequency decay waves satisfy the dispersion relation of T-G mode and IA mode respectively.

Figure 5 shows the spectrum containing the mode that appear in the *MHz* range with $f_o=f_1+f_2$. But it is difficult to verify the $k_{//}$-selection rule since the frequency spectrum of the decay wave is rather broad. Nevertheless, the low-frequency and high-frequency decay waves lie in the IC and T-G mode regions.

When the pump amplitude is increased beyond both thresholds we find that : (i) The spectroscopically measured T_e reaches a value which is roughly twice that of the initial T_e as shown in Fig. 6. (ii) The figure also indicates that electron density decreases. Such a decrease in density has also been observed by Hendel and Flick[6] in their study of IA decay instability. When the pump amplitude is several times the threshold, there is a saturation of T_e and the pump power alone is able to sustain a plasma in the machine with modified parameters.(iii) Concerning the IA decay wave, we further find that f_2 (IA) increases when T_e increases while always obeying $\omega/k_{//}=\sqrt{KT_e/m_i}$ and the corresponding decrease of f_1 (T-G mode) is such that $f_o=f_1+f_2$ remains fulfilled.

Two parametric instabilities have been simultaneously observed in our linear machine and these are accompanied by a doubling of electron temperature and a decrease in plasma density.

Acknowledgements. We thank F. Alberta, J. Neefs, F. Van Goethem and F. Van Thillo for their skilled technical assistance.

References.

[1] Hooke W.M. and Bernabei S., Phys. Rev. Lett., 29, 1218, 1972.

[2] Chu T.K., Bernabei S. and Motley R.W., ibid, 31, 211, 1973.

[3] Porkolab M., Proc. of Symposium on Plasma Heating in Toroidal Devices, Varenna, Sept. 4-17, 1974, p. 28.

[4] Chu T.K., Lee Y.C. and Porkolab M., ibid, p. 102.

[5] Bhatnagar V.P., Van Oost G., Messiaen A.M. and Vandenplas P.E., submitted for publication.

[6] Hendel H.W. and Flick J.T., Phys. Rev. Lett., 31, 199, 1973.

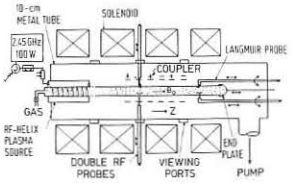

FIG. 1 SETUP

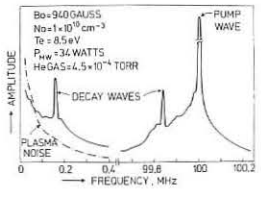

FIG. 4 IA INSTABILITY

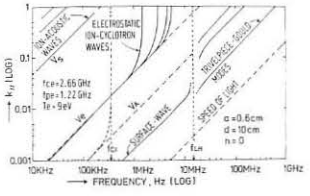

FIG. 2 DISPERSION DIAGRAM

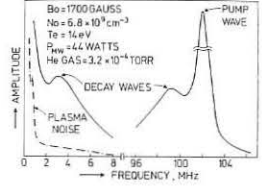

FIG. 5 IC INSTABILITY

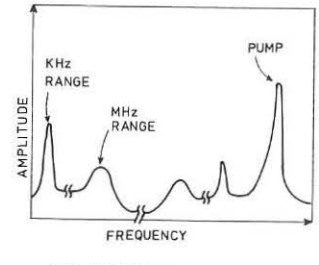

FIG. 3 SCHEMATIC SPECTRUM

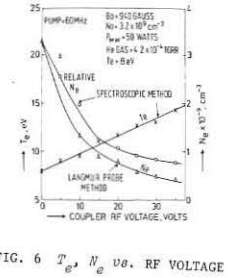

FIG. 6 T_e, N_e *vs.* RF VOLTAGE

QUASI-LINEAR APPROACH TO THE ABSORPTION OF AN RF FIELD AND HEATING OF A MAGNETIZED PLASMA

M. Bornatici
Department of Physics, University of Calabria, Cosenza, Italy
F. Santini
ASSOCIAZIONE EURATOM-CNEN sulla Fusione, Centro Gas Ionizzati
C.P. 65, 00044 Frascati, Rome, Italy.

ABSTRACT: The absorption of an RF electric field and heating of a parametrically unstable magnetized plasma are discussed in the quasi-linear approximation. Comparative heating of electrons and ions is considered for the resonant parametric excitation of a lower-hybrid and an ion acoustic mode.

INTRODUCTION: The possibility of transforming the electromagnetic energy of an intense RF electric field into thermal energy of plasma particles through the excitation of parametric instabilities is considered among the various schemes proposed for the heating of a thermonuclear plasma. Particular attention is given to the frequency range around the lower hybrid resonance [1] where instabilities can be prametrically excited via both the three wave resonant interaction and the mechanism of inverse nonlinear Landau damping. To estimate the rate of plasma heating due to an instability requires a nonlinear description of the instability which gives the level of fluctuation at which the instability saturates [2]. A quasi-linear description of the instability although insufficient to give a full solution of the heating problem allows nevertheless to compare the ion and electron heating to establish whether an efficient direct heating of the ions is possible. On the other hand, once the level of saturation of the instability is known the electron and ion heating rates are formally obtained from the quasi-linear energy equations.

Here by making use of the quasi-linear approximation we evaluate the absorption of an homogeneous RF (lower hybrid) field and derive how the electron and ion temperatures increase for a plasma which is unstable with respect to the resonant decay instability.

OUTLINE OF THE GENERAL PROCEDURE: The presence of a spatially homogeneous and monochromatic pump field $\underline{E}_p(t) = \frac{1}{2}(\underline{E}_0 e^{-i\omega_0 t} + c.c.)$ is described by expanding the distribution function $\mathcal{F}_\alpha$ of particles of species α (and the self-consistent electrostatic field) in terms of harmonics of the pump frequency ω_0,

$$\mathcal{F}_\alpha(\underline{x},\underline{v},t) = \sum_{n=-\infty}^{\infty}\left\{F_\alpha^{(n)}(\underline{u},t) + \sum_{\underline{k}\neq 0} f_{\alpha\underline{k}}(\underline{u},\omega_{\underline{k}}+n\omega_0) e^{-i\int_0^t \hat{\omega}_{\underline{k}}\,dt' + i\underline{k}\cdot(\underline{x}-\underline{x}_\alpha)}\right\} e^{-in\omega_0 t} \quad (1)$$

Here each component $F_\alpha^{(n)}(\underline{u},t)$ of the background distribution function and $\hat{\omega}_{\underline{k}}(t) = \omega_{\underline{k}}(t) + i\gamma_{\underline{k}}(t)$ are slowly varying functions of time; $\underline{u} = \underline{v} - \underline{v}_\alpha$ is the particle velocity in the frame oscillating with velocity $\underline{v}_\alpha$, $d\underline{u}/dt = \Omega_\alpha \underline{u} \times \hat{\underline{z}}$ with $\Omega_\alpha = q_\alpha B_0/m_\alpha c$, $\underline{B}_0 = \hat{\underline{z}} B_0$ and $d\underline{v}_\alpha/dt = \underline{v}_\alpha = \frac{1}{2}\underline{M}_\alpha(\omega_0)\cdot\underline{E}_0 e^{-i\omega_0 t} + c.c.$ where $\underline{M}_\alpha(\omega_0)$ is the mobility tensor of the species α.

Expansion (1) is now used in Vlasov equation to obtain an equation for the $\underline{k} = 0$ part of the distribution function (in fact this corresponds to an infinite number of equations, one for each $F_\alpha^{(n)}$) and an equation for $f_{\alpha\underline{k}}$ where we disregard the nonlinear terms. By combining these equations one is left with a set of quasi-linear-type equations for $F_\alpha^{(n)}$ which can then be used to express the velocity moments of $F_\alpha^{(n)}$ in terms of the fluctuating self-consistent field.

ABSORPTION OF THE RF FIELD: The anomalous absorption of the pump field by the particles of species α is related to the work, averaged over the pump period $2\pi/\omega_0$, performed by the pump on the particles,

$$\langle \underline{E}_p(t)\cdot\underline{j}_\alpha(t)\rangle = q_\alpha \langle \underline{E}_p(t)\cdot\int \underline{u}\sum_n F_\alpha^{(n)}(\underline{u},t)\, e^{-in\omega_0 t}\, d^3u\rangle = q_\alpha \mathrm{Re}\left\{\underline{E}_0^*\cdot\int \underline{u}\, F_\alpha^{(1)}(\underline{u},t)\, d^3u\right\} \quad (2)$$

By making use of the equation for the first hamonic of the background distribution function $F_\alpha^{(1)}$ one finds that, at the lowest significant order in the pump field, $\langle \underline{E}_p(t)\cdot\underline{j}_\alpha(t)\rangle \sim \phi_{\underline{k}}^*(\omega_{\underline{k}})\,\phi_{\underline{k}}(\omega_{\underline{k}}-\omega_0)$, with $\phi_{\underline{k}}$ the Fourier component of the potential. We note that in the random phase approximation this term would be zero. By making use also of Poisson's equation and the expression for the growth rate $\gamma_{\underline{k}}$ [1],

$$\langle \underline{E}_p(t)\cdot\underline{j}_\alpha(t)\rangle = 4\sum_{\underline{k}}\omega_0\left[\gamma_{\underline{k}}\frac{\partial\varepsilon'_{\underline{k}}(\omega_0-\omega_{\underline{k}})}{\partial(\omega_0-\omega_{\underline{k}})} + \varepsilon''_{\underline{k}}(\omega_0-\omega_{\underline{k}})\right]\frac{b_{\alpha\underline{k}}\varepsilon'_{\alpha\underline{k}}}{b_{\underline{k}}^2(\varepsilon'_{\underline{k}}(\omega_{\underline{k}}))^2}\sum_\beta b_{\beta\underline{k}}\varepsilon'_{\beta\underline{k}}\cos(\chi_{\alpha\underline{k}}-\chi_{\beta\underline{k}})\,\mathcal{E}_{\underline{k}} \quad (3)$$

where $\varepsilon_{\underline{k}}(\omega_{\underline{k}}) = \varepsilon'_{\underline{k}} + i\varepsilon''_{\underline{k}} = 1 + \sum_\alpha \varepsilon_{\alpha\underline{k}}(\omega_{\underline{k}})$ is the (linear) dielectric function with absence of pump field; $b_{\alpha\underline{k}} = e^{i\chi_{\alpha\underline{k}}}\,\underline{\kappa}\cdot\underline{M}_\alpha(\omega_0)\cdot\underline{E}_0/\omega_0$, $\chi_{\alpha\underline{k}}$ is a phase angle; $\mathcal{E}_{\underline{k}}(\omega_{\underline{k}}-\omega_0) = \kappa^2|\phi_{\underline{k}}(\omega_{\underline{k}}-\omega_0)|^2/8\pi$ is the spectral energy density.

From (3) one gets the average work performed by the RF field on the plasma [3],

$$\langle \underline{E}_p(t)\cdot\underline{j}(t)\rangle = \langle \underline{E}_p(t)\cdot\sum_\alpha \underline{j}_\alpha(t)\rangle = 2\sum_{\underline{k}}\omega_0\left[\gamma_{\underline{k}}\frac{\partial\varepsilon'_{\underline{k}}(\omega_0-|\omega_{\underline{k}}|)}{\partial(\omega_0-|\omega_{\underline{k}}|)} + \varepsilon''_{\underline{k}}(\omega_0-|\omega_{\underline{k}}|)\right]\mathcal{E}_{\underline{k}}(\omega_0-|\omega_{\underline{k}}|) \quad (4)$$

From (3) and for $\Omega_i^2 \ll \omega_0^2 \ll \Omega_e^2$ it follows $|\langle \underline{E}_p\cdot\underline{j}_i\rangle/\langle \underline{E}_p\cdot\underline{j}_e\rangle| = O(\Omega_i/\omega_0)$ so that the absorption of the pump takes place essentially through the electrons, $\langle \underline{E}_p\cdot\underline{j}\rangle \simeq \langle \underline{E}_p\cdot\underline{j}_e\rangle$.

ENERGY BALANCE AND PLASMA HEATING: The time variation of the kinetic energy density of particles of species α, averaged over the period $2\pi/\omega_0$, $\partial(n_0 K_\alpha)/\partial t = m_\alpha/2\,\langle\left[v^2\,\partial F_\alpha^{(0)}/\partial t\right]d^3u\rangle$, at lowest order in the pump amplitude is expressed by the equation:

$$\frac{\partial(n_0 K_\alpha)}{\partial t} = 2\sum_{\underline{k}}\left\{\left[\gamma_{\underline{k}}\frac{\partial(\omega_{\underline{k}}\varepsilon'_{\alpha\underline{k}}(\omega_{\underline{k}}))}{\partial\omega_{\underline{k}}} + \omega_{\underline{k}}\varepsilon''_{\alpha\underline{k}}(\omega_{\underline{k}})\right]\mathcal{E}_{\underline{k}}(\omega_{\underline{k}},t) + \right. \quad (5)$$

$$\left. + \text{same term with } \omega_{\underline{k}} \to \omega_0 - |\omega_{\underline{k}}|\right\},$$

a result which is independent of the phase relationship of the unstable modes. The terms on the r.h.s. of (5) proportional to $\gamma_{\underline{k}}$ refer to the sloshing energy, while the terms proportional to the imaginary parts of the dielectric susceptibilities $\varepsilon''_{\alpha\underline{k}}$ are related to the thermal energy of the particles of species α, i.e., characterize the rate of heating of the particle species $\partial(n_0 T_\alpha)/\partial t$. By using (5) and the Manley-Rowe relation one obtains the energy conservation $\frac{\partial}{\partial t}\left[\sum_\alpha n_0 K_\alpha + \mathcal{E}_\infty\right] = \langle \underline{E}_p\cdot\underline{j}\rangle$, where $\mathcal{E}_\infty \equiv \sum_{\underline{k}}\left[\mathcal{E}_{\underline{k}}(\omega_{\underline{k}},t) + \mathcal{E}_{\underline{k}}(\omega_0-|\omega_{\underline{k}}|,t)\right]$ and, at the lowest order in $\omega_{\underline{k}}/\omega_0$,

$$\frac{\partial(n_0 T)}{\partial t} \equiv \frac{\partial}{\partial t}\left(\sum_\alpha n_0 T_\alpha\right) = 2\sum_{\underline{k}}\omega_0\,\varepsilon''_{\underline{k}}(\omega_0-|\omega_{\underline{k}}|)\,\mathcal{E}_{\underline{k}}(\omega_0-|\omega_{\underline{k}}|,t) \quad . \quad (6)$$

FINAL REMARKS: As a specific application, we consider the resonant decay of the pump into a lower-hybrid and an ion acoustic mode in a Tokamak-like plasma. With $\omega_0 = \omega_{pi,max} = 3\omega_{pi}$, (i.e., $n_0 \simeq 10^{13}$, $n_{max} = 10^{14}$ cm^{-3}), T_e = 300 eV, B_0 = 50 kG, E_0 = 750 V/cm and a RF power input of 1 MW, we obtain $\gamma_{\underline{k}} \simeq 2.10^7\,\mathrm{sec}^{-1}$ and $\sum_{\underline{k}}\mathcal{E}_{\underline{k}}(\omega_0-|\omega_{\underline{k}}|)/n_0 T_e \simeq 5.10^{-5}$. By comparing (6) and (4), only 5% of the absorbed RF energy goes into thermal energy, i.e., before wave saturation, the pump energy is mainly converted into wave and sloshing energy. Also from (5), $(\partial T_e/\partial t)/(\partial T_i/\partial t) \gg M$. One can conclude, therefore, that the q.l. regime of the instability hardly affects the ions.

In the presence of nonlinear saturation, it is reasonable to assume that (6) is still valid with $\varepsilon''_{\underline{k}}$ representing also the nonlinear dissipation, if in such regime ($\gamma_{\underline{k}} = 0$, $\mathcal{E}_{\underline{k}} = \text{const}$) $\mathcal{E}_{\underline{k}}/n_0 T \ll 1$. Indeed, this is in agreement with the request of a heating time $\tau_h \simeq 1$ msec, since from (6), $\mathcal{E}_{\underline{k}}/n_0 T \simeq 1/2\tau_h\,\omega_0\,\varepsilon''_{\underline{k}}$ which is satisfied for the above plasma figures. Whether the saturation occurs at that turbulence level and what is the ratio $\varepsilon''_{eff}/\varepsilon''_{\underline{k}} \simeq (\partial T_e/\partial t)/(\partial T_i/\partial t)$ is related to the specific nonlinear phenomena, which can occur.

ACKNOWLEDGMENT: Useful discussions with Dr. Engelmann are acknowledged.

REFERENCES

1) M. Porkolab: Phys.Fluids 17, 1432 (1974 and references herein.
2) A. Rogister: Phys.Rev.Letters 34, 80 (1975)
3) I. Fidone and G. Granata: to be published.

ON THE THEORY OF ELECTRONCOUSTIC WAVES IN PLASMA

M.L.Tsintsadze, D.D.Tskhakaya

Institute of Physics, Academy of Sciences of the Georgian SSR, Tbilissi, USSR

Abstract: The character of electroacoustic waves in plasma with the negative dielectric permittivity at the strong HF fields when the HF wave pressure is greater than that of hydrodynamical is investigated. Under these conditions the electroacoustic wave is the wave of compession.

The propagation of the electromagnetic waves in plasma can be accompanied by the electrostriction effects which are manifesting in the fact that HF field pressure changes the density and at the same time the medium dielectric permittivity. These modulation processes lead to the generation of the sound oscillations which are propagating in plasma with the negative dielectric permittivity in a form of solitons /1/. In these works HF electromagnetic field was assumed weak,

$$E_m^2 < 2\left|\varepsilon(\omega_0)\right| \frac{\omega_0^2}{\omega_L^2} E_c^2 , \qquad (1)$$

where

$$\varepsilon(\omega_0) = 1 - \frac{\omega_L^2}{\omega_0^2} , \qquad \omega_L^2 = \frac{4\pi e^2 n_0}{m_e} ,$$

$$E_c^2 = \frac{4 m_e \omega_0^2 T_e}{e^2} , \qquad T_e >> T_i ,$$

n_0- nonperturbed density of particles, ω_0 -HF field frequency. The condition /1/ is equal to that of HF pressure smallness in comparison with the hydrodynamical pressure. In the case of stationary waves, when all values depend upon the argument $\xi = x - ut$ the relative perturbation of the density is $\frac{n-n_0}{n_0} = \frac{V}{u}$, where V - is the projection of the hydrodynamical velocity onto X axis (we consider small perturbations $V << u$). Since the hydrodynamical pressure is greater than that of HF, the force caused by the full (hydrodynamical + high frequency) pressure is directed against the wave propagation. Hence, $V < 0$ and always we have the wave of exhaustion $n - n_0 < 0$. However, if HF pressure is greater than hydrodynamical one, the full force changes its direction, the velocity being $V > 0$, and the soliton has a character of the compression wave.

The electromagnetic wave propagation is described by the system of Maxwell equations and the equations of the plasma hydrodynamics. We will not restrict the amplitude value of HF field assuming that electrons in HF field may possess high velocity (up to relativistic values). With HF field the search values contain together with the slow dependence upon the time, the fast dependence with the characteristic time $2\pi/\omega_0$. The fast changeable ion motion is neglected. If the spatial dependence is considered sufficiently smooth $\lambda >> \frac{|V|}{\omega_0}$ (λ - the characteristic distance of the variation of slow or fast changeable values) the procedure described in /2/ can be used. By means of averaging over the period $2\pi/\omega_0$ the fast changeable motion can be isolated from the slow one. Since we take into account the relativistic character of the motions of electrons in the transvers HF field the momentum of the fast changeable motion may be found in a form of /3/:

$$P_x = P_0(\xi)\cos(\omega_0 t - \varkappa_0 \xi) , \quad P_y = P_0(\xi)\sin(\omega_0 t - \varkappa_0 \xi) .$$

When the condition of the quasineutrality is realized the equation of fast changeable motion has a form

$$\frac{d^2 P_0}{d\xi^2} - \frac{\omega_0^2}{c^2}\left\{\left|\varepsilon(\omega_0)\right| - \frac{u^2}{c^2 - u^2}\right\} P_0 \left\{K_0 + 1\right\}^{-1}\left\{1 - 2\frac{K_0}{K_m}\right\} = 0 \qquad (2)$$

$$K_0 = \left(1 + \frac{P_0^2}{m_e^2 c^2}\right)^{1/2} - 1 , \qquad K_m = \left(1 + \frac{P_0^2}{m_e^2 c^2}\right)^{1/2} - 1 ,$$

where P_m - maximum value of electron momentum. The momentum P_0 is connected with HF field amplitude by $P_0 = \frac{e E_0}{\omega_0}$. The propagation speed of the sound wave and the relative change of the density are determined by the expressions

$$u^2 = s^2 + \frac{m_e}{m_i} K_m \frac{1}{A} c^2 ,$$

$$\frac{n - n_0}{n_0} = A \frac{K_0}{K_m} << 1 ,$$

where $s^2 = \frac{T_e}{m_i}$ and the value A determines the maximum deviation of the density from its value n_0 on the infinity $\xi \to \pm\infty$. For a compression waves $A > 0$, and for the waves of exhaustion $A < 0$. The value A satisfies the equation:

$$A^2 + 2\left\{\frac{\omega_0^2}{\omega_L^2}\left|\varepsilon(\omega_0)\right| - \frac{s^2}{c^2} - \frac{1}{2}\left(\frac{\omega_0^2}{\omega_L^2} + \frac{m_e}{m_i}\right) K_m\right\} A - \qquad (3)$$

$$- 2\frac{m_e}{m_i} K_m = 0 .$$

$u^2 << c^2$ is accounted for the above formulas. If $\left|\varepsilon(\omega_0)\right| > \frac{u^2}{c^2}\frac{\omega_L^2}{\omega_0^2}$ the equation (2) has a solution vanishing on the infinity /1/. In the nonrelativistic limit $P_0^2 << m_e^2 c^2$ this solution has a form $P_0(\xi) = P_m \operatorname{ch}^{-1}\left\{\frac{\omega_0}{c}\left(\left|\varepsilon(\omega_0)\right| - \frac{u^2}{c^2}\right)^{1/2}\xi\right\}$

The analysis of the solution of equation (3) leads to the following conclusions: if $\frac{m_e}{m_i} K_m > 2\left|\varepsilon(\omega_0)\right| \frac{s^2}{c^2}\frac{\omega_0^2}{\omega_L^2}$ the only solution satisfying the conditions

$$\left|\varepsilon(\omega_0)\right| \frac{\omega_0^2}{\omega_L^2} > \frac{u^2}{c^2} > 0 \qquad (4)$$

has a form

$$A = a + \left\{a^2 + 2\frac{m_e}{m_i} K_m\right\}^{1/2} , \qquad (5)$$

$$a = \frac{1}{2}\left(\frac{\omega_0^2}{\omega_L^2} + \frac{m_e}{m_i}\right) K_m - \left|\varepsilon(\omega_0)\right| \frac{\omega_0^2}{\omega_L^2} + \frac{s^2}{c^2} .$$

For realization of the first condition (4) it is necessary that $\left|\varepsilon(\omega_0)\right| > \frac{m_e}{m_i}\left(\frac{\omega_L}{\omega_0}\right)^4$. As it follows from (5) $A > 0$, we have the compression wave and $u^2 > s^2$. If $K_m >> 2\left|\varepsilon(\omega_0)\right|$ we obtain in the nonrelativistic limit

$$\frac{n - n_0}{n_0} = \frac{1}{2}\frac{\omega_0^2}{\omega_L^2}\frac{P_m^2}{m_e^2 c^2} \operatorname{ch}^{-2}\left\{\frac{\omega_0}{c}\left(\left|\varepsilon(\omega_0)\right| - \frac{u^2}{c^2}\right)^{1/2}\xi\right\} .$$

For the weak HF fields , $\frac{m_e}{m_i} K_m < 2\left|\varepsilon(\omega_0)\right| \frac{s^2}{c^2}\frac{\omega_0^2}{\omega_L^2}$ (this condition is equal to that of (1)), the solution of the equation (3), satisfying the conditions (4) leads to the results of /1/.

References

1. V.P.Gurovich, V.I.Karpman. J.Exp.teor.fiz., 56, 1952 (1969).

V.I.Karpman, "Nonlinear Waves in Dispersing Media", M. Nauka, 1973.

2. L.M.Gorbunov, Uspekhi Fiz. Nauk., 109, 631 (1973).

3. A.I.Akhiezer, R.V.Polovin, J.Exp.Teor.Fiz., 30,915 (1956).

Electromagnetic Resonance Cones in a Bounded Inhomogeneous Plasma

F. Leuterer

Max-Planck-Institut für Plasmaphysik, EURATOM-Association, D-8046 Garching bei München

Abstract: We study the performance of a simple azimutally symmetric gap for coupling r.f. power into a plasma filled waveguide. Power flow and input impedance are computed in terms of normal modes.

We consider a cylindrical waveguide of radius a, filled with a cold inhomogeneous plasma and oriented along a magnetic field. To a gap of width d around the plane z = o we apply an r.f. voltage $U = U_o e^{i\omega t}$. The boundary conditions for the electromagnetic fields to be met are

$$E_\varphi(z,a) = 0$$
$$E_z(z,a) = U_o \cdot \frac{1}{d} \quad \text{for } -d/2 \le z \le +d/2 \tag{1}$$

By superposition of two independent solutions $y_\alpha^{(1)}$ and $y_\alpha^{(2)}$ we get the unique solution for the fields in the waveguide

$$y_\alpha(k,r) = \left[\Delta_{\alpha 3}(k,r)/\Delta_{13}(k,a)\right] \cdot E_z(k,a) \tag{2}$$

where $y_\alpha(k,r)$ is the electromagnetic field vector $y_\alpha = \{E_z, H_z, E_\varphi, H_\varphi, E_r, H_r\}$, and

$$\Delta_{\alpha 3}(k,r) = \begin{Vmatrix} y_\alpha^{(1)}(k,r) & y_\alpha^{(2)}(k,r) \\ y_3^{(1)}(k,a) & y_3^{(2)}(k,a) \end{Vmatrix} \tag{3}$$

The fields in coordinate space are obtained by reversing the Fourier transform in equ. (2). Since along the real k axis equ. (2) shows singularities whenever

$$\Delta_{13}(k = k_n, a) = 0 , \tag{4}$$

which is the dispersion relation for normal modes in the plasma filled waveguide, we apply residue calculus to obtain the following normal mode expansion for the fields:

$$y_\alpha(z,r) = U_o \sum_n \frac{F_{\alpha 3}(k_n,r)}{k_n d} \begin{cases} e^{-ik_n(z+d/2)} - e^{-ik_n(z-d/2)} & \text{, if } z > d/2 \\ e^{+ik_n(z-d/2)} - e^{+ik_n(z+d/2)} & \text{, if } z < -d/2 \\ -2 + e^{-ik_n(z+d/2)} + e^{+ik_n(z-d/2)} & \text{, if } |z| < d/2 \end{cases} \tag{5}$$

with $F_{\alpha 3}(k_n,r) = \Delta_{\alpha 3}(k_n,r) \Big/ \frac{\partial}{\partial k}\left[\Delta_{13}(k,a)\right]_{k=k_n}$

Computing Poynting's vector and integrating over the cross-section we can evaluate the power flow along the waveguide and also the input admittance of the gap which is:

$$Z^{-1} \cdot Z_o = 2\pi\alpha \sum_n F_{43}(k_n,a)\left[H_n - i G_n\right] \tag{6}$$

with $H_n = 2(\sin k_n d - k_n d)/(k_n d)^2$; $G_n = (\sin k_n d/2 / k_n d/2)^2$; $Z_o = \sqrt{\mu_o/\varepsilon_o}$.
A more rigorous theoretical derivation can be found in /1/. We have numerically computed the fields, the power flow and the input impedance for the parameters $\omega/\omega_c = 0.4$; $\omega_p^2(r)/\omega_c^2 = 0.3 \cdot \exp[-(r/a)^2]$; $\alpha\, \omega_c/c = 5$, for which we do not yet have a lower hybrid layer in the plasma. But depending on α we may have a cutoff layer $\omega_p(r) = \omega$ within the waveguide. The main characteristic of the solution is shown in fig. 1 where we show the magnitude of the real part of the Poynting vector, $|\mathrm{Re}\{S(r,z)\}|$ as it develops due to interference of radial modes if we take more and more of them into account in computing $y_\alpha(r,z)$. The resultent maximum moves radially if we move away from the exciting gap, until it reaches the opposite wall where the energy is reflected. Its trajectory is known as the 'resonance cone' from a number of electrostatic calculations /2-4/. The power flow thus is spacially confined, its radial extent increasing with the gap width d. Integrating over the cross-section we get the axial power flow which is seen in fig. 2 for various plasma profiles how it develops with the number of modes being taken into account. For a homogeneous plasma, fig. 2a, we see that for a gap width d = o ($\delta(z)$-exciter) each further mode still contributes to the power flow, while for increasing gap width we reach pretty soon a saturation, i.e. the higher modes don't contribute anymore to the power flow. In this example of the homogeneous plasma this is solely due to the $(\sin k_n d/2 / k_n d/2)$ decrease of the external excitation of the higher modes. The resulting input impedance also shows kind of a saturation and is listed in table I.

Let us now look for effects due to a density profile. In fig. 2b we do not yet have the cutoff layer within the waveguide. In this case all the essential features remain the same as for a homogeneous plasma: There is still a pronounced maximum in the Poynting vector due to interference of the radial modes. For gap width d > o we get again saturation of the axial power flow.

For steeper profiles, where we get a cutoff layer within the waveguide, the axial power flow now shows saturation even in the case of a δ-function excitation although from the external spectrum, g(k) = 1, all the higher modes should be excited with equal strength. They are however less excited due to their rapidly increasing wave impedances. The onset of this saturation occurs the earlier the farer away the cutoff layer is from the wall. In fig. 2d for example only the first three radial modes are of importance. Lacking the higher order modes, the power flow is no longer confined to a narrow cone, but the 'cone' is smeared out over a large radial extent.

All profiles treated have one thing in common: the real part of the input impedance remains nearly independent of the gap width d within its range treated, although the actual distribution of the power flow changes with d. The imaginary part however is nearly proportional to d. This fact might be important in designing a coupling device for high power plasma heating.

References:

/1/ H. Derfler, Proc. Symposium on Plasma Heating Varenna, Italy, Sept. 4 - 17, 1974, page 91

/2/ H.H. Kuehl, Phys. Fluids 5, 1095 (1962)

/3/ R. Fisher, Thesis, Calif. Inst. of Technology, Pasadena, Cal. USA, 1970

/4/ R.J. Briggs, R.R. Parker, Phys. Rev. Lett. 29, 852 (1972)

Table I. Input impedances for the various profiles treated, $Z/Z_o = X + iY$.

α	∞	0.8	0.65	0.5
X	0.03	0.12	0.23	0.47
Y	0.044 $d\omega/c$	0.11 $d\omega/c$	0.15 $d\omega/c$	0.27 $d\omega/c$

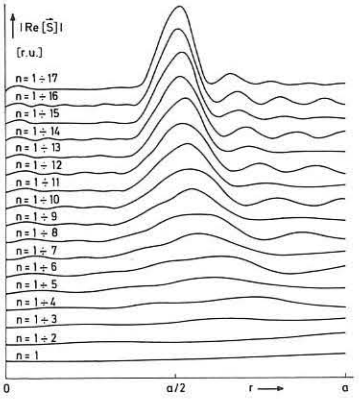

Fig. 1 Development of a resonance cone due to interference of up to 17 normal modes. Homogeneous Plasma, $\alpha =$; d = 0; $z\,\omega/c = 1.5$

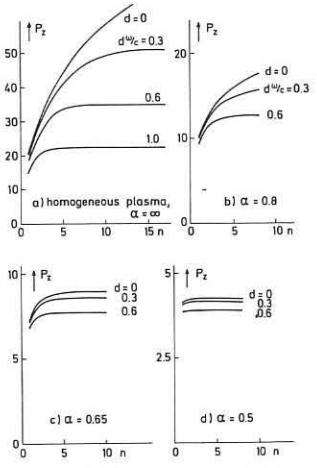

Fig. 2 Axial power flow vs. number of interfering radial modes.

ABSORPTION OF THE MICROWAVE POWER IN A TOROIDAL PLASMA

V. Kopecký, J. Musil, F. Žáček

Institute of Plasma Physics, Czechoslovak Academy of Sciences, Nademlýnská 600, 180 69 Prague 9, Czechoslovakia

Abstract: This paper deals with the experimental verification of the possibility of effective absorption of the microwave energy in the toroidal plasma at high magnetic fields satisfying condition $\omega < \omega_{ce}$, where ω and ω_{ce} are the frequency of microwaves and the electron cyclotron frequency respectively.

Recently has been shown that the microwave energy can be effectively absorbed in an inhomogeneous plasma also at magnetic fields which are higher then magnetic field corresponding to ECR, i.e. at $\omega_{ce}/\omega > 1$ [1-6]. This finding has the fundamental importance especially for h.f. heating of plasmas. The experimental results obtained up to now are, however, not sufficient to judge the perspective of such absorption for h.f. heating of CTR plasma. One of very important task is to verify this electromagnetic wave energy absorption and its efficiency in toroidal configuration, see for instance [4].

Such study was carried out in the toroidal device Intermezzo. Basic parameters of this device are following: stainless steel vacuum toroidal chamber, major radius 35cm, minor radius 4.7cm, limiter radius 3cm, continuous toroidal magnetic field of up to 2.5kG. Inside the vacuum chamber two identical spiral slow down structures are diametrically placed. These structures are coaxially fed from the magnetron 60 SA 51 (f_2= 2.35GHz, P = 0--2kW) or from the magnetron 62 SA 51 (f_1= 1.25GHz, P = 0-30kW) in pulses τ = 200-500μsec with repetition frequency f_{rep}= 50Hz. The absorption of the microwave energy at high magnetic fields $\omega_{ce}/\omega > 1$ requires a preionization [6]. The initial plasma is generated by the direct heated cathode and the plasma density N can be varied from N = 10^{10}cm^{-3} to N = 10^{12}cm^{-3}.

Main results of our experiments are given in figures.

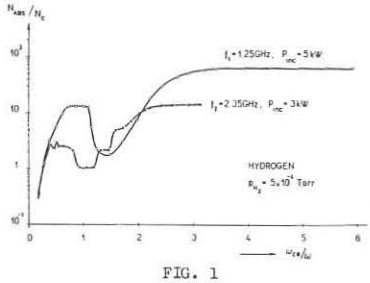

FIG. 1

Fig. 1 shows the dependence of a mean electron density N_{abs} of the hydrogen plasma created after absorption of the microwave power with frequency f_1= 1.25GHz and f_2= = 2.35GHz in the initial plasma on the magnetic field ω_{ce}/ω. Since the degree of ionization of our initial plasma was very small (≤ 1%) and practically all the absorbed energy went into neutral gas ionization, the density N_{abs} can be in the first approximation considered as a measure of the absorption of the microwave power in the initial plasma. From these measurements it is clearly seen that

(i) at high magnetic fields $\omega_{ce}/\omega > 1$ the absorption of the microwave power practically does not depend on the magnetic field;

(ii) the density of the plasma created at high magnetic fields $\omega_{ce}/\omega > 1$ is considerably higher than at low magnetic fields $\omega_{ce}/\omega < 1$;

(iii) at $\omega_{ce}/\omega \geq 2$ an overdense ($N/N_c \gg 1$) plasma can be generated; after absorption of the microwave power in the initial hydrogen plasma at pressure p = 1.5x10^{-4}Torr creates plasma with density

a) N/N_c = 15 for P_{inc}= 3kW and f_2= 2.35GHz

b) N/N_c ≃ 70 for P_{inc}= 5kW and f_1= 1.25GHz.

Fig. 2 shows the dependence of the power reflection coefficient $|R|^2$ of microwaves (f_1= 1.25GHz, P_{inc}= 100W) delivered into toroid by the first spiral structure on the density N of the plasma generated independently by the variable microwave power at frequency f_2= 2.35GHz by means of the second spiral structure. The plasma density N was regulated by the change of the microwave power f_2 from 0 to 2kW. The measurement was carried out at ω_{ce}/ω_1 = 2 and ω_{ce}/ω_1 = 4. The character of both curves given in Fig. 2 is the same. From these curves it can be seen that

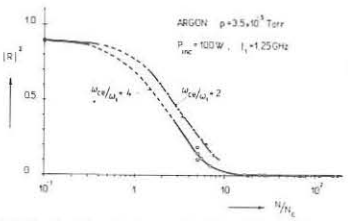

FIG. 2

(i) at $N/N_c \leq 1$ the reflection is high and the system slow down structure - plasma represents for the incident wave practically a short circuit;

(ii) in the interval $1 \leq N/N_c \leq 10$ the reflection strongly decreases from $|R|^2$ = 0.9 to $|R|^2$ = 0.1;

(iii) at $N/N_c \geq 10$ the reflection is very small ($|R|^2 \leq 0.05$) and the system slow down structure - plasma represents for the incident wave almost total impedance matching.

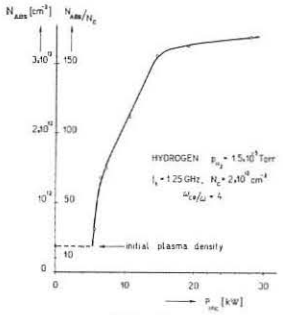

FIG. 3

The further important results of our measurements is the dependence of the mean electron density of the hydrogen plasma N_{abs}, created after absorption of the microwave energy f_1 in the initial plasma with N=2x10^{11}cm^{-3} at ω_{ce}/ω_1 = 4, on the incident power given in Fig. 3. This dependence can be divided into three regions:

(i) region of a strong increase of N_{abs}; here it is clearly seen the threshold of the incident power from which an absorption starts; this fact supports the idea that absorption mechanism is nonlinear one;

(ii) region of the linear increase of N_{abs} in the interval $P_{inc} \in \langle 7 \text{ to } 14 \rangle$ kW;

(iii) region of a slow increase of N_{abs} at $P_{inc} \gtrsim 14$kW.

The considerable deceleration of the density increase in third region is now under study. It is not excluded that the decrease of the density increase is caused by a strong decrease of the density of neutral particles. In this region the degree of plasma ionization is already high and it approaches to 50% (calculated from the mean electron plasma density).

Very important results of our measurements is also fact that the reflection of the microwave power delivered into a dense ($N/N_c \gg 1$) plasma is very low not only at small powers of incident wave (see Fig. 2) but that it remains almost zero also in the whole available interval of incident power P_{inc}= 0 to 30kW and the system slow down structure - dense plasma represents for the generator a matching load. We can expect that the same situation will take place also in the case when considerably higher powers P_{inc} > 30kW will be delivered into the dense plasma.

Conclusion: Our experiments clearly demonstrated the possibility of the efficient absorption of microwave energy in the dense ($N/N_c \gg 1$) toroidal plasma at high magnetic fields $\omega_{ce}/\omega > 1$. The existence of such absorption seems to us very promising for h.f. heating of CTR plasma. The plasma heating can be realized at relatively low frequencies in bands of cm and dm waves and this is great advantage. Today there are cm and dm generators of very high powers of the order of MW and greater which are sufficient to heat plasma in large volumes.

Very important is also the fact that the system slown down structure - dense ($N/N_c \gg 1$) plasma represents for the incident wave matched load and the microwave energy from generator can be practically without losses transferred into plasma.

The authors would like to thank Drs. J.Ďatlov and L.Kryška for developing of the directional couplers at f = 1.25GHz which enabled us to perform measurements given above.

References:

[1] Hotston E.S. et al.: Res. Rept. CLM - R78, 1968

[2] Aubert A.E. et al.: Appl. Phys. Lett. 18 (1971), 63

[3] Lisitano G. et al.: Appl. Phys. Lett. 16 (1970), 122
Phys. Rev. Lett. 26 (1971), 747

[4] Lisitano G. et al.: Res. Rept. IPP III/8 Garching, 1973

[5] Musil J., Žáček F.: Experimental study of the absorption of intense electromagnetic waves in a magnetoactive plasma, Academia, Prague 1975

[6] Kopecký et al.: Phys. Lett. 50A, No 4, 1974, 309

NONLINEAR BEHAVIOR AND STRONG DAMPING OF LARGE AMPLITUDE ALFVÉN WAVES

E. Berger, G. Müller, E. Räuchle and P.G. Schüller

Institut für Plasmaforschung, Universität Stuttgart, Federal Republic of Germany

Abstract: The influence of the amplitude of torsional Alfvén waves on wave field and wave damping in connection with plasma heating were observed experimentally. Strong wave damping is explained by turbulent resistivity.

Introduction: Propagation of large amplitude Alfvén waves and associated plasma heating was observed experimentally /1/. There results a steepening of wave fronts to switch on shocks because of the relatively low frequencies and large plasma radii. Strong wave damping was found at pertubation ratios B_φ / B_{oz} of about unity.

In this paper amplitude effects of almost monochromatically excited torsional Alfvén waves propagating in a cylindrical plasma parallel to a homogeneous axial (z-direction) magnetic field B_{oz} up to 9 kΓ are reported.

Experiment: Experiments were carried out in a quasistationary (200 µsec) plasma generated by a discharge between electrodes. Plasma parameters: length 1 m, diameter 5 cm, filling pressure 0.15 torr hydrogen, $n_e \approx 2 \cdot 10^{15}$ cm^{-3}, $T_e \approx T_i \approx 2$-3 eV. Alfvén waves with azimuthal wave amplitudes B_φ up to 5 kΓ were excited by a ringing capacitor discharge in a frequency range of 600 kcs/sec. A coaxial wave gun was used as antenna.

Measurements: In the case of small amplitudes ($B_\varphi \lesssim 100$ Γ) normal wave propagation was found. Under the condition of small nonlinearities ($B_\varphi \lesssim 500$ Γ) harmonics of the excitation frequencies were observed. Fig. 1 shows the original excited B_φ component of the wave at r = 8 mm (the point of maximal wave amplitude) and the B_z component at the same position, created by nonlinear wave-wave interaction. The B_z component is composed of a dc and a double frequency part. The nonlinear terms (vgrad)v and j x B in the equation of motion are responsible for the observed nonlinearity. Perturbation theory leads to the relation

$$B_z(2\omega_o) \propto B_\varphi(\omega_o)^2$$

which could be verified experimentally. The measured $B_z(2\omega_o)$ as function of B_φ is shown in figure 2.

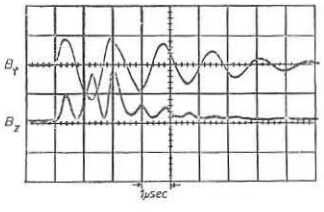

Fig. 1 : B_φ and B_z at r = 8 mm

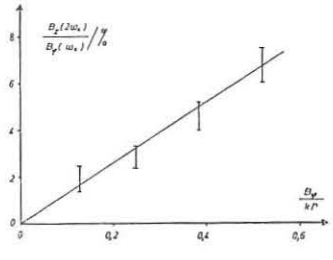

Fig. 2: Amplitude of double frequency B_z as a function of B_φ

For the above amplitude range, the damping decreased with increasing amplitudes. If the amplitudes are further raised, a strong increase of the damping was observed. Fig. 3 shows the observed damping constant d ($B_\varphi \propto e^{-dz}$) for two different magnetic field strengths B_{oz} = 5 kΓ and B_{oz} = 9 kΓ as a function of the wave amplitude B_φ.

In the low amplitude case, the Alfvén waves are damped by binary collisions (Spitzer's resistivity). The ohmic heating of finite amplitude wave causes an electron temperature raise connected with an increase in electrical conductivity, which leads to the reduced dissipation. Electron heating is observed by the appearence of multiply ionised impurity lines, such as O II, C III, CIV on the axis, where the wave current density is concentrated. Ion temperature increase up to 20 eV was measured by Doppler broadening of He II 4686 line. These measurements show that the electron temperature raises faster than the ion temperature.

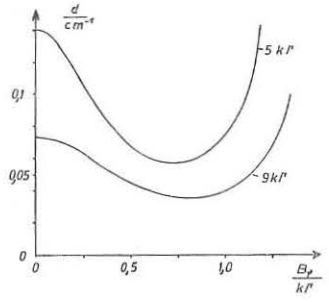

Fig. 3: Damping constant d ($B_\varphi \propto e^{-dz}$) as a function of the amplitude B_φ

Fig. 4: Normalized radial amplitude profile B_φ and connected current density j_z for two different wave amplitudes.

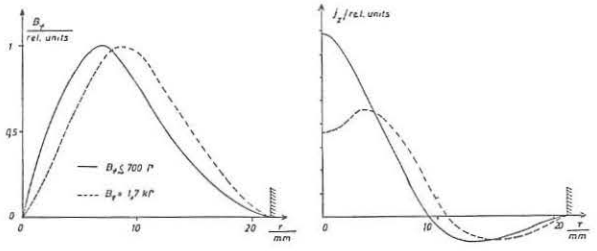

The region where the increase of the damping rate begins does not depend on the perturbation ratio B_φ / B_{oz} but on the amplitude B_φ only. At these amplitudes the current density j_z of the wave is so large on the axis that the electron drift velocity exceeds the ion sound velocity combined with $T_e > T_i$. This is the condition for the appearence of the ion sound instability, which results in a reduction of electrical conductivity and the strong wave damping. During the excitation of the wave electrostatic fluctuations were observed in the frequency range 50 Mcs/sec - 500 Mcs/sec by means of electrostatic probes, as used in /2/.

A decrease of the electrical conductivity on the axis leads also to a radial displacement of the wave field to the outer region. The dependence of the radial wave profile on the radial profile of the electrical conductivity is known under linear conditions /3/. The measured normalised profiles of $B_\varphi(r)$ and the related current densities $j_z(r)$ are shown in figure 4 for different wave amplitudes.

Conclusions: Nonlinear effects at the propagation of torsional Alfvén waves can be observed at perturbation ratios of some per cent already. At relatively small amplitudes of 10-20 %, strong wave damping is observed which does not depend on the perturbation ratio but on the wave amplitude only. This and the fact that the conditions for the ion acoustic instability are satisfied, leads to the conclusion that under the given experimental conditions the torsional Alfvén wave are damped by turbulent resistivity.

/1/ R.C. Cross and C.N. Watson-Munroe
Phys. Fluids 11, 557 (1968)

A.D. Craig and J.W.M. Paul
J. Plasma Phys. 9, 161 (1973)

/2/ S.M. Hamberger and J. Jancarik
Phys. Fluids 15, 825 (1972)

/3/ G. Müller, E. Räuchle, P.G. Schüller
Plasma Physics 15, 925 (1973)

R.F. HEATING BY MEANS OF BOUNDED ALFVEN WAVE RESONANCES IN MAGNETICALLY INHOMOGENEOUS PLASMAS.

A.M. MESSIAEN

Laboratoire de Physique des Plasmas - Laboratorium voor Plasmafysica
Association "Euratom-Etat belge" - Associatie "Euratom-Belgische Staat"
Ecole Royale Militaire - 1040 Brussels - Koninklijke Militaire School

Abstract : A gradient in the steady magnetic field such as occurs in large low aspect ratio tori only affects the magnetoacoustic resonance spectrum by internal coupling of different azimuthal modes. Furthermore the confluence between compressional and torsional Alfven waves increases strongly the absorption. This effect combined with the excitation of a bounded plasma resonance provides an attractive heating method.

Introduction. Recent heating experiments made in the ion cyclotron domain on the tokamaks TM-1[1] and ST[2] have shown the important role of the magnetoacoustic (M.A.) resonances [3,4] in coupling *rf* energy to the plasma. Even in large machines these resonances should play an important role [5]. Here the effect of steady magnetic field inhomogeneity on these resonances is investigated. This includes also the study of the effect of the confluence between the fast M.A. wave (characterized by the perpendicular wave number $k_{\perp 3}$; see details in 3,4) and the torsional Alfven wave ($k_{\perp 2}$). The behavior of $k^2_{\perp 2}$ and $k^2_{\perp 3}$ is given in fig.1 : the confluence occurs for $\omega = \omega_K$ and the zeroes of $k^2_{\perp 3}$ at $\omega = \omega_{S2}$ and ω_{S3}[4]. Typical absorption spectra in the homogeneous case are given in fig.2 for axisymmetric ($n=o$) and dipolar ($n=1$) excitation. Resonance "A" occurs at $\omega = \omega_K$ and the M.A. resonances for $\omega > \omega_{S3}$. Recent related work appears in ref.[6,7,8,9] and preliminary results of this study are given in [4].

Model. The problem is solved analytically using a plane slab model with $\frac{\partial}{\partial y}=o$ $\frac{\partial}{\partial z} = ik_{//}$ and $\bar{B}_o = B_o(x)\bar{1}z$ (see fig.3). Choosing an external $e^{-i\omega t}$ excitation characterized by $H_{za} = Fcosh(hx)exp(ik_{//}z)$ (with $h = \sqrt{k_{//}^2 - k_o^2}$) the model studied is analogous to the cylindrical case with an axisymmetric excitation, the correspondance between axes being $x \leftrightarrow r$, $y \leftrightarrow \theta$, $z \leftrightarrow z$. The exciting field induces a scattered field outside the plasma ($\propto exp(-h|x|)$). The fields induced in the plasma can be derived from the solutions of the following differential equations ($k_o^2 = \omega^2 \varepsilon_o \mu_o$) :

$$\left.\begin{aligned} &\left[\frac{d^2}{dx^2} + k_o^2\left(\frac{\varepsilon_1^2 - \varepsilon_2^2}{\varepsilon_1}\right) - k_{//}^2\right] B_x + ik_{//}^2 \frac{\varepsilon_2}{\varepsilon_1} B_y = o \\ &\left[\frac{d^2}{dx^2} + \frac{\varepsilon_3}{\varepsilon_1}\left(k_o^2\varepsilon_1 - k_{//}^2\right)\right] B_y - ik_o^2 \frac{\varepsilon_2}{\varepsilon_1}\varepsilon_3 B_x = o \end{aligned}\right\} \quad (1)$$

The ε 's are the cold plasma permittivity tensor elements (including phenomenological collision frequencies ν_e and ν_i and kinetic corrections of order zero in $k_\perp V/\omega_c$). Eq.(1) describes the fast (M.A.) and slow mode of Fig.1, where ω_K, ω_{S2} and ω_{S3} are now x dependent. Except near the confluence ($\omega_K(x)=\omega$), these modes are approximately decoupled and (1) can be then represented by

$$\left[\frac{d^2}{dx^2} + k^2_{\perp 3}(x)\right] B_{x_1} = o \; ; \quad B_{y_1} = \frac{ik_o^2\varepsilon_2}{X} B_{x_1} \quad (2)$$

$$\left[\frac{d^2}{dx^2} + k^2_{\perp 2}(x)\right] B_{y_2} = o \; ; \quad B_{x_2} = \frac{ik^2_{//}}{X}\frac{\varepsilon_2}{\varepsilon_3} B_{y_2} \quad (3)$$

with $B_x = B_{x_1} + B_{x_2}$; $B_y = B_{y_1} + B_{y_2}$; $k^2_{\perp 3} = X - \frac{\varepsilon_2^2 k_o^4}{X}$; $k^2_{\perp 2} = \frac{\varepsilon_3}{\varepsilon_1} X$; $X = k_o^2\varepsilon_1 - k_{//}^2$. $Re(X)=o$ defines the confluence plane. The slab problem is solved for $(k_{//}V_A)^2 \ll \omega_{ci}^2$ (region of the first M.A. resonances for typical values of large machines [5]), $B_o(x) = (1+\alpha x)^{-1/2} B_o(o)$ and constant density. Then $X = \bar{l}x + m$ is used as a new variable. The domain $Re(X)$ is divided in five domains (see fig.3) in which appropriate asymptotic solutions are derived. For $|X| < |\zeta| = |k_o^2 k_{//}^2 \varepsilon_2^2/\varepsilon_3|$, a fourth order differential equation is derived from (1)[4] and its solutions are given in [10]. This enables the proper connection of the solutions of (2) and (3) across the confluence. The tangential fields are then matched at $x = \pm a$ and a normalized absorbed power is computed ($\mathcal{P}'_{abs} = \left[\frac{P(x=-a) - P(x=a)}{2a\omega_o |F|^2}\right]$ with $P = Re[(\bar{E} \times \bar{H}^*).\bar{1}_z]$.

Discussion of the results. 1) The spectrum of magnetoacoustic resonances ($1,0$; $2,0$; $3,0$..) is only slightly affected by the inhomogeneity of B_o; they remain even if the confluence is in the plasma at the resonance frequency (see fig. 4). Of course, the fields inside the plasma become very asymmetrical (see fig.5). 2) The mean absorption level is strongly increased (even at very low ν) when the confluence $Re(X)=o$ lies in the plasma. The frequency zone in which this condition is fulfilled widens as α increases. This region of enhanced absorption has sharp edges and becomes the resonance A of fig.2 in the limit $\alpha \to o$. 3) The results pertaining to $\omega \ll |k_{//}V_e|$ or $\omega \gg |k_{//}V_e|$ are qualitatively similar except for the detailed coupling between E_y (fast wave) and E_z (slow wave) at the confluence (see fig.5). 4) If the homogeneous plasma is excited by a dipolar B_z field another set of resonances is excited ($0,1$; $1,1$; $2,1$ of fig.2). The first of these, ($0,1$), occurs near $\omega = \omega_K$ if $(k_{//}V_A)^2 \ll \omega_{ci}^2$ [3, 4, 5]. Inhomogeneity gives an internal coupling to the dipolar resonances even though the B_z excitation is symmetric[11]. This is seen in fig.4. In particular, for sufficiently high α, the first dipolar resonance ($0,1$) leads to strong enhancement of the field in the region with high damping due to the confluence. This last property suggests an interesting heating method for large machines : for well chosen ω, any exciting structure such that $k_{//}^2 \ll (\omega_{ci}/V_A)^2$ will excite the ($0,1$) resonance, enhancing absorption due to wave confluence. This heating is very effective : in the case of fig.4 the absorbed power P_{abs} is ~ 10 times larger than for electron TTMP at $T_e = 10^8 K$ (comparison made both near and far from a M.A. resonance). Contrary to TTMP, P_{abs} remains largely independent of T_e or ν down to very low values of these parameters.

References.
[1] Vdovin V. et al., VI Eur. Conf. Control. Fus., Contrib. papers p.553 (Moscow 1973)
[2] Adam J. et al., V Int. Conf. Control. Fus., paper IAEA-CN-33/A3-2 (Tokyo 74)
[3] Messiaen A., Vandenplas P., Weynants R., Koch R., Nuclear Fusion 15 (1975) 75
[4] Messiaen A., Proc. Symp. Plasma Heating Tor. Dev. Varenna (1974) p.55
[5] Messiaen A. Vandenplas P., V Int. Conf. Contr. Fus., paper IAEA-CN-33/C4-2 (Tokyo 1974) ; Phys. Letters 49A (1974) 475
[6] Hasegawa A., Chen L., Phys. Rev. Letters 32 (1974) 454
[7] Adam J., Takahashi H., Proc. Top. Conf. Plasma Heating (Lubbock 1974)
[8] Gould R., Int. Report, California Inst. of Technology, Pasadena (June 1974)
[9] Swanson D., Phys. Fluids, in press.
[10] Rabenstein A., Arch. Rational Mech. Anal. 1 (1958) 418
[11] In the cylindrical case there is internal coupling to all azimuthal modes.

The author thanks P. Vandenplas and D. Faulconer for stimulating discussions.

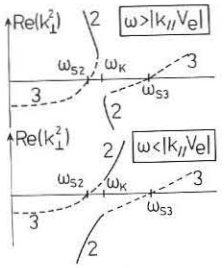

Fig.1. $k^2_{\perp 2}$ and $k^2_{\perp 3}$ versus ω.

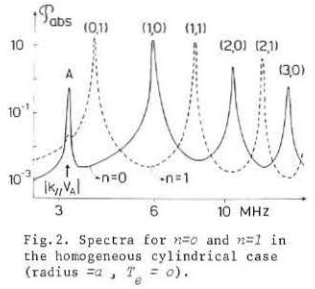

Fig.2. Spectra for $n=o$ and $n=1$ in the homogeneous cylindrical case (radius $=a$, $T_e = o$).

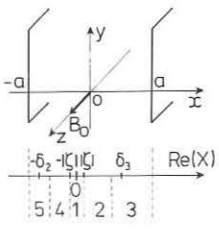

Fig.3. Slab with coordinate systems ($-\delta_2$ and δ_3 correspond to $\omega_{S2}=\omega$ and $\omega_{S3}=\omega$).

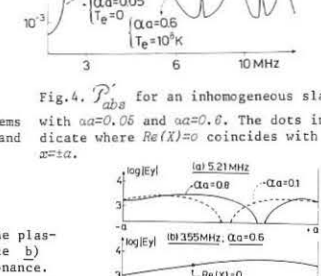

Fig.4. $\mathcal{P}'_{abs}$ for an inhomogeneous slab with $\alpha a = 0.05$ and $\alpha a = 0.6$. The dots indicate where $Re(X)=o$ coincides with $x = \pm a$.

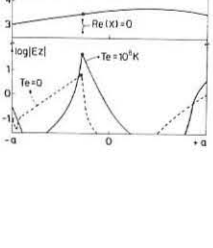

Fig.5. Behavior of $|E|$ inside the plasma a) $|E_y|$ for the ($1,0$) resonance b) $|E_y|$ and $|E_z|$ for the ($0,1$) resonance.

Parameters common to all figures : $B_o(x=o) = 45kG$; $N = 4\times10^{13} cm^{-3}$; $a = 100cm$; $k_o = 1,85\ 10^{-2} cm^{-2}$; *Deuterium*. $\nu_e = \nu_i = 25kHz$ when $T_e = o$ or electron Cerenkov damping $+\nu_i \simeq 2.5kHz$ when $T_e = 10^8 K$.

FILAMENTATION INSTABILITY OF AN ION-SOUND WAVE

E. CANOBBIO

ASSOCIATION EURATOM-CEA
Département de Physique du Plasma et de la Fusion Contrôlée
Service IGn - Centre d'Etudes Nucléaires
B.P.85 - Centre de Tri - 38041
GRENOBLE CEDEX (France)

ABSTRACT : Ion-sound waves propagating in a non-isothermal unmagnetized homogeneous plasma are unstable against modulation in the direction perpendiculat to their propagation for all amplitudes. The relevance of this and other more general instabilities from the viewpoint of plasma heating and confinement is briefly discussed.

THE GROUND STATE. We consider an unmagnetized homogeneous maxwellian plasma in the presence of an intense electrostatic wave

$$\vec{E}_o = 2\frac{E_o}{k_o}\vec{k}_o \cos(\vec{k}_o.\vec{r}-\omega_o t),\ \mathrm{Im}(E_o) = 0.$$

The ground state of the plasma is adequately described by the collisionless linear theory if /1/

$$\omega_o >> \nu_{ii} >> (\omega_o/k_o v_{ti})^3\, k_o v_{ti} |e\phi_o/T_i|^{3/2}, \qquad (1)$$

where ν_{ii} is the ion-ion collision frequency, $v_{ti} = (2T_i/m_i)^{1/2}$ is the ion thermal speed, and $\phi_o = -i E_o/k_o$. If we also assume

$$k_o v_{te} >> \omega_o >> k_o v_{ti} \quad \text{and} \quad k_o\lambda_D << 1 \qquad (2)$$

where λ_D is the Debye length, then

$$\omega_{pi}^2 >> \omega_o^2 = (k_o v_{ti})^2 .\ T_e/2T_i\ ;\ T_e >> 2T_i \qquad (3)$$

where ω_{pi} is the ion plasma frequency. Clearly, conditions (2) and (3) imply that in the pump the ions behave as a cold ideal fluid, while the electrons remain in thermal equilibrium. Moreover, in view of condition (1) we have $|e\phi_o/T_e| << \frac{1}{2}(2T_i/T_e)^{5/3} << 1$.

PERTURBATION OF THE GROUND STATE. We restrict our treatment to those three-waves parametric processes which involve a low frequency electrostatic wave $(\omega, \vec{k})$ with $|\omega| << \omega_o$, and with wave number $\vec{k}$ such that

$$\vec{k}.\vec{k}_o = 0, \text{ and } v_{te}^2 >> |\omega_\pm|^2/k_\pm^2 \equiv |\omega \pm \omega_o|^2/(\vec{k} \pm \vec{k}_o)^2 >> v_{ti}^2.$$

Here $\omega_\pm/k_\pm$ is the phase velocity of the side-bands whose presence in the plasma is required by the usual phase matching conditions.
Under the previous assumptions, $|\omega| << k\, v_{te}$, while $|\omega/k\, v_{ti}|$ is arbitrary. As a result, the electrons remain in thermal equilibrium both in the side-bands and the low-frequency mode. In contrast, the ions behave as a cold ideal fluid in the side-bands while at low-frequency the Vlasov equation is needed in order to describe their motion correctly.
Coupling between the two species as well as between the various modes is provided by the electrostatic potential which we Fourier expand in the following way :

$$\phi(\vec{r}, t)-\phi_o(\vec{k}_o.\vec{r}-\omega_o t) = \sum_{n=-\infty}^{\infty}\phi^{(n)}\exp i\left[(\vec{k}+n\vec{k}_o).\vec{r}-(\omega+n\omega_o)t\right].$$

The Fourier coefficients of the ion density may be found with the help of the Vlasov equation. We obtain

$$\begin{aligned} 4\pi e n_i^{(o)} &= -k^2\chi_i^{(o)}\phi^{(o)} - k^2\frac{e\phi_o}{T_e}\Sigma_\pm P_\pm\phi^{(\pm 1)} \\ 4\pi e n_i^{(\pm 1)} &= -k_\pm^2\chi_i^{(\pm 1)}\phi^{(\pm 1)} \mp \frac{e\phi_o}{T_e}\left[4\pi e n_i^{(o)} + 3\left(\frac{\omega_{pi}}{\omega_o}\right)^2\phi^{(o)}\right], \end{aligned} \qquad (4)$$

where $P_\pm = \pm\chi_i^{(o)}\,(1 \mp 2\,\omega/\omega_o) \mp (2\,\omega_{pi}/k\,v_{ti})^2 \times Z(x)$;

$$\chi_i^{(o)} = \chi_i(\omega, \vec{k}),\ \chi_i^{(\pm 1)} = \chi_i(\omega_\pm, \vec{k}_\pm)\ ;$$

$$\chi_i(\omega, \vec{k}) = \frac{2\omega_{pi}^2}{k^2 v_{ti}^2}(1 + x\,Z(x))\ ;\ x = \omega/kv_{ti}\ ;$$

here $Z(x)$ is the Fried and Conte Function. Higher order ($|n| > 1$) coefficients and corrections are negligible. We notice at this point that the effect of collisions would be simply to replace ω by $(\omega + i\,\nu_{ii})$ in Eqs. (4).

The electron-density Fourier coefficients corresponding to Eqs. (4) are given by the Boltzmann equilibrium equation.

THE DISPERSION RELATION. With the help of Poisson Equation we may obtain two homogeneous equations for $n_i^{(o)}$ and $n_e^{(o)}$ leading to the Dispersion Relation :

$$\frac{T_i}{T_e} + F(y) - Q\left[\frac{k_o^2}{k^2} - 3\right]\frac{1+(y/x_o)^2(1+2F(y))}{(y/x_o)^2 + \frac{1}{4}(k/k_o)^2(1+(y/x_o)^2)} = 0.$$

where :

$$y = -i\omega/kv_{ti},\ F(y) = 1-\sqrt{\pi}ye^{y^2}.\mathrm{erfcy},\ \text{and}\ Q = \left|\frac{e\phi_o\omega_{pi}}{T_e\omega_o}\right|^2.$$

As convective instabilities cannot develop in our case, only purely growing modes are possible. Marginal stability ($y = 0$) corresponds to curve A in the $(\sqrt{Q},\ (k/k_o)^2)$-plane (Fig. 1), while the growth rate becomes formally infinite on curve B as shown on Fig. 2 for several values of Q. Of course, our theory breaks down as soon as $|\omega| \to \omega_o$. As a matter of fact, very close to the curve B the instability becomes explosive in nature and has to be treated by a nonlinear theory similar to that of Ref. /2/. The main result here is that the amplitudes become infinite after a finite time $\sim |\phi_o|^{-2}$.

CONCLUSIONS. The purely growing mode described in this paper, is the low frequency version of the filamentation instability which produces standing density striations across the incident pump wave. Other instabilities may be found if we take $\vec{k}.\vec{k}_o \neq 0$. They include in particular induced Compton backscattering.
As it will be shown in a subsequent paper, filamentation and backscattering instabilities may occur, also in their explosive versions, in a variety of physical situations which include R.F. plasma heating and neutral beam injection. Althought parametric instabilities are usually quoted owing to their beneficial effects on heating, we should bear in mind that they may also constitute a potential danger from the point of view of confinement especially when they occur at the periphery of the plasma and the excited waves have rather long wave lengths. As indicated in Ref. /1/, such instabilities may explain easily both the level and the parameter dependence of the pumpout observed in the Transit Time magnetic pumping experiments. Recently, anomalous plasma behaviour has been observed also in an ion-cyclotron heating experiment /3/, when the RF-energy sent to the plasma exceeds a few hundred joules, independently of the power level. Althought our understanding of this matter is still very poor, one is tempted to attribute these phenomena to some explosive parametric instability. In this case, in fact, the product : (explosion time) x (RF-power of the pump) is a constant /2/. Then, depending on the value of this constant compared, for instance, with the thermal energy of the plasma, one might expect the instability be disruptive or not.
Similar byproducts of parametric instabilities may not be the exclusive privilege of RF-heating. Indeed, poloidal plasma rotations produced by high power neutral beam injection may also be expected to excite parametric instabilities with comparable effects.

REFERENCES. /1/ - E. CANOBBIO, IAEA Conference (TOKYO 1974), paper CN-33/C4-3
/2/ - V.E. ZAKHAROV, Soviet Physics JETP, 35, (1972), 908.
/3/ - J. ADAM et al., IAEA Conference (TOKYO 1974), paper CN-33/A3-2

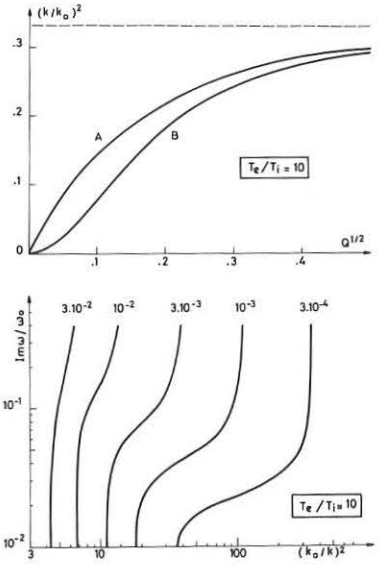

ALFVEN WAVE HEATING IN THE CONTINUUM BY KINK-LIKE MODES

A. Pochelon, R. Keller, F. Troyon, R. Gruber

Ecole Polytechnique Fédérale de Lausanne, Switzerland
Centre de Recherches en Physique des Plasmas

Abstract: The m=1 MHD spectrum of a screw-pinch is determined numerically. It is shown that modes in the Alfvèn continuum can have a kink-like behavior with the singularity deep in the center. Heating of the plasma by excitation of these modes is proposed.

Introduction: Heating by absorption of singular Alfvèn modes in the continuum has been suggested some time ago by W. Grossmann and J. Tataronis [1,2]. There are two main problems: the first is to understand the absorption and conversion mechanisms at the singular layer, the second is the problem of accessibility of the plasma core. We are concerned here with the second problem.

To gain some feeling for the spectrum and for the dependence of the modes structure on the various parameters of the equilibrium we use a 1D code based on a finite element expansion [3] which approximates well the continuum as well as the discrete part of the spectrum already with few points. As equilibrium we choose an infinite plasma cylinder of circular cross-section confined by an axial and an azimuthal field, surrounded by a concentric conducting shell, with:

$$B_z(r) = B_z(a)\sqrt{1-\beta\cdot(1-r^2/a^2)}\ ;\quad B_\theta(r) = 2\,B_\theta(a)\,\frac{r}{a}\,(1-\frac{r^2}{2a^2})$$

$$\rho(r) = \frac{\rho(o)}{2}\left[1+\rho_a+(1-\rho_a)\cos\frac{\pi r}{a}\right].$$

a is the plasma radius and R is the shell radius;

The m = 1 spectrum

The computed low-frequency part of the spectrum is shown in Fig. 1, for the following values of the parameters: $\beta = .2$, $\rho_a = .2$, $B_\theta(a)/B_z(a) = .02$, $R = 5$, representing a screw-pinch equilibrium. In abcisse we have the safety factor q at the plasma surface $q \equiv -ka\,B_z(a)/B_\theta(a)$; the frequency is normalized to an Alfvèn transit frequency $\Omega^2 \equiv \omega^2\,a^2\,\rho(0)/B_z^2(a)$.

The fast modes, also called magnetosonic, form a well separated discrete spectrum in the frequency range $1 \lesssim \Omega^2 \lesssim 10^3$; they are not visible on the scale of Fig. 1. The slow wave, or sound wave, continuum extends downwards to $\Omega = 0$ for all q. This is due to the assumption that it is the temperature which vanishes at the edge of the plasma and not the density. This is more reasonable than the inverse. The Alfvèn continuum is in an intermediate range of frequency, extending down to $\Omega = 0$ whenever q(r) vanishes somewhere in the plasma. The discrete mode which seems to pass through the continuums without loosing its character is the kink. For $q \gg 1$ it looks very much as the lowest member of the fast wave family. As q is lowered, it becomes lost in the Alfvèn continuum in the vicinity of $q = 1$. At the same time the weakly unstable internal kink mode, which is already unstable at $q = 2.3$, suddenly changes character, giving rise to the much more unstable external kink, as if the descending mode was reemerging from the continuum. As q becomes negative the kink becomes stable again, crossing the slow wave continuum with no change and eventually entering the Alfvèn continuum. As it approaches the continuum it retains its character of a global mode, except for a progressive peaking at the center which will turn into a singularity at the origin as it reaches the end-point of the continuum (Fig.2). For values of q and Ω near the point of contact the eigenfunctions in the continuum still look like a kink mode except for the singular surface deep in the plasma.

The heating scheme

We propose to make use of the good coupling between the core of the plasma and the vacuum surrounding the pinch by exciting a mode in the continuum which has a frequency Ω and a wavelength q in the vicinity of the merging point. Because of the long wavelength the excitation of the kink-like mode will be easy. The values of q and Ω are not critical as long as they are adjusted to keep the singular point in the core, which means staying close to the lower edge of the continuum.

It should be noted that the value of $|q|$ at the merging point is larger than the limit of stability of the external kink, but that it falls in the range of the internal kink which does not usually bring problems. It may be safer to push the operating $|q|$ above 2 and raise the heating frequency accordingly, while still having good coupling to the singular layer.

Extension to other configurations

The scheme is based on the fact that the lower boundary of the Alfvèn continuum at the merging point corresponds to modes having a singularity at the center of the plasma. In general the lower boundary is given by

$$\Omega^2 = \mathrm{Min}\left\{\ (k\,B_z + B_\theta/r)^2/\rho\mu_o\ \right\}$$

There are three possibilities: the minimum is reached at the center of the plasma, at the edge of the plasma and at some intermediate point. In the second case the kink will evolve differently near the merging point, peaking at the surface where the singularity will first appear. This is a bad case for the heating since it would be only peripheral. In the third case modes near the lower edge of the continuum have two singular points. Only the most exterior one is relevant. If it is deep enough the scheme will work just as well as in the first case.

Taking realistic profiles for pinches or Tokomaks we find that the second case never occurs, but the third case does occur frequently. It turns out that the minimum is very sensitive to details of the fields and density profiles, particularly on their relative widths. It should be noted that for sufficiently large values of $|q|$ the minimum always occurs at the center.

This work was supported by the Swiss National Science Foundation.

References

1) Tataronis, J.A., Grossmann, W., Z.Phys. 261, I & II (1973)

2) Tataronis, J.A., Grossmann, W., 2nd Top.Conf. on RF Plasma Heating Lubbock (19747

3) Appert, K., Berger, D., Gruber, R., Troyon, F., Computer Phys.Commun. (to appear).

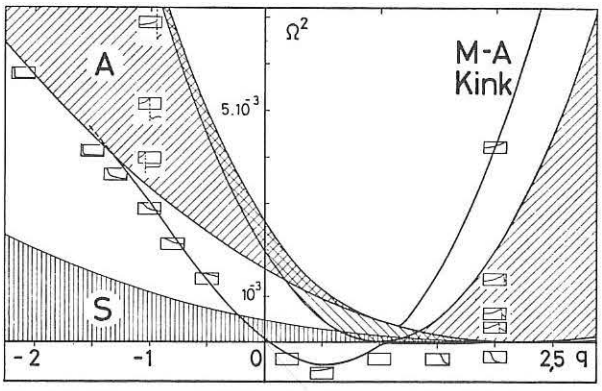

Fig. 1: Low-frequency part of the m=1 spectrum of a screw-pinch. S = slow-wave continuum, A = Alfvèn continuum. Singly hatched region = one singularity, doubly hatched region = two singularities. M.A. = magneto-acoustic.The internal kink is barely visible between q=1 and q=2.3. The radial component of the eigenvector is shown in the rectangles, the center being on the left.

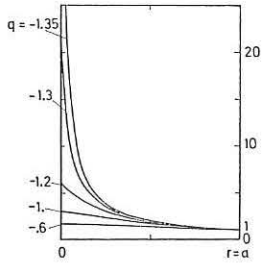

Fig. 2: Radial component of the eigenvector normalized to its boundary-value, for values of q on both sides of the merging point. At q=-1.35 the kink has already reached the continuum.

ALFVÉN WAVE HEATING OF FUSION PLASMAS

J. Kappraff
New Jersey Institute of Technology
Newark, New Jersey, U.S.A.

and

J.A. Tataronis and W. Grossmann
Courant Institute of Mathematical Sciences
New York University
New York, New York, U.S.A.

Abstract: In this paper we consider the effects of resistive dissipation on the energy absorption by the spatially localized Alfvén waves which form a part of the continuous spectrum of ideal magnetohydrodynamics (MHD). We demonstrate that the strong absorption rate found in ideal MHD is unaltered for plasma resistivities on the order of that found in Tokamaks, thus implying the possibility of effective heating of these machines by Alfvén waves.

It is well known that supplementary heating will be necessary to bring the Tokamak plasma into the ignition regime. One of the many methods currently proposed for Tokamak heating is through use of resonant Alfvén waves.[1] The basic theory of the energy absorption has been given by Tataronis[2] using the ideal MHD equations of motion. An extension of the plasma model to that of the guiding center plasma (GCP) has also been made and the results of these basically ideal (inviscid, perfectly conducting) models indicate the possibility of very effective energy absorption at frequencies much lower than ion cyclotron or lower hybrid. This paper concerns itself with an investigation of non-ideal effects on the energy absorption. In particular the effect of resistivity is investigated.

The bases of the absorption process in ideal MHD are the logarithmic singularities which occur in space in the distribution of the linearized plasma velocity of the Alfvén mode. These singularities render the continuum eigenfunctions of the linearized MHD operator non-square integrable and the energy content of the mode unbounded.[2] As an example of the rate at which energy can be transferred to these singular modes, we show in Fig. 1 a possible coil structure yielding a surface current $\underline{J}$ with periodicity λ along the z axis of the plasma column. We assume that the frequency of $\underline{J}$ is ω and we measure the absorption in terms of the real part of the impedence Z of the coil, where the real part of Z is a consequence of the singularities in the Alfvén mode.[2] Figure 2 shows the absorption rate for plasma parameters typical of the ST Tokamak. Since ideal MHD has no dissipation mechanisms, the energy absorbed is not transformed to heat. We therefore introduce here a non-zero resistivity in the fluid equations and calculate the Ohmic heating rate in the Alfvén mode. It will turn out to be identical to the ideal MHD absorption rate for the small resistivities found in Tokamaks.

The specific plasma configuration we study is identical to that of Ref. 2, namely, a planar sheet pinch with the equilibrium magnetic field, $\underline{B}$, parallel to the z-axis of an x,y,z Cartesian coordinate system. All equilibrium quantities depend on x alone. The plasma is confined to the region $-b < x < b$, and is surrounded by a vacuum region, where an externally supported sheet current is present parallel to the z-axis similar to Fig. 1. Assuming incompressibility, the linearized resistive equations are those of ideal MHD[2] but with Ohm's law in the form $(\underline{E}+\underline{v}\times\underline{B}) = \eta\underline{J}$.

We fourier analyze the perturbations with respect to time and the coordinate z and combine the linearized equations to form the following system:

$$(A\xi_x')' - k^2\xi_x = \frac{f\eta}{\omega\mu}(Q_x'''' - 2k^2Q_x'' + k^4Q_x) \qquad (1a)$$

$$Q_x'' = (k^2 + \frac{\mu i\omega}{\eta})Q_x - \frac{\omega\mu f}{\eta}\xi_x \qquad (1b)$$

where $f = kB(x)$ and $A(x,\omega) = \rho(\omega^2-\omega_a^2)$. Here k is the wave number along the z axis, η is the resistivity, ξ_x and Q_x are respectively the x components of the plasma displacement and the perturbed magnetic field, $\omega_a^2(x)$ ($\equiv f^2/\rho\mu$) is the square of the local Alfvén frequency, μ is the permeability of free space, primes (') denote partial differentiation with respect to x, and i has been written for $\sqrt{-1}$. If η is formally set equal to zero in Eq. (1a), one recovers the ideal MHD equation for ξ_x, the solutions of which can possess a logarithmic singularity about the zeros of A, $x_o(\omega)$, i.e., where ω equals the local Alfvén frequency. This singularity is not present for η different from zero, implying the existence of a resistive boundary layer for small η about $x_o(\omega)$. The energy which accumulates at x_o in ideal MHD is dissipated in this layer. To compute the rate of energy dissipation, the system (1) is scaled with respect to η and then solved in the resistive layer. The solutions are then matched to those of the outer regions describable by the ideal MHD equations.

The relevant scaling in the resistive layer, as established by Boris,[4] is $x-x_o \sim O(\eta^{1/3})$. Therefore, after introducing the normalized variable s by $(x-x_o)/a = \epsilon^{1/3}s$ where $s \sim O(1)$ and ϵ is dimensionless and of order η, the system (1) can be developed in η and combined to yield the following equation for ξ_x:

$$i\xi_x'''' + \alpha(s\xi_x')' = 0,$$

α depends on the equilibrium and is taken to be constant in the layer. The asymptotic form of the solutions to this equation are trivially shown to be the following:

$$\xi_x \sim \begin{cases} -\frac{i\pi}{2} + \ell n(-s) + c_1 + \ldots, & s \to -\infty \\ \frac{i\pi}{2} + \ell n(s) + c_2 + \ldots, & s \to \infty \end{cases} \qquad (2)$$

where c_1 and c_2 are constants. These asymptotic solutions are connected onto the ideal MHD solutions for ξ_x in the outer region by imposing continuity of (ξ_x'/ξ_x) at the limits of the boundary layer. Recognizing that to leading order, Eq. (2) is identical to the connection formula that one must impose across the logarithmic singularity in ideal MHD,[2] one concludes that the fields outside the resistive layer are identical, to leading order in η, with the corresponding fields found in Ref. 2. Since the impedance of the external coil is derived from the vacuum fields, one can then conclude that the coil impedance implied by the resistive equations assumed here is identical to the impedance found in Ref. 2 to leading order in η and hence that the absorption predicted by ideal MHD implies Ohmic heating in the resistive layer.

To obtain an estimate of the time required for the absorbed energy to be dissipated by the resistivity, we need the time behavior of the perturbed fields in the resistive layer. It is a straightforward calculation to derive $\xi_z(x,t)$ from the incompressibility condition $\xi_x' - ik\xi_z = 0$ and from the integral form of $\xi_x(x,\omega)$ in the resistive layer. After performing an inverse Fourier transform with an external force assumed at frequency ω_o, one finds

$$\xi_z(x,t) \sim e^{i\omega_o t}\int_o^{\bar{t}} \exp(-(t'/t_\eta)^3)\,dt' \qquad (3)$$

where $t_\eta^3 \sim 3/c^3$, c being a constant independent of η. Let t_h be the time at which $\bar{t} = 1$, i.e., $t_h = \eta^{-1/3}/c$. Then for $t << t_h$, Eq. (3) reduces to $\xi_z(x,t) \sim t\exp(i\omega_o t)$, which is the behavior of ξ_z found in ideal MHD,[2] while for $t >> t_h$, Eq. (3) implies a pure sinusoidal oscillation at ω_o. Therefore, for times up to t_h, one finds ξ_z growing linearly in t with the energy simply accumulating in the layer without dissipation. Beyond t_h, the fields saturate, and the absorbed energy is dissipated. We therefore take t_h as the heating time. It can be shown that t_h is related to the equilibrium fields in the following way:

$$t_h = \left(\frac{2\mu_o}{\eta\omega_o^2}\right)^{1/3}\left(\frac{2B'}{B} - \frac{\rho'}{\rho}\right)^{-2/3} \qquad (4)$$

A computation with parameters typical of the ST Tokamak yield $t_h \sim 10\mu$ sec. Since the confinement time t_c of Tokamaks is on the order of m sec., one has $t_h << t_c$. This fact together with the large absorption rates shown in Fig. 2 suggests significant energy transfer to the plasma.

One final estimate that we make here is that of the effective width of the resistive layer in Tokamak devices. This is accomplished from the relation $dW/dt = \int \eta J^2 d\tau$ as derived from the equations of motion. W is the total plasma energy and the integration is carried out over the resistive layer. By using for dW/dt the expression given in Ref. 2, one finds from the above relation Δx, the width of the resistive layer:

$$\Delta x = 8\pi\left(\frac{\eta}{\mu\omega_o}\right)^{1/3}\left(\frac{2B'}{B} - \frac{\rho'}{\rho}\right)^{-1/3}$$

For typical ST parameters this evaluates to about 10 ion Larmor radii.

References:

1. J.A. Tataronis and W. Grossmann, Z. Phys. 261, I and II (1973); W. Grossmann, M. Kaufmann and J. Neuhauser, Nuc. Fusion 3, 462 (1973).
2. J.A. Tataronis, J. Plasma Phys. 13, 87 (1975).
3. J.A. Tataronis and W. Grossmann, Proc. 2nd Topical Conf. on RF Plasma Heating, Lubbock, Texas, 1974, Paper A-6.
4. J. Boris, Thesis, Princeton Univ., Princeton, N.J., 1968.

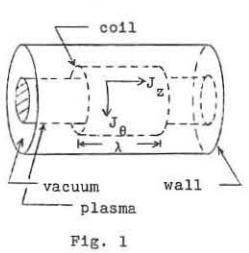

Fig. 1

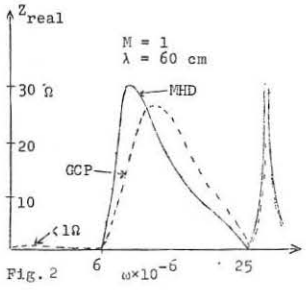

Fig. 2

EXPERIMENTS ON MAGNETOACOUSTIC OSCILLATIONS IN A ROTATING PLASMA

E. Tennfors, J. Bergström and M. Bureš
Royal institute of Technology,S-100 44 Stockholm 70, Sweden

Abstract: The damping of oscillations in a tuned external circuit is used to determine the coupling of RF-power to a rotating fully ionized plasma. The lowest magnetoacoustic resonance seems to offer the best coupling in the present case, but other resonances are also observed.

1. Introduction: In the internal ring device FLASK FIVB a fully ionized rotating plasma is created by means of crossed electric and magnetic fields. To enable magnetic shielding of the supports of the internal ring the rotation has to be stopped and the associated heating mechanisms replaced by some other method. The lowest magnetoacoustic resonances about 1 MHz has earlier been used for this purpose [1,2,3]. This resonance has also been studied by the excitation of eigenoscillations during the rotating phase [4,5]. The aim of the present work is to examine the coupling between the existing external coil systems and the plasma when the frequency is varied and the plasma is sustained by rotation.

2. Experimental arrangement: The FLASK FIVB [1,6] is run with an average magnetic field B_o=0.33 T in the mid-plane. The filling gas is hydrogen or deuterium with an initial pressure of 30×10^{-3} torr. The particle density is 10^{21} m^{-3}.

Two pairs of coils are available in the device. The coils earlier used for heating [1-5] (the "generator" coils) encircle the plasma about 10 cm above and below the mid-plane respectively. The other pair (the "pulse" coils) were used for the current pulse which excited the eigenoscillations [3,4] and are located closer to the mid-plane. The circuit is tuned by a variable capacitor and closed by an ignitron. The energy initially stored in the circuit is small compared to the plasma energy content.

3. Experimental results: The radial current J_r and the voltage ϕ_{12} across the rotating plasma are shown in Fig.1 as functions of time for a hydrogen plasma. The external ringing circuit is fired at t_o=400 μs when the voltage and thus the velocity of rotation is rather high. The damping of the current oscillations is determined for varying frequency and different combinations of the coils. A rogowski coil around the plasma measures the azimuthal plasma current J_φ. In addition to the forced oscillations, J_φ shows that eigenoscillations are excited. In the case of Fig.1, the eigenfrequency turns out to be 0.85 MHz while the external current oscillates at 2.15 MHz.

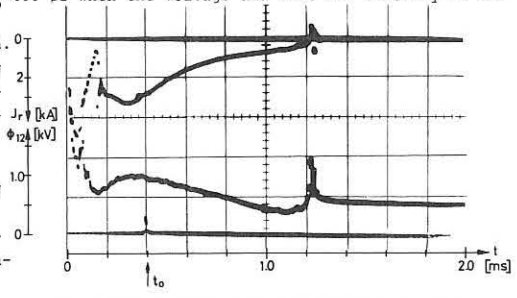

Fig.1.Radial current J_r and voltage ϕ_{12} for a rotating hydrogen plasma in FIVB.

The damping of the oscillations can be expressed in terms of an equivalent series, r_s, or parallel, R_p, resistance in the external circuit. $1/R_p$ is a measure of the total power loss in the system for a given voltage over the coils.

Fig.2 shows the r_s- and $1/R_p$- spectra for coupling between the "pulse" coils connected in series with currents in the same direction. Open circles refer to the damping in absence of the plasma. Both representations reveal a strong resonance just below 0.9 MHz in agreement with the measured eigenfrequency. An additional smaller peak is observed at ≈2.1 MHz. Parallel connection of the coils give higher frequencies and indicates a peak between 3.5 and 4 MHz. When the current is reversed in one of the pulse coils, only a weak resonance at ≈2.8 MHz is observed.

Fig.3 shows the situation for the "generator" coils, 10 cm above and below the mid-plane. Again, the coils are connected in series and carry currents in the same direction. The resonance now appears at ≈1.1 MHz. Part of the earlier observed discrepancy between the eigenfrequency and the optimum heating frequency ≈1.3 MHz [1-5] seems to be due to the location of the generator coils. The remaining difference may be explained by the change in resonance frequency with the velocity of rotation [4,5].With reversed current in one coil, the first resonance remains. This indicates an asymmetry in the coil-wall current system. Higher frequency resonances seems to be poorly coupled to the "generator" coils.

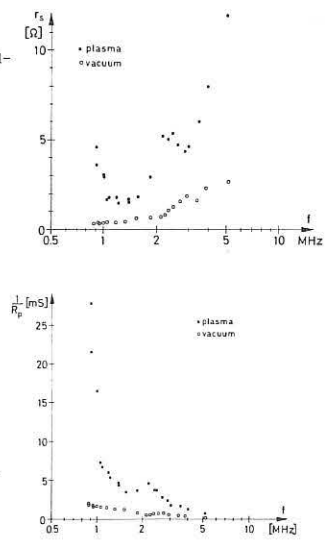

Fig.2.Equivalent resistance spectra for the "pulse" coils.

In part of the eigenoscillation measurements, [4,5] RF-power at 2.8 MHz was fed to the plasma by the "generator" coils with currents in opposite directions. The present results show no significant resonance there for hydrogen. For a deuterium plasma a small bump occurs around that frequency.

The level of $1/R_p$ in the cases earlier used for heating and the voltages then applied over the coils agree with the estimated power inputs of 0.5-1 MW.

The equivalent series resistance, r_s, increases steeply at higher frequencies in all the cases. It is not clear if this is a characteristic of the plasma or of the external circuits.

4. Conclusions: In the present set-up only the lowest magnetoacoustic mode can be used to increase the power to a few MW with reasonable coil voltages. The frequency has to be more carefully chosen than before and the "pulse" coils should be used to get the highest coupling.

The other peaks may grow with plasma temperature, but are poorly coupled to the present coil systems.

Earlier indirect estimates of RF-power coupled to the plasma [1-5] are confirmed by the present measurements.

This work has been supported by the Swedish Atomic Research Council and the Bank of Sweden Tercentenary Fund.

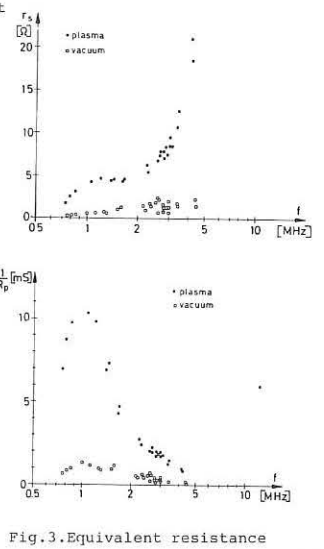

Fig.3.Equivalent resistance spectra for the "generator" coils.

References:

[1] B.Lehnert,J.Bergström,M.Bureš,E.Tennfors and B.Wilner, Plasma Physics and Controlled Nuclear Fusion Research, 1, IAEA, Vienna(1971),59.

[2] B.Lehnert,J.Bergström,M.Bureš,S.Holmberg and E.Tennfors, Physica Scripta,Vol.9,109-118,Stockholm(1974).

[3] B.Lehnert,J.Bergström,M.Bureš and E.Tennfors,Fourth Europ. Conf.on Contr.Fusion and Plasma Phys.,CNEN,p.102,Rome(1970).

[4] M.Bureš and E.Tennfors,Royal Institute of Technology,Stockholm,TRITA-EPP-72-84,(1972).

[5] M.Bures,E.Tennfors and B.Thorstensen,Sixth Europ.Conf.on Contr.Fusion and Plasma Phys.,Vol.I,p.575,Moscow(1973).

[6] E.Tennfors,J.Bergström and M.Bureš,Royal Institute of Technology,Stockholm,TRITA-EPP-74-24(1974).

EXPERIMENTAL INVESTIGATION OF THE INTERACTION OF MODULATED UHF OSCILLATIONS WITH PLASMA

S.I.Nanobashvili, G.I.Rostomashvili, N.L.Tsintsadze
Institute of Physics, Academy of Sciences of the Georgian SSR, Tbilissi, USSR

Abstract: The possibility of HF energy input to the ultrahigh frequency discharge plasma by means of UHF power modulation is experimentally shown in this paper, when the modulation frequency is equal to the ion-cyclotron one.

As it is known, recently heating by means of electromagnetic waves of UHF and HF ranges is successfully used as an additional method of plasma heating in thermonuclear devices. Methods are being worked out and experiments are in progress on the heating of both electron and ion components of plasma. It is taken into account that in the real thermonuclear devices, at temperatures close to thermonuclear ones, the energy exchange time between electrons and ions will be much less than the time necessary for its containment. Hence it is of no meaning, in which component the energy should be introduced. However, it is noteworthy, that for providing the greatest stability in the heating process it is desirable to have a possibility of realizing of independent heating of electrons and ions. As the experiments show, while the electromagnetic energy input into the thermonuclear devices in UHF range may be realized comparatively easily, in HF range essential technical difficulties have to be overcome.

Therefore, it is of interest to study the possibility of simulteneous HF and UHF energy input into the plasma by means of modulating of UHF oscillations with a low frequency. It is taken in mind, that the carrier (UHF) frequency should be close to the frequencies which are characteristic of plasma electron component and the modulation frequency- to the frequency of plasma ion component.In this paper the possibility of modulated UHF oscillation input into the magnetoactive plasma is experimentally investigated.The experiments were performed on the stationary device described in /1/. Plasma was created in the quartz vessel, dia.5.7cm, length 110cm (Fig.1).The vessel was located in the cylindrical waveguide intended for the propagation of the wave of TE_{11} type in 12 cm wavelength range.For matching with waveguide tract the end of the vessel was made of conical shape. The UHF radiation source operated in the continuous regime at the frequency of the order of 2.4GHz and power 20w.

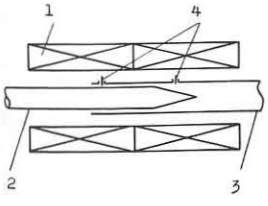

1. Solenoid
2. Quartz tube
3. Waveguide
4. Electrical prob

Fig.1

By means of a modulator it was possible to realize the modulation of UHF oscillations amplitude with adjustable modulation depth (up to tens percent) in the wide range of its frequency variation (50Hz to 5 MHz). The discharge vessel with the waveguide was located in the stationary homogeneous magnetic field which was smoothly changed from zero to electron-cyclotron value (H_e=850 Oe).In the described experiments argon was used as an operating gas. Plasma was formed in the electron-cyclotron resonance regime at the pressure of the operating gas in the vessel of the order of $7 \cdot 10^{-3}$torr.

In the course of the experiment the amplitude of the low frequency component of amplitude-modulated UHF power incident onto the plasma was registered by means of the probe introduced across the waveguide in the conical part of the discharge chamber. The detected signal from the probe was registered by the low frequency spectrum analyser. In the experiment the modulation frequency of UHF signal was smoothly changed at the fixed magnetic fields, the modulation depth being maintained at the same level. It turned out that the amplitude of low frequency component of modulated UHF signal has an explicitely expressed minimum when the modulation frequency (ω_m) approaches the ion cyclotron frequency (ω_{Hi}). This dependence is shown in Fig.2. One can see the analogy between this phenomenon and the decreasing of the voltage in lumped circuits which is associated with the decrease of the quality of the contour; in our case the modulation frequency at the ion-cyclotron resonance ($\omega_m = \omega_{Hi}$) is absorbed by the plasma. It is also experimentally established that with the change of the magnetic field shift of the frequency of the minimum takes place corresponding to the change of ion-cyclotron frequency. As concerns the change of the modulation depth, it does not practically affect neither the position of the minimum of the modulation frequency, nor the relative value of the minimum itself.

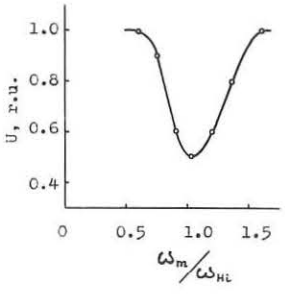

Fig.2

The experiments have shown that the change of the modulation depth in the wide range (from 0 to 50%) does not cause the appearance of the UHF signal supplied to the probe introduced in the end of the cylindrical waveguide and the limits of the range of plasma existence in the magnetic field do not change and coincide with the limits defined in /1/. It can be apparently concluded from these data that the amplitude modulation does not affect the efficiency of the absorption of UHF wave itself and does not change the mechanism of its absorption which was studied in many papers (see for example /2/).

Thus the performed experiments have shown the possibility of HF energy input into the plasma by means of UHF power modulation that allows to heat simultenеously both electron and ion components of plasma.

References

1. S.I.Nanobashvili, G.I.Rostomashvili, N.L.Tsintsadze. J.Techn.Fiz., 45, 445, 1975.
2. V.E.Golant, A.D.Piliya. Uspekhi Fiz.Nauk, 104, 413, 1971.

THE COLLISIONLESS DISSIPATION OF MICROWAVE RADIATION IN BOUNDED PLASMA

V.I.Barinov, I.R.Gekker, V.A.Ivanov, D.M.Karfidov

P.N.Lebedev Physical Institute, Moscow, USSR

Abstract: For initial conditions favouring and not favouring the linear transformation of waves, a series of experiments were performed on the interaction of S-band electromagnetic radiation with bounded isotropic collisionless plasma ($\ell \lesssim \lambda$) over a wide range $v_E/v_{Te}=10^{-5}$–6.

Collisionless plasma heating by electromagnetic radiation in the absence of an external magnetic field is a problem arising in the study of laser thermonuclear fusion. Model experiments in various ranges of wave length λ and of plasma size ℓ are important for a better understanding of the physical processes. For example, under laboratory conditions dissipation of microwave radiation is studied in a plasma with $\ell=(0.1\text{–}10)\lambda$ /1,2/. In this work we were founding conditions for the efficient collisionless dissipation of S-band electromagnetic radiation in a bounded plasma with $\ell \lesssim \lambda$.

The investigations were conducted on an installation (Fig.1) with H_{11} wave in a circular metal waveguide 10, the inner diameter of which was d=14cm $< \lambda_g$, where λ_g is the wave length in a vacuum waveguide. The flow 1 of collisionless plasma ($\nu/\omega \sim 10^{-5}$) created by a spark source 3 was injected into the region of interaction with the microwave through a diaphragm with a metal grid in the movable piston 2. Plasma velocity was $\approx 10^7$ cm/sec and electron temperature $T_e \approx 3$eV. Plasma density was measured by miniature, screened single-electrode probes 6 and 9. Multigrid probe 7 and probe-plate 8 analysed currents of fast electrons. A reflected microwave impulse power was registered by a direct coupler. The coefficient of microwave absorption $D^2=1-R^2$, where R^2 is the coefficient of microwave power reflection. The gas pressure was $\sim 10^{-6}$ torr.

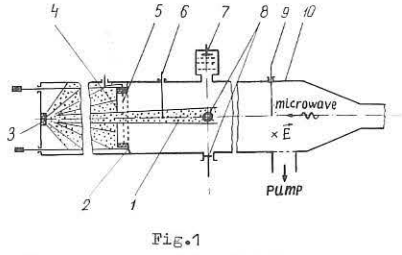

Fig.1

For the creation of initial conditions favouring the linear transformation of waves, the flow diameter was limited by a special diaphragm 4 with orifice $d_1=3\text{cm} \ll d < \lambda_g/3$. Piston 2 was placed at a distance of $\approx$70cm from source 3. The auxiliary plasma cut-off system 5 /4/ formed a sharp plasma flow front $\ell_f \sim 0.1\lambda_g$ (Fig.2a, the lower trace is a signal from probe 6 with and without plasma cutting) or short plasma bunch $\ell_\delta \sim \lambda_g/2$ (Fig. 2b, the lower trace is a signal from probe 6). The plasma density has a parabolic radial profile.

In weak fields ($v_E/v_{Te} \ll 10^{-5}$; $v_E=eE_0/m\omega$, E_0–maximum travelling wave field, $v_{Te}=\sqrt{T_e/m}$) the microwave absorption in a bunch $\ell_\delta < \lambda_g/2$ occured only if at a point on the axis at a distance $\lambda_g/4$ from the plasma cut-off system 2 the plasma density $n_0 > n_c$, where n_c is the "critical" density. The absorption increase with n_0 and D^2 amounted to tens persents (Fig.2a,b, upper trace is reflected microwave signal). This dissipation is associated with linear transformation and the experimental curve for D^2 correlate well with the theoretical calculation /5/.

An absorption process began instantly at all levels of electromagnetic field E_0 ($v_E/v_{Te}=10^{-5}$–6). For example, oscillograms of reflected microwave power in Fig.2c are for $v_E/v_{Te}=6$ and initial $n_0/n_c=2.5$. The higher impulse corresponds to the reflection from piston 2, the lower impulse to reflection from plasma flow, which has a length $\ell = \lambda_g$. For this plasma flow, the experimental curves of D^2 as a function of n_0/n_c and v_E/v_{Te} are plotted in Fig.3a. The experimental data are taken for $t=0.3\mu\text{sec} \gtrsim t_f$, where t_f is the duration of the microwave impulse front. If $v_E/v_{Te}=10^{-5}$–10^{-1}, values of D^2 are close to one another, but with the an increase of the value $v_E/v_{Te} > 0.1$ the coefficient D^2 decreases. This decrease can be attributed to intense plasma decay throughout the microwave impulse front. Complete decay of dense plasma ($n_0 > n_c$) takes place during $t \lesssim 0.5\mu$sec if $v_E/v_{Te} > 0.1$. In the dense plasma, fast electrons were generated along $\bar{E}$. The average energy of fast electrons ($n_0 \approx 1.5n_c$) was $\bar{\mathcal{E}}_e(\text{keV}) \approx 1.5E_0(\text{kV/cm})$. The current of fast electrons $j \sim E_0$ but reached saturation when $v_E/v_{Te} \gtrsim 0.5$. The maximum energy of accelerated electrons then exceeds by more than 10^3 times the thermal and oscillatory energy of electrons. The energy of ions in radial directions reached a value $\sim$10keV for $v_E/v_{Te} \sim 1$. If $n_0 < n_c$, microwave absorption and fast electrons had not been observed within the limits of sensitivity of the apparatus.

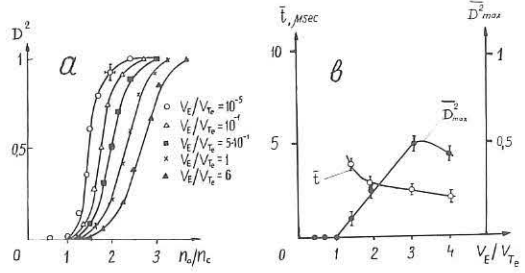

Fig.3

In the next series of experiments /6/, piston 2 was placed at a distance of 5cm from source 3. Now the initial diameter of plasma flow was 8 or 13cm. Plasma flow had practically homogeneous density distribution along the radius at a distance of 40cm from piston 2. This in combination with the high density gradient near the waveguide wall was a guarantee of the absence of intense linear transformation in the initial dense plasma. The microwave generator was switched on when the plasma flow was in the region of probe 6, which located at a distance of 70cm from plasma source 3. Maximum density was $n=2n_c$ at this point. The length of plasma front reached $\ell_f=(1\div2)\lambda_g$. In these experiments, intense absorption occured with a time delay, and if $v_E/v_{Te} \gtrsim 1$. Threshold field corresponds approximately to equality of wave pressure $E_0^2/8\pi$ and plasma pressure n_cT_e. In Fig.3b are plotted the averaged dependence of time delay $\bar{t}$ and D^2_{min} vs v_E/v_{Te}. A similar result was obtained also in the case of formation of sharp dense plasma front $\ell_f \approx 0.1\lambda_g$ at a distance of 70cm from source 3. For $v_E/v_{Te}=5$, oscillograms are presented in Fig.2d, where the upper trace is a reflected microwave signal and the lower trace is probe 6 signal.

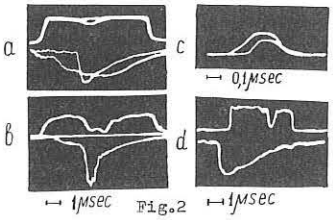

Fig.2

Investigations with two plasma probes placed in the same cross section at 40cm from probe 6 showed that during the time delay t plasma was retarded and deformed. The plasma front density increased especially at the centre of waveguide, where $\bar{E}^2$ was a maximum. Flow deformation was practically absent when $v_E/v_{Te} \lesssim 0.7$. If pulse duration $\tau > t$ and $v_E/v_{Te} > 1$, intense decay of plasma flow was observed. The control experiments showed that artificial deformation of plasma density profile can create the conditions for intense absorption even for a weak electromagnetic wave owing evidently to linear transformation.

Thus, in a bounded dense plasma with $\ell < \lambda$, intense and momentary collisionless microwave dissipation takes place in a strong field ($v_E/v_{Te} \sim 1$) if the initial conditions are favourable to linear transformation. In the opposite case, intense dissipation occured with a time delay, and only for $v_E/v_{Te} \gtrsim 1$. Deformation of plasma front preceedes the beginning of microwave absorption. This may indicate that occuring process is of the linear transformation type.

References:

/1/ STENZEL R.L., WONG A.Y., KIM H.C., Phys.Rev.Lett., 32, 654/1974/
/2/ BATANOV G.M., GOLANT V.E., Proc.XI Intern.Conf.on Phenom. in ionized gases, Prague, Invited paperes, 169/1973/
/3/ BARINOV V.I., KARFIDOV D.M., Plasma Physics /to be publ./
/4/ BARINOV V.I., Short Reports on Physics, PhIAN, №6, 8/1971/
/5/ PHEDOROV V.I., JYPh, 41, 680/1971/
/6/ BARINOV V.I., GEKKER I.R., IVANOV V.A., KARFIDOV D.M., Plasma Physics /to be published/

EXPERIMENTAL INVESTIGATION OF THE INFLUENCE OF LIMITERS IN r.f. HEATING DISCHARGES

A. Lietti

Ecole Polytechnique Fédérale de Lausanne - Switzerland
Centre de Recherches en Physique des Plasmas

Abstract: In linear rf discharges with diaphragms the current is not limited by the Kruskal-Shafranov condition but by the electron density of the gas surrounding the plasma column. The experiment agrees with a recent theory and accounts for previous controversial reports on the efficiency of limiters to improve oscillating field penetration. Energy transfer in the discharges have been investigated. At lower densities, anomalous conductivity has been observed.

The apparatus has already been described elsewhere [1]. Hydrogen gas is contained in a discharge tube of 15 cm diameter and 114 cm length which is equipped with end electrodes and situated within a solenoid which produces a 0.4 T axial constant field. The filling pressure ranges from 5 to 180 mTorr. To ensure breakdown at lowest pressure and partial preionisation, a 6 MHz, 40 KV prepulse is applied to two auxiliary electrodes. The 6 μs, 2.7 MHz, non decaying main discharge is produced by special line generators. The current ranges from 1 to 20 kA.
Two quartz diaphragms with an hole of 4 cm diameter and placed 74 cm apart, operate as limiters.

Controversial results have been reported about the efficiency of the limiters to control an rf axial current and to improve the penetration of the oscillating magnetic field [2-5]. In this experiment the dynamics of the plasma column has been investigated as follows: a) analysis of the voltage-current function [1]; b) magnetic probe measurements; c) image-converter camera photographs.
The result of these measurements is reported in Fig. 1 and 2. The existence of a critical current I_{cr} is evident. The expansion of the plasma column when $I > I_{cr}$ cannot be related to the Kruskal-Shafranov instability m = 1 mode, which occurs in unidirectional discharges, for the following reasons: 1) The column expands faster with increasing density (Fig. 2), the contrary could be expected in the case of K.S. instability. 2) Photographs do not show any m = 1 instability, but only symmetrical expansion of the column. 3) The growth rate of the K.S. m = 1 mode in the equivalent d.c. discharge has been estimated to be in all the experimental conditions smaller than the rate of change ω of the oscillating current. As a consequence, dynamical stabilisation would be expected. The observed expansion of the plasma column agrees with a recent theory [6] which considers the propagation of Alfvèn waves in the space between the diaphragms, the critical parameter being $\varepsilon = \omega L/2 V_A$ (L = tube length, V_A = Alfvèn speed). When $\varepsilon \ll 1$ the discharge is controlled by the limiters. The electron density in the space surrounding the plasma column has been deduced from interferometric measurements. We found that the density increases with current, and that $\varepsilon = 1$ corresponds to a current of 4 kA. In fact, we consider this result as approximate. The Alfvèn speed has been deduced from the estimated density, on the basis of the filling gas mass. This way impurities can somehow introduce an error. Even if we consider this point, we believe that the observed enhanced expansion of the plasma column, as well as the pressure dependance, agrees reasonably well with the theory.

The plasma produced by the discharge in the 15 - 20 kA range has been investigated as follows:
1) Average electron density has been measured with an He-Ne laser Mach-Zehnder interferometer [7]. Fig. 3 shows typical radial profiles, η being the ratio of the electron density to that which corresponds to complete ionisation of the filling gas.
Consider the discharge at 10 mTorr, 20 kA. We note that after 5 μs, η > 1, meaning that additional particles (wall interaction) increase the density.

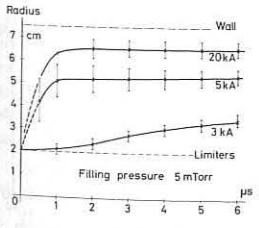

Fig. 1 Time evolution of the plasma column radius at different discharge currents.

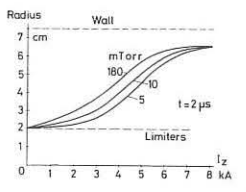

Fig. 2 Dependance of the plasma column radius on the current at different filling pressures.

2) The average transverse energy $W_\perp = k\,(n_e T_{e\perp} + n_i T_{i\perp})$ has been evaluated by diamagnetic measurements obtained by means of an electrostatically shielded loop in the center of the discharge tube. The measure has been carefully checked, as usual, to insure freedom from secondary effects originating from plasma mass motion and from rf spurious coupling. Fig. 4 shows the time evolution of the 10 mTorr, 20 kA discharge. From Fig. 5 a nearly linear dependance of $W_\perp$ and I_z^2 is deduced.
The electrical conductivity σ has been deduced from the skin depth measurement, which has been made by means of a probe introduced normally to the axis in the center of the discharge tube. Fig. 6 shows the time average of the skin depth and conductivity as a function of the filling pressure. We note that σ has a maximum, corresponding to a critical pressure p_{cr}. If $p > p_{cr}$, σ decreases. This behaviour agrees with a classical conductivity, the temperature indeed decreases with increasing pressure. On the contrary the decrease in σ if $p < p_{cr}$ shows an anomalous heating, which cannot be explained by the classical theory. At the lowest pressure an average electron temperature of $40 \cdot 10^4$ K° has been estimated in the 20 kA discharge. This results

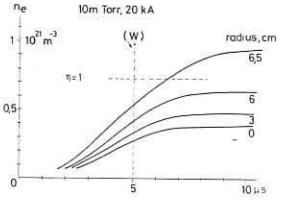

Fig. 3 Time evolution of the electron density at different radius. I_z = 20 kA

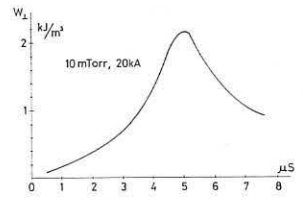

Fig. 4 Time evolution of the transversal energy density

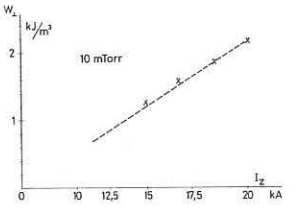

Fig. 5 Transversal energy density as a function of the current. The dotted line represents I^2 dependance.

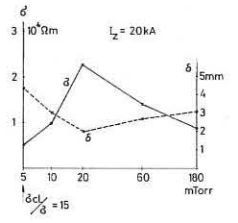

Fig. 6 Skin depth δ, and electrical conductivity σ as a function of the filling pressure

from simultaneous measurements of average density and thermal energy, as discussed before, and from the assumption $T_e \gg T_i$. On these grounds the measured conductivity is 15 times lower than the classical one. This shows that, at lower densities, the conductivity becomes anomalous in this discharge. We mention that the behaviour of σ as a function of pressure is consistent with previous measurements of the total electrical resistance of the discharge [1]. At the maximum thermal energy, shown in Fig. 4, the ratio of the drift velocity to the sound velocity has been estimated 1,3. Ion-acoustic instability can therefore produce the observed anomalous conductivity.

References:

[1] A. Lietti and M. Roux, Z. Angew. Math. Phys. 25, 674 (1974)

[2] V.P. Gordienko, L.V. Dubovoi and I.M. Roife, Sov.Phys.JETP 27, 185 (1968)

[3] L.V. Dubovoi, V.P. Fedyakov and V.P. Fedyakova, Sov.Phys.JETP 32, 805 (1971)

[4] G. Becker, O. Gruber and H. Herold, 4th Conf.Proc. Madison, Nuclear Fusion (IAEA 1971), Vol. I, p. 277

[5] F. Hofmann and A. Simik, Lab.Report 74 (1973) EPF, Centre de Recherches en Physique des Plasmas, Lausanne

[6] I.R. Jones, J.M. Peiry and F. Troyon, Nuclear Fusion 14, 497 (1974)

[7] A. Heym, Plasma Physics 10, 1069 (1968)

HEATING OF PLASMAS BY CURRENT-INDUCED TURBULENCE IN A SMALL TOKAMAK

H.W. Kalfsbeek, B. de Groot, T.G.A. Winkel,
H. de Kluiver, and H.W. Piekaar

Association Euratom-FOM
FOM-Instituut voor Plasmafysica
Rijnhuizen, Jutphaas, The Netherlands

Abstract: In a small Tokamak-like device hydrogen plasmas with densities between 3×10^{19} - 5×10^{20} m^{-3} are heated by induction of supercritical toroidal currents ($u > c_s$; ¼ T = 3 μs). Anomalous plasma conductivity has been deduced. Appreciable electron and ion heating occurs.

The apparatus

The vacuum vessel is a four-segmented quartz-torus, R = 0.46 m, r = 0.09 m. The torus is surrounded by a thick copper shell, divided into four 90° segments connected to heating and preionization banks. The shell serves for the toroidal current conduction as well as for plasma equilibrium. The main heating bank is 125 kJ, 50 kV. The maximum loop voltage is presently approximately 50 kV, corresponding to an E-field of 20 kV/m in the plasma. The current can be crowbarred at a preset time.

Plasma formation is brought about by r.f.-power capacitively coupled to the plasma volume in combination with a 10 kJ, 5 kV (¼ T - 70 μs) high inductance capacitor bank. Plasma densities could be varied between 3×10^{19} - 3×10^{21} m^{-3}. B_{tor} is 2 Tesla. Vertical field coils can slowly adjust the position of the plasma column.

Diagnostics

Data of voltage and plasma current are taken every 100 ns. The plasma resistance has been computed after correction for inductive terms. The plasma pressure and the position of the column have been deduced from diamagnetic loops and sets of sine-cosine and Mirnov coils, respectively. The plasma density has been monitored by microwave interferometry and laser Thomson-scattering diagnostics. The occurrence of ion-acoustic instabilities is sensitively demonstrated by the e.m.-radiation signals near f_{pi} (0.4 - 10 GHz).

The electron temperatures have been measured by Thomson-scattering with a ruby laser.

A preliminary determination of the ion energy distribution has been obtained by means of time of flight measurements of charge-exchanged neutrals near the periphery of the plasma column with a secondary emission detector.

Results and discussion

In Fig. 1 a, b, c, and d, voltage, current, radiation between 0.4 and 10 GHz, and plasma resistance are shown as a function of time for a specimen discharge.

Fig. 2a shows the energy density $w(\tau)$ of the same shot, both from $w(\tau) = V_{pl}^{-1} \int_0^\tau I^2(t)R(t)dt$ and the diamagnetic loop signal; Fig. 2b gives the corresponding poloidal β.

Voltage and current traces of numerous discharges show that up to 4 μs a strong anomalous resistivity exists. The termination of this anomaly is evident by the abrupt disappearance of e.m.-radiation in the ion-electron two-streaming and ion-acoustic regions.

Data for the effective resistance have been derived by $R(t) = \left[V(t) - L\frac{dI(t)}{dt}\right] / I(t)$, during the period of turbulence. A high first spike is always found during approximately 0.1 μs probably due to a skin-like current layer. This current layer diffuses rapidly onto a rather uniform current profile, as is confirmed by measurements of $B_\phi(r)$ with an array of small magnetic pick-up coils. From our resistivity data we find $\nu_{eff} \approx 0.5\,\omega_{pi}$. This value is accounted for by the mechanism of the growth and the saturation of strong ion-acoustic instabilities[1].

Evidently, below a certain threshold for the E-field and for too low a value of T_e/T_i, the turbulent friction rapidly diminishes, preferably first near the plasma axis, where the conditions for the onset for instabilities are marginal. This gives rise to a peaking up of the current profile (magnetic probe measurements) with an apparent increase in the real part of the plasma impedance by dL_{pl}/dt.

Therefore, the integral expression for the energy density $w(\tau)$ is only reliable up to the time of termination of plasma turbulence. After crowbarring the total current decreases rapidly, preferentially near the plasma (limiter) boundary at r = 0.085 m, due to skin effects resulting in a further steepening of the current profile. This deteriorates plasma confinement in the crowbar stage.

By insertion of the radial current profile in the afterglow, as measured with the magnetic multiprobe - the current decay can be completely accounted for by computer simulation.

In Figs. 3 and 4 the energy density, $w(\tau)$, in kJ/m³ and (T_e+T_i) in keV are given as functions of bank voltages and plasma density, respectively. Figure 4 also shows β_{pol} at t = 8 μs, derived from the diamagnetic loop signal. Diamagnetic loop data for $w(\tau)$ agree with those obtained from $\int_0^\tau I^2(t)R(t)dt$. At a density of 6×10^{19} m^{-3} T_e is 400 eV, as deduced from laser diagnostics. At lower densities the energy distribution is not completely Maxwellian, consisting of a colder part near 200 eV and a hotter tail of electrons heated up to 1000 eV.

Presumably in the skin region the ions are heated up to 1000 eV, whereas the ion temperature near the axis is a few hundred eV.

The position of the column never changed more than 1.0 - 1.5 cm during turbulence and afterglow. During the heating the q-value at the plasma boundary is never much below 1.

In conclusion

It has been found that effective electron and ion heating occurs in plasmas, near 10^{20} m^{-3} by strong ion-acoustic turbulence in a Tokamak-like device. No major plasma losses occur during the heating process. For plasma confinement after heating power crowbarring is found to be necessary.

Acknowledgement

The authors are greatly indebted to Prof. C.M. Braams for valuable discussions on the work's progress.

The careful design and the construction of the apparatus by the technical staff of the Institute is gratefully acknowledged. Thanks are due to Messrs C.J. Barth and A.G. Kuipers for their share in the laser measurements.

This work was performed under the Euratom-FOM association agreement with financial support from ZWO and Euratom.

References

[1] H. Schrijver, Physica 70 (1973) 358.

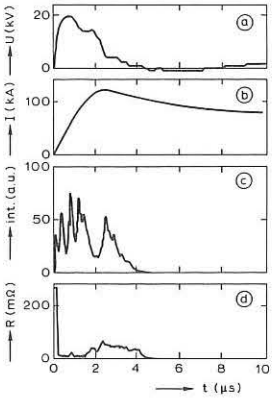

Fig. 1.
Some discharge characteristics:
a) voltage, b) current,
c) e.m.radiation 0.4 - 10 GHz,
d) resistance after correction for inductive terms.
B = 1.5 T; $n_p = 6\times10^{19}$ m^{-3};
V_c = 25 kV.

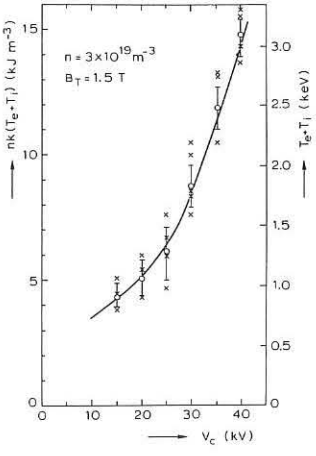

Fig. 3.
The energy density and temperature (at t = 4 μs) versus the bank voltage at constant electron density.

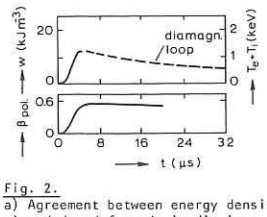

Fig. 2.
a) Agreement between energy densities deduced from Joule dissipation (up to 4 μs, full curve) with values from diamagnetic loop signals (dotted curve).
b) β_{pol}.
B = 1.5 T; $n_p = 6\times10^{19}$ m^{-3};
V_c = 25 kV.

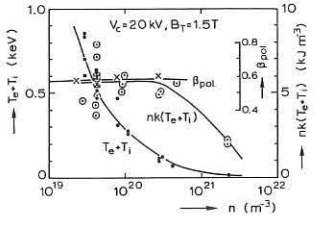

Fig. 4.
The energy density and the temperature (at t = 4 μs) and β_{pol} (at t = 8 μs) versus the electron density at a constant bank voltage.

PLASMA BEHAVIOUR IN STRONG ELECTRIC FIELDS : A COMPARISON BETWEEN COMPUTER AND LABORATORY EXPERIMENTS

S.M. HAMBERGER, L.E. SHARP, M. WOODWARD* and W.H.M. CLARK✓
Culham Laboratory, Abingdon, Oxon, OX 14 3DB, UK.
(Euratom/UKAEA Fusion Association)

The results of laboratory turbulent heating experiments and computer simulation are compared and contrasted for the cases of strong, quasi-steady applied electric fields, and shown to disagree quite markedly.

Many computer simulations[1,2] have been made to explore the response of collision-free plasma to quasi-steady ($T \gg \omega_{pe}^{-1}$), strong ($E \gtrsim m v_e \omega_{pi}/e$) applied electric fields. All show essentially the same behaviour, despite differences in dimensionality, T_e/T_i, etc: there is first a period of free-acceleration while the drift velocity $v_d(t)$ increases to $v_d \sim v_e(0)$; once $v_d \gtrsim v_e$, two-stream electrostatic instability occurs (with $k_\parallel \lambda_D \sim 1$); the ensuing turbulent fluctuations then scatter (heat) the drifting electrons until $v_e \gtrsim v_d$, thus removing the source of instability; the whole process then repeats indefinitely on a time scale $\sim 10\,\omega_{pi}^{-1}$. Thus the system stays close to marginal stability, i.e. $\langle v_d(t) \rangle \approx \langle v_e(t) \rangle$ where averaging is over times $\sim 10\,\omega_{pi}^{-1}$. Provided (as in the simulations) energy is conserved, it follows that (a) $v_d \simeq v_e \propto t$, i.e. the current and temperature increase indefinitely with time; (b) the effective collision frequency $\nu \approx t^{-1}$ and the conductivity $\sigma \approx \frac{ne^2}{m} t$. Hence the plasma responds as an inductive rather than a resistive circuit element (i.e. conductivity is an unsuitable parameter), while electrons still runaway despite the fluctuations, whose spectrum remains concentrated at short wavelength (ion-acoustic instability is too slow-growing to be important).

Table I - Parameters of the Two Laboratory Experiments

Configuration	TWIST	THESEUS
	Toroidal Stellarator	Linear Q-Machine
Plasma density (cm^{-3})	10^{12}	10^{9}
Ion	H^+	K^+
Plasma dimensions (cm)	r = 5 , R = 32	r = 1.5 , L = 80
Voltage pulse (max)	100 kV	100 V
E(V/cm) (max)	500	1
Pulse duration (μs)	0.3	2
I_{max} (A)	$\lesssim 10^4$	< 1
T_{eo} (eV)	$\sim$ 3	0.2
T_e (max) eV	$> 10^4$	20 - 80
$B_\parallel$ (kG)	3	3
Diagnostics	Magnetic, Microwaves, X-rays, etc.	Electron Wave Dispersion
Repetition rate (sec^{-1})	10^{-2}	10^{2}

TABLE II

	Stellarator	Q-Machine
$\frac{Ee}{m v_e \omega_{pi}}$	4	2 - 7
$\omega_{pi}\,\tau$	~ 200	~ 80
$\frac{\omega_{ce}}{\omega_{pe}}$	~ 1	~ 10
$\frac{\omega_{ci}}{\omega_{pi}}$	3×10^{-2}	3×10^{-2}

Quite different behaviour is, however, seen in two laboratory experiments which, although very dissimilar, both satisfy the necessary criteria (strong, quasi-steady E; sufficient energy confinement) and whose parameters are summarized in the Tables.

Typical results from TWIST[3] are shown in Fig.1: the conductivity, which is derived from the current and voltage waveforms while making a proper allowance for circuit inductance (i.e. introducing a self-consistent current distribution), remains approximately constant around the value $\sigma \simeq 0.5\left(\frac{M}{m}\right)^{\frac{1}{2}}\omega_{pe}$ found earlier at $\dot{I} = 0$ in strong electric fields[4]. The current waveform is resistive, and with peak value ~8 kA. A prediction based on the computer experiments (shown in Fig.1) would be a longer rising current pulse with maximum value ~ 50 kA (corresponding to an inductively limited current). Although the highly resistive phase clearly starts at the appropriate threshold for two-stream instability ($v_d \gtrsim 1.4\, v_e(0) \simeq 2 \times 10^8\,cm\,s^{-1}$) it persists well past current maximum, i.e. for $v_d/v_e \lesssim 0.1$. Electrostatic probe signals show a wide frequency spectrum[5] including evidence of two-stream instability, despite the fact that $v_d < v_e$. The electron temperature estimates (from X-ray spectra) are consistent with good confinement of the dissipated electrical energy.

Fig.1

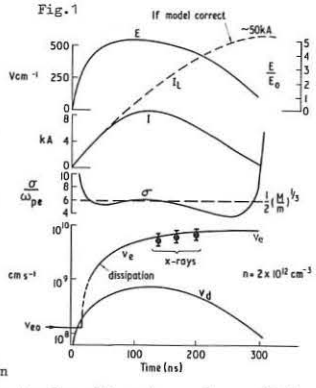

In the linear alkali-plasma experiment[6] the electrical data are supplemented by time resolved measurements of long-wavelength electron wave dispersion from which instantaneous values of n_e, v_d, v_e and higher moments of f(v) can be obtained. The solid points in Fig.2 show how σ varies with $v_d/v_e(0)$ for different applied fields: it falls rapidly when $v_d \gtrsim 1.3\, v_e(0)$ (the theoretical threshold for instability when $T_{eo} = T_{io}$) and reaches an approximately constant value which again corresponds closely to the empirical formula quoted above. The values of σ at peak current in two toroidal experiments are also shown for comparison, appropriately normalized. (In these cases $T_e(0) > T_i(0)$ so the threshold is less well-defined.) Typical temporal behaviour is shown in Fig.3: as in Fig.1, instability occurs when $v_d > v_e(0) \approx 2 \times 10^7\,cms^{-1}$, after which v_e rises faster than v_d so that $v_d < v_e$. The conductivity remains constant, while the rate of electron heating agrees well with the energy input up to $\tau \approx 1.0$-$2\,\mu s$ (depending on maximum temperature reached) after which some electron heat loss occurs.

Fig.2

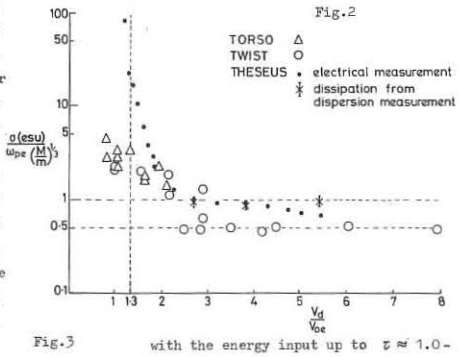

Fig.3

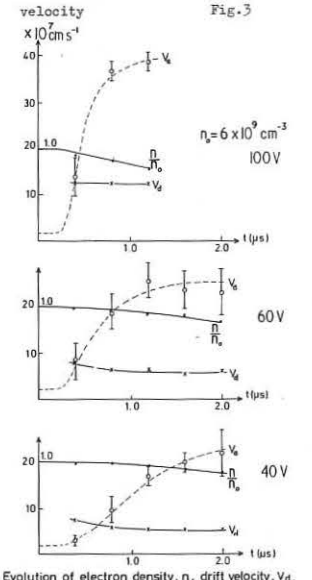

Evolution of electron density, n, drift velocity, V_d, and r.m.s. velocity V_e, (in the electron drift frame) for three different voltage pulses.

In the hope of reconciling this serious discrepancy we have tried various ways to make the simulations more realistic, e.g. by including: (a) 2-dimensions (to allow growth of off-axis modes) for various M/m; (b) an initial spectrum of ion-acoustic fluctuations; (c) skin-current profiles; (d) spatially periodic initial density perturbation (to simulate electron magnetic trapping, so allowing e-e interactions[2]); (e) a programmed variation in E to simulate the effect of circuit inductance on the current rise; (f) a sequence of constant E followed by constant current, etc. In no case does the result show any significant departure from the general asymptotic behaviour seen in the simple cases, i.e. $v_d \sim v_e \propto t$; $\sigma \propto t$, etc. An example of case (e) with M/m = 100, $E/E_o \approx 1$ is shown in Fig.4 which illustrates the same behaviour. Thus we are forced to conclude that some other form of plasma instability, probably not purely electrostatic in nature, must be involved in these situations.

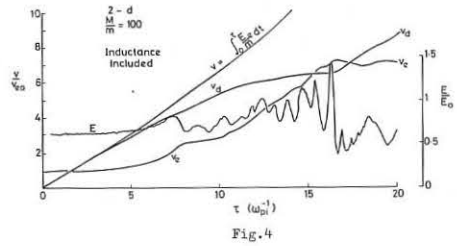

Fig.4

REFERENCES

[1] BORIS, J.P., DAWSON, J.M., ORENS, J.H. and ROBERTS, K.V., Phys. Rev. Letts., 25, 706, 1970.
BISKAMP, D. and CHODURA, R., Proc. IAEA (Madison), vol.II, 265, 1971.
MORSE, R.L. and NIELSON, C.W., Phys. Rev. Lett., 26. 3, 1971.
ORENS, J.H., NRL Memo No.2850, 1974.

[2] WHITFIELD, D.W.A., Ph.D. Thesis, University of Saskatchewan, Sept. 1971.

[3] HAMBERGER, S.M., JANCARIK, J., SHARP, L.E. and ALDCROFT, D.A. In 'Plasma Physics and Controlled Nuclear Fusion Research', IAEA (Madison), vol.II, 1971.

[4] HAMBERGER, S.M. and FRIEDMAN, M., Phys. Rev. Lett., 21, 674 (1968).

[5] HAMBERGER, S.M. and JANCARIK, J., Phys. Fluids, 15, 825 (1972).

[6] HAMBERGER, S.M. and CLARK, W.H.M., (These proceedings).

* Also at Mathematical Institute, University of Oxford.
✓ Also at Dept. of Engineering Science, University of Oxford.

ANOMALOUS RESISTANCE AND TURBULENT HEATING IN A Q-MACHINE

S.M. HAMBERGER and W.H.M. CLARK *

Culham Laboratory, Abongdon, Oxon, OX 14 3DB, UK.
(Euratom/UKAEA Fusion Association)

Anomalous resistance and non-classical electron heating are observed during the passage of large current pulses ($v_d > v_{eo}$, $t \sim 2\mu s$) along a Q-machine plasma column. The results are quantitatively consistent with those found in pulsed turbulent heating discharges in toroidal devices.

Results on the response of plasma to strong electric field pulses, analogous to those observed in toroidal turbulent heating experiments[1], have been obtained using a single-ended Q-machine plasma (K^+, $n \approx 6 \times 10^9$ cm^{-3}, $T_{eo} = T_{io} = 2500$ K, $r = 1.5$ cm, $L = 80$ cm, $B_\parallel = 2$ kG) operating under conditions such that effects caused by the electrodes (e.g. energy losses and sheath acceleration) are unimportant. A positive voltage pulse ($V \leq 100$ V, $t_r \simeq 20$ ns, length $\tau \approx 2\mu s$, repetition rate 100 s^{-1}) is applied to the cold end-plate (Fig.1(a)); as a result axial currents ≤ 600 mA, corresponding to $v_d/v_{eo} \sim 5 - 10$, are passed. For comparison, the temperature limited thermionic emission is ~ 6 A.

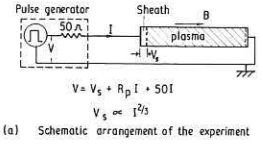

(a) Schematic arrangement of the experiment

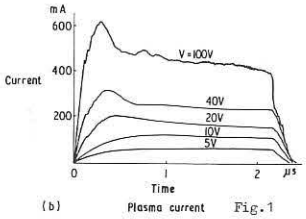

(b) Plasma current Fig.1

In addition to the conventional measurement of macroscopic quantities (e.g. V, I) Fig.1(b), the time- and space-resolved properties of the electron gas can be obtained unambiguously by measuring the dispersion of lightly damped, axially propagating electron plasma waves, launched from a fixed exciter probe with known frequencies ω (typically $\sim 500 - 800$ MHz). Using a fast (~ 0.3 ns) sampling technique, the local wavelength (and direction) of the excited waves can be found with a time resolution ~ 10 ns.

Measurements are made (a) in the unperturbed plasma ($t < 0$); (b) with electron drift; (c) against the drift (for $0 < t < \tau$). Typical results are shown in Fig.2 for $t = 0$, 300, and 1000 ns at a position half-way along the column.

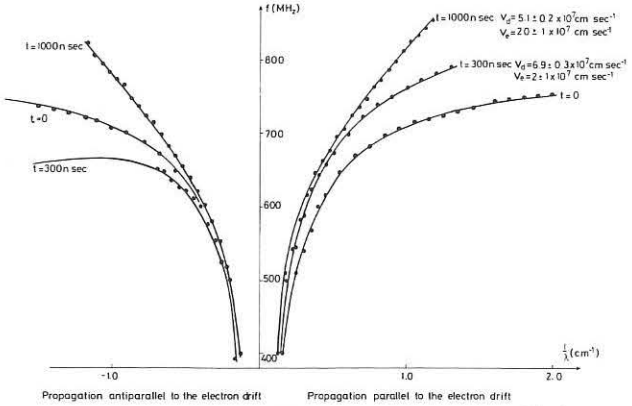

Typical measured dispersion curves for a pulse amplitude of 40V Fig.2

For wavelengths much longer than those of ion fluctuations expected to be excited by the current-drive instability ($k\lambda_D \sim 1$), the propagation depends on plasma properties averaged over many such fluctuations and therefore can be related to an appropriate space averaged distribution function f(v) parallel to B. For lightly damped waves ($v_\varphi = \omega/k \gg v_e$) the usual dispersion relation can be expressed as an expansion in moments of f(v), i.e. in $A_p = \int v^p f(v)\, dv$. If ω_o, ω^+, and ω^- correspond to frequencies of equal wavenumber $|k|$ for the 3 cases above, then by taking the ratios $\left(\frac{\omega^+}{\omega_o}\right)^2$ and $\left(\frac{\omega^-}{\omega_o}\right)^2$ for waves ω^+ and ω^- which have equal but opposite phase velocities $|v_\varphi|$, it can be shown that the even and odd moments are related by the following expressions

$$\frac{1}{2}\left\{\left(\frac{\omega^+}{\omega_o}\right)^2 + \left(\frac{\omega^-}{\omega_o}\right)^2\right\} = \frac{n}{n_o}\,(1 + 3A_2 x + 5A_4 x^2 \ \ldots)$$

$$\frac{1}{2}\frac{1}{\sqrt{x}}\left\{\left(\frac{\omega^+}{\omega_o}\right)^2 - \left(\frac{\omega^-}{\omega_o}\right)^2\right\} = \frac{n}{n_o}\,(2A_1 + 4A_3 x \ \ldots)$$

where $x = 1/v_\varphi^2$. In this way we can follow the development of n/n_o, $v_d \equiv A_1$, $v_e^2 \equiv A_2$, as well as the third and fourth moments. (In practice the results show that for times of interest, $n \approx$ const. and $v_d \approx I/\pi r^2 n_o e$.) Typical

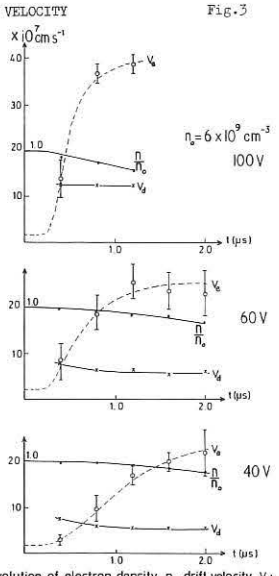

Fig.3 Evolution of electron density, n, drift velocity, V_d, and r.m.s. velocity V_e, (in the electron drift frame) for three different voltage pulses.

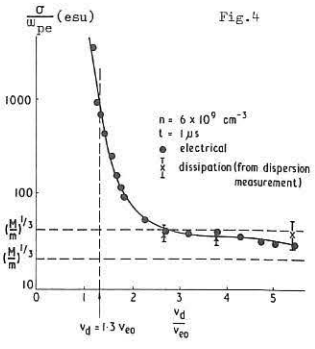

Fig.4

results are shown in Fig.3 for three pulse voltages. (Note that the electron temperature rises to $T_\parallel \sim 80$ eV.)

By subtracting the sheath voltage (assume the perveance measured under stable conditions ($v_d < v_{eo}$) remains constant) from that between the electrodes the resistance of the plasma column can be obtained. Fig.4 shows the mean conductivity normalized to ω_{pe} plotted against v_d/v_{eo} for $t = 1\mu s$, when the fluctuations are well established in each case. The conductivity, which is essentially constant throughout the pulse, falls sharply for $v_d \geq 1.3\, v_{eo}$ (which corresponds to the theoretical threshold for instability[3]) and reaches a roughly constant value for large v_d/v_{eo} in good agreement with that given by the empirical formula $\sigma \simeq 0.5 \left(\frac{M}{m}\right)^{\frac{1}{3}} \omega_{pe}$ found in high voltage toroidal discharges at higher densities[3].

The effective electron-ion collision rate ν (and σ) can also be obtained from the rate of increase of v_e, according to $\frac{d}{dt}(v_e^2) = 2\nu v_d^2$. Fig.5 shows a comparison between the measured increase in v_e^2 and that calculated for two values of ν or σ assuming parallel energy is conserved. The results (also shown in Fig.4 for comparison with the electrical measurements) are again consistent with the above formula.

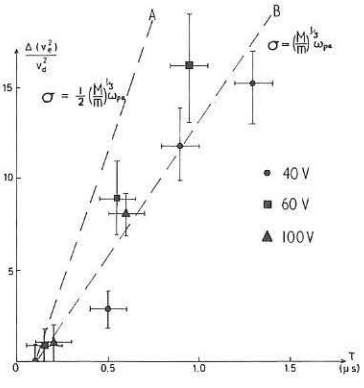

Estimation of the electrical conductivity, σ, from the electron 'heating' rate
Fig.5

Notice (Fig.3) that the maximum temperature reached (~ 80 eV for V = 100 V) depends on the energy confinement time which is given approximately by $L/v_d \sim 1\ \mu s$.

Measurements of A_3 and A_4 suggest that at least for part of each pulse the drifting velocity distribution is non-Maxwellian, with $\int v^3 f\, dv$ of opposite sign to v_d (i.e. towards the ion distribution).

Fluctuations with frequencies ≥ 3 MHz appear during the time when the resistance is high. Their frequency and wavelength spectra are currently being studied.

REFERENCES

1 HAMBERGER, S.M., JANCARIK, J., SHARP, L.E. and ALDCROFT, D.A., In 'Plasma Physics and Controlled Nuclear Fusion Research', (Madison, 1971), vol.II.

2 STRINGER, T.E., J. Nucl. Energy, Pt.C 6, 267 (1964).

3 HAMBERGER, S.M. and FRIEDMAN, M., Phys. Rev. Letts., 21, 674 (1968).

* Also at Dept. of Eng. Science, University of Oxford.

Mass Dependence of Ion Heating in Turbulently Heated Plasmas (THE MACH II)

K. Adati, H. Iguchi, Y. Ito,* T. Kawabe,** K. kawasaki,* T. Oda,* R. Sugihara and T. Yokota***

Institute of Plasma Physics, Nagoya University, Nagoya, Japan
* Faculty of Science, Hiroshima University, Hiroshima, Japan
** Also Plasma Physics Group, Physics Dept., University of Tsukuba, Ibaragi, Japan
***Physics Dept., Kyoyobu, Ehime University, Matsuyama, Japan

ABSTRACT Mass dependence of ion heating (He^+, Ar^+, Kr^+ and Xe^+) in turbulently heated plasmas is experimentally investigated. It is found that the resultant ion temperature at the peak state of heating is nearly proportional to the mass of ion. A model of the mechanism for ion heating is proposed.

A previous paper [1] describes linear turbulent-heating experiments in which argon ions mixed as test particles in the helium plasma are heated almost simultaneously to about 20 eV under a condition that an applied heating voltage is a little higher than the threshold voltage [2].

Further studies have been made of the mass dependence of the resultant temperatures of ions in the similar experiments performed by using THE MACH II device [3], the heating voltage having been much higher than the critical value. The device has a pair of hollow electrodes with an inner diameter of 3 cm, separated by 135 cm from each other. A hydrogen plasma produced by a titanium washer gun is introduced through the electrodes in the discharge tube, where a longitudinal and mirror magnetic field is applied. Its initial density and temperature are about 5×10^{12} cm^{-3} and 8 eV, respectively. After the heating voltage is applied, the electron temperature rises to several tens eV in the first 1 μs and then further increases up to 10 keV, coincident with abrupt grow of the resistance of the plasma. The detailed experimental procedure and the plasma behavior are shown in earlier papers [3].

The ion heating is estimated from the observed Doppler profiles of the ion spectral lines, by using a multichannel Echelle spectrometer. The line profiles have been measured along a chord through the center of the cross section of the plasma column. Both the Zeeman and the Stark effects are all small compared with the Doppler effect to these lines in the present experiments. To supply the test ions, a mixture gas is filled in the vessel at a pressure of 2×10^{-4} Torr, before the titanium washer gun is fired. The mixture gas consists of helium (84 %) as the main ingredient and four kinds of gases (4 % each) as test ions; neon, argon, kripton and xenon.

Fig. 1 shows typical examples of the energy distributions of the ions at various times after the onset of the heating current. Each ion line width considerably increases after 0.5 μs and reaches a peak value at about 1 μs, a little bit before the resistive hump takes place in the heating current-voltage curve. At this time the energy distribution fuctions seem to consist of two components except the case of the helium ion.

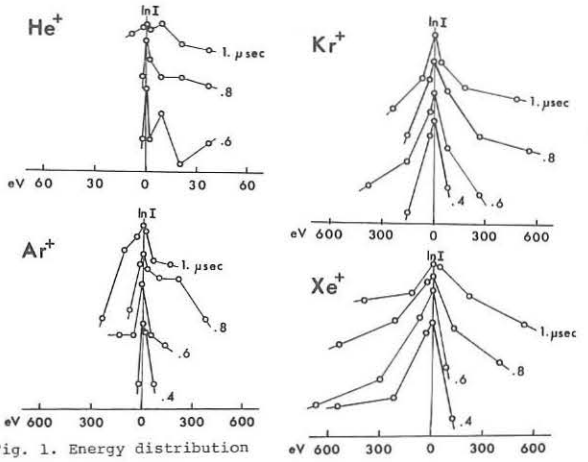

Fig. 1. Energy distribution functions of the ions with different masses.

The lower component of each test species is heated to only about 100 eV and there appear no clear mass dependence in the heating. It also seems that the energy at the transition points from the lower component to the higher one in the distribution curves are nearly proportional to the ion mass.

Fig. 2 shows a mass dependence of the resultant temperature of the higher components at 1 μs. Note that the ion temperature increases with the ion mass almost proportionally. Therefore, a mechanism may exist for the ion heating giving almost the same average speed to the ions with different masses; the ions being trapped in a certain wave in the plasmas are accelerated to its phase velocity. The above explanation may also be supported by the fact that the ion energy profiles have two components with different temperatures except the helium ion, a main ingredient of the plasma.

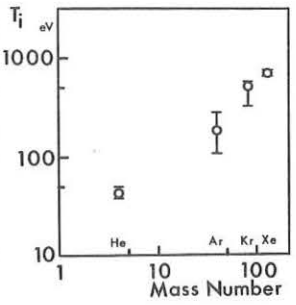

Fig. 2.

The authors would like to thank Professor K. Watanabe of Osaka City University for his kindness to take care of the group. They also appreciate encouragement by Professor H. Takeyama of Hiroshima University. This work was carried out under the cooperative research program at the Institute of Plasma Physics, Nagoya University.

REFERENCES

[1] K. Adati, T. Kawabe, T. Oda, Y. Takezaki, T. Yokota, T. Uyama and K. Watanabe, Phys. Rev. Letters, 29(1972)1223.

[2] K. Adati, R. Sugihara, T. Uyama and K. Watanabe, Proc. VIIth European Conf. on Contr. Fusion and Plasma Physics, Moscow, 1973, Vol. 1, p 561.

[3] Y. Nakagawa et al, Vth IAEA Cof., paper CN-33/C3-3, Tokyo, 1974.

DETERMINATION OF MICROFIELDS IN A TURBULENT PLASMA BY OPTICAL AND FAR-INFRARED SPECTROSCOPY

W.R. Rutgers and H.W. Kalfsbeek
Association Euratom-FOM, FOM-Instituut voor Plasmafysica, Rijnhuizen, Jutphaas, The Netherlands

Abstract: In a turbulent heating experiment we observe three consecutive phases. Phase I: electrons are heated and e.m.radiation with frequencies below f_{pe} is emitted. Phase II: Langmuir and ion-acoustic oscillations are present. Radiation up to 10 f_{pe} is observed. Phase III: radiation spectrum consisting of discrete maxima at $n \cdot f_{pe}$ caused by strong Langmuir turbulence.

Experiment: A schematic drawing of the plasma heating experiment TURHE is given in Fig. 1. A plasma with a diameter of 0.011 m and a density between $2 \cdot 10^{19}$ m^{-3} and $2 \cdot 10^{20}$ m^{-3} is formed by a hollow cathode arc discharge. The plasma is made turbulent by discharging a high voltage capacitor through it. The electrons are accelerated in the electric field creating a beam-plasma type of instability. The nonlinear streaming instability generates fluctuation fields in the frequency domain $0.1\ f_{pe} < f < 0.5\ f_{pe}$. This phase can last for a few hundreds of nanoseconds. The electrons are heated from about 10 eV to several keV during this time which will be denoted as phase I. In the next 1 to 3 microseconds the ratio of drift velocity over the ion sound velocity $u/c_s > 1$ and $T_e/T_i \gg 1$. In this period, denoted as phase II, strong ion-acoustic oscillations grow unstable accompanied by electron Langmuir oscillations. Ion heating takes place mainly by nonlinear Landau damping. Temperatures up to $T_i = 3$ keV were reached[1].

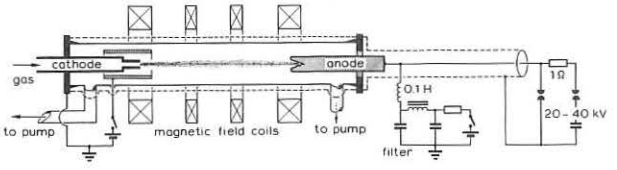

Fig. 1. Schematic drawing of the linear turbulence heating experiment TURHE.

Results from optical measurements: The fields of electron Langmuir waves ($f \sim f_{pe}$, the electron plasma frequency) and ion-acoustic waves ($f \sim f_{pi} = \sqrt{m_e/M_i}\ f_{pe}$) were measured in helium from the spectral profile of forbidden helium lines (e.g. 2^1P-4^1F at 4920 Å) and its satellites at $\pm f_{pe}$. A field strength of about 10^6 V/m was determined for both the high and the low frequency oscillations[2] during phase II. In hydrogen turbulent microfields have been determined from the profiles of hydrogen Balmer lines H_α, H_β, and H_γ. The fields give rise to Stark splitting of hydrogen energy levels. From the frequency splitting and the intensity of the different Stark components measured in two polarizations it is possible to calculate from an optical spectral profile the field strength of ion-acoustic waves and Langmuir waves. We found values from $2 \cdot 10^6$ V/m up to $5 \cdot 10^6$ V/m for the ion-acoustic waves, depending on the voltage applied to the plasma column[4]. The corresponding field strength of high-frequency oscillations is between 10^6 V/m and $3 \cdot 10^6$ V/m.

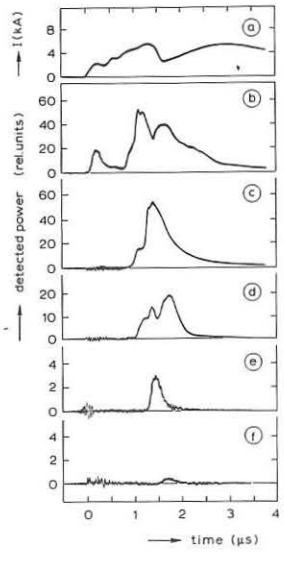

Fig. 2.
Emitted e.m.radiation as a function of time for a helium discharge.
a) discharge current, b) total radiation between 40 and 1000 GHz,
c) after transmission through a wire-mesh filter 55 - 135 GHz,
d) 95 - 230 GHz, e) 190 - 460 GHz,
f) 430 - 1130 GHz.

Far-infrared measurements: The microfields in the plasma also cause e.m.radiation which is measured with a liquid helium-cooled InSb detector. In Fig. 2b the measured radiation, picked up by a circular light pipe (diameter 0.025 m) placed at 12 cm from the plasma column is shown as a function of time for a helium discharge. The radiation is also measured after passing through different band-pass filters (wire-mesh filters) shown in Figs. 2c... 2f, and a low-pass filter (polythene grating). From this observation it is obvious that during phase I the radiation contains frequencies below f_{pe} while during phase II radiation with frequencies up to 10 f_{pe} is emitted. During phase II the intensity decreases as $f^{-\alpha}$ with α from 2.5 for high densities ($n \approx 10^{20}$ m^{-3}) to $\alpha = 4$ for low densities ($n \approx 2.5 \cdot 10^{19}$ m^{-3}). In Fig. 3 this is shown for low density hydrogen and helium discharges ($n \approx 4 \cdot 10^{19}$ m^{-3}). For a limited density range we do not observe a gradual transition to a normal resistive regime at the end of the heating phase but a current dip accompanied by a strong burst of radiation (see Fig. 4). This current dip has previously also been recognized by Watanabe et al.[4]. The frequency spectrum of the radiation emitted in phase III is spectrally resolved with a far-infrared spectrometer.

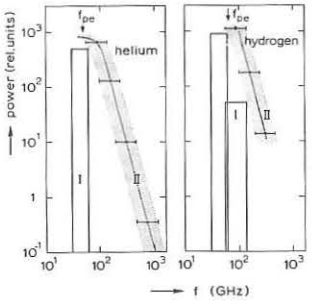

Fig. 3. Emitted e.m.radiation measured with a low-pass polythene grating filter (40-70 GHz) and four wire-mesh filters. Full line: f^{-4} spectrum.
I t = 0 - 300 nanoseconds
II t ∿ 2 microseconds.

Strong Langmuir turbulence ($W/nkT > m_e/M_i$, W is the energy in the fluctuations) causes radiation, not only at f_{pe} and $2f_{pe}$ as reported earlier[1], but also at higher harmonics as shown in Fig. 5. After correction for the bandwidth of the spectrometer the intensity decreases as f^{-3}. In phase III ion-acoustic oscillations can hardly grow unstable because the ratio T_e/T_i has been decreased to about $T_e/T_i \approx 3$. On the other hand strong Langmuir turbulence is excited by bunches of electrons, accelerated in the external electric field. Density depressions of about 50 Debye length can be formed in which the high-frequency oscillations are trapped. The cavity shrinks in the course of time to about one Debye length and decays afterwards with generation of e.m.radiation.

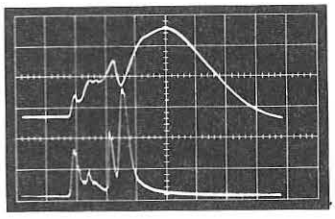

Fig. 4.
Upper trace: discharge current as a function of time.
Lower trace: total e.m.radiation
Time scale: 1 μs/large division,
phase I: t = 0-0.3 μs;
phase II: t = 0.3 - 1.6 μs;
phase III: t = 1.6 - 2.0 μs.

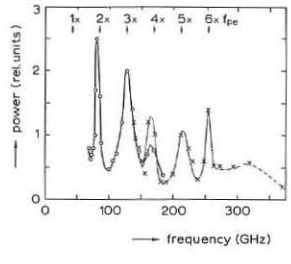

Fig. 5.
Frequency spectrum of e.m.radiation during phase III measured with a far-infrared spectrometer.
$n = 2.5 \cdot 10^{19}$ m^{-3}, V = 45 kV/m.

Acknowledgement

The authors wish to thank Dr. H. de Kluiver for continuous stimulations and Prof. C.M. Braams for valuable discussions.

This work was performed under the Euratom-FOM association agreement with financial support from ZWO and Euratom.

References

[1] H. Schrijver et al., Proc. 5th Int. Conf. on Plasma Phys. and Contr. Nucl. Fusion Res., Tokyo, 1974, CN 33/C3-1.
[2] W.R. Rutgers, submitted to Z. Naturforsch.
[3] W.R. Rutgers and H.W. Kalfsbeek, Z. Naturforsch. 30A (1975) in press.
[4] Y. Nakagawa et al., Proc. 5th Int. Conf. on Plasma Phys. and Contr. Nucl. Fusion Res., Tokyo, 1974, CN 33/C3-3.

MICROWAVE SCATTERING FROM A TURBULENTLY HEATED PLASMA

L.E. SHARP and S. MROWKA*

Culham Laboratory, Abingdon, Oxon, OX 14 3DB, UK
(Euratom/UKAEA Fusion Association)

The electron density fluctuation spectrum during the turbulent heating of a plasma has been derived from the scattering of $\lambda = 2.4$mm and 8.8mm microwave beams. There is evidence of ion sound fluctuations, ($k_\perp B$) while late in the heating phase large amplitude, long wavelength, high frequency fluctuations $k_\perp B$ are observed whose origin has not yet been identified.

The density fluctuation spectrum which occurs during the current driven turbulence in a toroidal hydrogen plasma has been examined from the scattered radiation of $\lambda_o = 2.4$mm and 8.8mm wavelength microwave beam. The heating current ($\tau \sim 300$ns) is produced by electromagnetic induction of a strong electric field ($50\,kV\,m^{-1}$) parallel to the axial confining field (0.3 tesla) of a stellarator (TWIST)[1].

Figure 1 shows typical waveforms for the applied electric field, the induced current, the electric conductivity and the electron thermal v_e drift v_D and sound speeds c_s. The observations are concerned with the density fluctuations during the first 300ns during which most of the electrical dissipation occurs. Within this period the density (typically $2 \times 10^{18}\ m^{-3}$) remains essentially constant while the electron energy typically increases from ~ 10eV to as high as 30keV depending on operating conditions[1].

From linear theory we should expect the most unstable wavenumbers to be $\leq \lambda_D^{-1}$, thus during the observation the corresponding fluctuation wavelengths will increase from 120μm to 6mm.

When $v_D > c_s$ ion sound can be generated within the Cerenkov cone of angle $\cos^{-1}(v_D/c_s)$ and with frequencies $0 < \omega < \omega_{pi}$. For $v_D > v_e$ a fluid (two-stream) type instability can occur. In the frame of the ions the characteristic frequency is $\omega^* \sim \frac{1}{2}(m_i/m_e)^{1/6}\omega_{pi} = 1.7\,\omega_{pi}$ for hydrogen. For $n = 2 \times 10^{18}\ m^{-3}$ we should expect fluctuation frequencies $\nu \sim 600$MHz for the latter and $\nu \sim 280$MHz for the ion sound turbulence.

Considering the limitation of presently available signal sources and experimental access, the most suitable probing wavelengths were $\lambda_o = 2.4$ mm and 8.8 mm. With $\lambda_o = 2.4$ mm the fluctuations could be measured at $\phi = 90^\circ$, 70°, 30° and 0° with respect to the current and with $\lambda_o = 8.0$ at $\phi = 90^\circ$. The respective fluctuation wavenumbers are 2.7 - 4.5 mm^{-1} and 0.8 mm^{-1}. The minimum detectable fluctuation level of the system were respectively $S(k) = 6 \times 10^4$ and 2×10^4 set by the plasma radiation level. Heterodyne detection followed by a multichannel filter array allowed the spectrum $S(k, \omega)$ to be obtained simultaneously at eight frequencies. For frequencies below 150 MHz, $S(k, \omega)$ was derived from the Fourier transform of the heterodyne video signal.

In Fig.2, $S(k, \omega)$ for $\phi = 90^\circ$ is plotted as a function of frequency for T = 100, 150 and 250ns, where the data points represent the ensemble averaged spectrum of 10 individual sets of results. The open symbols are obtained from the filter array and the filled symbols from the Fourier analysis. After T = 150ns the spectrum is seen to widen rapidly to include components $\nu \sim 800$MHz well above ν_{pi} and ν^* and to maintain this distribution for some 150ns after which the scattered signal falls rapidly below the plasma radiation level. At the same time the conductivity is observed to increase rapidly, suggesting an overall reduction in the turbulence level. The fluctuation spectrum $S(k,\omega)$ at $\tau = 250$ns is plotted in Fig.3 for $\phi = 90^\circ$, 70°, 30° and 0° for $\lambda_o = 2.4$mm and in Fig.4 at $\phi = 90^\circ$ for $\lambda_o = 8.8$mm. Although $v_D > v_e$ (Fig.1) for a short period and the electrical conductivity is consistant[2] with the electrostatic two-stream instability, the scattering measurements were unable to detect the associated density fluctuations as the fastest growing wavenumber is outside the instrumental range. Fig.2 shows a weak maximum (corresponding to $S(k) \sim 10^5$) in the spectrum at T = 150 ns which may arise from a cross field ion sound instability[3] although we have been unable to detect a similar peak for smaller ϕ. Thus a limit of $S(k) < 2 \times 10^4$ can be set for ion sound fluctuations parallel to the current at this wavenumber.

Just after maximum current (T > 120ns) Fig.3 shows clearly that high frequency components at $k \sim 3.5\ mm^{-1}$ increase considerably as ϕ is increased, i.e. they have wave-vectors predominantly perpendicular to the current, with $S(k_\perp) = 10^6 \gg S(k_\parallel) \leq 10^5$, The frequency range extends well above those associated with electrostatic fluctuations (i.e. ν_{pi}, ν^*). Fig.4 ($\varphi = 90^\circ$, $\lambda_o = 8.8$ mm) shows an even wider spread of frequency with fluctuations detectable near ν_{pe} and with $S(k_\perp) \sim 8 \times 10^5$, comparable with those at $\lambda_o = 2.4$mm.

It is difficult to reconcile such wide frequency and wavelength spectra with electrostatic modes of oscillation, while those wavelengths observed appear not to be associated with any particular frequency. Thus it appears that the conditions observed corresponds to a high level of strong plasma turbulence. Considering that intense microwave continuum radiation[4] ($\sim 10^5$ x black body at $T = 10^4$ eV) is observed during this time, it is possible that the density fluctuations arise as a result of some form of electromagnetic (rather than electrostatic) instability. It has not, however, been possible to identify the origin of such an instability.

REFERENCES

1 HAMBERGER, S.M. et al., Proc. Conference on Plasma Physics and Controlled Nuclear Fusion Research, Madison, 1971, vol.II, p.37.

2 HAMBERGER, S.M. and JANCARIK, J., Phys. Fluids, 15, 825 (1972).

3 BISKAMP, D. and HORTON, W., Max. Planck Institute Report IPP 6/124, 1974.

4 HAMBERGER, S.M. et al., Proc. Conference on Controlled Fusion and Plasma Physics, Grenoble, August 1972, vol.II, p.245.

* Also at Department of Engineering Science, University of Oxford.

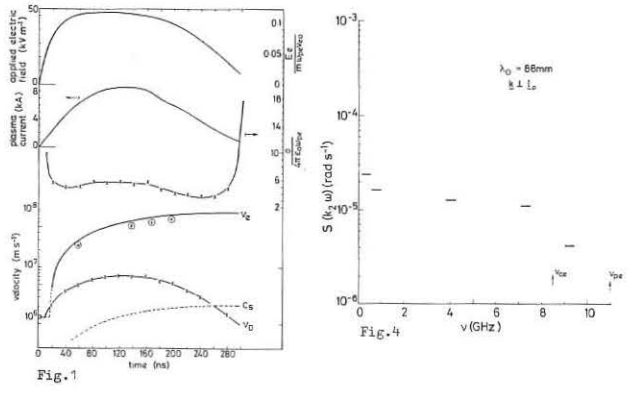

Fig.1

Fig.4

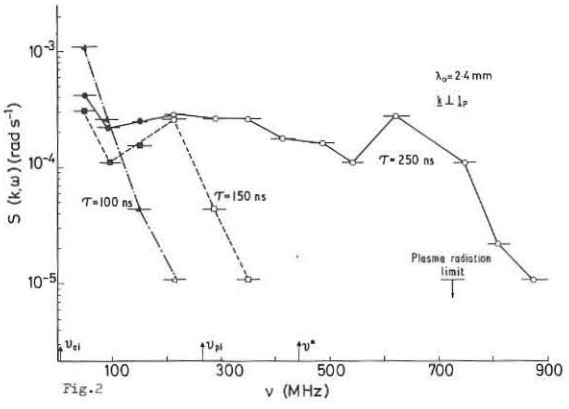

Fig.2

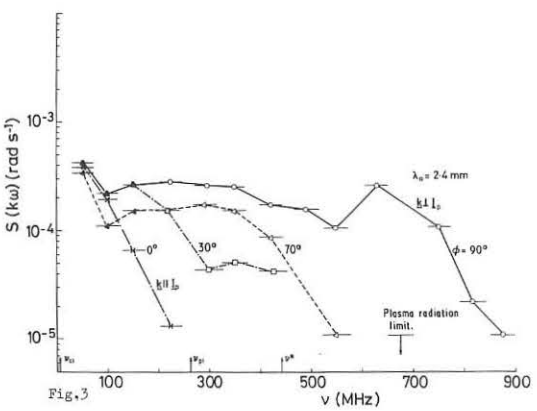

Fig.3

NUMERICAL RESULTS FOR THE HIGH FREQUENCY CONDUCTIVITY OF A TURBULENT PLASMA*

K.H. Spatschek, P.K. Shukla, and M.Y. Yu
Institut für Theoretische Physik
Ruhr-Universität, 463 Bochum, F.R. Germany

Abstract: A consistent derivation of the high-frequency conductivity of a fully developed turbulent plasma is presented. Numerical results are given for Langmuir and ion-acoustic turbulence.

We investigate the a.c. conductivity (1,2) of a plasma in a turbulent steady-state described by a strong turbulence theory (3). Accordingly, for electrostatic turbulence, the velocity-space diffusion tensor in the equation for the space-averaged one-particle distribution function of a homogeneous plasma in an external electric field $E_o \hat{e}_z \sin\omega_o t$ is

$$\underset{\sim}{D}_j(v) = \frac{e_j^2}{m_j^2}\int_0^\infty d\tau \sum_{\underset{\sim}{k},m,n} \underset{\sim}{\hat{k}}\,\underset{\sim}{\hat{k}}\, S(\underset{\sim}{k},t;\tau) J_n(\underset{\sim}{k}\cdot\underset{\sim}{\varepsilon}_j) J_m(\underset{\sim}{k}\cdot\underset{\sim}{\varepsilon}_j) \exp\left\{-i(n\omega_o - \underset{\sim}{k}\cdot\underset{\sim}{v}')\tau - \beta_j\tau^2 + i(n-m)\omega_o t\right\}, \quad (1)$$

where $\underset{\sim}{v}' = \underset{\sim}{v} + \underset{\sim}{\varepsilon}_j \omega_o \cos\omega_o t$, $\underset{\sim}{\varepsilon}_j = e_j \underset{\sim}{E}_o/m_j\omega_o^2$ and $\beta_j = \frac{1}{2}(k^2 D_{jzz})^{2/3}$. We note that β_j and $S(\underset{\sim}{k},t;\tau)$ are functions of the a.c. field. From the appropriate dispersion relation (4), one obtains $S(\underset{\sim}{k},t;\tau) = [1 + (\underset{\sim}{k}\cdot\underset{\sim}{E}_o/2\omega_o^2)R]S^0$, where $R = \lambda^+_{+\underset{\sim}{k}} \exp[i\omega_o(t-\tau)] + \lambda^-_{+\underset{\sim}{k}} \exp[-i\omega_o(t-\tau)] - \lambda^+_{-\underset{\sim}{k}} \exp(i\omega_o t) - \lambda^-_{-\underset{\sim}{k}} \exp(-i\omega_o t)$. Here, $S^0 = \langle|\delta E^0_{\underset{\sim}{k}}(\omega_{\underset{\sim}{k}})|^2\rangle \exp(-i\omega_{\underset{\sim}{k}}\tau)$, with $\langle|\delta E^0_{\underset{\sim}{k}}|^2\rangle$ being the steady-state fluctuation spectrum in the absence of the a.c. field. We have defined $\lambda^\pm_{\underset{\sim}{k}} = \mp\varepsilon^{-1}_{NL}(\omega_{\underset{\sim}{k}} \pm \omega_o)\sum_j e_j\left[\chi^{NL}_j(\omega_{\underset{\sim}{k}} \pm \omega_o) - \chi^{NL}_j(\omega_{\underset{\sim}{k}})\right]/m_j$. Here, ε_{NL} and $\chi^{NL}_j(\omega_{\underset{\sim}{k}})$ are respectively the nonlinear dielectric function and susceptibility including resonance broadening effects (4,5), i.e., $\chi^{NL}_j = \omega^2_{pj} G'\left[(\omega_{\underset{\sim}{k}} - \underset{\sim}{k}\cdot\underset{\sim}{v}_{dj})/\sqrt{2}\,k\,\bar{v}_{Tj}\right]/2k^2\bar{v}^2_{Tj}$, where $\bar{v}^2_{Tj} = v^2_{Tj} + 2\beta^0_j/k^2$, $\beta^0_j = \beta_j(E_o = 0)$, and v_{Tj} is the thermal velocity. In deriving the above equation, the averaged distribution function $\langle f_j\rangle$ is taken to be Maxwellian with a d.c. drift velocity v_{dj}.

The conductivity is obtained by taking the velocity moment of the kinetic equation (3) and integrating over $\underset{\sim}{v}$ and τ. We obtain for $\underset{\sim}{k}\cdot\underset{\sim}{\varepsilon}_j \ll 1$, $m_e/m_i \ll 1$ the dissipative part

$$\underset{\sim}{\sigma}_d = \frac{e^2}{4\pi\omega_o^3 m_e^2}\sum_{\underset{\sim}{k}} \underset{\sim}{k}\underset{\sim}{k}\,\langle|\delta E^0_{\underset{\sim}{k}}|^2\rangle\, \mathrm{Im}\left\{\left[\frac{\chi^{NL}_i(\omega_{\underset{\sim}{k}} - \omega_o) - \chi^{NL}_i(\omega_{\underset{\sim}{k}})}{\varepsilon_{NL}(\omega_{\underset{\sim}{k}} - \omega_o)}\right]\left[\chi^{NL}_e(\omega_{\underset{\sim}{k}} - \omega_o) - \chi^{NL\,*}_e(\omega_{\underset{\sim}{k}})\right] - \frac{m_e\beta^0_e(\lambda^-_{\underset{\sim}{k}} - \lambda^-_{-\underset{\sim}{k}})}{2e\,k^2\bar{v}^2_{Te}}\left[2\chi^{NL}_e(\omega_{\underset{\sim}{k}}) + \omega_{\underset{\sim}{k}}\frac{\partial}{\partial\omega_{\underset{\sim}{k}}}\chi^{NL}_e(\omega_{\underset{\sim}{k}})\right]\right\}. \quad (2)$$

At saturation, the linear growth $\sum_j \gamma^L_j$ of the ion-acoustic instability is balanced by the nonlinear damping $\gamma^{NL}_i - \gamma^L_i$ produced by ion resonance broadening (5). For $\gamma^{NL}_i \ll \omega_{\underset{\sim}{k}}$, and assuming that the spectrum is peaked at $\underset{\sim}{k} \simeq (\sqrt{2}\,\lambda_e)^{-1}\hat{e}_z$, we obtain

$$(2\psi)^{3/2} e^{-\psi} = \frac{1}{(k\lambda_e)^2}\left(\frac{\omega_{\underset{\sim}{k}}}{\omega_{pi}}\right)^2\left[\frac{v_{de}}{v_{Te}} - \frac{1}{k\lambda_e}\left(\frac{m_e}{m_i}\right)^{1/2}\frac{\omega_{\underset{\sim}{k}}}{\omega_{pi}}\right], \quad (3)$$

where $\psi = \omega^2_{\underset{\sim}{k}}/2k^2\bar{v}^2_{Ti}$, and $\omega_{\underset{\sim}{k}} \approx 0.82\,\omega_{pi}$. From eq.(2) the fluctuation field energy density for ion-sound turbulence can be calculated as $\sum_{\underset{\sim}{k}}\langle|\delta E^0_{\underset{\sim}{k}}|^2\rangle = (14.8/\sqrt{2\pi})8\pi\, n\, T_e\left[\omega^2_{\underset{\sim}{k}}/(4\psi\,\omega^2_{pi}) - T_i k^2\lambda_e^2/2T_e\right]^2$, $\lambda_e = v_{Te}/\omega_{pe}$. Next, as origin of the Langmuir turbulence, we take the beam-plasma instability. Saturation occurs through electron resonance broadening due to both the plasma and beam electrons. Thus, $\gamma^{NL}_e + \gamma^{NL}_b = 0$, where the subscript b indicates beam quantities. Noting that $\beta^0_b = \beta^0_e$ and $\omega_{\underset{\sim}{k}} \gg k\,v_{Te}$, we obtain for $n_b \ll n_e$ and $T_b \ll T_e$ in place of eq.(3),

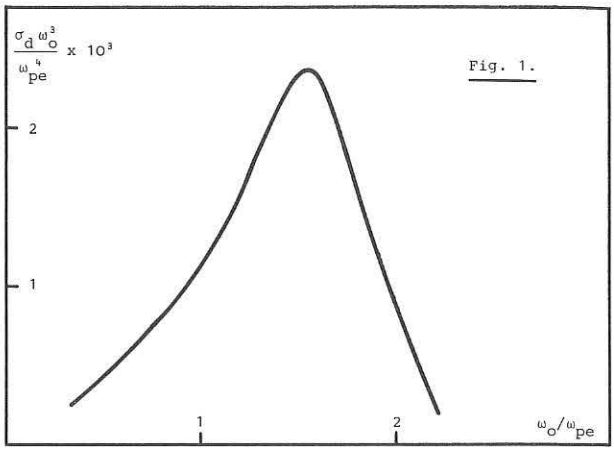

Fig. 1.

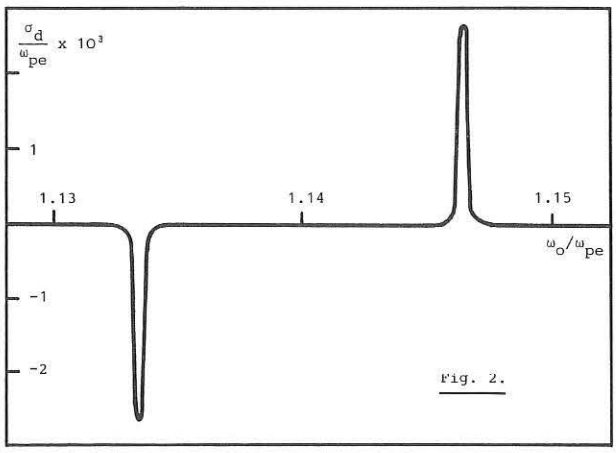

Fig. 2.

$$\sqrt{\psi}\, e^{-\psi} = \frac{n_b T_e}{2\sqrt{\pi} n_e}\,\frac{1 + 2\beta^0_e(\omega_{pe}\,k\lambda_e)^{-2}}{T_b + 2\beta^0_e(\omega_{pe}\,k\lambda_e)^{-2}T_e}\,\mathrm{Im}\,G'\left(\frac{\omega_{\underset{\sim}{k}} - k v_{db}}{\sqrt{2}\,k\,\bar{v}_{Tb}}\right), \quad (4)$$

where $\beta^0_e/\omega^2_{pe} = \omega^2_{\underset{\sim}{k}}/(4\psi\,\omega^2_{pe}) - k^2\lambda_e^2/2$, and $\omega_{\underset{\sim}{k}}$ is the solution of $1 + \chi^{NL}_e + \chi^{NL}_b = 0$. We have assumed that $\langle f_b\rangle$ is Maxwellian. For a peaked spectrum, the fluctuation field energy density is then $\sum_{\underset{\sim}{k}}\langle|\delta E^0_{\underset{\sim}{k}}|^2\rangle = (14.8/\sqrt{2\pi})\,8\pi\, n_e T_e\left[\omega^2_{\underset{\sim}{k}}/(4\psi\,\omega^2_{pe}) - k^2\lambda_e^2/2\right]^2$.

For ion-acoustic turbulence, the conductivity in Fig. 1 ($T_e/T_i = 100$, $v_{de}/v_{Te} = 0.1$; $\omega_{\underset{\sim}{k}} = 0.69\,\omega_{pi}$, $k\lambda_e = .71$) shows a broad peak above ω_{pe}. The reason is that $\mathrm{Im}[1/\varepsilon^{NL}(\omega_{\underset{\sim}{k}} - \omega_o)]$ is non-vanishing over a broad frequency range $|\omega_{\underset{\sim}{k}} - \omega_o| \simeq \sqrt{3}\,k\,v_{Te}$. Therefore, our result can be attributed to electron Compton scattering. For the case of Langmuir turbulence (Fig. 2; $v_{db}/v_{Te} = 5$, $T_b/T_e = 10^{-2}$, $n_b/n_e = 10^{-3}$; $\omega_{\underset{\sim}{k}} = 1.14\,\omega_{pe}$, $k\lambda_e = 0.25$), the conductivity shows two spikes with opposite signs above ω_{pe}. This may be attributed to a three-wave interaction among the turbulent mode, the a.c. field, and the ion-sound wave. For $\omega_o < \omega_{\underset{\sim}{k}}$, energy is extracted from the turbulent modes, resulting in negative conductivity. On the other hand, for $\omega_o > \omega_{\underset{\sim}{k}}$, energy flows from the a.c. field to the ion-sound waves and the turbulent modes, leading to positive conductivity.

* Supported by SFB "Plasmaphysik Bochum/Jülich".

[1] J. Dawson and C. Oberman, Phys. Fluids 5, 517 (1962).
[2] K. Nishikawa and Y.H. Ichikawa, Phys.Fluids 12, 2563 (1969).
[3] T.H. Dupree, Phys. Fluids 9, 1773 (1966).
[4] B.Bezzerides and J.Weinstock, Phys.Rev.Lett.28, 981 (1972).
[5] A. Sleeper et al.,Phys. Rev. Lett. 29, 343 (1972).

Anomalous Ion Heating and Thermal Energy Transport

B.Coppi, F. Pegoraro and G. Rewoldt
Massachusetts Institute of Technology, Cambridge, Mass., U.S.A.

tract: The enhanced ion heating, resulting from current driven modes about the ion plasma frequency when a fraction of the electron popula-n is trapped and the circulating electron distribution tends to run-y as a whole, is treated and compared with the experimental observa-ns. A new dissipative trapped ion mode driven by the impurity density dient is found and shown to produce outflow (decontamination) of impuri-s but also enhanced ion thermal conductivity.

Current driven modes with $\omega/k_{\parallel} > (\Delta B/B)^{1/2} v_{the}$ can be excited in re-es where a fraction $(\Delta B/B)^{1/2}$ of the electron population is trapped the applied electric field is such that the circulating electron di-ibution tends to runaway as a whole (slide-away regime) [1]. The relevant es are electrostatic, with potential $\tilde{\phi} = \tilde{\phi}_k \exp(-i\omega t + ik_{\perp} r_{\perp} + ik_{\parallel} \ell)$ and treated in a simplified geometry where ℓ indicates a distance along agnetic field line. We consider the frequency range $\Omega_i < \omega < \Omega_e$, = $eB/(cm_j)$ being the gyrofrequency of species j, and transverse waveleng-such that $\rho_i^{-1} < k_{\perp} < \rho_e^{-1}$, where $\rho_j \equiv v_{thj}/\Omega_j$. Therefore the ions can treated as unmagnetized and the relevant wave-particle resonances are the form

$$k_{\perp} v_{\perp})_i + k_{\parallel} v_{\parallel})_i = \omega = k_{\parallel} v_{\parallel})_e .$$

ce the region of positive slope in the electron distribution is produc-by the circulating electrons $v_{\parallel})_e \gtrsim (\Delta B/B)^{1/2} v_{the}$, effective ion ting can be produced only if $v_{\parallel})_i \sim v_{thi}$. Therefore $k_{\perp}/k_{\parallel} \gtrsim$ $/B)^{1/2}(v_{the}/v_{thi})$ and longitudinal energy of the current carrying ctrons is transferred mostly as transverse energy to the ions. The nsverse momentum in the electron-wave resonance is taken up by the magnetic eld while the longitudinal momentum exchanged between circulating elec-ns and ions prevents the first population from running away and produ- a finite resistivity. Considering the electron distribution composed by two Maxwellians in the longitudinal direction, the relevant spersion relation can be written as

$$\lambda_{De}^2 = (T_e/T_i) W(\omega/kv_{thi}) + (n_1/n) W(\omega - k_{\parallel} u_1/k_{\parallel} v_{the}) + [n_o T_e/(n T_{eo})]$$
$$W(\omega/k_{\parallel} v_{theo})$$

re λ_{De} is the electron Debye length, the subscript 1 refers to circulat-electrons and zero to trapped electrons, and W is the well known dau integral. We can see that the solution of this equation for ω real two branches, one roughly corresponding to ω_{pi}, the ion plasma fre-ncy, and the other to $k_{\parallel} \omega_{pe}/k$. The lower branch has a lower thres-d, as measured by $\xi = u_e/v_{the}$ where $u_e = J/(ne)$ is the total elec-n drift velocity. A quasilinear analysis of the effects of these modes been carried out and correlated with the onset of fluctuations, ob-ved in plasmas produced by the Alcator device, and of sharp ion heating $<\xi>$, an average taken over the plasma cross section, becomes larger n a critical value. The observed spectrum is sharply peaked around in the range 350 ÷ 700 MHz and has been seen to extend up to 4GHz. The analysis of electron-loss cone modes, in order to explain the enhanced emission, over the thermal level, of electron cyclotron radiation has also been carried out. [2]

2. We have found a new mode, in the trapped ion regime, that is standing along the magnetic field lines, has odd electrostatic potential around the point of minimum field, and whose growth rate depends on the collision frequency of trapped ions and on the density gradient of the impurity population. This is of the order of

$$\gamma \sim \left(\frac{L}{\lambda_{ieff}}\right)^{1/2} \frac{v_{thi}}{r_{nI}} \left(\frac{L}{r_n}\right) (k \rho_i)^2 \frac{Z_{eff}}{Z}$$

where L is the magnetic field periodicity length, $\lambda_{ieff} = (v_{thi}/\nu_i)(\Delta B/B)^{3/2}$ the effective mean free path of trapped ions, r_n and r_{nI} the density gradient scale distance for the main ions and impurity ions respectively, Z and Z_{eff} the impurity and the plasma effective charge number respectively. The considered mode is unstable if impurities are accumulated at the center of the plasma column, so that $d\ell n n_I/d\ell n n_i > 0$ if

$$\frac{d\ell n T_i}{dr} \left(\frac{d\ell n n_i}{dr}\right)^{-1} > \frac{2}{3}$$

Thus the instability produces and outflow of impurities (decontamination) [3], for a typical relative temperature gradient that is more realistic and smaller than that predicted by the collisional transport theory. In particular, for values of the actual ion temperature gradient between the two critical temperature gradients, we can have a situation in which the impurities are concentrated at the outside of the column, with the collisional inward impurity flux balanced by the outward impurity flux due to the impurity-driven modes. At the same time anomalous ion thermal energy transport is produced but this occurs at a slower rate than that for impurity particle transport. [4]

* Supported in part by the U.S.E.R.D.A.

[1] B.Coppi, A.Oomens, R.Parker, L.Pieroni, F.Schüller, S.Segre and R. Taylor, M.I.T. Report PRR-7417 (Cambridge, Mass., 1974), to be published.

[2] B.Coppi, F.Fegoraro and G.Rewoldt, M.I.T. Report PRR-758 (Cambridge, Mass., 1975), to be published.

[3] B.Coppi, Phys.Rev.Letters, 31, 1443 (1973).

[4] B.Coppi, G.Rewoldt and T.Schep, M.I.T. Report PRR-754 (Cambridge, Mass., 1975), to be published.

EARLY STAGES OF THE EVOLUTION OF THE ELECTRON DISTRIBUTION FUNCTION UNDER AN APPLIED ELECTRIC FIELD.

A.Airoldi Crescentini, E.Lazzaro, A.Orefice

Laboratorio di Fisica del Plasma del CNR - Ist. di Fisica
via Celoria, 16 - Milano - Italy

ABSTRACT: We search informations on the early stages of the evolution of the electron distribution function, in a collisional, fully ionized plasma, under the influence of a realistic axial electric field. A simulation of the magnetic trapping effect expectable in a toroidal device is included and discussed.

We employ an electron kinetic equation with a Landau collision operator:

$$\frac{\partial f_e}{\partial t} - \frac{e}{m}\underline{E}\cdot\frac{\partial f_e}{\partial \underline{v}} = \frac{\gamma_e}{2}\sum_{s,i,j}\frac{n_s}{m_s}\frac{\partial}{\partial v_i}\int d\underline{v}'\,\frac{\partial^2|\underline{v}-\underline{v}'|}{\partial v_i\,\partial v_j}\cdot \left\{ m_s f_s(\underline{v}')\frac{\partial f_e}{\partial v_j} - m_e f_e(\underline{v})\frac{\partial f_s}{\partial v_j'}\right\} \qquad (1)$$

The species (electrons and ions) are labelled by "s"; $\underline{E}$ is along z, Λ_s is the coulomb logarithm and

$$\gamma_s = 4\pi n e^4 \Lambda_s Z_s/m_e^2 \quad ; \quad \eta_s = \gamma_s/\gamma_e \equiv Z_{eff}$$

Integrating eq.(1) over $d\underline{v} = dv_x\,dv_y$ and using $\underline{u} = \underline{v}/v_o$; $\tau = \gamma_e t/\pi v_o^3$; $E_c = m_e\gamma_e/e\pi v_o^2$; $F(u_3,\tau) = v_o^3\int d\underline{u}_\perp f_e$ where $v_o = v_{thermal}$ (t=0), we obtain[1] an equation formally similar to the one obtained by Field and Fried[2]:

$$\frac{\partial F}{\partial \tau} + \frac{\partial}{\partial u_3}\left\{\left[\frac{E}{E_c} - \psi(u_3,\tau)\right]F\right\} = \frac{1}{2}\frac{\partial}{\partial u_3}\left(D\frac{\partial F}{\partial u_3}\right) \qquad (2)$$

In our equation

$$\psi = \sum_s \eta_s\psi_s = \pi v_o\sum_s \eta_s\frac{m_s}{m_e+m_s}\left\langle \frac{u_3}{2}\frac{\partial^2 h_s}{\partial u_3^2} - \frac{m_e}{m_s}\frac{\partial h_s}{\partial u_3}\right\rangle \quad ; \quad D = \sum_s \eta_s D_s = \frac{\pi}{v_o}\sum_s \eta_s\left\langle\frac{\partial^2 g_s}{\partial u_3^2}\right\rangle$$

and h_s, g_s are the usual "potential functions" of Rosenbluth, McDonald and Judd. The averages ψ and D have then the meaning of dynamical friction and diffusion coefficients respectively. We evaluate the collision integrals h_s, g_s with the substitution of a maxwellian f_i for the ions, in the limit $m_e/m_i \to 0$, centered in $u_3 = 0$, and of a suitable maxwellian f_e for the electrons:

$$f_e = \pi^{-3/2} v_o^{-3}\lambda^{-3}(\tau)\exp\left\{-\frac{u_\perp^2 + [u_3 - W(\tau)]^2}{\lambda^2(\tau)}\right\} \qquad (3)$$

where the electron drift $W(\tau)$ and the function $\lambda(\tau) = v_{th}(\tau)/v_o$ keep somewhat into account the nonlinearity of the problem. We assume that the averages ψ, D may be made over a single weight function, which is taken to be the transverse electron maxwellian:

$$\varphi_\perp = \pi\lambda^{-2}(\tau)\exp\left\{-\frac{u_\perp^2}{\lambda^2}\right\} \qquad (4)$$

The following basic relation hold between ψ_s and D_s:

$$\psi_s(u_3,\tau) = \frac{u_3 - \delta_{es}W(\tau)}{\lambda^2}D_s(u_3,\tau) \qquad (5)$$

where

$$D_s(u_3,\tau) = 2\pi\lambda\frac{\partial^2}{\partial u_3^2}\int_0^\infty d\rho\,\rho\,e^{-\rho^2}\beta_s\left(\sqrt{\rho^2 + \left(\frac{u_3 - \delta_{es}W_s}{\lambda}\right)^2}\right) \qquad (6)$$

with $\beta_s(r) = \left(r + \frac{\epsilon_s^2}{2r}\right)erf\left\{\frac{r}{\epsilon_s}\right\} + \frac{\epsilon_s}{\sqrt{\pi}}e^{-\frac{r^2}{\epsilon_s^2}}$; $\epsilon_s = v_{th,s}/v_{th,e}$

Plots of ψ_s, D_s, ψ, D are shown in fig.(1).
Energy conservation requires that

$$\lambda^2(\tau) = 1 + 2\int_0^\tau d\tau\,\frac{E(\tau)}{E_c}\bar{u}_3(\tau) - \bar{u}_3^2(\tau) \quad \text{with} \quad \bar{u}_3(\tau) = \int du_3\,u_3 F. \qquad (7)$$

Momentum conservation suggests to choose the drift $W(\tau)$, in the electron maxwellian, so as to avoid a non-physical momentum exchange in the e-e collisions: we are induced therefore to assume

$$W(\tau) = \bar{u}_3(\tau) \qquad (8)$$

In figs.(2),(3),(4) we show the evolution of the reduced electron distribution function, of its drift $W(\tau)$, of the thermal velocity normalized on v_o ($\lambda = v_{th}/v_o$) and of the electric conductivity normalized on the Spitzer value, σ/σ_{sp}, with $E/E_c = .3$
As $\lambda(\tau)$ grows, the total effective friction force $\psi(u_3,\tau)$ decreases, thereby allowing an acceleration of the electron population. The corresponding evolution of the electron distribution function is towards a situation in which it deviates progressively from a drifting maxwellian, developing a high energy tail. Anyway, it is apparent that e-e collisions, when properly considered through a nonlinear term, do not allow a strong departure from a maxwellian, at least for the values of time and electric field examined here. It is seen that, after a transient time, the conductivity σ settles slightly over the Spitzer value. The evolution of the electron temperature and drift agrees with Dreicer's results[3]; our model clarifies the effectiveness of e-e collisions on the kinetic behavior.

Even though our model, as it stands, is not suitable to study 3-dimensional effects as those due to a magnetic field, it seems interesting to simulate the magnetic trapping effect expected, in the banana regime, in a Tokamak device[4]. For this purpose, we impose an electric field of the form

$$\underline{E} = H\left(|u_3| - u_\perp\epsilon^{1/2}\right)\underline{E} \qquad (9)$$

where ϵ simulates a toroidal inverse aspect ratio. The introduction of (9) into eq.(1) leads to the substitution in eq.(2) of the term E/E_c with

$$\frac{E}{E_c}\left\{1 - exp\left[-u_3^2/\epsilon\lambda^2\right]\right\} \qquad (10)$$

The evolution of $F(u_3,\tau)$ in this case is shown in fig.(5). As can be seen, the reduced distribution function undergoes, as time goes on, a much stronger deformation than in the preceding cases, developing a second bump at high velocities. However in this case our model is obviously much less plausible, so that this last result must be taken as merely indicative.

REFERENCES

(1) A.Airoldi Crescentini, E.Lazzaro, A.Orefice: Rep.FP 43 (1974)

(2) E.C.Field, B.D.Fried: The Phys.of Fluids 7, 1937 (1964)

(3) H.Dreicer: Phys. Rev. 115, 238 (1959)

(4) B.Coppi, R.Pozzoli, G.Rewoldt, T.Schep: Proc. 5th Int. Conf. on Plasma Physics and Controlled Nuclear Fusion IAEA-CN-33/A 14-4, (1974).

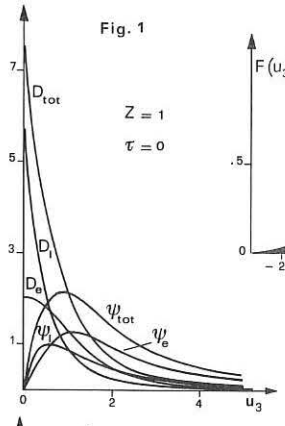

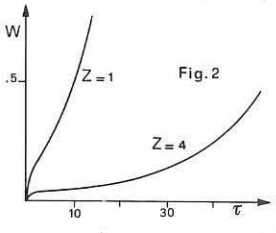

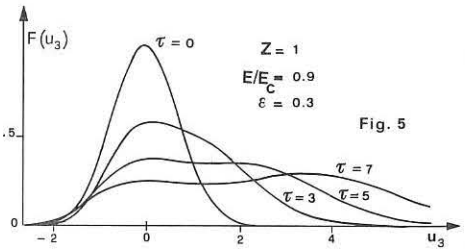

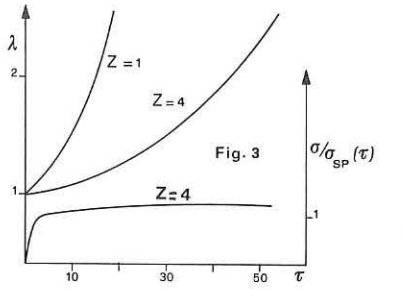

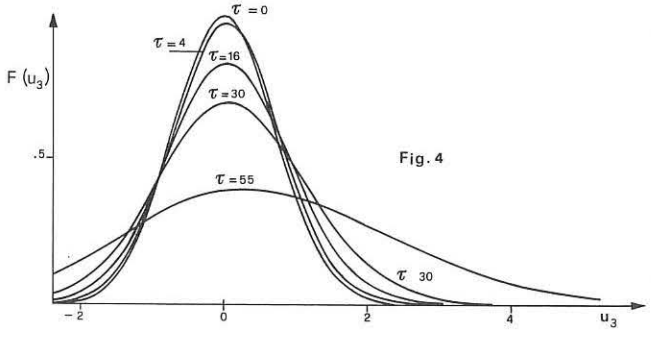

THE TRAPPED ELECTRON INSTABILITY

R.N. FRANKLIN * and R. MacKINLAY *

Culham Laboratory, Abingdon, Oxon, OX 14 3DB, UK.
(Euratom/UKAEA Fusion Association)

The deformation of the electron distribution function in the presence of a large amplitude electron plasma wave is evaluated in the approximation of constant wave amplitude, for various initial distributions. The stability of plasma for frequencies near the main wave frequency is examined. We establish for this model a general requirement for the initial distribution to be unstable, and comment on the relevance to the experimental situation.

The initial observation by Wharton et al[1] of the generation of sidebands by a large amplitude electron plasma wave propagating at phase velocities such that a significant number of particles are trapped in the potential wells of the wave has led to a large number of theoretical treatments and a number of more detailed measurements[2]. It still cannot be said that there is good agreement between experiment and theory to the extent that all features are well understood. Some of the difficulties arise because experimentally the amplitude of the main wave is a function of position. The various theoretical approaches can largely be divided into those that consider the temporal evolution of some initially given distribution in phase space, and those that take a stationary distribution function and examine the stability of plasma to excitation of other frequencies by the parametric process of mode coupling. This paper describes some results obtained by adopting the former or 'quasilinear' approach which sheds light on some of the theoretical work (Brinca[3]) and some experiments.

In the approximation of constant main wave amplitude, the trapped and untrapped particle orbits can be found in closed form (O'Neil[4]). For a given initial distribution function at time $t=0$ the paths of particles in phase space can be followed and the spatially averaged distribution function $\bar{f}(v,t)$ found. Waves with phase velocity V_φ such that $\frac{\partial \bar{f}}{\partial v}(v,t)\Big|_{V_\varphi}$ is positive, will be unstable according to linear theory. The time evolution of fluctuations in the plasma can then be obtained by examining A_w, the logarithm of the wave amplitude, where $A_w = \int_o^t \gamma\left(\frac{\omega}{k}, t\right) dt$ and γ is the linear growth or damping rate. Brinca[3] gave such a treatment for a linear (two-term Taylor) approximation to a Maxwellian. However, the variation of energy with orbit was not properly taken into account in the space averaging of $f(x,v,t)$. Fig.1 shows the results of determining $\bar{f}(v,t)$ numerically for a small amplitude wave. For this case, there are no waves in the resonant region for which there is any cumulative growth. We are able to recover the results of O'Neil[4] for $V_\varphi = \omega_o/k_o$, showing the oscillatory time dependence of the main wave amplitude. In Fig.2, A_w is plotted against V_φ for a large amplitude wave and an initially spatially uniform Maxwellian distribution, indicating that for large amplitude there is the possibility of growth for some frequencies. However, a plot of $f(x,v,t)$ over phase space at different times reveals that the effects are associated with 'just-trapped' particle orbits which would not be present experimentally for times long enough to cause our observed growth.

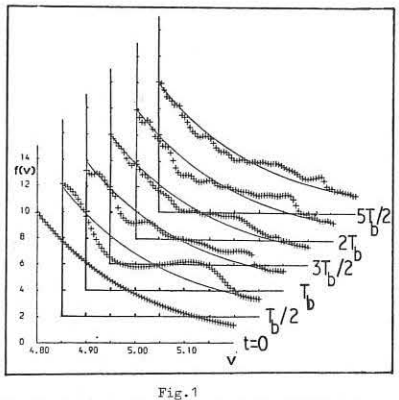

Fig.1
$\bar{f}(v,t)$ shown at intervals of $T_b/2$ for conditions $\omega_o/k_o = 5.0\, C_e$, $e\varphi_o/K_B T_e = 0.005$, $(C_e^2 = K_B T_e/m)$ and $\bar{f}(0) = 10^8$

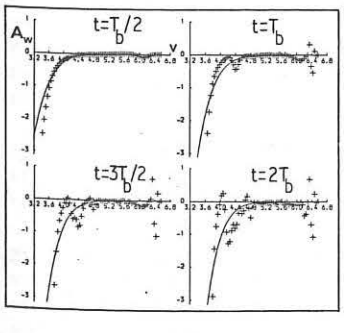

Fig.2
A_w is plotted against velocity for the same conditions as Fig.1 except $e\varphi_o/K_B T_e = 0.5$. The unbroken line represents Landau damping. The 'just-trapped' growth can clearly be seen.

The model can be taken further by examining initial distribution functions other than Maxwellian. We have examined various initial distributions using the 'quasilinear' model, with the empirical result that if $f(x,v,t=0)$ is a monotonically decreasing function of velocity, the plasma is stable except for the 'just-trapped' cases already mentioned. For a 'gentle bump-in-tail' initial distribution one would expect instability without trapping (as indeed we observe); however, the effect of trapping is to modify this behaviour substantially. Fig.3 shows the distortion of an initial gentle bump-in-tail distribution at half a bounce period, $T_b/2$, in the presence of a large amplitude wave. The growth associated with this distribution is shown in Fig.4, where A_w is plotted against V_φ for various times, showing the departure from exponential growth expected for no trapping. We have thus established the general requirements for instability on a quasilinear model, namely there must be an initial inverted trapped particle distribution.

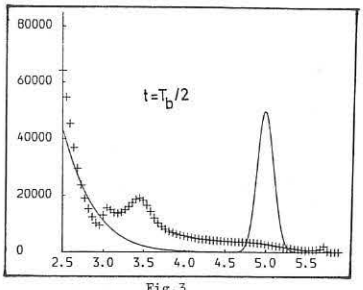

Fig.3
$\bar{f}(v,t)$ is shown at $t=T_b/2$ for a bump-in-tail initial distribution. Here, $\omega_o/k_o = 4.2\, C_e$ and $e\varphi_o/K_B T_e = 0.5$.

The experimental results of Barbian[5] and Jahns and Van Hoven[6] show significant distortion of the distribution function from the Maxwellian measured in the absence of perturbation at distances from the exciting antenna, short compared with the bounce length λ_b, (the equivalent of T_b in the temporal case). Thus the experimental situation appears to be one in which the effective initial distribution is not Maxwellian, but closer to a 'bump-in-tail' state similar to the case treated in Figs.3 and 4.

We conclude that deformation of the distribution function near the exciting antenna can be an important influence on the trapped particle instability as observed experimentally. Simultaneous measurements of the spatial evolution of the distribution function (and of test wave growth rate) 'quasilinear' theory is adequate, or whether it would be more appropriate to use a parametric coupled-mode model.

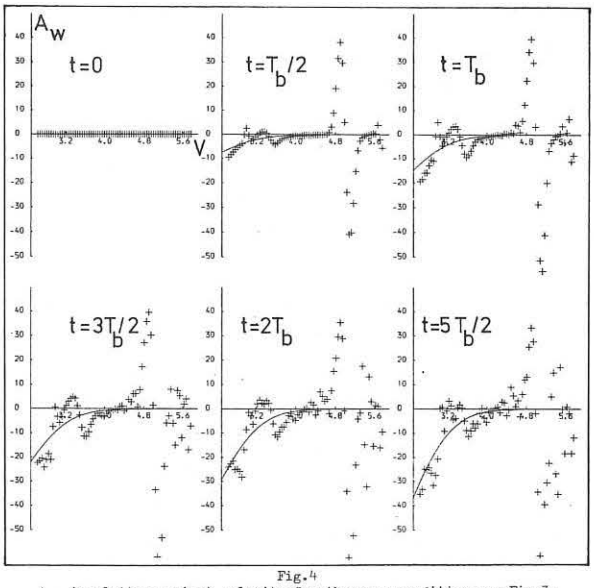

Fig.4
A_w is plotted against velocity for the same conditions as Fig.3, showing wave growth due to the bump-in-tail distribution

REFERENCES

1 WHARTON, C.B., MALMBERG, J.M. and O'NEIL, T.M., Phys. Fluids, 11, 1761 (1968).

2 FRANKLIN, R.N., HAMBERGER, S.M., IKEZI, H., LAMPIS, G. and SMITH, G.J. Phys. Rev. Letts., 28, 1114, (1972).

3 BRINCA, A.L., J. Plasma Phys., 7, 385 (1972).

4 O'NEIL, T.M., Phys. Fluids, 8, 2255 (1965).

5 BARBIAN, E.P., 6th European Conference on Controlled Fusion and Plasma Physics, Moscow, (1973).

6 Van HOVEN, G. and JAHNS, G., Phys. Fluids, 18, 80 (1975).

* Also at Dept. of Engineering Science, University of Oxford.

NONLINEAR SHIFT IN WAVE NUMBER OF AN ELECTRON PLASMA WAVE

E.P. Barbian

EURATOM-FOM Association Contract

FOM-Instituut voor Atoom- en Molecuulfysica, Kruislaan 407, Amsterdam/Wgm.

Abstract: The nonlinear shift in phase of an electron plasma wave is experimentally demonstrated by the measurement of the wave number shift of a transmitted small-amplitude test wave in the presence of a large-amplitude wave.

Introduction: The damping of large-amplitude electron plasma waves deviates considerably from the exponential attenuation as described by the Landau theory. If these waves are propagated through a collisionless and homogeneous plasma, then after the initial damping which is still governed by the linear damping rate, we do observe nonlinear oscillations of the wave amplitude. Morales and O'Neil [1] pointed out that in this nonlinear situation both, oscillations in phase as well as in amplitude are to be expected. These authors start from an initial-value problem and describe the case with the wave number fixed and the frequency modified by oscillations in time. Both oscillations can be explained by equations describing the conservation of energy and the conservation of momentum. In an experiment the frequency is fixed and instead of oscillations in frequency the wave number of the transmitted wave will undergo nonlinear oscillations and it is this case whereupon we want to put our attention.
Theoretical and experimental work carried out so far concentrated on the oscillation of wave amplitudes, mainly initiated by the calculations of O'Neil [2] and others and by the observations of Malmberg and Wharton [3]. This work concerned both electron [4] and ion waves [5] and emphasized the role of trapped particles [6] and recently the strong influence of the wave particle interaction on the growth of the sideband instability [7,8,9]. Attention to the non-linear phase shift as a complimentary case to the amplitude oscillation was then given by Morales and O'Neil [1] and others [10,11] and in recent experimental work this phase shift was demonstrated [12,13]. The measured decrease of the wave number appeared to be a few percent only in agreement with theory. The change of the wavenumber can be much larger, however, if a test wave of small amplitude is used in the presence of a large amplitude wave, as will be discussed here.

Theoretical wave number shift: Together with the calculation of the damping of the large-amplitude electron plasma wave Morales and O'Neil [1] presented a time-varying frequency shift $\delta\Omega$, which attains after several oscillations the value $\delta\Omega = -1.63\,\Omega_o$ with

$$\Omega_o = \left(\frac{eE_o k}{m}\right)^{\frac{1}{2}} \frac{\omega_p^2}{k^3} \left(\frac{\partial^2 f_o}{\partial v^2}\right)_{v_p} \left(\frac{\partial \varepsilon}{\partial \omega}\right)^{-1} \qquad (1)$$

where $\omega_B = \left(\frac{eE_o k}{m}\right)^{\frac{1}{2}}$ represents the bouncing frequency of the trapped particles, ω_p the plasma frequency, k the wave number, $\left(\partial^2 f_o/\partial v^2\right)_{v_p}$ the second derivative of the electron velocity distribution at the value of the phase velocity v_p. The factor $\left(\partial\varepsilon/\partial\omega\right)^{-1}$ can be determined from the dispersion formula for electron plasma waves adjusted for the experimental case of a warm plasma ($v_t^2 = kT/m$) using the dispersion relation

$$\varepsilon = 1 - \frac{\omega_p^2}{\omega^2} - \frac{3v_t^2 k^2}{\omega^2} \qquad (2)$$

By an analytic transformation the calculated shift in frequency (1) can be transformed into the real experimental situation of a fixed frequency and we get

$$\delta k = \delta\Omega/(-v_g) \qquad (3)$$

where v_g is the wave group velocity, which is experimentally determinable from the measured dispersion curve $\omega = f(k)$ in agreement with (2).

The experiment: The electron plasma waves are transmitted through the plasma column of a Q-machine [8]. The wave number ($k = 2\pi/\omega$) is measured by an interferometer, the plasma datas ($\omega_p = 127 \times 10^6\ s^{-1}$, kT = 0.19 eV) can be determined from the measured dispersion. The density is constant along the plasma column (90 cm long, B-field: 2200 Gauss) within a few percent. An energy analyzer mounted behind the movable cold end-plate can be used to measure the spatial evolution of the distribution under the influence of a large plasma wave [8].

Observations: When moderate large waves are excited at $\omega = 1.1\,\omega_p$ we observe the oscillation of the amplitude with a bounce wave number $k_B = 0.16\ cm^{-1}$. All parameters in Eq. (1) can be determined with a good accuracy in the quiescent plasma. By using the measured datas $\omega_B = 9.3 \times 10^6\ s^{-1}$; $k = 2.35\ cm^{-1}$, $\omega = 137 \times 10^6\ s^{-1}$; $v_t = 1.83 \times 10^7\ cm\ s^{-1}$; $v_p/v_t = 3.2$; $v_p/v_g = 1.95$ and calculating the second derivative of the undisturbed distribution we get for the asymptotic value of the wave number shift in Eq. (3): $\delta k = 0.14\ cm^{-1}$ or $\delta k/k = 0.06$ which is still a measurable quantity, though very small. The maximum shift determined from the interferometer plot of the large wave itself reached a value of $\delta k/k = 0.06$ with an asymptotic value of 0.04.

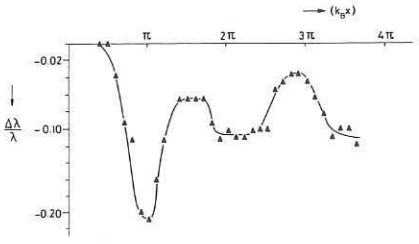

Fig. 1. Shift in wavelength versus distance from the emitter probe (at x=0). The bounce wave number ($k_B = 0.16\ cm^{-1}$) of the main wave is deduced from its amplitude modulation.

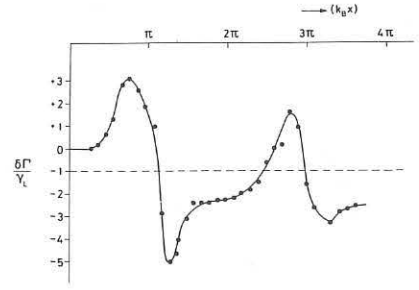

Fig. 2. Shift in damping coefficient versus distance. The linear Landau damping γ_L is measured with a small amplitude wave.

The wave number shift can be observed in a much more pronounced way if we use test waves. Together with the main wave which undergoes an amplitude modulation with $k_B = 0.16\ cm^{-1}$ the test waves (30 dB smaller in initial amplitude) are launched by a probe. Their phase velocity is chosen to interact with the strongly humped part of the distribution which is known from measurement. Under these conditions now a much stronger shift of k (or λ) is observed (see Fig. 1). The change in λ is 20% at its most, with an asymptotic value $\delta\lambda/\lambda = 0.8$.
In Fig. 2 we demonstrate the change of the damping rate at the same parameters. The zero damping ($\delta\Gamma/\gamma_L = -1$) is attained both for the main wave (not shown) and the test wave (Fig. 2) at the same value of $k_B x \approx 2.5\,\pi$. Both curves have the same characteristics as the calculated curves of Morales and O'Neil [1]. The oscillation in $\Delta\lambda$ appears twice as often in space than the oscillation in $\delta\Gamma$ which has the same period as the amplitude modulation k_B. This behaviour is explained by theory as the change in kinetic energy takes place with twice the rate of the change in momentum.
One remark might be added concerning the enhanced damping of the test wave (up to 4 times γ_L) after the initial damping (γ_L), and again after one period $k_B x$. This is a special item which can be related to the interaction with the positive slope of the humped distribution which is established by the main wave. This situation was theoretically described by Brinca [7] and is related with the physcial picture of the sideband instability.

Acknowledgement: The author thanks Dr. H. Hopman for valuable discussions and Mr. E. Gerlofsma for technical assistance.

References:

[1] G.J. Morales and T.M. O'Neil, Phys.Rev.Letters 28, 417 (1972).
[2] T.M. O'Neil, Phys.Fluids 8, 2255 (1965).
[3] J.H. Malmberg and C.B. Wharton, Phys.Rev.Letters 19, 775 (1967).
[4] R.N. Franklin, S.M. Hamberger and G.J. Smith, Phys.Rev.Letters 29, 914 (1972).
[5] H. Ikezi, Y. Kiwamoto, K. Nishikawa and K. Mima, Phys.Fluids 15, 1605 (1971).
[6] W.L. Kruer and I.M. Dawson, Phys.Fluids 13, 2747 (1970).
[7] A.L. Brinca, J.Plasma Phys. 7, 385 (1972).
[8] E.P. Barbian, Proc.of the Sixth Europ.Conf.on Controlled Fusion and Plasma Physics, Moscow, 465 (1973).
[9] G. Van Hoven and G. Jahns, Phys.Fluids 18, 80 (1975).
[10] A. Lee and G. Pocobelli, Phys.Fluids 15, 2351 (1972) and 16, 1964 (1973).
[11] S. Tsai, J.Plasma Phys. 11, 213 (1974).
[12] P.I. Vidmar, I.H. Malmberg and T.P. Starke, Phys.Rev.Letters 34, 646 (1975).
[13] H. Sugai and E. Märk, Phys.Rev.Letters 34, 127 (1975).

ION ACOUSTIC WAVES IN A DENSITY GRADIENT

N. D'Angelo
Danish Space Research Institute, Lyngby, Denmark,
and Research Establishment Risø, Roskilde, Denmark
and
P. Michelsen and H.L. Pécseli
Association Euratom - AEK, Danish Atomic Energy Commission
Research Establishment Risø, Roskilde, Denmark

Abstract: The propagation of ion acoustic waves in a density gradient was investigated experimentally. A transition between damping and growth in relative wave amplitude was observed at a wavelength $\lambda_c = 2\pi l_n$, where l_n is the e-folding length for the density gradient.

Ion acoustic waves are known to play an important role in problems of absorption and reflection of laser radiation in inhomogeneous plasmas[1]. We investigated the linear properties of these waves in density gradients[2] in order to improve the knowledge of the basic processes. Study is also relevant for the problem of the heating of the solar corona[3].

The experiment was conducted in a Cs-plasma column of a single-ended Q-machine. The plasma density was $1\text{-}5\times10^{9}$ cm^{-3} and the neutral gas pressure $\leq 10^{-5}$ mm Hg. A (variable) density gradient along the direction of the magnetic field (2-3000 gauss) was produced by surrounding a portion of the plasma column with a metal tube. The more negatively biased this tube, the steeper the density profile.

Measurements were performed with a Langmuir probe movable along the column axis. The probe was a flat metal disc oriented normal to the axis. The zero-order axial density profile was obtained through measurements of the probe floating potential and the relation $\varkappa T_e \frac{\partial n}{\partial x} = en\frac{\partial \varphi}{\partial x}$ between density and potential gradients. With the same probe the flux was observed to decrease along the axis when moved away from the generating plate, thus showing the presence of radial plasma losses. When the zero-order plasma behaviour is analysed on the basis of continuity and momentum equations, including a radial loss term, agreement is found with the measured zero-order quantities.

Ion-acoustic waves were excited by a grid immersed in the plasma (normal to the axis of the column) between the generating plate and the metal tube. The wave measurements were performed with the probe floating electrically, since $\frac{\tilde{n}}{n} = \frac{e\tilde{\varphi}}{\varkappa T_e}$ ($\tilde{n}$ is the perturbed density, $\tilde{\varphi}$ is the perturbed potential). The results of the wave measurements are summarized in Fig. 1. At any frequency, f, the corresponding wavelength is indicated by a cross. Above f ≈ 2 kHz the waves are damped as they propagate away from the grid, and δ_d (with triangles pointing upward) is the damping distance. Below f ≈ 2 kHz the waves grow; δ_g (with triangles pointing downward) is the growth distance. The measurements of Fig. 1 were performed with a tube bias of -30 volt, which corresponds to $l_n \sim 12$ cm. From Fig. 1 we note first that the phase velocity $f\lambda$ is constant ≈ $1.2\cdot10^{5}$ cm/s and for f ≥ 3 kHz, the ratio $\delta_g/\lambda \approx 0.5$, both quantities being independent of frequency as normally found for propagation of ion-acoustic perturbations in uniform plasmas when $T_e = T_i$. Secondly, for f ≤ 1 kHz, the growth distance $\delta_g = 2l_n$ is independent of frequency as predicted by a hydrodynamic model. Finally at f ≈ 2 kHz, δ_d and δ_g become large, as expected at the frequency of transition between growth and damping.

In Fig. 2 we show the observed relation between l_n and λ_c. The uncertainty is represented by a rectangle. Assuming a linear relationship, the best fit to the measured points is very close to the line $\lambda_c = 2\pi l_n$.

As already mentioned, our results for the low frequency part are predicted by a hydrodynamic model. For the high frequency part our measurements do not differ from those found in uniform plasmas and can be explained from a collisionless description. The transition region where $\lambda = \lambda_c$ has been considered by Parkinson et al.[3]. They considered an isothermal, exponential atmosphere, acted upon by the solar gravity, in which ion acoustic waves propagate, and found a critical wavelength $\lambda = 2\pi l_n$ (when $T_i = T_e$). The overall agreement between our measurements and their results indicates that they apply to ion-acoustic wave behaviour in density gradients no matter how the gradients are produced.

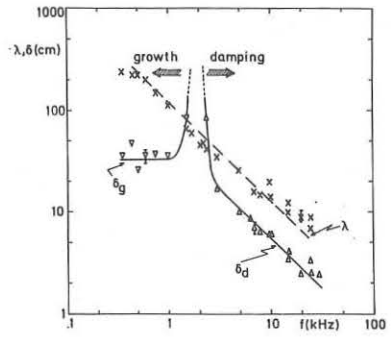

Fig. 1. The wavelength λ, and the damping, δ_d, or growth δ_g, distance vs. the wave frequency f.

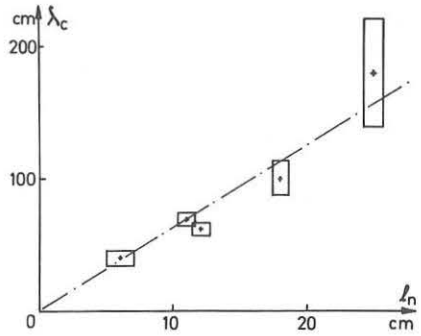

Fig. 2. The critical wavelength λ_c vs. the gradient e-folding length l_n.

References:

1) V.N. Tsytovish, L. Stenflo, H. Wilhelmsson, H.-G. Gustavson and K. Østberg, Physica Scripta 7, 241 (1973).

2) N. D'Angelo, P. Michelsen and H.L. Pécseli, Phys. Rev. Lett. 34, (May 1975).

3) Parkinson and K. Schindler, J. Plasma Physics 3, 13 (1969).

Parametric Instabilities Arising from Whistler Wave Resonance Cone

R. W. BOSWELL

European Space Research & Technology Centre
Noordwijk, Netherlands

Abstract: Experimental results are presented which show that the parametric decay of whistler mode waves launched from a point source are associated with the large electric field of the group velocity resonance cone.

Most work on the right hand polarised wave which propagates below the electron gyro frequency, the so-called whistler mode, has been carried out using either a plane wave theory or including cylindrical boundary conditions. However, in many applications, such as laboratory experiments and in the ionosphere, the source region is small compared to a wavelength and a theory including all possible allowed wave vectors is required to satisfactorily describe the radiation pattern. Theoretical work (1,2) and experimental observations (3,4) have shown the existence of a resonance cone where the electric field of the wave becomes very large. The radiation pattern in the far field has been measured (5,6) showing that the field of the resonance cone is still approximately 10dB above the wave fields.

Previous experiments (7,8) on parametric decay of the whistler wave have not considered the effect of the resonance cone on the wave fields, leading to doubtful estimates of the instability threshold electric field and the mechanism of the decay processes.

The experiment was carried out in a large volume magneto-plasma with an experimental length of 120 cms and diameter of 60 cms, the steady magnetic field B_o of 128 gauss being uniform to $\pm$ 0.6% over this volume.

A plasma was formed by RF ionisation in argon gas at a pressure of 8×10^{-4} torr with a density of approximately 5×10^{10} cm^{-3} and electron temperature of 3eV.

The waves were launched from a small 1 cm magnetic loop antenna and received on an electric probe with an exposed area 4 mm long and 1 mm in diameter which could be rotated about the transmitter on a circle of 28 cm radius. Although the decay instability could be produced over a range of pump frequencies, it was strongest when the pump frequency was approximately 0.7 of the gyro frequency f_c. For these conditions the axial whistler wavelength was 6 cm.

Figure 1 shows the high and low frequency decay spectra for an input power of about 10 watts. From the received signal, the amplitude of the pump can be estimated to be a few volts per metre. The frequency difference between the two high frequency waves can be seen to be equal to the low frequency wave thereby satisfying the energy conservation condition $\omega_1 = \omega_2 + \omega_3$.

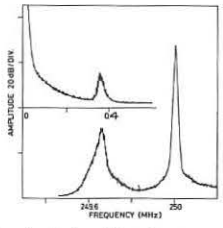

Fig. 1 High and Low Frequency Decay Spectra

The electric fields of the pump wave and decay wave are shown in Figures 2a) and 2b) as a function of angle to B_o for a pump frequency of 250 MHz, which was approximately $0.7f_c$. Taking into account thermal corrections, the theoretical angle for the resonance cone is 43 degrees.

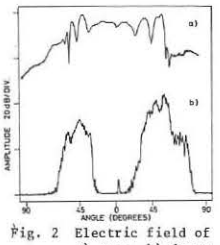

Fig. 2 Electric field of a) pump, b) decay

The structure outside the cone is due to a slow plasma wave which has been analysed by Kuehl (9). The electric field of the decay whistler can be seen to be directly associated with the large electric field of the pump resonance cone and its structure, whilst the whistler waves which propagate inside the resonance cone have a wave field which is below threshold for the parametric instability and no decay occurs.

In a theoretical analysis by Porkolab (10) it was found that this instability had a minimum threshold for excitation if the low frequency acoustic wave had wavelengths perpendicular and parallel to B_o which were approximately equal, i.e. the wave was travelling at 45 degrees to B_o. Since this is nearly the resonance cone angle the instability should occur over a small range of frequencies around $f = 0.7\ f_c$ for pump fields just above threshold; much higher fields being required for frequencies outside this range. This is in good agreement with our experimental measurements.

It should be noted that Porkolab (7) has measured two different types of decay occurring at the same frequency ($f=0.69f_c$). The first is probably due to the interaction between the cone field and the plasma wave which is associated with the cone and not with the boundary effects. The second decay involved two whistlers and produced a low frequency acoustic wave with a wavelength about five times longer than that predicted by the linear dispersion relation.

This apparent contradiction can be resolved by studying the radiation pattern of the antenna used to launch the waves (6). Since the whistler waves are propagated out of a cone, the wavefronts are formed by the addition of many wave vectors. Consequently, close to the cone and at an appropriate radial distance from the transmitting antenna it is possible to satisfy the momentum conservation relation and also the dispersion relation for the acoustic waves.

A resonance cone also exists in the first pass band for the cyclotron harmonic (Bernstein) waves and similar parametric interactions should occur in this frequency range.

References

(1) H. H. Kuehl. Phys. Fluids 17 1275 (1974)
(2) N. Singh & R. W. Gould. Radio Science 6 1151 (1971)
(3) R. K. Fisher & R. W. Gould. Phys. Fluids 14 857 (1971)
(4) A. Gonfalone. J. Phys. (Paris) 33 521 (1972)
(5) R. W. Boswell & A. Gonfalone. To be published in Physics Letters (May 1975)
(6) R. W. Boswell. Submitted to Phys. Rev. Lett. March 1975
(7) M. Porkolab et al. Phys. Rev. Lett. 29 1438 (1972)
(8) C. Christopoulos. PhD Thesis University of Sussex (1974)
(9) H. H. Kuehl. Phys. Fluids 16 1311 (1973)
(10) M. Porkolab. Nuclear Fusion 12 329 (1972)

DAMPING OF PLASMA WAVES IN HOT WEAKLY INHOMOGENEOUS MAGNETIZED PLASMA

S.S.Pešić

Atomic Physics Laboratory,"Boris Kidrič" Institute-Vinča
P.O.Box 522,11001 Beograd,Yugoslavia.

Abstract The propagation and damping of small amplitude quasi-longitudinal plasma waves in hot plasma in the presence of weak density and magnetic field gradients is studied. The efficiency of the wave energy thermalization in the LH frequency range is discussed.

The propagation and damping of externally driven quasi-longitudinal plasma(electrostatic) waves with finite $k_{//}$ in hot homogeneous magnetized plasma has been studied in details /1/. In order to give an insight into the lower hybrid (LH) heating of thermonuclear plasmas and to make the results pertinent to the present LH experiments in toroidal devices,in this paper we study the propagation and spatial damping of quasi-longitudinal plasma waves in hot plasma in the presence of weak density and magnetic field gradients.

We consider the wave propagation in hot plasma whose parameters depend only on one coordinate. The static magnetic field is orthogonal to the direction of plasma inhomogeneity. Regarding the plasma as a homogeneous medium having the physical local properties of the actual plasma,we have solved numerically for a wide range of plasma parameters the full dispersion equation governing small amplitude quasi-longitudinal waves in hot magnetized plasma /2/,

$$D(\omega,\vec{k},C_\beta)=k^2+\sum_\alpha \sum_{n=-\infty}^{\infty} \frac{2\omega_{p\alpha}^2 e^{-\lambda_\alpha} I_n(\lambda_\alpha)}{v_{t\alpha\perp}^2}\left\{\frac{T_{\alpha\perp}}{T_{\alpha//}}+\left(z_{n\alpha}\frac{T_{\alpha\perp}}{T_{\alpha//}}-\frac{n\omega_{b\alpha}}{v_{t\alpha//}}\right)Z(z_n)\right\}=0 \qquad (1).$$

Here the C_β's represent the steady state plasma parameters, $v_{t\alpha\perp,//}^2=2\kappa T_{\alpha\perp,//}/m_\alpha$, $\lambda_\alpha=k_\perp^2 v_{t\alpha\perp}^2/2\omega_{b\alpha}^2$, $z_{n\alpha}=(\omega-k_{//}V_{//}+n\omega_{b\alpha})/k_{//}v_{t\alpha//}$ and and Z(z) is the plasma dispersion function. The results obtained hold in quasi-homogeneous plasma under the condition that the steady state plasma parameters are slowly varying within a wavelength. The magnetic field and density inhomogeneity of toroidal plasmas are gentle enough(except in a narrow region near the plasma edge of inconsequential importance for the subject under consideration) to make this local plasma description appropriate. Consequently,the plasma density is allowed to have a density profile $n=n_0\{1-(x/X)^\gamma\}$,where $\gamma=3,4,..$,whose characteristic length is left unspecified. The magnetic field intensity is assumed to vary as r^{-1},while the ratio between the major torus radius and the plasma radius is taken to be 6. In what follows the following dimensionless parameters are used frequently: λ_i is the square of the ratio between the ion Larmor radius and the perpendicular wavelength,and $h=\omega/\Omega_b$ is the ratio between the angular frequency and the ion cyclotron frequency.

In travelling in the direction of increasing density the resonant electromagnetic mode slows down and reaches a density region at which its phase velocity becomes close to that of plasma waves(in Fig.2. the electromagnetic and plasma waves are labelled CPS and HPS,respectively). The wave propagation up to this layer is not materially affected by the particle thermal motion. However in the afore mentioned density region the two waves lose their separate identity,merge smoothly and convert one to the other. The wave conversion takes place at the density $/3,4/\omega_p^2/\omega_{pr}^2\simeq 1-2.5q^2 v_{ti}(m_e/m_i)^{1/2}/c$ where $q^2=\omega_{pr}^2/\omega^2$. In the flat-topped toroidal plasma the wave conversion occurs relatively far from the cold wave resonance position. Anticipating the results concerning the damping of plasma waves in quasi-homogeneous plasma,we conclude that in order to communicate the wave energy to the bulk of charged particles the wave conversion should occur near the maximal density. The above observation indicates that the problem of frequency tracking of the maximal density is overestimated at least at small variation (up to 20%) of the maximal density. If the waves are launched in the direction of increasing density and magnetic field,the cold wave resonance position displaces towards higher densities,passes on the other side of the plasma column and finally disappears as the maximal density decreases. However,the conversion between electromagnetic and plasma waves occurs at high densities even in absence of the cold wave resonance.

The wave behaviour in hot quasi-homogeneous plasma can be qualitatively examined by means of the dispersion curves for plasma waves with finite $k_{//}/1/$. The lower hybrid dispersion curves represented on Fig.1. are typical ones in a large scale of parameters considered. When the the waves are launched in the direction of increasing density and magnetic field,the resonant electromagnetic mode converts into a backward fast plasma wave. Moving radially inwards this wave encounters a branch point (the locus of this point is labelled A in Fig.2.). It should be pointed out that throughout this paper we consider only the least damped plasma mode which in long time in absence of collisions is dominant in the plasma. We refer to this solution of the dispersion relation (1) as the principal mode. The solution trajectories of the other spatial modes can be found in Ref./1/. Beyond the branch point A the principal mode becomes outward-moving forward wave. As the wave travels farther,another branch point is reached (see Fig.2.) at which the principal mode converts into an inward-moving slow wave. A similar wave behaviour occurs when the waves are launched in the direction of increasing density and decreasing magnetic field intensity.

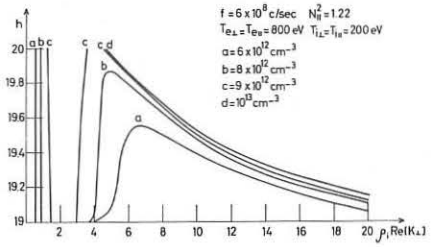

Fig.1.-The lower hybrid dispersion curves

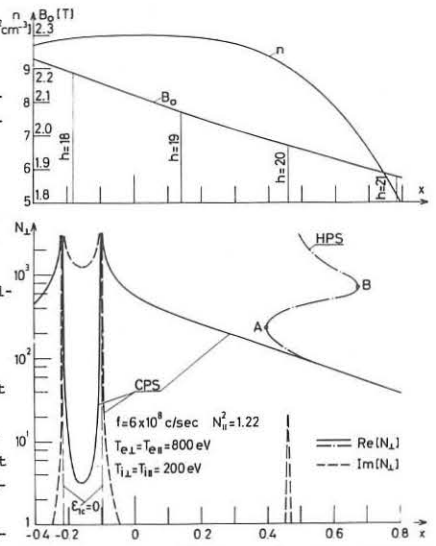

Fig.2.-The perpendicular refractive indices of electromagnetic and plasma waves.

The previous discussion reveals that in the presence of magnetic field gradients the principal mode is trapped between adjacent harmonics of the ion cyclotron frequency. At low ion temperatures the wave field amplification in this region can be sufficiently high to excite parametric effects. However,the wave field amplification decreases for increasing the ion temperature /3,5/ and the linear collisionless harmonic ion cyclotron interaction(or the collision-restored Cerenkov interaction) becomes the dominant process in the wave energy thermalization. The damping of the excited plasma waves by the harmonic ion cyclotron collisionless interaction is important only in the vicinity of the harmonics of the ion cyclotron frequency (see Fig.2.). The efficiency of the wave damping during its first encounter with the harmonic of the ion cyclotron frequency depends on the quantity $N_{//}v_{ti}h$ and the value of λ_i at which the harmonic occurs. Namely,the imaginary part of the wave refractive index increases and the region in which an efficient damping occurs enlarges considerably(in the case represented on Fig.2. it is large a few Larmor radii) for increasing the quantity $N_{//}v_{ti}h$. If at the harmonic λ_i is sufficiently larger than the critical value at which the ion cyclotron damping starts to be effective(this value is of the order of h) the wave is efficiently damped at its first encounter with the harmonic.

REFERENCES

1. Pešić S.S.,Plasma Physics 15(1973)193.
2. Stix T.H.,THEORY OF PLASMA WAVES,Mc Graw-Hill,New York(1962)
3. Pešić S.S.,Ph.D.Dissertation,University of Paris,May 1973.
4. Pešić S.S.,Lectures given at the VII YSPIG(1974),Rovinj, Yugoslavia.
5. Pešić S.S.,UPee-74/11,University of Padova(1974).

INVESTIGATION OF HIGH-TEMPERATURE PLASMA OBTAINED BY HYDRODYNAMICAL EFFECT OF SHOCKING AND HEATING

M.A.SULTANOV

(Tajik State University, Dushanbe, USSR)

ABSTRACTS: The possibility of obtaining dense high-temperature plasma at the collision of two supersonic plasma fluxes (SPF) in air under the atmosphere pressure in shown. The cause of plasma heating is shock wave (SW) multiple reflection from the discharge chamber sides.

INTRODUCTION: The question of high-temperature plasma obtained under laboratory conditions (except thermo-nuclear devices [1] and MC-generators [2]) is of great theoretical and practical value. For example, on the base of powerful high-current pulse discharges (PHCD) it is possible to obtain SPF at the collision of which shock-compreseed plasma volumes (SCPV) are formed with high temperature and density readings.

RESULTS: The discharge loop regime at C=1 200 μF, V=3 kv, was used. The flux parameters before the collision were as follows the entrance velosity is 12-16 km/sec, Mach number - 8-12, SPF temperature $\sim$2.6 ev, adiabatic index γ for theoretical evalutions was takes as 1.25.

As it can be seen from space-time scanning, oscillogram, high-speed frames and plasma spectrograms at the moment of the two symmetrical SPF collision in the middle of the discharge chamber parallel to direction (fig.1) SCPV is formed with the parameters difference to those of the spreading SPF; it is confinted from the SW discharge chamber side. At the same time SCPV is a zone of intensive luminescence of rather high density and temperature with a high gradient of N_e and T_e. The evidence can be obtained by frame scanning normal to AB direction where light and dark volumes of plasma cluster can be noticed. The SCPV obtained speads radially with supersonic speed; for the given regime it equals to 4-6 km/sec.

The spectrum of plasma obtained has strong linear and continuous radiation (fig.3).both in longitudinal and transverse sections: it consist mainly of the lines of electrode disintegration material, and those of air components. The continuous spectrum is due to braking and recombination radiation. The analysis of the linear plasma spectrum shows that all the lines of neutral and single ionized atoms are recorded in absorption. In the line loops of the same degree of ionization the intensity maximum displacement take place, its value permits to measure the plasma temperature [3,4] . In the neutral atom line takes place symmetrical, and in the ion line loop - assymmetrical self-reversal.

When considering intensity distruction of continuous and linear radiation in various sections its maximum value can be noticed off the discharge chamber cutoft. It can be explained by a SW formatio in the middle of a discharge gap and by radial SCPV spread ; .

DISCATION: At the two symmetrical SPF collisions, according to the hydrodynamics laws, SW formation is observed accompanied by symmetrical reflected SW propagation. Since electrodes are confinded by dielectric Walls of large size, multiple SW off the discharge axis; the sharp change of SW off the discharge axis; the sharpe change of plasma parameters is observed at the same point. Being plasma parameters is increasing on account of reflected from the opposive sides, SW contributes to additional heating of plasma and makes it denser. The fact that the hydrodynamics effects are the cause of SCPV formation can be proved by asymmetry in ion line loops.

Quantitative measurements of asymmetric ion line self-reversal with high constants make us to believe that the main cause of their broadening in more powerful discharges is Stark-effect and high pressure at a shock wave. Under the Stark-effect, which must be of statistical character at high densities, the line broadens asymmetrically, while the statistical wing joins the centre of the line from the shorter or longer wave length directions, depending on the constant quadratic effect sign.

Quantitative parameters obtained for the given discharge loop regimes showed that in this way plasma with the temperature more 40 ev and electron concentration $\sim 10^{19}$ sm^{-3} can be obtained. The same results are observed in ion lines of highly ionized air.

For quantitative explanation of the effect observed theoretical evalutions from gas-hydrodynamic can be considered. For this purpose, first of all, the main hydrodynamics equations and Renkin-Gugonio ratios were made. A unidimentional plane problem is to be solved to form the equation of confinuity, quantity of motion, energy constancy and enhalpy.

Thus, the use of hydrodynamical effect of shocking and heating is the most practical under laboratory conditions for obtaining plasma with high values of T_e and N_e on the PNPD basis.

The proposed technique and the results of our investigations may be used to keep and increase the life-time of both low-temperature and high-temperature plasma, to obtain high density radiation sources, for additional plasma heating with the help of multiple SW reflection etc.

REFERENCES:

1. L.A.Artsimovich. Controlled termo-nuclear reactions. Moscow, 1962.
2. A.D.Sakharov. Doklady Akademii Nauk SSSR, 165, 65, 1965.
3. A.Bardocz, T.Vörös. J. Quant. Spectr. Radiat. Transfer., Pergamon Press, 6, 193, 1966.
4. M.A.Sultanov. US National Bureau of Standards, Washington, 232.07.1974.

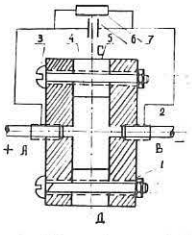

Fig.1. The scheme of discharge chamber: 1-dielectric plates, 2-electrodes, 3-clamps, 4-plasma volume, 5-barries, 6-condenser batterys, 7-high voltage rectifier.

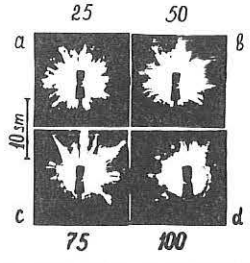

Fig.3. Fragments of insequenses of high-speed scanning at registration of differ times. Ciphers shows the time discharge.

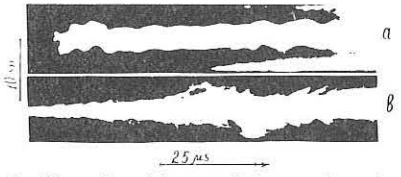

Fig.2. Time of continuous photoscanning at collisions of two SPF: longitutinal (a) and transversal (b) sections.

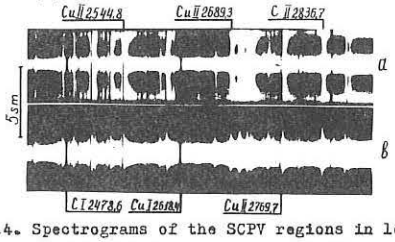

Fig.4. Spectrograms of the SCPV regions in longitutinal (a) and transversal (b) sections.

ON THE POSSIBILITY OF PLASMA ASSELERATION AND HEATING IN THE HIGH-CURRENT PULSE DISCHARGE IN A CUMULATIVE ZONE

M.A.SULTANOV

(Tajik State University, Dushanbe, USSR)

ABSTRACTS: At the interaction of two or more supersonic plasma fluxes (SPF) at different angles of slope an efficient acceleration and heating of plasma in a cumulative zone occurs. Some parameters of the acceleration plasma flux were measured, the gas-dynamical nature of the phenomenon observed is supposed.

INTRODUCTION: The method of obtaining plasma with the help of cumulative effects is widely used in the fields of high-temperature plasma and controlled thermo-nuclear fusion [1-4]. Under the laboratory conditions of special interest in the cumulative method of obtaining fluxes in explosive and shock plasma devices. Additionaly in the cumulative zone it is possible to study different physical processes, such as: plasma irregularity, large-scale, anomalous light scattering, mechanism of heating and so on.

As the experimental studies show, such processes take place at SPF cumulativity at different angles of slope and in high-current pulse discharge (HCPD). In connection with it, in the present paper a possibility of acceleration and heating plasma fluxes in cumulative zone at the interaction of two SPF at 0^0, 30^0, 45^0, 60^0 and 90^0 angle of slope is investigated.

RESULTS: The investigation took place on the basis of powerful pulse discharges by the method of continuous scanning and frame shooting, as well as by spectroscopic measurements of main parameters. The structures of accelerated plasma flux and those of free SPF were compared [5]. As investigations show a spase-time inhomogeneity along the flux axis takes place and some other phenomena which had not been observed at a single SPF study (fig.1). The structure of plasma formation consists of three separate luminescence fronts: anodic, cathodic and a shock wave being formed at their interaction. After the interaction different gas-dynamical parameters of the flux alter depending on the angle of slope. The highest increase in parameters takes place at the SPF interaction with 60^0 angle of slope. For example, when the length of the dark space is 48 mm, the speed of SPF entrance from the inlet of the discharge chamber is 12 km/sec and in cumulative zone - 14 km/sec This is most clearly seen in the high-speed frames (fig.2). The structure of plasma fluxes on the high-speed frames sharply differs in each case. At the parallel electrode position (0^0 angle) in the flux structure the formation is observed of two quasi-electrode "bumpy-structures" (from anode and cathode torches) followed by one more and then by the repeated first two "bumpy-structures" after the interaction, when the of slope is 60^0 at the point of two SPF collision only one "bumpy-structure" occurs. In the first two variations (fig.2,a,b) before the anodic and cathodic torches collisions a periodical pattern in their structure was observed, characterized by shock wave formations as intensive points at equal distances from one another with different gas-dynamical parameters. Such a picture is more clearly seen in the initial discharge stage.

The above said can be proved by the investigation of spectroscopic properties of the accelerated flux characterized by in intensive luminescence zones, by broadening of ion line loops and neutral atom loops, and by an efficient displacement of intensity maximum in spectrum region. In general, plasma spectrum character depending on the SPF angle differs both in intensity of radiation of electrode material components lines, and in alteration or radiation and self-reversal lines loops. The differences are seen both in new lines formation and continuum intensity growth in one spectrum and in vanishing or their intensity in the other one.

All the above written was proved by quantitative measurements of plasma temperature and concentration (fig.4). Temperature and concentration values are the lowest at 0^0 angle of slope and the largest at 60^0. In cumulative zone, for example, at 0^0 T_e = 1.8 ev, at 60^0 - 3.1 ev; N_e - 1.1×10^{17} and 2.5×10^{17} sm^{-3} respectively; the accelaration of a plasma flux is 5-6 km/sec^2.

DISCUSSION: Under the conditions when presure in the discharge chamber is much higher than of the atmosphere, the flux being ejected from the cylinder outlet is subjected to supersonic broadening. In the initial stage of the pulse two "bumpy-structures" from anode and cathod torches are formed, which in some moments fuse forming a single "bumpy-structure". After the maximum jet broadening behind the nozzle the narrowing takes place: the jet becomes denser, which is accompanied by the increase of flux parameters. It is known that in the maximal narrowing zone some acceleration of the flux takes place. This region is a cumulative zone, as well, where besides the flux acceleration the increase of its parameters takes place.

Thus, at two or more SPF interactions with different angles of slope the formation of complex gas-dynamical structure as a system of wave compression and thinning, shock and cumulative waves takes place. Shock wave form and structure in certain regimes of a discharge loop depends on the angle of electrode position in a discharge chamber; for example, a bridge-shaped shock wave can be formed.

The results of our investigations can be practically used in heating and increasing life-time, plasma and gas flows acceleration in the cumulative zone, SPF formation, in jet engineering etc.

REFERENCES:

1. A.D.Sakharov. Uspehi fizich. Nauk, Sov`et, 88, 725, 1966.
2. L.V.Al`tshuller. Uspehi fiz. Nauk, Sov`et, 85, 196, 1965.
3. Physics of Hifh Energy Density. Edited by P.Caldirola and by H.Knoepfel. Academic Press, New-York, London, 1971.
4. Y.V.Afanas`ev, V.A.Gribkov, O.N.Krokhin, V.Y.Nikulin, G.V. Sklizkov, M.A.Sultanov. Preprint N 87, Lebedev`s Institute, Moscow, 1973.
5. M.A.Sultanov. JTF, Sov`et, 44, 759, 1974.

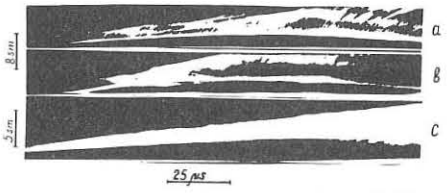

Fig.1. Time continuous scanning of cumulative zone at 0^0 (a), 60^0 and free SPF (c).

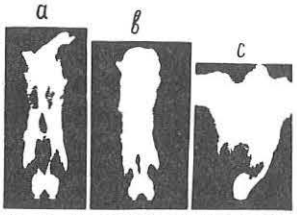

Fig.2. Fragments of the sequenses of high-speed scanning after 150 μs of impulse at 0^0 (a), 60^0 (b), single SPF (c).

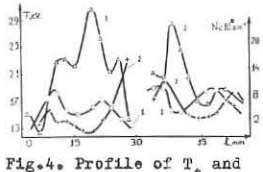

Fig.4. Profile of T_e and N_e at 0^0 (1), 30^0 (2) and 60^0 (3).

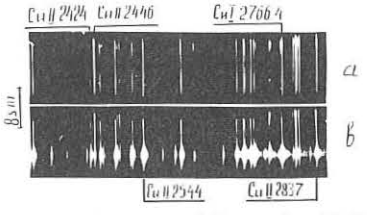

Fig.3. Spectrograms of the region in cumulative zone at 0^0 (a) and 60^0 (b).

HEATING AND IONISATION IN MHD SHOCK WAVES PROPAGATING INTO PARTIALLY IONIZED PLASMA

L. Bighel, A.R. Collins, N.F. Cramer and C.N. Watson-Munro

School of Physics, University of Sydney, NSW, Australia

Abstract: A model of the structure of MHD switch-on shocks propagating in a partially ionized plasma, in which the primary dissipation mechanism is friction between ions and neutrals, is here compared favourably with experimental results. Four degrees of upstream ionization were studied, ranging from almost complete to very small ionization.

Introduction

Studies of shock structure previously obtained on SUPPER II indicate that the principal heating process in ionizing shocks is ion-neutral collisions (1). This series of experiments extends this work to examine the effects on shock structure of varying the neutral component in the upstream plasma. Four shocks were studied and their method of preparation differed only in the level of preionization. T_e, T_i and n (electron density) profiles were obtained for four shocks and these profiles compared with a model of shock structure based on ion-neutral friction.

Experiment

The SUPPER II plasma vessel is a stainless steel cylindrical shock tube. At each end of the vessel is a Pyrex endplate, in one of which is a short central electrode. The vessel was filled with 120 mtorr of helium and embedded in an axial magnetic field of 0.25 tesla.

The test plasma was prepared by driving a low power ionizing shock into the vessel. This shock was launched by discharging a 30 kA, 40 μsec half period, current pulse between the central electrode and the vessel wall. The plasma thus formed was allowed to settle to a quiescent state before launching the main shock. Since the initial plasma was rapidly cooling, varying the time between plasma preparation and shock preparation effectively controlled the level of preionization.

The shock waves were launched by discharging, at the appropriate time, a radial current pulse with half period 16 μsec and peak current 150 kA. The shock waves were all similar in behaviour with an axial velocity of 10^5 m/sec.

Electron density and temperature profiles were determined by 90° Thomson scattering of a 150 MW ruby laser beam. The ion temperature was estimated by measuring the Doppler broadening of the HeII line at 468.6 nm.

Theory

The calculation of heating and ionization in the shock wave is similar to that in (1) for an ionizing shock in a 1 tesla field, i.e. the current and magnetic field profiles are assumed known and fed in to calculate the heating. However, this calculation is more complete in that all terms in the species energy equations are retained, including the adiabatic compression term.

The ions and atoms are assumed to have the same temperature, and ionization assumed to occur through electron-neutral ionizing collisions. Any second ionization of the helium is neglected. Dissipation terms in the energy equations (1) are calculated using Cowling's model of partially ionized plasma (2), the most important of these being the ion-neutral friction term.

Compression in the shock is calculated from the known switch-on field B_θ by means of the integrated overall momentum and energy conservation equations (3) (neglecting ionization energy). The resultant relation depends on the radial electric field, which is zero for the shock propagating into a non-zero upstream electron density and for the ionizing shock takes the value satisfying the Chapman-Jouguet condition (4).

Discussion

(i) Highly ionized upstream plasma (n = 2 x 10^{21} m^{-3}, 50% ionization) (Figs. 1a,1b). Computation with 50% ionization and the observed B_θ rise time of 1 μsec gives little heating and equal ion and electron temperatures. To gain good agreement with experiment it is necessary to assume that the upstream neutrals have been centrifuged to the walls, leaving 100% ionized upstream plasma. Also we assume a rise time of 0.2 μsec (i.e. the observed rise time of n and T_e) and a resistivity 5 times the classical value. This enhancement in resistivity could be due to the ion-acoustic instability discussed in (5).

(ii) Upstream ionization 25% (n = 10^{21} m^{-3})(Figs. 2a,2b). Ions, neutrals and electrons are heated about equally, in agreement with observation. The rise time in B_θ used is 0.2 μsec.

(iii) Upstream ionization 6% (n = 2.4 x 10^{20} m^{-3}) (Figs. 3a,3b) A B_θ rise of 0.5 μsec gives strong ionization and ion heating, as is observed.

(iv) Ionizing shock (Figs. 4a,4b). The initial electron density is due to photoionization from the hot rear of the shock. Strong ion and neutral heating is observed in excellent agreement with experiment.

Acknowledgements

Support for this work has been provided by the Australian Research Grants Committee, the Australian Institute of Nuclear Science and Engineering, the University of Sydney Research Grants Committee and the Science Foundation for Physics within the University of Sydney.

References

(1) Bighel, L., Cramer, N.F., Millar, D.D. and Niland, R.A., Phys. Letts. 44a, 449 (1973).

(2) Cowling, T.G., Mon. Not. R.A.S. 116, 114 (1956).

(3) Leonard, B.P., J. Plasma Phys., 7, 133 (1972).

(4) Chu, C.K. and Gross, R.A., Advances in Plasma Physics 2, 139 (1969).

(5) Craig, A.D. and Paul, J.W.M., Plasma Phys., 9, 151 (1973).

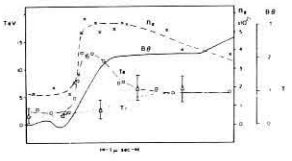

Fig. 1a

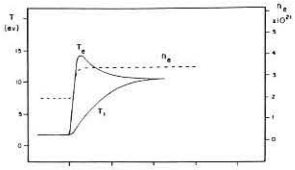

Fig. 1b

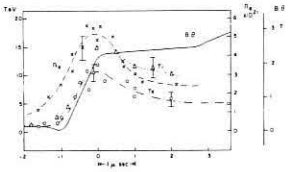

Fig. 2a

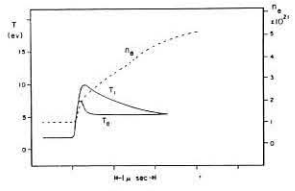

Fig. 2b

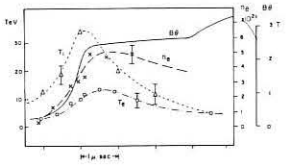

Fig. 3a

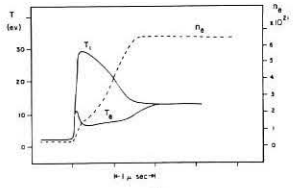

Fig. 3b

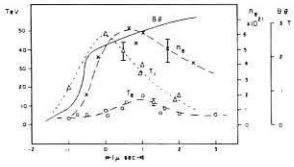

Fig. 4a

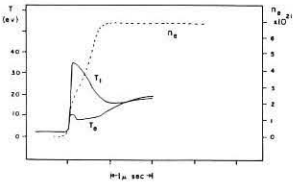

Fig. 4b

OHM'S LAW IN COLLISIONLESS SHOCK WAVE

J.G.Lominadze, A.D.Pataraya

Institute of Physics, Academy of Sciences of the Georgian SSR, Tbilissi, USSR

The structure of the collisionless shock wave propagating across the magnetic field in two component plasma consisting of hot electrons and cold ions is studied in the paper. The quasilinear kinetic equation for the electrons being in the weak magnetic field is investigated.

The electron cyclotron frequency is considered small in comparison with Langmuir electron frequency $\Omega_e \ll \omega_p$ i.e. $\frac{eH}{mc} \ll \sqrt{\frac{4\pi n_0 e^2}{m}}$. A two-dimensional case in the plane accross the magnetic field is considered. An anisotropic distribution of the ion-sound oscillation spectrum was obtained. In addition, the plasma effective resistance was found.

Let us investigate the quasilinear equation for electrons, which is written as /1/

$$\frac{\partial \bar{f}_e}{\partial t} - \frac{e}{m}\left\{\vec{E} + \frac{1}{c}[\vec{v}\vec{H}]\right\}\frac{\partial \bar{f}_e}{\partial \vec{v}} = \frac{\partial}{\partial v_\alpha} D_{\alpha\beta}\frac{\partial \bar{f}_e}{\partial v_\beta} \qquad (1)$$

where $\bar{f}_e$ is the electron distribution function

$$D_{\alpha\beta} = \frac{e^2}{m^2}\int k_\alpha k_\beta |\Phi_k|^2 \pi\, \delta(\vec{k}\vec{v} - \omega)\,\frac{d\vec{k}}{(2\pi)^2} \qquad (2)$$

Here Φ_k is the potential of fluctuational electrostatic field.

Further, the magnetic field strength $\vec{H}$ is directed along axis z .

We search for the solution of the equation (1) according to the perturbation theory. The value proportional to the electric field strength is taken as the small parameter.

$$\bar{f}_e = n_0\left\{f_e^{(0)} + f_e^{(1)} + f_e^{(2)}\right\}, \qquad (3)$$

where $f_e^{(0)} = A_0 e^{-\frac{v^2}{v_0^2}}$ (4)

$$f_e^{(1)} = \frac{e}{m\Omega_e}\left(E_x\cos\varphi - E_y\sin\varphi\right)\frac{\partial f_e^{(0)}}{\partial v_\perp} \qquad (5)$$

$$f_e^{(2)} = \left(\frac{e}{m\Omega_e}\right)^2\left\{-\frac{E_x^2 - E_y^2}{4}\cos 2\varphi - \frac{E_x E_y}{2}\sin 2\varphi\right\}\times$$
$$\left(\frac{\partial^2 f_e^0}{\partial v_\perp^2} - \frac{1}{v_\perp}\frac{\partial f_e^0}{\partial v_\perp}\right) + \frac{e}{m\Omega_e^2}\left\{-\cos\varphi\left[E_x(\hat{A}_1 - \hat{A}_3) + E_y\hat{A}_2\right]\frac{\partial f_e^{(0)}}{\partial v_\perp} + \sin\varphi\left[-(\hat{A}_1 - \hat{A}_3)E_y + \right.\right. \qquad (6)$$
$$\left.\left. + \hat{A}_2 E_x\right]\frac{\partial f_e^{(0)}}{\partial v_\perp}\right\},$$

$$\hat{A}_1 = \frac{1}{v_\perp}\frac{\partial}{\partial v_\perp}\left[v_\perp \hat{A}\left(\frac{\omega}{\kappa v_\perp}\right)^2\frac{\partial}{\partial v_\perp}\right], \qquad (7)$$

$$\hat{A}_2 = \frac{1}{v_\perp}\frac{\partial}{\partial v_\perp}\left[\hat{A}\left(\frac{\omega}{\kappa v_\perp}\right)\sqrt{1 - \left(\frac{\omega}{\kappa v_\perp}\right)^2}\right] + \frac{2}{v_\perp}\hat{A}\left(\frac{\omega}{\kappa v_\perp}\right)\sqrt{1 - \left(\frac{\omega}{\kappa v_\perp}\right)^2}\frac{\partial}{\partial v_\perp}, \qquad (8)$$

$$\hat{A}_3 = \frac{1}{v_\perp^2}\hat{A}\left[1 - \left(\frac{\omega}{\kappa v_\perp}\right)^2\right], \qquad (9)$$

$$\hat{A} = \frac{e^2}{m^2}\,\frac{\pi}{(2\pi)^2}\,\frac{2}{v_\perp}\int d\kappa\,\frac{\kappa^2 |\Phi_k|^2}{\sqrt{1 - \left(\frac{\omega}{\kappa v_\perp}\right)^2}} \qquad (10)$$

Here φ and $v_\perp$ are the polar coordinates of the macroscopic velocity of electrons

$$A_0 = \frac{1}{v_{Te}^2}\,\frac{\Gamma\left(\frac{4}{5}\right)}{\pi\,\Gamma\left(\frac{2}{5}\right)\Gamma\left(\frac{3}{5}\right)}, \qquad (11)$$

$$v_0^2 = \frac{1}{v_{Te}^2}\,\frac{\Gamma\left(\frac{2}{5}\right)}{\Gamma\left(\frac{4}{5}\right)} \qquad (12)$$

$v_{Te} = \sqrt{\frac{T_e}{m}}$ is the thermal velocity of electrons $\Gamma(n)$ - is gamma-function.

The distribution function (4) was obtained in /1/.

The shock wave is propagating along axis x , and hence the x component of the current in the wave front is equal to Zero. From this condition we obtain the following relationship between x and y components of the electric field strength

$$E_x = \frac{\Omega_e}{\nu_0} E_y \qquad (13)$$

where

$$\nu_0 = \frac{\omega_p^2 \bar{W}}{n T_e v_{Te}}\,\frac{1}{4\sqrt{\pi}^2\sqrt{2}}\left[\frac{\Gamma\left(\frac{4}{5}\right)}{\Gamma\left(\frac{2}{5}\right)}\right]^{5/2} \qquad (14)$$

here

$$\bar{W} = \int \frac{\kappa |\Phi_\kappa|^2}{8\pi}\, d\vec{\kappa} \qquad (15)$$

Using the formula (3-6), it is easy to find the y component of the current.

It has a form of

$$j_y = \frac{\omega_p^2}{4\pi\nu_0}\left(1 + \frac{\nu_0^2}{\Omega_e^2}\right)E_y \qquad (16)$$

From (16) one can write the following expression for the effective conductivity

$$\sigma_{eff} = \frac{\omega_p^2}{4\pi\nu_0}\left(1 + \frac{\nu_0^2}{\Omega_e^2}\right) \qquad (17)$$

and from the above expression it is possible to obtain the value of the effective collision frequency

$$\nu_{eff} = \frac{\nu_0}{1 + \frac{\nu_0^2}{\Omega_e^2}} \qquad (18)$$

We study the ion-sound oscillation of the weakly turbulent plasma across the magnetic field in the shock wave front. The maximum increament value (the increment has the negative sign) is determined for the angle φ_k , between the wave vector and axis x .

$$tg\,\varphi_k = \frac{\Omega_e}{\nu_0} \qquad (19)$$

If we introduce $\Theta = \pi + 2\varphi_k$ and $\nu_0 \ll \Omega$, $tg\Theta = \frac{2\nu_{eff}}{\Omega_e}$ which coincides with the result obtained in /2/,

The increment of the ion-sound oscillations has zero value in the direction of x axis $(k_y = 0)$. In this case

$$E_y = \frac{H v_s}{c}\ ; \quad v_s = \sqrt{\frac{T_e}{M}} \qquad (20)$$

It is the solution of the equation $rot\vec{E} = -\frac{1}{c}\frac{\partial \vec{H}}{\partial t}$ in the system of the shock wave moving with the velocity close to the velocity of ion-sound wave $(v \geq v_s)$.

References

1. A.A.Galeev, R.Z.Sagdeev. Voprosi teorii plasmi, issue 7 Moscow, Atomizdat, 1973.

2. D.Biskamp, R.Chodera, C.T.Dam. Phys.Rev.Lett.vol.34, N.3, 1975.

HEATING OF PLASMA BY A COLLISIONLESS SHOCK IN THE LONGITUDINAL MAGNETIC FIELD AT VARIOUS ALFVEN MACH-NUMBER

T.A. EL-KHALAFAWY, M.M. EL-NICKLAWY, A.B. BESHARA, M.B. ETEIBA and N.I. RUDNEV+)
Atomic Energy Authority, Cairo, Egypt

Abstract: The paper presents results of experimental studies on longitudinal collisionless shocks at Alfven-Mach numbers $M_A \geq M_c$. It is shown that the dependence of plasma temperature on M_A- both at and behind the wave front-becomes substantially nonlinear at $M_A \geq (1,5 \div 2)$.

The principal experimental results include data on plasma temperature measurements through its diamagnetism in the two regions of the shock wave-at the front and in the piston (Figs. 1 and 2). From Figs. 1 and 2 it follows that substantial lack of correspondence to the law of dependence of the plasma temperature on the discharge current is observed, - both at the front (curve 2) and in the piston (curve 3) - starting from the Mach numbers $M_A \geq 1,5$.

A strong damping of the fields in the wave at $M > M_c \geq (1,5 \div 2)$ and the temperature jump in this region indicate to the existence of a nonlinear mechanism of dissipation and transformation of the wave energy into transverse energy of the plasma particles $W_\perp$.

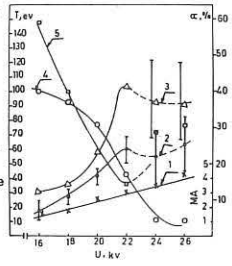

Fig.1. T=f(U); 1- M_A; 2- T_f; 3- T_p; 4- α_f=(Be) z=24cm/(Be)z=12cm; B_{oz}=.5KG.

It can be readily seen that plasma temperature rises in proportion to the amplitude of the magnetic field (Fig. 3 in which the point at $B_{oz}=0.3$ kG is taken from /1/). A considerable lack of reproducibility, at $M_A \geq 3$, indicates to instability of the heat flux in a given cross-section, (z=24 cm). This results from a transient character of processes in the wave at $M \gg M_c$ as well as statistical straggling of the cross-section Z in which the overturning of the wave takes place. The temperature dependencies and magnetic structure of the shock wave allow to break the continuum of Mach numbers into three regions, provisionally: 1) $M_A=(1.2 \div 2)$, that is the region of a regular oscillatory structure of the wave front, 2) $M=(2 \div 3)$, the region of a turbulent structure of the front, and 3) $M > 3$, the region in which the wave is always upset and the front is broadened.

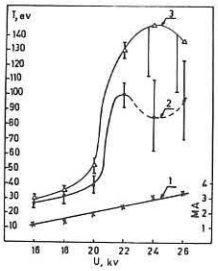

Fig.2. T=f(U); 1- M_A; 2- T_f; 3- T_p; B_{oz}=0.8 KG.

Fig. 4 a,b shows oscillograms of the B_θ- field in the wave together with the diamagnetic signal (the lower beam). Fig. 4a 1,2 illustrates the case when generation of the sinusoidal wave at frequency $\sim \omega_{Bi}$ with amplitude, rising with time, is possible in the first and second regions of M_A. As a rule, the temperature rise is step-by-step according to the oscillation frequency. Given in Fig. 4b 1, the oscillogram shows minimum front width at the upper boundary of the first region of M_A ($\Delta_f \lesssim 2$ cm. at velocity $v_f=4,6.10^7$cm./sec.) and h.f. oscillations at the maximum of the signal. In this case, the plasma temperature is about 50 eV that corresponds to a free-path length of the charged particles, l=75 cm > L, where L is the linear size of the system. In case of bigger M_A, i.e. 2÷3, a turbulent structure of the front is observed (Fig. 4b 2) and a dissipation length is found within the short wave region. The conditions of super-critical Mach numbers ($M_A > 3$) are characterized by the broadened front with h.f. oscillations (Fig. 4b 3), or by a "foot" (Fig. 4a 3) with a sharp splash of diamagnetic signal.

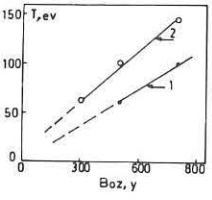

Fig. 3. $T_{max}=f(B_{oz})$. 1- T_f; 2- T_p.

In the first region of $M_A=(1,2 \div 2)$, the oscillations propagate ahead of the wave front that is due to the ion dispersion and wave group velocity growth $\partial\omega/\partial\kappa$. Estimated experimentally, the wavelength of these oscillations (in the radius r=3 cm) coincides, to the accuracy of 50%, with the wavelength calculated by formula /2/ within $\theta = 20°-30°$.

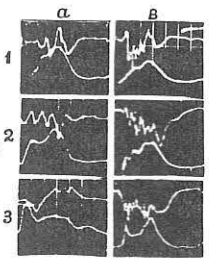

Fig. 4 a- B_{oz}=0.5KG; 1- M_A=2.4; 2- M_A=3; 3- M_A=4; b- B_{oz}=0.8KG. 1- M_A=2; 2- M_A=2.5; 3- M_A=3.5.

$$\lambda \approx 2\pi M_A \cos\alpha \cdot c/\omega_{pi} \left(M_A^2-1\right)^{1/2} \cdot \left(M_A^2-\cos^2\alpha\right)$$

For example, $\lambda_{exp}=(4 \div 10)$ cm. at $B_{oz}=0.8$ KG and $M_A \simeq 2$, whereas $\lambda_{th}=7$ cm. A considerable disparity between rated and experimental is attributed to inhomogeneity of the plasma density in and variation of the Mach number along the radius as well as variation of angle θ between wave vector K and B_{oz}. Since (for a given angle θ) the value of λ_{th} in the interval of M_A from 1,5 to 2 greatly decreases, such a coincidence of λ_{th} and λ_{exp} can be considered acceptable ($\sim 50\%$) and, hence, the oscillations are Wistler oscillations. It is electrons that are predominantly heated in such regular electromagnetic fields i.e. in the first region inequality $T_e > T_i$ is satisfied.

In the second region ($M_A=2 \div 3$) one can observe both a turbulent structure of the front that is probably due to the development of a multistream motion of ions, and oscillations near the ion cyclotron frequency. Both the conditions of generating ion-cyclotron wave by a longitudinal beam of electrons and ions $m_e v_g^2 \theta/m_i \ll \omega_{pi}^2 \beta^2 (1+\cos^2\theta)/2\omega_{Be}^2 \ll 1$; $(3 \cdot 10^{-4} \ll 2.8 \cdot 10^{-3} \ll 1)$ at $\beta \ll 1$ and $\omega/\kappa > v_{Ti}$ and the conditions of generating the multistream ion-ion instability $M_A > M_c = 1 + 3/4 \left(8\pi n_i \kappa \overline{T_{ei}}\right)/B_i^2)^{1/3} = 1.3 \div 1.5$ at $B_i = (0.5 \div 0.8)\kappa G$ and $n_{imax} = 5 \cdot 10^{13} cm^{-3} \gg n_c \simeq 10^{11} cm^{-3}$ and $v_d > v_{Te} > v_S = (T_e/m_i)^{1/2}$ are satisfied by a large margin. A nonlinear rise in the plasma temperature with rising M_A, i.e. non-adiabatic heating, is observed both in generating ion-cyclotron wave and in the case of turbulent shock waves. Under the conditions of ion-ion double-flow instability ($M_A \gg M_c$), either predominantly short-wave ($\lambda \ll \rho_e = mcv_e/eB$) electrostatic instabilities, or electromagnetic-with a longer wavelength- oscillations /3/ $\lambda \sim c/\omega_{pe}$ and $\omega \sim (\omega_{Be}\omega_{Bi})^{1/2}$ can be excited in the shock wave and lead, by way of transforming into the plasma oscillations due to the Cherenkov absorption of plasma waves, to ion heating.

From the Rankine-Hugoniot relations it follows that at $M_A > 3,5$ the value of β_2 is larger than 1, whereas for $B_{oz}=0.8$ KG and at $M_A > 3,5$ the ratio of gaskinetic pressure to magnetic pressure $\beta_{exp} = 8\pi n_2 kT/B_{oz}^2 = 0.44$. Hence, the plasma temperature is not limited by β but, probably, by ion Larmor radius.

REFERENCES

/1/ El-Khalafawy, T.A., et al., IAEA-CN-33/HG-4 Vienna (1975).
/2/ Stringer, T.E., Plasma Physics, 5 (1963), 89.
/3/ Kadomtsev, B.B., Proc. Plasma Phys. and Problem of Contr. Therm. Reactions, 4, Publ; by USSR Academy of Sciences (1958), 364.

+) On leave from the Atomic Energy State Committee, USSR.

NONLINEAR SPACE-TIME EVOLUTION OF THE ELECTRON CYCLOTRON INSTABILITY IN A BEAM-PLASMA EXPERIMENT

J.A.C. Cabral and M.E.F. Silva

Laboratório de Electrodinâmica - Complexo Interdisciplinar

Instituto Superior Técnico - Lisboa - Portugal

ABSTRACT- We analyse the space-time evolution of the electron cyclotron instability bursts. Their "group velocity", after saturation, becomes negative. A low frequency wave starts to grow approximately when the cyclotron bursts saturate.

1.- SPACE-TIME ANALYSIS OF THE CYCLOTRON BURSTS: - In our cylindrical interaction chamber (L=75 cm; Ø=8 cm) a 2 KeV-10 mA electron beam creates its own Helium plasma ($p= 6 \times 10^{-4}$ Torr; B_o=112 Gauss). Under these conditions ($n_e=1.3 \times 10^9$ cm^{-3}; T_e=5.3 eV), we observed sharp cyclotron peaks (450 MHz) close to the upper hybrid frequency. The cyclotron instability appears under the form of rapid bursts (~100 ns). These ones were analysed with a fast sampling scope, triggered by the highest amplitude bursts occurring at z_o=53 cm. In this way we defined a space-time domain running in space (z) from 30 to 73.2 cm and in time (τ) from 0 to 110 ns. By the use of a convenient delay, the instant of trigger is set at τ=50 ns. In this space-time domain we can make cuts along lines of constant z or constant τ. Keeping τ=Cte we made several "instantaneous pictures" of the bursts along space, (Fig. 1). In this figure we can observe the large coherence length of these bursts as well as their temporal growth, saturation and further decrease in amplitude. A complementary set of measurements was done by obtaining 10 cuts along lines of constant z. These temporal analysis of the bursts confirmed the measurements of Fig. 1 on the 60 common points of space-time. Fig. 2 shows the results of this double analysis in the form of an altitude topographic map for the amplitude of the cyclotron bursts in a two-dimensional space-time chart. In this figure we represent with small circles the position of the centre of gravity of the bursts for several values of τ. We see that the "group velocity" during the growth period of the bursts is very small. As soon as the bursts saturate the group velocity becomes negative and of the order of -3×10^8 cm s^{-1}. This backward movement of the cyclotron bursts shall be explained in another paper also submitted to this Conference [1].

2.- POSSIBLE CAUSES FOR THE BURST DESTRUCTION: - a)- TRAPPING:- By measuring the axial velocity distribuition function of the beam electrons, when leaving the plasma, we could show that trapping of the beam electrons in the wave potential well can not occur, as the wave phase velocity is smaller than the minimum velocity of these electrons [2]. b)- INFLUENCE OF REFLECTED WAVES:- By analysing the two instantaneous pictures of the instability E-field, obtained for two values of τ separated by 1/4 of an oscillation period we found that these two field structures are separated in space by 1/4 of a wavelength, the movement being towards the collector. This fact was verified in every stage of nonlinear devellopment of the bursts. Therefore the cyclotron wave packet is only composed by incident waves (k>0). Reflected cyclotron waves are unimportant as their group velocity, due to the anomalous dispersion of the plasma, is positive, and so the reflected field struture is forced to stay pushed against the collector. c)- WAVE-WAVE INTERACTION:- Given the former considerations the nonlinear evolution of the bursts is probably related to some local phenomenon, occurring near the regions of space-time where the bursts attain their maximum amplitude. The most natural phenomenon would be the modification of the plasma density by the excitation of the cyclotron instability above some threshold value. In order to observe, in a qualitative way, these possible density variations, we analysed the ion saturation current to a Langmuir probe in the same space-time domain in which we analysed the instability E-field. Results are presented in Fig. 3 where we can observe: - while the bursts grow the "density" is relatively high and it falls rather quickly when we approach the collector; - as soon as the bursts saturate (τ=50 ns) the plasma "density" drops and we observe the formation of a long "valley" with two deep wells; - As time goes on we observe the rise of a high "density" hump, later followed by another "density" minimum for τ=110 ns; - Therefore, during the destruction phase of the cyclotron bursts we wittness the formation of a periodic structure on the plasma "density" in space-time, representing the spontaneous excitation of a low frequency oscillation; - Identical analysis, made for other values of the axial magnetic field, between 60 and 135 Gauss, revealed similar patterns for the evolution in space-time of both the E-field of the instability and the plasma "density".

3.- CONCLUSIONS: - The field structure of the cyclotron instability travels backwards after saturation; - a low frequency "density" wave appears in close correlation with the nonlinear development of that instability; - A qualitative explanation for these two facts shall be given in [1] based upon the consideration of a nonlinear three-wave interaction process, of the parametric decay type, involving the cyclotron wave, the "density" wave and another mode of our beam-plasma system.

REFERENCES -

[1] - CABRAL, J.A.C. (1975) - 7th Europ. Conference on Controlled Fusion and Plasma Physics, Lausanne.

[2] - CABRAL, J.A.C.; HOPMAN, H.J. (1970) Plasma Physics 12, 759.

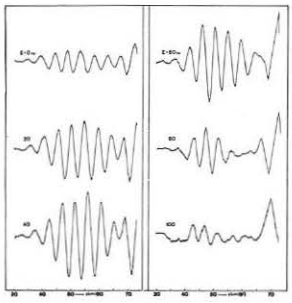

Fig. 1 - "Instantaneous pictures" of the bursts in space.

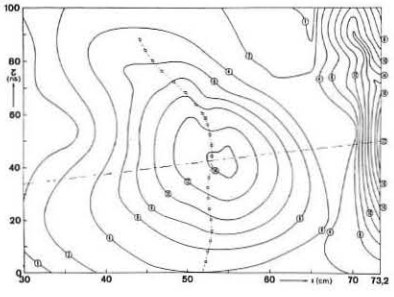

Fig. 2 - Space-time analysis of the instability electric field.

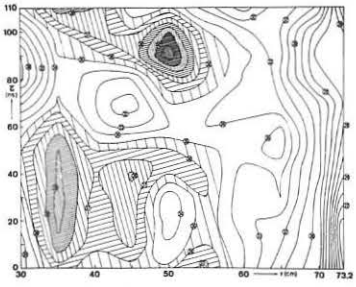

Fig. 3 - Space-time analysis of the plasma "density". Darker areas represent higher "densities".

A QUALITATIVE EXPLANATION FOR THE SATURATION AND DECAY OF THE ELECTRON CYCLOTRON INSTABILITY IN A BEAM-PLASMA SYSTEM

J.A.C. Cabral

Laboratório de Electrodinâmica - Complexo Interdisciplinar

Instituto Superior Técnico - Lisboa - Portugal

ABSTRACT - We show that the saturation and subsequent destruction of the electron cyclotron bursts is due to a parametric decay process which originates strong density fluctuations in the plasma.

1- EXPERIMENTAL EVIDENCE FOR A PARAMETRIC DECAY:- In another paper, also submitted to this Conference [1], we presented some experimental results suggesting that the low frequency density oscillation is a direct nonlinear effect of the growth of the cyclotron instability above some threshold level. A possible mechanism which would lead to the growth of this density wave is the parametric decay:- indeed, the main cyclotron wave (ω_o, k_o) might decay into that density wave (ω_2, k_2) and another mode (ω_1, k_1) of our system, satisfying the synchronism conditions: I) $\omega_o=\omega_1+\omega_2$ and II) $k_o=k_1+k_2$. To chek on the first of these conditions we injected a monochromatic wave at z=43 cm and we looked for changes in the excited frequency spectrum at z=53 cm. The beam-plasma parameters were the same as in [1] except B_o=60 Gauss. This value of the magnetic field permitted the best results. We verified that the injected waves only modified the spontaneous frequency spectrum if their frequency was close to f_2 (density wave) or to f_o-f_2. In Fig. 1 we show the result of the injection of a h.f. wave with f_1=208 MHz. In this figure we observe a large increase in the amplitude of the spectrum around f_2=27 MHz. The main frequency of the cyclotron wave packet was f_o=235 MHz. A complementary check was made by injecting a l.f. wave with f_2=27 MHz. In Fig. 2 we see that the injection of this wave resulted in the appearence of a large hump in the spectrum around f_1=208 MHz (f_o=235 MHz). These measurements permit us to conclude that relation I) is indeed verified. The same conclusion holds for other values of B_o. To check on the second synchronism condition, we determined the value of k_o from the cyclotron wavelength (λ_o=4,7 cm) taken from Fig. 1 of [1]. An estimate for k_2 can be taken from Fig. 3 of the same paper, where we can see that λ_2 is of the order of 40 cm, and that k_2 is negative. So, condition II) can only be fulfilled if $k_1>k_o$:- this means that this parametric decay process is only possible if the b-p system will have anomalous dispersion around f_o. In Fig. 3 we have drawn a simplified and semi-quantitative dispersion diagram, taking into consideration the numerical results obtained in [1]. This figure illustrates the parametric decay of the cyclotron wave (A) into waves (B) and (C) satisfying both synchronism conditions. Points (A) and (C) were experimentally determined and point (B) was located in k by the use of equation II). As point (B) qualitatively fits the expected dispersion curve for the cyclotron waves, this parametric process is likely to occur under our experimental conditions. The value for the group velocity of the cyclotron waves, taken from this figure ($v_g=-8\times10^8$ cm s^{-1}), agrees, in order of magnitude, with the one we experimentally determined in [1].

2- INTERPRETATION OF THE RESULTS:- A qualitative explanation for the nonlinear evolution of the cyclotron instability in a b-p system is as follows:- a- Let us assume that when the plasma density, driven by some steady state ion oscillation, attains a certain threshold value [2] [3], the cyclotron instability starts to grow exponentially according to linear theory. b- the instability is absolute and so it grows in time everywhere. An amplitude is reached at which we must consider nonlinear processes. c- by this time the b-p system has devellopped a first order density perturbation with frequency f_o, thus becoming parametrically driven by the cyclotron instability (A) that behaves like a pump wave. The system permits now the growth of two new waves, (B) and (C), satisfying the synchronism relations. d- a fraction of the energy extracted from the electron beam by the cyclotron wave is delivered to both parametrically generated waves. This explains the saturation of the instability. e- as the density wave grows, the dispersion of the plasma changes accordingly, through local variations of ω_{pe} and ω_{uh}. The density fluctuations, now with frequency f_2, are strong enough to leave the initially unstable zone (square around A) out of the instantaneous dispersion diagram. f- The cyclotron wave packet is forced to readjust itself to the new dispersion conditions by adjusting its k values. Therefore the cyclotron wave becomes uncoupled from the beam waves and this explains the backward movement of field structure after saturation ($v_g<0$). g- The cyclotron wave reduces its amplitude as it is now the only source of energy to the growth of the two new waves and it finally vanishes. h- The density wave also damps away, in about 500 ns, because the next cyclotron bursts, excited when the plasma density is momentarily high, do not grow above the threshold level for the occurrence of nonlinear phenomena [4]. i- Probably, the excitation of another high amplitude burst can only take place after the density wave has been completely damped. Then, the ion wave leads again the plasma density, smoothly towards the critical value above which the excitation of the cyclotron instability takes place. j- The cyclotron wave grows and the closed cycle of events just described repeats itself.

REFERENCES

[1]- CABRAL, J.A.C.; SILVA, M.E.F. (1975) - 7th Europ. Conference Controlled Fusion and Plasma Physics, Lausanne.

[2]- CABRAL, J.A.; HOPMAN, H.J. (1970) Plasma Physics 12, 759.

[3]- HOPMAN, H.J.; MATITTI, T.; KISTEMAKER, J. (1968) Plasma Physics 10, 1051.

[4]- CABRAL, J.A.C.; SILVA, M.F.E. (1973) - 6th Europ. Conference Controlled Fusion and Plasma Physics, Moscow, 525.

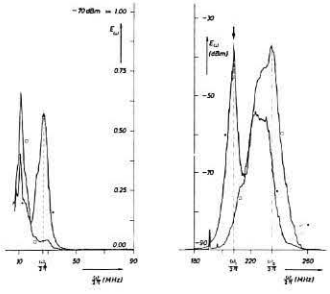

Fig. 1 - Injection of a high frequency wave.

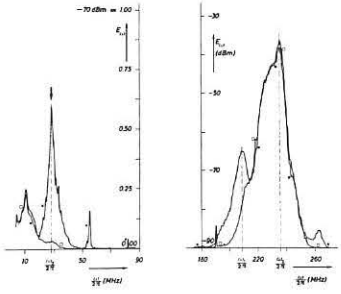

Fig. 2 - Injection of a low frequency wave.

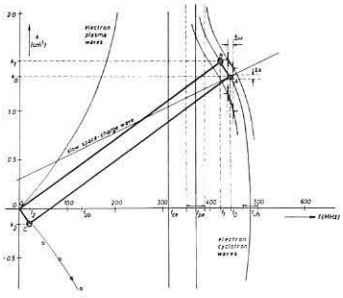

Fig. 3 - Semi-quantitative dispersion diagram.

NON-LINEAR INTERACTION OF WAVES IN AN INHOMOGENEOUS BEAM-PLASMA MEDIUM

V.V. DOLGOPOLOV+), R.N. EL-SHERIEF, M.M. EL-SIRAGY and A.M. HUSSEIN

Atomic Energy Authority, Cairo, Egypt

Abstract: The authors consider the formation of waves at double frequency at the inlet of a beam into a plasma. They show that these waves can play a greater part in the beam interaction with plasma than the waves at basic frequencies, even in the case of a weak non-linearity.

Wave interaction in a homogeneous, infinite, weakly non-linear medium is known to be feasible provided the sum of frequencies and the sum of wave vectors of the interacting waves are zero. In a region where the medium is substantially inhomogeneous, the wave vector's component directed along the medium inhomogeneity expands into a continuum of values, i.e. the concept of wave vector loses its sense. Therefore, the waves which do not interact in a homogeneous medium, can do so in an inhomogeneous medium. The wave interaction at combination frequencies in a sharply bounded /1/, or weakly inhomogeneous /2/, plasma can give an example.

We consider here a non-linear interaction, viz. the formation of waves at double frequencies, with a homogeneous low-density electron beam propagating in an inhomogeneous plasma.

When the beam density is small as compared with the plasma density and beam Langmuir frequency is small as compared with the wave frequency, the wave phase velocity is close to the beam velocity. In this case, non-linear interaction associated with the plasma can be neglected as compared with that associated with the beam. Then, assuming that the x-axis is directed along the beam propagation and all values are only dependent on one spatial coordinate x, we shall obtain - for describing the electrostatic oscillations - the folowing system of equations:

$$\left.\begin{aligned} &\frac{\partial v}{\partial t}+(u+v)\frac{\partial v}{\partial x}=-\frac{e}{m}E,\quad \frac{\partial n}{\partial t}+\frac{\partial}{\partial x}\{(n_b+n)(u+v)\}=0,\\ &\frac{\partial v'}{\partial t}=-\frac{e}{m}E,\quad \frac{\partial n'}{\partial t}+\frac{\partial}{\partial x}\{n_p(x)\cdot v'\}=0,\quad \frac{\partial E}{\partial x}=-4\pi e(n'+n), \end{aligned}\right\} \quad (1)$$

where u and n_b the velocity and density of the unperturbed beam respectively ($u>0$); $n_p(x)$ -the unperturbed electron plasma density, v, n and v', n' are the perturbations of the velocity and density of the beam and those of the plasma respectively, associated with electrostatic field E.

Suppose, the oscillations are excited by a monochromatic external source with frequency ω placed on the left from the plasma volume. Then, in the case of a weak non-linearity ($|n|\ll n_b$, $|v|\ll u$), any value describing the oscillations $f(x,t)$ can be represented in the form:

$$f(x,t)=f_1(x)\cdot e^{-i\omega t}+f_2(x)\cdot e^{-i2\omega t}+\dots\dots+C.C.\,, \quad (2)$$

where $|f_{n+1}|\ll|f_n|$.

From relations (1),(2) we obtain

$$\frac{d^2\mathcal{E}}{dx^2}+\frac{k^2}{\varepsilon}\cdot\mathcal{E}=0 \quad (3),\qquad \frac{d^2\mathcal{E}_2}{dx^2}+\frac{k^2}{\varepsilon_2}\cdot\mathcal{E}_2=R \quad (4),$$

where

$$\mathcal{E}=\varepsilon\cdot e^{-i\frac{\omega}{u}x}\cdot E_1(x),\quad \mathcal{E}_2=\varepsilon_2\cdot e^{-i2\frac{\omega}{u}x}\cdot E_2(x),\quad k=\frac{\omega_b}{u},\quad \omega_b=\left(\frac{4\pi e^2 n_b}{m}\right)^{1/2},$$

$$\varepsilon(x)=1-\frac{\omega_p^2}{\omega^2},\quad \varepsilon_2(x)=1-\frac{\omega_p^2}{4\omega^2},\quad \omega_p(x)=\left(\frac{4\pi e^2 n_p}{m}\right)^{1/2},\quad \frac{\omega_b}{\omega}\ll 1,$$

$$R=-i\cdot\frac{2e\omega}{mu\omega_b^2}\cdot\left[\left(\frac{d\mathcal{E}}{dx}\right)^2-\frac{k^2}{2}\cdot\frac{\mathcal{E}^2}{\varepsilon}\right] \quad (5)$$

Eqs. (3);(4) give the fields at basic and double frequencies for an arbirary dependence of plasma density on x.

We shall solve these equations for the case of a semi-bounded, homogeneous plasma, then

$$\varepsilon=\varepsilon_2=1 \text{ at } x<0\,,\quad \frac{\partial\mathcal{E}}{\partial x}=\frac{\partial\mathcal{E}_2}{\partial x}=0 \quad \text{at} \quad x>0 \quad (6)$$

From (3)-(5) it follows that functions $\mathcal{E}(x)$ and $\mathcal{E}_2(x)$ and their first derivatives over x are continuous at the point $x=0$.

Taking it into account, we have:

$$\mathcal{E}=A\cdot e^{i\frac{k}{\sqrt{\varepsilon}}x}+B\cdot e^{-ikx}\quad x<0\,,\quad \mathcal{E}=A_0\cdot e^{i\frac{k}{\sqrt{\varepsilon'}}x}+B_0\cdot e^{-i\frac{k}{\sqrt{\varepsilon'}}x}\quad x>0\,, \quad (7)$$

where

$$A_0=\frac{1}{2}\left[(1+\sqrt{\varepsilon'})\cdot A+(1-\sqrt{\varepsilon'})\cdot B\right],\quad B_0=\frac{1}{2}\left[(1-\sqrt{\varepsilon'})\cdot A+(1+\sqrt{\varepsilon'})\cdot B\right], \quad (8)$$

A and B are the constants.

Inserting expressions (7) into (5), we can write the solutions of Eq. (4) in the form:

$$\mathcal{E}_2=A_2\cdot e^{i2kx}+B_2\cdot e^{-i2kx}+C_2 \quad \text{at } x<0\,, \quad (9)$$

$$\mathcal{E}_2=G_+\cdot e^{i\frac{k}{\sqrt{\varepsilon_2'}}x}+G_-\cdot e^{-i\frac{k}{\sqrt{\varepsilon_2'}}x}+A_{20}\cdot e^{i\frac{2k}{\sqrt{\varepsilon'}}x}+B_{20}\cdot e^{-i\frac{2k}{\sqrt{\varepsilon'}}x}+C_{20}\quad x>0\,, \quad (10)$$

where $A_2=q\cdot A^2$, $B_2=q\cdot B^2$, $C_2=2q\cdot AB$, $A_{20}=q\cdot\varepsilon_2 A_0^2$, $B_{20}=q\cdot\varepsilon_2 B_0^2$,

$$C_{20}=2q\cdot\frac{\varepsilon_2}{\varepsilon}A_0B_0\,,\qquad q\equiv -i\cdot\frac{e\omega}{mu^3k^2}\,,$$

G_+ and G_- are the integration constants determining amplitudes of the second harmonics (i.e. waves at double frequency which propagate - in homogeneous regions of the medium - irrespective of the waves with basic frequency). Using expressions (9) and (10), we can find G_+ and G_- from the continuity condition of functions $\mathcal{E}_2(x)$ and $d\mathcal{E}_2/dx$ at the point $x=0$.

In the case of a beam instability ($\varepsilon_2<0$), G_+ yields amplitude of a rising wave whereas G_- gives that of a damping wave. Therefore, we give the expression for G_+ only:

$$G_+=i\cdot\frac{e\omega}{4mu\omega_b^2}\cdot\left(\alpha_+A^2+\alpha_-B^2+\beta\cdot AB\right), \quad (11)$$

where $\alpha_\pm=\frac{\varepsilon_2}{2}\left(\varepsilon+\frac{1}{\varepsilon}\right)-2\pm 4\cdot\sqrt{\varepsilon_2'}\cdot(\varepsilon_2-1)$, $\beta=2\cdot\left[2(\varepsilon_2-1)-\varepsilon_2\left(\varepsilon-\frac{1}{\varepsilon}\right)\right]$.

Amplitude of a rising second harmonic is found here as a function of amplitudes of the beam oscillation at basic frequency in vacuum.

From the above it follows that in case $\varepsilon_2<0$, the fields of the second harmonics will considerably exceed those of the waves with basic frequency at a sufficient depth from the plasma surface - even if the conditions for applicability of the approximation of weak non-linearity are satisfied. The obtained results are valid if width of a transition plasma-vacuum layer is smaller than $1/k$.

REFERENCES

/1/ A.R. Barakate, V.V. Dolgopolov and N.M. El-Siragy (1978), Plasma Physics, 17, 89;

/2/ N.S. Erokhin, V.E. Zakharov and S.S. Moiseev (1969), Zh. eksp. teor. Fiz. 56, 179.

+) On leave from the Atomic Energy State Committee, USSR.

WAVE COUPLING IN A NARROW INHOMOGENEOUS LAYER OF THE MAGNETOACTIVE PLASMA

V.V. DOLGOPOLOV[+], N.M. EL-SIRAGY and Y.A. SAYED

Atomic Energy Authority, Cairo, Egypt

Abstract: Effect of the magnetic field on wave coupling in a narrow inhomogeneous plasma layer is studied on example of the generation of the second harmonics. It is shown that, due to the magnetic field, the intensity of the second harmonics radiation from the plasma layer can sharply increase.

With the advent of powerful sources of monochromatic electromagnetic waves-lazers, the interest to nonlinear interaction of these waves in the plasma has now become greater. But in most theoretical works (e.g. see /1,2/) this interaction has been only studied in the approximation of weakly inhomogeneous,plasma, or homogeneous semi-bounded plasma with a sharp boundary. In /3/ the authors considered nonlinear interaction with the formation of waves at double frequencies in a narrow, arbitrarily inhomogeneous layer of isotropic plasma. Here, we consider this effect for the case of magnetoactive plasma.

The initial system of equations for the components of the electromagnetic field $\vec{E}$ and $\vec{H}$ and the perturbations of the density n and velocity $\vec{v}$ of plasma electrons will be such:

$$[\nabla,\vec{E}] = -\frac{1}{c}\frac{\partial \vec{H}}{\partial t}, \quad [\nabla,\vec{H}] = \frac{1}{c}\frac{\partial \vec{E}}{\partial t} - \frac{4\pi e}{c}(n_0+n)\vec{v}, \quad \frac{\partial n}{\partial t} + \{\nabla,(n_0+n)\vec{v}\} = 0,$$
$$\frac{\partial \vec{v}}{\partial t} + (\vec{v}\nabla)\vec{v} = -\frac{e}{m}\left\{\vec{E} + \frac{1}{c}[\vec{v},\vec{H}_0+\vec{H}]\right\}, \qquad (1)$$

where n_0 -the unperturbed density of plasma electrons ($\frac{\partial n_0}{\partial t} = 0$), $\vec{H}_0$ is the constant magnetic field.

In the case of monochromatic external field with frequency ω and a weak nonlinearity, any value $f(\vec{r},t)$ describing the steady state oscillations in plasma, making allowance for the terms proportional to square amplitude, can be represented in the form:

$$f(\vec{r},t) = f_1(\vec{r})\, e^{-i\omega t} + f_2(\vec{r})\, e^{-i2\omega t} + \text{c.c.} \qquad (2),$$ where, $|f_2(\vec{r})| \ll |f_1(\vec{r})|$.

As in /3/, we consider that n_0 is an arbitrary, continuous function of x in the region $0 \leqslant x \leqslant a$, equal to zero at $x \leqslant 0$ and $x \geqslant a$ and is independent of y and z . $\vec{H}_0$ is directed along the z-axis. The wave vector of s-polarized electromagnetic wave incident on a plasma, lies in the plane xoy . Then, the electromagnetic field is independent of z .

In this case, representing $\vec{E}$, $\vec{H}$, n and $\vec{v}$ in the form of (2), we obtain from the system of equations (1) in the zero (linear) approximation of the theory of perturbations that:

$$\frac{\partial^2 E_z}{\partial x^2} + \varkappa^2 E_z = 0 \qquad (3); \qquad H_x = n E_z, \qquad H_y = i\frac{c}{\omega}\frac{\partial E_z}{\partial x} \qquad (4);$$

where $E_z(\vec{r}) = \mathcal{E}(x)\, e^{iky}$, $\varkappa(x) = \frac{\omega}{c}\sqrt{\varepsilon - n^2}$, $\varepsilon(x) = 1 - \frac{\Omega^2}{\omega^2}$, $\Omega(x) = \left(\frac{4\pi e^2 n_0}{m}\right)^{1/2}$, $n = \frac{kc}{\omega}$.

Allowing for the second term in (2), in the next approximation we shall obtain from (1) the following equation for the magnetic field of p-polarized wave at double frequency (s-polarized waves are not generated in our case):

$$\frac{\partial}{\partial x}\left(\frac{1}{\varepsilon_1}\frac{\partial H}{\partial x}\right) + \mathcal{K}^2 H = \mathcal{R}, \qquad (5)$$

where

$$H \equiv H_{2z}, \qquad \mathcal{K}^2(x) = \left(\frac{2\omega}{c}\right)^2 - \frac{(2k)^2}{\varepsilon_1} + 2k\left(\frac{\partial}{\partial x}\frac{\varepsilon_2}{\varepsilon_1^2-\varepsilon_2^2}\right), \qquad \varepsilon_\perp(x) = \frac{\varepsilon_1^2-\varepsilon_2^2}{\varepsilon_1},$$

$$\mathcal{R} = \frac{2e}{mc\omega}\left\{-\frac{\partial}{\partial x}\left[\frac{\varepsilon_2}{\varepsilon_1^2-\varepsilon_2^2}\left(E_z\frac{\partial E_x}{\partial x} + k\frac{2\omega}{\omega_H}\varepsilon_3 E_z^2\right)\right] + 2k\frac{\varepsilon_2}{\varepsilon_1^2-\varepsilon_2^2}\left(\frac{2\omega}{\omega_H}\varepsilon_3 E_x\frac{\partial E_x}{\partial x} + kE_z^2\right)\right\}, \qquad (6)$$

$$\varepsilon_1(x) = 1 - \frac{\Omega^2}{4\omega^2-\omega_H^2}, \qquad \varepsilon_2(x) = \frac{\omega_H}{2\omega}\cdot\frac{\Omega^2}{4\omega^2-\omega_H^2}, \qquad \varepsilon_3(x) = 1 - \frac{\Omega^2}{4\omega^2}, \qquad \omega_H = \frac{eH_0}{mc}.$$

Suppose, width of the plasma layer a is small as compared with the wavelengths

$$|\varkappa a| \ll 1, \qquad ka \ll 1, \qquad \left(\frac{2\omega}{c}\right)^2 a\left|\int_0^a dx\,\varepsilon_\perp\right| \ll 1 \qquad (7)$$

and $n^2 \neq 1$. Then the solution of (3), that is corresponding to wave incidence on the plasma from the left side, can be approximately written in the form:

$$E_z \approx E_0\, e^{ik_0 x}, \qquad (8)$$

where $k_0 = \frac{\omega}{c}\sqrt{1-n^2}$, $\frac{\partial E_0}{\partial x} = 0$.

Since $\mathcal{R} = 0$ at $x < 0$ and $x > a$, the solution of (5) in vacuum must take the form of waves radiating from the plasma layer to both sides:

$$H(x) = H_-\, e^{-i2k_0 x} \quad \text{at } x \leqslant 0, \qquad H(x) = H_+\, e^{i2k_0(x-a)} \quad \text{at } x \geqslant a, \qquad (9)$$

where H_+ and H_- are the constants as related to x . Taking into account (7), one can look for the solution of (5) in the region $0 \leqslant x \leqslant a$ using the method of successive approximations /4/:

$$H(x) = H^{(0)} + H^{(1)} + \cdots \qquad (10)$$

As a result, we have:

$$H^{(0)} = B + \int_0^x dx'\,\varepsilon_\perp\,(A + \int_0^{x'} dx''\,\mathcal{R}), \qquad H^{(1)} = -\int_0^x dx'\,\varepsilon_\perp \int_0^{x'} dx''\,\mathcal{K}^2 H^{(0)}, \qquad (11)$$

where $0 \leqslant x \leqslant a$, A and B are the integration constants.

From relationships (9)-(11) and from the continuity condition for functions $H(x)$ and $\frac{\partial H}{\partial x}$ at the points $x=0$ and $x=a$, we shall find amplitudes of the magnetic field of the second harmonics (waves with double frequency) in vacuum:

$$H_\pm = -\frac{i}{4k_0}\cdot\int_0^a dx\,\mathcal{R} - i\frac{k}{2k_0}\cdot\int_0^a dx\,\frac{\varepsilon_2}{\varepsilon_1}\int_0^x dx'\,\mathcal{R} \pm \frac{1}{2}\cdot\int_0^a dx\,\varepsilon_\perp\int_0^x dx'\,\mathcal{R}. \qquad (12)$$

In (12) we have omitted the terms proportional to a^2 .

Using expressions (6) and (8) in (12), we have

$$H_\pm = \frac{eE_0^2}{mc\omega}\cdot\int_0^a dx\,\frac{\varepsilon_2}{\varepsilon_1}\left\{\frac{k}{\varepsilon_1^2-\varepsilon_2^2}\left[i\frac{k}{k_0}\left(\frac{2\omega}{\omega_H}^2\varepsilon_3 - \varepsilon_1\right) + \frac{2\omega}{\omega_H}\varepsilon_1\varepsilon_3 - \varepsilon_2\right] \mp \left(ik_0 + \frac{2\omega}{\omega_H}k\varepsilon_3\right)\right\}. \qquad (13)$$

In the case of a low-density plasma when $\left|\frac{\Omega^2}{4\omega^2-\omega_H^2}\right| \ll 1$, expression (13) takes on the form

$$H_\pm = \frac{4\pi e^3 N}{m^2 c\omega(4\omega^2-\omega_H^2)}\cdot\left[-i\frac{\omega_H}{2\omega}\left(\frac{k^2}{k_0}\pm k_0\right) + (1\mp 1)k\right]\cdot E_0^*, \qquad (14)$$

where $N = \int_0^a n_0(x)\,dx$ is the total number of electrons per unit surface of the plasma layer.

It follows from (13) and (14) that, in the case of magnetoactive plasma, generation of the second harmonics increases sharply when incidence angle of the waves with basic frequency goes to $\frac{\pi}{2}$ i.e. $k_0 \to 0$ (we note that at $k_0 \leqslant k \ll ka$ our consideration becomes inapplicable).

Also, from (14) it can be readily seen that, at low densities of a plasma ($\Omega \ll \omega$), the amplitudes of waves at double frequencies increase sharply when ω_H approaches 2ω . However, as it follows from (13), a similar effect does not exist at $\Omega \gtrsim \omega$.

In the case of a low-density magnetoactive plasma, as distinct from the case of isotropic plasma, the second harmonics are radiated from the plasma layer to both sides.

REFERENCES

/1/ Fidone J., Granata G. and Teichman J. (1971) Phys. Fluids, 14, 737.

/2/ Alanakyan Yu.R. (1965) Soviet Phys.-tech. Phys., 10, 1202.

/3/ Dolgopolov V.V., El-Siragy N.M. and Sayed Y.A. (1974) J. Plasma Physics, 12, 15.

/4/ Stepanov K.N. (1965) Zh. tech. Fiz., 35, 1849.

[+] On leave from the Atomic Energy State Committee, USSR.

SPATIALLY RESOLVED INSTABILITY MEASUREMENTS WITH A HEAVY ION BEAM PROBE

W. C. Jennings, R. L. Hickok, and J. C. Glowienka
Plasma Dynamics Laboratory
Rensselaer Polytechnic Institute
Troy, New York 12181 USA

Abstract: A heavy ion beam probe has been used to make simultaneous measurements of the amplitude and phase of both density and space potential fluctuations in an energetic arc plasma. Detailed comparison with theoretical predictions identifies a 70 KHz coherent oscillation as a Kelvin-Helmholtz instability localized to a region of strong fluid shear.

INTRODUCTION

Unambiguous identification of instabilities in high energy density plasmas has been exceedingly difficult. This is primarily due to the lack of space and time resolved measurements of both plasma density and space potential. We have now demonstrated that ion beam probing can provide the required information. The present work is concerned with the detailed comparison of theoretical predictions and experimental data for a Kelvin-Helmholtz instability in an energetic arc discharge. The techniques, however, can be extended to larger plasma systems and in particular, should be applicable to the study of trapped particle modes in Tokamaks.

An ion beam probe diagnostic system is shown schematically in Fig. 1. A beam of singly charged primary ions is directed through the plasma normal to the confining magnetic field. Some of these are converted to doubly charged secondary ions by electron impact. The intensity of the secondary ion beam provides a measure of the plasma density and electron temperature at the location where the secondary ions were created.[1] The energy difference between the primary and secondary beams is a direct measure of the plasma space potential.[2] Typical space resolution is 0.6 cm^3 and time resolution is less than 10 μsec, allowing detailed measurements of low frequency plasma instabilities.

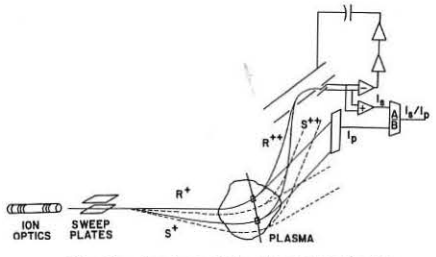

Fig. 1: Ion Beam Probe Diagnostic System

EXPERIMENTAL MEASUREMENTS

The instability study was carried out in an energetic hollow cathode discharge which was operated with a solonoidal magnetic field of ≤ 2 kgauss. This arc produced a 3 cm diameter He plasma with a peak density of the order of 10^{14} cm^{-3} and an electron temperature of ≈ 10 eV.[1] The plasma was subject to a strong coherent instability at a frequency of approximately 70 KHz.

Figure 2 shows a typical beam probe profile measurement along a plasma diameter. The central trace is the fluctuating component of the plasma density and shows strong radial localization and essentially zero amplitude at the center of the plasma. The second trace is the time-averaged space potential profile along the same diameter. Detailed examination of space potential profiles shows that there is a reversal in the radial electric field and that the instability is maximum in this region of strong fluid shear. Both traces in Fig. 2 are asymmetric whereas the corresponding time-averaged density distribution possesses cylindrical symmetry. Space potential fluctuations are somewhat noisier and show the same characteristics as the density fluctuations except the radial location of the peak amplitude is slightly smaller.

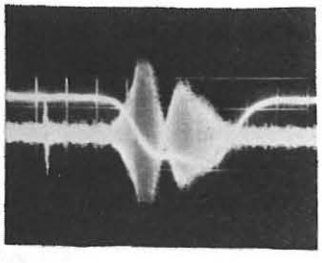

Fig. 2: Fluctuating Density Amplitude and Time-Averaged Space Potential Along a Diameter of the Plasma

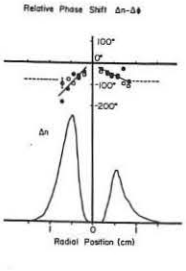

Fig. 3: Fluctuating Density Amplitude and Density-Space Potential Phase Difference Along a Diameter of the Plasma

Figure 3 shows similar radial plot of the fluctuating density amplitude along with the density-space potential phase angle. Since both density and space potential fluctuations are measured simultaneously, this phase difference can be directly measured. Almost all the variation in phase angle is due to the space potential phase. Density phase measurements show a nearly constant phase on either side of the plasma. There is an ≈ 180° phase shift at the center, establishing an m = 1 azimuthal mode.

Variation of the axial magnetic field causes large changes in the characteristics of the instability, as shown in Fig. 4. The left hand oscillograms show the fluctuating density and the time-averaged space potential along a chord that is tangent to the peak amplitude radius. The right hand oscillograms are spectrum analyzer traces of the density signal. As the magnetic field increases the gradients in the space potential become more pronounced. This leads to larger instability amplitude and increased coherence. Similar variation in the space potential profile can be produced by varying the arc current while maintaining the magnetic field constant. This also leads to the same type of behavior for the fluctuation spectra and clearly demonstrates that the radial space potential profile is the dominant parameter controlling the instability.

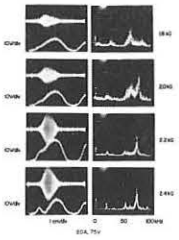

Fig. 4: Effect of Changing the Confining Field. Left Hand Oscillograms: Top Trace is Fluctuating Density Amplitude, Lower Trace is Time-Averaged Space Potential Along an Off-center, Detector Line. Right Hand Oscillograms: Spectrum Analyzer Trace of Density Signal.

COMPARISON WITH THEORY

The ability to make space and time resolved measurements of both density and space potential permits us to make a detailed comparison with theoretical predictions. The strong dependence on the space potential profile and the localization to the region of maximum fluid shear suggest a Kelvin-Helmholtz instability. We have compared the measurements with predictions based on a model developed by Jassby.[3] This model predicts localization to regions of maximum shear, $e\tilde{\phi}/kT_i >> 1$, and a large variation in the density-space potential phase angle in the region of the maximum shear. The experimental results are in excellent agreement with the predictions. The localization and phase variation are shown in Fig. 3 and the measured value of $e\tilde{\phi}/kT_i > 25$.

We have also used a general flute model developed by Rosenbluth and Simon[4] to predict the eigenfrequency of the instability and the radial eigenfunctions of density and space potential. The model takes the form of a radial wave equation which must be evaluated numerically. The analysis was made specific to the present experiment by using a rotation profile determined from the space potential measurements. Figure 5 shows the measured and calculated radial profiles for the amplitude and phase of the density fluctuations. The calculated eigenfrequency is 135 KHz compared with the experimentally observed frequency of 70 KHz. The agreement is very good, considering that the model utilizes a linear perturbation analysis and assumes cylindrical symmetry while the measurements are made in a non-linear regime and show definite asymmetry. Similar agreement is obtained for the amplitude and phase of the space potential fluctuations.

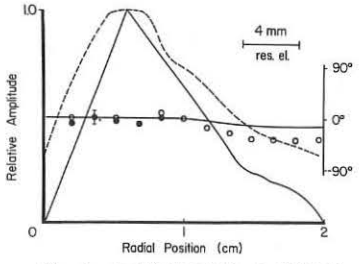

Fig. 5: Amplitude and Phase of Density Fluctuations vs Radius. Dotted Lines and Points are Experimental Data. Solid Lines are Theoretical Predictions.

CONCLUSIONS

A heavy ion beam probe is capable of providing the space and time resolved measurements of density and space potential in high energy density plasmas that are necessary in order to obtain an unambiguous identification of plasma instabilities. Excellent agreement between theory and experiment has been obtained for a Kelvin-Helmholtz mode in an energetic arc.

REFERENCES

1. R. E. Reinovsky, J. C. Glowienka, A. E. Seaver, W. C. Jennings and R. L. Hickok, IEEE Trans. Plasma Science, PS-2, 250 (1974).
2. F. C. Jobes and R. L. Hickok, Nucl. Fusion, 10, 195 (1970).
3. D. L. Jassby, Phys. Fluids, 15, 1590 (1972).
4. M. N. Rosenbluth and A. Simon, Phys. Fluids, 8, 1300 (1965).

†Work Supported by ERDA Contract AT(11-1)-2229

ION-BEAM PLASMA INTERACTION AT THE ION CYCLOTRON FREQUENCY

A. Goede, P. Massmann, H.J. Hopman, J. Kistemaker

Association Euratom - FOM

FOM-Instituut voor Atoom- en Molecuulfysica, Kruislaan 407, Amsterdam
The Netherlands

Abstract: Injecting an energetic He^+-ion beam obliquely into a magnetized plasma, we observe the excitation of ion cyclotron harmonic waves (ICHW), propagating azimuthally across the applied magnetic field. These measurements are discussed in the framework of the linear theory of electrostatic instabilities in a homogeneous Maxwellian plasma, traversed by a monoenergetic ion beam.

Experiment: A He^+-ion beam (energy 10 keV, density 10^7 cm^{-3}) is injected into a beam created plasma column (density 10^7 - 10^8 cm^{-3}, electron temperature 5 eV, length 1 m, diam. 2 cm), which is confined in an uniform magnetic field B (up to 6 kG). The beam is injected with a small but finite divergence, which gives the beam ions a velocity component v_{oz} parallel and $v_{o\perp}$ perpendicular to $\vec{B}$. We have the following ordering in velocities: $c_s < v_{o\perp} << v_{the}$ and $v_{oz} \lesssim v_{the}$ (v_{the} is the electron thermal velocity, c_s the acoustic velocity). Most measurements have been done in Helium at a pressure of 2.8×10^{-5} Torr. Under this condition we have the following parameter range: $0.9 < \omega_p/\omega_{ci} < 8$, and $0.7 < \omega_{pb}/\omega_{pi} < 2$ where $\omega_p^2 = \omega_{pi}^2 + \omega_{pb}^2$ (ω_{pi} and ω_{pb} are the plasma frequencies of plasma and beam ions, ω_{ci} is the ion cyclotron frequency). The observed waves are picked up by two Langmuir probes. Their phase velocities are determined from the phase shift of the wave as a function of probe distance.

Measurements: In this system we observe the excitation of waves, which are connected to the ion cyclotron harmonics. Fig. 1 gives frequency and amplitude as function of B. The oscillations are observed in a rather wide range of B-field values. However, the amplitude of the wave does not remain constant when varying B. It shows definite maxima as shown in the lower half of Fig. 1. One can distinguish three instability regions. In these regions the number of cyclotron turns made by the beam ions increase from ½ to 3/2. The frequency difference $(\omega - \omega_{ci})$ is weakly proportional to the plasma density. By taking H_2 or Ne instead of He as a target gas, we checked that the frequency of the excited waves is connected to the cyclotron frequency of the plasma ions and not with the ions of the beam.

Wave propagation measurements in axial and radial direction do not show a clear phase shift. The magnitude of the azimuthal phase velocity v_{ph} is in the order of 10^4 m/s, measured at the edge of the plasma column. The measurements have been done in the three instability regions of the B-field. Only the propagation of the first harmonic has been studied. Written in terms of the cyclotron frequency and the beam radius a, we get the experimental relation for the azimuthal phase velocity: $v_{ph} = (0.9 \pm 0.2)a\omega_{ci}$. This means $v_{ph} \approx v_{o\perp}$, supposing $v_{o\perp} \approx a\omega_{ci}$. From the frequency and phase velocity it follows that the instabilities near ω_{ci} are n = 1 modes.

Theory: From our measurements it follows that we should focus on slow waves, propagating across the magnetic field, with a frequency near the ion cyclotron frequency and its harmonics. The instability frequency shows a weak dependence on the plasma density. Since the waves are connected to the ions of the plasma, we may consider the waves as plasma modes, driven unstable by the presence of the beam.

The electrostatic dispersion curves for plasma waves with $k_z = 0$ in the low frequency regime, the so-called ion Bernstein waves, exhibit the above mentioned properties [1]. Ion Bernstein waves are essentially undamped. When the propagation direction deviates a small amount from exact perpendicularity, they become Landau damped by the plasma electrons. However, the measurements of Fig. 2, show no measurable phase shift in axial direction. Assuming the phase shift to be less than 0.1 μs over 40 cm, it means that $\omega/k_z > 4v_{the}$ and $\omega/k_z > 6v_{oz}$ (ω/k_z is the axial phase velocity). Hence, electron Landau damping can be neglected and the approximation $k_z = 0$ is justified. As a consequence the perpendicular beam velocity component is supposed to be the wave driving mechanism, since a resonance between parallel beam velocity and wave does not exist if $k_z = 0$.

To work out this hypothesis, consider a collisionless magnetized plasma, which is taken uniform and infinite. The propagation characteristics of small amplitude electrostatic plasma waves are given by the Harris dispersion relation [2]. When we substitute a Maxwellian for the plasma and a δ-function for the velocity distribution and assume $k_\perp \rho_e >> 1$, we get the following dispersion relation for pure perpendicular propagation:

$$\sum_{n=1}^{\infty}\left[\frac{\omega_{pi}^2}{\omega_{ci}^2}\,\frac{e^{-\lambda_i} I_n(\lambda_i)}{\lambda_i} + \frac{\omega_{pb}^2}{\omega_{ci}^2}\,\frac{1}{\mu}\,\frac{d\,J_n^2(\mu)}{du}\right]\frac{2\,n^2\omega_{ci}^2}{\omega^2 - n^2\omega_{ci}^2} = 1 + \frac{\omega_{pe}^2}{\omega_{ce}^2}$$

(J_n and I_n are the Bessel and modified Bessel function, $\lambda_i = \frac{1}{2} k_\perp^2 \rho_i^2$, $\mu = k_\perp v_{o\perp}/\omega_{ci}$, ρ_s = Larmor radius species s.)

This dispersion relation is formally identically to that for electron cyclotron waves which has been treated before by Tataronis and Crawford [3]. They showed that this dispersion relation contains unstable wave solutions around the cyclotron harmonics. Also they proved that these instabilities are absolute in nature. We have numerically solved this equation for the ions, taking μ real and ω complex. In fig. 3 a specific conditions is plotted. We find a rather strong instability at $\omega \approx 1.5\ \omega_{ci}$ and the subsequent harmonics. The magnitude of the growth rate is about $\mathrm{Im}\ \omega/\omega_{ci} \approx 0.2$, which means a growth of about 10 dB per cyclotron period. The value of the instability wavenumber is $\mu \approx 4$. This is about 35% larger than the experimentally found value. The instability frequency is about 7% too high. The experimentally found increase in instability frequency with density is present in our model. The instability threshold is strongly dependent on the parameter ω/ω_{ci}. At high B-field the theory does not predict instability, contrary to our experimental results.

Discussion: In his ion beam-plasma experiment Gabovich presumably observed the same type of instability as we did [4]. His interpretation however differs from ours. He attributes the excitation of the ion cyclotron harmonic waves to the spatial inhomogeneity of the beam-plasma system. Indeed the radial density gradient is not negligible and the azimuthal propagation suggests drift waves. It is thus possible that the instability is an ion cyclotron drift wave (ICDW), which was recently investigated by Hendel and Yamada [5]. However, in our experiment the ion drift frequency is a factor ten smaller than the ion cyclotron frequency and also our phase velocity is proportional to B, unlike the phase velocity of ICDW which are inversely proportional to B. So in our experiment we do not expect a strong influence of the density gradient on the wave propagation. However, the instability threshold is lowered by inhomogeneity.

References:

[1] R.W. Fredericks, J.Plasma Phys. 2 (1968) 365.
[2] E.G. Harris, Plasma Phys. 2 (1961) 138.
[3] J.A. Tataronis, F.W. Crawford, J.Plasma Phys. 4 (1970) 231.
[4] M.D. Gabovich, I.A. Soloshenko, Sovjet Phys. -Techn.Phys. 15 (1970) 184.
[5] H.W. Hendel, M. Yamada, Phys.Rev.Lett. 33 (1974) 1076.

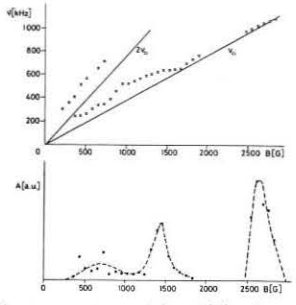

Fig. 1 Dependence of instability frequency and amplitude on the magnetic field.

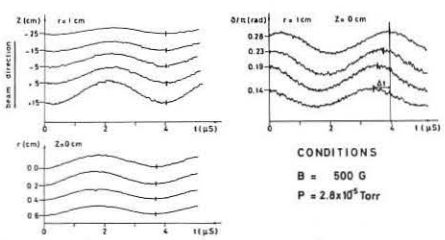

Fig. 2 A typical set of raw wave propagation measurements. In axial or radial direction we do not find a clear phaseshift. In azimuthal direction the phaseshift corresponds to a phasevelocity of 8×10^3 m/s in the ion-gyration direction.

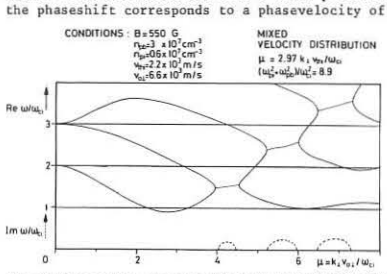

Fig.3 Dispersion of perpendicular propagating ion cyclotron waves in a plasma with a velocity distribution which consists of a mixture of a Maxwellian and a δ-function. Low B-field case.

ION BEAM EXCITATION OF ELECTROSTATIC ION-CYCLOTRON WAVES

N. Rynn, H. Böhmer, and J. P. Hauck
Physics Department, University of California
Irvine, California, USA 92664

Abstract: Electrostatic ion-cyclotron waves are excited by a cesium ion beam injected into a cesium plasma in a Q-machine. Strong interactions are observed. Spatial growth rates are measured as a function of beam and plasma parameters.

We present evidence for the excitation of electrostatic ion-cyclotron waves by the interaction of a cesium ion beam having a small perpendicular velocity component with a cesium plasma. Our objective is plasma ion heating which has already been observed in this laboratory[1] for the case of electron-current driven electrostatic ion cyclotron waves (ICW).

The Q-machine was operated in the single ended mode with the final electrode of the ion beam source terminating the plasma (Fig. 1). Considerable care was taken to insure that the observed modes were driven by the ion beam current and were not spurious modes driven by electron current from any electrodes. The ion beam was produced by a porous tungsten plug and focussed by Pierce electrodes. The beam is characterized by currents in the range 1 μA to 1 mA, energies of 30 eV to 1 keV and densities in the range 10^7 to $10^9 cm^{-3}$; it is nearly monoernergetic.

The beam was injected in a region of converging magnetic field. The perpendicular velocity, $v_\perp$, of the beam was controlled by varying the radial position of the ion injector. Typically $v_\perp$ is in the range $1 - 6 \times 10^5 cm\ sec^{-1}$, corresponding to perpendicular energies of about 1 - 25 eV and Larmour radii of 0.3 - 2 cm. The perpendicular velocity is thus several times the ion thermal velocity and comparable to the perpendicular phase velocity of the IC waves. Beam particle trajectories are shown schematically in Fig. 1. The beam is focussed in this way because of the converging magnetic field at the injection point.

When a beam of these characteristics is injected into a plasma of density of the order of $10^8 cm^{-3}$, modes are observed at frequencies just above the ion cyclotron frequency, f_{ci}. The steady state level of the observed turbulence depends strongly on the beam parameters (Fig. 2). At low beam densities relatively narrow linewidth modes are excited, whereas for strong beams a highly turbulent state obtains, characterized by a strong increase of broadband noise from 0 to 200 kHz and above.

These modes persist over a range of magnetic fields varying from 3 kG to 7.5 kG, the maximum field available.

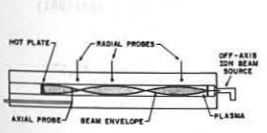

Fig. 1: Schematic of Q-machine and ion beam setup.

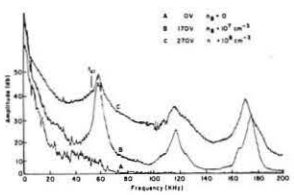

Fig. 2: Frequency spectrum of the mode amplitudes. B = 4.65 kG, $n_p = 3 \times 10^8 cm^{-3}$

Their frequencies are in the range nf_{ci} to $(n + 0.2)f_{ci}$, being slightly higher than the ion cyclotron frequency and its harmonics. Typically, several harmonics are present with the third harmonic frequently dominating near onset.

The dispersion relation for ion beam driven ion-cyclotron waves can be derived following the method of Tatronis and Crawford.[2]

For low beam densities and no damping, the final result is the dispersion relation for "normal" ion cyclotron waves,

$$\omega = n\omega_{ci}\left(1 + \frac{\Delta_n}{1 + \Delta_n}\right) \; ; \; \Delta_n = \frac{T_e}{T_i} e^{-s_i} I_n(s_i) \quad .$$

For small values of $s_i = (k_\perp \rho_i)^2$ the ion cyclotron mode frequency is approximately f_{ci} while for larger values of s_i the frequency increases to a maximum at $s = 1.5$ to 1.18 f_{ci} for $T_e/T_i = 1$. Here we have assumed that $k_\perp = m/r_b$. The azimuthal mode number m is a small integer. Since the observed frequencies are in the range $f = 1.18\ f_{ci} - 1.2\ f_{ci}$ the modes are identified as the electrostatic ion-cyclotron modes.[3]

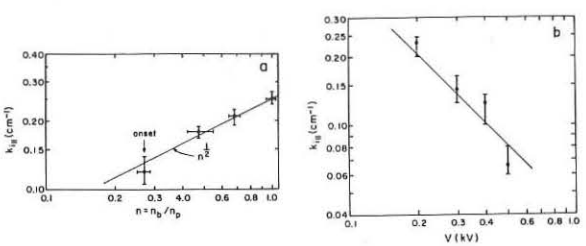

Fig. 3: (a) Beam density dependence ($V_b = 200$ V), and (b) Beam energy dependence ($n_b \sim 10^8 cm^{-3}$) of the spatial growth rate B = 4 kG, $n_p = 3 \times 10^8 cm^{-3}$.

We have also measured the axial wavelength and spatial growth rate of the modes using an axially movable probe. The wavelength was measured using a cross correlation technique. The axial wavelength is selected by the beam velocity such that $\lambda_\parallel = (1 \pm 0.2) v_{o\parallel}/f_{ICW}$.

We observe the amplitude of these waves to grow exponentially for about 30 cm from the injection point. The growth rate increases as the beam source is moved further off axis and with increasing beam current; it decreases at high beam velocities and is relatively independent of the magnetic field strength (Fig. 3). It can be shown that these general features are in qualitative agreement with a theoretical expression for the growth rate, but the experimental growth rate is much larger than the theoretical value.

This work was supported by National Science Foundation Grant #GP-39031X.

References

1. N. Rynn, D. R. Dakin, D. L. Correll, and Gregory Benford, Phys. Rev. Letters 33, 765 (1974).
2. J. A. Tatronis and F. W. Crawford, J. Plasma Physics 4, 231 (1970).
3. W. E. Drummond and M. N. Rosenbluth, Phys. Fluids 5, 1507 (1962).

RELAXATION OF ENERGETIC ION BEAM IN A TURBULENT PLASMA

K.Ishii, A.Itakura, H.Ishizuka, S.Hagiwara, S.Kojima
Department of Physics,Tokyo University of Education
Bunkyo-Ku, Tokyo, 112 Japan
and
S.Miyoshi, K.Yatsu and T.Kawabe
Institute of Physics, the University of Tsukuba
Ibaraki-Ken, 300-31 Japan

Abstract: The enchanced relaxation of an energetic ion beam has been studied experimentally in a turbulent plasma. The broadening of spectrum and loss of the beam energy were investigated as a function of level of turbulence. The results were explained by the theory of stochastic process.

The investigation of relaxation process of ion beams in plasmas is important from the point of view of plasma heating and formation of two component plasma. Collisionless thermalization of an ion beam in the plasma was studied theoretically (1) and experimentally (2) under the condition that the beam velocity was comparable to the ion sound velocity. In this paper we report the experimental results on relaxation of an energetic ion beam in a turbulent plasma and an interpretation based on the theory of stochastic process.

The experimental apparatus (OHTSUKA II) is shown in Fig.1(length:2 m, diameter of the chamber: 13 cm, strength of the magnetic field: 3 kG). The helium ion beam was generated by a multi-aperture ion source (3) and injected into the chamber on the axis along the magnetic field from one end of the device and analysed with an electrostatic analyser at the

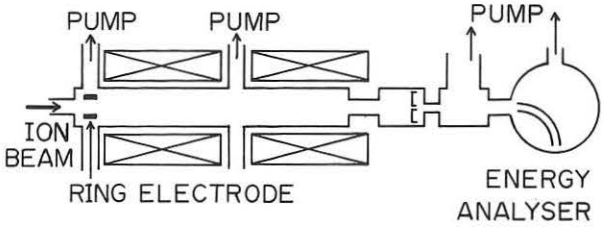

Fig.1 Schematic diagram of the experimental apparatus

opposite end. The energy and current of the beam were typically 1.5 keV and 5o mA,respectively. The plasma was produced by ionizing the helium gas in the chamber with a pressure of 3×10^{-4}Torr by ion beam itself. Parameters and fluctuations of the plasma were measured by Langmuir probes. The density and the temperature of the plasma were $10^{10}cm^{-3}$and 20 eV, respectively. The diameters of both the beam and the plasma were 3 cm each.

As the fluctuations in the beam-produced plasma were quite small, turbulent fluctuations were excited by applying dc high voltage on a ring electrode surrounding the plasma column and drawing current through the plasma. The potential of the plasma on the axis did not change to affect on the beam dynamics. In this way three types of oscillations were excited: low frequency fluctuations with a turbulent spectrum, 100 kHz fluctuation and 8 MHz fluctuation. The first one had a broad frequency spectrum from 1 kHz to 200 kHz with and amplitude of about 30 V. The second one had a width of the frequency spectrum of 20 kHz, an intensity of 3 V, an azimuthal mode number of zero, and a longitudinal wave length of 20 cm. This fluctuation was referred to as an ion acoustic wave. The frequency of the third fluctuation was close to the ion plasma frequency, and the azimuthal mode number of it was 1. When the ring voltage was increased, the frequency spectrum of the fluctuations did not change, while the intensities of all three types increased.

Typical examples of the energy distribution of the ion beam at different values of the ring voltage are shown in Fig.2. When the ring voltage was applied up to 1.0kV, the width of the energy distribution $\Delta E/E$ changed from less than 0.8 to 5.4 %. The relation between the energy spread $\Delta E/E$ and the amplitude of the 100 kHz fluctuations ($\delta\varphi$) is shown in Fig.3. The energy spread had also same dependence on the low frequency fluctuations, while it had somewhat different tendency on the amplitude of the 8 MHz fluctuations. Therefore we conclude that the low frequency fluctuations and the ion sound waves are responsible for anomalous energy relaxation of the ion beam.

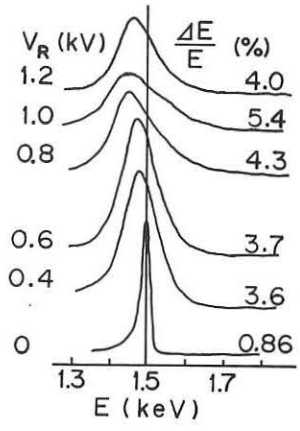

Fig.2 Energy distribution of ion beam for different values of ring voltage V_R.

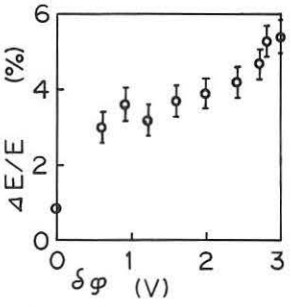

Fig.3 Energy spread of ion beam vs potential fluctuation.

According to the theory by Ichimaru(4), when the beam velocity V_b is much larger than the phase velocity of the wave, the wave-particle interaction brings about the change of the thermal energy of the beam (K_b) which is written as

$$\frac{d}{dt}K_b \simeq -\sum_{\kappa}\int d\omega \frac{\vec{k}\cdot\vec{V_b}}{4\pi} I_m\chi_b \langle |E^2(\vec{k},\omega)| \rangle \qquad (1)$$

where χ_b is susceptibility of the beam, and k,ω and $\langle |E|^2 \rangle$are the wave number, angular frequency and the ensemble average of the fluctuation field, respectively. Equation (1) leads to the energy spread of the beam (dE_b) given simply by

$$dE_b \simeq 4e\,\delta\varphi\,(L\gamma/V_b)^{1/2} \qquad (2)$$

where γ is linear growth rate of the fluctuation and L is the interaction length. If γ could be replaced by the inverse of correlation time (τ_c), then the equation (2) would become the one deduced from the stochastic approaches of difusion in velocity space. By giving the measured values of $\delta\varphi$ and τ_c, we obtained an energy spread of 5 % which agreed with the measured value.

The authors thank Professor S.Ichimaru of the University of Tokyo for his fruitful discussions.

References:

(1) A.A.Vedenov, E.P.Velikhov and R.Z.Sagdeev, Sov.Phys.Usp.4,332(1961)
(2)A.G.Borisenko and G.S.Kirichenko, Sov.Phys.JETP. 33,2o7(1971).
(3)K.Yatsu, K.Uehara, S.Hagiwara and S.Kojima, Rev.Sci.Instrum. 45,570 (1974).
(4)T.Tange and S.Ichimaru, J.Phys.Soc.Japan 36,1437 (1974).

AUTHOR INDEX

L.

M.

U.

V.

W.

Y.

Z.